Imperial College
London

Alternating Injection of Steam and CO_2 For Thermal Recovery of Heavy Oil

A thesis

submitted to the Department of Earth Science and Engineering

Imperial College London

in part fulfilment of the requirements for the degree of

Doctor of Philosophy

in

Petroleum Engineering

by

Kazeem Akintayo Lawal

August 2011

Declaration

*I declare that this thesis: "**Alternating Injection of Steam and CO_2 for Thermal Recovery of Heavy Oil**", is the outcome of my own original thoughts, works and analyses, while any ideas and information from other people and sources are duly acknowledged in line with the current standard practice in petroleum engineering and related disciplines.*

_____

Kazeem Akintayo Lawal

Dedication

All my teachers, formal and informal, for building me!

In memory of Sikiru Ayinde Balogun (Barrister), for the inspiration through your works, and for giving Fuji music to the world.
Sun ree o, Barry Wonder, Mr *Fuji*.

My granny, for nursing me at infancy, when I had very remote chances of survival.
Iya Alade, thanks for the sacrifice.

The custodians of our culture, for preserving our heritage in the face of the intrusions through the Sahara and the Atlantic. *Isese a gbe wa ooo (ase)*!

Abstract

A combination of rising oil demand and declining supply from the conventional sources is drawing global attention to the vast heavy-oil resources. These are commonly developed with steam-based processes which, in most cases, burn fossil fuel to generate the required steam. However, tightening constraints on fuel, water, and the environment are some of the factors currently fuelling the interests in enhancements to the traditional steaming operations. To mitigate some of the steam-related issues, we introduce two new thermal recovery methods, namely: (i) alternating-injection of steam and CO_2 (SAC), and (ii) alternating-injection of steam and flue-gas (SAF).

The primary objective of this research is to assess the technical and commercial feasibility of these new processes. To achieve this objective, we employ a combination of analytic modelling, numerical simulations and experimental studies, investigating the reservoir heat-transport aspects of steam-based processes, asphaltene-induced formation impairment, as well as the key controls on reservoir dynamics and project economics.

In this work, the concepts of first-contact condensation (FCC) and multiple-contact condensation (MCC) have been introduced as additional mechanisms of heat-transport in steam-based processes. Hence, the traditional conductive-convective heat equations have been extended. Solutions of these equations indicate that laboratory and field observations are better rationalised, hence eliminating the current practice of employing unrealistic effective permeability and thermal diffusivity to explain these observations. We also provide conditions under which petroleum reservoirs may be analysed as adiabatic systems, and establish the relative influence of reservoir and operating parameters on reservoir heat-transport.

Considering the asphaltene-precipitation potentials of CO_2 and flue-gas, new models have been formulated for describing asphaltene-induced impairment of the permeability of porous media which, in turn, have been analysed as either closed (non-flowing) or open (flowing) systems. Application of the models to rationalise the experimental results from common porous media, which include sandstone, carbonate and glass-bead, validates their robustness. As a further test on the robustness of the proposed models, their main underlying assumptions have been validated with a set of capillary-flow experiments, which approximate asphaltene deposition at pore scale.

As a case study for reservoir simulations, the Nigerian heavy-oil deposit has been examined. The sensitivity of reservoir response to reservoir, geometric (number and design of wells) and operating parameters has been quantified. From these results, a realistic set of dynamic-simulation models has been constructed for the Nigerian deposit. Within the parameter-space explored, the main subsurface uncertainties are reservoir geometry, permeability distribution as well as fluid and

relative-permeability models. In addition, all the processes, namely steam-alone, SAC and SAF, are vulnerable to geometric and operating parameters.

On the net effect of in-situ asphaltene removal, the alternating-injection processes would only yield higher oil recovery than the steam-alone process if there is significant in-situ deasphalting such that the oil-viscosity reduction effect overrides the permeability impairment effect. Otherwise, the miscibility of these gases in the oil-phase is not sufficiently high to take advantage of the reduction of crude viscosity by dilution.

Finally, within the range of parameters evaluated, the three processes are technically and commercially feasible for the Nigerian deposit investigated. However, in terms of economics and robustness against commercial risks, the order is SAC > steam-alone > SAF. The reservoir model, oil price and costs are found to be the main determinants of project risks. Given the limitations of this research and the uncertainties in the input data used for analyses, we complete the work by outlining the scope for further studies.

Acknowledgements

The credit for this work goes to my supervisor, Prof. Velisa Vesovic, for his insights and understanding during this study. Most importantly, thanks for allowing me an "infinite" domain, rather than a perching spot, to explore original ideas. Velisa, with this thesis, I hope I have been able to articulate most of our fascinating thoughts in a way to make our research group take pride in this work. If not, please bear with me, as there is always a room for improvement.

I would like to thank the Nigerian Government (Petroleum Technology Development Fund), for sponsoring my PhD studies at Imperial College London (ICL). To Dr. F.B.O. Dayo of Triple 'E' Systems Associates Ltd., Lagos, Nigeria, I am grateful for cultivating and nurturing my interests in energy and climate-related issues.

I also acknowledge all the authors whose works were consulted in the course of this research. Thanks for sharing your great ideas. Much appreciation to Prof. M.A. Rahaman of the Geology Department, Obafemi Awolowo University, Ile-Ife, Nigeria, for providing vital materials on the geosciences of the Nigerian heavy-oil deposit. Prof., I still cherish those telephone conversations and the attempt at visiting me at Imperial. Thanks to Dr. N. Riesco of Earth Science & Engineering Department ICL, for providing the FORTRAN compiler used for some aspects of this work.

My gratitude goes to Prof. G.C. Maitland and Dr. E. Hendriks for accepting to serve as my internal and external examiners, respectively. I am grateful for the meticulous review of my draft thesis, with the resulting comments contributing to the quality of the final thesis.

On the experimental aspects of this research, the credits go to Drs. E.S. Boek and J.P. Crawshaw, both of the Chemical Engineering & Chemical Technology Department, ICL. John, I sincerely value your contributions in setting up the experimental rig. Edo, thanks for those stimulating discussions, and the encouragement to publish some of the exciting asphaltene-study results in *Energy & Fuel* – "the asphaltene journal". In the same spirit, I acknowledge Qatar Petroleum, Qatar Science & Technology Park, and Shell, for providing, through the Qatar Carbonates & Carbon Storage Research Centre at ICL, the facilities used for the experiments. Additional thanks to Shell, for providing the South-American heavy-oil sample used in the experimental study.

Finally, four sets of people really deserve this "PhD Degree". They are: (i) my parents and siblings, for their compliments, earn the 'P'; (ii) my friends, for their support, take the 'h'; (iii) my uncle, J.A. Olaboye, and cousin, Opeyemi, in her own little but crucial capacity, merit the 'D'; and (iv) my wife and children, for their steadfastness in the last 2+ years, during which I "abdicated" my responsibilities, certainly own the 'Degree'. Folayemi and Gbemisola, I'm sorry for not being around to supervise your school works, take you out, and partake of the fun times. Damilola, *aya mi owon*, I'm sorry for not being available for the "pillow" talks. With these wonderful people, I'm convinced that my garment of honour remains intact. *E seun ooo*!

Contents

Declaration 2
Dedication 3
Abstract....4
Acknowledgements....6
Contents....7
List of Tables....12
List of Figures....14
List of Publications....21
Nomenclature....22

1 Introduction....27
1.1 The SAC Concept....28
1.2 Study Objectives....30
1.3 Thesis Outline....30

2 Literature Review....32
2.1 Steam-Injection Processes....32
2.1.1 Current Status and Challenges....34
2.1.2 Process Improvements....35
2.2 Modelling Steam-Injection Processes....36
2.2.1 Analytic Models....36
2.2.2 Numerical Models....43
2.2.3 Experimental Models and Field Studies....46
2.3 Analogy from Industrial Processes....51
2.4 Chapter Summary....52

3 Modelling Heat-Transport in Petroleum Reservoirs....54
3.1 Domain Definition and Modelling....54
3.1.1 Mass Balance....56
3.1.2 Momentum Balance....57
3.1.3 Heat Balance....58
3.1.4 Initial and Boundary Conditions....65
3.2 Numerical Solution....65
3.2.1 MCC Model....66
3.2.2 FCC Model....66
3.2.3 Numerical Convergence....67
3.2.4 Optimum Mesh Sizes- MCC....68
3.2.5 Optimum Mesh Sizes- FCC....70

3.2.6 Numerical Program……..71
3.3 Example Application……71
3.4 Results and Discussion……71
3.5 Reservoir Zoning by Heat-Transfer Mechanisms……..……80
3.6 Further Critiques of Current Reservoir-Heating Models…… 82
3.7 Relaxing Key Assumptions Underlying the Heat-Transport Models……86
3.7.1 Influence of Pressure-Drop on Reservoir-Heating……..…86
3.7.2 Time-scale for Reaching Local Thermal Equilibrium……..89
3.8 Chapter Summary……..…92

4 Heat-Transport for Systems with Non-Isothermal Boundaries…… 94
4.1 A Review of Current Methods of Modelling Boundary-Thermal Losses…….. 94
4.2 Formulation of Boundary Thermal-Loss Model…… 96
4.2.1 Overall Heat-Transfer Coefficients……98
4.2.2 Temperatures of Cap and Base Rock……98
4.2.3 Numerical Schemes……99
4.2.4 Boundary Conditions……100
4.2.5 Solution of PDE under Conducting Boundaries……..103
4.3 Effects of Relative Location of Sink Saturants……..103
4.3.1 Simulation Design……105
4.3.2 Interpretation of Simulation Results..…… ….. 105
4.3.3 Relative Location of Sink Saturants……..106
4.4 Parametric Studies……..116
4.4.1 Effect of Boundary Thickness……..…116
4.4.2 Effect of Reservoir Thickness……..…117
4.4.3 Effect of Injection Temperature…….. 118
4.4.4 Effect of Heat-Transfer Coefficient of Fluids Adjacent to Boundaries…..118
4.5 Characterisation of Thermal Floods for Adiabatic Analysis……..…119
4.5.1 Effect of Boundary Conductive-Resistance……..…120
4.5.2 Effect of Permeability on Minimum R_{th}……..…122
4.6 Further Tests of Robustness of the Adiabatic Criterion……...123
4.7 Chapter Summary……..……..125

5 Asphaltene-Induced Formation Damage……..126
5.1 Theoretical Studies……..…...127
5.1.1 Formation-Impairment Model……..……127
5.2 Damage in Closed Systems……..…130
5.2.1 Model Validation for Closed Systems……..……..130
5.2.2 Validation Results for Closed Systems……...…132
5.2.3 Dynamics of Deposition in a Closed System……...…133

5.3 Damage in Open Systems……138
5.3.1 Deposition under Dynamic Conditions……140
5.3.2 Validation of Open-System Models……145
5.3.3 Towards Predictive Open-System Models……155
5.4 Experimental Investigation of Asphaltene Deposition in Capillary Flow…… 158
5.4.1 Hydraulic Design……162
5.4.2 Data-Interpretation Models ……164
5.4.3 Experimental Results and Discussion……166
5.5 Chapter Summary……170

6 Reservoir-Simulation Model for Nigerian Heavy-Oil Deposit……172
6.1 Status of the Nigerian Heavy-Oil Sector…… 172
6.2 Geology……175
6.3 Petrophysics……177
6.4 Wettability, Relative Permeability and Capillary Pressure……179
6.5 Thermal Properties and Aquifer Model……181
6.6 Reservoir Datum and Initial Conditions…… 182
6.7 Fluid Model……182
6.8 Reservoir Model……188
6.9 Well Model……190
6.10 Assessment of Subsurface Uncertainties……192
6.10.1 Single-Variable Sensitivity…… 192
6.10.2 Multi-Variable Sensitivity (Experimental Design) ……194
6.11 Final Simulation Models…… 205
6.12 Chapter Summary……206

7 Optimisation of the Steam-Alone Process……207
7.1 Optimisation Studies…… 207
7.1.1 Basis for Discriminating the Optimisation Variables…… 208
7.1.2 Reference Development Concept……209
7.2 Optimisation of Fixed Design Factors…… 210
7.3 Optimisation of Variable Design Factors…… 224
7.4 Summary of Optimum Development Concepts…… 233
7.5 Chapter Summary……234

8 Alternating Injection of Steam and CO_2 for Heavy-Oil Recovery……236
8.1 Co-injection versus Alternating-Injection of Steam and CO_2……236
8.2 Basic Process Engineering and CO_2 Emissions Inventory……238
8.3 Compressor Power Consumption……239
8.4 CO_2 Emissions due to Steam Generation and Compression Works……240

8.5 Optimisation of the Alternating-Injection Processes……..241
8.6 Final Injection and Production Schemes……..…… 245
8.7 Comparing Steam-alone and Alternating-Injection Processes……...245
8.8 Chapter Summary……..……..248

9 Reservoir / Fluid-Property Heterogeneities and Deasphalting……..... 249
9.1 Permeability Heterogeneity (Layering) ……..…..... 249
9.2 Viscosity Heterogeneity (Layering) ……..... 252
9.3 Relative-Permeability Heterogeneity (Layering) ……..…..... 253
9.4 Rock-Thermal Conductivity Heterogeneity (Layering) ……..…..… 253
9.5 Permeability-Impairment Due to CO_2-Induced Deasphalting……..... 254
9.6 Viscosity-Reduction Due to CO_2-Induced Deasphalting……..…… 255
9.7 Effects of Dispersion……..…… 256
9.8 Final Simulations……..……..… 258
9.9 Chapter Summary……..……..... 265

10 Economics and Risk Analysis……..267
10.1 Economic Model…… 267
10.1.1 CAPEX and OPEX Elements……...268
10.1.2 Revenue and Penalty……...270
10.1.3 Fiscal Terms……...271
10.2 Parameter Space and Sensitivity Analysis……271
10.3 Risk Analysis……273
10.4 Chapter Summary……...278

11 Conclusion and Future Work……..…279
11.1 Specific Conclusions……..…….. 280
11.1.1 Heat-Transport Modelling……280
11.1.2 Asphaltene-Induced Impairment……..…281
11.1.3 Numerical Reservoir-Simulations……...282
11.1.4 Economics and Risk Analysis……..282
11.2 Future Work……283
11.2.1 Heat-Transport Modelling……283
11.2.2 Asphaltene-Induced Impairment……283
11.2.3 Numerical Reservoir-Simulations……284
11.2.4 Feasibility of Alternating-Injection of Steam and CO_2……..284

Appendices

A Thermophysical and Transport Properties……..285

A.1 Mixing Rules……286

B Estimation of Condensation Rate……287

C Spatial Variation of Latent Heat Due to Pressure-Drop……288

D Lumped-Parameter System Analysis ……290
D.1 Reservoir and Surroundings are Non-Interacting……290
D.2 Reservoir and Surroundings Interact……292

E Estimating Heat-Transfer Coefficients in Porous Media……293

F Sensitivity of Other Processes to Boundary Thermal Losses……295
F.1 Non-Condensing Steam ……295
F.2 Flue Gas (50% CO_2, 50% N_2) ……295

G Numerical Integration of Asphaltene-Deposition Model……296

H Asphaltene-Induced Impairment in a Capillary Tube……297

I Some Additional Results of Uncertainty Assessment……298

J Estimation of CO_2 Emissions……299
J.1 Boiler Emissions……299
J.2 Compressor Emissions……300

K Analysis of Compositional Grading……301

L Additional Economic Results……303

References……304

List of Tables

3.1 Base-case Rock and Fluid Data……..……..…71
4.1 Base-case Rock and Fluid Data……...105
4.2 Full-Factorial Design for Saturants under MCC-Heating
(*G* = gas-saturated, *L* = liquid-saturated) ……..107
4.3 Full-Factorial Design for Saturants under CO_2-Heating……...110
4.4 Full-Factorial Design for Saturants under Conduction-Heating……..114
5.1 Summary of Reference Experiments and Validation Results……131
5.2 Summary of Benchmark Datasets……...……..146
5.3 Summary of Validation Results……....147
5.4 Parameters of the Universal Curves for the Datasets of Fadili *et al.* (2009) ……152
5.5 Numerical Values of Some Hydraulic-Design Parameters……..163
5.6 Range of Total-Injection Rate……...163
5.7 Matrix for Sensitivity Studies……....164
6.1 Average Net Thicknesses (metres) ……177
6.2 Average Porosity and Bitumen Saturations (fraction) ……177
6.3 Average Permeability, K_v / K_h, Rock Compressibility and Skin Factor……...178
6.4 Input Data for Corey-type Relative-Permeability Functions……....180
6.5 Estimated Thermal Properties for Nigerian Bituminous Rocks…….. 181
6.6 Aquifer Properties…….. 182
6.7 Estimated R_{si} and B_{oi} for Nigerian Bitumen (Lawal, 2011a; Lawal & Adenuga, 2010) ……184
6.8 Pseudocomponent Groups for the Nigerian Bitumen (Lawal & Adenuga, 2010) ……185
6.9 Correlations Used for the PC Parameters (Lawal, 2011b) ……185
6.10 Phase-Distribution of Components……...188
6.11 Area (X-Y) Dimensions of Sector Model……..……....189
6.12 Definition of Main Subsurface Uncertainties……..194
6.13 ED Matrix for the Steam-alone Process……195
6.14 Results Matrix for Steam-alone Process……197
6.15 Proxy Model Constants for Steam-alone Process……....199
6.16 Responses and Inferred Probabilistic Realisations for Steam-alone Process……200
6.17 Results Matrix for the SAC Process……201
6.18 Proxy-Model Constants for the SAC Process……202
6.19 Responses and Inferred Probabilistic Realisations for the SAC Process……203
7.1 Reference State for Optimisation……....210
7.2 Some Optimum States for the Steam-alone Process…….. 234
8.1 Injection Streams for Co- and Alternating-Injection of Steam and CO_2……237
8.2 Some Optimum Variables for the Alternating-Injection Processes……245
8.3 Injection Fluids and Rates for the Different Processes……...245

9.1 Assumed Vertical Distributions of Some Properties……251
9.2 Input Data and Estimated Model Parameters for the Open-system Model……255
9.3 Molar Compositions (in fractions) before and after Deasphalting (Average) ……256
9.4 Performance Summary (High Case) ……260
9.5 Performance Summary (Base Case) ……261
9.6 Performance Summary (Low Case) ……261
10.1 CAPEX Components……269
10.2 OPEX Components……270
10.3 Revenue and Penalty Components……270
10.4 Fiscal-Term Components……271
10.5 Range of Economic Variables for Sensitivity Analysis……272
10.6 Design Matrix and Output for the SAC Process……274
10.7 Summary of Economic Analysis……276
F.1 Full-Factorial Design for Saturants in Non-Condensing Steam Process ……295
F.2 Full-Factorial Design for Saturants in Flue-Gas Process……295
J.1 Some Input Factors for Emission Calculations (Herold, 2003; IPCC, 1997)……300
L.1 Design Matrix and Output for the Steam-alone Process……303
L.2 Design Matrix and Output for the SAF Process……303

List of Figures

1.1 Conceptual Model of Alternating Injection of Steam and CO_2……29
2.1 Bitumen Development with CSS and SAGD……33
2.2 Schematics of Slope and Ceiling Drainages in SAGD (adapted from Albahlani and Babadagli (2009)) ……38
3.1 Simplified Model of Gravity-Driven Counter-current Flow at Liquid-Steam Interface…..55
3.2 Pore-scale Processes for Counter-current Flow (Sjølyst, 2006) ……55
3.3 Comparison of Analytic & Numeric Solutions (Pure Conduction) ……72
3.4 Convergence Test- MCC (N_t = 50, B_{ref} = 0.18) ……72
3.5 Convergence Test- MCC (N_Z = 50, K_{vo} = 1 D, K_{vs} = 10 D, B_{ref} = 0.18) ……73
3.6 MCC- Effect of Condensate Production……73
3.7 FCC- Effect of Condensate Production (100 mD, 400 days) ……73
3.8 Response of Superconductor FCC……73
3.9 Decoupling Condensation Effect……75
3.10a MCC- Effect of Permeability……75
3.10b Laboratory *SAGD* Temperature Profile, Permeability Effect (Nasr *et al.*, 2000) ……75
3.11 MCC- Effect of Heating Time……76
3.12 Laboratory *SAGD* Temperature Profile, Time Effect (Nasr *et al.*, 2000) ……76
3.13 Experimental Steamflood Temperature Profile (Hornbrook *et al.,* 1991) ……76
3.14 FCC- Effect of Heating Time……77
3.15 FCC- Effect of Steam Quality (100 mD) ……77
3.16 MCC- Effect of Injection Temperature (150 days) ……78
3.17 Heating a Tight (0.1 mD) Formation……78
3.18 Comparison of Heating Processes (100 mD, 400 days) ……78
3.19 C'_p (Volume-basis, ρc_p) of Steam, CO_2 & N_2……79
3.20 Viscosity of Steam, CO_2 and N_2 (250 ^oC) ……79
3.21 MCC- Effect of Reservoir Thickness (200 mD) ……80
3.22 MCC- Effects of Oil & Condensate Drainage……80
3.23 Temperature Profile under MCC Heating……81
3.24 Temperature Profiles under Conductive-Convective and Pure Conductive Heating……81
3.25 Temperature Profiles ahead of a Non-condensing Thermal Front……84
3.26 Effect of Permeability on Temperature Profile ahead of a Condensing Thermal Front…..84
3.27 Effect of Time on Temperature Profile Ahead of a Slow Thermal Front (0.5 mD) ……85
3.28 Effect of Time on Temperature Profile Ahead of a Fast Thermal Front (500 mD) ……85
3.29 Effect of Pressure-Drop on Delivery of Sensible Heat……87
3.30 Effect of Pressure-Drop on Delivery of Latent Heat……87
3.31 Effect of Pressure-Drop on Heating (MCC) ……88
3.32 Effect of Pressure-Drop on Heating (CO_2) ……88

3.33 Differential Volume with All Elements Initially at Different Temperatures……...89
3.34 Effect of Time on LTE……92
3.35 Effect of Convective-Coefficient on LTE……..... 92
3.36 Effect of Heat-transfer Perimeter on LTE……....92
4.1 Reservoir and Adjacent Heat Sinks…….... 98
4.2 Grid Configuration at the Cap-rock……....101
4.3 Average Temp for Different Boundary Saturants (MCC) ……..……..107
4.4 Average Temp for Selected Boundaries (MCC) ……...107
4.5 Cap/Base-rock Heat Fluxes for Specific Boundary Realisations (MCC) ……..109
4.6 Evolution of Caprock Temperature for Different Boundaries (MCC) ……..……109
4.7 Total Heat-Flux for Specific Boundary Saturants (MCC) ……..……..……109
4.8 Average Temp for Different Boundary Saturants (CO_2) ……...…111
4.9 Average Temp for Selected Boundaries (CO_2) ……....111
4.10 Cap-rock Unproductive Heat-Flux for Specific Boundary Realisations (CO_2) ……..112
4.11 Evolution of Caprock Temperature for Different Boundaries (CO_2) ……..……112
4.12 Total Unproductive Heat-Flux for Specific Boundary Realisations (CO_2) ……..…...113
4.13 Average Temp for Different Boundary Saturants (Conduction) ……...……..114
4.14 Average Temp at “Early” Times (Conduction) ……..…114
4.15 Average Temp for Selected Boundaries (Conduction) ……...……..……...115
4.16 Underburden Heat-Flux for Different Saturants (Conduction) ……...……....115
4.17 Normalised Responses of Some Heating Processes (Adiabatic Scenarios) ……... 116
4.18 Normalised Responses of Some Heating Processes (Non-Adiabatic Scenarios) ……..…116
4.19 Effect of Boundary-Thickness on Average Temp (MCC) ……..…… 117
4.20 Effect of Boundary-Thickness on Total Heat Loss (MCC) ……..……..… 117
4.21 Effect of Reservoir-Thickness on Average Temp (MCC) ……..……....117
4.22 Effect of Reservoir-Thickness on Total Heat Loss (MCC) ……..……..…117
4.23 Effect of Reservoir-Thickness on Average Temp (CO_2) ……..…… 118
4.24 Effect of Reservoir-Thickness on Cumulative Total Heat Loss (MCC) ……..118
4.25 Effect of Injection-Temp on Average Temp (MCC) ……....118
4.26 Effect of Injection-Temp on Total Heat-Loss (MCC) ……..…… 118
4.27 Effect of Boundary Fluids' Heat-Transfer Coefficient on Average Temp (MCC)……..... 119
4.28 Effect of Boundary Fluids' Heat-Transfer Coefficient on Total Heat-Loss (MCC)……... 119
4.29 Effect of Boundary Fluid on Average Temp, R_{th} = 0.01 m^2 K W^{-1} (MCC) ……..……...120
4.30 Effect of Boundary Fluid on Cap / Base Rock Heat Loss, R_{th} = 0.01 m^2 K W^{-1} (MCC)…...120
4.31 Effect of Boundary Fluid on Average Temp, R_{th} = 0.01 m^2 K W^{-1} (CO_2)……..121
4.32 Effect of Boundary Fluid on Cap/Base Rock Heat-Loss, R_{th} = 0.01 m^2 K W^{-1} (CO_2)…….…121
4.33 Effect of Boundary Fluid on Average Temp, R_{th} = 15 m^2 K W^{-1} (MCC) ……121
4.34 Effect of Boundary Fluid on Total Heat Loss, R_{th} = 15 m^2 K W^{-1} (MCC)……..……..121
4.35 Sensitivity of Average Temp to R_{th} in a Convective (1,000 mD) Reservoir (CO_2) ……...122
4.36 Sensitivity of Total Heat Loss to R_{th} in a Convective (1,000 mD) Reservoir (CO_2)…..……122

4.37 R_{th_min} for Approximate 'Adiabatic' Behaviour……..123
4.38 Approximating Adiabatic Conditions for Different Thickness but Same K_v and R_{th} (MCC)……..124
4.39 Fractional Total Heat-Loss for Different Reservoir Thickness but Same K_v and R_{th} (MCC) ……124
4.40 Fractional Total Heat-Loss for Different Initial Temperature but Same K_v and R_{th} (MCC) ……124
4.41 Fractional Total Heat-Loss for Different Injection Temperature but Same K_v and R_{th} (MCC) ……..124
5.1 Axial View of Asphaltene-inflicted Pores……128
5.2 Data of Sharma *et al.* (1992), Core 1……...132
5.3 Data of Sharma *et al.* (1992), Core 2…… 132
5.4 Data of Sharma *et al.* (1992), Core 3……...132
5.5 Optimising Data of Sharma *et al.* (1992), Core 3……132
5.6 Matched *n* versus Estimated Pore-throat Radius: All Data……133
5.7 Schematic of Asphaltene-Floc Deposition in a Closed System……134
5.8 Effect of Initial Permeability on Damage Rate……137
5.9 Effect of Initial Porosity on Damage Rate……137
5.10 Effect of Maltene Viscosity on Damage Rate……..138
5.11 Effect of Asphaltene-Aggregate Size on Damage Rate……138
5.12 Schematic of Asphaltene-Suspension Flow Process……141
5.13 Data of Minssieux *et al.* (1998) - Run GV10……148
5.14 Data of Minssieux *et al.* (1998) - Run GP9……..148
5.15 Data of Minssieux *et al.* (1998) - Run GF2……..149
5.16 Validating Minssieux *et al.* (1998), Run GF3: Using fitted GF2 Parameters……149
5.17 Data of Minssieux *et al.* (1998) - Run HMD26……150
5.18 Data of Mendoza *et al.* (2009): Limestone……150
5.19 Data of Shedid and Abbas (2005) - Run 1……151
5.20 Data of Shedid and Abbas (2005) - Run 2……151
5.21 Universal Fit for Test 2, 1, 5 of Fadili *et al.* (2009) ……152
5.22 Universal Fit for Test 4 and 6 of Fadili *et al.* (2009) ……..152
5.23 Datasets 2, 6, 3 of Fadili *et al.* (2009) ……153
5.24 Data of Todd *et al.* (1990) – their Dataset 2……153
5.25 Data of Minssieux *et al.* (1998) - Run GV5……..155
5.26 Sensitivity on n, λ_o and τ for the Fit to the Run 1 in Shedid & Abbas (2005)……155
5.27 Asphaltene-Precipitation Curves for the Crude Oil (after Li (2011))……159
5.28 Schematic of the Asphaltene-Deposition Experiment in a Capillary Tube (Modified after Boek et al. (2010b))……160
5.29 The Experimental Rig……160
5.30 Unfiltered Datasets (Run 4) ……..167

5.31 Effect of Flowrate on Conductivity Impairment……..167
5.32 Effect of Flowrate on Deposition……167
5.33 Comparison of Thickness-Estimation Models…… 167
5.34 Effect of Precipitant Concentration on Deposition ……..169
5.35 Deposition for Different Precipitants……169
5.36 Plan-View Photographs of Capillary Internals at Selected Times (Run 2) ……....170
6.1a Tar Outcrop Belt of Southwestern Nigeria (after Enu (1985)) ……....173
6.1b Some Exposed Tar-bearing Section at Agbabu, Southwestern Nigeria
(Source: Tribune Newspapers (2011)) ……..173
6.2 Geologic N-S Cross-section of the Stratigraphy of Nigerian Tarsand Units
(after Enu, 1985)…… ……..176
6.3 Oil-Water Relperm Model (Base-Case) ……....181
6.4 Gas-Oil Relperm Model (Base-Case……....181
6.5 Reference Viscosity-Temperature Relationships for Nigerian Heavy Oil……184
6.6 Viscosity Matched to PC Schemes (Lawal, 2011b) ……..186
6.7 PC Viscosities of Matched 3-PC Model (Lawal, 2011b) ……...186
6.8 Gas-Liquid (Oleic) Equilibrium Ratios for CH_4……187
6.9 Gas-Liquid Equilibrium Ratios for Maltene……..187
6.10 Gas-Liquid Equilibrium Ratios for Asphaltene……...187
6.11 Gas-Liquid (Oleic) *K*-values for CO_2……187
6.12 Gas-Liquid (Oleic) *K*-values for N_2……..188
6.13 Base-case Reservoir Geometry and Permeability ($K_x = K_y$) Field……189
6.14 Well Configuration and Initial Oil Saturation Field (Base Case) ……..191
6.15 Generic Wellbore Configuration (after Stone *et al.* (2002); Carpenter & Dazet (1992).....192
6.16 Tornado Plot for STOIIP (MMstb) ……193
6.17 Tornado Plot for Discounted Oil Recovery (MMstb) ……193
6.18 Steaming Runs 1, 12 and 14 (Oil Recovery) ……..196
6.19 Steaming Runs 1, 12 and 14 (CSOR) ……196
6.20 N_p vs. R_f……....198
6.21 N_p vs. N……198
6.22 R_f vs. W_i……198
6.23 R_f vs. C_{SOR}……198
6.24 C_{SOR} vs. T_{WOR}……198
6.25 C_{SOR} *vs.* C'_{SOR}……198
6.26 Model Adequacy for N……..200
6.27 Model Adequacy for W_i……200
6.28 Oil RF for Steaming and Alternating-Injection Runs (All Runs) ……203
6.29 Oil RF for SAC (Low-Viscosity Runs)……205
6.30 Oil RF for SAC (High-Viscosity Runs)……205
7.1 Effect of Well Type on Oil Recovery……212

7.2 Effect of Wellbore Radius on Oil Recovery and CSOR……..……..……..212
7.3 Effect of Wellbore (Horizontal) Length on Oil Recovery……..…….. 213
7.4 Effect of Number of Wellpairs on Oil Recovery (Unequal Total Injection Rates)……..…..214
7.5 Effect of Number of Wellpairs on Oil Recovery (Equal Total Injection Rates) ……214
7.6 N_x versus Wellpair Count……..……..……..……215
7.7 Effect of Vertical Well-spacing on Oil Recovery……..……..……215
7.8 Effect of Vertical Well-spacing on Average Reservoir Temperature……..……215
7.9 Steam-Chamber Geometry after 7 Years for 20-m Vertical Spacing……..……216
7.10 Effect of Wellpair-Spacing on Oil Recovery……..……..……217
7.11 Steam-Chamber Geometry after 6 Years for Selected Wellpair Spacings……..……..217
7.12 Instantaneous Temperature Profiles for Conductive-Heating of Inter-well Volume……218
7.13 Schematic of Staggered-Well Configuration (Plan View) ……..……..……220
7.14 Effect of Well-Staggering on Oil Recovery……..……..……..…220
7.15 Conceptualised Heat and Mass Flow Paths for Different Well-Placement Patterns……..221
7.16 Effect of Producer-Producer Spacing on Oil Recovery……..…….. 221
7.17 Steam-Chamber Geometry after 3 Years for Selected Producer Spacing……222
7.18 Effect of Injector-Injector Spacing on Oil Recovery……..……..…….. 223
7.19 Effects of Well-Arrangement on Oil Recovery……..……..…….. 224
7.20 Oil Recovery for Different Injection Streams……..……..……..……225
7.21 Enthalpy In-place for Different Injection Streams……..……..……..225
7.22 Effect of Injection-Temperature on Oil Recovery……..……..…….. 226
7.23 Average Reservoir-Pressure for Different Injection Temperatures……..……...226
7.24 Steam-Chamber Geometry after 15 Years for 225 and 275 ^oC Runs……..……...227
7.25 Effect of Injection-Temperature on CSOR……..……..……..……...227
7.26 Effect of Injection-Temp on Enthalpy In-place……..……..…….. 227
7.27 Effect of Injection-Temperature on Enthalpy Injected……..……..…….. 227
7.28 Viscosity-Temperature Characteristics of the Bitumen (Base-case)…….. 228
7.29 Effect of Injection-BHP on Oil Recovery……..…….. 229
7.30 Effect of Injection-BHP on CSOR……..……..……229
7.31 Effect of Injection-BHP on Enthalpy Injected……..……..…….. 229
7.32 Effect of Injection-Rate Per Well on Oil Recovery……..……..……....230
7.33 Effect of Injection-Rate Per Well on CSOR……..……..……....230
7.34 Effect of Injection-Rate Per Well on Cumulative Injection……..……..……231
7.35 Effect of Subcool-Temperature on Oil Recovery……..……..……232
7.36 Effect of Steam-Quality on Oil Recovery and CSOR……..……..……233
7.37 Variation of Enthalpy In-place for the Runs……..……..……....233
8.1 Performance Plots for Co- and Alternating-Injection of Steam and CO_2……..……237
8.2 Proposed Process Scheme for Steam-alone Process……..…….. 238
8.3 Process Scheme for Alternating Steam and CO_2 (SAC) Injection Process……..…... 239
8.4 Process Scheme for Alternating Steam and Flue-gas (SAF) Injection Process……..……239

8.5 Total CO_2 Intensity for Compression of Boiler CO_2……241
8.6 Total CO_2 Intensity for the SAF Process…….. ……241
8.7 Effect of Cycle Time on Oil Recovery for SAC……242
8.8 Effect of Cycle Time on CSOR for SAC……242
8.9 Effect of Gas-Production on Oil Recovery (SAC)……243
8.10 Effect of Gas-Production on CO2 Injection (SAC)……243
8.11 Effect of Gas-Production Constraint on CO_2 Re-Production (SAC) ……243
8.12 Effect of Gas Constraint on Time Variation of Net CO_2-Retention (SAC)…… 244
8.13 Cumulative Injection-Enthalpy for Different Processes…… 247
8.14 Average Formation-Temperature for Different Processes……247
8.15 Oil Recovery for Different Processes…… . 248
9.1 Estimated Oil-Mobility Profiles at Initialisation (Base Case) ……252
9.2 Schematic of Oil-Phase Compositions in the Homogenous & Heterogeneous Models…. 253
9.3 Effects of Some Property Heterogeneities on the Alternating-Injection Process……254
9.4 Effects of Asphaltene-induced Permeability and Viscosity Reduction on Oil Recovery… 255
9.5 Effects of Dispersion on the SAC Process……257
9.6 Gas-Saturation Profiles for theSAC Process (Topmost Layer after 15 Years)……257
9.7a Oil Production for the Steam-alone Process……258
9.7b Water Production and Steam Consumption for the Steam-alone Process……258
9.8a Oil Production for the SAC Process……259
9.8b Water Production and Steam Consumption for the SAC Process……259
9.8c CO_2 Injection and Recovery for the SAC Process……259
9.9a Oil Production for the SAF Process……259
9.9b Water Production and Steam Consumption for the SAF Process……259
9.9c CO_2 Injection and Recovery for the SAF Process……260
9.10 Comparison of CSOR for the Different Processes…… 263
9.11 Effects of CO_2-Composition on Performance of the SAF Process……263
9.12 Distribution of Temperature after 40 Years……264
9.13 Distribution of Gas-Saturation after 40 Years……265
10.1 Tornado Plot for NPV ($ mln) – SAC Process……273
10.2 VIR-NPV Crossplot for the SAC Process…… 274
10.3 Expectation Curves for NPV……276
10.4 Expectation Curves for VIR…… 276
D.1 Lumped Model of Injector-Reservoir-Surroundings System…… 290
D.2 Reservoir and Surrounding Responses (Non-Interacting Subsystems in Series)……291
D.3 Reservoir and Surrounding Responses (Interacting Subsystems in Series)……292
I.1 Reverse Cumulative Probability for N_p…… 298
I.2 Reverse Cumulative Probability for W_i…… 298
I.3 Reverse Cumulative Probability for R_f……298
I.4 Reverse Cumulative Probability for C_{SOR}…… 298

I.5 Reverse Cumulative Probability for N_{p_CO2}……..……..……..……..……..……..…....298
I.6 Reverse Cumulative Probability for G_{CO2}…….……..……..……..……..…….. 298
K.1 Schematic of Oil-Phase Compositions in the Homogenous and Heterogeneous Model
……..301

List of Publications

Lawal, A. K. (2011). "Reconciling and Improving the Volumetrics of Nigerian Heavy Oil and Bitumen Resources". Paper 150802 presented at Nigeria Annual SPE Int. Technical Conf. & Exhibition, Abuja, 30 Jul – 3 Aug.

Lawal, A. K. (2011). "Validation of a Pseudocomponent Scheme for Nigerian Heavy Oil and Bitumen". Paper 150815 presented at Nigeria Annual SPE Int. Technical Conf. & Exhibition, Abuja, 30 Jul – 3 Aug.

Lawal, A.K. and Adenuga, A.O. (2010). "Pseudo-components for Nigerian Heavy Oil and Bitumen". Paper 136954 presented at Nigeria Annual SPE Int. Conf. & Exhibition, Calabar, 31 Jul - 7 Aug.

Lawal, A.K. and Vesovic, V. (2010). "Modelling Asphaltene-Induced Formation Damage in Closed Systems". SPE Paper 138497 presented at Abu Dhabi Int. Petroleum Exhibition & Conf., Abu Dhabi, 1-4 Nov.

Lawal, A.K. and Vesovic, V. (2010). "Modelling Multiple-Contact Condensation of Heat-Transporting Fluids in Thermal Floods". Paper 130568 presented at SPE EUROPEC/EAGE Annual Conf. & Exhibition, Barcelona, 14–17 Jun.

Lawal, A.K. and Vesovic, V. (2009). "Analytic Investigation of Convection During Conduction Heating of a Heavy-Oil Reservoir". Paper 124072 presented at SPE Annual Technical Conf. & Exhibition, New Orleans, 4-7 Oct.

Lawal, A.K. and Vesovic, V. (2009). "A Model of First-Contact Condensation in a Heavy-Oil Reservoir Heated by a Condensable Fluid". Poster 13492 presented at Int. Pet. Tech. Conf., Doha, 7-9 Dec.

Lawal, A.K., Vesovic, V. and Boek, E.S. (2011). "Modelling Permeability Impairment in Porous Media due to Asphaltene Deposition under Dynamic Conditions", *Energy & Fuels* (in review).

Lawal, A.K. and Vesovic, V. (2011). "Assessment of Asphaltene-induced Formation Damage in Quiescent Environments". Poster presented at 2011 PetroPhase Conf., London, 10-14 Jul.

Lawal, A.K., Crawshaw, J.P., Boek, E.S. and Vesovic, V. (2011). "An Experimental Investigation of Asphaltene Deposition in Capillary Flow", to be submitted to *Energy & Fuels*.

Lawal, A.K. and Vesovic, V. (2011). "First-Contact Condensation for Reservoir-Heating by a Condensable Fluid", to be submitted to *J. Can. Pet. Tech*.

Lawal, A.K. and Vesovic, V. (2011). "Multiple-Contact Condensation in Steam-Assisted Gravity Drainage", to be submitted to *J. Can. Pet. Tech*.

Nomenclature

A : cross-sectional area, m^2

a : temperature exponent in the oil μ-T power law model (**Eq. 3.9)**, dimensionless

a_x : scalar multiplier, dimensionless

B : scalar multiplier, dimensionless

B_{oi} : initial oil formation-volume factor, rb/stb

c_p : isobaric specific heat capacity, J kg^{-1} K^{-1}; Btu lbm^{-1} $^oF^{-1}$ in **Eq. A.1**

C_{CO2} : carbon-emissions penalty, $ mln

C_d : fiscal depreciation, $ mln

c_f : fraction of carbon oxidised

C_{SOR} : cumulative steam-oil ratio, stb/stb

C_t : thermal capacitance, J m^{-2} K^{-1}

$\bar{c}_t$: total compressibility of reservoir, Pa^{-1}

D : capillary internal diameter; reservoir depth, m

D_a : asphaltene-floc diameter, m

D_p : pore diameter, m

E : energy, J; electric voltage gradient, v m^{-1}

E^T : transpose of electric voltage gradient, v m^{-1}

$\dot{E}_{net}$: thermal power, W

e_f : fuel emission factor, ton C /TJ

e_t : deposit thickness at time t, m

F : convection term, m s^{-1}; input-factor to proxy models, dimensionless

f : precipitant-to-solvent volumetric ratio, dimensionless

f_c : condensable fraction (mass) of steam, fraction

f_{cw} : mass fraction of condensate produced, fraction

f_s : steam quality at reservoir inlet, fraction

G : scalar multiplier, dimensionless; gas-storage capacity of reservoir, m^3

G_{CO2} : net mass of CO_2 retained in the reservoir, kton

G_R : transfer function, dimensionless

G_{RV} : gross-rock volume, m^3

g : gravitational acceleration, m s^{-2}

g_p : rate of heat generation in the moving solid per unit volume; W m^{-3}

H : vertical distance between injection plane and caprock, m

h : space-step size, m; local convective heat-transfer coefficient, W m^{-2} K^{-1}

h_i : water specific enthalpy, J kg^{-1}

K_r : relative permeability, dimensionless

K_v : effective vertical permeability, m^2

k : time-step size, s

L : length, m

L_c : specific latent heat of condensation, J kg^{-1}

L_e : minimum entrance (exit) length for fully-developed flow, m

M_g : gas molar mass, kg mol^{-1}

m : constant in **Eq. 6.1**, K

m_c : mass-rate of steam condensation per unit volume, kg s^{-1} m^{-3}

N : dimensionless number; pore-volumes; oil-volume; number of pseudocomponents

N_{CF} : net cash-flow, $ mln

N_p : volume of oil produced, m^3

N_{PV} : net present value, $ mln

N_t : number of grids on the time axis

N_z : number of grids on the space axis

n : exponent of the permeability-porosity power-law model, dimensionless

n_w : number of wellpairs

P : perimeter of heat-transfer surface, m

PV : number of pore-volumes injected, m^3

Q : flowrate, m^3 s^{-1}

q : heat-flux rate, W m^{-2}

R : volumetric ratio of solvent and precipitant to crude, dimensionless

R_f : recovery factor, dimensionless

R_o : universal gas-constant, J mol^{-1} K^{-1}

R_p : reservoir-drainage radius, m

R_{si} : initial ga-oil ratio, scf/stb

R_{th} : conductive-resistance, m^2 K W^{-1}

R_v : gross revenue, $ mln

r : pore-radius, m (μm in **Eqs. 5.32** and **5.34**)

r_D : discount rate, %

S : saturation, fraction

T : temperature, K; ^oF in **Eq. A.1**

T_r : reference temperature corresponding to ρ_{or} (**Eq. 3.10**), K

T_{WOR} : total water-oil ratio, stb/stb

t : time, s

t_m : operating lifetime, s

U : overall heat-transfer coefficient, W m^{-2} K^{-1}

V : volume, m^3

v : Darcy velocity, single-particle settling velocity, m s^{-1}

v_{or} : oil velocity corresponding to ρ_{or} and μ_{or} (**Eq. 3.12**), m s^{-1}

v_{sr} : steam velocity corresponding to ρ_{or} (**Eq. 3.11**), m s^{-1}

$\vec{v}_s$: steam-velocity vector, m s^{-1}

W : water volume, m^3

x : mole fraction

x_a : mass fraction of asphaltene in suspension

x_a' : mass fraction of asphaltene adsorbed

x_p : mass fraction of asphaltene in deposit

z : distance, m

Z_g : compressibility factor, dimensionless

Greek Symbols

α : bulk thermal-diffusivity, $m^2\ s^{-1}$

α_m : dispersion coefficient, $m^2\ s^{-1}$

β : coefficient of isobaric oil-thermal expansion, K^{-1}

ε : Lennard-Jones parameter, K^{-1}; local truncation error, $K\ s^{-1}$

γ : specific heat ratio, dimensionless

γ_o : oil specific-gravity (water = 1)

κ : bulk thermal-conductivity, $W\ m^{-1}\ K^{-1}$

λ : overall filtration-coefficient, m^{-1}

λ_o : oil thermal-conductivity, $Btu\ hr^{-1}\ ft^{-1}\ ^oF^{-1}$

η : thermal efficiency, fraction

μ : dynamic viscosity, $N\ s\ m^{-2}$

μ_{or} : viscosity asymptote (maximum) in the oil μ-T power law model (**Eq. 3.9)**, $N\ s\ m^{-2}$

$\Omega_{\mu,\kappa}$: collision integral

O : order of local truncation error

ϕ : effective porosity, fraction

Ψ_x : fraction of bulk volumetric heat-capacity contributed by fluid x (oil or steam)

ρ : density, $kg\ m^{-3}$

ρ_{or} : reference oil density in the isobaric thermal-expansion model (**Eq. 3.10**), $kg\ m^{-3}$

τ : time constant, s

σ : bulk electrical-conductivity, $\Omega^{-1}\ m^{-1}$

$\sigma E.E^T$: electrical power density, $W\ m^{-3}$

θ : reservoir dip (to horizontal), degrees

ξ : distance ahead of the front into the colder zone, m

Subscripts

a : asphaltene, ambient conditions, surroundings

b : base-rock

c : condensate, caprock, original crude, carbonate, colder fluid

ca : capillary number, CAPEX
cm : colder fluid-matrix interface
D : dimensionless
d : damaged
f : front
G : gravity number
g : gas mixture, glass-bead
h : heating fluid
hc : heating-colder fluid interface
i : initial, space counter (numerical scheme), component, injected
j : time counter (numerical scheme)
L : latent/condensate
m : mixture, maltene, matrix
o : oil, stabilized
op : OPEX
Pe : Peclet number
p : phase, precipitant, produced
Re : Reynolds number
r : rock, reservoir, royalty
ref : reference
s : steam, sandstone, solvent
ss : steady-state
T : total
t : tax
w : water
wc : connate water

Superscripts

‘ : discounted
* : time-constant
b : steam generator (boiler)
comp : compressor

Abbreviations

AAPG : American Association of Petroleum Geologists
AIChE : American Institute for Chemical Engineers
API : American Petroleum Institute
ASTM : American Society for Testing and Materials
BP : British Petroleum
CAPEX : Capital Expenditure
CSOR : Cumulative Steam-Oil Ratio
CSS : Cyclic Steam Stimulation
CVI : Capillary-Volume Injected
CWE : Cold-Water Equivalent
DOE : Department of Energy
ETF : Education Trust Fund
FCC : First-Contact Condensation
FG : Federal Government
IEA : International Energy Agency
IPCC : Intergovernmental Panel on Climate Change
JCPT : Journal of Canadian Petroleum Technology
JPT : Journal of Petroleum Technology
KRPC : Kaduna Refining & Petrochemical Company
MCC : Multiple-Contact Condensation
NCG : Non-Condensable Gas
NPV : Net Present Value
OPEX : Operating Expenditure
PV : Pore Volume
PVT : Pressure-Volume-Temperature
SAC : Steam Alternating CO_2
SAF : Steam Alternating Flue-gas
SAGD : Steam-assisted Gravity Drainage
SAGP : Steam-assisted Gas Push
SIAM : Society for Industrial and Applied Mathematics
SPE : Society of Petroleum Engineers
SPEFE : SPE Formation Evaluation
SPEPF : SPE Projects & Facilities
SPERE : SPE Reservoir Engineering
SPEREE : SPE Reservoir Evaluation & Engineering
VIR : Value-to-Investment Ratio

Chapter 1

Introduction

The International Energy Agency (IEA), in its world energy outlook for the period 2008-2035 (IEA, 2010), projects a global primary-energy demand rate of about 300 million barrels of oil-equivalent per day (mb/d). From its current share of 30%, the demand for crude oil is expected to grow steadily, reaching some 100 mb/d by the year 2035. However, within this 27-year period, the production from conventional oil sources is predicted to peak at about 70 mb/d, leaving some 30 m/d oil-supply gap to be partly filled by heavy-oil sources (IEA, 2010). With the projected significance of heavy-oil to future energy supply, it becomes understandable why this unconventional resource has continued to attract the attention of energy developers and policy makers (Lee, 2009; Hart, 2008). The current and projected high oil prices, the relatively lower exploration costs and their vast in-place volumes (~ 6 trillion barrels) are additional factors fuelling the interests in heavy-oil resources (IEA, 2010; Meyer *et al.*, 2007; Rogner, 1997).

Generally, heavy crude refers to oil whose in-situ density and viscosity are in excess of 0.934 g/cm^3 (< 20 ^{o}API) and 100 cP, respectively (Meyer *et al.*, 2007). In this broad classification are natural bitumen, extra-heavy oil, viscous oil, and tar. By definition, natural bitumen is oil with density and viscosity exceeding 1 g/cm^3 (< 10 ^{o}API) and 10,000 cP, respectively (Meyer *et al.*, 2007; Speight, 1991). Although commonly used interchangeably with bitumen, heavy oil and extra-heavy oil are different. Whereas heavy oil has density of 0.934-1.0 g/cm^3 (10-20 ^{o}API) and in-situ viscosity of 100-10,000 cP (Speight, 1991), extra-heavy oil is denser than 1 g/cm^3 (< 10 ^{o}API) but less viscous than 10,000 cP (de Ghetto *et al.*, 1995). In some formations, bitumen viscosity in excess of 1 million centipoise has been reported (Bazyleva *et al.*, 2010; Law, 2004).

In most cases, owing to flow barriers and baffles that impede the natural advection and diffusion processes on one hand (Besong, 2009; Nasrabadi *et al.*, 2006) and microbial activities on the other hand (Larter *et al.*, 2008; Koopmans *et al.*, 2002), it is not unusual to discover all these oil variants, including gas, coexisting in the same geologic system (Larter *et al.*, 2008; Roche, 2008; Law *et al.*, 2003a; 2003b). These subtle differences notwithstanding, their characteristic high viscosity renders them virtually immobile under reservoir conditions, even with the induction of fractures and imposition of extreme pressure gradients, as applicable in the process of cold heavy-oil production with sand – CHOPS (Zhang and Dusseault, 2004). Given their typical coexistence and similar dynamic behaviours, in this work, we do not distinguish between these unconventional crude types, hence we use the terms heavy oil, viscous oil, extra-heavy oil, tar and bitumen interchangeably.

Broadly speaking, there are two commercially successful methods for developing heavy-oil reservoirs. These are surface mining and in-situ recovery. Where the deposit is relatively shallow, within 75 m from the surface, surface-mining is often employed (Charpentier *et al.*, 2009; E & P, 2007). However, only about 5-20% of known resources are accessible to the current mining technologies (Elliot, 2008; Das and Butler, 1994). Huge capital expenses, land degradation and

solid-waste problems are additional drawbacks of the surface-mining method (Butler, 1998). Consequently, the in-situ techniques account for most of the commercial production.

As the uneconomic mobility of the heavy crudes is primarily due to the high viscous forces retaining them within the reservoir pores (Polikar *et al.*, 1986), successful in-situ techniques are premised on downhole reduction of the viscosity. This is achieved either by adding heat or diluting with some solvents, or a combination of both processes (Rezaei *et al.*, 2010; Nasr *et al.*, 2003; Butler, 1994; Butler and Mokrys, 1993). Processes that utilise heat are regarded as thermal while those that are based on dilution, such as vapour extraction (VAPEX), are the non-thermal methods (Das and Butler, 1998). Commercially, the thermal processes are more successful because of the stronger dependency of oil viscosity on temperature compared to composition (Law, 2004; Svrcek and Mehrotra, 1989). Common thermal methods are steam-injection and in-situ combustion (Nadella, 2010).

Steam-based processes, most of which generate steam by burning fossil fuels, currently account for some 98% of commercial production from thermal techniques (Nadella, 2010). However, fossil-based steam generation is faced with several issues relating to CO_2 emissions, water management, and fuel costs. Although there are still debates on whether it causes global warming (IEA, 2010; IPCC, 1997) or cooling (Sorokhtin *et al.*, 2010, 2007), it is generally believed that CO_2 has negative impacts on the climate, hence CO_2–curtailment is attracting much interest (IEA, 2010). Added to these is the thermal inefficiency, as a significant percentage (> 60%) of the injected heat is expended through flowline and wellbore losses as well as heating up non-productive portions of the reservoir, including matrix, connate water and the adjacent formations (Valbuena *et al*., 2009; Yee and Stroich, 2004; Doan *et al.*, 1999). With these limitations, there is increasing pressure to enhance conventional steaming processes (E & P, 2007).

In order to take advantage of the decrease of heavy-oil viscosity by dilution (Law, 2004; Svrcek and Mehrotra, 1989), researchers have proposed enhancements to the basic steam-injection techniques. In this regard, the potentials of adding a solvent or CO_2 to the injected steam have been studied (Butler, 2004; Nasr *et al.*, 2003). As will be discussed in Chapter 2, the prohibitive solvent costs and the limitations on CO_2 concentration in the injection stream are some of the challenges currently facing these “improvements”. At present, commercial-scale implementation is still protracted (E & P, 2007).

As a further improvement to the steam-based techniques, we are introducing the alternating-injection of steam and CO_2 which, for brevity, is referred to as the steam-alternating-CO_2 (SAC) process. In the following section, we outline the basic features of this new thermal-recovery method.

1.1 The SAC Concept

Conceptually, SAC entails injecting steam and CO_2 in cycles while oil is continuously produced. In terms of the injection procedure, this scheme is similar to the water-alternating-gas (WAG) process, which has been successful in the development of relatively light oil reservoirs (Mane,

2007; Sanchez, 1999). Despite this apparent operational similarity, the recovery mechanisms of the two processes are significantly different. For example, while WAG is a cold process, SAC is thermal, taking advantage of both temperature and miscibility effects on viscous and capillary forces (Bazyleva *et al.*, 2010; Saeed, 2010; Law, 2004).

Fig. 1.1 illustrates the application of SAC in a generic two-pad development. This depicts a hypothetical case in which each pad has three injector-producer pairs. Typically, a field is developed as several pads, with each pad consisting of multiple injector-producer pairs (Gipson *et al.*, 2002). While pad **A** is on steam, hot CO_2 (or flue gas) is injected in pad **B**, with oil produced from both pads. After a period of time, the injected fluids are switched between pads. Again, oil production continues. In principle, for a water-wet formation, while one pad (steaming) undergoes imbibition, the other pad (CO_2 injection) is primarily on drainage cycle. As a result, at pad level, the overall process may be viewed as a repeating cycle of imbibition and drainage processes, in which the saturation of water (wetting phase) increases and decreases, respectively. Although the process engineering is not the main focus of this research, we assume that the CO_2 and steam lines (dashed lines) are easily interchangeable, such that the transport of a particular fluid to the target pad is readily implemented through appropriate headers. In the current example, CO_2 is injected at the same temperature as steam.

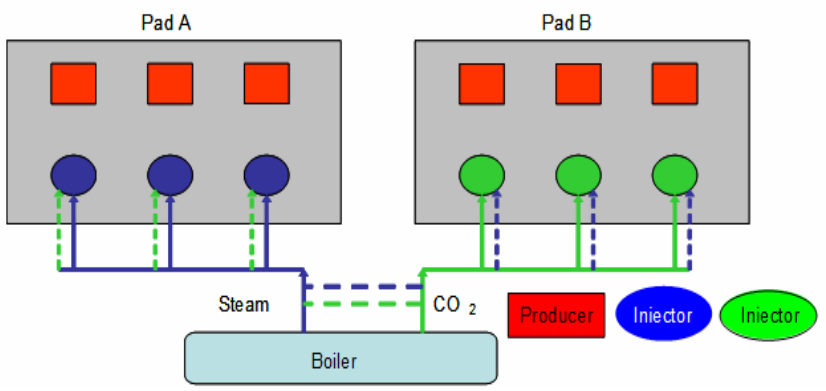


Fig. 1.1: Conceptual Model of Alternating Injection of Steam and CO_2

In this scheme, CO_2 is sourced from the flue-gas exhausts of steam generation. Because the steam-generating facilities would continuously be on-stream, the supply of process CO_2 is virtually guaranteed. Hence, from a CO_2 viewpoint, the overall process is self-sustaining, as the required CO_2 is generated and utilised within the same system. In effect, the scheme may be considered as converting some of the steam injectors in the conventional steam-injection processes to hot-CO_2 injectors.

Owing to the displacement of some steam injectors, steam consumption per unit oil recovery is expected to decrease. With reduced unit steam requirements, the unit fuel consumption, CO_2 emissions as well as the volumes of process water (for steam generation) and waste-water (from production) are expected to decline.

Furthermore, some of the injected CO_2 would be trapped within the formation (Bachu *et al.*, 2004). As a result, in comparison to a conventional steam-alone project of comparable scope, SAC would achieve a net reduction in the amount of CO_2 released into the atmosphere. With this underground carbon storage, additional revenue could accrue from carbon-credit claims (Law, 2004), further improving its competitiveness.

In principle, the SAC process requires high-quality CO_2. However, capturing CO_2 from flue gas, which is typically about 90% N_2 and 10% CO_2 (Nogueira and Mamora, 2005), is currently a major challenge, especially for large-scale applications such as those envisaged here (Kumar *et al.*, 2010; Bentein, 2009; Aimard *et al.*, 2007). To mitigate this challenge, we consider the case in which the flue-gas is injected directly, thus bypassing the challenging CO_2-capture step. We refer to this other process as alternating injection of steam and flue-gas, or simply steam-alternating-flue gas (SAF).

However, CO_2 and flue-gas are proven precipitants of asphaltenes which, in turn, cause considerable production problems (Dahaghi *et al.*, 2008; Srivastava *et al.*, 1999a; Leontaritis and Mansoori, 1988). On the other hand, in-situ asphaltene removal (deasphalting) reduces oil viscosity and density, hence upgrading the market value of produced oil (Luo *et al.*, 2010; Luo and Gu; 2007, 2005). Ideally, for a credible assessment of the SAC and SAF processes, it is imperative to understand the net impact of these opposing deasphalting effects on project performance.

1.2 Study Objectives

The main objective of the current study is to assess the technical and commercial feasibility of the SAC and SAF processes through:

- understanding the heat-transport aspects of steam-based operations in petroleum reservoirs;
- gaining insights into the mechanisms of asphaltene-induced impairment of porous media;
- identifying the main reservoir, geometric (well) and operating parameters that control the performances of steam-based extraction methods;
- understanding the net effect of deasphalting-induced reduction of crude viscosity and formation permeability on the performance of steam-based processes;
- establishing the main factors that govern the economics and commercial risks of steam-based recovery projects; and
- defining scope for further research.

In order to achieve the outlined objectives, we employ a combination of analytic modelling, numerical simulations and experiments.

1.3 Thesis Outline

Divided into 11 chapters, this thesis presents the work done, results obtained and analyses performed to achieve the outlined objectives and the conclusions drawn.

Chapters 1 and 2 are introductory, setting the research motivation and background. The basic principles of the proposed recovery methods are also presented. Previous works on steam-based processes are reviewed, with their limitations highlighted.

In Chapter 3, improved heat-transport models which include two novel condensation mechanisms are developed and solved. For the finite-difference solution schemes, criteria for numerical convergence are discussed. The simulation results are shown to be consistent with laboratory and field observations. To assess the robustness of the models, some underlying assumptions are relaxed and the effects quantified.

Chapter 4 extends the heat-transport treatments to non-isothermal boundaries, formulating new models for describing reservoir-boundary thermal losses. From simulations, we highlight the importance of reservoir boundaries and the fluids in adjacent formations on the heat-transport during steam-injection operations.

The physics of asphaltene deposition and formation impairment is described in Chapter 5. For the analysis of formation impairment, the concept of open and closed systems is introduced. The resulting asphaltene-impairment models are extensively validated against published experimental datasets. We also discuss the experiments performed, in-house, to evaluate some of the assumptions underlying our theoretical treatments.

The Nigerian heavy-oil system is examined in Chapter 6, with a set of generic reservoir-simulation models constructed for it. Effects of subsurface uncertainties on bitumen extraction by the steam-alone and alternating-injection processes are presented. In Chapters 7 and 8, we perform optimisation studies on the steam-alone and alternating-injection processes, respectively. Chapter 8 also quantifies the amounts of process CO_2 associated with the steam-alone, SAC and SAF methods.

Impacts of reservoir and fluid-property heterogeneities on the recovery methods are presented in Chapter 9. For the alternating-injection methods, the net effects of the reduction of oil viscosity and reservoir permeability due to in-situ deasphalting are highlighted. On the relative competitiveness of the steam-alone, SAC and SAF processes, Chapter 10 presents simple analysis of project economics and commercial risks.

Chapter 11 provides concluding remarks and the scope for extending this work, while the appendices (**A**-**L**) present additional results and information in support of the analyses leading to the conclusions reached.

Chapter 2

Literature Review

Enhanced oil recovery methods, which may be thermal or non-thermal, refer to the class of techniques that achieve crude production by altering the original oil properties (Schlumberger, 2011). While the thermal processes primarily utilise heat to alter the crude properties, most non-thermal processes depend on dilution. As they account for some 70% of the current total production from heavy crudes, the thermal methods are generally regarded as the standard techniques for the in-situ exploitation of these resources (Nadella, 2010).

At present, about 98% of the output from thermal methods is attributed to steam-injection processes (Nadella, 2010). In the industry, the popularity of the steam-injection techniques is evident in the number of projects that are currently on-stream, in planning or at various stages of construction (Roche, 2008; Hart, 2006). Similarly, within the petroleum-engineering research community, steam-related subjects have continued to attract considerable interests, as inferred from the volume, diversity and contemporariness of related publications (Gu *et al.*, 2011; Valbuena *et al.*, 2009; Shin, 2008; Marx and Langenheim, 1959). These and other reasons explain why the current research focuses on the steaming processes.

This chapter describes the basic principles of the common steam-injection methods, their current state of application and the associated challenges. Current efforts at mitigating some of these challenges are also discussed. Relevant details on the modelling and the field performances of these processes and their variants are presented. To augment our understanding of steam-based exploitation of petroleum reservoirs, we consider some industrial processes in which steam is routinely utilised and well-monitored. However, in reviewing the previous modelling efforts, we highlight the limitations of the various approaches and studies. From this review, the scope for further developments in this area is outlined.

2.1 Steam-Injection Processes

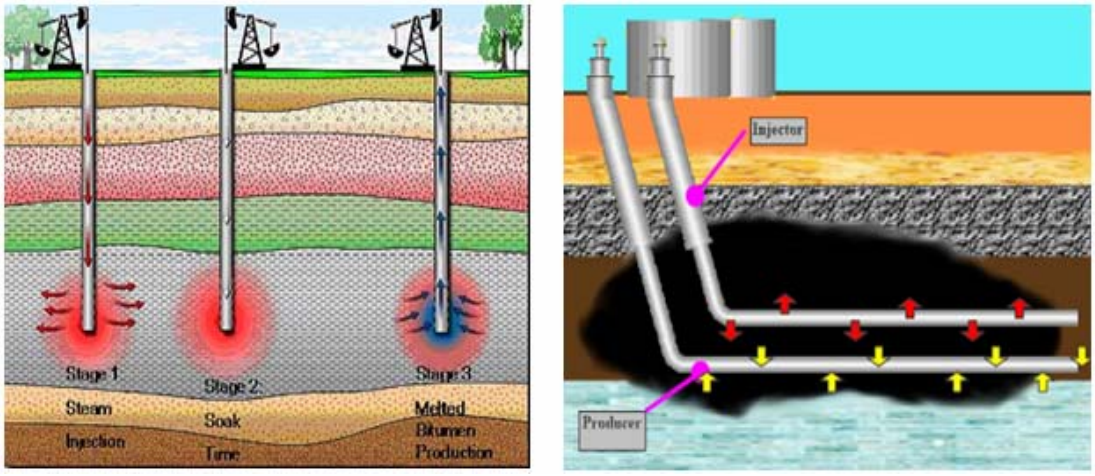
The steam-injection recovery method refers to all enhanced-oil production techniques that utilise steam as the main vehicle for transporting heat to the reservoir. With the heat, reservoir temperature is raised and oil mobility increases due to reduced viscosity. Compared to other fluids, a major advantage of steam is the enormous amount of latent heat released during its condensation. Depending on how the steam is injected, common variants of this technique are cyclic steam stimulation (CSS), steamflooding, and steam-assisted gravity drainage (SAGD). However, they are all characterised by the heat-transfer mechanisms of conduction, convection and condensation (Akin, 2005).

CSS is characterised by a cycle of inject, soak, and produce. As illustrated in **Fig. 2.1a**, steam is injected over a period of time. Then, injection is stopped, leaving the reservoir to “soak” the injected

heat over another time interval. Afterwards, production commences through the same well, continuing until it is no longer economic. Subsequently, another inject-soak-produce cycle begins. Depending on the project economics, more than five cycles may be implemented before abandonment (Meyer *et al.*, 2007). Typically, CSS recovery does not exceed 30% of the oil-volume within the project area (E & P, 2007; Butler, 1998; Farouq-Ali, 1994).

In contrast to what obtains in CSS, steamflooding utilises multiple wells and involves continuous injection and production. In addition to oil mobilisation by increased temperature, this process depends on pressure drive to push the mobilised oil towards the producers. Once the oil has been mobilised, the displacement process can be seen as some form of water flooding. But unlike water flooding in which cold water drives light oil, steam and water condensate are the main drivers of mobilised oil in the case of steam flooding. In suitable formations, the recovery factor for this process is about 60 % (Green and Willhite, 1998).

SAGD is a relatively new technology (Butler, 1998). In its basic form (**Fig. 2.1b**), this process involves a pair of parallel horizontal producer and injector placed close to the bottom of a thick formation. Typically, the injector is about 4-10 m above the producer (Chen *et al.*, 2008). While steam is injected through the injector, gravity drives mobilised oil and condensate to the producer (Butler, 1994). Unlike CSS and steamflooding, steam injection in SAGD is more gradual, allowing the steady development and expansion of a steam chamber (Dusseault, 2001). In principle, the so-called steam chamber is an accumulation of steam that is on the verge of condensation (**Fig. 2.1b**). In appropriate reservoirs, recovery efficiency of 50-75 % has been quoted (Dusseault, 2001). To a large extent, the competitiveness of SAGD is due to the employment of horizontal wells which, for the same pressure drawdown, typically achieve much higher injectivity and productivity than their vertical counterparts (Butler, 1994). In the later parts of this thesis, we compare performances of horizontal and vertical-well SAGD.



(a) CSS (Alberta Geological Survey, 2009) **(b) SAGD (S & S Geological Consultants Inc., 2008)**

Fig. 2.1: Bitumen Development with CSS and SAGD

Although they differ in mechanisms, operating strategies and scope of applicability, the steam-based techniques have the common challenge of utilising steam to optimally heat-up the reservoir. This explains why, in some applications, it may be more competitive to combine the methods. For example, SAGD could be operated as CSS (Edmunds *et al.*, 1994). In the Primrose East project (Canada), there was a firm plan to start-up with CSS then use SAGD as a follow-up process (Hart, 2006).

2.1.1 Current Status and Challenges

In the last 10 years, high oil prices have been driving investments in steam-injection projects, with several commercial-scale projects at various stages of planning and completion (Roche, 2008; Yeung, 2007; Hart, 2006). Currently, a significant fraction of the global production from bituminous deposits is based on steam injection (Meyer *et al.*, 2007; Oil & Gas, 2006). The proliferation of these steam-based technologies notwithstanding, they are currently faced with a number of challenges, most of which relate to water sourcing and treatment, carbon management and the security of energy supply.

In Canada, wastewater management is a major concern for SAGD operators (Jimenez, 2008; O'Rourke *et al.*, 1997). Despite reusing produced water for steam generation in the Kern River field (California), net water-cut is still an operational challenge (Waldron, 2005). Similar issues prevail in the CSS process at the Cold Lake field, Canada (Hart, 2006). Apparently, as the fields mature, imperatives for produced water-handling become more pronounced.

Veil *et al.* (2009), in discussing water issues related to heavy-oil production, identified water sourcing, wastewater management and disposal as major operational issues and cost centres. As mitigation, they recommended that during project planning, water supplies should be given similar consideration as oil reserves. From a sustainability viewpoint, such analysis is useful in assessing the competitiveness of a pool of potential projects.

Following a performance review of several SAGD projects in Canada, Jimenez (2008) concluded that steam-related issues vis-à-vis lack of steam, long boiler shutdowns and premature loss of confined injectors, account for disappointing performances observed in about 35% of the projects considered. Similarly, in the Kern (California) and Duri (Indonesia) fields, steam is reportedly the single largest operating expenditure (Zalan *et al.*, 2003). In addition, several workers (Shin, 2008; Edmunds and Chhina, 2001) have shown that steam-oil ratio (SOR) has a greater influence on SAGD economics than oil production rate.

Partly due to steam-based in-situ recovery methods, the heavy-oil industry has consistently been a major net polluter (CAPP, 2008; Environment Canada, 2007). In most cases, fossil fuel is burnt for the generation of steam. As will be shown in Chapter 8, with the common fuels, about 35 - 65 kg of CO_2 is generated per barrel of cold-water equivalent (CWE) steam. Given that the average production and SOR of steam-based processes are 1.3 million b/d and 4 b/b, respectively (Shin, 2008; Meyer *et al.*, 2007; Oil & Gas, 2006), we estimate that these processes make an annual contribution of at least 70 Mtons of CO_2 into the global atmosphere. Please bear in mind that this

estimate is limited to the upstream sector of steam-based oil production, suggesting that the actual emissions from the upstream and midstream operations would be higher.

From the foregoing, it is clear that the steam-based methods, as currently understood, would need to be improved if they are to remain competitive in the medium to long term. In the next section, we discuss some process improvements, including the management of CO_2 emissions, which have been proposed.

2.1.2 Process Improvements

In the light of the issues raised in the preceding section, there have been efforts at enhancing the conventional steaming processes. Conceptually, the enhancements have centred on improving the thermal and microscopic-displacement efficiencies (Al-Bahlani and Babadagli, 2009). In this regard, the ideas of co-injection and wind-down have attracted significant interests.

2.1.2.1 Co-Injection Processes

In co-injection, steam is injected in combination with some additives. Generally, the additive can either be a solvent or a non-condensable gas (NCG), or some combinations of these (Butler, 2004, 1997; Nasr *et al.*, 2003). The main functions of the additives are to extend the steam chamber and reduce oil viscosity beyond what is obtainable from the steam-alone process (Butler, 2004; Nasr *et al.*, 2003). Among the common NCG additives are CO_2, flue-gas and natural gas (Butler, 2004; Klins, 1984; Miller and Jones, 1981). On the other hand, most of the solvent additives are light hydrocarbons such as propane, butane and naphtha (Ayodele *et al.*, 2009; Nasr *et al.*, 2003, 1987).

In the case of solvent co-injection, the additive vaporises in the formation, travelling to the leading edge of the steam chamber where it dissolves into the cold bitumen, diluting and mobilising the oil (Sharma and Gates, 2010). One major concern of this process is the recovery of the solvent, which is a key contributor to project costs (Hart, 2006). On the other hand, NCG may accumulate above the steam chamber, forming a thermal-insulation layer that curtails heat losses to the adjacent formation (Butler, 2004; 1997). But NCG usually reduces the steam saturation-temperature, undermining the release of latent heat (Butler, 2004).

Considering the solvent costs and the effect of NCG on the saturation-temperature of steam, their concentration in the injection stream is often limited. In the case of NCG, its concentration is typically < 1 mol. % (Ayodele *et al.*, 2009; Yee and Stroich, 2004; Butler, 2004). As will be shown in Chapter 8, process engineering analysis indicates that for every mol of steam generated from fossil combustion, about 200 mol of CO_2 would be released. Given the maximum steam:CO_2 injection ratio of 99:1 allowed for the NCG co-injection process, as stated above, it follows that this process may not be feasible for simultaneous oil recovery and large-scale CO_2 disposal. In Chapter 8, with CO_2 as the additive, we compare the performances of the co- and alternating-injection methods.

2.1.2.2 Wind-Down Process

As a steam-injection project approaches maturity, its economic competitiveness diminishes, primarily due to declining thermal efficiency. In order to continue oil production at relatively lower costs, the substitution of steam with CO_2, N_2 or flue-gas has been proposed (Bagci *et al.,* 2008; Law, 2004; Yee and Stroich, 2004). In this case, unlike what applies in co-injection, the injection of steam ceases while the operation continues with the injection of NCG only.

From simulation studies, the technical feasibility of the process was established (Bagci *et al.,* 2008; Law, 2004). Although oil recovery for the wind-down process was reportedly lower than that of steam-alone, there were significant savings in steam consumption, water production and CO_2 emissions. However, to the best of our knowledge, the economic feasibility of this process remains to be presented.

From a carbon-management viewpoint, a key concern of the wind-down process is the delayed injection of CO_2. In other words, prior to commencing CO_2 injection, the emissions associated with the steam used in running the project would, in principle, be released into the atmosphere. Indeed, the simulation studies by Bagci *et al.* (2008) and Law (2004) appear to lend credence to this concern, as it was concluded that both oil recovery and CO_2 storage are jeopardised by the early commencement of wind-down.

A less obvious concern is that related to a scenario in which the operation is based on only one steam generator. Given that CO_2 or flue-gas would only be available when the generator is in operation, the cessation of steam generation implies there is no 'cheap' CO_2. As a consequence, it might be necessary to import CO_2, which might increase the project costs.

Considering the outlined challenges, it is necessary to develop a technique, such as the alternating-injection process, that could accelerate CO_2 storage while ensuring the continuous supply of 'cheap' CO_2 or flue-gas to run the process sustainably. In the next section, we review some of the current methods of modelling steam-injection processes with or without NCG.

2.2 Modelling Steam-Injection Processes

In this section, we review some of the approaches previously taken to study steaming processes and their variants. Attention is drawn to the relative strengths and weaknesses of these approaches and results.

2.2.1 Analytic Models

Conventionally, analytic modelling is the first step in understanding a recovery process. Ideally, they describe the fundamental relationship between an output variable and the various variables that influence its outcome. As they are internally consistent, they are useful for performing and rationalising experimental results (Butler, 1987), as well as upscaling laboratory results (Pujol and Boberg, 1972). The following is a review of some of the analytic models developed for steam-injection processes.

The modelling of CSS treats the operation as a form of reservoir stimulation (enlarged wellbore). Hence, the reservoir is idealised as a radial two-zone system with a step-temperature profile, in which the heated (stimulated) zone is instantly raised to the steam temperature while the "cold" (unstimulated) zone remains at the initial temperature (Simangunsong *et al*., 2006; Jones, 1977; Seba and Perry, 1969; Davidson *et al*, 1967; Boberg and Lantz, 1966). As the heated radius is central to the current theories, several models have been proposed for its estimation (van Lookeren, 1983; Marx and Langenheim, 1959). In all the models, heat exchange between heated and cold zones is limited to conduction. In subsequent discussions, we refer to these cold and hot-region approximations as two-zone models.

One of the main aspects of CSS modelling is the assumption of steam-zone geometry. Different shapes and geometry have been employed with mixed success (Jones, 1992; Godze *et al.*, 1989; Gontijo and Aziz, 1984; Seba and Perry, 1969; Boberg and Lantz, 1966). However, performance of 14 injectors in the Tia Juana field (Venezuela) indicated that only 20-70 % of the reservoir thickness actually received steam (de Haan and Schenk, 1969). This observation suggests that if a reservoir section does not receive steam, it can still be heated up by conduction.

Performances of the current models are generally not satisfactory. Although they may work reasonably for some systems conforming to majority of the inherent assumptions, they perform poorly in most situations (Burns, 1969). In field applications, obtaining a reasonable "history" match typically requires downscaling predicted oil profile by a factor of two to four (Jones, 1992; Sylvester and Chen, 1988). As argued above, this is partly a consequence of exaggerating the heat transport in most two-zone approximation models. As part of the current research, we highlight conditions under which the two-zone models may be appropriate.

From a critical review of available CSS models, Jones (1992) expressed doubt on the possibility of having a universal model that applies to all situations. He identified complex heat and fluid flow reversals as well as multiple reservoir mechanisms as the bane of conventional analytic models. As an alternative, process-specific modelling, which considers individual phases, was advocated. Owing to the inconsistency of various CSS models, Robertson (1998) proposed a criterion for selecting the most "appropriate" model. However, the so-called "appropriate" model could still be in error by more than 50%.

In order to rationalise steamflood performances, various attempts have been made at describing the shape of the steam-condensation front. However, these have recorded limited success (Chandra and Mamora, 2005; Palmgren and Bruining; 1992; van Lookeren, 1983), as the resulting models often give poor predictions of oil production (Jones, 1981). In essence, this and the earlier discussions suggest that our current understanding of the key physics of CSS and steamflooding is incomplete.

Similar to the CSS and steamflooding, the existence of a steam chamber is central to the SAGD theory (Edmunds *et al.*, 1994; Butler *et al.*, 1981). Consequently, most of the related studies have been dedicated to understanding steam-chamber geometry and dynamics (Sharma and Gates, 2010; Ito *et al.*, 2004; Tarhuni *et al.*, 2004; Sasaki *et al*., 2002; Butler and Stephens, 1981).

Excellent reviews of SAGD studies, including issues and knowledge gaps, are available (Albahlani and Babadagli; 2009, 2008).

SAGD processes are characterised by two types of fluid flow- ceiling and slope drainage (**Fig. 2.2**). Whereas ceiling drainage is a counter-current override (buoyancy drive) of steam, oil and condensate (Edmunds, 1994), slope drainage involves heated oil and condensate draining from around the steam chamber (Butler, 1994). Despite the fundamental differences in the flow mechanisms, almost all SAGD theories are premised on slope drainage (Sharma and Gates, 2010; Akin, 2005; Reis, 1992; Butler and Stephens, 1981). For ceiling drainage, Butler (1987) proposed the steam-fingering theory, in which steam fingers are at the leading edge of the rising front (Ito and Ipek, 2005). However, analyses indicate that the ceiling drainage matches observations in numerical simulations more closely (Farouq-Ali, 1997). Hence, in principle, models based on the slope-drainage (Sharma and Gates, 2010; Akin, 2005; Butler, 1994; Reis, 1992) may be less robust.

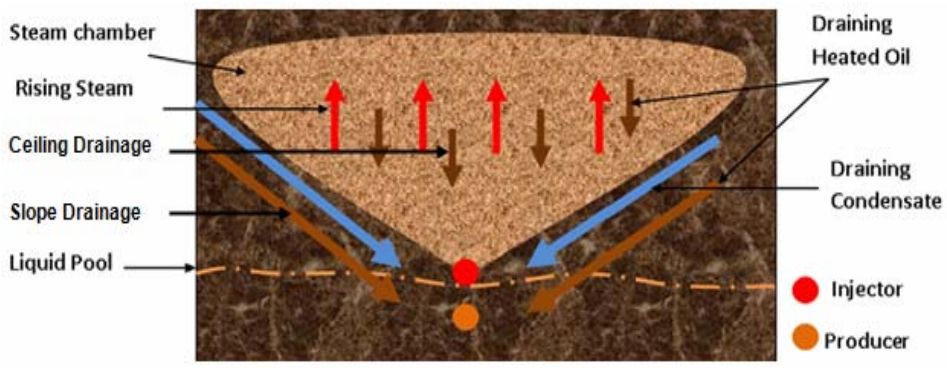


Fig. 2.2: Schematics of Slope and Ceiling Drainages in SAGD (adapted from Albahlani and Babadagli (2009))

With several simplifying assumptions, Butler *et al.* (1981) developed an analytic model to predict oil-rate in a slope-drained SAGD process. It was assumed that a steam chamber always exists and is connected to the producer. Using the concept of heat conduction in a moving solid (Ozisik, 1993; Carslaw and Jaeger, 1959), the chamber is taken to be a moving "heat source". Heat transfer ahead of the chamber is by steady-state conduction. Over-prediction of experimental results and subsequent works by Butler and co-workers (Butler, 1994; Butler and Stephens, 1981) triggered modifications of the original theory. Most of these modifications reflect uncertainties of chamber geometry and dynamics.

Subject to a quasi steady-state advancement of the steam chamber and conductive heat transfer, the temperature distribution into the cold oil sand ahead of the chamber has been approximated by the following expression (Sharma and Gates, 2010; Akin, 2005; Reis, 1992; Butler, 1985; Butler *et al.*, 1981).

$$T^* = \frac{T - T_r}{T_s - T_r} = \exp\left(-\frac{a_x U \xi}{\alpha}\right), \tag{2.1}$$

where T is the temperature at distance ξ ahead of chamber front; T^*, dimensionless temperature; U, chamber interface velocity normal to the interface; α, reservoir thermal diffusivity; a_x is a constant, equals 1 in Butler models and 0.4 in Reis (1992); subscripts *r* and *s* refer to reservoir and steam, respectively.

Eq. 2.1 is based on a simplification of the moving-solid conductive-convective heat transfer equation for a semi-infinite system (Ozisik, 1993; Carslaw and Jaeger, 1959). However, the Butler-type models (Sharma and Gates, 2010; Akin, 2005; Reis, 1993, 1992; Butler, 1985; Butler *et al.*, 1981) retained only the first term of the series expansion of the error function.

For emphasis, most of the early efforts on the original Butler model have focused on the heat-transport approximation of **Eq. 2.1**. As a result of these modifications, different multipliers have been introduced into the model for estimating the oil-rate of SAGD processes (Butler, 1985). Consequently, it is not unusual to see production forecasts differing by up to a factor of two (Akin, 2005; Reis, 1992, Butler, 1985; Butler and Stephens, 1981; Butler *et al.*, 1981).

In recent times, researchers are beginning to consider more rigorous approaches to improve the Butler models. Instead of the simple assumption of quasi-steady temperature profile in front of the chamber, Alali *et al.* (2009) employed a transient distribution. However, in spite of its complexity, their model still does not address one of the fundamental aspects of the heat transport in steam processes, namely condensation.

Still on the improvement of Butler's model, Sharma and Gates (2010) incorporated the effects of temperature-induced oil-saturation gradient and the resulting spatial variation of relative permeability (Corey-type) on the dynamics of oil at the chamber front. As a result, a new model was developed. Although it was "successfully" validated against published experimental and field data, there are some fundamental issues with this model.

By fixing the oil saturation at the edge of the chamber at its residual value, the derivation by Sharma and Gates (2010) apparently overlooked two important points. First, it does not account for the fact that, under gravity, a substantial fraction of the draining oil would pass (vertically and laterally) through the vicinity of the chamber edge as it travels towards the producer (Mohammadzadeh *et al.*, 2010), thereby raising the local oil saturation above residual. As a complementary remark, because gravity drive is more favourable (density and viscosity effects) to steam condensate than mobilised oil, the latter would experience greater hold up, hence increased local resaturation, as both fluids flow to the producer.

Secondly, the authors implicitly assume that oil desaturation (water imbibition), besides being spontaneous, is proportional to temperature, and that steam cannot co-exist with mobile oil. These assumptions clearly contradict several field reports where the analyses of seismic and production data indicate significant lag time (up to 4 years in high-permeability sands) before a steam zone can be regarded as reaching residual oil saturation for the specific depletion process (Baker *et al.*, 2010). To underscore our critique of these "sophisticated" models, some of their reported performances against field observations were not very impressive (Sharma and Gates, 2010).

From a critical evaluation of the current models that are premised on the moving "heat-source" approximation, we are of the opinion that their fundamental limitation is the implied hypothesis that the time scales for heat and steam propagation are similar (Sharma and Gates, 2010), explaining the viewpoint that chamber front is identical to thermal front. As we shall show with our improved models and field data, this assumption is not valid for: (i) situations where the heat-carrying fluid is condensable and formation is of high permeability; (ii) conduction is the dominant heat-transfer mechanism; or (iii) there is a considerable preheating (superposition) effect, in which the zone ahead of the front is already being heated up by conduction before the arrival of the front.

The dominant heat-transfer mechanism during SAGD is still contentious. While Farouq-Ali (1997) argued for convection, Edmunds (1999) supported conduction. But Doan *et al.* (1998) indicated that though conduction dominates the early stages of SAGD, convection becomes increasingly important with continuous steam injection. Attempts at using the moving-conduction theory to match field data were not convincing, as they required unrealistically high thermal diffusivity and velocity (Birrell, 2001; Closmann and Smith, 1983). Conversely, detailed numerical studies by several researchers indicated the dominance of convection (Ito and Suzuki, 1999). Field data also provide evidence of fluid movement ahead of the steam front (Aherne and Maini, 2008). At least on the basis of this evidence, it is necessary to incorporate convection (sensible heat) into realistic heat-transport models of SAGD.

However, the tricky aspect of convection is phase change. Despite acknowledging phase changes, very few models include latent heat of condensation in their description and solution of heat-transport problems in petroleum reservoirs. To their credit, Yortsos and Gavalas (1982; 1981a, b) incorporated condensation in their models. But the models neither indicate how the pressure drop resulting from steam flow would impact the condensation dynamics and reservoir heating (Closmann, 2010) nor include the temperature-dependency of oil properties (e.g. viscosity) and their impact on the dynamics of the advancing front. With anticipated large contributions of latent heat, it is imperative to have a good understanding of the mechanisms of condensation as well as front dynamics during the heating of heavy-oil reservoirs.

As an improvement over the first generation of models, researchers are beginning to consider the contribution of convection (sensible heat) ahead of the steam chamber, especially at the steam-oil interface (Sharma and Gates, 2010; Gotawala and Gates, 2010). However, current interest appears to be motivated by the phenomena of channelling caused by non-uniform permeabilities, and fingering, which results from viscosity contrasts between steam and oil. Furthermore, current treatments have not quantified the effects of flow-induced pressure drop on steam condensation.

In order to establish the lower limits of convection, Lawal and Vesovic (2009) used the Nusselt number to quantify free convection in heavy-oil reservoirs under conductive heating. Despite its simplicity, this model closely approximates: (i) the heating of matrix block through an adjacent fracture (Al-Rabaani *et al.*, 2008; Pooladi-Darvish *et al.*, 1994); (ii) steam channelling (Closmann, 1984), including micro-channelling due to geomechanical changes (Ito, 1984); and (iii) heat exchange between two sand layers separated by a vertical flow barrier. Given that steam and

resident oil are effectively not in direct contact, this representation, in principle, eliminates the effects of forced-convection phenomena of channelling and fingering espoused by some workers to make a case for convection ahead of the chamber (Gotawala and Gates, 2008; Butler, 1987). From their analyses, Lawal and Vesovic (2009) concluded that free convection is significant, especially in the vicinity of the heat source. However, the magnitude of free convection further away from the heat source depends, among other factors, on the rock and fluid properties as well as the duration of heating and imposed temperature gradient.

Most of the models for estimating heated volume are based on heat balance, suggesting that both steam and condensation zones must always exist within the reservoir (Jones, 1977). However, intuition and studies on tight / heterogeneous systems indicate otherwise (Al-Rabaani *et al.*, 2008; Collins, 2007b; Yang and Butler, 1992; Satter, 1967). In their interpretation of SAGD pressure falloff data, Tarhuni *et al.* (2004) deduced the permeability-dependency of steam-zone geometry. Similarly, experimental and numerical studies of matrix-heating via steam-injection into fractures indicate negligible steam penetration into the matrix block (Sumnu *et al.*, 1996; Pooladi-Darvish *et al.*, 1994).

From this review, it is clear that almost all existing theories on steam-injection (CSS, steamflood, or SAGD) can be related to the concept of a condensation zone (or interface) sandwiched between steam and "cold" oil zones. In principle, this conforms to the two-zone approximation (step-temperature function). Apparently, when steam does *not* condense or where a non-condensable heating fluid, such as CO_2, is used, this concept breaks down. Therefore, a robust description of condensation dynamics is warranted in order to develop representative heat-transport models.

2.2.1.1 Theory of Steam-Fingering

In order to account for the general underestimation of steam-chamber growth by the conduction-based models on one hand and the use of non-physical fitting parameters by the conductive-convective equations on the other hand, the theory of steam fingering has been developed (Gotawala and Gates, 2010; Butler, 1987). It is generally believed that pointed fingers, which result from viscous instabilities, account for the convective heat-transport at the edges of the chamber. Hence, advances in this area have generally focused on the characterisation of finger geometry and dynamics (Gotawala and Gates; 2010, 2008; Sasaki *et al.*, 2002, 2001; Butler, 1987). However, this theory is limited to ceiling drainage (Reis, 1992; Butler, 1987).

According to Gotawala and Gates (2008), the maximum vertical velocity of the steam fingers, and by extension, the steam chamber (Gotawala and Gates, 2010), is given by:

$$U_{\max} = \frac{k\ k_{rs} g\left(\rho_o - \rho_s\right)}{\mu_s}\left\{\frac{\rho_s L_c}{\left(T_s - T_r\right)\left[\rho_c c_c + 0.5 A_{m2}\phi\Delta S_o\left(\rho_o c_o + \rho_w c_w\right)\right]}\right\}, \qquad (2.2)$$

where k is absolute permeability; k_{rs}, steam relative permeability; g, gravitational acceleration; ρ_s, ρ_o and ρ_w are steam, oil and water densities, respectively; c_c, c_o and c_w are chamber, oil and water specific heat capacities, respectively; ΔS_o is mobile oil saturation in the chamber; ϕ, porosity; T_s, μ_s

and L_c are steam temperature, dynamic viscosity and latent heat, respectively; T_r, initial reservoir temperature; A_{m2} is a constant, relating to the oil viscosity-temperature relationship.

Although **Eq. 2.2** emphasises that the rate of chamber (finger) rise is proportional to the latent heat of steam, it however suggests, unrealistically, that for a non-condensing heating fluid, such as hotwater and CO_2, the heated (isothermal) chamber does not rise, and in fact, may not exist. Considering that SAGD production is purported to be strongly linked to the chamber volume (Edmunds *et al.*, 1994), it implies that processes that rely on heating by either conduction or sensible enthalpy may not be successful. But some operations, such as conduction-heating, may not even have a distinct condensation zone yet production is due to reservoir-heating (Al-Rabaani *et al.*, 2008; Collins, 2007b; Yang and Butler, 1992; Satter, 1967). This raises fundamental questions on the validity of **Eq. 2.2** and similar fingering models (Butler, 1987).

By employing a procedure that is similar to Butler (1987), but using the first seven terms of the series expansion of the error function in the exact solution of the semi-infinite slab conduction equation (Ozisik, 1993; Carslaw and Jaeger, 1959), Gotawala and Gates (2008) developed "improved" models for describing the dimensions of steam fingers and chamber growth (**Eq. 2.2**). However, in the analysis leading to their final expression, the mass-conservation principle was violated, questioning its internal consistency. Specifically, their analysis suggests that oil drains at the same velocity as the rising steam finger (see their ***Eqs. 14*** and ***18***) which, in essence, implies that steam and oil have comparable densities. Apparently, where steam and oil have similar densities, the buoyancy drive, which is the primary fluid-flow mechanism, ceases to exist.

The fundamental error in the derivation of **Eq. 2.2** partly explains the counter-intuitive inference that the rate of chamber growth decreases with increasing steam-oil ratio. To the contrary, oil removal and steam replacement at the interface is basically an ablation (successive removal of materials at the surface of a solid. For example, consider the melting of a candle, especially the gradual advancement of the melting front into the colder wax), rather than a displacement process (Edmunds *et al.*, 1994). Therefore, the removal of interface oil and the resulting chamber advancement is primarily governed by the availability and absorption of thermal energy which, in turn, is roughly indicated by the steam-oil ratio and thermal diffusivity. For emphasis, this critique also applies to the work of Butler (1987).

With the steam-fingering theory, Butler (1987) attempted to 'match' the field data reported by Closmann and Smith (1983), who had earlier analysed the same data with the conduction-convection equation. The front velocity estimated in the two works differed by about 400%. To 'force' a match (within 48% deviation), Butler (1987) increased the reference effective permeabilities of oil and steam by 25 and 400%, respectively. In other words, steam flow had to be increased significantly in order to increase the amount of convection obtainable with steam fingers. Elsewhere, Closmann (1995) also advocated the use of permeability as a fitting parameter, apparently oblivious of the fact that, in most cases, permeability is usually known within a certain range of uncertainties.

In summary, it can be deduced from the foregoing discussions that current analytic models are not robust for rationalising the performances of steam-injection processes. In general, their shortcomings can be attributed to the inadequate description of the heat-transport aspects of these processes. Essentially, this explains why they typically require unrealistically high permeability and thermal diffusivity to explain experimental datasets.

2.2.2 Numerical Models

In most cases, the complexity of the process precludes developing useful analytic models. Hence, numerical simulations are usually employed for detailed study of steam-injection processes. Besides aiding the decision-making process, numerical models are also used for rationalising experimental observations (Li and Chalaturnyk, 2009; Sasaki *et al.*, 2002). Here, we review some of the previous numerical-simulation studies, most of which were based on finite-difference simulators, highlighting the relevant results and the shortcomings of such works.

To understand SAGD mechanisms in the Hangingstone reservoir (Canada), Ito and Susuki (1999) conducted a 3D simulation study. The sandstone formation contains 1000 Pa s bitumen at in-situ conditions. From their simulations, which included geomechanical changes, they concluded that heat transfer is dominated by the convective energy transported by steam condensate both within and ahead of the chamber.

Employing experimental and numerical methods, Nasr *et al.* (2000) investigated effects of permeability and initial gas-saturation on SAGD countercurrent and co-current flows. According to them, the heating rate improved with permeability. However, considering that the in-situ fluid was water, with its relatively temperature-independent density and viscosity, their conclusion that the countercurrent steam-front advances at a constant velocity should be taken cautiously.

To history-match their SAGD experimental data, Sasaki *et al.* (2002) constructed a 3D numerical model. The relative-permeability function was found to be vital for explaining the chamber shape and oil recovery. In spite of considerable tweaking of the parameters of the physical model, the "matched" cumulative oil recovery still deviated by 18% from the experimental result, notwithstanding that, of all performance parameters, oil production is often the most trivial to match. A visual observation of the corresponding oil rates reveals much larger deviations between the "matched" and experimental profiles. An earlier history-match of the same experiment resulted in a 24% deviation between the numerical and laboratory results (Sasaki *et al.*, 2001).

Bennion *et al.* (1985) discussed the temperature-sensitivity of relative-permeability functions and their implications for the numerical simulation of CSS processes. It is worthwhile to report that most simulation studies in the literature did not include temperature effects on relative permeabilities (Li and Chalaturnyk, 2009; Bagci *et al.*, 2008; Law, 2004; Nasr *et al.*, 2000), and this may somewhat undermine their conclusions.

Using a heterogeneous 2D simulation model of a typical Cold Lake (Canada) formation saturated with a 30 Pa s oil, Lei *et al.* (2010) assessed the impacts of relative-permeability curves on SAGD dynamics. Within the range of parametric values studied, they highlighted the significant

sensitivity of SAGD process to relative-permeability assumptions, leading to the recommendation that the robustness of potential projects against relative-permeability uncertainties should always be evaluated. They also suggested that efforts be made to reduce these uncertainties, prior to large-scale project development, through acquisition and analysis of representative data. With experimental design, response-surface method and Monte Carlo simulations, Yang *et al.* (2009) employed detailed 3D numerical simulations to stress the sensitivity, via the end points and residual saturations, of a commercial SAGD project to temperature-dependent relative permeabilities. However, the use of an unrealistic steam residual-oil saturation (as low as 0 %), compared to experimental low of about 5% (Frauenfeld *et al.*, 1988), casts some doubt on the conclusions from their work. Elsewhere, Kisman and Yeung (1995) did not notice any significant impact of relative-permeability uncertainties on the performance of the Burnt Lake (Alberta), containing 13.6 ^{o}API (0.975 g/cm^3) and 26 Pa s crude.

From an extensive review of experimental data and subsequent semi-empirical analysis, Saeed (2010) concluded that, through the influence of oil viscosity and interfacial tension on residual oil-saturation, thermal recovery methods are susceptible to temperature-induced changes in relative-permeability functions, and these changes should be adequately incorporated in numerical simulation studies. According to the author, these effects are equally important in both sandstone and carbonate media.

For reservoirs, such as those in the Surmont field (Canada), containing either an overlying water zone or a gas-cap, Law *et al.* (2003a, b) performed laboratory and field-scale studies on the main mechanisms governing oil and steam movement during SAGD process. These top zones were established as thief zones, serving as sinks for steam, oil and heat, hence jeopardising SAGD performance. Specifically, it was concluded that an initial gas-cap has greater detrimental effect on oil recovery than a top water-zone. However, a higher quantity of heat (steam) was reportedly lost to the water zone than the gas cap, an observation explained by the higher thermal conductivity for water-saturated sand.

The above explanation by Law *et al.* (2003a, b) is not convincing. First, thermal diffusivity, not thermal conductivity, controls conductive heat transfer which, from the temperature profiles presented, was dominant ahead of the advancing steam chamber. Secondly, for porosity/saturation-weighted thermophysical properties, it is the rock properties that often govern the bulk behaviour of porous media (see Appendix **A**). As a result, for the same petrophysical parameters, the difference in the thermal diffusivities of gas-saturated and water-saturated columns should not be so significant that it would cause such a difference in conductive heat-transport. To substantiate our position, as part of the current research (see Chapter 4), we show that it is the heat-transfer coefficient, rather than thermal conductivity (or diffusivity), that can satisfactorily explain the magnitude of contrasting thermal losses noted for the top gas and water-zone models.

Zabel *et al.* (2010) assessed the effects of uncertainties in heavy-oil properties, namely live viscosity and saturation pressure (solution gas), on the performances of primary recovery and SAGD in a typical Faja (Venezuela) reservoir. They found that primary recovery is more sensitive to

solution-gas uncertainties because of its stronger dependence on foamy oil and solution-gas drive mechanisms. On the other hand, they noted that live-viscosity uncertainties have controlling influence on SAGD because its performance is more reliant on oil-viscosity reduction.

Based on a stochastic model of shale and sand distribution, Chen *et al.* (2008) performed 3D numerical simulation to evaluate SAGD performance in heterogeneous formations with 8.8 ^{o}API (1.009 g/cm^3), 1000 Pa s heavy oil. Where the reservoir geology consists of long, continuous shale or high percentage of shale, SAGD performance was sub-optimal, which is a consequence of poor chamber growth and fluid hydraulics. For systems with poor vertical communication, hydraulic fracturing was recommended. However, no mitigation was provided for reservoirs with random shale distribution, as fracturing may not be practical.

Gotawala and Gates (2010) also employed 3D numerical simulation, utilising a generic reservoir model based on Cold Lake properties and heavy oil of 17.6 ^{o}API (0.949 g/cm^3) and 127.95 Pa s, to study how steam-chamber development and geometry are affected by permeability heterogeneity. Among other findings, they reported non-uniform steam chamber, and recommended that permeability distribution should be considered in the placement of SAGD wells. Similarly, for intelligent completions, inflow control valves should be placed and operated according to permeability (transmissibility) distribution. Analysis of time-lapse seismic and production data have also underscored the role of geologic heterogeneities on steam-chamber growth and SAGD performance (Zhang *et al.*, 2007).

Gates *et al.* (2008a, b) and Larter *et al.* (2008) examined fluid-property heterogeneities, focusing on the susceptibility of the SAGD process to spatial variation of oil viscosity. From their simulation studies, they established that SAGD processes are vulnerable to the non-uniform distribution of oil viscosity.

Leung (1983) performed three-dimensional (3D) simulation of concurrent CO_2 and steam-injection in CSS and steamflood processes, using Athabasca-type sand saturated with oil of 10 ^{o}API (1 g/cm^3) and 1380 Pa s. CO_2 reportedly concentrated at the leading edge of the steam-condensation zone. For CSS, oil recovery increased significantly (~ 36%) over that of steam-alone. In high and normal-compressibility systems, the incremental benefits were attributed to the effects of oil-viscosity reduction and solution gas-drive, respectively. However, in steamflood, recovery was mainly accelerated, and contribution of CO_2 swelling to incremental recovery was minor, due to decreasing gas solubility at high temperature. Instructively, as an alternative to reservoir preheating, the author recommended preceding steam injection with CO_2. A key shortcoming of this study is that it did not evaluate potential crude destabilisation and the dynamic consequences of asphaltene precipitation that might occur due to CO_2 injection (Dahaghi *et al.*, 2008).

Using 14 ^{o}API (0.973 g/cm^3) and 2000 cP dead oil, Hong and Ault (1984) reported that CO_2 accelerated oil recovery from a conventional steamflood, but the ultimate recovery remained similar. This was attributed to reservoir pressurisation by the CO_2. Surprisingly, rather than depend on CO_2 quantity, oil recovery was reported to be proportional to heat input, as recovery deteriorated with reduction of steam quantity. As the simulation was based on single-component oil, we cannot

ascertain how the presence of dissolved gas and other lighter ends would have influenced their conclusion on the role of CO_2.

As part of the efforts towards implementing downhole steam generation, Bader *et al.* (1981) and Fox *et al.* (1981) compared the performances of steamflood with and without NCG. They observed that gas addition accelerated oil production by about 30% but no significant impact on ultimate recovery. It is noteworthy that their NCG was a mixture of combustion gases i.e. flue gas.

Claridge and Dietrich (1983) performed 3D simulation of immiscible CO_2 as steam additive (2-20 mol. %) to stimulate a sample of Cold Lake bitumen (10 ^{o}API, 135 Pa s) in the presence of dissolved gas (50 scf/stb). Although adding CO_2 reportedly jeopardised the recovery expected from steam-alone, they observed that CO_2 penetrated deep into the reservoir, promoting injector-producer communication. By the deep penetration, CO_2 "conditions" the reservoir for a steamflood. This observation provides motivation for reservoir preheating, as entailed in our proposed alternating-injection method.

As at date, we have not come across any published work on the potential impacts of the spatial variation of formation thermal properties and relative permeabilities, especially where distinct facies, such as sand, intra-reservoir shale, and mixtures of these primary facies, have been mapped. However, in the later parts of the current study, we address this issue.

In conclusion, the limitations of the results of the numerical-simulation studies are appreciated. In particular, the impacts of numerical dispersion and instability have been highlighted (Nasr *et al.*, 1996; Esmail, 1985; Closmann and Smith, 1983). It is believed that the development of robust convergence criteria would reduce these problems (Rossen and Dalton, 1990). In Chapter 3, based on finite-difference analysis, we develop simple convergence criteria for the solution of our heat-transport equations.

2.2.3 Experimental Models and Field Studies

In order to assess the feasibility of new developments as well as validate analytic and numerical models, experiments are usually conducted. They also provide information on some of the parameters required in analytic and numerical models. The following is a discussion of some previous experiments on steam-based processes, including the use of NCG as additives.

In a 1D physical model, Paracha (1985) studied the effects of concurrent CO_2 and steam injection on oil samples of 15, 20, and 26 ^{o}API (0.966, 0.934, and 0.898 g/cm^3). Although CO_2 addition was found to increase oil recovery significantly, the effect reportedly reduced with oil density, and was sensitive to the CO_2/steam volumetric ratio injected.

For the purpose of bitumen development, Nasr *et al.* (1987) conducted experiments on the impacts of co-injecting CO_2, N_2 and flue-gas with steam, in both continuous and cyclic modes. Although all the additives proved beneficial to oil recovery, CO_2 was shown to yield higher improvements than either N_2 or flue-gas. But in the continuous injection process, no significant difference was recorded in the enhancements offered by N_2 and flue-gas. They attributed the

similarity of the results of the steam-N_2 and steam-flue gas processes to the dilution of CO_2 by the high concentration of N_2 in the flue-gas; hence, in principle, the two processes were essentially N_2 additives. Contrary to expectations, despite the use of known asphaltene precipitants, they did not notice any asphaltene-related problems (Dahaghi *et al.*, 2008; Srivastava *et al.*, 1999a). Perhaps, the duration of these tests was probably not long enough for asphaltene precipitation, aggregation and deposition to manifest. We address this issue in Chapter 5.

Employing a 2D physical simulator, Frauenfeld *et al.* (1988) studied the response of a Cold Lake-type crude, 10.5 ^{o}API (0.996 g/cm^3) and 100 Pa s, to the co-injection of steam and CO_2. They reported that adding CO_2 would only improve oil recovery relative to pure-steam injection in a CSS if the heavy oil has no solution gas initially (dead oil). Within the range studied, production enhancement, attributed to probable flashing of light ends during pressure drawdown, increased with CO_2-steam mass ratio. For live heavy oil (28 scf/stb), adding CO_2 was found to be detrimental to steam. Although the authors reported a recovery loss of ~ 3%, subsequent analysis of the same data by Schenk (1989) suggested the loss probably exceeded 40 %. However, the temperature contour plots showed that higher temperatures were obtained in steam-only than the co-injection runs.

From a high-pressure 1D laboratory displacement study, Hornbrook *et al.* (1991) evaluated the effects of simultaneous injection of CO_2 and steam on the recovery of West Sak (Alaska) crude oil, 19.2 ^{o}API (0.939 g/cm^3) and 35.4 cP. They also found that the presence of a free-gas phase reduced the ultimate recovery of a conventional steamflood. However, as long as the effective mixing temperature exceeded the steam saturation-temperature at prevailing pressure, the presence of CO_2 reportedly increased oil recovery (~ 15% higher) while reducing the formation temperatures and heat input.

Experimentally, Metwally (1990) conducted a 1D study of the impacts of CO_2 and methane on the performance of steam-injection processes with a sample of oil, 13.5 ^{o}API (0.976 g/cm^3) and 5450 cP, from the Lindberhg field, Alberta. Although there was significant injectivity improvement when NCG was co-injected with steam, greater injectivity increase was noted when a gas slug was injected prior to steaming. However in both procedures, the presence of NCG jeopardised oil recovery, as it resulted in lower microscopic displacement efficiency (higher residual oil saturation) compared to the steam-only process. Subsequent numerical simulations, based on two-component oil model, corroborated their laboratory results.

With 1D and 3D physical models, Bagci and Gumrah (2004) detailed the effects of CO_2 and methane on the development of 12.4 ^{o}API (0.983 g/cm^3) oil by steam injection. From sensitivity studies, they established the importance of optimum injection ratio, and found that the optimum CH_4/steam ratio depended on the model dimensions. However, their optimum CO_2/steam ratio was at variance with that of a 19.2 ^{o}API (0.939 g/cm^3) oil reported by Hornbrook *et al.* (1991). If we ignore differences in experimental conditions and other factors, a comparison of these two independent results would suggest that the optimum CO_2/steam injection ratio increases as the oil becomes heavier.

On the other hand, contrary to the conclusion from the 1D work of Bagci and Gumrah (2004), the 1D experiments by Pursley (1975) showed that steam-CH_4 yielded higher amounts of oil than steam-CO_2 despite that a similar crude (12.4 ^oAPI) was used by both authors.

In another 1D test on 12 ^oAPI (0.986 g/cm^3) oil, Sedaee Sola and Rashidi (2004) established an optimum CH_4/steam ratio that differed from that of Bagci and Gumrah (2004), despite the similarity of the crudes. However, the incremental benefits of improved/accelerated recovery and steam injectivity were validated. In contrast, for propane-steam, Rivero and Mamora (2002) observed that production acceleration and injectivity enhancements were independent of injection ratio for a sample of Hamaca field (Venezuela) crude, 8 ^oAPI (1.014 g/cm^3) and 25 Pa s at reservoir conditions.

Recently, Zhang *et al.* (2009) proposed the application of a carbamide surfactant as steam additive. Apart from the claim that this additive would enhance steam conformance, they showed that at high temperature, carbamide would decompose to CO_2 and NH_3, both of which are NCG. Due to their higher diffusion rates, the authors argued, these decomposition products improve chamber expansion and, at the same time, dissolve in the oil to make it swell and decrease its viscosity by as much as 80 %. From the results of a field test presented, although accelerated production was obtained with carbamide, the ultimate recovery and steam consumption did not show significant improvement over the steam-only process. However, it remains to be demonstrated whether the accelerated recovery compensates the overall costs of carbamide.

In principle, most of the foregoing studies were steamflood experiments. As specifics, researchers have also examined CSS and SAGD processes, including the effects of NCG additives.

Using 2D scaled experiments, Nasr *et al.* (1996) studied the dynamics and injection strategies of a SAGD process. The initialisation and development of the steam chamber were found to be very sensitive to permeability. Furthermore, for the same operating pressure, injection strategy based on the control of enthalpy (steam quality) was more effective than that based on rate control. However, a complementary numerical study was inconclusive due to numerical problems, including unusual sensitivity to grid sizes.

Yang and Butler (1992) conducted 2D experiments on SAGD sensitivity to reservoir heterogeneities (geologic). Although the work was limited to vertical heterogeneity (two layers), the early-time and late-time dynamics were controlled by the properties of the injection and production zones, respectively. The overall performance is somewhere between the performances of a homogenous formation consisting of either of the two layers. For such layered systems, Butler (2004) suggested injecting steam into the more permeable layer. Although no work has been published in this regard, it is expected that a good understanding of the impact of thermal heterogeneity (spatial variation of thermal properties) would make useful contribution to the current body of knowledge on thermal processes.

Working with a cylindrical 1D model and Athabasca (Canada) tar sand, Briggs *et al.* (1982) investigated the effects of adding CO_2 and naphtha to steam in a CSS process. Although adding CO_2 enhanced oil recovery, this was attributed to supplementary drive energy provided during the depletion phase of the CSS process.

Steam-assisted gas push (SAGP), involving concurrent injection of steam and NCG, is a variation of SAGD. Although most SAGP studies reported steam savings (up to 38%), oil recovery was jeopardised (up to 30%) (Butler, 2004). In general, the gas forms an 'insulating' layer at the upper part of the chamber thereby reducing heat loss to the overburden. However, the gas reduces the effective steam temperature. A consequence of this cooling effect is a reduction in reservoir-heating rate, which manifests as declining production, relative to the steam-only process, as oil-viscosity increases (Jiang *et al.*, 2000a).

Canbolat *et al.* (2004) assessed the effect of steam, steam-CO_2 and steam-butane mixtures on oil productivity and recovery from SAGD-style development of a sample from the Bati Raman field (Turkey), consisting of limestone saturated with 12.4 ^{o}API (0.983 g/cm^3), 600 cP oil at initial conditions. Relative to the steam-only process, although steam-oil ratio showed slight improvement with the presence of NCG's, oil rate and recovery reduced significantly with increasing fraction of NCG, even when higher injectivity was engineered by injecting the steam-gas mixtures at higher pressure. Performance also varied with the vertical separation of producer and injector.

Mohammadzadeh *et al.* (2010) examined the pore-scale events of hybrid SAGD, entailing co-injection of *n*-C_5, *n*-C_6 or *n*-C_7 solvent with steam, in glass micromodels. Oil properties included 8.3 ^{o}API (1.012 g/cm^3), 70,000 cP and 17.4 wt. % asphaltene. Among other findings at the pore-level (dominated by capillary forces), they discovered that the gravity-capillary balance accounts for oil drainage and, due to local condensation of injected vapours, water-in-oil and solvent-in-water emulsions coexist at the interface of in-situ oil and gaseous (vapour) injectants. Of interest was the observation of localised entrapment of steam and vapourised solvent, a situation that would undermine the condensation process and, depending on the prevailing thermal diffusivity, impede the propagation of latent heat. Asphaltene precipitates clogged flowpaths, but mobilised fluids were able to define new paths.

A major limitation of most laboratory models is the difficulty of maintaining adiabatic conditions. For example, glass 'windows', created on the walls of the physical models, are typically used for visual observation of the processes. Through these windows, excessive heat losses are incurred, undermining the results and consistency of experiments (Jiang *et al.*, 2000a, b). Recently, Albahlani and Babadagli (2009, 2008) attributed the limitations of typical laboratory models to poor model insulation, non-representative physical models, and pressure-induced sand-grain movements, which create false permeability increase, exaggerating the productivity, injectivity and ultimate recovery.

A plausible reason for the inconsistency of laboratory results is the magnitude of heat losses typically incurred. With approximately 60-75% of heat input typically lost to the surroundings (Sasaki *et al*., 2002, 2001), the credibility of quantitative analysis of heating mechanisms from laboratory-

based data is suspect. Recognising that latent heat often constitutes at least 35% of steam enthalpy, the chances of meaningful study of condensation-heating in the laboratory are very slim. Accordingly, inferences from typical studies need to be taken cautiously. In particular, conclusions from these investigations should be put in context.

In order to reduce thermal losses, Demiral and Erdogmus (2003) used computerised tomography (CT) to study SAGD production mechanisms, thus eliminating the observation windows. However, the use of water as the in-situ fluid makes it difficult to evaluate the effects of temperature-dependent fluid properties on heat transfer and fluid production.

With CT, Alajmi *et al.* (2008) monitored the steam zone, condensate (hot water) bank and oil movement in a 1D (horizontal) steamflood experiment. About 50% of the pore volume was reportedly occupied by condensate. As expected, rate of steam-zone advancement was affected by heat loss to the surroundings and produced fluids. The retention of relatively large volume of condensate is a manifestation of 'inefficient' drive mechanism. Unlike SAGD, where gravity continuously drains condensate and mobile oil, the piston-like displacement in steamflood favours trailing zones, hence continuous expansion of condensate bank.

The co-injection of steam and NCG has also been implemented in the field. In separate CSS field tests, co-injection of steam and air reportedly accelerated oil production (Rintoul, 1979; Meldau *et al.*, 1981). Complemented with reservoir simulations, Meldau *et al*. (1981) argued that higher pressure drive and convective heat-transfer were the main factors accounting for the improved performances observed in a pilot conducted in the Paris Valley field (California) containing 10.5 ^{o}API (0.996 g/cm^3) oil of initial viscosities 227 and 23 Pa s in the upper and lower lobes, respectively. However, with the use of dead oil, their single-component model gives no insight into the role of initial solution gas. Elsewhere, Clark *et al.* (1964) reported increased productivity from the use of flue gases.

Zhang *et al.* (2000) performed simultaneous injection of steam and flue gas[*] (80-85% N_2, 10-15% CO_2), including a foaming agent, in a CSS project in the Chinese blocks Jin-45 and Jin-7, containing 3350 cP crude. Apart from the benefits of improved and accelerated oil recovery over that of steam-alone, they noted better steam conformance, reduced operating costs and emissions, as well as delayed water production. They attributed these benefits to pressure support, dilution-induced reduction of oil-viscosity as well as interfacial tension, and diffusion-induced expansion of heated volume.

As a summary, the effects of NCG on the recovery mechanisms of steam-based processes are not fully understood. While some researchers reported improved/accelerated oil recovery (Simangunsong *et al.*, 2006; Sedaee Sola and Rashidi, 2004; Harding *et al.*, 1983; Redford and McKay, 1982; Pursley, 1975), others indicated otherwise (Jiang *et al.*, 2000a; Jiang *et al.*, 2000b; Metwally, 1990; Frauenfeld *et al.*, 1988). To improve the current understanding of the physics of these processes, a key question needs to be addressed. What aspects of the overall process are

[*] Although the authors refer to it as "fuel" gas, it should read "flue" gas.

being influenced by the additives? Is it the heat transport, injectivity, microscopic displacement, macroscopic sweep, or some combinations of these? In the course of investigating the physics of our alternating-injection process, we address some of these questions.

2.3 Analogy from Industrial Processes

Some industrial applications, such as steam filtration (Gerl and Stahl, 1996), thermal dewatering (Berger *et al*., 1999), and remediation of underground contaminants (Bruining and Marchesin, 2006; Schmidt *et al.*, 2002), involve direct steam injection into porous media. In principle, these well-monitored processes should offer useful insights for the analyses of petroleum reservoir-heating.

Crone and co-workers (2002) argued for inclusion of both spatial and transient temperature gradients, in addition to complex solid-fluids heat exchange, in realistic models of these processes. The works by Crone *et al.* (2002) and Bergins *et al.* (2005) concluded that matrix-fluids heat exchange dominates heat transfer in industrial processes. They studied the heating of porous media by condensing steam but ignored heat transfer due to phase change (latent heat) in their models. Whereas condensation effects were included, Bruining and Marchesin (2006) neglected conduction, and did not provide explicitly, an estimate of the condensation rate. However, for most petroleum-reservoir applications, the assumption of local thermal equilibrium (LTE), which ignores matrix-fluid heat gradient, is usually sufficient (Bergins *et al.*, 2005; Crone *et al*., 2002; Prats, 1982). Apparently, the relatively large time-scale of petroleum reservoir-heating and the characteristic low flow velocity, which promotes longer contacts, provide good arguments for LTE. However, as part of this research, we probe the robustness of this assumption for the analysis of thermal oil-recovery methods in general.

Although not a porous medium, Siow *et al.* (2007) presented a two-phase model describing laminar film condensation from steam-air mixtures in declining (dipping) parallel-plate channels. They observed that produced condensate films became thinner and moved faster as the plate channel became more vertical (increasing angle of declination). Of interest was the conclusion that NCG (air) decreases heat-transfer rate but this undesirable effect diminishes as the channels become vertical. Additionally, a condensation “cessation” point was identified, as some point downstream of the inlet, at which the vapour (steam) has everywhere cooled to the lowest temperature within the system.

For horizontal channels, Siow *et al.* (2002) reported condensation studies on vapour-gas mixtures. Similar studies on channels of vertical orientation were carried out by Siow *et al.* (2004) for steam-air mixtures. The results indicate that both vertical and horizontal orientations are limiting cases of the declining orientation earlier discussed by Siow *et al.* (2007) for vapour-gas mixtures.

No and Park (2002), using an analogy of the conservation laws, derived a condensation model for steam-NCG mixture in a vertical tube. The model predictions were reportedly in excellent agreement with the experimental datasets of Park and No (1998), Kuhn (1995) and Siddique *et al.* (1993). Their results, valid for tubes with isothermal walls, indicate that the total heat-transfer

coefficient decreases as the condensing fluid flows through the tube. However, this conclusion is arguable, as the converse (increasing heat-transfer rate) might be true if there had been a fluid (colder) outside the tube flowing countercurrently to the condensing stream. In essence, this work underscores the conventional wisdom of putting experiments in context as against generalising their findings.

From the preceding review, the analyses of most non-porous media (e.g. ducts and channels) used as heat exchangers often focus on characterising the condensate-film thickness and heat-transfer coefficients. Whereas these systems have specific condensation surfaces (usually the walls) and non-physical contacts of the fluids, in porous media, the fact that the heating and heated fluids are always in direct contact precludes the possibility of a fixed condensation plane. Furthermore, continuous mixing of fluids renders the theory of film thickness unrealistic in porous media applications such as the heating of petroleum reservoirs. However, at least in qualitative terms, some of the deductions from these industrial systems should still be relevant for the analysis of petroleum reservoirs undergoing steam-injection.

A major difference between steam injection into petroleum reservoirs and industrial porous media is the nature of the in-situ fluids. While most industrial porous media are saturated with water or some fluids of relatively simple properties, oil sands contain crude with complex behaviours, whose reliable description is vital. In conclusion, although industrial processes do complement our understanding of the complex mechanisms of reservoir-heating, they are not substitutes for rigorous analyses of the latter.

2.4 Chapter Summary

Several aspects, including modelling and field performances, of the steam-based oil-recovery methods have been reviewed. From the discussion in this chapter, we conclude that the following issues remain to be resolved:

- mechanisms of steam condensation and its impact on reservoir-heating. Current treatments do not model condensation explicitly (see Chapters 3 and 4);
- criteria for numerical convergence of simulation models at minimal computational costs. No clear guideline currently exists (see Chapter 3);
- impacts of adjacent formations and boundary characteristics, including intra-reservoir top/bottom gas and water zones, on reservoir-heat containment (Chapter 4);
- kinetics and the net effect (interplay of viscosity-reduction and permeability damage) of potential deasphalting, due to the presence of NCG, on reservoir dynamics (see Chapters 5 and 9);
- detailed analysis of the influence of surface and subsurface parameters on steam-based processes (see Chapters 6 and 7);
- effects of NCG on oil recovery and energy consumption by steam processes. Previous studies reported conflicting results (see Chapters 8 and 9);
- influence of thermal and relative-permeability heterogeneities. Existing literature is limited to permeability and oil-viscosity heterogeneities (see Chapter 9); and

- overall cost-benefit analysis, including sourcing, compression, transportation, and injection, of NCG as additives to steaming processes (see Chapter 10).

We believe that the resolution of these issues would make significant contribution to the current body of knowledge on this subject. However, in the context of this work, resolving these issues is a first step in fulfilling the primary objective of this research, namely investigating the technical and commercial feasibility of the proposed scheme of alternating injection of steam and CO_2 for the development of bituminous reservoirs. Because it is currently the most efficient and popular of the steam-injection methods (Roche, 2008; Hart, 2006; Butler, 1998), SAGD is the reference case in this research. However, where necessary, we refer to ideas relating to CSS and steamflooding.

Chapter 3

Modelling Heat-Transport in Petroleum Reservoirs

The injection of heat-carrying fluids, usually steam, is a common thermal operation for developing viscous-oil deposits (Edmunds *et al.*, 1994; Farouq-Ali, 1994). In these operations, heating is the primary mechanism for enhancing in-situ oil mobility (Carcoana, 1992; Prats, 1982). However, despite their critical role, the heat-transport aspects of the process are still not fully understood (Birrell, 2001; Jones, 1992). As discussed in the last chapter, this limitation, to a large extent, accounts for the poor analysis and predictability of these processes (Albahlani and Babadagli, 2009; Jones, 1992; Butler, 1987).

When a saturated vapour, such as steam, is injected and comes into contact with the colder reservoir, the vapour condenses, releasing its latent heat to the colder reservoir. Although virtually all SAGD theorists acknowledge the importance of condensation in the overall heat transport, its contribution is not adequately included in the theoretical description of this process (Sharma and Gates, 2010; Akin, 2005; Birrell, 2001; Reis, 1992; Butler, 1985; Closmann and Smith, 1983). In order to establish the upper bounds of the steam-alone process, which is the reference case in the current research, we need to account for condensation. With this, we would have a good basis to assess the heating performance of proposed alternating-injection process, as neither CO_2 nor flue-gas is condensable within the anticipated operating conditions.

In this chapter, we extend the traditional convective-conductive treatments of heat-transport in petroleum reservoirs by explicitly including the contributions of condensation. We introduce two mechanisms of condensation, namely multiple-contact and first-contact condensation. For these mechanisms, mathematical models are derived and solved, with considerable attention given to the convergence of the solution schemes. For simplicity, the present analysis is limited to the case of reservoirs with isothermal boundaries; non-isothermal boundaries are considered in the next chapter. The direct application of the new formulations to real problems is presented. We then proceed to examine the robustness of the new models to some of the underlying assumptions. Throughout this study, our reference is steam, although the ideas presented herein can easily be extended to other heat-conveying saturated vapours.

3.1 Domain Definition and Modelling

Fig. 3.1 shows the domain of study. Heating fluid is introduced via the injector, placed above the producer. Injector and producer are parallel to the reservoir bed. Through the producer, a hot mixture of oil and condensate (for condensed steam) is drained. The model, incorporating heat transport by conduction, convection and phase change, is characterised by countercurrent flows induced by density contrasts. **Fig. 3.2** provides a lucid description of countercurrent flow at the pore-scale. Reservoir dynamics are governed by the conservation equations, applied over the interval z to $z+dz$.

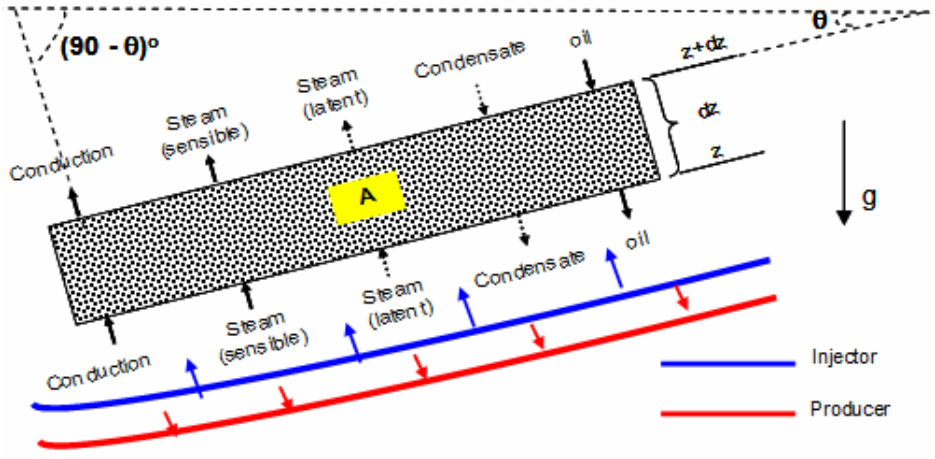


Fig. 3.1: Simplified Model of Gravity-Driven Counter-current Flow at Liquid-Steam Interface

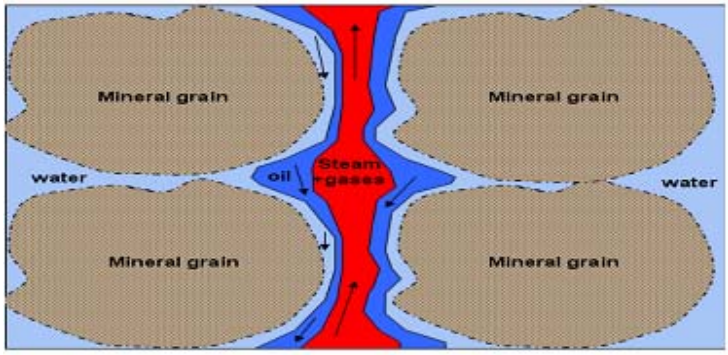


Fig. 3.2: Pore-scale Processes for Counter-current Flow (Sjølyst, 2006)

With a combination of steam diverters (Zhang *et al.*, 2009) and horizontal wells, and noting that the well length is roughly of the same order as the reservoir dimensions, fluid flow would reasonably approximate 1-D. The condition of buoyancy drive presumes that injection pressure is just at the reservoir pressure which, in turn, is below the fracture pressure but greater than oil saturation pressure at all temperatures. With continuous voidage replacement by fluid injection, reservoir pressure should be fairly constant.

By implementing appropriate steam-trap control strategy, the escape of live steam (heating fluids) would be minimal (Doan *et al.*, 1999; Ito and Susuki, 1999; Edmunds, 1998). There are practical methods for achieving uniform steam conformance. These include the injection of foamed steam (Gotawala and Gates, 2009; Patzek, 1996) and keeping production below the critical rate for coning /cresting (Yang and Wattenbarger, 1991). Although studies reported interactions between fluid flow and geomechanical behaviour during steam-injection operations (Li and Chalaturnyk, 2009; Collins, 2007b), conditions exist, such as below fracture pressure, that permit ignoring these effects. In general, there are field performances that support the dominance of gravity drive in similar operations (Vogel, 1992).

Although the model description closely approximates SAGD systems, in principle, the applicability is not limited to SAGD and its variants. Some non-conventional methods, such as

thermally-assisted gas-oil gravity drainage (Al-Rabaani *et al.*, 2008; Ikwumonu *et al.*, 2007; van Wunnik and Wit, 1992), may also be rationalised with the proposed theories.

By examining effects of capillary pressure on heavy-oil systems under steam floods, Pujol and Boberg (1972) concluded that viscous forces are of much greater importance than capillary forces in high-viscosity oils (> 100 Pa s). Hence dynamics of such systems is largely independent of capillarity. Considering that capillary pressure is primarily controlled by fluid saturations, it is reasonable to infer that the effect of relative permeability, which is also saturation-dependent, would be comparably insignificant.

Despite the complexity of steam-injection processes, the foregoing suggests that certain simplifying assumptions can be made. In order to take advantage of analytical approach, we make some assumptions. First, we treat fluids as single phase, although in real life, multiphase flows exist. As a result, saturation-dependent relative-permeability and capillary-pressure effects are ignored. This allows the use of a constant, but not necessarily equal, effective permeability for all the fluids. A similar simplification is implicit in the analyses of earlier workers (Akin, 2005; Reis, 1992; Butler, 1987). The other assumptions governing subsequent mathematical models are:

- 1-D, homogenous and isotropic system subject to buoyancy drive;
- there is local thermal equilibrium between the matrix and fluids;
- flow is countercurrent (ceiling drainage) and normal to the reservoir's plane of dip;
- reservoir pressure changes negligibly and there are no chemical reactions;
- heated oil does not vapourise, and condensate flash to steam is negligible;
- only steam can condense, and live steam is not produced;
- steam, NCG, condensate and oil are immiscible;
- steam of constant quality and temperature is injected; and
- negligible geomechanical changes.

In the later part of this chapter, the assumptions of local thermal equilibrium and negligible pressure-drop are relaxed in order to assess the sensitivity of the proposed models to these assumptions.

3.1.1 Mass Balance

The following analysis assumes that only steam, condensate and oil are present. Application of the mass-conservation law, over the differential element *dz* during the time interval *dt*, yields the following overall mass balance for time-invariant saturations:

$$\rho_s v_s\big|_z + \rho_w v_w\big|_{z+dz} + \rho_o v_o\big|_{z+dz} \approx \rho_s v_s\big|_{z+dz} + \rho_w v_w\big|_z + \rho_o v_o\big|_z . \tag{3.1}$$

where ρ_s, ρ_w, and ρ_o are the densities of steam, water (condensate) and oil, respectively. v_s, v_w, and v_o are the corresponding velocities.

Eq. 3.1 describes a three-phase countercurrent flow i.e. upward steam-flow is balanced with an equal mass flux of oil and condensate flowing downward. That is, the resultant mass flux of the system is zero.

3.1.2 Momentum Balance

We assume that the flow is laminar and each phase moves with a Darcy (superficial) velocity. Therefore, neglecting skin effect (additional pressure drop due to formation damage and flow restriction related to the completion of the wells), phase velocity and gravity potential are coupled by the Darcy equation (Dake, 1977):

$$v_p = \frac{K_{vp} g (\Delta \rho_p) \cos \theta}{\mu_p}, \tag{3.2}$$

where K_v is the effective vertical permeability; g, the gravitational acceleration; and θ is the reservoir dip as illustrated in **Fig. 3.1**. μ_p is the phase viscosity and $\Delta\rho$ is the buoyancy drive for the phase. Subscript p denotes the flowing phase.

In **Fig. 3.1** and **Eq. 3.2**, the angle θ effectively refers to the local inclination of the interface (as the fluids are assumed to be completely immiscible) of the rising steam and falling oil and steam-condensate within a differential element of thickness dz. Thus in the limiting case $\theta = 0$, the interface is moving vertically, and we have a perfect horizontal interface, which gives maximum buoyancy drive. Conversely, when $\theta = 90^o$, it implies that a gravity-driven interface does not exist, suggesting that other mechanisms are driving the fluids. In essence, $g \cos\theta$ is a resolution of the vector quantity g, in the flow (defined as normal to the bedding plane) direction depicted in **Fig. 3.1**.

In **Eq. 3.2**, the effective permeability is kept constant, both in time and space, for each phase. Although Kv_p, assumed to depend on saturation only, should change as the saturations of the fluids vary between reservoir positions and at different times. However, behind the steam front, due to the continuous presence of the different streams (steam, oil and water); we can assume that the fluid saturations would be reasonably constant, especially in the mid to late times. On the other hand, the region ahead of the front is primarily saturated with oil, implying that saturation changes due to multiphase flow in this region would be negligible. As a result, K_{vo} ahead of the front should also be constant. As we will show in the later part of this chapter, deep into the colder oil ahead of the front, the primary heating mechanism is conduction, implying zero flux of steam and condensate. In this conduction-dominated region, only the oil mobilised by conductive-heating flows. This simplifying assumption on K_{vp} allows us to develop analytic models for gaining useful insights into the heat-transport aspects of this process. This notwithstanding, in chapters 6-9, we use numerical simulations to conduct rigorous assessment of saturation-induced changes (in time and space) in effective permeabilities on both heat and mass transport.

The following defines the density driving force for each phase.

$$\Delta\rho_s = \rho_w - \rho_s; \qquad \Delta\rho_w = \rho_w - \rho_s; \qquad \Delta\rho_o = \rho_o - \rho_s. \tag{3.3}$$

Because $\rho_w >> \rho_s$ and $\rho_o >> \rho_s$ in reality, we could have employed $\Delta\rho_s = \Delta\rho_w \approx \rho_w$ and $\Delta\rho_o \approx \rho_o$, as used by other workers (Sharma and Gates, 2010; Akin, 2005). However, in the current study we retain the differences for better accuracy.

3.1.3 Heat Balance

In the case of steam injection, when saturated steam comes into contact with the colder formation, three heat-transfer mechanisms are usually at play. These are conduction, convection and condensation. By conduction, heat is propagated through the body of the bulk formation, consisting of the rock and the saturating water, oil and possibly, gas. Convection conveys the sensible heat. This results from the flow of the fluids, which include the inflowing heat carrier(s) and the outflowing heated fluids. Heat transfer by condensation is due to the latent heat released as the steam undergoes a phase change. In principle, condensation is a special form of convection, involving latent heat rather than sensible heat.

Ideally, the heat balance equation for a steam-injection process must account for the three mechanisms. However, as would be discussed in the later parts of this chapter, current heat-transfer treatments do not include condensation (Sharma and Gates, 2010; Akin, 2005; Birrell, 2001; Reis, 1992; Butler, 1985; Closmann and Smith, 1983), despite being a key contributor to the overall behaviour of steam-injection processes. Compared to the injection of non-condensing heat carriers such as CO_2 and N_2, the latent heat gives steam an important comparative advantage.

If the heating fluid condenses, we hypothesise that this may occur by either of two mechanisms. These are multiple-contact condensation (MCC) and first-contact condensation (FCC). While the FCC model is based on instantaneous phase change, the MCC theory assumes that the injected steam condenses progressively as it traverses the reservoir. In the following sections, we derive mathematical models that describe the proposed condensation mechanisms.

In principle, the MCC and FCC are different ways of describing the same process of steam condensation. The main difference lies in how the latent heat from steam condensation is released, which influences how this quantity is incorporated into the heat equations. In the FCC process, we assume that all the “available” latent heat is released at the first colder plane encountered by the advancing steam. By colder plane, we mean the plane, in the direction of steam movement, which is at a lower temperature than the saturation-temperature of the advancing steam. On the other hand, in the MCC process, the “available” latent heat is released over a succession of colder planes ahead of the front. Therefore, while there is a latent-heat gradient in the MCC process, a gradient does not exist in the FCC process.

We recognise that the injected steam may not fully condense in the MCC and FCC processes. This position is supported by reports of significant production of live steam in laboratory and field studies (Alajmi *et al.*, 2008). Although part of the reproduced steam can be attributed to the flashing of some water condensates (result from steam condensation), from an energy-balance viewpoint, we can account for these events by penalising the gross latent heat, hence the use of the term

"available" latent heat. In principle, these events can be treated as a consequence of limited condensation.

In general, limited condensation can be attributed to two factors: (i) not all the injected steam makes contact with a colder surface; and (ii) the contact time between the steam and colder surface(s) is too short to achieve complete condensation. For example, some of the upward flowing steam may get trapped in dead voids (unconnected pores), localised regions (de Haan and Schenk, 1969), within downward flowing hot oil (Mohammadzadeh *et al.*, 2010), or stuck behind shale streaks (Chen *et al.*, 2008; Yang and Butler, 1992; Closmann and Smith, 1983), preventing them from reaching the colder surfaces. Similarly, excessive pressure drawdown from the producer could force the steam within the colder region to detour and move towards the producer rather than stay in contact with the colder plane (Doan *et al.*, 1999; Ito and Susuki, 1999; Edmunds, 1998). Therefore, in order to account for the limited condensation, we introduce the quantity f_c, which represents the effective mass-fraction of the injected steam that eventually condenses within the domain of interest. Given the factors that influence limited condensation, it is apparent that f_c cannot be predicted with high confidence. Hence, in this study, we treat it as a model-fitting parameter, which ranges from 0 to 1.

In the above discussion, the condensation refers to the dry-steam (saturated) component of the injected steam, which is characterised by the steam-quality, f_s. The steam quality is the mass-fraction, ranging from 0 to 1, of the dry steam present in the injected mixture of saturated steam and its condensate. In practice, f_s at the injector-reservoir interface is reasonably known (Valbuena *et al.*, 2009). Hence, in our work, we treat f_s as a known input parameter.

As a result of steam condensation, water condensate is generated in-situ. Due to buoyancy, the condensate flows downward, carrying some sensible heat along. Ideally, one would expect all the condensate, as determined by f_c, to be drained at the producer. However, several factors, which include dead voids, presence of flow barriers and the re-vapourisation of the condensate, limit the net amount of condensate production. To account for the limited production of the generated condensates, hence the sensible heat, we introduce the quantity f_{cw}, referring to the effective mass-fraction of the in-situ condensate that eventually reaches the producer. As explained in the case of f_c, several factors preclude reliable prediction of f_{cw}. Hence, in the current work, it is an adjustable parameter, ranging from 0 to 1.

Throughout this study, the quantities f_c, f_s, and f_{cw} are taken to be global quantities that represent the average behaviour over the entire heating domain and time. Hence, they are independent of position, time and temperature. Apart from f_s that can reasonably be engineered in practice, the others are simply adjustable parameters.

3.1.3.1 Multiple-Contact Condensation

Adding condensation gradient to conduction, convection and accumulation terms, MCC heat balance is:

$$\begin{aligned} &-\kappa A\frac{\partial T}{\partial z}\Big|_z + \rho_s A v_s c_{p_s} T\Big|_z + \rho_o A v_o c_{p_o} T\Big|_{z+dz} + \rho_w A v_w c_{p_w} T\Big|_{z+dz} + \left(-f_c \rho_s A v_s L_c\big|_z\right) \\ &= -\kappa A\frac{\partial T}{\partial z}\Big|_{z+dz} + \rho_s A v_s c_{p_s} T\Big|_{z+dz} + \rho_o A v_o c_{p_o} T\Big|_z + \rho_w A v_w c_{p_w} T\Big|_z + \left(-f_c \rho_s A v_s L_c\big|_{z+dz}\right) + \rho A c_p dz\frac{\partial T}{\partial t} \end{aligned} \quad , \quad (3.4)$$

where κ, ρ, and c_p are the thermal conductivity, density and specific heat capacity of bulk reservoir, respectively. T is temperature and L_c, the specific latent heat of steam condensation (vapourisation). f_c is the mass fraction of steam condensed. Again, subscripts *s*, *o* and *w* refer to steam, oil and water, respectively.

The above equation assumes that the steam and the formation attain local thermal equilibrium (LTE) instantaneously; hence they have the same temperature T at the plane z. In the later part of this chapter, we analyse the time scales for reaching LTE and conditions under which LTE may be violated.

Assuming all the mobile hot water comes from steam (condensate), then:

$$\rho_w v_w = f_c \rho_s v_s \,. \quad (3.5)$$

Suitability of **Eq. 3.5** is supported by the SAGD experiment conducted by Law *et al.* (2003a). The results showed that despite the presence of unconfined water zone above the oil zone, mass rates of produced condensate and injected steam were approximately the same (<1% deviation). Similar conclusion was reached when a large gas-cap overlaid the oil zone.

From **Eqs. 3.4** and **3.5**, we have a nonlinear partial differential equation (PDE).

$$\alpha\frac{\partial^2 T}{\partial z^2} - \Psi_s\frac{\partial(v_s T)}{\partial z} + \Omega_c\frac{\partial(v_s L_c)}{\partial z} + \Psi_o\frac{\partial(v_o T)}{\partial z} + \Omega_w\frac{\partial(v_s T)}{\partial z} = \frac{\partial T}{\partial t}\,, \quad (3.6)$$

in which

$$\alpha = \frac{\kappa}{\rho c_p}\,;\quad \psi_x = \frac{\rho_x c_{p_x}}{\rho c_p}\,;\quad \Omega_c = \frac{\rho_s f_c f_s}{\rho c_p}\,;\quad \Omega_w = \frac{\rho_s f_c f_s f_{cw} c_{p_w}}{\rho c_p}\,. \quad (3.7)$$

where f_s is the steam quality and f_{cw}, the net fraction of condensate withdrawn from the heating domain. Subscript *x* refers to the phase.

Although Yortsos and Gavalas (1981a, b) had proposed a similar PDE as our **Eq. 3.6**, the following are some improvements over their equation:

- inclusion of the term f_c, which accounts for limited condensation of a condensable fluid. In Yortsos and Gavalas model, we can infer that f_c = 1; and
- addition of the term f_{cw}, accounting for the retention of some of the water condensate. In Yortsos and Gavalas model, it is apparent that f_{cw} = 1.

We further enhance our model by incorporating:

- temperature-dependency of oil viscosity and density (see below); and
- the effects of pressure-drop (see later part of this chapter).

Considering that much of the dependent variables (v_o, v_s, and L_c) in **Eq. 3.6** are functions of temperature, scope exists for explicitly building the temperature dependence into the PDE. For example, the following simplifications can be made to the condensation contribution:

$$\frac{\partial(L_c v_s)}{\partial z} = L_c \frac{\partial v_s}{\partial z}; \qquad \frac{\partial v_s}{\partial z} = \frac{\partial v_s}{\partial T}\frac{\partial T}{\partial z} \tag{3.8}$$

taking into account that the latent heat will be realised at the saturation temperature, hence L_c is invariant. The dependence of the steam velocity on temperature is a direct result of the change of oil density (see **Eqs. 3.2** and **3.3**) with temperature, as the steam properties, ρ_s and μ_s, evaluated at injection conditions are not dependent on the change in the reservoir temperature.

Eq. 3.8 assumes that L_c, which is evaluated at the injection temperature T_s, is independent of the steam position. Ideally, there is pressure-drop due to steam flow. Noting that saturated steam is injected, we would expect some drop in saturation temperature, hence L_c would change. Although we ignore this effect in the current analysis, we assess the impact of this assumption in the later part of this chapter. Because steam (heating fluid) properties are always evaluated at injection conditions, they are constant.

For the sake of mathematical convenience, the following temperature-dependence (**Eq. 3.9** is empirical) is assumed for heavy-oil viscosity and density (Al-Rabaani *et al.*, 2008; McCain, 1990; Jones, 1977).

$$\mu_o = \mu_{o_r} T^a, \tag{3.9}$$

$$\rho_o = \rho_{o_r}\left[1 - \beta\left(T - T_r\right)\right]. \tag{3.10}$$

where a and β are empirical constants. T_r is a reference temperature for oil viscosity μ_{or}, and density ρ_{or}.

In line with **Eq. 3.8**, and the assumed equation-of-state, the following is the steam-velocity gradient.

$$\frac{\partial v_s}{\partial z} = \left(\frac{-K_{vs} g \rho_{o_r} (\cos\theta)\beta}{\mu_s}\right)\frac{\partial T}{\partial z} \equiv -v_{s_r}\beta\frac{\partial T}{\partial z}. \tag{3.11}$$

Similar analysis for the oil yields the following velocity gradient:

$$\frac{\partial v_o}{\partial z} = -\frac{K_{vo} g \rho_{o_r}\cos\theta}{\mu_{o_r}}\left(\frac{a(1+\beta T_r)}{T^{(a+1)}} + \frac{\beta(1-a)}{T^a}\right)\frac{\partial T}{\partial z} \equiv -v_{o_r}\left(\frac{a(1+\beta T_r)}{T^{(a+1)}} + \frac{\beta(1-a)}{T^a}\right)\frac{\partial T}{\partial z}, \tag{3.12}$$

Using the above equations in the PDE, we reduce **Eq. 3.6**,

$$\alpha \frac{\partial^2 T}{\partial z^2} + F \frac{\partial T}{\partial z} = \frac{\partial T}{\partial t} \quad , \qquad (3.13)$$
$$Conduction + Convection = Accumulation$$

where the convective term F is

$$F(T) = F_o(T) + F_w(T) - F_s(T) + F_L(T), \qquad (3.14)$$

$$F_o(T) = \Psi_o v_{o_r} \left[\frac{(1+\beta T_r)(1-a)}{T^a} - \frac{\beta(2-a)}{T^{(a-1)}} \right], \qquad (3.15)$$

$$F_w(T) = \Omega_w v_{s_r} \left[1 - 2\beta T + \beta T_r \right], \qquad (3.16)$$

$$F_s(T) = \Psi_s v_{s_r} \left[1 - 2\beta T + \beta T_r \right], \qquad (3.17)$$

$$F_L(T) = -\Omega_c v_{s_r} \beta L_c \,, \qquad (3.18)$$

where F, F_o, F_w, and F_s denote the effective, oil, water, and steam convection terms respectively. F_L is the convection *equivalence* of condensation-heating. All the terms have velocity dimensions.

3.1.3.2 First-Contact Condensation

If all the condensable fraction of steam condenses immediately, we derive

$$\alpha \frac{\partial^2 T}{\partial z^2} - \Psi_s \frac{\partial (v_s T)}{\partial z} + \Omega_{c1} - \Omega_{cx} + \Psi_o \frac{\partial (v_o T)}{\partial z} + \Omega_w \frac{\partial (v_s T)}{\partial z} = \frac{\partial T}{\partial t}, \qquad (3.19)$$

in which

$$\Omega_{c1}(T) = \frac{m_c L_c}{\rho c_p}; \quad \Omega_{cx}(T_i) = \frac{m_c h_i}{\rho c_p}; \quad m_c = \frac{f_c f_s \rho_s v_s}{z_f}, \qquad (3.20)$$

where Ω_{c1} is the absolute contribution of FCC to reservoir-heating; Ω_{cx} is heat-source at initial reservoir temperature, T_i; $h_i(T)$ is the specific enthalpy of water at T_i and it is given by $h_i = c_{pw}(T_i - T_{ref})$. T_{ref}, which is the reference temperature for estimating enthalpy, is set to 0 °C. (Ω_{c1} - Ω_{cx}) is net heat gained due to instantaneous condensation of the heating fluid. This is simply the change in reservoir-enthalpy caused by the instantaneously condensing steam; m_c is the condensation rate per unit volume, derived in Appendix **B**; and z_f is the vertical distance covered by the front.

As will be shown shortly, the quantity m_c is a local quantity, which is determined by f_c, f_s, as well as rock and fluid properties. Considering its dependency on f_c, an uncertain fitting parameter, m_c is also an adjustable parameter. However, whereas f_c is a constant global quantity, m_c varies with position, time and temperature.

The foregoing estimation of the initial reservoir specific enthalpy h_i, assumes that the reservoir is initially filled with water, hence the use of c_{pw}. The consideration of the initial enthalpy allows us to

have a proper account of the net amount of heat introduced by the instantaneously condensing steam in the FCC process. Without discounting this initial enthalpy, the net heat input in the FCC process would be over-estimated.

In the MCC process, because all the temperature terms are differentials, the effect of initial reservoir enthalpy cancels out. Conversely, the FCC model includes this variable because the latent-heat term is released instantaneously. Hence, in the case of FCC, we have:

$$\alpha \frac{\partial^2 T}{\partial z^2} + F \frac{\partial T}{\partial z} + \Omega_1 = \frac{\partial T}{\partial t} \quad , \qquad (3.21)$$
$$Conduction + Convection + Source = Accumulation$$

where

$$\Omega_1 = \Omega_{c1} - \Omega_{cx} . \qquad (3.22)$$

where Ω_1 denotes a net heat 'source', which is steam latent-heat less initial reservoir enthalpy.

Eqs. 3.13 and **3.21** include all the heat-transport mechanisms (conduction, convection and condensation) in steam-injection processes. As would be expected, in the case of a non-condensing heat carrier (e.g. hot CO_2), L_c = 0 and m_c = 0, reducing the equations to the traditional conductive-convective model (Closmann and Smith, 1983). And where there is a fluid-flow barrier, $F = 0$, further simplifying the equations to the conduction model (Alali *et al.*, 2009; Pooladi-Darvish *et al.*, 1994; Butler *et al.*, 1981; Satter, 1967). On the evidence of this internal consistency, it can be concluded that the new models are major improvements over the current treatments of the heat-transport of steam-injection processes.

The convective term F is given by

$$F(T) = F_o(T) + F_w(T) - F_s(T) . \qquad (3.23)$$

The absence of condensation term in **Eq. 3.23** distinguishes it from corresponding MCC term (**Eq. 3.14**). The terms F_o, F_w, and F_s are as defined for the MCC model (**Eq. 3.15 - 3.17**). Basically, **Eq. 3.21** is a convective-conductive model with a source term which, in turn, depends on steam-injection rate and temperature as well as reservoir properties and initial conditions. Hence, the maximum temperature that can be reached during the reservoir-heating process is limited by the source (steam) temperature.

In the literature, various forms of **Eq. 3.21** have been derived for a number of applications that involve heat generation by an in-situ source such as electrical, chemical, and nuclear processes (Ozisik, 1993; Cornwell, 1977; Bird *et al.*, 1960). For example, McGee and Vermeulen (2007) used the following model to describe heat-transfer mechanisms during electrical-heating of oil sands,

$$\nabla.(\kappa \nabla T) - \rho_s c_{p_s} \vec{v}_s . \nabla T + \sigma E . E^T = \frac{\partial(\rho c_p T)}{\partial t} \quad . \qquad (3.24)$$
$$Conduction + Convection + Electrical\ Source = Accumulati\ on$$

where E is the electric voltage gradient, E^T is the transpose of E, and σ is the electrical conductivity.

The model, structurally the same (in 1-D) as our **Eq. 3.21**, has the electrical-source term analogous to our heat-source term (FCC). This notwithstanding, as much as we are aware, the current heat-flow model with an explicit source-term has not been used to describe heating by a condensable fluid, such as steam, in petroleum reservoirs. A review of available reservoir-heating models would substantiate this point (Sharma and Gates, 2010; Alali *et al.*, 2009; Akin, 2005; Reis, 1992; Butler, 1985; Closmann and Smith, 1983; Yortsos and Gavalas, 1981).

McGee and Vermeulen (2007) noted that the source-term causes an instantaneous energy distribution, resulting in *uniform temperature increase everywhere in the spatial domain*. Although this observation provides a benchmark for the FCC model, it is worth pointing out that their result implies that the source-term always exists everywhere in their problem domain; hence its effect on the system temperature is felt uniformly, rather than localised.

In our models, relative-permeability comes in through the effective permeability, which affects the phase velocities (**Eq. 3.2**). As relative permeability depends on fluid-saturation, there may be concerns on the variation of effective permeabilities due to fluid-saturation changes. While noting the validity of this concern for conventional oil reservoirs, we postulate that it is not critical for heavy-oil reservoirs under thermally-assisted gravity-drive, as inferred from previous works (Akin, 2005; Reis, 1992; Butler, 1987).

During heat-mobilisation of heavy oil, we believe that temperature distribution is much more important than saturation profile. A review of some previous modelling efforts would substantiate this position (Alali et al., 2009; Akin, 2005; Reis, 1992; Butler, 1987). Gravity-drainage is a countercurrent process, where mobile oil and water are ‘immediately’ drained and replaced by steam. This hinders the ‘stable’ coexistence of steam and mobile liquids, thereby trivialising effects of saturation-induced relative permeability dynamics, as long as mobile oil and water exist. For such buoyancy-dominated processes, flow reversals undermine conventional theories on relative permeabilities (Cao and Aziz, 1999).

On the significance of relative permeability, there is a key issue to be addressed: are conventional relative-permeability data suitable for gravity-drainage processes? While conventional relative-permeability experiments and correlations are based on co-current and diffuse multiphase flow (Kjosavik *et al.*, 2002; Corey, 1954), our process is dominated by counter-current and segregated flows, making conventional relative-permeability models unrealistic. In principle, while co-current flow is a “displacement” process, in which steam/condensate pushes the oil in the same direction, counter-current flow is more of “substitution”, whereby steam replaces oil. Hence, the latter can be approximated as a single-phase flow (Farouq-Ali, 1997). Moreover, influence of temperature on fluid saturations and relative permeabilities is still inconclusive (Polikar *et al.*, 1986; Maini and Batycky, 1983; Miller and Ramey, 1983).

Nasr *et al*. (2000), after “matching” their steam-water experiments, reported significant differences between the “matching” counter-current and co-current relative permeability functions. At all saturations, they observed that the magnitude of co-current relative permeability was consistently higher than corresponding counter-current process. Similarly, Bourbiaux and

Kalaydjian (1990) reported that for any water saturation, the relative permeabilities that enabled reasonable match of oil recovery rates in countercurrent experiments were about 30% lower than the conventional co-current relative permeabilities. Considering that most numerical simulations are based on co-current relative permeability models, predicting performances of countercurrent systems is inherently optimistic (Nasr *et al.*, 2000).

With the approach discussed so far, we have simplified the complex problem of reservoir-heating and production to energy equations (**Eqs. 3.13** and **3.21**), which solutions provide the temperature profile and an 'indication' of oil mobility over time. In the following sections, the solutions are developed.

3.1.4 Initial and Boundary Conditions

The following constitute the initial (IC) and boundary (BC) conditions. We have two fixed boundary conditions corresponding to steam injector and caprock,

$$T(z,0) = T_i; \quad t < 0, \tag{3.25}$$

$$T(0,t) = T_s; \quad t \geq 0, \tag{3.26}$$

where T_i is the initial reservoir-temperature prior to heating (or after preheating).

Possible options for the second BC are

$$\kappa \frac{dT}{dz} = 0 \Rightarrow T(H,t) = T_i; \quad t \geq 0, \tag{3.27a}$$

$$\kappa \frac{dT}{dz} = q(t); \quad t \geq 0, \tag{3.27b}$$

$$T(\infty,t) \approx T_i; \quad t \geq 0, \tag{3.27c}$$

where **Eq. 3.27a** represents an isothermal insulating caprock (negligible heat loss), while **Eq. 3.27b** models a conducting rock which has a time-dependent heat flux. A specific form of this generalised model was used by van der Maas and Maldonaldo (1997) as well as Hassid (2002), to approximate semi-infinite behaviour. **Eq. 3.27c** describes a semi-infinite reservoir.

One drawback of **Eq. 3.27c** is the difficulty of applying it in numerical codes (Vinsome and Westerveld, 1980). In Chapter 4, we present an improved form of **Eq. 3.27b**, which is the most robust of the BC's.

3.2 Numerical Solution

The inherent nonlinearity of **Eqs. 3.13** and **3.21** precludes analytic solutions. Hence, we employ numerical solution. For its relative simplicity, the finite difference scheme (FDS) is used, and the drive for computational efficiency, favours an implicit scheme (Smith, 1985).

Using the Crank-Nicolson method (Crank and Nicolson, 1947) on a uniform grid spacing *h*, and timestep *k*, while assuming central and forward difference formulae for $\partial T/\partial z$ and $\partial T/\partial t$, respectively, the PDE terms are approximated as follows.

$$\alpha\frac{\partial^2 T}{\partial z^2}\approx\frac{\alpha}{2h^2}\left(T_{i+1,j+1}-2T_{i,j+1}+T_{i-1,j+1}+T_{i+1,j}-2T_{i,j}+T_{i-1,j}\right), \tag{3.28}$$

$$F\frac{\partial T}{\partial z}\approx\frac{F}{2h}\left(T_{i+1,j+1}-T_{i,j+1}+T_{i+1,j}-T_{i,j}\right), \tag{3.29}$$

$$\frac{\partial T}{\partial t}\approx\frac{1}{k}\left(T_{i,j+1}-T_{i,j}\right);\ h\ =\ \delta z\ ;\ k\ =\ \delta t\ . \tag{3.30}$$

3.2.1 MCC Model

In the case of the MCC equation (**Eq. 3.13**), we obtain the following numerical scheme:

$$-\left(\frac{\alpha}{2h^2}\right)T_{i-1,j+1}+\left(\frac{\alpha}{h^2}+\frac{F}{2h}+\frac{1}{k}\right)T_{i,j+1}-\left(\frac{\alpha}{2h^2}+\frac{F}{2h}\right)T_{i+1,j+1}\approx\left(\frac{\alpha}{2h^2}\right)T_{i-1,j}-\left(\frac{\alpha}{h^2}+\frac{F}{2h}-\frac{1}{k}\right)T_{i,j}+\left(\frac{\alpha}{2h^2}+\frac{F}{2h}\right)T_{i+1,j}, \tag{3.31}$$

$$F(T)=F\left(T_{i,j}\right)=F_o\left(T_{i,j}\right)+F_w\left(T_{i,j}\right)-F_s\left(T_{i,j}\right)+F_L\left(T_{i,j}\right), \tag{3.32}$$

with one of the convection terms given by

$$F_o(T)=\Psi_o v_{o_r}\left[\frac{(1+\beta T_r)(1-a)}{T_{i,j}{}^{a}}-\frac{\beta(2-a)}{T_{i,j}{}^{(a-1)}}\right]. \tag{3.33}$$

3.2.2 FCC Model

Applying the foregoing procedure to the FCC equation (**Eq. 3.21**) yields

$$-\left(\frac{\alpha}{2h^2}\right)T_{i-1,j+1}+\left(\frac{\alpha}{h^2}+\frac{F}{2h}+\frac{1}{k}\right)T_{i,j+1}-\left(\frac{\alpha}{2h^2}+\frac{F}{2h}\right)T_{i+1,j+1}\approx\left(\frac{\alpha}{2h^2}\right)T_{i-1,j}-\left(\frac{\alpha}{h^2}+\frac{F}{2h}-\frac{1}{k}\right)T_{i,j}+\left(\frac{\alpha}{2h^2}+\frac{F}{2h}\right)T_{i+1,j}+\Omega_1\,. \tag{3.34}$$

The heat-source term for the next timestep and grid is estimated from

$$\Omega_1=\Omega_{c1}-\Omega_{cx};\quad \Omega_{cx}\left(T_i\right)=\frac{\dot{m}_c h_i}{\rho c_p}, \tag{3.35a}$$

$$m_c\approx\frac{f_c f_s \rho_s K_{vs} g\rho_{o_r}\left[1-\beta\left(T_{i,j}-T_r\right)\right]}{H\mu_s}, \tag{3.35b}$$

Note that in **Eq. 3.34**, the heat-source term Ω_1, is only active behind the advancing front of the condensable heating-fluid (e.g. steam). In other words, as soon as the condensing front passes a particular location that is colder than the zone which it just traverses, it releases all (depending on the fractional condensation, f_c) its latent heat instantaneously. The released heat is assumed to be shared equally throughout the zone behind the advancing front at that instant. Therefore, in principle, the variable *H* in **Eq. 3.35b** refers to the current vertical distance covered by the mobile

heating fluid. *H* only takes on its maximum value (reservoir thickness), when the front reaches the reservoir-overburden boundary.

3.2.3 Numerical Convergence

For computational efficiency, it is necessary to employ the optimum number of grids for the implementation of the numerical schemes of **Eqs. 3.31** and **3.34**. In order to develop simple guidelines for first-order selection of the optimum grid sizes, it is imperative to investigate the convergence of these schemes, in the course of which we can derive an expression for the local truncation error associated with the schemes. Hence, the analysis presented in this section is a precursor to the study on the optimum mesh sizes, as presented in sub-section **3.2.4**.

Employing direct analysis to establish convergence of an FDS is tedious, and may not be justified (Morton and Mayers, 2005; Stikwerda, 2004). However, with the Lax-Richtmyer equivalence theorem, which indicates that consistency and stability guarantee convergence (Richtmyer and Morton, 1967), convergence can be demonstrated cheaply. In this work, we employ simple theories on consistency and stability to examine the convergence of the proposed numerical scheme (**Eq. 3.31**).

3.2.3.1 Local Truncation Error

In the following analysis, we estimate the local truncation error, which is a requirement for assessing numerical convergence. We assume a continuous and differentiable $T(z,t)$, and that $\frac{\partial^2 T}{\partial z \partial t} = \frac{\partial^2 T}{\partial t \partial z}$.

Let *Y* be the PDE (**Eq. 3.13**) and $\varepsilon_{i,j}$ the truncation error of the scheme. Expressions for these terms are:

$$Y = \alpha \frac{\partial^2 T}{\partial z^2} + F\frac{\partial T}{\partial z} - \frac{\partial T}{\partial t}, \tag{3.36}$$

$$\varepsilon_{i,j} = Y_{i,j}(T) = \left(\frac{\alpha}{2h^2}\right)T_{i-1,j} - \left(\frac{\alpha}{h^2} + \frac{F}{2h} - \frac{1}{k}\right)T_{i,j} + \left(\frac{\alpha}{2h^2} + \frac{F}{2h}\right)T_{i+1,j} + \left(\frac{\alpha}{2h^2}\right)T_{i-1,j+1} - \left(\frac{\alpha}{h^2} + \frac{F}{2h} + \frac{1}{k}\right)T_{i,j+1} + \left(\frac{\alpha}{2h^2} + \frac{F}{2h}\right)T_{i+1,j+1}. \tag{3.37}$$

Taylor's expansion of the terms about point (ih, jk), yields

$$\begin{aligned}\varepsilon_{i,j} \approx{}& \alpha\left(\frac{\partial^2 T}{\partial z^2}\right)_{i,j} + F\left(\frac{\partial T}{\partial z}\right)_{i,j} - \left(\frac{\partial T}{\partial t}\right)_{i,j} + \frac{Fh}{2}\left(\frac{\partial^2 T}{\partial z^2}\right)_{i,j} - \frac{k^2}{6}\left(\frac{\partial^3 T}{\partial t^3}\right)_{i,j} + \frac{\alpha h^2}{12}\left(\frac{\partial^4 T}{\partial z^4}\right)_{i,j} - \frac{k^3}{24}\left(\frac{\partial^4 T}{\partial t^4}\right)_{i,j} \\ &+ \frac{\alpha k}{2}\left(\frac{\partial^3 T}{\partial z^2 \partial t}\right)_{i,j} - \frac{k}{2}\left(\frac{\partial^2 T}{\partial t^2}\right)_{i,j} + \frac{Fk}{2}\left(\frac{\partial^2 T}{\partial z \partial t}\right)_{i,j} + \frac{Fh^3}{24}\left(\frac{\partial^4 T}{\partial z^4}\right)_{i,j} + \frac{\alpha k^2}{4}\left(\frac{\partial^4 T}{\partial z^2 \partial t^2}\right)_{i,j} + \frac{\alpha k^4}{48h}\left(\frac{\partial^5 T}{\partial z \partial t^4}\right)_{i,j} \\ &- \frac{k^4}{120}\left(\frac{\partial^5 T}{\partial t^5}\right)_{i,j} + \frac{Fh^4}{120}\left(\frac{\partial^5 T}{\partial z^5}\right)_{i,j} + \frac{\alpha h^4}{720}\left(\frac{\partial^6 T}{\partial z^6}\right)_{i,j} + \frac{Fh^5}{720}\left(\frac{\partial^6 T}{\partial z^6}\right)_{i,j} - \frac{\alpha k^6}{720h^2}\left(\frac{\partial^6 T}{\partial t^6}\right)_{i,j} + \ldots\end{aligned}. \tag{3.38}$$

Given that $T_{i,j}$ is the solution of the PDE (**Eq. 3.36**), the differentiability of $T(z,t)$, and ignoring higher differential terms, $\varepsilon_{i,j}$ is approximately

$$\varepsilon_{i,j} \approx \frac{Fh}{2}\left(\frac{\partial^2 T}{\partial z^2}\right)_{i,j} - \frac{k^2}{6}\left(\frac{\partial^3 T}{\partial t^3}\right)_{i,j} + \frac{\alpha h^2}{12}\left(\frac{\partial^4 T}{\partial z^4}\right)_{i,j} + O\left(h^4 + k^3\right). \tag{3.39}$$

This shows that local truncation error of the proposed numerical scheme is of order $O\left(h + h^2 + k^2\right)$. However, for pure conduction ($F = 0$), we have $O\left(h^2 + k^2\right)$. The latter is in agreement with other independent analyses of the Crank-Nicolson scheme (Lapidus and Pinder, 1980; Stikwerda, 2004).

3.2.3.2 Consistency

By definition (Smith, 1985), an FDS is consistent with a PDE if the solution of the scheme converges to the solution of that PDE as the mesh sizes tend to zero (grid refinement). Mathematically,

$$h \to 0 \quad k \to 0\,; \;\Rightarrow \varepsilon_{i,j}(T) \to 0\,. \tag{3.40}$$

Applying these conditions in **Eq. 3.39**, consistency is established, as $\varepsilon_{i,j} \to 0$.

As it conforms to **Eq. 3.40**, we conclude that the proposed numerical scheme (**Eq. 3.31**) is *unconditionally* consistent with the PDE (**Eq. 3.13**).

Given that the Crank-Nicolson method, the basis of our FDS, is unconditionally stable (Smith, 1985), and having demonstrated consistency of the scheme in the preceding section, we conclude that our numerical scheme (**Eq. 3.31**) is *unconditionally convergent*.

3.2.4 Optimum Mesh Sizes- MCC

Having shown that our numerical scheme is convergent, we now develop simple rules for selecting the optimum number of simulation grids and time steps. First, we need some exact solution for this purpose.

For a finite system of thickness *H*, governed by **Eqs. 3.25**-**3.27a**, the exact solution of **Eq. 3.13** for pure conduction is (Bird *et al.*, 1960)

$$T(z,t) = T_s - 2(T_s - T_i)\left\{\sum_{n=0}^{\infty} \frac{(-1)^n}{\left(n + \frac{1}{2}\right)\pi} e^{-4\left(n+\frac{1}{2}\right)^2 \pi^2 \frac{\alpha t}{H}} \cos\left(n + \frac{1}{2}\right)\frac{2\pi z}{H}\right\}. \tag{3.41}$$

However, being a series and considering the nature of its terms, it is difficult to implement **Eq. 3.41** in **Eq. 3.39**. Hence, this solution is no longer considered in this analysis.

As an alternative, for the limiting case of a semi-infinite system (**Eqs. 3.25**, **3.26** and **3.27c**), with constant convection (*F*), the exact solution of **Eq. 3.13** is (Carslaw and Jaeger, 1959).

$$T(z,t) = T_i + \left(\frac{T_s - T_i}{2}\right)\left\{erfc\left(\frac{z+Ft}{2\sqrt{\alpha t}}\right) + e^{\frac{-Fz}{\alpha}}erfc\left(\frac{z-Ft}{2\sqrt{\alpha t}}\right)\right\}. \quad (3.42)$$

With mixed success, steady-state approximations of this solution have been used to describe the heating of oil sands (Akin, 2005; Birrell, 2001; Reis, 1992; Butler, 1985). But, one drawback of this expression is the difficulty of implementing it in **Eq. 3.39**. However, in this work, we employ it for the limiting cases in which either conduction or convection (no condensation) is the dominant heating mechanism.

3.2.4.1 Conduction-Dominated Process ($F = 0$)

Incorporating **Eq. 3.42**, with $F = 0$, into **Eq. 3.39** and setting the principal part to zero, we derive the following as the condition for numerical convergence.

$$\frac{h}{k} = \frac{1}{t}\sqrt{\left.\frac{\left(z^4 - 20\alpha t z^2 + 60\alpha^2 t^2\right)}{2\left(z^2 - 6\alpha t\right)}\right|_{i,j}}. \quad (3.43)$$

Considering that *z* and *t* are variables, **Eq. 3.43** indicates that the gridding 'velocity' (h/k) is not constant. This offers scope for dynamic gridding as simulation progresses in the *t* and *z* axes.

The upper-bound of the convergence criterion can be established by assuming a limiting system of thickness *h*, heated for time *k*. Setting $t \to k$ and $z \to h$ in **Eq. 3.43**, we obtain a mesh relationship,

$$k \le 0.212 h^2/\alpha, \quad (3.44)$$

indicating the 'minimum' grid-size that would ensure numerical convergence for a time-step size, *h*.

To account for the different possibilities, we generalise the convergence criterion

$$0 < k \le B h^2/\alpha. \quad (3.45)$$

where *B* is a positive constant.

As a comparison, the following is the convergence criterion for the explicit finite-difference approximations of the conduction equation (Dehghan, 2004; Smith, 1985).

$$k \le h^2/6\alpha. \quad (3.46)$$

For the same accuracy, using *B* = 0.212 would result in a simulation design that is some 30% cheaper than the conventional explicit scheme. With *B* = 2, we could reduce the computational costs of the explicit scheme by a factor of 12.

In principle, we expect the results to be independent of the value of *B* used. However, for some applications such as thin systems or problems with large transient times, caution should be exercised in applying the criterion 'rigidly'. Recalling that this criterion is based on a constant-convection semi-infinite theory (**Eq. 3.42**), caution should be exercised when applying it to the analysis of finite systems or where the net convection (velocity) term varies significantly.

Computationally, dynamic (variable) gridding is more efficient. For problems that have long transient times, it might be pragmatic to use a smaller time-step (B = 0.212) initially, increasing it gradually as the simulation progresses (consistent with **Eq. 3.45**). A similar approach has been applied elsewhere (Giles and Carter, 2006; Forsyth and Vetzal, 2002).

3.2.4.2 Convection-Dominated Process ($F \neq 0$)

When convection is important, using **Eq. 3.42** in **Eq. 3.39** yields a complex expression, which cannot be solved uniquely as done for the conduction case. Therefore, we use a different approach in this case.

At steady-state and neglecting heat loss, we can infer a "conduction-equivalence" of convection,

$$\alpha_{convection} = \kappa / \rho c_p \equiv Fh\,. \tag{3.47}$$

For 'total' conduction, which entails adding conduction and convection, **Eq. 3.45** becomes:

$$0 < k \le \frac{Bh^2}{\alpha + Fh}, \tag{3.48}$$

where $(\alpha + Fh)$ is apparent thermal diffusivity. Because F is not known at start-up, it is reasonable to assume initial velocity (**Eq. 3.2**) of injected heating fluid. Being the highest possible velocity, it results in the maximum time-step size (or minimum number of time-steps) that guarantees convergence.

As a remark, we emphasise that the grid-selection criteria of **Eqs. 3.45** and **3.48** are premised on the assumption that the solutions of the heat-transport equations (**Eqs. 3.13 and 3.21**) are continuous and differentiable at all times and everywhere within the simulation domain. When these conditions are not satisfied, the criteria are not applicable.

3.2.5 Optimum Mesh Sizes- FCC

Performing the preceding analysis for the FCC equation does not yield a useful relationship. Therefore, we recommend that the MCC-based criteria be used for simulating the FCC. For a fixed number of space grids N_z, and convergence objective, a sensitivity study indicates that the FCC requires more time-steps than the MCC. With this observation, the following holds

$$N_{t-FCC} \ge G N_{t-MCC}; \quad G > 1\,. \tag{3.49}$$

where G is a scalar multiplier, and N_t is the number of time steps.

As there is no method for estimating G, we take advantage of the current practice of upscaling reservoir dynamic models, essentially by trial-and-error, (Ekrann and Mykkeltveit, 1995; Stone, 1991; Kyte and Berry, 1975). This entails the use of **Eq. 3.48** to create a small (coarse) model of the system. N_t sensitivity is then performed by gradual increment of G until satisfactory convergence results. This 'optimum' G will then be applied in the full model. Obviously, the result is

non-unique, and changing the parameters of the model or N_z might necessitate a G update. However, due to space constraint, this "improvised" approach is not discussed here.

3.2.6 Numerical Program

A FORTRAN program has been written for the numerical schemes (**Eqs. 3.31** and **3.34**). Procedure for estimating required thermophysical and transport properties is presented in Appendix **A**. It should be noted that properties of the rock, connate water and oil (thermal diffusivity) are evaluated at the average of initial and heating fluid temperatures, and are not updated with time. On the other hand, heating fluid properties are estimated at injection conditions but not updated with time as there is always a fresh injection stream (steam or NCG) at the same temperature.

In each time-step, the numerical schemes yield a system of simultaneous equations in temperature. This system is solved with the tridiagonal matrices method (Koenig, 1998). Additionally, for the FCC model, we ensure that the heat-source term is only implemented behind the advancing thermal front at any instant. Similarly, the instantaneous mass-rate of condensation is averaged for the region behind the front.

3.3 Example Application

The base-case input data**,** typical of Athabasca oil sands (Dusseault, 2001), are listed in **Table 3.1**. Sensitivity studies are performed, evaluating effects of process, petrophysical and operating variables on the heating process. In simulating the FCC, 500 mD was found to be too high for the base-case simulation time of 100 days, masking the impacts of other variables. Hence, specifically for the FCC, K_{vs} = 100 mD. The reservoir is finite, bounded by insulating cap and base rocks kept at initial temperature.

Table 3.1: Base-case Rock and Fluid Data

T_i, °C	0	ρ_r, kg/m^3	2600	f_s	1
T_{cap}, °C	0	κ_r, W m^{-1} K^{-1}	2	API, degree	9
T_s, °C	250	c_{pr}, J kg^{-1} K^{-1}	900	β, K^{-1}	400 x 10^{-6}
H, m	50	K_{vs}, mD	500, 100	ρ_o @ 0 °C, kg/m^3	990
ϕ	0.2	K_{vo}, mD	500	μ_o @ 0 °C, Pa s	1.27 x 10^{85}
S_o	0.8	θ, degree	0	a	-33.25
S_w	0.2	α, m^2/s	9.0 x 10^{-7}	Reservoir	Finite

3.4 Results and Discussion

Except stated otherwise, oil is not withdrawn. This was implemented in the simulations by setting K_{vo} = 0. Furthermore, the results are generally for f_c = 1 and f_{cw} = 0 after 100 heating days in the case of MCC but 400 days for the FCC process.

To ascertain its robustness, the numerical code was first validated against an analytic solution (**Eq. 3.42**), in a simple case of conduction-heating for which analytic solution is available. **Fig. 3.3** indicates an excellent agreement between the numerical and analytic solutions at different times.

The code was further tested for numerical convergence by choosing the optimum time and grid steps, in line with the proposed gridding criteria. For an arbitrary MCC problem, we invoke the gridding criterion of **Eq. 3.45** in all but one case. As an example, for N_t = 50 and B = 20.2, N_z is 106. Similarly, for N_t = 50 and B = 0.18, N_z = 2900. The same procedure applies to all the other cases except N_z = 27. Conversely, for the same N_t = 50 and B = 20.2, we deliberately use N_z = 27, which is ~ 25% of the optimum 106.

Results of the average temperature over time are shown in **Fig. 3.4** for the various cases examined. Although the simulation maintains its convergence above the optimum grids, the performance degrades significantly below the optimum. From this example, we conclude that the gridding criterion is suitable for the intended class of problems and solution scheme.

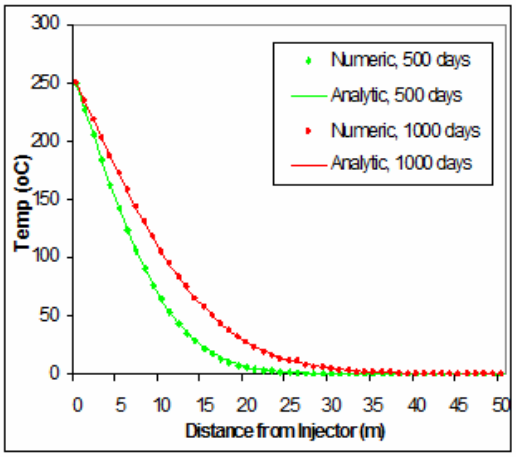


Fig. 3.3: Comparison of Analytic & Numeric Solutions (Pure Conduction)

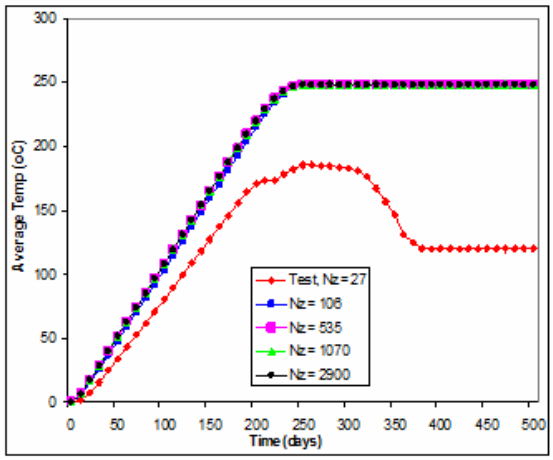


Fig. 3.4: Convergence Test- MCC (N_t= 50, B_{ref} = 0.18)

Fig. 3.5 illustrates the temperature profiles for different B's after 10 heating days for the MCC. Despite wide disparity in the number of grids (factor of 28), all the profiles, but one, converge. The test case (B = 20.2), coarser than the recommended maximum (B = 5.05) by factor of four, shows serious numerical instability (oscillations). While the other results yield average temperature of 82.5±0.4 ^{o}C for the lower 30 m, corresponding value for the test case is 153 ^{o}C. This further confirms the appropriateness of the criterion, at least in the cases considered.

Figs. 3.6 and **3.7** depict effects of condensed steam-fraction (f_c) and withdrawn condensate-fraction (f_w) on the MCC and FCC, respectively. In both cases, heating-rate increases with condensed steam while condensate removal cools the reservoir. However, the cooling effect of condensate removal is more pronounced for high f_c. That is, the lower the amount of condensed fluid, the lower the sensitivity of reservoir-heating to condensate drainage. From an energy-

conservation viewpoint, this suggests that it is beneficial to minimise condensate production, as this improves heat accumulation within the reservoir, hence the reservoir-heating rate.

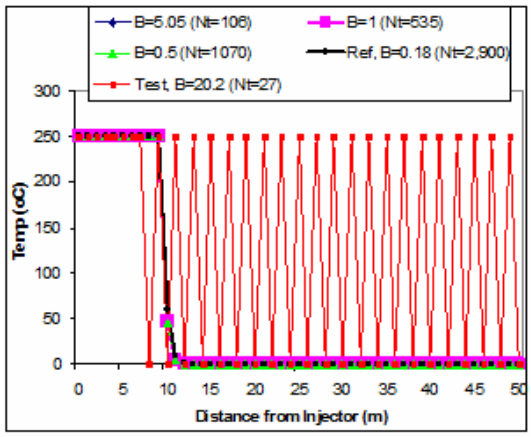


Fig. 3.5: Convergence Test- MCC
(N_Z = 50, K_{vo} = 1 D, K_{vs} = 10 D, B_{ref} = 0.18)

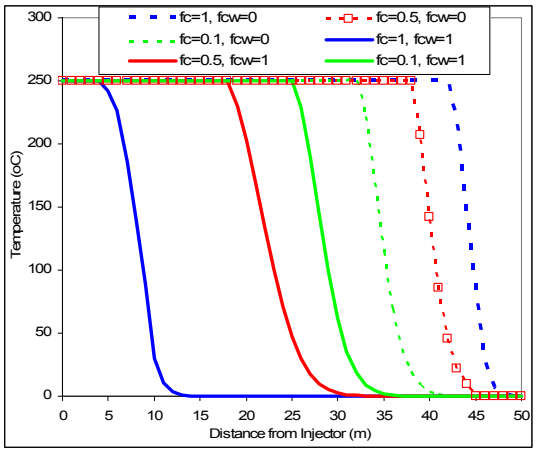


Fig. 3.6: MCC- Effect of Condensate Production

For comparison, we run a hypothetical case in which latent-heat is released uniformly in the reservoir (z_f = H) rather than restricted behind the front. In principle, the former scenario may be approximated if we imagine vertical steam injectors placed above the horizontal injector, with all wells injecting steam continuously. This may also be approximated if we place heat generators, such as electric heater, in the vertical plane above the horizontal injector. For discussion, we refer to the hypothetic FCC as “superconductor-FCC” while the more realistic case is simply called FCC.

For the same set of parameters, **Fig. 3.8** shows the temperature profiles for the superconductor FCC after 100 days. Compared to the MCC and FCC processes (**Figs. 3.6** and **3.7**), this process has a different profile. However, a constant-temperature interval is evident in all cases. For discussion purposes, we refer to these isothermal intervals as “condensation” zones.

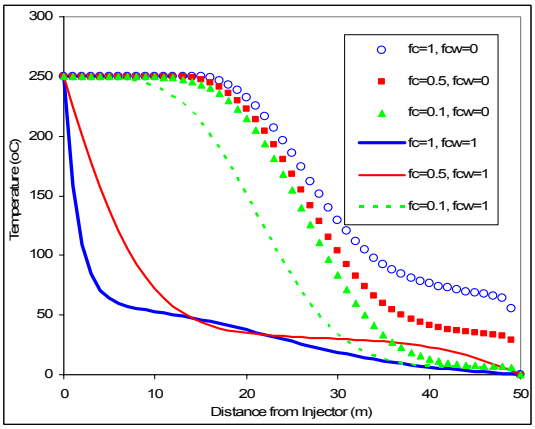


Fig. 3.7: FCC- Effect of Condensate Production

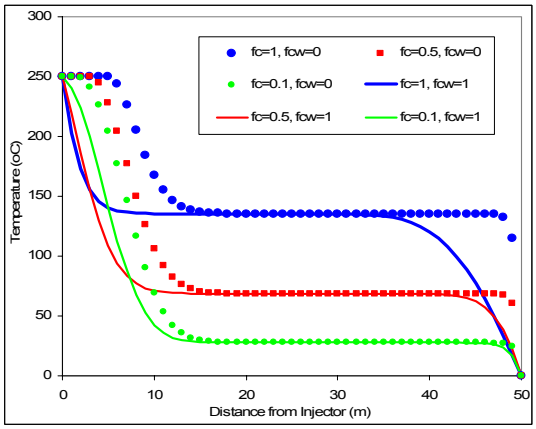


Fig. 3.8: Response of Superconductor FCC

Whereas the MCC and FCC have their condensation zones at the injection temperature, prior to reaching steady-state, the condensation zone of the superconductor-FCC is not at injection conditions. Moreover, unlike the other processes that have expanding condensation zones, that of the superconductor-FCC has a fairly constant thickness at all times. However, with increasing rate of condensation and condensate retention, the latter also approaches the injection temperature.

The MCC and FCC profiles indicate an advancing inlet-temperature front preceded by a short interval of conduction-heating (evident by the concave downward trend). On the other hand, the condensation zone of the superconductor-FCC occupies over 70% of reservoir thickness and, via conduction/convection, exchanges heat with the boundaries. Discounting boundary effects in **Fig. 3.8**, the reservoir is heated uniformly. This is in excellent agreement with the observations from the electric-heating of an oil sand (McGee and Vermeulen, 2007). In our case, the instantaneously propagating and condensing steam (superconductor FCC) replaces their electrical source (heater), in which electric heaters covered much of the reservoir area. To rationalise the superconductor-FCC process, the formation may be viewed as some super-conductor of heat, which allows instantaneous heat propagation throughout its body.

Figs. 3.7 and **3.8** indicate that, for the same conditions, the FCC process offers slightly lower rate of heating than its superconductor counterpart. This is due to the restriction placed on the distribution of latent heat. Whereas the FCC model limits the distribution to the region behind the front, the other distributes it uniformly along the entire reservoir thickness at all times.

In the case of MCC, it may be argued that the so-called “condensation zone” is just a steam zone, which results from continuous injection without production. For the same K_{vs} = 0.5 D system, **Fig. 3.9** shows that after 100 heating days, the steam front would have advanced ~42 m under MCC as against some 28 m for non-condensing steam. In order to match the MCC’s front-propagation rate, while insisting on non-condensing steam, the ‘known’ effective permeability would need to be doubled. In general, the amount of permeability “adjustment” increases with the in-situ permeability (Lawal and Vesovic, 2010a). This probably explains why Butler (1987) had to increase the reference steam effective permeability by a factor of four (and nine) to match the field data reported by Closmann and Smith (1983). This example highlights the pitfall in the current practice of tracking thermal front by fitting thermocouple data to conductive-convective models (Birrell, 2001); as such models do not consider steam condensation.

As shown in **Fig. 3.10a**, although permeability has a profound effect on heating-rate, the significance is less pronounced at low values. The impact is non-linear, as a 5-fold permeability increase from 20 mD does not yield appreciable improvement in heating-rate. As reference, **Fig. 3.10b** shows the experimental data reported by Nasr *et al.* (2000). A qualitative comparison of **Figs. 3.10a** and **b** reveals that their results are consistent with the MCC model, with the minor difference towards the colder boundaries attributed to the boundary conditions, as the latter was obtained from a semi-infinite system. In the next chapter, we extend our models to semi-infinite systems. Additionally, a close evaluation of **Figs. 3.9** and **3.10** shows that the heat-front becomes sharper

with permeability, suggesting that as the formation becomes more permeable, conductive-heat transfer reduces ahead of the front.

The sensitivity on permeability also reveals the pitfall in modelling the reservoir as two isothermal regions, i.e. hot and cold zones. From these results (see also **Fig. 3.18**), models based on step-temperature profiles (Marx-Langenheim, 1959; Jones, 1977; Seba and Perry, 1969) may not be valid in all cases.

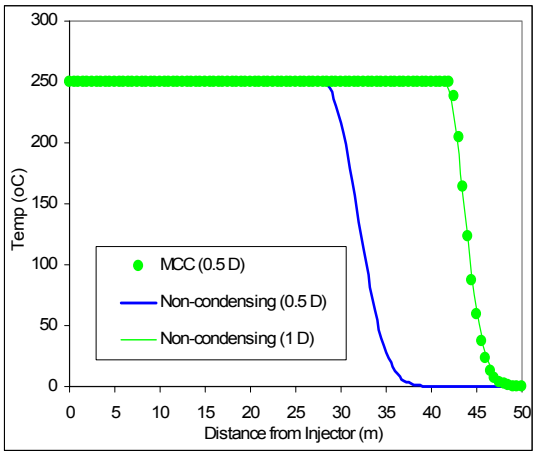


Fig. 3.9: Decoupling Condensation Effect

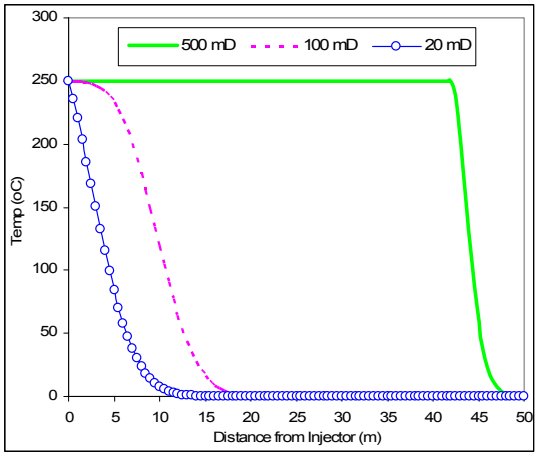


Fig. 3.10a: MCC- Effect of Permeability

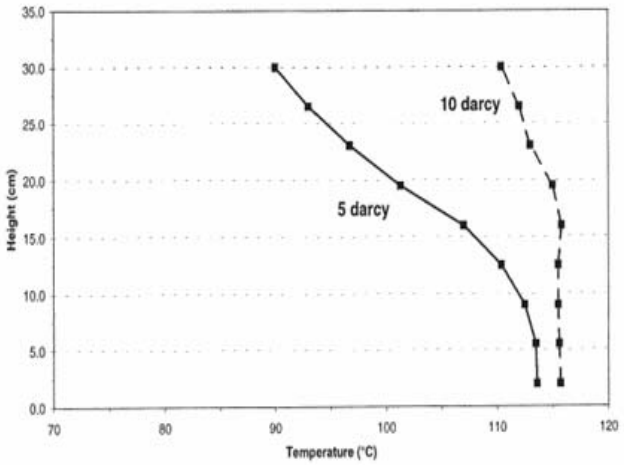


Fig. 3.10b: Laboratory *SAGD* Temperature Profile, Permeability Effect (Nasr *et al.*, 2000)

Figs. 3.11-3.14 highlight the dependence of temperature profile on the heating duration. In the MCC and FCC cases, the fronts continue advancing at the injection temperature. From these results, a clear correlation is evident between the amount of heating and elapsed time. In particular, the MCC model shows good consistency with the experiment results of Nasr *et al.* (2000), presented here as **Fig. 3.12**. Although it was a steamflood experiment, characterised by co-current flow and semi-infinite behaviour, the data (**Fig. 3.13**) of Hornbrook *et al.* (1991) generally conform to the MCC and FCC theories (pore volume injected is equivalent to heating time). The heating rate

also increases with steam-quality (**Fig. 3.15**), resulting from the positive effect of steam quality on latent heat.

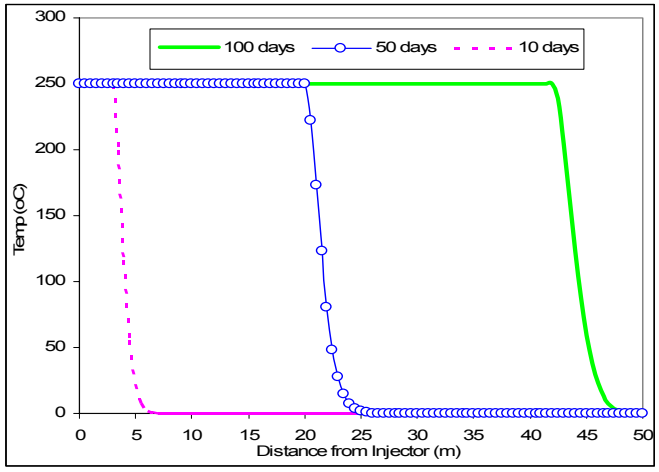


Fig. 3.11: MCC- Effect of Heating Time

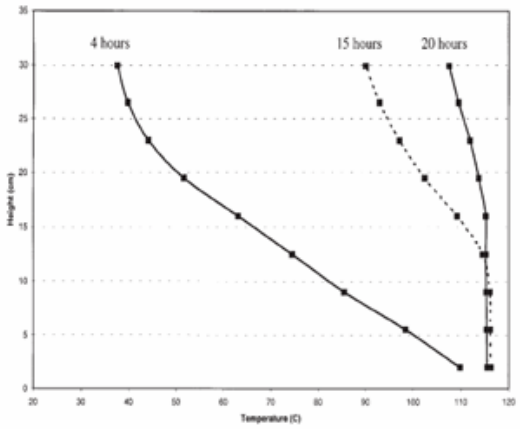


Fig. 3.12: Laboratory *SAGD* Temperature Profile, Time Effect (Nasr *et al*., 2000)

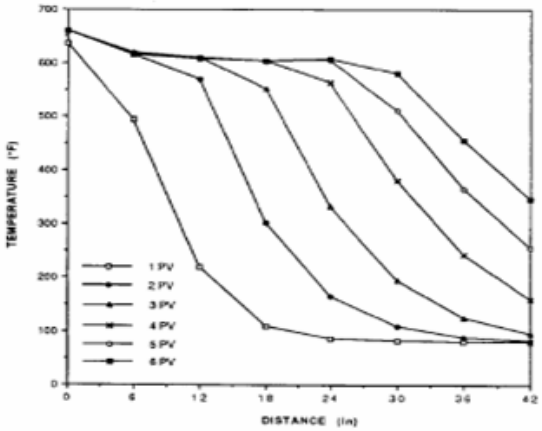


Fig. 3.13: Experimental *Steamflood* Temperature Profile (Hornbrook *et al.,* 1991)

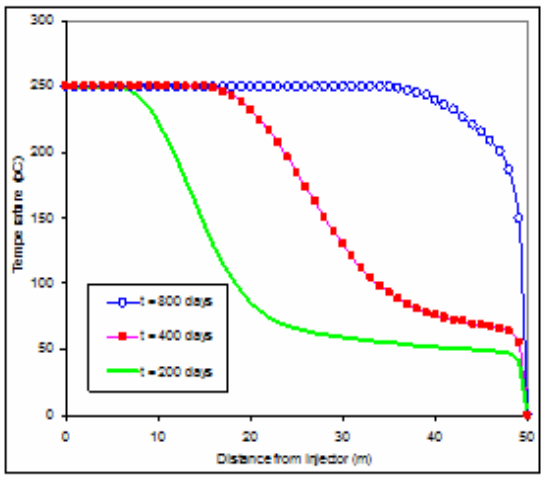


Fig. 3.14: FCC- Effect of Heating Time

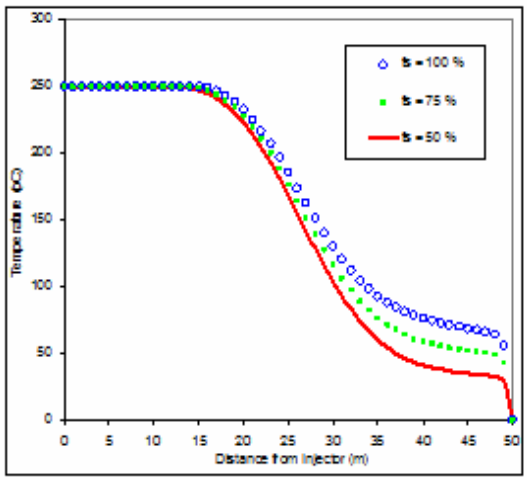


Fig. 3.15: FCC- Effect of Steam Quality (100 mD)

As our simulations account for temperature-dependence of rock and steam properties, **Fig. 3.16** indicates that heating-rate improves with temperature for the same initial conditions (0 ^{o}C). Contrary to conventional opinion, which advocates low-temperature (pressure) injection, high-temperature actually enhances the heating rate. Although low-temperature minimises the amount of heat injected, high-temperature minimises the *net* amount of heat injected, as more heat is recoverable from the produced fluids (Collins, 2007a) and retained in the formation. As noted by Collins (2007b), the beneficial effects of geomechanics are more pronounced at high temperatures. However, as the critical temperature is approached, the latent heat decreases dramatically, making high-temperature steaming less optimal. Hence, for every scenario, there exists some optimum operating temperature, which must be investigated.

As shown in **Fig. 3.17**, regardless of the heating process, conduction is dominant in tight formations. Despite the release of latent heat by condensed steam, poor mobility (permeability) hinders heat flow into the formation. This affirms the general theory that conduction controls fracture-matrix heat exchange (Sumnu *et al.*, 1996; Pooladi-Darvish, 1994; Closmann, 1984; Bodvarsson and Tsang, 1982).

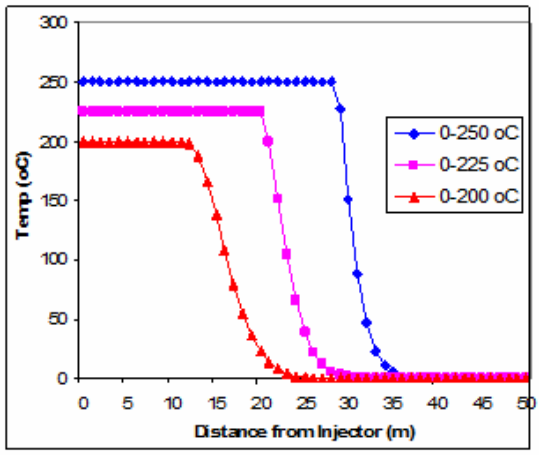


Fig. 3.16: MCC- Effect of Injection Temperature (150 days)

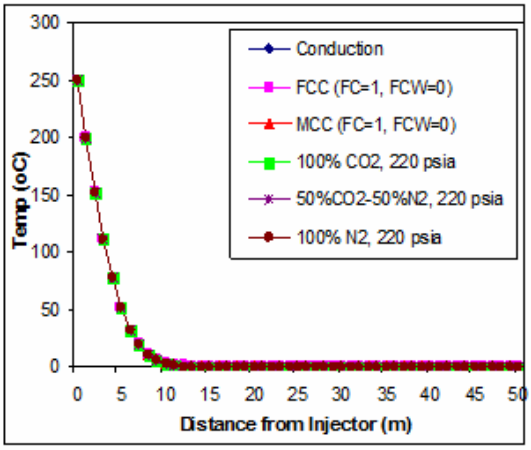


Fig. 3.17: Heating a Tight (0.1 mD) Formation

Following 400 days of injection, **Fig. 3.18** depicts the temperature profiles for various heating processes, in which all the non-steam processes have the heating fluids injected at the saturation pressure (4 MPa) of 250 ^{o}C steam. From the results, it is clear that steam, whether condensing or not, is a better heat carrier than CO_2 and N_2 as well as their mixture. In essence, these results illustrate the potential negative impacts that the presence of either CO_2 or N_2 would have on reservoir-heating by steam. Hence, from a reservoir-heating viewpoint, we may infer that the SAC and SAF processes are not likely to achieve the same performance as a steam-alone process, but SAC offers a better alternative than the SAF.

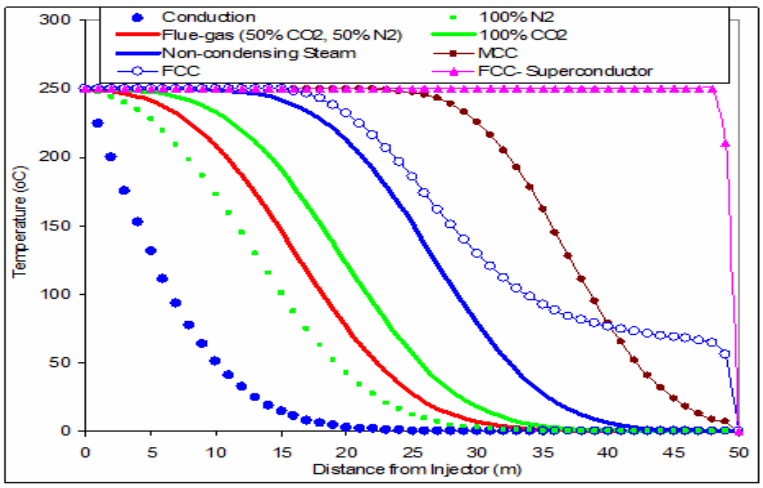


Fig. 3.18: Comparison of Heating Processes (100 mD, 400 days)

On a mass-basis, saturated steam has greater (factor of 2) specific heat than N_2 and CO_2. However, as depicted in **Fig. 3.19**, on volumetric-basis, CO_2 has the highest capacity to transport sensible heat. Importantly, this relative superiority increases with temperature. On the other hand, for the same effective permeability, CO_2 and N_2 are less mobile (viscosity effect) than saturated steam (**Fig. 3.20**). With a combination of higher heat-capacity and mobility, steam and CO_2 are

better heat carriers than N_2. However, at the temperature of study, the mobility effect (steam about 44% more mobile than CO_2) overrides specific-heat effect (c'_p of steam ~26% less than CO_2), hence non-condensing saturated-steam is superior to CO_2 as a heat carrier. With the contribution of latent-heat, it is clear why the condensing-steam cases are much more effective in **Fig. 3.18**.

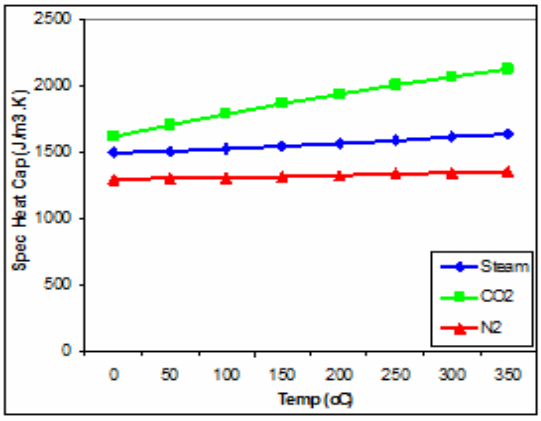


Fig. 3.19: C'_p (Volume-basis, ρc_p) of Steam, CO_2 & N_2

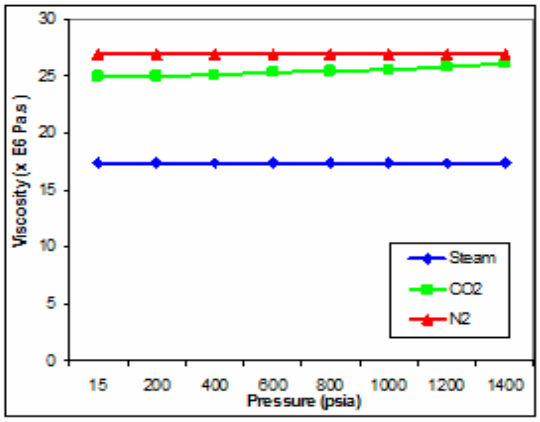


Fig. 3.20: Viscosity of Steam, CO_2 and N_2 (250 °C)

Effects of formation thickness on the heating rate are presented in **Fig. 3.21** where, for the sake of objective comparison, a dimensionless distance has been defined to normalise the reservoir thicknesses. As one would expect, thinner reservoirs take less time to heat. However, for the same operating conditions and permeability, the thermal front tends to be sharper in thicker formations. This can be rationalised by the longer time it takes for the influence of the colder isothermal-boundary to manifest in thicker formations, where the system initially behaves as semi-infinite. In the next chapter, we investigate the effects of reservoir thickness on the rate and magnitude of thermal losses to the surroundings, and how these losses influence overall reservoir heating.

In the discussions that follow, except where stated otherwise, we use dimensionless temperature and distance:

$$T_D = \frac{T - T_i}{T_s - T_i}, \tag{3.50}$$

where T, T_s and T_i are the real, injection and initial temperatures, respectively.

$$z_D = z/H\ , \tag{3.51}$$

where H is reservoir thickness measured from the injector to the caprock; and z, referenced to the injector, is the position corresponding to temperature T.

For the same effective permeability of 100 mD, **Fig. 3.22** illustrates how the heating rate responds to the withdrawal of condensate and heated (mobilised) oil in an MCC process. As expected, heating is most effective when hot fluids are retained, though this is not attractive from the viewpoint of oil revenue. Conversely, the instantaneous drainage of all mobile hot fluids causes the slowest heating-rate. These results provide additional justification for implementing steam-trap

control, as this, in effect, delays the production of heat-carrying oil and condensate while mitigating the escape of live steam (Ito and Susuki, 1999; Edmunds, 1998). By steam-trap, we refer to the difference between the steam saturation temperature and the temperature of the produced hot oil / condensate (CMG, 2010a). In general, the production of live steam reduces with the allowable steam-trap. Additionally, **Fig. 3.22** indicates that it is more beneficial to drain hot oil rather than condensate. This is due to condensate (in this case, water) having a higher heat-capacity than oil.

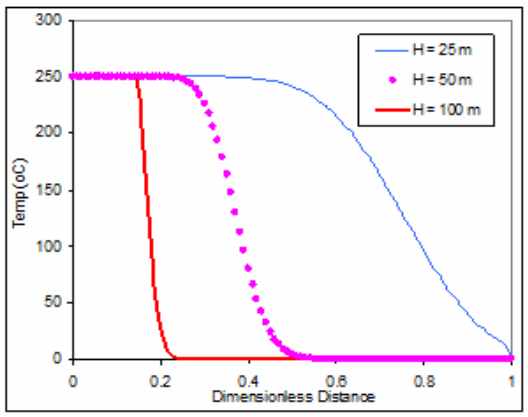


Fig. 3.21: MCC- Effect of Reservoir Thickness (200 mD)

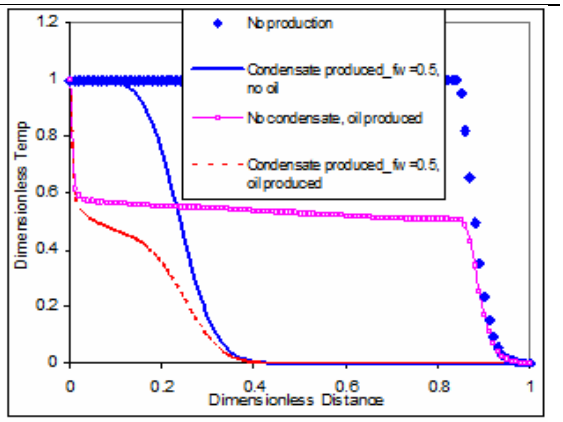


Fig. 3.22: MCC- Effects of Oil & Condensate Drainage

3.5 Reservoir Zoning by Heat-Transfer Mechanisms

In this section, we revisit the common assumption that conduction is the primary heat-transfer mechanism at the leading edge of an advancing thermal front. As discussed in Chapter 2, this assumption and the argument of a quasi-stationary system are the basis of SAGD theories (Alali *et al.*, 2009; Birrell, 2001; Reis, 1992; Butler, 1985). By drawing an "analogy" with the well-established problem of heat conduction in a moving solid (Ozisik, 1993; Carslaw and Jaeger, 1959), theorists have modelled heat transfer in reservoir steam-injection processes as a moving boundary problem, with the following PDE (Alali *et al.*, 2009; Birrell, 2001; Reis, 1992; Closmann and Smith, 1983)

$$\alpha \frac{\partial^2 T}{\partial z^2} - v_s \frac{\partial T}{\partial z} = \frac{\partial T}{\partial t}, \tag{3.52}$$

which for a semi-infinite system, has the exact solution (Carslaw and Jaeger, 1959)

$$\frac{T - T_r}{T_s - T_r} = \frac{1}{2}\left\{ erfc\left(\frac{z - v_s t}{2\sqrt{\alpha t}}\right) + \exp\left(\frac{v_s z}{\alpha}\right) erfc\left(\frac{z + v_s t}{2\sqrt{\alpha t}}\right)\right\}. \tag{3.53}$$

where v_s is the linear velocity of the steam front.

Owing to the quasi-stationary argument, the exact solution (**Eq. 3.53**) is approximated as (Sharma and Gates, 2010; Akin, 2005; Reis, 1992; Butler, 1985)

$$\frac{T - T_r}{T_s - T_r} = \exp\left(-\frac{a_x v_s \xi}{\alpha}\right), \tag{3.54}$$

where a_x is a scalar multiplier, which varies from one author to the other (Reis, 1992; Butler, 1985); ξ is distance measured ahead of the front into the colder zone.

We set up a hypothetical problem in which reservoir-heating is accomplished by each of MCC, conduction and convection (non-condensing) processes. After a sufficiently long period of heating, the prevailing temperature profiles are analysed and the reservoir delineated into zones according to differences in temperature signatures. With this information, the thermal front is mapped, and the dominant heat-transport mechanisms at its leading edge, analysed. **Figs. 3.23** and **3.24** are the instantaneous results (i.e. at a given time).

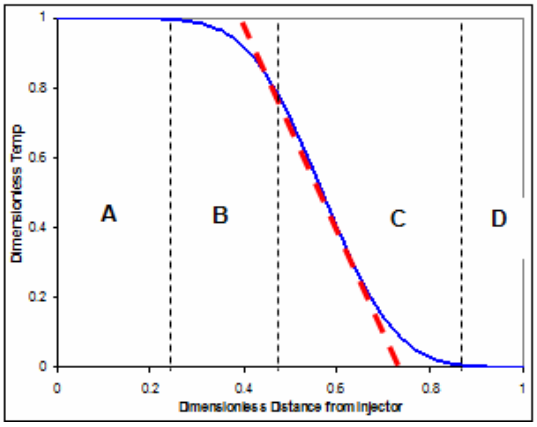


Fig. 3.23: Temperature Profile under MCC Heating

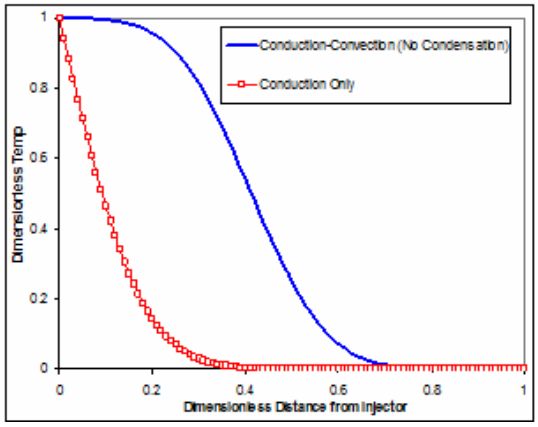


Fig. 3.24: Temperature Profiles under Conductive-Convective and Pure Conductive Heating

As shown in **Fig. 3.23**, a maximum of four zones can be identified at any instant. Although, as further depicted in **Fig. 3.24**, the relative thickness of the zones depends on the stage and prevailing process (conduction or convection), some or all of the following zones can be observed:

- A: condensation zone / region already covered by the front.
- B: convection zone.
- C: conduction zone.
- D: unperturbed zone.

In **Fig. 3.23**, zone *A* is that interval within which the temperature corresponds to that at the injection plane. In essence, either this is where condensation occurs or, in the absence of condensation, this is the area covered by the travelling heating-fluid. Zone *C* is that region characterised by a concave downward (exponential decay) temperature profile, which is characteristic of the conduction equation (Ozisik, 1993; Bird *et al.*, 1960). Zone *B*, described by a concave upward temperature profile, is dominated by convective heat-transfer. Alternatively, zone *B* is defined by the point of deviation from the injection temperature and a tangent to the conduction response. Finally, there is a zone *D* that is yet to be penetrated by the diffusing heat.

Fig. 3.24 indicates that only two zones (*C* and D) exist in the conduction process while the conduction-convection process exhibits the four zones, although its zone *A* is shorter than that of

the MCC process (**Fig. 3.23**) at the same instant, which is simply due to the absence of condensation-heating, hence slower heating-rate, in the former.

Based on this classification, we may argue that the so-called phenomena of fingering (Gotawala and Gates, 2008; Butler, 1987) and micro-channelling (Sasaki *et al.*, 2002, 2001) are probably physical manifestations of the convection zone depicted here as zone *B*. And as presented in **Fig. 3.24** for the conductive-convective process, it can be deduced that this fingering and micro-channelling phenomena, in principle, are not restricted to condensable heat carriers, e.g. steam, because the temperature profile is characteristic of convective processes involving a moving fluid, even if it does not condense. By this analysis, it follows that reservoir-dynamic models that rely on the concept of two isothermal zones (Simangunsong *et al*., 2006; Godze *et al.*, 1989; Gontijo and Aziz, 1984; Jones, 1977; Seba and Perry, 1969; Davidson *et al*, 1967; Boberg and Lantz, 1966; Marx and Langenheim, 1959) do not account for zones *B* and *C*, rendering the models less adequate when these zones are not negligible. From our analysis, as long as the heating medium is mobile (convection) and there is no flow barrier, the convective region would always exist. Given this limitation, it follows that steamflood oil-recovery models (Prats, 1982; Williams *et al.*, 1980; Myhill and Stegemeyer, 1978) that are premised on the frontal oil-displacement theory of Marx and Langenheim (1959) and its variants (Ramey, 1964), need to be employed with caution.

3.6 Further Critiques of Current Reservoir-Heating Models

In addition to the reviews presented in Chapter 2, we consider six other limitations of the analytic models commonly used to describe heat-transport in petroleum reservoirs.

1. ***Heat Flux due to Other Fluids.*** A cursory look at **Eq. 3.52** and our MCC model (**Eq. 3.13**) would suggest that the two models are the same. However, this is misleading. Unlike the MCC model, **Eq. 3.52** does not account for the other components of the convective flow vis-à-vis heat removal by oil and condensate, and most importantly, heat addition that would accompany the condensation process.

2. ***On the Heat-Source Term.*** Supposedly, **Eq. 3.52** takes after the problem of moving solid (heat source), formulated as (Carslaw and Jaeger, 1959):

$$\alpha \frac{\partial^2 T}{\partial z^2} - v_s \frac{\partial T}{\partial z} = \frac{\partial T}{\partial t} - \frac{g_p}{\rho c_p}, \tag{3.55}$$

where g_p is a heat-source term, referring to the heat-generation rate in the moving solid per unit volume.

In the supposed analogy, steam is analogous to the moving solid. While typical moving-solid applications, such as welding and grinding, involve the in-situ generation of heat (e.g. friction) in the solid (Ozisik, 1993), in the case of condensable fluids, the in-situ heat source is that due to phase change.

Comparing **Eqs. 3.52** and **3.55**, it is evident that the latter does not describe heat generation in the body (steam) moving with velocity v_s, hence it is not adequate for describing the intended system. As a result, in the context of our discussion, perhaps a more appropriate descriptor for the current heat-transfer models based on **Eq. 3.52** is a *moving isothermal plane* (advancing at velocity v_s), rather than the intended moving heat-source process. In other words, the current models implicitly treat the advancing steam as a moving-boundary which does not undergo phase change, relying on just advective heat-transport. Hence, in a strict sense, **Eq. 3.52** should not be applied to reservoir-heating that uses condensable heat-carriers such as steam. In general, any analysis based on **Eq. 3.52** may be inherently pessimistic because it ignores an important contributor to heat propagation. By missing the source term, **Eq. 3.52** is incapable of giving correct estimates of the location of the thermal front, hence the use of unrealistic effective permeability and thermal diffusivity to explain field results (Birrell, 2001; Butler, 1987).

3. ***Is Conduction the Dominant Mode of Heat Transfer Ahead of Front?*** Current models assume the dominance of conduction ahead of the front (Sharma and Gates, 2010; Akin, 2005; Reis, 1992; Butler, 1985). From the analysis presented on **Figs. 3.23** and **3.24**, the immediate region ahead of the front is convective, and its thickness may not be negligible. Hence, assuming conduction ahead of the front would underestimate the temperature profile and, consequently, oil production. Indeed, the drive to correct the typical poor prediction of heat transport and oil recovery by the analytic models (Sharma and Gates, 2010; Akin, 2005; Birrell, 2001; Closmann and Smith, 1983) was one of the motivations for developing the so-called fingering theory (Gotawala and Gates, 2008; Butler, 1987), the use of different scalar multipliers (**Eq. 3.54**) and other modifications (Akin, 2005; Reis, 1992; Butler, 1987). However, as we shall show shortly, although the assumption of conduction ahead of the front may be valid under some conditions, that of steady-state is less satisfactory.

4. ***Validity of Quasi-Stationary Assumption ahead of Front.*** Besides assuming the dominance of conduction ahead of the front, current theories treat conduction as being at steady-state, hence the use of **Eq. 3.54** for the temperature distribution. We now investigate the adequacy of this assumption.

We set up the simple case of heating a 500 mD formation by a non-condensing fluid such as CO_2. Hence, the primary heating mechanisms are conduction and convection, with no fluid produced. After 10 and 20 heating-days, we track the temperature profiles ahead of the thermal front (beyond zone *A*).

As shown in **Fig. 3.25**, we have a set of five solutions. Two of these are based on the exact conduction-convection equation (**Eq. 3.53** and our numerical scheme for the MCC). The other two are obtained from the exact (unsteady-state) conduction equation ($v_s = 0$ in **Eq. 3.53**). The last profile uses **Eq. 3.54** but $a_x = 1$ (Butler, 1985). The dimensionless distance is defined relative to the thermal front, according to **Eq. 3.51**.

In this example, the results suggest that the steady-state profile is a poor approximation of the conduction equation. On the other hand, despite the absence of condensation, conduction is not a good representation of the actual conduction-convection process that governs the region of interest.

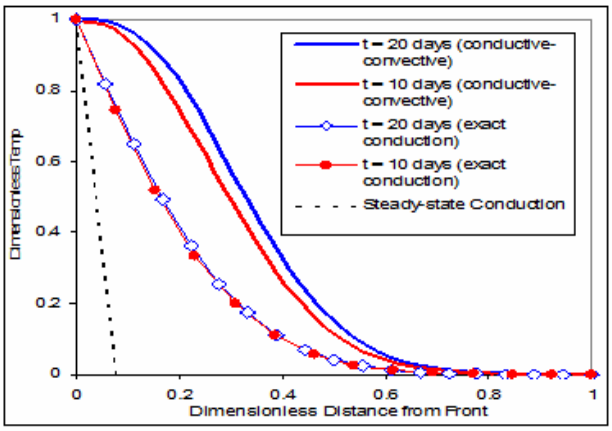


Fig. 3.25: Temperature Profiles ahead of a Non-condensing Thermal Front

5. ***When is it valid to assume steady-state conduction ahead of advancing thermal front?***

At the other extreme of complexity, we consider an example involving a condensable fluid (MCC). Here, according to the exponential arguments of **Eq. 3.54**, we analyse permeability effect on the temperature distribution ahead of the front. We consider steam permeabilities of 50, 5 and 0.5 mD which, for the parameters listed in **Table 3.1** and **Eq. 3.7**, correspond to rising front velocities of $2.7x10^{-5}$, $2.7x10^{-6}$ and $2.7x10^{-7}$ m/s, respectively. For each case of permeability (velocity), we solve the MCC model (**Eq. 3.13**) to obtain the front-leading profile. We also use **Eq. 3.54** to estimate the steady-state temperature profile.

Fig. 3.26 shows the results of heating a 20-m reservoir for 100 days. Obviously, the steady-state assumption is only reasonable for the 0.5 mD case, degrading significantly as the velocity (permeability) increases. As a result, we generalise that the steady-state assumption may only be valid at very low front velocity (low permeability), which promotes conduction.

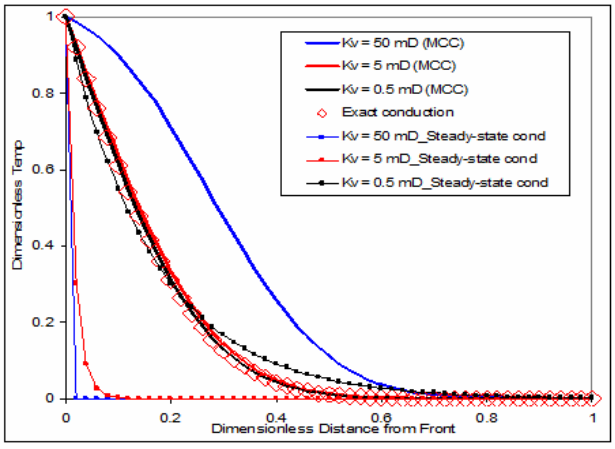


Fig. 3.26: Effect of Permeability on Temperature Profile ahead of a Condensing Thermal Front

6. ***Superposition Effect.*** Consider a plane *z* somewhere ahead of the front. Before the front (condensation plane) reaches *z* at time *t*, this plane would have been sensing the effect of the propagating heat (not necessarily the isothermal front) due to conduction and convection. In contrast to this physical realism, the current quasi-steady approximation (**Eq. 3.54**) appears to indicate that the heating of plane *z* only commences just when the isothermal front is within the vicinity of *z*, ignoring the heat that would have been accumulating at this plane prior to this time (< *t*). This phenomenon of heat accumulation (preheating), which is time dependent, is what we refer to as the superposition effect.

We study the superposition effect in low and high-permeability formations characterised by conductive and convective-heat transport, respectively. Here, we track the instantaneous temperature profile ahead of the travelling front (at 250 ^{o}C) after 5, 1000 and 5000 days of commencing injection in the case of the tight system and 0.1, 20 and 100 days, for the permeable formation. In principle, if there was no superposition, the temperature profile ahead of the moving front should be time-invariant.

Fig. 3.27 shows the temperature distribution at the leading edge of the front at various times, including that based on quasi-steady assumption. First, despite the dominance of conduction in this example, it is evident that the leading profile is not constant, and the quantity of accumulated heat (related to the integral of the profiles) ahead of the front increases over time. Clearly, being a time-independent model, **Eq. 3.54** cannot explain these two observations.

Results for the convection-dominated example are shown in **Fig. 3.28**. Compared to the tight-reservoir case, despite the much smaller time scale, superposition effect is more pronounced in the permeable formation. Within the same time frame, both the temperature profile and accumulated heat ahead of the front change faster in a convection-dominated system than the conductive case.

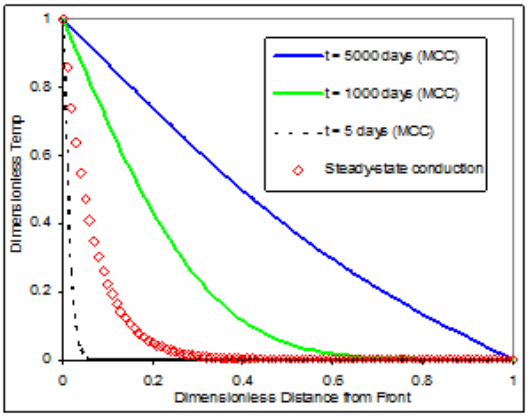


Fig. 3.27: Effect of Time on Temperature Profile Ahead of a Slow Thermal Front (0.5 mD)

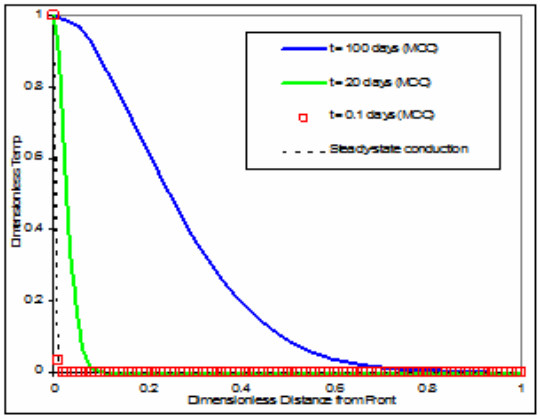


Fig. 3.28: Effect of Time on Temperature Profile Ahead of a Fast Thermal Front (500 mD)

In general, whether the process is dominated by conduction or convection, superposition effect is not negligible, especially at intermediate times and distances. As a complement, other workers

(Yortsos and Gavalas, 1981a) have also questioned the apparent disregard of preheating by step-temperature theories, which underlie some reservoir-heating models (Marx and Langenheim, 1959).

Our analyses agree with the conclusion reached by Yortsos and Gavalas (1981a, b) that the Marx-Langenheim model (hence the step-temperature profile) is only valid at early times in convection-controlled (high-permeability) processes. However, the definition of early times is not that straightforward, due to its dependence on the length scale of the problem (see **Fig. 3.21**), the condensation mechanism (**Figs. 3.6 - 3.8**) – if a condensing fluid is used, prevailing boundary conditions (see the next chapter) and other factors. It is also necessary to point out that, contrary to the argument of Yortsos and Gavalas (1981a, b), the release of latent heat may not be critical for the emergence of a step profile (see **Fig. 3.9**).

3.7 Relaxing Key Assumptions Underlying the Heat-Transport Models

In the mathematical formulation of the heat-transport models, we ignored pressure drop due to the flow of the heat-conveying fluid. Additionally, it was assumed that the heating fluid, heated fluid and matrix are always at the same temperature. However, under some conditions, which include low thermal diffusivity, large matrix size, and small fluid-matrix contact area, the assumption of local thermal equilibrium (LTE) may not be valid (Crone *et al.*, 2002; Prats, 1982; Jenkins and Aronofsky, 1954). The following analyses examine the appropriateness of neglecting pressure-drop and possible lack of LTE.

3.7.1 Influence of Pressure-Drop on Reservoir-Heating

Because the temperature and pressure of a saturated steam are coupled, flow-induced pressure drop would trigger a corresponding saturation-temperature drop (Closmann, 2010). To estimate the cooling effect of pressure drop on flowing steam, we employ:

$$\frac{dT}{dz} = \frac{dT}{dP}\frac{dP}{dz}. \tag{3.56}$$

For a buoyancy-driven flow, the pressure gradient is given by:

$$\frac{dP}{dz} = -(\Delta\rho)g\,. \tag{3.57}$$

With dT/dP estimated from the steam tables (Appendix **C**) and noting that

$$\frac{dL_c}{dz} = \frac{dL_c}{dT}\frac{dT}{dz}, \tag{3.58}$$

we obtain the following as the changes in T and L_c due to flow-induced drop in steam pressure,

$$\frac{dT}{dz} = -948.524\,(\Delta\rho)g\,(T_s - 273.15)^{-3.2553}, \tag{3.59}$$

$$\frac{dL_c}{dz} = \frac{-46.5251x10^5(\Delta\rho)\left(11048.6-176.810T_s+0.487683T_s^{\,2}-4.85508x10^{-4}T_s^{\,3}\right)}{\left(7184500+11048.6T_s-88.4050T_s^{\,2}+0.162561T_s^{\,3}-1.21377x10^{-4}T_s^{\,4}\right)^{1/2}(T_s-273.15)^{3.2553}}. \quad (3.60)$$

In the case of non-condensable heating gases (sub-critical conditions) such as CO_2 and N_2, application of the real-gas equation gives

$$\frac{dT}{dz} = -\frac{(\Delta\rho)gM_g}{\bar{z}_g\bar{\rho}_g R_o}. \quad (3.61)$$

where $\bar{z}_g$ and $\bar{\rho}_g$ are gas compressibility-factor and density, averaged over the range of pressure change. M_g and R_o are molar mass and Universal gas-constant, respectively.

We implement **Eqs. 3.59** and **3.61** in our MCC code to estimate the heating-fluid temperature at its current position, while treating the specific heat c_p as a function of temperature, hence updated with new temperature. With updated c_p, the effect of pressure-drop on sensible heat is thus estimated. But in the case of steam, the latent heat is also updated.

For steam, we implement **Eqs. 3.59** and **3.60** to estimate the effect of pressure-drop on the net quantities of deliverable sensible and latent heats, respectively. We consider saturated steam injected at different temperatures in the range 140-360 ^oC, travelling over 10, 20 and 100 m. The results are shown in **Figs. 3.29** and **3.30**. In an operation characterised by a constant injection rate, although the delivery sensible heat decreases with pressure-drop, the increase in the latent heat compensates for the sensible-heat reduction. As a result of these opposite effects, the net change in the total heat is negligible (maximum is 5.6% within 140-360 ^oC for 100 m distance). Hence, for this buoyancy-driven system, it is not expected that pressure-drop due to steam flow would have significant impact on the reservoir-heating rate.

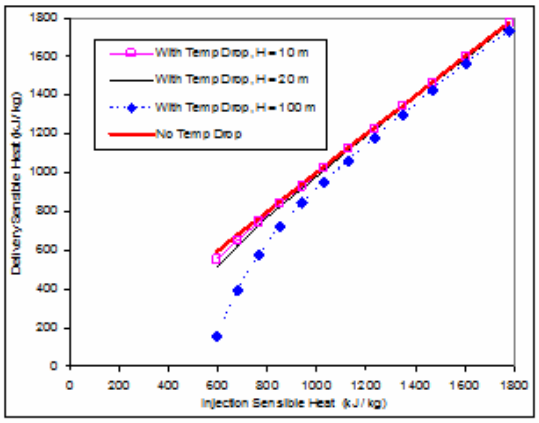


Fig. 3.29: Effect of Pressure-Drop on Delivery of Sensible Heat

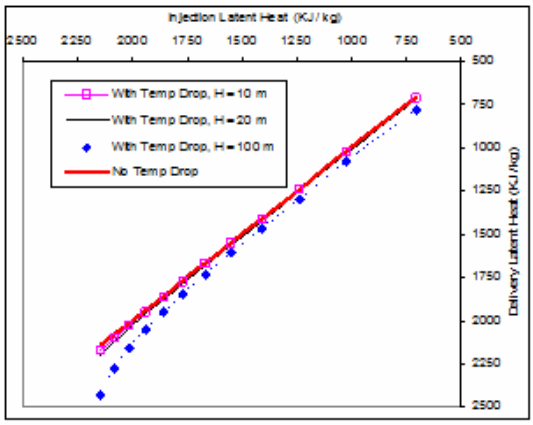


Fig. 3.30: Effect of Pressure-Drop on Delivery of Latent Heat

It is interesting to note that temperature has the opposite effect on the sensible and latent heats of steam, such that at low temperatures when latent heat is maximum, sensible heat is minimum and vice-versa, resulting in a total heat that is fairly temperature-independent (< 5% variation from

50-360 ^{o}C). This explains the negligible effect of pressure-drop on the total heat and, expectedly, reservoir-heating rates should not be much impacted for a constant mass-rate.

Fig. 3.31 shows the results for MCC in two different reservoirs, 50 and 100 m thick, but of equal permeability (100 mD). In these cases, the dynamics is not sensitive to pressure-drop. Nonetheless, the anticipated trend of increasing pressure-drop with formation thickness still manifests, as maximum deviations (MD) of 0.5 and 0.9% are obtained for the 50 m and 100 m systems, respectively.

As an example of a non-condensable heating-fluid, we examine CO_2. Within the range studied, $\overline{Z}_g$ and $\overline{\rho}_g$ of CO_2 are 0.95 and 35 kg/m^3, respectively. Again, injection rate is kept constant. As shown in **Fig. 3.32**, the effect of pressure-drop is more significant. While MD of the 50 m formation is 3.8%, the 100 m system is about 7%, indicating that the effect of pressure-drop is more pronounced in thicker reservoirs. Compared to steam, pressure-drop has a higher impact on the CO_2 process because the latter, being non-condensable, lacks the latent heat that would compensate for the loss of sensible heat. In short, the smaller the contribution of the latent heat and the thicker the formation, the greater is the influence of pressure-drop on the heating rate.

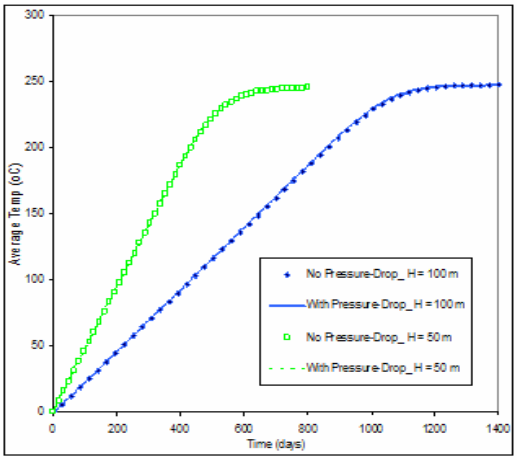


Fig. 3.31: Effect of Pressure-Drop on Heating (MCC)

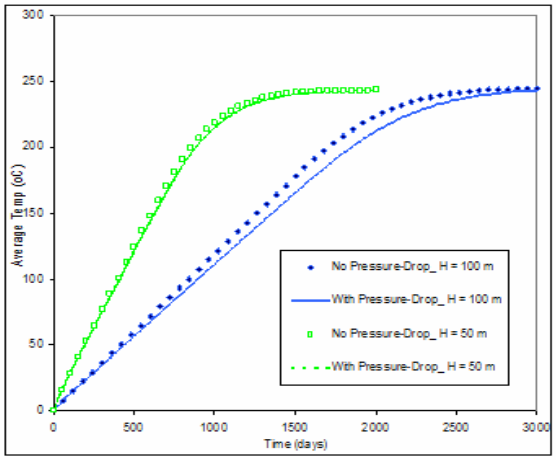


Fig. 3.32: Effect of Pressure-Drop on Heating (CO_2)

For a constant-rate process, this analysis suggests that the effects of pressure-drop would probably be important for non-condensing heat carriers in formations exceeding 100 m in thickness. As most heavy-oil reservoirs do not have a continuous thickness up to 100 m (Dusseault, 2001; Enu, 1985), it can be concluded that "equivalent" pressure-drop in a buoyancy-driven system is not likely to have significant impacts on the heat-transport models developed in this work, and the deductions made from them are valid.

Please note that the foregoing conclusion assumes a constant mass-rate, implying that increased back-pressure is overcome by increased injection pressure. Otherwise, the effect of pressure-drop may be significant. Considering that the general practice is to maintain the injection mass-rate (Closmann, 2010; Bagci *et al.*, 2008; Barillas *et al.*, 2006), we conclude that, whether the

heat-transporting fluid is condensable or not, the effect of pressure-drop on reservoir-heating is not likely to be pronounced, providing the reservoir is not thicker than 100 m and buoyancy is the main flow mechanism.

3.7.2 Time-scale for Reaching Local Thermal Equilibrium

To investigate the appropriateness of ignoring possible time-lag between the temperatures of the three elements (fluids and matrix), we employ a pore-level analysis.

Fig. 3.33 is a differential volume (thickness *dz*) of a saturated pore and matrix. The heating fluid, colder fluid, and matrix are at temperatures T_h, T_c and T_m, respectively. The pore diameter is D_p. We seek to establish the conditions and time-scales for T_c and T_m to attain T_h, in response to the disturbance caused by introducing the heating stream at T_h.

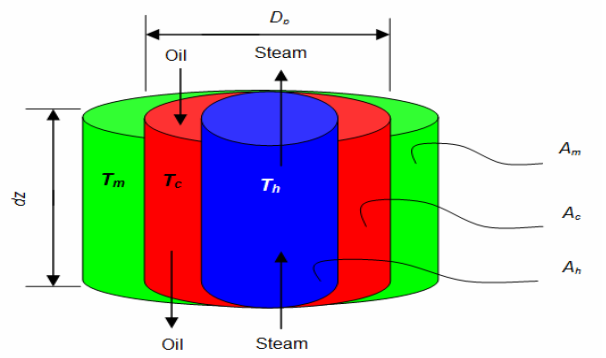


Fig. 3.33: Differential Volume with All Elements Initially at Different Temperatures

In the following analysis, we make further assumptions:

- There is no phase change.
- Oil is wetting phase (adheres to matrix). Thus, heating fluid is always at the core of the pore.
- Heating and heated fluids have the same flow cross-section i.e. pore is evenly shared between them.
- All elements have equal thermal diffusivity and cross-sectional area for heat accumulation ($A_h = A_c = A_m = A$).
- The fluids strictly flow in parallel without mixing. That is, they only exchange heat through their outermost layers (interface) in contact. However, there is negligible radial temperature gradient within each element.

Although our reference heating fluid has been steam, which undergoes phase change, for simplicity in the analysis that follows, we consider a hypothetical non-condensing heating fluid, for example hot water and CO_2. By ignoring the contribution of latent heat to the overall heat transfer, the results obtained from this simplified analysis would give the upper limits of the time-scale for reaching local thermal equilibrium (LTE). Ideally for the same conditions, LTE would be reached earlier in the case of steam.

Subject to the stated assumptions, we derive the following 1-D heat balances for the heating fluid, colder fluid and matrix, respectively.

$$\alpha\frac{\partial^2 T_h}{\partial z^2}-\Psi_s\frac{\partial\left(v_s T_h\right)}{\partial z}-\frac{hP_{hc}}{\rho A c_p}\left(T_h-T_c\right)=\frac{\partial T_h}{\partial t}, \tag{3.62}$$

$$-\alpha\frac{\partial^2 T_c}{\partial z^2}+\Psi_o\frac{\partial\left(v_o T_c\right)}{\partial z}+\frac{hP_{hc}}{\rho A c_p}\left(T_h-T_c\right)-\frac{hP_{cm}}{\rho A c_p}\left(T_c-T_m\right)=\frac{\partial T_c}{\partial t}, \tag{3.63}$$

$$-\alpha\frac{\partial^2 T_m}{\partial z^2}+\frac{hP_{cm}}{\rho A c_p}\left(T_c-T_m\right)=\frac{\partial T_m}{\partial t}, \tag{3.64}$$

where *P* is perimeter of heat-transfer surface; *h* is local convective heat-transfer coefficient. Subscripts "hc" and "cm" refer to heating-colder fluid interface and colder fluid-matrix interface, respectively. P/A is effective surface area per unit volume (Sissom and Pitts, 1972), and hP/A is the *volumetric* convective heat-transfer coefficient (Rice and Do, 1995).

For a cylindrical pore-throat, the following are applicable:

$$P_{hc}=\pi D_p/2, \tag{3.65}$$

$$P_{cm}=\pi D_p, \tag{3.66}$$

$$A=\pi {D_p}^2/16, \tag{3.67}$$

where D_p is estimated from permeability and porosity ϕ (Stolz and Graves, 2003):

$$D_p=2\sqrt{k/\phi}. \tag{3.68}$$

In order to derive analytic solution for **Eqs. 3.62**-**3.64**, we make additional simplification. We neglect the thermal resistance between the colder fluid and matrix i.e. $T_c\approx T_m$. Hence, the system reduces to

$$\alpha\frac{\partial^2 T_h}{\partial z^2}-\Psi_s\frac{\partial\left(v_s T_h\right)}{\partial z}-\frac{hP_{hc}}{\rho A c_p}\left(T_h-T_c\right)=\frac{\partial T_h}{\partial t}, \tag{3.69}$$

$$-2\alpha\frac{\partial^2 T_c}{\partial z^2}+\Psi_o\frac{\partial\left(v_o T_c\right)}{\partial z}+\frac{hP_{hc}}{\rho A c_p}\left(T_h-T_c\right)=2\frac{\partial T_c}{\partial t}. \tag{3.70}$$

Solving **Eqs. 3.69** and **3.70** by Laplace transform while assuming constant physical properties and ignoring thermal conduction $\alpha\to 0$, we obtain the following Laplace-domain solutions

$$\overline{T}_h(z,s)\approx\frac{\left(T_s\,e^{m_2H}-T_o\right)e^{m_1z}-\left(T_s e^{m_1H}-T_o\right)e^{m_2z}}{\left(e^{m_2H}-e^{m_1H}\right)s}, \tag{3.71}$$

$$\overline{T}_c(z,s) \approx \frac{\left(T_s e^{m_2 H} - T_o\right)\left(\omega_2 m_1 + \omega_3 + s\right)e^{m_1 z} - \left(T_s e^{m_1 H} - T_o\right)\left(\omega_2 m_2 + \omega_3 + s\right)e^{m_2 z}}{\omega_3\left(e^{m_2 H} - e^{m_1 H}\right)s}, \quad (3.72)$$

for a system of thickness H and isothermal boundaries, T_s and T_o. The parameters are

$$\omega_2 = \Psi_s v_s \; ; \; \omega_3 = hP_{hc} / \rho A c_p \; ; \; \chi_2 = \Psi_o v_o \, , \quad (3.73a)$$

$$m_1, m_2 = \frac{\left(\omega_2\omega_3 - \omega_3\chi_2 + 2\omega_2 s - \chi_2 s\right) \pm D_c}{2\omega_2\chi_2}, \quad (3.73b)$$

$$D_c = \sqrt{\left(\chi_2 + 2\omega_2\right)^2 s^2 + 2\left(\chi_2 + 2\omega_2\right)\left(\omega_2\omega_3 + \omega_3\chi_2\right)s + \left(\omega_2\omega_3 - \omega_3\chi_2\right)^2} \, . \quad (3.73c)$$

As these Laplace forms are not amenable to analytic inversion, we employ the method of Schapery (1962) to gain first-order insights into the responses (Hassanzadeh and Pooladi-Darvish, 2007). The estimates of the instantaneous deviations in T_h and T_c from their initial conditions at time t and position z are

$$\Delta T_h(z,t) \approx \left\{ s\overline{T}_h(z,s) \right\}_{s = 1/1.781\,t}, \quad (3.74)$$

$$\Delta T_c(z,t) \approx \left\{ s\overline{T}_c(z,s) \right\}_{s = 1/1.781\,t}. \quad (3.75)$$

To assess robustness of the LTE assumption, we consider a pore-level simulation using **Eqs. 3.74** and **3.75**. Key pore parameters are 0.01 m, 1000 mD, 0.2 and 2 W m^2 K^{-1} for H, k, ϕ and h, respectively. As will be shown in Chapter 4, the assumed heat-transfer coefficient is on the low side, which should favour the lack of LTE. Non-condensing steam, at 250 ^oC, is injected into the pore containing 1000 cP oil. The heat-transfer perimeter is estimated with **Eq. 3.65**, which assumes the steam occupies 50% of pore diameter; hence heat-transfer perimeter is 50% of pore circumference.

Fig. 3.34 shows the temperature profiles of the heated and heating fluids at different times. From the results, thermal equilibrium is reached as early as 1 min after injection of steam. Although not shown here, we found that transfer lag is limited to the first 30 sec of injection for the system considered. As field-scale simulations typically have time-steps on the order of hours and days, we conclude that thermal equilibrium would essentially be instantaneous for realistic problems.

The influence of heat-transfer coefficient is illustrated in **Fig. 3.35**. Within the time-scale of 0.01 days (~ 14 min), the heating and heated systems attain thermal equilibrium as long as h > 0.05 W/m^2K. But typical liquid systems are characterised by h > 50 W/m^2K (see Chapter 4), implying that in realistic pores, thermal equilibrium would most likely be instantaneous. In fact, with h = 50 W/m^2K, it is estimated that equilibrium would be reached within 1 sec of the steam coming into contact with the oil-matrix system.

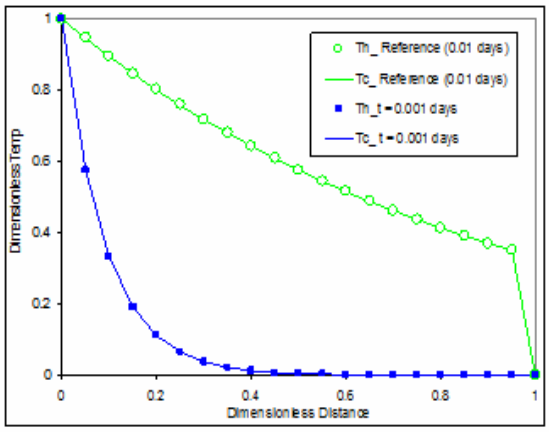


Fig. 3.34: Effect of Time on LTE

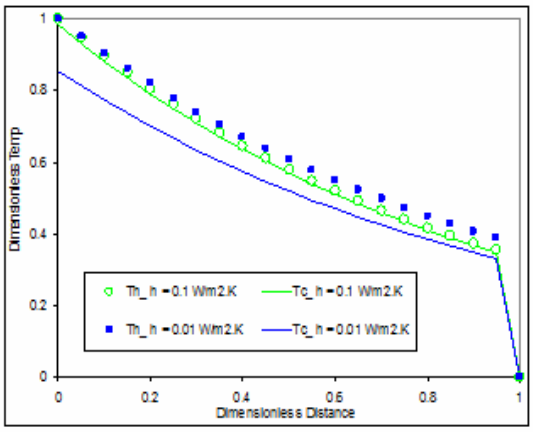


Fig. 3.35: Effect of Convective-Coefficient on LTE

Finally, impacts of heat-transfer surface are shown in **Fig. 3.36**. While the base case treats heat-transfer perimeter as 50% of the pore-perimeter, we also evaluate 0.5 and 0.05%. In this example, lack of LTE may only be an issue if the injected fluid occupies less than 0.08% of the pore diameter. Except in the case of significant steam bypass, possibly due to flow barrier/baffles, thermal equilibrium remains satisfactory for the analysis of petroleum reservoirs, particularly at typical time scales.

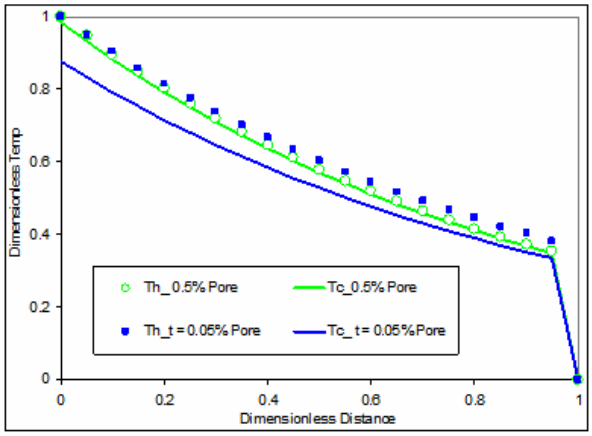


Fig. 3.36: Effect of Heat-transfer Perimeter on LTE

3.8 Chapter Summary

As improvements over the current treatments of heat-transport in petroleum reservoirs, the concepts of MCC and FCC are introduced to account for the contributions of condensation to the overall heat transfer. For a buoyancy-driven system and realistic fluid properties, mathematical models of these concepts have been formulated. Limited to isothermal boundary conditions, numerical schemes have been developed to solve the resulting 1-D nonlinear differential equations. Rigorous studies on the convergence (stability and consistency) of the proposed numerical schemes have led to the development of useful criteria for selecting the size of simulation grids.

Considering typical characteristics of heavy-oil pools, several simulations were conducted to gain insights into the relative influences of a number of operating and petrophysical parameters. Among other findings, these numerical experiments indicate that the proposed convergence criteria are sufficiently robust. Most importantly, apart from being validated with published experiments, the simulations show that including condensation (MCC and FCC) mechanisms into current conductive-convective models of SAGD and other steaming processes would eliminate the need to apply unrealistic permeabilities and thermal diffusivities in order to fit experimental dataset.

Finally, some of the main assumptions underlying the mathematical models are relaxed. In spite of the relaxation, neither the performances nor the inferences of the models are compromised. The analysis clearly shows that within the realistic range of reservoir and process parameters, the proposed models are sufficiently robust for practical applications.

Chapter 4

Heat-Transport for Systems with Non-Isothermal Boundaries

In the previous chapter, the overlying and underlying formations were assumed to be isothermal, hence potential heat exchange at the boundaries was neglected. But in practice, boundary temperatures do vary (Vinsome and Westerveld, 1980), which limits the applications of the models in Chapter 3. In the current chapter, we address boundary thermal losses and relevant issues relating to cap and base rocks.

4.1 A Review of Current Methods of Modelling Boundary-Thermal Losses

Numerically, the detailed approach for treating this problem is to invoke the finite-difference technique, though the finite-element equivalence is also available (Lewis *et al*., 1985). In its most rigorous applications, the overburden and underburden are explicitly described by grid blocks (discretised), which may extend to the surface and far below the base rock. In most thermal simulators, about 40-55 % of grid blocks in the vertical direction would be inactive for fluid flow, as they are specifically reserved to model heat losses (Schlumberger, 2009), thus the finite-difference form of the energy balance is solved in these domains. The main drive is “accurate” description of dynamics of the semi-infinite boundaries that enclose the reservoir system. At “infinite” ends of the boundaries, the reservoir is in thermodynamic equilibrium with the “ultimate” sinks. While this approach is computationally intensive, the high accuracy that would result may not always have much impact on project decisions (Vinsome and Westerveld, 1980).

In order to achieve computational efficiency, some approximate methods have been published. Most of these methods are hinged on the same principle, in which the boundary is modelled as a semi-infinite heat conductor that can be described by the transient 1-D conduction equation (Carslaw and Jaeger, 1959). Some “fitting” functions are used to approximate the temperature profile into the cap or base rock, hence the so-called semi-analytic approach. These functions, generally arbitrary, are required to satisfy the conduction equation through the boundaries and the semi-infinite conditions. By semi-infinite, the boundary inlet temperature equals that at interface with the reservoir, but there is negligible temperature change at its “infinite” end. The fitting parameters, influenced by reservoir-boundary interface temperature and boundary thermal conductivity, are updated every time step (Vinsome and Westerveld, 1980; Weinstein, 1972).

As might be expected, the fitting functions are of varied form and complexity. Vinsome and Westerveld (1980) proposed a relatively simple exponential decaying function to fit the temperature profile. But Chase and O’Dell (1973) applied the more rigorous principles of variational calculus, assuming a cubic polynomial. In his papers, Weinstein (1972, 1974) also implemented variational

techniques but the fitting functions, which include repeated integral of the complementary error function, are much more complex, leading to relatively cumbersome solution procedure.

For finite-element techniques, the use of infinite element to map a semi-infinite domain onto the finite element region has been proposed (Lewis *et al*., 1985; Zienkiewicz and Morgan, 1983). But results are sensitive to the mapping functions, and the procedure for calculating the mapping parameters is inconclusive. A semi-analytic approach is one of the options being evaluated to mitigate these concerns (Lewis *et al*., 1985).

Despite their widespread application, these semi-analytic methods have four major drawbacks. First, they are independent of boundary geometry (thickness). Second, solutions are very sensitive to the fitting function (and number of parameters) used. Third, there is no precise way to assess, *a priori*, appropriateness or otherwise of adiabatic assumption. Finally, they do not account, explicitly, for the effects of the type of fluids that saturate adjacent geologic formations.

The simulation of laboratory-scale models poses a unique challenge to both the full discretisation and semi-analytic approximation methods. As laboratory physical models are often characterised by relatively thin boundary walls, usually in centimetres, they prove difficult for the conventional techniques of modelling thermal losses through boundaries. For this class of systems, the concept of “infinitely” long boundary characterised by smooth temperature profile, which decays towards its end is questionable. The modest wall thickness makes the wall-ambient interface a point of sharp temperature discontinuity. In applying the full-discretisation method, how does one discretise the surroundings which, technically, consist of convecting air layers and not rigid, stationary solid layers?

Given the foregoing limitations of existing methods of modelling boundary losses, the current study seeks to achieve the following objectives:

- develop a computationally efficient method for modelling thermal losses to the cap and base rocks;
- assess the impact of heat losses on the rate of reservoir-heating;
- establish criterion for assessing, *a priori*, validity of the adiabatic assumption; and
- understand the influence of fluids, present in the vicinity of boundaries and within adjacent formations, on the rate of heat efflux.

In this work, we propose an approach that is fundamentally different from previous methods. The principle of heat exchanger is used to model the boundary-sink system. Here, the boundary is a conductive “wall” through which two fluid-saturated systems (reservoir and adjacent formations), which are at different temperatures, exchange heat but not mass. As we are not interested in the temperature distribution along the wall, but the wall’s thermal resistance, this completely eliminates the need for the debatable temperature-profile fitting functions. As the main objective is to estimate heat losses and their impacts on reservoir-heating, accurate description of the boundary dynamics may not be of much benefit. Thus, for the intended purpose, the proposed method is pragmatic. Additionally, rather than solve for the heat losses through some iterative procedure, our proposed

method solves it simultaneously with the other parts of the solution domain. This would further alleviate storage and computing costs.

4.2 Formulation of Boundary Thermal-Loss Model

Conceptually, the system of reservoir and adjacent formations can be viewed as a heat exchanger. Typical heat exchangers consist of two moving fluid streams of different temperatures, separated by a conducting wall, that exchange heat yet do not mix. That is, while the streams exchange heat through the wall, owing to the non-permeability of the wall, there is no mass transfer between them. In our case, the reservoir, boundary and adjacent formations are analogous to the hotter fluid, wall and colder fluid, respectively.

We use the domain in **Fig. 3.1** but how include the terms Q_{cap} and Q_{base}, denoting net heat exchange with the cap and base rocks, respectively. The following assumptions underlie the subsequent 1-D analysis:

- Both cap and base rocks are in contact with sinks of infinite volumes, whose temperatures remain constant at their initial reservoir conditions.
- The sinks consist of adjacent geologic systems saturated by either gas or liquid.
- Cap and base rocks are of uniform thickness throughout their contacts with the reservoir.
- Cap rock, base-rock and reservoir have same cross-sectional area for heat flow.
- Thermophysical properties of cap/base rocks and adjacent fluids are constant.
- Heat-transfer between injection plane and base-rock is by conduction.
- Thermal resistances in the direction of heat flow (normal to reservoir dip) are in series.

The first assumption implies that the time-scale for heating the reservoir is negligible compared to that of the adjacent sinks. This argument is substantiated in Appendix **D**. In this Chapter, the terms cap and base rocks refer to the distinct layer (shale, siltstone or evaporite) that separates the reservoir from the overburden (overlying formation) and underburden (underlying formation), respectively.

In reality, reservoirs are bounded laterally and vertically by other geologic systems that are also saturated with some fluids, which may or may not be the same as that of the subject reservoir. Even within the reservoir, fluids immediately underneath (say, gas) the caprock and above (say, water) the base rock may differ from that being targeted (heavy oil).

By assuming infinite volumes (relative to subject reservoir) for the adjacent sinks, absorbed heat instantly diffuses throughout the sink, such that there is no significant change in its bulk temperature during the operating lifetime. Although this assumption yields upper bounds for thermal losses, in principle, the over-estimation partly compensates for lateral losses tacitly ignored in this 1-D model.

The field data reported by Closmann and Smith (1983) suggests the dominance of thermal conduction below a horizontal steam-heated fracture in an oil sand. Taking the fracture as

analogous to an injection plane, it is reasonable to apply the conduction equation between the injector and underburden.

At the cap and base rocks, the FCC model (**Eq. 3.21**) becomes (where we have used the notation Δz in place of dz in order to avoid confusion)

$$\alpha\frac{\partial^2 T}{\partial z^2}+F\frac{\partial T}{\partial z}+\Omega_1-\frac{Q_{loss}}{\rho c_p A\Delta z}=\frac{\partial T}{\partial t}, \tag{4.1}$$

where Q_{loss} refers to either the cap or base rock i.e. Q_{cap} and Q_{base}, respectively.

For the other layers, we simply set:

$$Q_{loss}=0. \tag{4.2}$$

The expressions $Q_{cap}/A\Delta z$ and $Q_{base}/A\Delta z$, representing $Q_{loss}/A\Delta z$, are the rates of boundary heat losses per unit volume of the differential element of thickness Δz. For a reservoir of thickness H (above injector), and gross volume AH, the PDE becomes:

$$\alpha\frac{\partial^2 T}{\partial z^2}+F\frac{\partial T}{\partial z}+\Omega_1-\frac{Q_{loss}}{\rho c_p AH}=\frac{\partial T}{\partial t}. \tag{4.3}$$

By treating the reservoir-caprock-top sink and reservoir-base rock-bottom sink as some form of heat exchangers, Q_{cap} and Q_{base} can be estimated from:

$$Q_{cap}=U_c A\left(T_c-T_a\right), \tag{4.4}$$

$$Q_{base}=U_b A\left(T_b-T_a\right), \tag{4.5}$$

where U_c and U_b are overall heat-transfer coefficients of reservoir-caprock-sink and reservoir-baserock-sink systems, respectively. T_a is temperature of surrounding media which, in spite of continuously absorbing heat from the reservoir, are assumed isothermal. T_c and T_b are instantaneous temperatures of cap and base rocks (boundaries), respectively.

From **Eqs. 4.3** - **4.5**, the following describe the FCC at other layers, the cap and base, respectively

$$\alpha\frac{\partial^2 T}{\partial z^2}+F\frac{\partial T}{\partial z}+\Omega_1=\frac{\partial T}{\partial t}, \tag{4.6a}$$

$$\alpha\frac{\partial^2 T}{\partial z^2}+F\frac{\partial T}{\partial z}+\Omega_1-\frac{U_c\left(T_c-T_a\right)}{\rho c_p H}=\frac{\partial T}{\partial t}, \tag{4.6b}$$

$$\alpha\frac{\partial^2 T}{\partial z^2}+F\frac{\partial T}{\partial z}+\Omega_1-\frac{U_b\left(T_b-T_a\right)}{\rho c_p H}=\frac{\partial T}{\partial t}. \tag{4.6c}$$

Using the same procedure, the MCC process is governed by:

$$\alpha\frac{\partial^2 T}{\partial z^2}+F\frac{\partial T}{\partial z}=\frac{\partial T}{\partial t}, \tag{4.7a}$$

$$\alpha\frac{\partial^2 T}{\partial z^2}+F\frac{\partial T}{\partial z}-\frac{U_c\left(T_c-T_a\right)}{\rho c_p H}=\frac{\partial T}{\partial t}, \tag{4.7b}$$

$$\alpha\frac{\partial^2 T}{\partial z^2}+F\frac{\partial T}{\partial z}-\frac{U_b\left(T_b-T_a\right)}{\rho c_p H}=\frac{\partial T}{\partial t}. \tag{4.7c}$$

Note that until $T_c > T_a$ or $T_b > T_a$, the system's behaviour remains adiabatic. And where any of the cap and base layers are thermal insulators, we simply set $U_b = 0$ and $U_c = 0$ as the case may be. Again, the FCC term Ω_1 only applies to the volume behind the front.

4.2.1 Overall Heat-Transfer Coefficients

Fig. 4.1 illustrates the reservoir system, with the adjacent fluids, cap/base-rock geometries and sinks. With the boundary regions treated as heat exchangers, the overall heat-transfer coefficients, assumed constant throughout the operating period, are estimated as follows (Bird *et al.*, 1960).

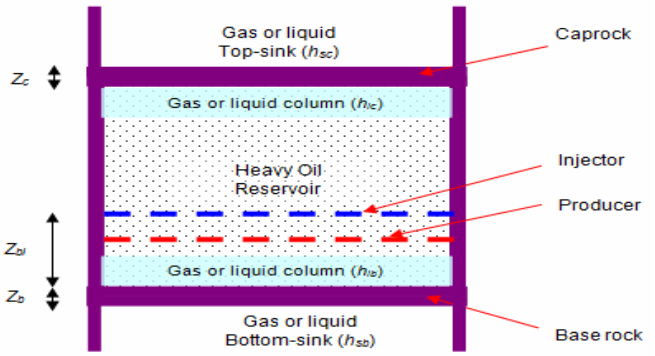


Fig. 4.1: Reservoir and Adjacent Heat Sinks

$$U_c=\left[\frac{1}{h_{ic}}+\frac{Z_c}{\kappa_c}+\frac{1}{h_{sc}}\right]^{-1};\quad U_b=\left[\frac{1}{h_{ib}}+\frac{Z_b}{\kappa_b}+\frac{1}{h_{sb}}\right]^{-1}, \tag{4.8}$$

where h_{ic} and h_{sc} are heat-transfer coefficients of layer just below and above the caprock, respectively; Z_c is caprock thickness in flow direction, and κ_c is caprock thermal conductivity. Similar notations apply to the base-rock vis-à-vis h_{ib} refers to the layer just before base-rock (within reservoir), and h_{sb} applies to the medium below (sink) the base rock. A simple procedure, built on the assumption that a porous medium is equivalent to a bundle-of-tubes, is proposed for estimating the heat-transfer coefficients (Appendix **E**).

4.2.2. Temperatures of Cap and Base Rock

In **Eqs. 4.6** and **4.7**, T_c and T_b are required to estimate rates of heat loss through the cap and base rocks, respectively. While T_b can be estimated explicitly using the isothermal injection plane as

reference, T_c is only obtainable implicitly from the solution of the entire system with the boundary conditions.

Assuming the subsystem between injection plane and base-rock behaves as a semi-infinite thermal medium, T_b can be estimated from (Carslaw and Jaeger, 1959):

$$T_{base} \approx T_i + (T_s - T_i) erfc\left(\frac{Z_{bi}}{2\sqrt{\alpha t}}\right), \tag{4.9}$$

where Z_{bi} is the vertical distance between injector and base-rock (**Fig. 4.1**); t is elapsed time; α is reservoir thermal diffusivity; T_s and T_i are injection and initial temperatures, respectively.

In **Eq. 4.9**, we ignore the influence of fluid (oil, live steam, condensate, water influx or gas) convection to the producer on the conduction profile between injector and base-rock. In practice, beyond the start-up period, instantaneous temperatures at injector and producer are generally comparable. Although technically, the producer is the appropriate heat 'source' to the base-rock, the usually short vertical separation, typically ~ 5 m (Sharma and Gates, 2010), between injector and producer should justify using the injector as heat 'source' for estimating base-rock temperatures. Besides, the fact that the injector is a more obvious isothermal source makes it a more convenient reference, in **Eq. 4.9**, than the producer.

4.2.3 Numerical Schemes

Using the approach adopted for the finite system to discretise **Eqs. 4.6** and **4.7**, we obtain the following implicit numerical schemes for the FCC and MCC processes, respectively.

$$\begin{aligned} &-\left(\frac{\alpha}{2h^2}\right)T_{i-1,j+1}+\left(\frac{\alpha}{h^2}+\frac{F}{2h}+\frac{1}{k}\right)T_{i,j+1}-\left(\frac{\alpha}{2h^2}+\frac{F}{2h}\right)T_{i+1,j+1} \\ &\approx \\ &\left(\frac{\alpha}{2h^2}\right)T_{i-1,j}-\left(\frac{\alpha}{h^2}+\frac{F}{2h}-\frac{1}{k}\right)T_{i,j}+\left(\frac{\alpha}{2h^2}+\frac{F}{2h}\right)T_{i+1,j}+\Omega_1^j-\frac{U\left(T_{boundary}^j-T_a\right)}{\rho c_p H} \end{aligned}, \tag{4.10}$$

$$\begin{aligned} &-\left(\frac{\alpha}{2h^2}\right)T_{i-1,j+1}+\left(\frac{\alpha}{h^2}+\frac{F}{2h}+\frac{1}{k}\right)T_{i,j+1}-\left(\frac{\alpha}{2h^2}+\frac{F}{2h}\right)T_{i+1,j+1} \\ &\approx \\ &\left(\frac{\alpha}{2h^2}\right)T_{i-1,j}-\left(\frac{\alpha}{h^2}+\frac{F}{2h}-\frac{1}{k}\right)T_{i,j}+\left(\frac{\alpha}{2h^2}+\frac{F}{2h}\right)T_{i+1,j}-\frac{U\left(T_{boundary}^j-T_a\right)}{\rho c_p H} \end{aligned}. \tag{4.11}$$

At the intermediate grids, $U=0$. However, at the cap rock, we set $U=U_c$ and $T_{boundary}^j=T_c^j$. Corresponding expressions at the base are $U=U_b$ and $T_{boundary}^j=T_b^j$. The terms Ω_c^j, T_c^j and T_b^j are evaluated at the preceding time-step, j.

4.2.4 Boundary Conditions

Neglecting heat storage in the cap and base rocks (interface layers), the following provides an estimate of time-dependent heat fluxes to and fro the boundaries, where heat flow to the boundary is approximated by 'effective' conduction and bulk flow (forced convection). For simplicity, heat supplied by condensation as well as that removed by produced oil and condensate in the vicinity of the boundaries are ignored. To some extent, these neglected sources should cancel one another.

$$T(z,0) = T_i \qquad t < 0\ , \tag{4.12}$$

$$T(0,t) = T_s \quad t \geq 0\ , \tag{4.13a}$$

$$z = H\ ;\quad -\kappa_R \frac{dT}{dz} + \rho_s c_{p_s} v_s dT = q(t) \quad t \geq 0, \tag{4.13b}$$

where κ_R is reservoir thermal conductivity.

Eq. 4.13b is the BC for systems with conducting boundaries. In our case, (**Eq. 4.13a**) refers to the isothermal injection plane while **Eq. 4.13b** describes caprock, as the heating fluid, under buoyancy, effectively convects towards the cap-rock rather than the base-rock.

For a conduction-dominated system, the forced-convective term in **Eq. 4.13b** is negligible. However, depending on the system characteristics and time-scale, it may be necessary to consider free convection as a complement to conductive-heat transfer to the caprock (Lawal and Vesovic, 2009).

Given the heat-exchanger concept and the definition of *q (t)*, **Eq. 4.13b** can be re-written as:

$$-\kappa_R \frac{dT}{dz} + \rho_s c_{p_s} v_s dT = -U_c (T - T_a)\cdot \tag{4.14}$$

A similar, but less rigorous, approach for approximating derivative boundary conditions is routinely used elsewhere, though for the simpler problem of conduction-heating. In those applications, there is no convection term on the supply side, and the boundary thickness is ignored hence the use of surrounding convective-coefficient rather than overall coefficient (Gerald and Wheatley, 1989; Sukhatme, 1989; Cornwell, 1977; Robenstein, 1972). However, in this study, we consider bulk heat-flow, and use the more realistic overall heat-transfer coefficient, incorporating both geometry and thermophysical properties of the boundary. To complete the mathematical description of our problem, we need to implement **Eq. 4.13b** in the numerical schemes given in **Eqs. 4.10** and **4.11**.

4.2.4.1 At the Caprock

To incorporate the caprock BC, we create a 'fictitious' grid (N_{z+2}) beyond the caprock into the sink. **Fig. 4.2** depicts the three-grid configuration, centred at the caprock ($z = H$).

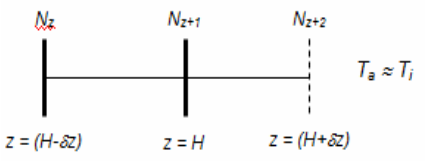


Fig. 4.2: Grid Configuration at the Cap-rock

Application of the central-difference formula to **Eq. 4.14** gives

$$-\kappa_R \frac{\left(T_{N_{z+2},j} - T_{N_z,j}\right)}{2h} + \rho_s c_{p_s} v_s \left(T_{N_z,j} - T_{N_{z+2},j}\right) \approx -U_c \left(T_a - T_{N_{z+1},j}\right). \tag{4.15}$$

Therefore, at time-step *j*, the temperature of the 'fictitious' grid, in terms of preceding grids, is given by:

$$T_{N_{z+2},j} \approx \frac{T_{N_z,j}\left(2h\rho_s c_{p_s} v_s + \kappa_R\right) - 2hU_c\left(T_{N_{z+1},j} - T_a\right)}{2h\rho_s c_{p_s} v_s + \kappa_R}. \tag{4.16}$$

Corresponding scheme at time-step (*j+1*) is:

$$T_{N_{z+2},j+1} \approx \frac{T_{N_z,j+1}\left(2h\rho_s c_{p_s} v_s + \kappa_R\right) - 2hU_c\left(T_{N_{z+1},j+1} - T_a\right)}{2h\rho_s c_{p_s} v_s + \kappa_R}. \tag{4.17}$$

4.2.4.1.1 Caprock in MCC Model

Applying **Eq. 4.11** at the caprock ($i = N_{z+1}$), we obtain the following, which includes 'fictitious' grid ($i = N_{z+2}$):

$$\begin{aligned} &-\left(\frac{\alpha}{2h^2}\right)T_{N_z,j+1} + \left(\frac{\alpha}{h^2} + \frac{F}{2h} + \frac{1}{k}\right)T_{N_{z+1},j+1} - \left(\frac{\alpha}{2h^2} + \frac{F}{2h}\right)T_{N_{z+2},j+1} \\ &\approx \\ &\left(\frac{\alpha}{2h^2}\right)T_{N_z,j} - \left(\frac{\alpha}{h^2} + \frac{F}{2h} - \frac{1}{k}\right)T_{N_{z+1},j} + \left(\frac{\alpha}{2h^2} + \frac{F}{2h}\right)T_{N_{z+2},j} - \frac{U_c\left(T_{N_{z+1},j} - T_a\right)}{\rho c_p H} \end{aligned}. \tag{4.18}$$

To eliminate the 'fictitious' grid, we combine **Eqs. 4.16**-**4.18**, yielding:

$$\begin{aligned} &-\left(2h\rho_s c_{p_s} v_s + \kappa_R\right)\left(\frac{\alpha}{h^2} + \frac{F}{2h}\right)T_{N_z,j+1} + \left\{\left(2h\rho_s c_{p_s} v_s + \kappa_R\right)\left(\frac{\alpha}{h^2} + \frac{F}{2h} + \frac{1}{k}\right) + U_c\left(\frac{\alpha}{h} + F\right)\right\}T_{N_{z+1},j+1} \\ &\approx \left(2h\rho_s c_{p_s} v_s + \kappa_R\right)\left(\frac{\alpha}{h^2} + \frac{F}{2h}\right)T_{N_z,j} - \left\{\left(2h\rho_s c_{p_s} v_s + \kappa_R\right)\left(\frac{\alpha}{h^2} + \frac{F}{2h} - \frac{1}{k}\right) + U_c\left(\frac{\alpha}{h} + F\right)\right\}T_{N_{z+1},j} + 2U_c T_a\left(\frac{\alpha}{h} + F\right) \\ &- \frac{\left(2h\rho_s c_{p_s} v_s + \kappa_R\right)}{\rho c_p H}\left\{U_c\left(T_{N_{z+1},j} - T_a\right)\right\} \end{aligned}. \tag{4.19}$$

A similar analysis for the FCC yields

$$-\left(2h\rho_s c_{p_s} v_s + \kappa_R\right)\left(\frac{\alpha}{h^2}+\frac{F}{2h}\right)T_{N_z,j+1} + \left\{\left(2h\rho_s c_{p_s} v_s + \kappa_R\right)\left(\frac{\alpha}{h^2}+\frac{F}{2h}+\frac{1}{k}\right) + U_c\left(\frac{\alpha}{h}+F\right)\right\}T_{N_{z+1},j+1}$$
$$\approx$$
$$\left(2h\rho_s c_{p_s} v_s + \kappa_R\right)\left(\frac{\alpha}{h^2}+\frac{F}{2h}\right)T_{N_z,j} - \left\{\left(2h\rho_s c_{p_s} v_s + \kappa_R\right)\left(\frac{\alpha}{h^2}+\frac{F}{2h}-\frac{1}{k}\right) + U_c\left(\frac{\alpha}{h}+F\right)\right\}T_{N_{z+1},j} + 2U_c T_a\left(\frac{\alpha}{h}+F\right) + \Omega_1\left(2h\rho_s c_{p_s} v_s + \kappa_R\right)$$
$$-\frac{\left(2h\rho_s c_{p_s} v_s + \kappa_R\right)}{\rho c_p H}\left\{U_c\left(T_{N_{z+1},j} - T_a\right)\right\} \qquad (4.20)$$

4.2.4.2 At the Injection Plane

We are also interested in the dynamics at the other mathematical 'boundary', which is the injection plane. As a remark, temperature profile below (including at base-rock) the injection plane is estimated from the conduction equation, referenced to the injection plane. Hence, we do not need to invoke some 'fictitious' grids as used for the cap-rock. Rather, the known isothermal behaviour of the injection plane must be preserved in all numerical schemes, and the instantaneous heat-flux through the neighbouring base-rock updated accordingly.

4.2.4.2.1 Injection Plane in MCC Model

Applying **Eq. 4.11** at the injection plane, we have:

$$-\left(\frac{\alpha}{2h^2}\right)T_{1,j+1} + \left(\frac{\alpha}{h^2}+\frac{F}{2h}+\frac{1}{k}\right)T_{2,j+1} - \left(\frac{\alpha}{2h^2}+\frac{F}{2h}\right)T_{3,j+1}$$
$$\approx \qquad (4.21)$$
$$\left(\frac{\alpha}{2h^2}\right)T_{1,j} - \left(\frac{\alpha}{h^2}+\frac{F}{2h}-\frac{1}{k}\right)T_{2,j} + \left(\frac{\alpha}{2h^2}+\frac{F}{2h}\right)T_{3,j} - \frac{U_b\left(T_b^j - T_a\right)}{\rho c_p H}$$

Noting that the injection plane is maintained at temperature T_s at all times, **Eq. 4.21** reduces to the following equation with two unknowns T_2 and T_3 at next time-step ($j+1$).

$$\left(\frac{\alpha}{h^2}+\frac{F}{2h}+\frac{1}{k}\right)T_{2,j+1} - \left(\frac{\alpha}{2h^2}+\frac{F}{2h}\right)T_{3,j+1}$$
$$\approx \qquad (4.22)$$
$$\left(\frac{\alpha}{h^2}\right)T_s - \left(\frac{\alpha}{h^2}+\frac{F}{2h}-\frac{1}{k}\right)T_{2,j} + \left(\frac{\alpha}{2h^2}+\frac{F}{2h}\right)T_{3,j} - \frac{U_b\left(T_b^j - T_a\right)}{\rho c_p H}$$

Application of the foregoing analysis to the FCC,

$$\left(\frac{\alpha}{h^2}+\frac{F}{2h}+\frac{1}{k}\right)T_{2,j+1} - \left(\frac{\alpha}{2h^2}+\frac{F}{2h}\right)T_{3,j+1}$$
$$\approx \qquad (4.23)$$
$$\left(\frac{\alpha}{h^2}\right)T_s - \left(\frac{\alpha}{h^2}+\frac{F}{2h}-\frac{1}{k}\right)T_{2,j} + \left(\frac{\alpha}{2h^2}+\frac{F}{2h}\right)T_{3,j} + \Omega_{c1}^j - \frac{U_b\left(T_b^j - T_a\right)}{\rho c_p H}$$

4.2.5 Solution of PDE under Conducting Boundaries

To obtain the temperature profile in MCC, **Eqs. 4.11**, **4.19** and **4.22** are solved simultaneously at every time-step. On the other hand, prediction of temperature distribution in the case of FCC requires solving **Eqs. 4.10**, **4.20** and **4.23** at every time-step.

As illustration, we derive the system of equations for a reservoir discretised into N_z grids on the z-axis. The injection plane and caprock are represented by grids $i = 1$ and $i = N_{z+1}$, respectively. For an FCC model, the following equations are applicable.

Injection Plane ($i = 1$):

$$\left(\frac{\alpha}{h^2}+\frac{F}{2h}+\frac{1}{k}\right)T_{2,j+1}-\left(\frac{\alpha}{2h^2}+\frac{F}{2h}\right)T_{3,j+1} \approx \left(\frac{\alpha}{h^2}\right)T_s-\left(\frac{\alpha}{h^2}+\frac{F}{2h}-\frac{1}{k}\right)T_{2,j}+\left(\frac{\alpha}{2h^2}+\frac{F}{2h}\right)T_{3,j}+\Omega_1^j-\frac{U_b\left(T_b^j-T_a\right)}{\rho c_p H} \quad (4.24)$$

Intermediate grids ($i = 2, 3, \ldots, N_z$):

$$-\left(\frac{\alpha}{2h^2}\right)T_{i-1,j+1}+\left(\frac{\alpha}{h^2}+\frac{F}{2h}+\frac{1}{k}\right)T_{i,j+1}-\left(\frac{\alpha}{2h^2}+\frac{F}{2h}\right)T_{i+1,j+1} \approx \left(\frac{\alpha}{2h^2}\right)T_{i-1,j}-\left(\frac{\alpha}{h^2}+\frac{F}{2h}-\frac{1}{k}\right)T_{i,j}+\left(\frac{\alpha}{2h^2}+\frac{F}{2h}\right)T_{i+1,j}+\Omega_1^j \quad (4.25)$$

Caprock ($i = N_{z+1}$):

$$-\left(2h\rho_s c_{p_s} v_s+\kappa_R\right)\left(\frac{\alpha}{h^2}+\frac{F}{2h}\right)T_{N_z,j+1}+\left\{\left(2h\rho_s c_{p_s} v_s+\kappa_R\right)\left(\frac{\alpha}{h^2}+\frac{F}{2h}+\frac{1}{k}\right)+U_c\left(\frac{\alpha}{h}+F\right)\right\}T_{N_{z+1},j+1} \approx \left(2h\rho_s c_{p_s} v_s+\kappa_R\right)\left(\frac{\alpha}{h^2}+\frac{F}{2h}\right)T_{N_z,j}-$$

$$\left\{\left(2h\rho_s c_{p_s} v_s+\kappa_R\right)\left(\frac{\alpha}{h^2}+\frac{F}{2h}-\frac{1}{k}\right)+U_c\left(\frac{\alpha}{h}+F\right)\right\}T_{N_{z+1},j}+2U_c T_a\left(\frac{\alpha}{h}+F\right)+\Omega_1\left(2h\rho_s c_{p_s} v_s+\kappa_R\right)-\frac{\left(2h\rho_s c_{p_s} v_s+\kappa_R\right)}{\rho c_p H}\left\{U_c\left(T_{N_{z+1},j}-T_a\right)\right\} \quad (4.26)$$

From the foregoing, it is clear that at any instant, there are N_z algebraic equations in N_z unknown temperature points. This well-posed system of simultaneous equations is easily solved.

4.3 Effects of Relative Location of Sink Saturants

There are natural occurrences of bituminous deposits in communication with gas and/or water zones. Unlike gas-cap occurrences, top-water systems are not common. Nevertheless, whether a water-zone underlies or overlies an oil sand depends on the density contrast between in-situ oil and water (Doan *et al.*, 1999). The following are some field examples of both types.

Husky's Tucker oil sand project (Alberta) has bottom water. Despite recording key feats during its construction, as evident in the costs and schedule, the operational phase was disappointing (Roche, 2008). With a cumulative steam-oil-ratio (CSOR) of 20 bbl/bbl (industry best is 2.5-3 bbl/bbl (Roche, 2008)), independent analysis of the performance highlighted considerable thermal

inefficiencies, attributed to heat loss (including steam short-circuiting) to the underlying water-zone. Placing wells (injectors and producers) too close to the water layer was identified as the main cause of the sub-optimal results and, as "optimisation strategies"; there were plans to re-position some wells (Roche, 2008).

Encana's Borealis project (Canada), scheduled for start-up in 2015, has water-zone overlying bitumen within the McMurray formation. To mitigate operational problems expected from this occurrence, Encana plans to inject air, prior to steaming, into the top zone to displace the water (Roche, 2008). That is, if this proposal for an "air blanket" is successfully implemented, the deposit would have been converted from top-water to top-air. It would be interesting to understand the implications of this proposal on reservoir dynamics and project performance.

The widely reported ConocoPhillips' Surmont lease (Canada) is uniquely challenging for thermal recovery (Roche, 2008; Law *et al*., 2003a, b). Besides having contiguous gas-cap and mobile water-zone above the oil sand, there is pressure-depletion in the gas-cap due to gas production from a communicating reservoir.

For systems devoid of initial top-gas, artificial gas-caps may be created by injecting gas. For example, in simulating CO_2 sequestration into the Kartaltepe Field, a mature oil deposit in Turkey, Pamukcu and Gumrah (2008) observed that a significant fraction of injected CO_2 accumulated in the upper zones of the formation. A similar observation was earlier reported by Law (2004) and Bagci *et al.* (2008). In qualitative terms, these simulation results are consistent with available laboratory and field data (Yee and Stroich, 2004; Jiang *et al*., 2000a, b).

As much as we are aware, there is no record of a natural formation where gas layer underlies an oil sand within the same continuous reservoir. This notwithstanding, we conceptualise the following scenarios as being consistent with this uncommon, yet interesting, case of underlying bottom gas (*gas-like* zones).

- Gas leakage from an underlying formation (at higher pressure) into the subject reservoir.
- Accumulation of live steam and/or flashed condensate in the vicinity of the producer, placed very close to the base-rock.
- Vapourisation of bottom-water as a result of prevailing temperature and pressure.
- Vapourisation of oil in the vicinity of the base rock.
- The period following gas injection in systems where the injector is positioned in the lower part of the formation. Typically, gas plume does not rise instantly, and there exists a slower higher-saturation trailing edge in the vicinity of injection point (Silin *et al*., 2009; Riaz and Tchelepi, 2008).
- Capillary/hydrodynamic trapping of injected gas in the lower part of the reservoir (Bryant *et al.*, 2008).

The foregoing scenarios motivated our interest to evaluate all possible combinations of gas and liquid layers in the neighbourhood of cap and base rocks. Results from this robust study should improve the current design and analysis of similar systems in practice.

In this Chapter, we retain most of the data used in Chapter 3. Although sensitivity studies are performed, we use lower base-case permeability and formation thickness in order to highlight the magnitude of boundary losses relative to injected heat. In addition to the data listed in **Table 3.1**, specific data for the current analysis is presented in **Table 4.1**, where the thermal conductivity is estimated from Somerton (1958).

Table 4.1: Base-case Rock and Fluid Data

Variable	Magnitude	Variable	Magnitude
T_{cap}, °C	0[ζ]	κ_c, W m^{-1} K^{-1}	1.366
H, m	20	Z_c, m	1
K_{vs}, mD	100	Base rock	Shale
K_{vo}, mD	0	κ_b, W m^{-1} K^{-1}	1.366
Boundaries	Non-isothermal	Z_b, m	1
Cap rock	Shale	Z_{bi}, m	5

4.3.1 Simulation Design

To study non-adiabatic effect in relation to sink saturants, we employ a two-level (low and high) full-factorial experimental design (ED), as discussed in Montgomery (1976). We examine different heating processes. For each process, ED requires 16 simulation runs to fully assess the effects of sink saturants only. For comparison, cases of adiabatic and isothermal (cap rock maintained at initial temperature) boundaries are included.

In studying the effect of sink-saturants, we consider the fluid that fills the vicinity of cap and base rocks. There are four factors, representing the two sides (top and underneath) of each of cap and base-rock boundaries. In this case, the two levels are gas and liquid saturants. Combining these two levels with the four possible factors results in 16 (2^4) simulation runs in the case of sink-saturants.

4.3.2 Interpretation of Simulation Results

The PDE is second-order in space but first-order in time. Being first-order in time, the average reservoir temperature can be treated as a variable, thus simplifying this distributed-parameter system into a lumped problem. Simple investigations of reservoir-sink interaction for lumped (perfectly mixed) systems are presented in Appendix **D**, indicating there is a time-lag between the responses of the reservoir and the surroundings, which justifies the use of lumped analysis for the reservoir.

In this work, we employ the lumped-parameter analysis to assess the average reservoir-behaviour in a steam-injection process in which there are heat losses to adjacent formations.

[ζ] Applicable for the case of isothermal boundaries.

Although this simplifies the real physical situation, such analysis has been used successfully for industrial systems (Khalil, 1982).

In principle, the adjacent sinks may be viewed as controllers, aiming to keep the reservoir temperature at its pre-injection value (steady-state). Hence, we employ the principle used for the analysis of industrial control systems. As performance indicators for reservoir-heating, we use the following parameters (Marlin, 1995; Coughanowr, 1991; Stephanopoulos, 1984).

- **Steady-state Temperature, T_{ss}:** stabilised average temperature attained.
- **Steady-state Time, t_{ss}:** time to reach T_{ss}. It is a fair indication of the speed of response.
- **Steady-state Deviation, δ:** a measure of relative deviation between the source temperature T_s and T_{ss}. In the current context, it generally indicates departure from a perfect adiabatic performance.

$$\delta = 100\left(T_s - T_{ss}\right)/T_s \ . \tag{4.28}$$

4.3.3 Relative Location of Sink Saturants

In this section, all the possible locations of gas and liquid columns are covered. The impacts of the relative locations of these columns on reservoir-heating and thermal losses are evaluated.

4.3.3.1 Heating by MCC

Table 4.2 presents the 16 runs for the MCC process (100% steam condensation) while **Fig. 4.3** shows the performance plots. Apart from the isothermal case (run 18), with steady-state deviation of ~ 3%, the other runs are consistently within 1.5 ^{o}C (<1%) of the ultimate adiabatic performance. In terms of ultimate temperature and deviation, run 10, consisting of only gas saturants, gives the best heating performance while the exact converse, run 9, with only liquid saturants, provides the least attractive result.

Fig. 4.4 compares adiabatic, isothermal and the limits (runs 9 and 10) of non-adiabatic responses. Considering the consistency between the adiabatic and non-adiabatic behaviours, it can be concluded that in this case of MCC heating, thermal recovery operation can satisfactorily be modelled as adiabatic. However, an isothermal assumption is less suitable.

Having established runs 9 and 10 as the lower and upper limits of performance, respectively, we examine scenarios of homogenous saturants in either boundary. These refer to filling either sides of a boundary with one fluid while the other boundary is saturated, on either sides, by another fluid i.e. runs 14 and 1.

The variation of rate of heat loss through overburden and underburden are shown in **Fig. 4.5** for runs 1, 9, 10 and 14. Within the first 30 days, there is no appreciable heat-flux through the base rock for all runs. Between 30 and 120 days, heat flux to the bottom sink ramps up, then goes

asymptotic. Although runs 9 and 14 are essentially the same, they show marked differences from runs 1 and 10, where lower rates of underburden thermal losses are estimated.

Table 4.2: Full-Factorial Design for Saturants under MCC-Heating (*G* = gas-saturated, *L* = liquid-saturated)[↑]

Run	Base Sink	Bottom	Cap	Cap Sink	T_{ss} (°C)	t_s (days)	δ (%)
1	*G*	*G*	*L*	*L*	*248.8*	*264*	*0.5*
2	L	G	G	L	249.0	243	0.4
3	G	L	L	G	249.2	240	0.3
4	G	L	L	L	248.8	279	0.5
5	G	G	G	L	249.0	237	0.4
6	L	G	L	G	249.2	243	0.3
7	G	L	G	L	249.0	240	0.4
8	G	L	G	G	249.3	237	0.3
9	*L*	*L*	*L*	*L*	*248.7*	*243*	*0.5*
10	*G*	*G*	*G*	*G*	*249.3*	*237*	*0.3*
11	L	G	L	L	248.7	237	0.5
12	L	G	G	G	249.3	243	0.3
13	L	L	L	G	249.2	252	0.3
14	*L*	*L*	*G*	*G*	*249.3*	*249*	*0.3*
15	G	G	L	G	249.2	237	0.3
16	L	L	G	L	249.0	249	0.4
17	Adiabatic boundaries $(U_b = U_c = 0)$				250	249	0
18	Isothermal boundaries				243.1	234	2.8

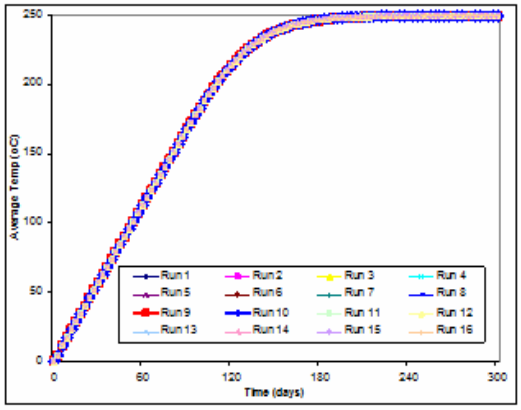


Fig. 4.3: Average Temp for Different Boundary Saturants (MCC)

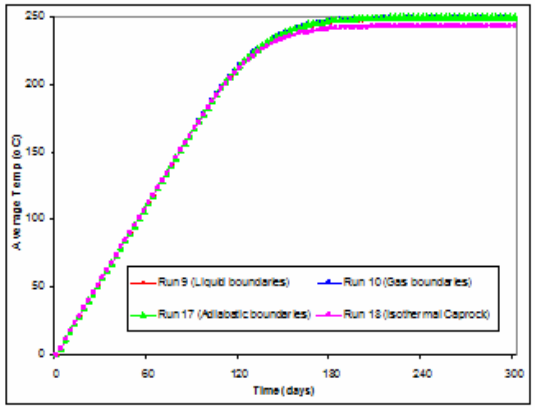


Fig. 4.4: Average Temp for Selected Boundaries (MCC)

[↑] For gas, h = 12 W m^{-2} K^{-1}. For liquid, h = 500 W m^{-2} K^{-1}.

The similarity of runs 9 and 14 for underburden heat flux is not unexpected. This can be explained by the fact that both have either sides of the base-rock saturated with liquid, hence same base overall heat-transfer coefficient, despite the difference in overburden saturants. That both runs 1 and 10 also have gas-saturated bottoms, despite contrasts in cap rock fills, explains their similar underburden heat flux. Because liquid-saturated porous media have higher overall heat-transfer coefficient than the gas-saturated ones, the higher rate of underburden heat loss observed in runs 9 and 14 is understandable.

Within the first 90 days, heat flux through the cap rock is negligible in all the runs. Subsequently, cap-rock losses are noticeable, increasing sharply over the next 50 days, then more slowly until reaching steady-state after 220 days. The rate of overburden heat losses in runs 1 and 9 consistently exceeds that of the pair 10 and 14. At steady-state, the rate in the former is twice that in the latter. We interpret the steady-state as roughly coinciding with the time when the advancing front effectively reaches the cap-rock. It is noteworthy that the asymptotes coincide with the respective steady-state times in **Table 4.2**.

The earlier argument for the base-rock losses applies to the cap rock observations. In the vicinity of the cap rock, runs 1 and 9 are both liquid-saturated, despite contrasting underburden saturants. Conversely, runs 10 and 14 assumed gas-filled overburden neighbourhood but dissimilar underburden fills. Owing to higher overall heat-transfer coefficient associated with liquid systems, runs 1 and 9 consistently show poorer thermal insulation capacity than runs 10 and 14.

For the overburden response, the difference between the pairs increases over time, until it stabilises. This can be attributed to increasing temperature difference, which is the driver of heat flux, between the cap-rock and the surroundings (sustained at initial temperature). Because MCC and other convective (non-zero permeability) processes involve propagation of a thermal front, at early times, the cap-rock is mainly being heated by conduction; hence only modest temperatures are achieved. When the thermal front eventually reaches the vicinity of the boundary, the saturants on either sides of the caprock play key roles in heat retention. From **Fig. 4.6**, illustrating the variation of temperature at the reservoir-overburden interface, there is evidence of the temperature-dampening effect of the boundary saturants. Consequently, we deduce that where the cap-rock heat loss dominates reservoir behaviour, the temperature-regulating effect of heat sinks would mainly manifest as the front approaches the cap-rock, or in conduction-controlled systems, when the neighbourhood of the cap rock is sufficiently hot.

This overburden-heating mechanism contrasts sharply with that of the base-rock, which is heated by conduction. Hence, in the base-rock, the ultimate temperature is attained gradually and asymptotically after a relatively longer time. The insignificant base-rock heat flux within the first 30 days is an indication that this time is insufficient to conductively heat up the base rock by a heat source 5 m away. In this study, convective-heating is favourable to the cap-rock because of our assumption of buoyancy-driven flow, allowing continuous upward migration of the less dense heat-transporting fluids.

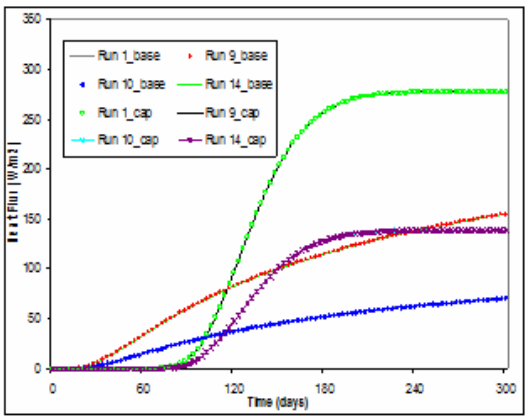


Fig. 4.5: Cap/Base-rock Heat-Fluxes for Specific Boundary Realisations (MCC)

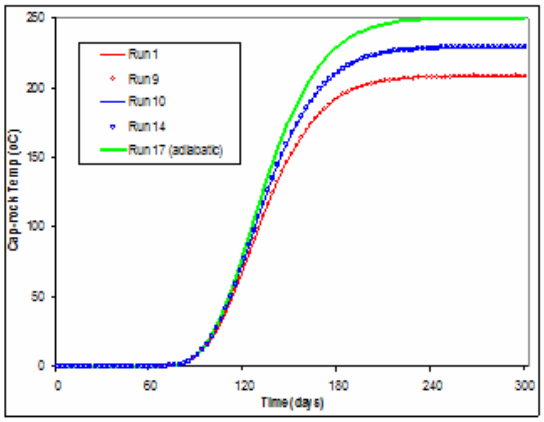


Fig. 4.6: Evolution of Caprock Temperature for Different Boundaries (MCC)

Fig. 4.7 highlights the combination of overburden and underburden heat fluxes for selected runs. Within the first 90 days, runs 1 and 10 behave similarly while runs 9 and 14 constitute another identical pair. However, in terms of long-term heat conservation, the increasing order of attractiveness is run 9 < 1 < 14 < 10. From the worst to the best, this order is consistent with the performances depicted in **Fig. 4.3** and summarised in **Table 4.2**. Based on the relative boundary losses in this example, the caprock is more vulnerable. Hence, it is apparent that a key success factor is to reduce the overall heat-transfer coefficient of the overburden fluids. However, whether this is justified in view of the theoretical limits set by the adiabatic result (**Fig. 4.4**) is a decision to be premised on economics and other factors.

Accounting for heat-loss affects both heat conservation and reservoir temperature but it appears that the effect is more pronounced on heat conservation. While the ultimate average temperatures of runs 1, 9, 10 and 14 are within 1% of each other, variation of total heat flux is up to 52%. In this example, it can be concluded that though the engineering of boundary fluids might not improve heating performance (hence oil recovery) significantly, its effect on overall thermal efficiency is promising.

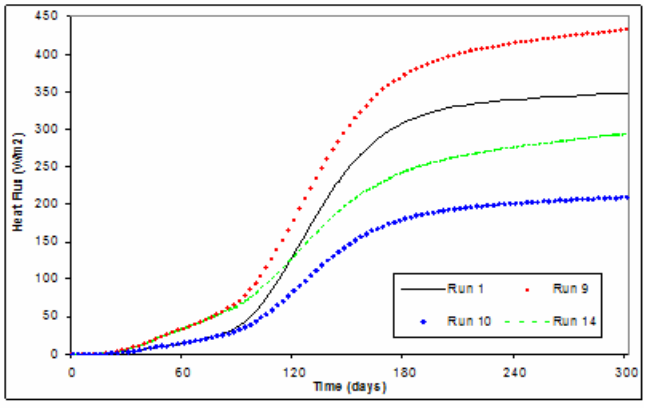


Fig. 4.7: Total Heat-Flux for Specific Boundary Saturants (MCC)

4.3.3.2 Heating by CO_2

As an example of non-condensing convective-heating, we consider CO_2. Although we also studied the cases of non-condensing steam, flue-gas (50% CO_2, 50% N_2) and N_2 heating, space consideration limits this discussion to just the case of CO_2. However, most of the inferences obtained for the CO_2 apply to the other convection processes, in which the heating fluid is not condensable. .

To discount the effect of pressure, this analysis assumes CO_2 pressure equals steam-saturation pressure (3.973 MPa) at the injection temperature (250 ^oC). However, we do not consider the potential permeability-impairment due to CO_2-induced precipitation of asphaltenes.

Table 4.3 presents the simulation runs for this case while the results are plotted in **Fig. 4.8**. As observed with the MCC, the non-adiabatic runs are less effective than the adiabatic scheme. Similarly, the isothermal scenario is the least attractive while runs 9 and 10 still set the lower and upper bounds of non-adiabatic performance, respectively (**Fig. 4.9**).

Table 4.3: Full-Factorial Design for Saturants under CO_2-Heating

Run	Base Sink	Bottom	Cap	Cap Sink	T_{ss} (^oC)	t_s (days)	δ (%)
1	*G*	*G*	*L*	*L*	*239.2*	*1185*	*4.3*
2	L	G	G	L	240.8	1245	3.7
3	G	L	L	G	242.2	1305	3.1
4	G	L	L	L	239.2	1215	4.3
5	G	G	G	L	240.9	1395	3.6
6	L	G	L	G	242.1	1185	3.2
7	G	L	G	L	240.8	1185	3.7
8	G	L	G	G	243.1	1455	2.8
9	*L*	*L*	*L*	*L*	*239.1*	*1200*	*4.4*
10	*G*	*G*	*G*	*G*	*243.1*	*1350*	*2.8*
11	L	G	L	L	239.2	1305	4.3
12	L	G	G	G	243.0	1245	2.8
13	L	L	L	G	242.1	1290	3.2
14	*L*	*L*	*G*	*G*	*243.0*	*1410*	*2.8*
15	G	G	L	G	242.2	1260	3.1
16	L	L	G	L	240.7	1170	3.7
17	Adiabatic boundaries $(U_b = U_c = 0)$				250	1455	0
18	Isothermal boundaries				228.2	1095	8.7

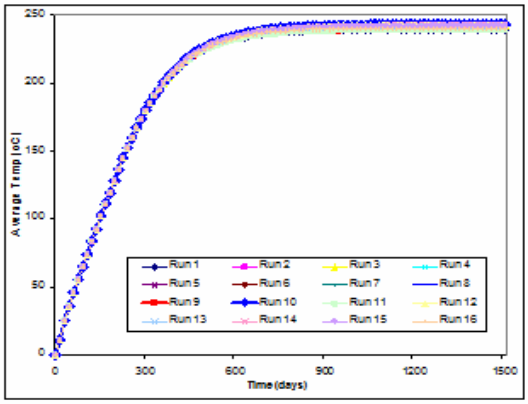


Fig. 4.8: Average Temp for Different Boundary Saturants (CO_2)

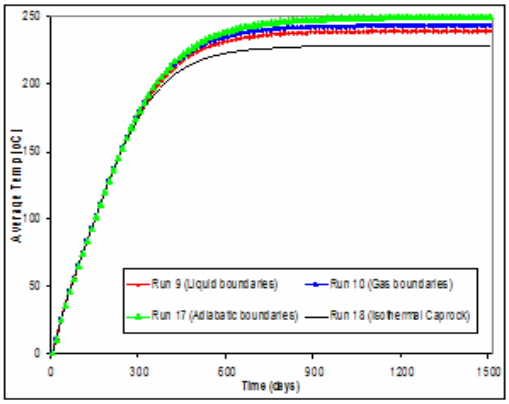


Fig. 4.9: Average Temp for Selected Boundaries (CO_2)

With an ultimate temperature-deviation of 2.8-8.7% (including isothermal run), compared to the range 0.3-2.8% for MCC, it follows that the CO_2 process is more sensitive to boundary conditions. Comparing their steady-state times, the CO_2–heating is slower. Hence, we infer that as a heating process becomes more effective, it is less sensitive to the nature and configuration of boundary saturants because the rate of heat supply to the reservoir significantly exceeds that of heat loss through the reservoir boundaries. Therefore, modifying the boundary conditions is not likely to have significant impacts on a relatively fast heating process. Furthermore, the results indicate that for relatively fast heating processes, the adiabatic assumption may be reasonable, providing the time-scale is not large.

For emphasis, deviation from adiabatic assumption declines with effectiveness of the heating process, even when it is apparently “non-adiabatic”. Here, the understanding differs slightly from the conventional definition of “adiabatic” system, which refers to “zero” heat flux. In the current analysis, we consider “adiabatic” when the rate of replenishing lost heat significantly exceeds that at which the heat is being lost. In principle, when the rate of heat supply to the reservoir boundaries significantly exceeds that of leakage through the same boundaries, the net impact is an “attenuated” effect of heat loss on the overall energy availability. Hence, the average system-behaviour is adiabatic.

Fig. 4.10 shows instantaneous heat flux through the cap rock for selected runs 1, 9, 10 and 14. The behaviour is consistent with the delayed response observed for the MCC process. The striking similarity in the overburden fluxes between runs 1 and 9 on one hand as well as runs 10 and 14 on the other is also pronounced. Again, this is explained by the similarity of the overburden saturants within either pairs. As highlighted under MCC heating, **Fig. 4.11**, which shows the variation of reservoir-overburden interface temperature, complements this discussion.

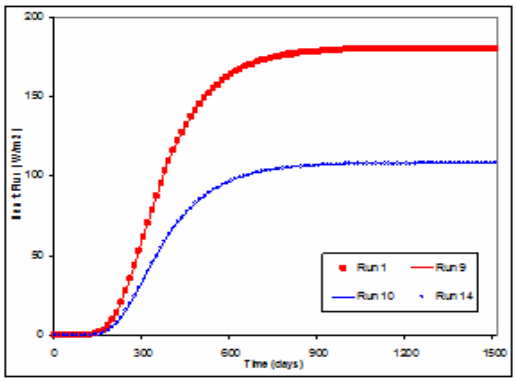


Fig. 4.10: Cap-rock Unproductive Heat-Flux for Specific Boundary Realisations (CO_2)

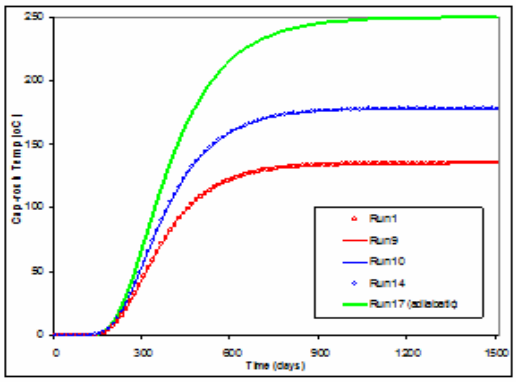


Fig. 4.11: Evolution of Caprock Temperature for Different Boundaries (CO_2)

Fig. 4.12 depicts the variation of the total heat-flux. Along with **Fig. 4.10**, a close evaluation would reveal that the contribution of overburden losses is negligible (< 5%) within the first 200 days, but steadily rises to about 40% after 400 days. Apparently, while the time-scale here is long enough for conductive heat-transport to the base rock to manifest, it is not sufficient for convection to the caprock to dominate.

Fig. 4.13 shows the instantaneous total heat-fluxes for selected runs. From the viewpoint of energy-conservation, run 10 is the most efficient while run 9 is the least competitive. Between these limits are runs 1 and 14 in that order. But in the context of final temperature (**Table 4.3**), the scenario of run 14 is better than run 1. Generally, while it is clear that runs 10 and 9 are the most favourable and least attractive, respectively, the choice between runs 1 and 14 would need to be based on further studies.

As it is not common for thermal-flood projects to be operated for just 200 days, an important message is that the engineer needs to have a good understanding of the minimum time-scale needed for the effects of key mechanisms to manifest. Apparently, only the mechanisms that are likely to have significant impacts on the project objectives would deserve appropriate accounting and possible mitigation.

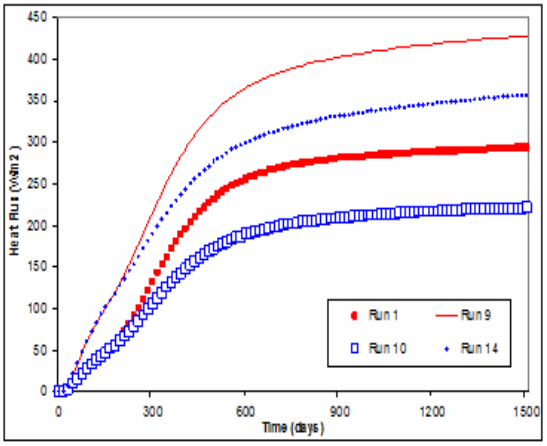


Fig. 4.12: Total Unproductive Heat-Flux for Specific Boundary Realisations (CO_2)

4.3.3.3 Conduction-Dominated Heating

In order to ensure pure conduction-heating in this case, reservoir-permeability was set to zero. However, for the estimation of boundary heat-transfer coefficients, the base-case permeability of 100 mD was used.

A summary of the runs and the results is given in **Table 4.4**. Generally, the steady-state times are much longer than those for the convective-heating processes of MCC and CO_2. Comparing the adiabatic cases, this heating rate is about ten times slower than the performance of CO_2 heating, the slower of the convective processes. Ranging from 43 to 50%, its steady-state temperature-deviation is much larger than the convective cases. These indicate that the conductive process, though more stable in terms of the relative magnitude of losses, is much more sensitive to thermal instability induced by energy interactions with the surroundings.

Considering the magnitude of steady-state temperature deviations, it can be concluded that in a conductive process, the adiabatic assumption is not a good approximation for both isothermal and non-adiabatic operations. Nevertheless, consistent with the observations made for the other processes, runs 9 and 10 are the limiting scenarios.

Fig. 4.13 illustrates how the average temperature varies over time. Within the first 1000 days, the system behaves as if it were infinite, as the dynamics is largely independent of boundary fluids. Subsequently, boundary effects are evident, though masked by the time-scale in **Fig. 4.13**. To facilitate comparison, **Fig. 4.14** amplifies the first 4,000 days of **Fig. 4.13**. Unlike the adiabatic result, **Fig. 4.14** indicates that most of the non-adiabatic responses are within their respective stabilised states around 4,000 days.

Table 4.4: Full-Factorial Design for Saturants under Conduction-Heating

Run	Base Sink	Bottom	Cap	Cap Sink	T_{ss} (°C)	t_s (days)	δ (%)
1	*G*	*G*	*L*	*L*	*132.9*	*4400*	*46.8*
2	L	G	G	L	136.1	5600	45.6
3	G	L	L	G	139.5	5200	44.2
4	G	L	L	L	132.9	4800	46.8
5	G	G	G	L	168.9	8000	32.4
6	L	G	L	G	139.5	5600	44.2
7	G	L	G	L	136.1	5200	45.6
8	G	L	G	G	142.3	5200	43.1
9	*L*	*L*	*L*	*L*	*132.8*	*4400*	*46.9*
10	*G*	*G*	*G*	*G*	*142.4*	*9200*	*43.0*
11	L	G	L	L	132.9	5200	46.8
12	L	G	G	G	142.3	5600	43.1
13	L	L	L	G	139.5	6000	44.2
14	*L*	*L*	*G*	*G*	*142.3*	*6800*	*43.1*
15	G	G	L	G	139.5	5200	44.2
16	L	L	G	L	136	5200	45.6
17	Adiabatic boundaries $(U_b = U_c = 0)$				250	15400	0
18	Isothermal boundaries				125	1460	50

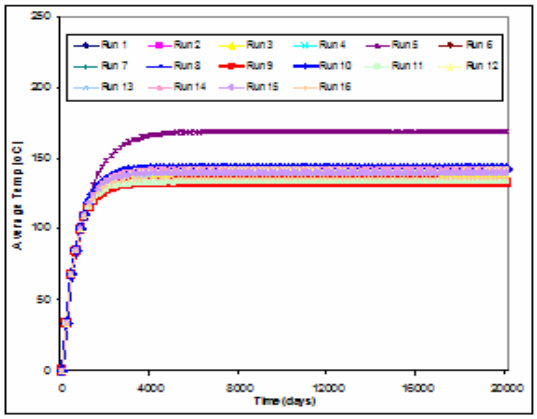


Fig. 4.13: Average Temp for Different Boundary Saturants (Conduction)

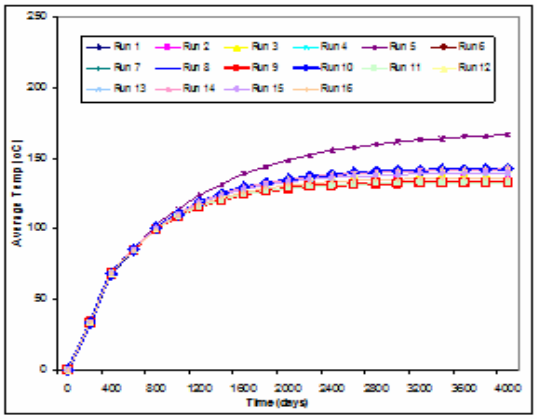


Fig. 4.14: Average Temp at "Early" Times (Conduction)

Fig. 4.15 affirms the assertion that the early-time behaviours are independent of boundary assumptions. After about 1000 days, the non-adiabatic and isothermal-overburden responses deviate sharply from the adiabatic trend. However, almost immediately, the isothermal and non-adiabatic systems show clear but consistent contrasts in their individual dynamics.

Fig. 4.16 illustrates the variation of underburden heat-fluxes that correspond to the average temperatures in **Fig. 4.13**. In contrast to the convective cases, the underburden heat-loss controls reservoir dynamics. The reason for this is the relative distance of the two candidate sinks from the heat source. While the base-rock is only 5 m away from the injection plane, which is the heat

source, the cap rock is about 20 m away. Recalling that heat-transfer is strictly by conduction in this case, it is understood why the underburden is the dominant heat-sink in this case. Within the simulation time considered, the underburden consistently accounts for over 90% of total unproductive instantaneous heat flux.

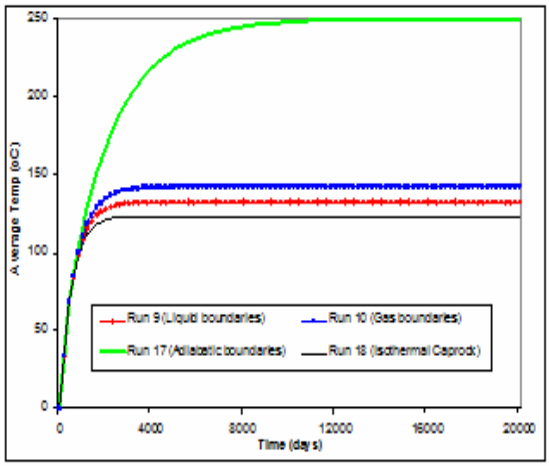


Fig. 4.15: Average Temp for Selected Boundaries (Conduction)

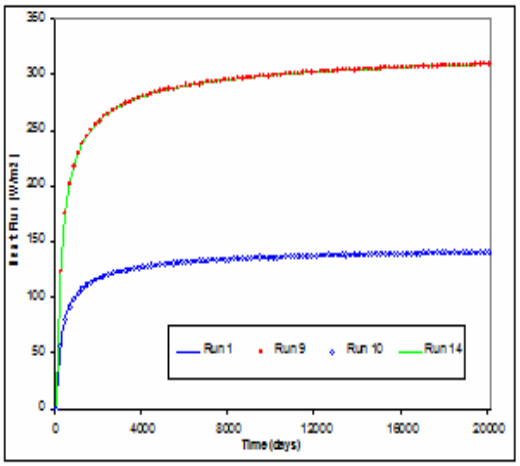


Fig. 4.16: Underburden Heat Flux for Different Saturants (Conduction)

A comparison of all the results suggests that the convective processes have higher rate of heat losses than the corresponding conduction cases. However, all the convective cases yield performances that agree more closely (the worst case is within 7%) with the adiabatic behaviour than does conductive-heating, where the closest agreement is a 43% deviation. This substantiates our earlier argument that the balance of the rates of heat supply and removal gives a better indication of adiabatic dynamics than just the magnitude of heat removal. In essence, the results indicate that the susceptibility to the effects of heat leakage increases with deceasing permeability (increasing conduction).

For greater clarity, we use normalised temperature and time scales to compare the responses of the various heating processes. Reference temperature and time are 250 ^{o}C and 20,000 days, respectively. **Figs. 4.17** and **4.18** depict the results for the adiabatic and non-adiabatic scenarios, respectively. The results for the other heating processes are presented in Appendix **F**.

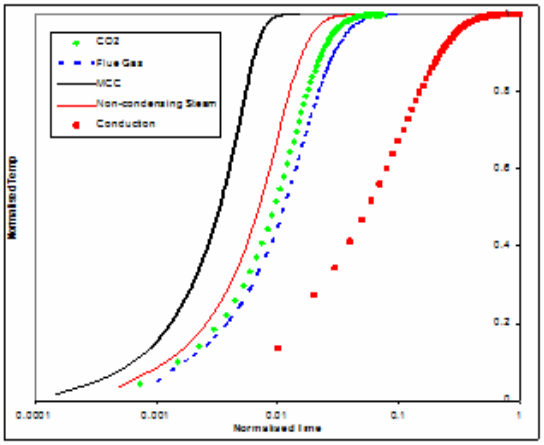


Fig. 4.17: Normalised Responses of Some Heating Processes (Adiabatic Scenarios)

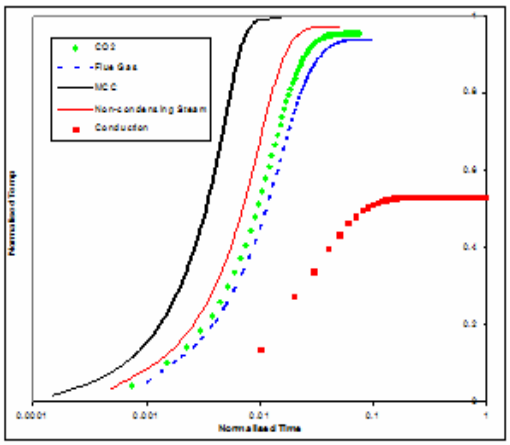


Fig. 4.18: Normalised Responses of Some Heating Processes (Non-Adiabatic Scenarios)

4.4 Parametric Studies

In this section, we perform single-variable analysis to quantify the effects of selected variables on reservoir-heating and thermal losses.

4.4.1 Effect of Boundary Thickness

Fig. 4.19 shows the average temperature for an MCC process in which the thickness of the boundaries (cap and base rocks) is set to 0.1, 1 and 10 m. Reservoir-heating improves with boundary thickness. Compared to the scenario where adiabatic assumption is valid, steady-state deviations of 2.1, 0.5 and 0.1% are obtained for the 0.1, 1 and 10 m systems, respectively.

From **Fig. 4.20**, it is deduced that heat-containment is sensitive to the thickness of reservoir boundaries within the range examined. However, the sensitivity of heat loss to boundary-thickness is higher than that of average temperature. While the stabilised temperatures for 0.1, 1 and 10 m boundaries are within 2% of one another, relative deviation of heat leakages is more than a factor of 40. In this particular case, for a 10-fold increase in the thickness of overburden and underburden, though heating performance might be improved by just 2%, heat savings might be over 40-fold.

Qualitatively, we found the same results for the case of CO_2-heating, but the impacts are higher than the MCC. In both cases, we notice that if both cap and base rocks are thicker than 1 m, the effect of boundary thickness is relatively suppressed. So, could it be that a boundary-thickness of 1 m is a sufficient criterion for assessing the thermal characteristics of reservoirs under steam-injection? We attempt to answer this question with subsequent sensitivity studies.

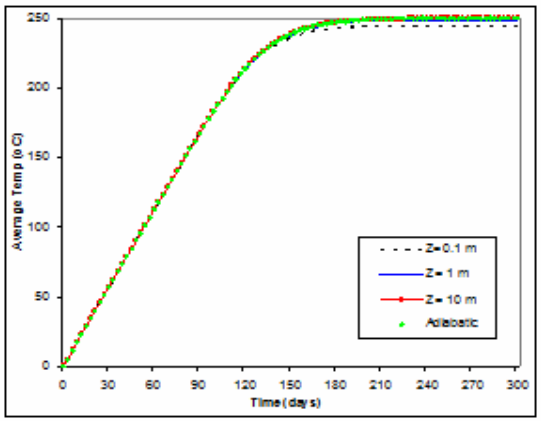


Fig. 4.19: Effect of Boundary-Thickness on Average Temp (MCC)

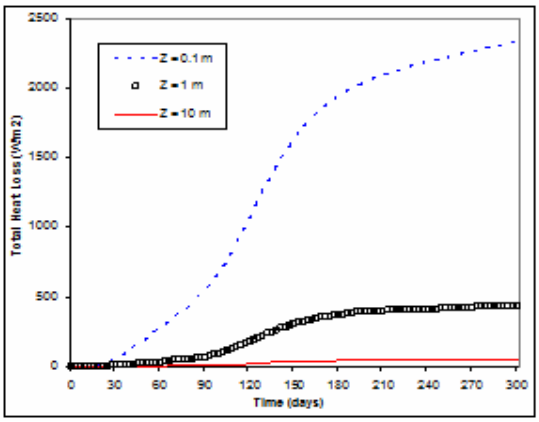


Fig. 4.20: Effect of Boundary-Thickness on Total Heat Loss (MCC)

4.4.2 Effect of Reservoir Thickness

Figs. 4.21 and **4.22** depict the performances for reservoir thicknesses of 10, 20 and 40 m. As would be expected, heating-rate increases with decreasing reservoir thickness. However, although heat loss is accelerated in the thin systems, the late-time results indicate the rate of heat-loss is not quite sensitive to the formation thickness. Although more pronounced, similar results are obtained for the CO_2 case (**Fig. 4.23**). In essence, the accelerated heat-loss partly explains the less competitiveness of thermal methods in thin formations (Hart, 2006).

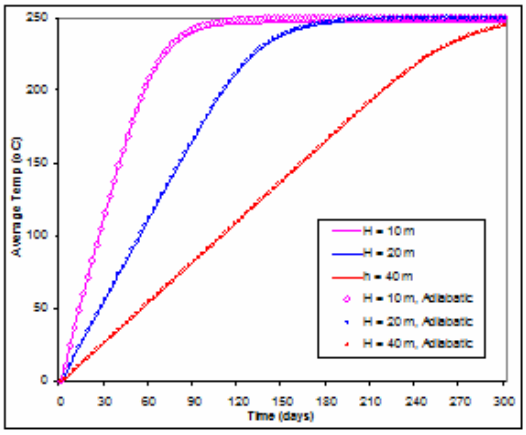


Fig. 4.21: Effect of Reservoir-Thickness on Average Temp (MCC)

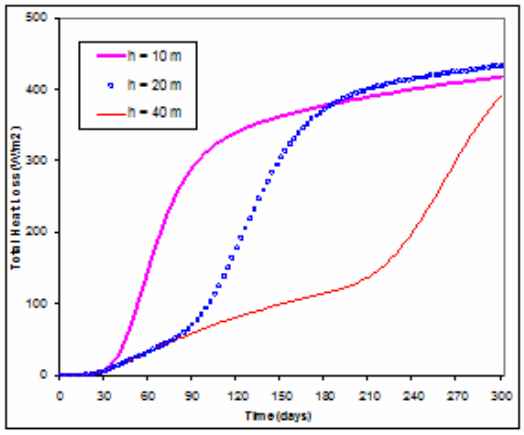


Fig. 4.22: Effect of Reservoir-Thickness on Total Heat-Loss (MCC)

For greater clarity on how the formation thickness affects thermal efficiency, we consider cumulative heat losses rather than just instantaneous losses. **Fig. 4.24** shows temporal variation of cumulative total heat-loss (in GJ m^{-2}) for the three thicknesses and two processes under discourse. From these results, it is evident that the quantity of heat-loss to adjacent strata varies inversely as the reservoir thickness. It is interesting to note that the same conclusion was reached by Gomaa (1980) on the basis of rigorous reservoir-simulation studies.

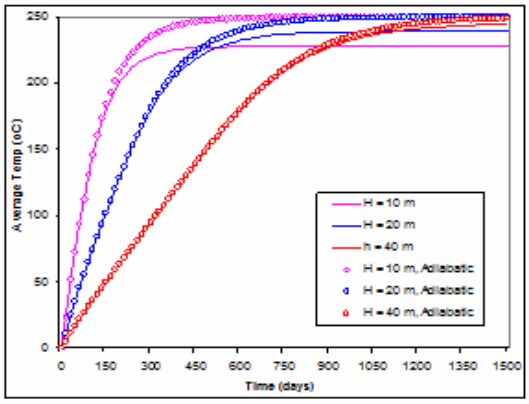


Fig. 4.23: Effect of Reservoir-Thickness on Average Temp (CO_2)

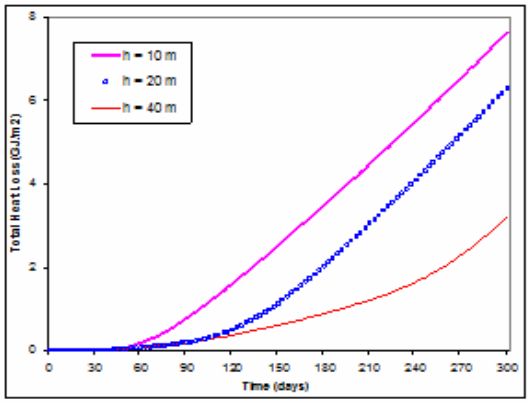


Fig. 4.24: Effect of Reservoir-Thickness on Cumulative Total Heat-Loss (MCC)

4.4.3 Effect of Injection Temperature

Figs. 4.25 and **4.26** show the results for the MCC, operated at 200, 250 and 300 ^{o}C injection temperatures. Although it results in increased heat-leakage, higher temperature accelerates the heating process. As would be expected, heat-flux is proportional to the heating temperature (actually it is the temperature difference between the source and sink but here, sink is at 0 ^{o}C). However, the dependence of heat-flux on the injection temperature is non-linear, as can be seen from the relative magnitude of the fluxes in **Fig. 4.26**.

By these results, it is not likely that maximum heat-conservation (favoured by low-temperature) and accelerated heating (offered by high-temperature) could be achieved at the same time. Hence, choosing between high and low injection temperatures calls for rigorous analysis. This point would be revisited in Chapter 7, when discussing the optimisation of a steam-injection process.

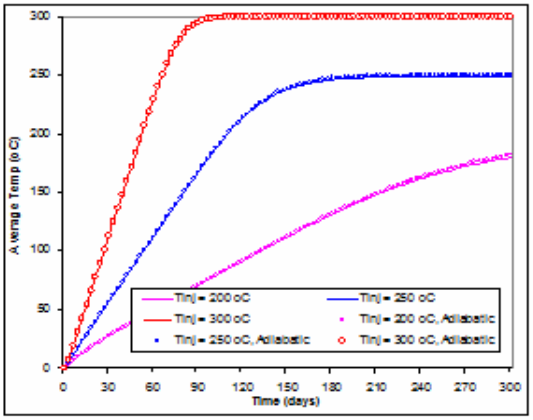


Fig. 4.25: Effect of Injection-Temp on Average Temp (MCC)

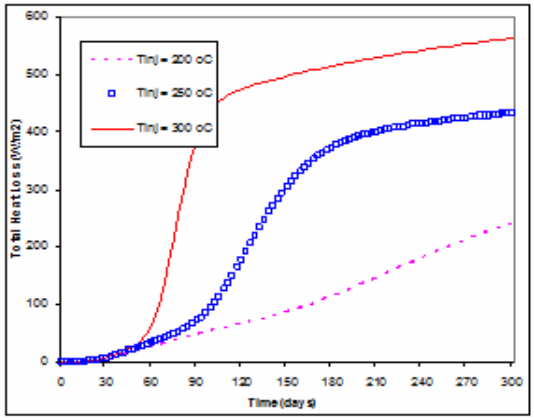


Fig. 4.26: Effect of Injection-Temp on Total Heat-Loss (MCC)

4.4.4 Effect of Heat-Transfer Coefficient of Fluids Adjacent to Boundaries

Given the range of input data assumed, we estimate that the heat-transfer coefficients of gas and liquid-filled porous-media lie within 0.1-20 and 60-1000 W m^{-2} K^{-1}, respectively. It is interesting

to note that this range coincides with the 2-25 and 50-1000 W m^{-2} K^{-1}, which describe the free-convection of gas and liquid in industrial systems, respectively (Cengel and Boles, 2002). In the following discussion, we use the full range of estimated coefficients to rationalise how the nature of sink fluid, its flow regime and thermodynamic properties affect heat-transport in the reservoir.

Fig. 4.27 illustrates the temporal variation of the average temperature in the case of MCC. In this example, the rate of reservoir-heating is largely independent of the fluid that saturates the layers adjacent to the overburden and underburden. However, the effect is more pronounced on the loss (**Fig. 4.28**), indicating that, for the same set of conditions, gas-filled boundaries provide better heat containment than their liquid-filled counterparts.

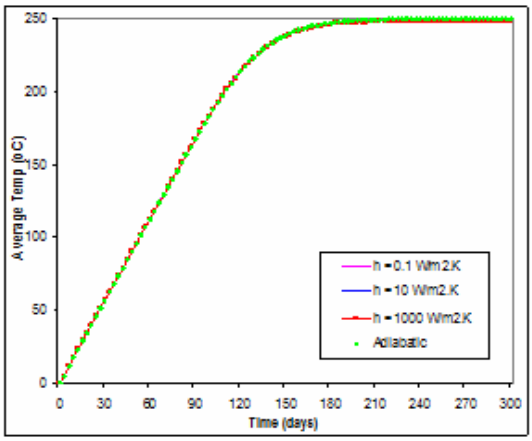


Fig. 4.27: Effect of Boundary Fluids' Heat-Transfer Coefficient on Average Temp (MCC)

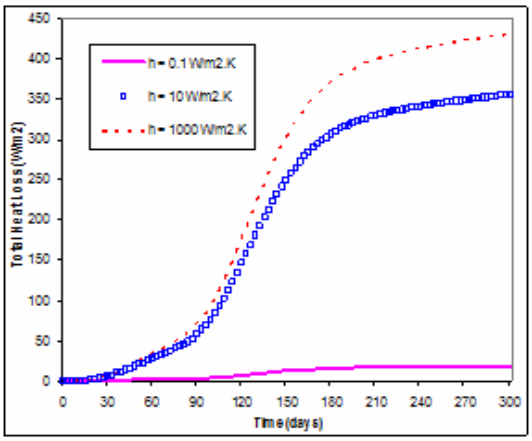


Fig. 4.28: Effect of Boundary Fluids' Heat-Transfer Coefficient on Total Heat-Loss (MCC)

4.5 Characterisation of Thermal Floods for Adiabatic Analysis

In Chapter 3, for isothermal boundary conditions, we established that permeability is an important in-situ parameter affecting reservoir-heating. But from the analyses in the current chapter and Appendix **D**, we deduce that the boundary-thickness and thermal conductivity also have much influence on reservoir-heating. Therefore, we investigate the prospects of using reservoir-permeability as well as boundary-thickness and conductivity for "characterising" steam-injection processes. While permeability influences the rate at which heat is supplied to the boundaries, a combination of boundary conductivity and thickness uniquely determines the thermal-insulation quality of the boundaries. By "characterisation", we mean the ability to predict whether the average system dynamics would be approximately adiabatic; hence allow the use of the simpler adiabatic analysis.

From **Eq. 4.8** and Appendix **D**, we infer that the conductive-resistance R_{th}, defined below, is a suitable candidate for the thermal characterisation of reservoir boundaries, as it combines both the boundary geometry and conductivity.

$$R_{th} = Z/\kappa\,, \tag{4.29}$$

where Z and κ refer to the cap and base-rock, as appropriate.

We conduct an iterative analysis, in which we fix other parameters and evaluate the effects of R_{th} and heat-transfer coefficient. We begin by perturbing only R_{th}, and evaluating the effects on the heating-rate and heat-flux to the surroundings. Here, we assume that:

- Cap and base rocks have the same conductive-resistance.
- Except stated otherwise, injector-base rock distance is 5 m while reservoir thickness and permeability are 20 m and 100 mD, respectively.

The first assumption simplifies the analysis while the second ensures there is sufficient time for boundary heat-fluxes and their effects to manifest.

4.5.1 Effect of Boundary Conductive-Resistance

Fig. 4.29 shows the average temperatures for the MCC when R_{th} = 0.01 m^2 K W^{-1}. With the exception of the 1,000 W m^{-2} K^{-1} case, heating is not quite sensitive to the boundary saturants (convective coefficients). Although the temperature effect is not significant, the insulation capacity of overburden and underburden varies inversely as the convective-coefficients of the adjacent fluids.

Fig. 4.30 presents instantaneous overburden and underburden heat fluxes. Within the simulation time, while cap-rock heat-flux has reached steady-state, the base rock is still in transient. However, it is clear that reservoir-surrounding heat flux depends on the type of boundary saturant. Similar analysis shows greater sensitivity in the case of CO_2 heating (**Figs. 4.31** and **4.32**).

On these results ($R_{th} \leq 0.01$ m^2 K W^{-1}), we revisit the planned replacement of the top water by air in Encana's Borealis project (Roche, 2008). In this case of low conductive-resistance of the boundaries, it may be beneficial to "engineer" the boundary fluids, at least from a heat-containment perspective.

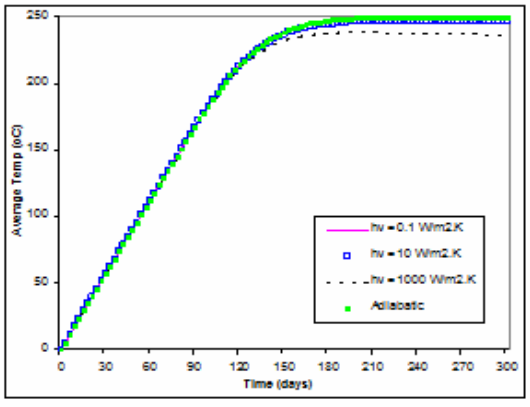


Fig. 4.29: Effect of Boundary Fluid on Average Temp, R_{th} = 0.01 m^2 K W^{-1} (MCC)

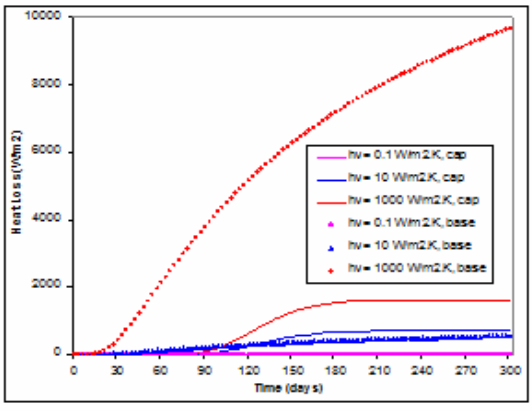


Fig. 4.30: Effect of Boundary Fluid on Cap / Base Rock Heat Loss, R_{th} = 0.01 m^2 K W^{-1} (MCC)

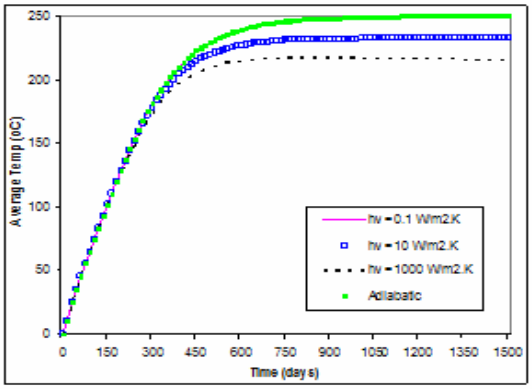


Fig. 4.31: Effect of Boundary Fluid on Average Temp, R_{th} = 0.01 m^2 K W^{-1}(CO_2)

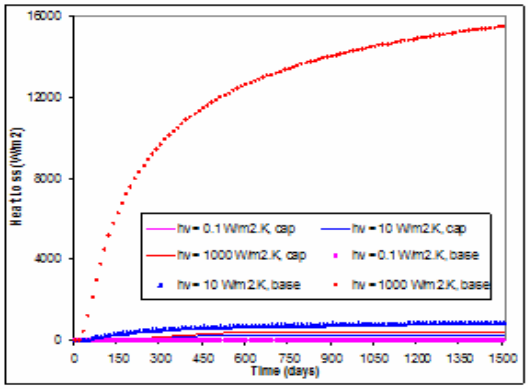


Fig. 4.32: Effect of Boundary Fluid on Cap/Base Rock Heat-Loss, R_{th} = 0.01 m^2 K W^{-1} (CO_2)

We perform the foregoing analysis for several R_{th}, including 0.1, 1 and 10 m^2 K W^{-1}. However, space constraint limits the next discussion to the case of 15 m^2 K W^{-1}, found to be the minimum boundary-resistance required for "satisfactory" adiabatic result in the current example. Our definition of "satisfactory" is based on the maximum heat-efflux not exceeding 1% of the net heat injected. Apparently, this minimum would not be 15 m^2 K W^{-1} if the current cut-off of 1% is changed.

In the case of R_{th} = 15 m^2 K W^{-1}, the MCC results are illustrated in **Figs. 4.33** and **4.34**. The temperatures of the approximate adiabatic and theoretical adiabatic cases are virtually the same. In all cases, the difference between the temperatures is within 0.5%. On the other hand, when the heat losses for R_{th} = 0.01 and 15 m^2 K W^{-1} are compared, 99% of the heat-loss in the former is saved. It is interesting to note that the same deduction was made from the case of CO_2 heating.

In conclusion, for the 20 m thick, 100 mD formation studied, 15 m^2 K W^{-1} is the minimum boundary conductive-resistance required to achieve adiabatic conditions. When this condition is satisfied, the average system dynamics is not likely to depend on the type of fluids in the vicinity of the cap and base rocks. Given this condition, any re-engineering of fluids in the neighbourhood of the boundaries is not likely to achieve significant improvement on reservoir performance.

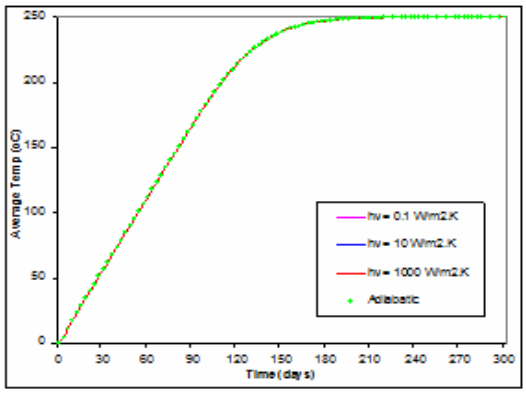


Fig. 4.33: Effect of Boundary Fluid on Average Temp, R_{th} = 15 m^2 K W^{-1} (MCC)

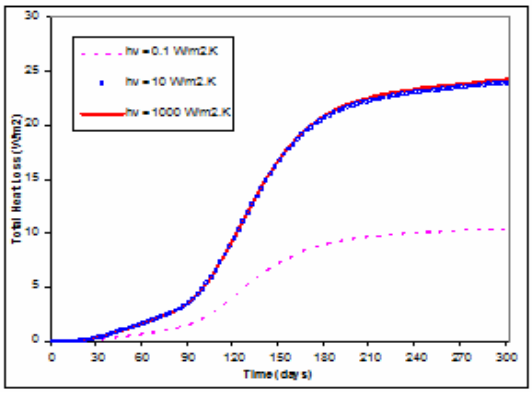


Fig. 4.34: Effect of Boundary Fluid on Total Heat Loss, R_{th} = 15 m^2 K W^{-1} (MCC)

4.5.2 Effect of Permeability on Minimum R_{th}

We now investigate the sensitivity of minimum conductive-resistance to formation permeability, while keeping other factors constant. In the case of dependency, we establish the minimum R_{th} for a set of permeabilities. In principle, the results from this limited set should be relevant for practical purposes. However, the following discussion presents the results for the case of CO_2 heating, which is more vulnerable to heat losses than the MCC.

Figs. 4.35 and **4.36** show the results in the case of k_{vs} = 1000 mD for selected R_{th}. In this example, all the temperature responses are in excellent agreement with the adiabatic behaviour. However, the case of 0.5 m^2 K W^{-1} violates the criterion of limiting the steady-state relative heat-flux to 1 %. Hence, we infer that the 1000 mD system requires that $R_{th} \geq 1$ m^2 K W^{-1} in order to behave as an adiabatic system.

Following the foregoing procedure, we obtain a simple relationship between minimum R_{th} (R_{thmin}) and permeability (**Fig. 4.37**), in which R_{thmin} reduces with increasing permeability. In general, this simple correlation indicates that given the same boundary properties, the effect of thermal losses on convective processes would be less severe compared to conductive processes.

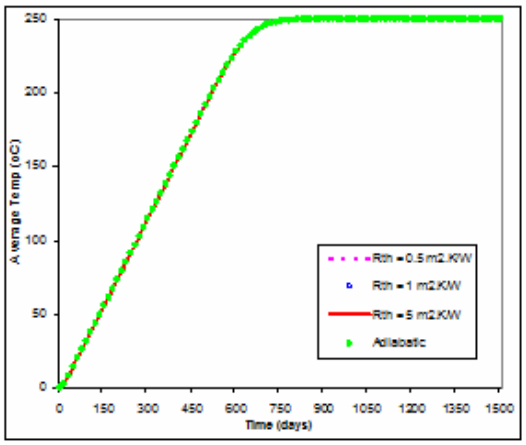


Fig. 4.35: Sensitivity of Average Temp to R_{th} in a Convective (1,000 mD) Reservoir (CO_2)

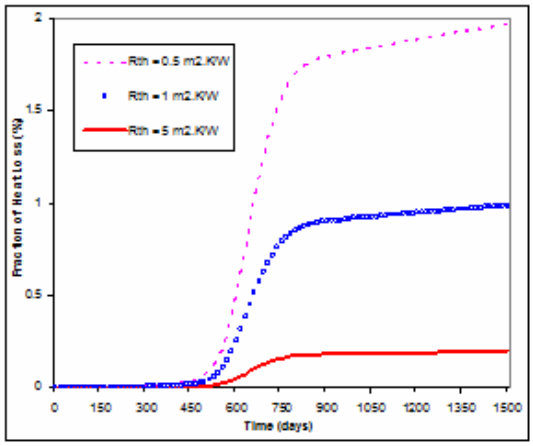


Fig. 4.36: Sensitivity of Total Heat Loss to R_{th} in a Convective (1,000 mD) Reservoir (CO_2)

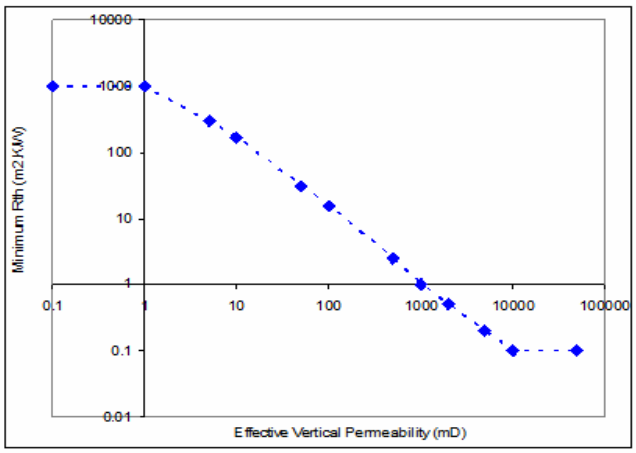


Fig. 4.37: R_{th_min} for Approximate 'Adiabatic' Behaviour

For the range of heat-transfer coefficients (*h*) studied, we found that R_{th} correlates very well with the overall heat-transfer coefficient, *U*. In fact, we observe that R_{th} is roughly the reciprocal of *U*, as the effects of the heat-transfer coefficients are less significant. This finding is quite important for practical applications. In essence, it implies that R_{th} is sufficient for characterising the heat-containment potentials of a reservoir, even with limited knowledge about the boundary saturants.

Given the reservoir permeability, in line with the preceding argument, we only need to estimate R_{thmin} from **Fig. 4.37** and compare it with R_{th} of the subject formation boundaries. If $R_{th} \geq R_{th\,\min}$, it is likely that some 99% of heat injected would not leak through the boundaries. If otherwise, we may consider re-engineering the boundary fluids to make up the shortfall in the insulation capacity of the boundary layers. An obvious example of fluid re-engineering is the creation of a "gas-blanket" around the top and bottom boundaries. In principle, the existence of such gas layers explains why the SAGP process typically yields better thermal performance than its SAGD counterpart (Butler, 2004; 1998). Therefore, the prospect of the SAC and SAF processes to generate a top-gas column may lead to better thermal efficiencies than the steam-alone process. We revisit this issue in Chapter 9.

In principle, the issue of engineering the boundary fluids should be viewed as a way of augmenting the deficit by the natural boundaries in heat containment. Although we do not have information on the characteristics of the formation(s) in the Encana's Borealis project (Roche, 2008), we recommend that analysis of the type presented here should be perfomed to justify the proposed displacement of the original water column in order to create a top air-column.

4.6 Further Tests of Robustness of the Adiabatic Criterion

Finally, we conduct additional checks on the proposed adiabatic criterion (**Fig. 4.37**). We evaluate its sensitivity to reservoir thickness and injector position. Here, we consider formation thickness of 10, 20 and 30 m while the injector is just 0.1 m above the base-rock. These cases are

much different from the thickness of 20 m and injection-underburden distance of 5 m used to develop the criterion.

Fig. 4.38 presents the results for different reservoir thickness. Although heating-rate varies inversely as reservoir-thickness, the adiabatic and 'approximate' adiabatic solutions agree very closely. As depicted in **Fig. 4.39**, although instantaneous heat flux varies with reservoir-thickness, the steady-state behaviours are the same, within 1% of injection rate. Note that in this case, the heat loss is immediate because of the proximity of the injector to the base-rock.

The responses for different initial and injection temperatures are shown in **Figs. 4.40** and **4.41**, respectively. Again, the results confirm the isothermal-boundary analysis (Chapter 3) that reservoir-heating improves with injection temperature (pressure). As its performance is not affected by formation thickness, injector position and injection temperature, we conclude that the proposed criterion of permeability-dependent conductive-resistance is sufficient for evaluating prospective adiabatic dynamics.

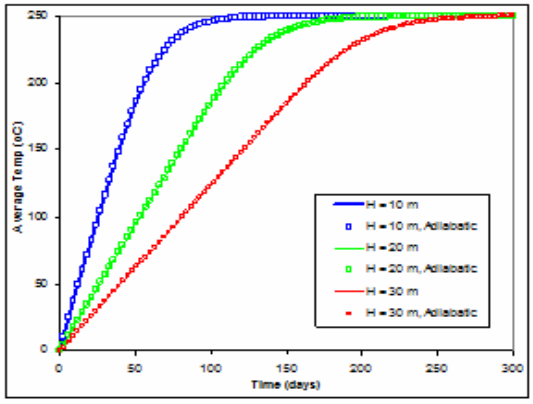


Fig. 4.38: Approximating Adiabatic Conditions for Different Thickness but Same K_v and R_{th} (MCC)

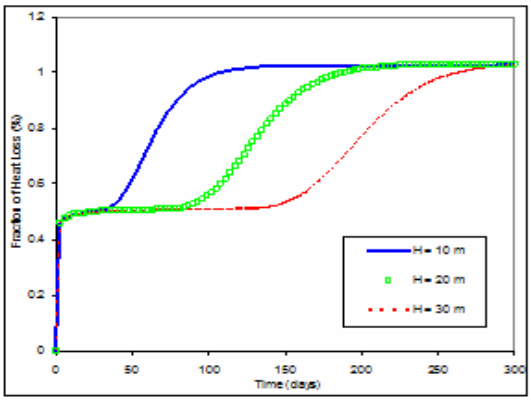


Fig. 4.39: Fractional Total Heat-Loss for Different Thickness but Same K_v and R_{th} (MCC)

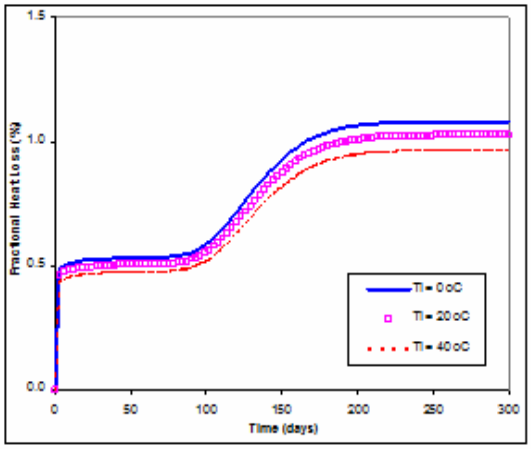


Fig. 4.40: Fractional Total Heat-Loss for Different Initial Temp but Same K_v and R_{th} (MCC)

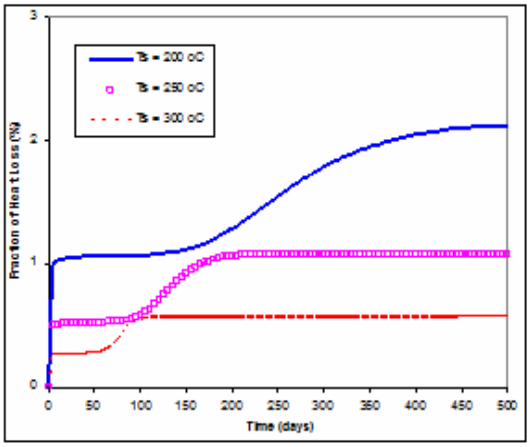


Fig. 4.41: Fractional Total Heat-Loss for Different Injection Temp but Same K_v and R_{th} (MCC)

4.7 Chapter Summary

Taking advantage of the well-established heat-exchanger theory, the heat-transport models, which include FCC and MCC, have been extended to reservoir systems with non-isothermal boundary conditions, with the primary objective of understanding the impacts of thermal losses through the reservoir cap and base rocks on the overall heating process. As part of this novel approach, methods of estimating the heat-transfer coefficients of porous media have been formulated. Additionally, we have investigated how the fluids in the vicinity of the boundaries on one hand, and the characteristics of the boundary layer on the other hand, affect the performances of thermal floods.

From single-variable parametric studies and multi-variable experimental design, it is established that thermal floods become increasingly sensitive to boundary thermal losses if the rate of heat supply by the process is less than that of heat removal through the boundaries. In other words, sensitivity to heat losses declines with effectiveness of the prevailing heating process.

Regardless of the prevailing method of thermal recovery and the nature of boundary fluids, conditions under which the adiabatic assumption would yield satisfactory results are presented. Specifically, it is demonstrated that reasonable information on the formation permeability and the conductive resistances of the boundaries are sufficient for assessing the suitability of potential thermal floods for adiabatic analysis on one hand, and evaluating the performance risks of “modifying” the boundary fluids on the other hand.

Chapter 5

Asphaltene-Induced Formation Damage

When crude oil is analysed in terms of the polarisability and polarity of the components, it is essentially a mixture of saturate, aromatic, resin and asphaltene, with polarity increasing in that order (Fan and Buckley, 2002). Typically, asphaltene is a key component of heavy oils (Bowden *et al.*, 2009). However, despite their role in defining the bulk properties of crude, the chemistry of asphaltenes is not well established (Badre *et al.*, 2006; Jamaluddin *et al.*, 2002). Instead, they are generally understood to be polar, polyaromatic, friable and infusible solid, existing as microcolloidal suspension in crude oil (Badre *et al.*, 2006; Srivastava *et al.*, 1999a). One way of classifying them is that they are that fraction of crude that is soluble in light aromatic solvents such as toluene and xylene but insoluble in excess of light alkanes, particularly *n*-pentane and *n*-heptane (Nabzar and Aguiléra, 2008; Hamadou *et al.*, 2008; Zekri *et al.*, 2001; Srivastava *et al.*, 1999a). Under appropriate conditions vis-à-vis temperature, pressure and compositional changes (Fisher *et al.*, 2003; Hirschberg *et al.*, 1984), crude oil may be destabilised to precipitate, flocculate and deposit asphaltene particles (aggregates). Severity of the problem is more pronounced when active precipitants, such as CO_2 and N_2, come into contact with crude oil (Dahaghi *et al.*, 2008; Srivastava *et al.*, 1999a). Considering that our proposed alternating-injection process involves CO_2, which is a proven precipitant, it is pertinent to investigate potential asphaltene-related problems.

Productivity and injectivity decline due to asphaltene deposition is a common operational problem in petroleum engineering (Kokal *et al.*, 2003; Cenegy, 2001). As solid deposits, asphaltenes plug the pores and throats, reducing in-situ permeability (Minssieux *et al.*, 1998; Ali and Islam, 1997). Their formation-degrading effects of permeability impairment and wettability alteration have been previously investigated and analysed (Nasri and Dabir, 2009; Hamadou *et al.*, 2008; Shedid, 2001; Leontaritis *et al.*, 1994; Leontaritis, 1989). Downstream, asphaltenes may deposit in pipelines and heat exchangers, resulting in considerable cost, energy and safety penalties (Machietto *et al.*, 2011; Leontaritis and Mansoori, 1988).

Although several models exist for induced permeability damage (Mendoza de la Cruz *et al.*, 2009; Wang and Civan, 2001; Minssieux *et al.*, 1998; Ali and Islam, 1998; 1997), they rely on fitting a large number of adjustable parameters and their overall predictive performance is not as good as one would expect. Some of the difficulties stem from our limited understanding of the physics of the process, which is evident in the different approaches and assumptions used in the cited works.

An important observation is that virtually all the current models were developed for open systems or the so-called flow processes. An open system involves continuous introduction of asphaltene mixture into the porous medium, leading to progressive increase in the in-situ asphaltene concentration. In other words, open systems are characterised by accumulative effects. But a critical evaluation of typical field occurrences would reveal that the asphaltene deposition is

more consistent with the closed system model. In a typical operation, asphaltene-free injectants such as CO_2, natural gas, or flue gas are introduced into the oil reservoir. Although the injection streams are asphaltene-free, the injectants are asphaltene precipitants. Hence, their contact with the native crude causes the precipitation, flocculation and eventual deposition of native asphaltenes. Thus, at no time during reservoir development would the in-situ asphaltene concentration exceed the initial value because no fresh stream of asphaltene comes in. This scenario contrasts sharply with the usual laboratory procedure (Fadili *et al.*, 2009; Sim *et al.*, 2005), where an asphaltene suspension is continuously injected (several pore-volumes) into a porous medium. The filtration effect of the medium allows building-up the in-situ concentration beyond the initial value. We are of the opinion that, the latter, which is an accumulative process, is a poor approximation of typical field occurrences. Hence in order to model the effects of formation plugging in flow processes, we initially consider non-flow processes (closed system), with an additional advantage that, due to simplicity, they offer more fundamental physical insights. As they are non-accumulative, the closed-system analysis should yield the lower limits of formation impairment, and provide useful inferences for the more complex flow processes that entail deposition under dynamic conditions.

In this Chapter, we conduct theoretical studies on the key mechanisms of formation impairment in closed and open systems. The resulting mathematical models are validated with published experimental datasets, representing common porous media such as sandstone, carbonate and glass-bead. Finally, we design and conduct independent set of experiments to further validate and characterise the asphaltene-damage models proposed in this work. While acknowledging wettability alteration as an aspect of asphaltene-induced formation damage (Amin *et al.*, 2011, 2010), the current research is limited to the impairment of permeability, porosity and pore-throat.

5.1 Theoretical Studies

In order to simplify the complex problem of asphaltene-induced formation damage of petroleum reservoirs, we delineate the reservoir into two zones, namely closed and open, indicating areas that conform to the closed (non-flowing) and open-system (flowing) approximations, respectively. In this section, we formulate important expressions that describe the impairment of some porous-media properties. The models presented herein are applicable to both closed and open systems.

5.1.1 Formation-Impairment Model

We postulate that asphaltene flocs adhere to the pore walls (in a water-wet system, adjacent to the connate water) and that the deposits form multiple layers, originating from the wall (Minssieux *et al.*, 1998). **Fig. 5.1** depicts the ideal symmetric deposition and the more realistic asymmetric deposition models. Note that the asymmetric model may be applicable in the case of asphaltene flocs exceeding a critical size, above which gravity becomes important. In principle, in order to estimate the fraction of the flow path clogged by the deposits, in this work we are more interested in the equivalent pore volume occupied by the deposits, rather than the geometry of deposition.



(a) Symmetric Deposition **(b) Asymmetric Deposition**

Fig. 5.1: Axial View of Asphaltene-inflicted Pores

5.1.1.1 Porosity-Reduction Model

In the following derivation, we exploit the colloidal and reconstitution theories of heavy oil (Nabzar and Aguiléra, 2008; Luo and Gu, 2007, 2005; Hénaut *et al.*, 2001; Kawanaka *et al.*, 1989; Pfeiffer and Saal, 1940), allowing for the existence of distinct solid and liquid phases. Assuming that the equivalent pore volume (less connate water), V_c, is occupied by crude oil, we can partition it between the volume occupied by maltene (asphaltene-free oil), V_m, and the volume occupied by the deposited asphaltene, V_a,

$$V_c = V_m + V_a \,. \tag{5.1}$$

Recognising that asphaltene deposits plug the flow path, for unit-mass of mixture in the pore, the remaining fraction of initial pore volume available for flow after deposition of all asphaltene is,

$$\frac{V_{post-damage}}{V_{original}} \equiv \frac{V_m}{V_c} = \frac{(1-x_a)\rho_c}{\rho_m}, \tag{5.2}$$

where ρ_c is the density of original crude, ρ_m is the maltene density and x_a is the mass fraction of asphaltene in the original crude. In other words, for every gram of heavy oil transported through the pore-throats, there is potential to precipitate and deposit, under suitable conditions, x_a grams of asphaltene particles. Consistent with **Eq. 5.1**, we obtain a simple mixing rule for the density of the crude oil in terms of x_a,

$$\rho_c = \frac{\rho_m \rho_a}{x_a \rho_m + \rho_a (1-x_a)}, \tag{5.3}$$

where ρ_a is asphaltene density. Assuming that ρ_m and ρ_a are constant, **Eqs. 5.2**-**5.3** indicate that the asphaltene concentration, measured by x_a, is the primary control of the plugging of pore-volume. This conforms to the reconstitution principle underlying published dependency of crude rheology on asphaltene content (Luo and Gu, 2005; Chakma *et al.*, 1994). Consequently, the problem somewhat simplifies to understanding the dynamics of in-situ asphaltene concentration.

Making use of **Eqs. 5.2**-**5.3** allows us to express the change in porosity, following asphaltene deposition and adsorption, in terms of quantities known beforehand,

$$\frac{V_{post-damage}}{V_{original}} \equiv \frac{\phi_{post-damage}}{\phi_{original}} \equiv \frac{\phi_d}{\phi_i} = \left(1 - \frac{x_a \rho_c}{\rho_a}\right). \tag{5.4}$$

It must be emphasised that the pore volume, as used here, refers to the connected porosity, ϕ. If the deposition is accumulative, for instance in processes involving continuous flow of asphalted crude, both ρ_c and x_a are time dependent quantities within the porous system.

5.1.1.2 Permeability and Pore-radius Impairment Models

At the lowest level of homogeneity vis-à-vis flow unit, permeability k, and porosity ϕ, are reasonably correlated with power-law functions (Bernabe *et al.*, 2003; David *et al.*, 1994),

$$k \propto \phi^n , \tag{5.5}$$

where n is the exponent of the power-law relationship. The exponent n is nearly always treated as an adjustable parameter, which characterises the intrinsic flow properties of the porous medium including its lithology and facies (Lawal and Onyekonwu, 2005; Bernabe *et al.*, 2003). For most rock types, n falls within the range 2-10 (Fazelipour, 2005; Sisavath *et al.*, 2003; Ring *et al.*, 1994), though $n > 20$ and $n < 2$ have been used to describe some uncommon rock evolution processes and rock types (Bernabe *et al.*, 2003; David *et al.*, 1994).

Combining **Eqs. 5.4** and **5.5**, we derive the ratio of damaged and original permeability,

$$\frac{k_{post-damage}}{k_{original}} \equiv \frac{k_d}{k_i} = \left(1 - \frac{x_a \rho_c}{\rho_a}\right)^n . \tag{5.6}$$

Furthermore, we can obtain the following relationship between the damaged and undamaged pore sizes,

$$\frac{r_{post-damage}}{r_{original}} \equiv \frac{r_d}{r_i} = \left(1 - \frac{x_a \rho_c}{\rho_a}\right)^{(n-1)/2} , \tag{5.7}$$

by making use of the result that the average pore radius can be estimated from permeability and effective porosity (Stolz and Graves, 2003; Amaefule *et al.*, 1993),

$$r = \sqrt{k/\phi} . \tag{5.8}$$

In summary, **Eqs. 5.3**, **5.4**, **5.6** and **5.7** describe a consistent approach to estimate the extent of formation damage induced by asphaltene deposition. However, as most realistic processes involve continuous deposition, there is a need to take into account that x_a will change with time. Hence, in subsequent discussions on flow (open systems) processes, we replace x_a by the term x_p, which denotes the instantaneous concentration of deposited asphaltenes. Consequently, we have the following set of damage models for damage under dynamic conditions,

$$\rho_c(t) = \frac{\rho_m \rho_a}{\rho_m x_p(t) + \rho_a (1 - x_p(t))} , \tag{5.9}$$

$$\frac{\phi_d(t)}{\phi_i} = \left(1 - \frac{x_p(t)\rho_c(t)}{\rho_a}\right), \tag{5.10}$$

$$\frac{k_d(t)}{k_i} = \left(1 - \frac{x_p(t)\rho_c(t)}{\rho_a}\right)^n, \tag{5.11}$$

$$\frac{r_d(t)}{r_i} = \left(1 - \frac{x_p(t)\rho_c(t)}{\rho_a}\right)^{(n-1)/2}. \tag{5.12}$$

In section **5.3**, we describe the derivation of a model that predicts the time-variation of deposited concentration, $x_p(t)$.

5.2 Damage in Closed Systems

Although less common than the flow processes, "non-flow" experiments have also been performed. These include cases of asphaltene suspensions left to "age" in cores (Kocabas, 2003; Sharma *et al.*, 1992). In the study conducted by Sharma *et al.* (1992), the injection of one pore-volume (PV) of asphalted oil and precipitants can be regarded as a batch process. Similarly, experimental procedures that involved following a forward-flooding operation with reverse-flooding are also taken to approximate a closed system (Kocabas, 2003). Additionally, the so-called static experiments, such as those reported by Shedid and Abbas (2005), whereby cores are first soaked in asphaltene solution then withdrawn to age, may also be classified as closed. Further example of static experiment was recently performed by Al-Huraibi and Belhaj (2010), in which an electrolytic cell was set-up using graphite electrodes and asphalted crude oil. Asphaltene precipitation and deposition was induced by electrical charge through the solution.

In order to further our understanding of the complex physics of formation plugging under flowing conditions, we implement the set of semi-analytic models derived above. The set of equations **5.3**, **5.4**, **5.6** and **5.7** describes asphaltene-induced porosity reduction, pore-throat damage and permeability impairment in closed systems (under "stagnant" conditions). The model is validated by optimising a single adjustable parameter by recourse to the experimental data. Further, we present simplified dynamics of asphaltene deposition under non-flow conditions. In principle, results from closed systems offer key insights and can be used as benchmarks for the more complex flow (open) processes which, with the elapse of time, are inherently accumulative of asphaltene deposits, and have relatively shorter time scales of induced damages.

5.2.1 Model Validation for Closed Systems

Proposed model for permeability damage under static conditions is used to analyse the results of experiments performed by Sharma *et al.* (1992) and Kocabas (2003), conducted on sandstone and carbonate media, respectively. Key experimental data for both experiments are summarised in **Table 5.1**, which also includes results of model validation to be discussed shortly.

Table 5.1: Summary of Reference Experiments and Validation Results

Source	Core	Medium	Medium Properties		Oil Properties		Matching Results	
			Permeability (mD)	Porosity (fraction)	Oil API	Asphaltene content (wt. %)	Parameter *n*	AAD (%)
Sharma *et al.* (1992)	1	Sandstone	236	0.2786	21.2 – 25.7	0 – 12.8	7.7	6.9
Sharma *et al.* (1992)	2	"	2380	0.3267	21.2 – 25.8	0 – 12.8	3	2
Sharma *et al.* (1992)	3	"	1520	0.3125	21.2 – 25.9	0 – 12.8	5.5	4
Kocabas (2003)	VF1	Carbonate	12.66	0.20	24.4	3.7	5.2	0.9
Kocabas (2003)	SU2	"	7.8	0.16	24.4	3.7	7.2	0.9
Kocabas (2003)	WF1	"	4.85	0.16	24.4	3.7	10	6.6

Sharma and co-workers (Sharma *et al.*, 1992) have measured the effect of asphaltene deposition by noting changes in the oil-water relative permeability curves, absolute permeability, displacement performance and oil recovery for three different sandstone cores. Test-set 1 was based on consolidated core, while Test-sets 2 and 3 used unconsolidated cores.

Each Test-set involved four runs performed on the same core. Thus, a total of 12 runs were conducted. For each run, asphaltene was introduced into the core by simultaneous injection of precipitant and crude oil. The degree of asphaltene deposition in each run was achieved by varying the precipitant/oil injection ratio, hence varying the density of injected asphalted mixture. Concentration of deposited asphaltene in run 1 through 4 was 0, 5.1, 9.9 and 12.8 wt%, respectively. Permeability damage for each run was related to the corresponding steady-state asphaltene deposition of 0, 5.1, 9.9 and 12.8 wt%.

Kocabas (2003) conducted a series of experiments on carbonate cores (**Table 5.1**) with the primary objective of characterising asphaltene deposition effect on permeability impairment in carbonate systems. Relative effects of damage mechanisms, such as adsorption and mechanical plugging, were quantified through flow reversal and solvent injection. The relative contributions of convection and dispersion to the overall transport process were also analysed.

Although the experiment, in the forward-flooding mode, was inherently a flow process, with the implementation of reverse-flooding, the net behaviour should approximate no-flow, as the resultant injection was approximately zero. In particular, the injection of cyclohexane, neither an asphaltene precipitant nor solvent, in the reverse flow was consistent with the objective of accounting for adsorption effect. For our purpose of studying a closed system, we are primarily interested in the ratio of permeabilities after flow reversal and before forward flooding. The results of this ratio are available for three cores.

5.2.2 Validation Results for Closed Systems

In order to validate the proposed model (**Eqs. 5.3**, **5.4**, **5.6** and **5.7**), knowledge of density and its variation is required. The density of crude mixture was estimated, using a simple mixing rule (**Eq. 5.3**) from asphaltene mass fraction as well as densities of maltene (asphaltene-free oil) and asphaltene, taken to be 900 and 1160 kg/m^3, respectively (Mehrotra and Svrcek, 1987).

Given representative information about the fluid properties, **Eq. 5.6** implies that the parameter *n* is sufficient to describe permeability reduction for a no-flow process. Hence, this parameter was optimised within the physical range of 2-10 by minimising the average absolute deviation (AAD) between experimental and model data points.

Figs. 5.2-5.4 show the fitting results for the three experimental sets conducted by Sharma *et al.* (1992). We need to emphasise that the ‘‘best’’ match is unique, as there exists a global minimum of AAD that corresponds to just one value of *n*. However, the global minimum is relatively shallow indicating that the accuracy of the experimental data set will play a major role in determining parameter *n*. **Fig. 5.5**, where AAD was plotted against *n,* illustrates the situation for the data pertaining to Core 3. Although *n* = 5.5 was the optimal value, the parameter *n* in the range *n* = 4.8 - 6 would give equally reasonable match.

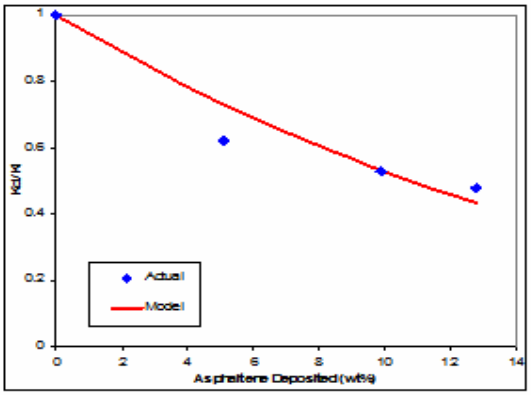


Fig. 5.2: Data of Sharma *et al.* (1992), Core 1

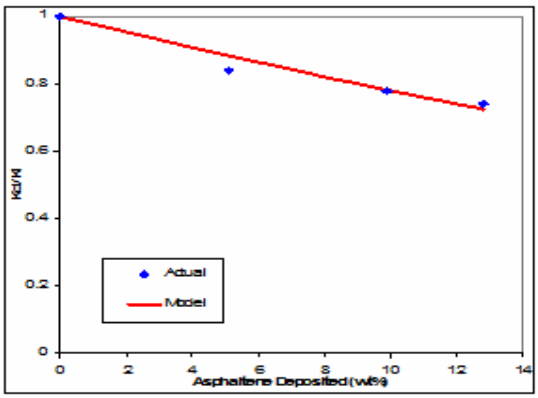


Fig. 5.3: Data of Sharma *et al.* (1992), Core 2

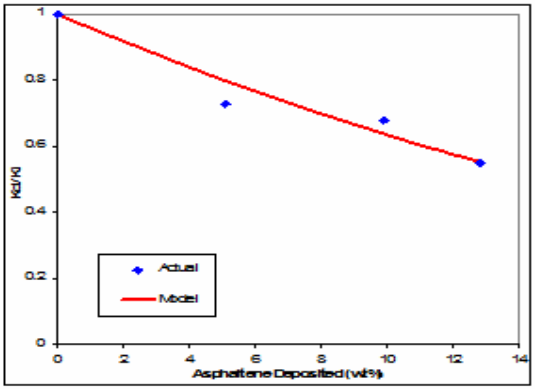


Fig. 5.4: Data of Sharma *et al.* (1992), Core 3

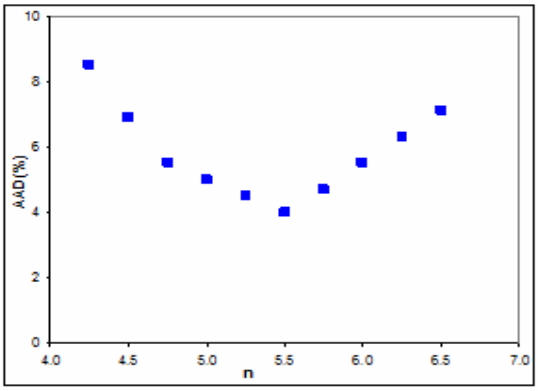


Fig. 5.5: Optimising Data of Sharma *et al.* (1992), Core 3

The datasets of Kocabas (2003) were analysed in a similar fashion to determine the value of parameter *n*. It should be noted that unlike the experiments of Sharma *et al.* (1992) that evaluated effects of asphaltene content on the damage kinetics in the same core, those of Kocabas (2003) were based on a single asphaltene concentration. Consequently, while the optimisation of *n* used multiple data points in each of the experiments of Sharma *et al.* (1992), those of Kocabas (2003) were based on single-point. In this case, the sensitivity of parameter *n* to the accuracy of data, which is unknown, is higher than for the data of Sharma *et al.* (1992). For instance, an error of 1% in a ratio of permeabilities, see **Eq. 5.6**, would change the parameter *n* by the order of 10%.

Notwithstanding the possible large error bars associated with the evaluation of the parameter *n*, we explored a fundamental relationship between matched value of parameter *n* and the initial pore-throat radius, estimated as ($\sqrt{k/\phi}$). **Fig. 5.6** illustrates the relationship, whereby the value of parameter *n* decreases with the increasing pore-throat radius - an indication of greater rock quality. Although we have no information on the accuracy of the two experimental datasets used in the analysis and hence cannot estimate the accuracy of *n* obtained, a linear relationship can be discerned, for the data from the same source, between *n*, an indicator of medium's hydraulic quality and pore radius, which is also an important hydraulic parameter (Stolz and Graves, 2003). These results underscore the appropriateness, at least on flow-unit scale, of using *n* as a quantitative indicator of rock hydraulic quality. This would be revisited shortly, in the discussion of the open-system model.

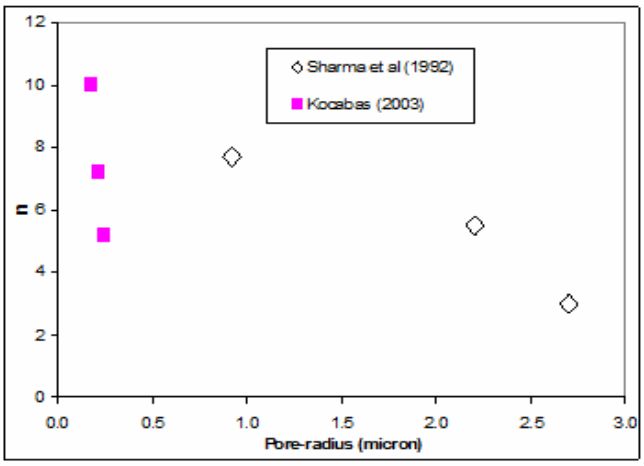


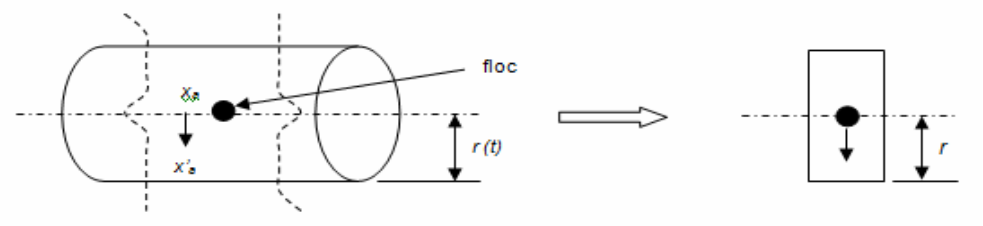
Fig. 5.6: Matched *n* versus Estimated Pore-throat Radius: All Data

5.2.3 Dynamics of Deposition in a Closed System

As long as asphaltene particulates remain in solution or suspension, they are not likely to cause significant problems (ignore bridging and staining effects). However, on being deposited and subsequently adsorbed onto the pore walls, the effective pore volume is reduced. In this section, a simple analysis of the deposition dynamics of asphaltene aggregates is presented. It is assumed

that: (a) deposits are adsorbed (layering) immediately (b) neither deposition nor adsorption is reversible (c) gravity is the dominant force.

Fig. 5.7a depicts a cylindrical pore of radius *r*, with an asphaltene floc being deposited from the centre of the pore in a direction normal to the pore axis. We assume that two phases (liquid oil and solid asphaltene) are present. For simplicity, we develop a 1-D model (**Fig. 5.7b**), taking *r* as our primary direction. We further assume the average behaviour and replace the deposition from the interior of the pore by the deposition from the centre of the pore. Hence, allowing us to define the dynamics by a single characteristic time. Although *r* is time-variant, decreasing with the layering of deposits, we ignore this dependency in the following simplified formulation to obtain a semi-steady state (relative to *r*) analysis.



(a) Actual Configuration **(b) 1-D Simplification**

Fig. 5.7: Schematic of Asphaltene-Floc Deposition in a Closed System

In the following analysis, we consider that the liquid system trapped within the pore-enclosure consists of two liquid subsystems, namely the suspension and deposit. The suspension is a binary system of asphaltene and maltene, with the mass-fraction of the former being x_a. Similarly, the deposit is an asphaltene-maltene mixture but with asphaltene mass-fraction x_a' at any instant. Furthermore, the suspended flocs are assumed to be in a 'queue' such that they are deposited in succession. In reality, this is a fair assumption considering that the suspended particles are not likely to be of the same size, hence would experience different settling velocities, reducing the likelihood of having an instantaneous total depletion of the asphaltenes in the suspension. In addition, using typical rock and fluid properties with floc diameter in excess of 1 nm, we found that the time scale for Brownian motion of the flocs is negligible in relation to that of sedimentation. A similar inference was drawn by other workers (Boek *et al.*, 2010c). As a result, the following analysis ignores dispersion.

Neglecting concentration gradient of asphaltene along the adsorption surface (pore walls) i.e. lumped-parameter analysis, the dynamics of floc deposition can be described by:

$$\rho_c v_s x_a = \rho_c v_s x'_a + \rho_c r \frac{dx'_a}{dt}, \tag{5.13}$$

where v_s is the settling velocity, x_a and x'_a are asphaltene contents (mass-fraction) of the suspension and deposit respectively, and *r* is the average pore-radius. The above mass balance ignores

kinetics of precipitation and flocculation, treating them as instantaneous (Leontaritis *et al.*, 1994). **Eq. 5.13** can be presented as:

$$x_a = x'_a + \tau \frac{dx'_a}{dt}, \tag{5.14}$$

where the single characteristic time-constant is given by

$$\tau = r/v_s . \tag{5.15}$$

We estimate the initial travel distance from initial permeability and porosity thus (Stolz and Graves, 2003):

$$r \approx \sqrt{k_i/\phi_i} . \tag{5.16}$$

We reiterate that this travel distance is time-invariant (same argument is implicit in **Eq. 5.13**) and ignore the effects of asphaltene deposition. Although we could have used **Eq. 5.15** to account for the change in *r*, we refrain from doing so in the present analysis as to maintain the simplicity and keep to the spirit of the previous assumptions made about the average behaviour.

Assuming spherical asphaltene flocs moving under creeping flow conditions (N_{Re} << 1), and taking mixture settling velocity as that of asphaltene flocs dispersed in a continuous phase of maltene, the settling velocity can be estimated from Stokes' law (Tchobanoglous *et al.*, 2003):

$$v_s \approx \frac{(\rho_a - \rho_m) g D_a^{\,2}}{18 \mu_m}, \tag{5.17}$$

where μ_m is the maltene viscosity and *g* is gravitational acceleration.

Although preceding expression for terminal velocity only holds in a gravity-dominated system, we assume that the net effect of other forces such as electrostatic and van der Waals (Al-Huraibi and Belhaj, 2010; Tchobanoglous *et al.*, 2003) would only be to increase the aggregate diameter, D_a without affecting other variables, thus increasing the settling velocity. In principle, the idea of settling velocity is restricted to a single-particle. Here, we are interested in the deposition of a floc, whose existence results in a very dilute suspension; such that the effect of the remaining dispersed particles on this settling floc is negligible.

Strictly speaking, the 'settling' velocity given by **Eq. 5.17** holds when interstitial velocity of the bulk flow is less than (or equal to) this terminal velocity of asphaltene flocs. If it is not, flocs deposition (hence adsorption) rate would be reduced, thereby increasing the time constant. Under the latter scenario, floc entrainment is increased, favouring mechanical entrapment and plugging in the net direction of flow. However, in practice, mechanical plugging (which results when asphaltene-floc size either compares with or exceeds the size of the pore-throat) is easily "treated" by flow reversal (back-flushing), with minimal impacts on adsorption-induced damage (Kocabas, 2003).

By substituting **Eqs. 5.16** and **5.17** into **Eq. 5.15**, the time-constant is expressed as:

$$\tau \approx \frac{18\,\mu_m \sqrt{k_i / \phi_i}}{(\rho_a - \rho_m) g D_a^2}, \tag{5.18}$$

where the maltene density ρ_m, if unknown, can be estimated from known ρ_a and ρ_c according to **Eq. 5.3**,

We recognise that the floc diameter, D_a is a source of major uncertainty. Based on filtration measurements, sizes larger than 100 nm (Leontaritis *et al.*, 1994) and up to 500 nm (Sim *et al.*, 2005) have been reported. On the other hand, Minssieux *et al.* (1998) indicated that their simulation model required a size of 5-20 nm to match their experimental data. Consequently, we limit our studies to the range D_a = 5–500 nm, and arbitrarily assume an average diameter of 200 nm for our simulations. In our opinion, this large range of aggregate diameter is a fair reflection of the complexity of forces (e.g. gravity and electrostatic) that act on the particulates as well as the nature of rock surfaces (Hamadou *et al.*, 2008; Tchobanoglous *et al.*, 2003).

The solution of **Eq. 5.14** yields the following relationship between 'adsorbed' and 'available' (suspension) asphaltene mass fractions

$$x'_a(t) = x_a\left(1 - e^{-t/\tau}\right), \tag{5.19}$$

where *t* is elapsed time.

As we are dealing with a closed system (constant-mass), this implies that although asphaltene adsorption is continuous it would ultimately (asymptotically) reach a state where all the initial mass of dispersed particles is deposited. However in practice, it may be assumed that steady-state is reached at 3τ, corresponding to some 95% of the final value.

Shedid and Abbas (2005) monitored the concentration of deposited asphaltene with time in static experiments conducted on carbonate rocks. Their data, which exhibited a clear asymptote, can reasonably be approximated with a first-order function such as that in **Eq. 5.19**. However, only about 36% of the initial asphaltene content was adsorbed at "steady-state". We suspect that the relatively low steady-state adsorption was probably due to ineffective precipitation and flocculation processes. This position is supported by the observation that neither a precipitant nor flocculant was reportedly used during the experiments.

5.2.3.1 Simulating Dynamics of a Closed System

For an arbitrary set of reference data ρ_a = 1.16 g/cm^3, ρ_m = 0.9 g/cm^3, x_a = 0.3, n = 3, we simulate effects of petrophysics, fluid and asphaltene properties on the dynamics of a hypothetic batch process. Except when stated otherwise, other base-case parameters are k = 500 mD, μ_m = 100 cP, D_a = 200 nm, and ϕ = 0.3. Our batch process, basically a deposition study, consists of uniformly distributed asphaltene aggregates (after precipitating) on the verge of deposition. There is no mass exchange with the surroundings. The following analyses are based on **Eqs. 5.3** and **5.6** as well as

Eqs. **5.15**-**19**. Given our interest in the rate of deposition in a closed system, the simulation of **Eqs. 5.3** and **5.6** entails replacing x_a with x_a' in these equations. In turn, the temporal variation of x_a' is updated according to **Eq. 5.19**. It is worth stating that most of the inferences from the following plots (**Figs. 5.8**-**5.11**) of simulation results can easily be deduced from the time-constant (**Eq. 5.18**); nevertheless the plots provide additional illustrations to support the ensuing discussion.

Fig. 5.8 illustrates how initial permeability influences rate of damage. Although the same amount of damage would ultimately be observed, impairment is accelerated in less-permeable systems. However, the dependency is nonlinear. Conversely, **Fig. 5.9** indicates that the rate of damage correlates positively with initial porosity but the effect is relatively weak. The steady-state is also independent of initial porosity.

Dependence of maltene viscosity (hence, mixture viscosity) on permeability reduction is depicted in **Fig. 5.10**. Noting that viscosity was perturbed by a factor of four compared to permeability's five, it can be concluded that oil viscosity has greater influence on the damage rate. Although not shown, ultimate impairment is independent of viscosity.

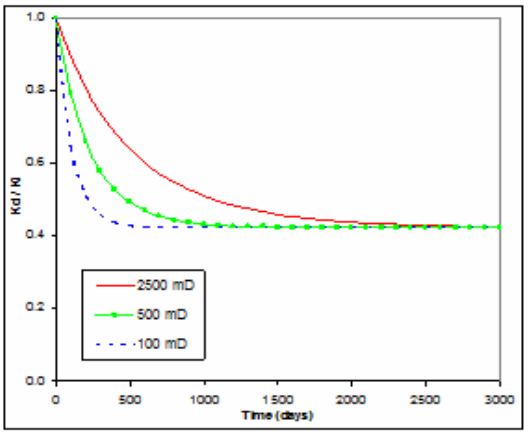


Fig. 5.8: Effect of Initial Permeability on Damage Rate

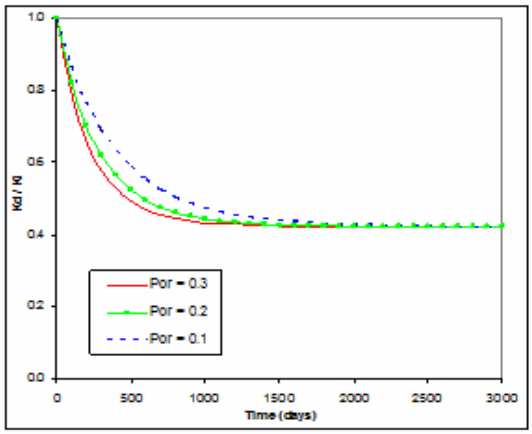


Fig. 5.9: Effect of Initial Porosity on Damage Rate

The viscosity effect is particularly useful as it partly explains the current somewhat counter-intuitive findings of more severe formation damage in lighter oil compared to heavy oil systems despite that the latter is naturally characterised by much higher asphaltene content (Minssieux *et al.*, 1998; Nghiem and Coombe, 1997; de Boer *et al.*, 1995; Hirschberg *et al.*, 1984). Current opinion attributes this to relatively higher content of asphaltene precipitants (low molecular weight paraffins) such as C_3, *n*-C_5 and *n*-C_7 in light oils, whereas heavy oils characteristically contain comparatively higher fraction of asphaltene solvents (light aromatic hydrocarbons) such as benzene and toluene (Nghiem and Coombe, 1997; Sheu and Storm, 1995). While the foregoing may influence the rate of precipitation (due to concentration of particulates), our results indicate that crude viscosity is the key control of deposition rate. This is quite consistent with the observations made by Al-Huraibi and Belhaj (2010) that, over the same time interval, higher voltage was required to stimulate asphaltene deposition in heavy oil systems in comparison to light crudes. Ignoring other

effects, for comparable deposition rate, **Eq. 5.18** stipulates that higher voltage is theoretically equivalent to increasing the effective gravitational acceleration to compensate for high crude viscosity. Apparently, the damage rate in a closed system correlates positively with "effective" body force (*g*), which in theory could be due to gravity, electricity, and / or magnetism.

As would be expected, our results indicate that impairment rate depends strongly on the dimensions of asphaltene flocs (**Fig. 5.11**). However, the final damage is not sensitive to the size of aggregates, a result which is not unexpected in a batch system.

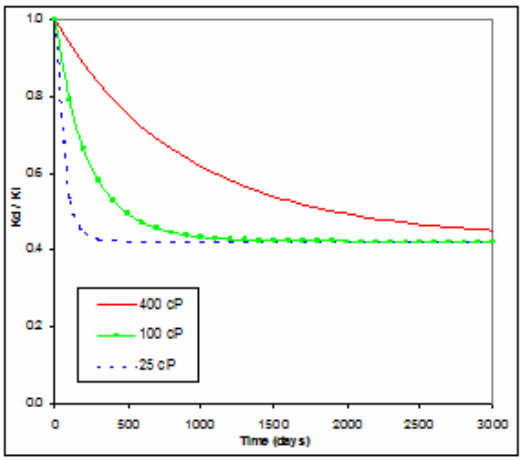


Fig. 5.10: Effect of Maltene Viscosity on Damage Rate

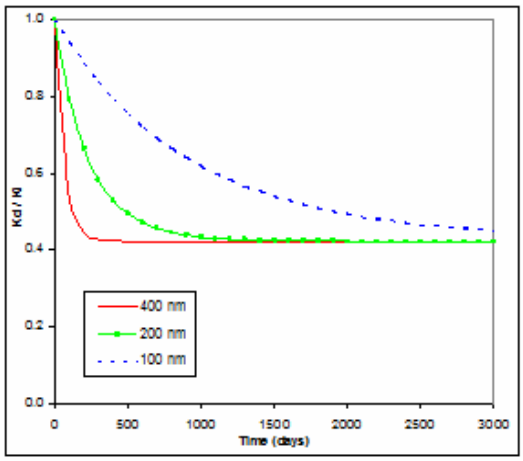


Fig. 5.11: Effect of Asphaltene Aggregate Size on Damage Rate

Based on these simulation results, it can be concluded that among crude-oil properties, oil viscosity and asphaltene floc size, have the greatest influence on the rate of asphaltene-induced permeability impairment in a closed system. Consequently, to control asphaltene-related problems in the porous media, it might be more rewarding (subject to economics and other considerations) to increase in-situ oil viscosity or / and mitigate aggregation of precipitates. However, because increasing oil viscosity is counterproductive (reduced productivity, increased transport costs, etc), we advocate the latter option. The latter option indeed agrees with our current understanding of the natural role of resin in crude oil, which is to stabilise asphaltene. It is understood that resins play this role by reducing the aggregation of asphaltenes (Hirschberg *et al.*, 1984; Koots and Speight, 1975). The use of dispersants, as part of the chemical control strategy, is in line with the philosophy of curtailing particulate aggregation (Amro, 2005). Similarly, the promising application of laser technology for the treatment of asphaltene deposition problems may also be viewed in the context of the latter option (Zekri *et al.*, 2001).

5.3 Damage in Open Systems

Historically, deep-bed filtration (DBF) models have been used to rationalise the formation damage induced by various solid particulates invading the pore space of oil reservoirs, leading to impaired recovery of hydrocarbons. Early work on DBF filtration modelling has been reviewed by

Herzig *et al.* (1970). These models describe particles moving in terms of concentration fields, without explicitly representing the pore space, and include the flow continuity, mass-balance, and kinetic equations for the release of suspended particles. Recently, the sand production problem in oil recovery as a consequence of erosion of sand particles has been successfully studied following a similar approach (Vardoulakis *et al.*, 1996). In addition, Wennberg *et al.* (1996) studied band formation due to fines deposition in porous media. The invasion of particulates from drilling fluids and injection water in reservoir rock has been studied by a combination of experiments and DBF modelling (Bailey *et al.*, 2000; Pang and Sharma, 1997). The DBF theory has also found application in the analysis of synchrotron X-ray experiments (Boek *et al.*, 2010c).

Wojtanowicz *et al.* (1987) presented another set of models based on the DBF and chemical-reaction kinetics. The models describe common pore-blocking mechanisms, such as bridging (cake formation) and entrainment, as well as particle re-mobilisation. However, the practical application of this set of sophisticated models is limited to the diagnosis (pattern recognition) of permeability impairments, partly because of the high number of empirical parameters (> 10).

Models based on surface-excess theory (Gruesbeck and Collins, 1982) have also been used to describe the deposition of precipitated asphaltene in reservoir rock (Wang and Civan, 2005; 2001; Ali and Islam, 1998; 1997). However, the number of fitting parameters used in these studies is often such that the problem is overdetermined and their predictive value is limited. For example, the model proposed by Ali and Islam (1998, 1997) includes over 15 adjustable parameters. One possible way forward to enhance the predictive properties of DBF and other models is to link them to detailed studies of the deposition of colloidal asphaltene in well-defined capillaries (Boek *et al.*, 2008) and to use a multi-scale modelling approach to rationalise the results (Boek *et al.*, 2010a, b).

Unlike water injection operations in which particulates are introduced into the reservoir and are more prone to surface filtration in the vicinity of the inlet, asphaltene suspensions are generated in-situ and flow outwards. Although the latter is more consistent with the DBF theory, the theory may not be quite valid in regions around production wells because of potential drawdown-induced local accumulations. However, with adequate surveillance and regular treatment of near-wellbore accumulations (Leontaritis *et al.*, 1994; Galoppini and Tambini, 1994; Baker *et al.*, 1992), the models proposed in the current research should still be suitable for these susceptible areas. As laboratory studies of asphaltene problems typically involve injection of suspensions, investigators need to be wary of potential surface filtration, though internal filtration is intended, and make necessary allowances for such.

There have been several experiments to elucidate the kinetics and dynamics of asphaltene precipitation. Here, we focus on the dynamics and summarise some of the main recent findings of relevance to the development of the current model. Yudin *et al.* (1998) examined the kinetics of asphaltene aggregation in toluene-heptane mixtures. They reported the existence of a threshold concentration of precipitant (heptane), below which there was no noticeable aggregation. Above this threshold however, the aggregation rate increased markedly. Moreover, the threshold

precipitant concentration depended on both the origin and concentration of asphaltenes in the crude. They also noted that there is a direct relationship between aggregation rate and the concentrations of asphaltene and precipitant.

In another experimental investigation of the kinetics of asphaltene precipitation, Maqbool *et al.* (2009) noted that regardless of precipitant concentration, asphaltene precipitation follows the same trend in which it increases gradually at early times, then goes asymptotic at late times, although the initial kinetics may be masked in very fast reactions. However, both the steady-state quantity of precipitates and the time to reach the plateau are sensitive to precipitant concentration; while the former increased with concentration, the latter decreased sharply.

Rastegari *et al.* (2004) made some instructive observations on the effects of asphaltene and precipitant concentration as well as shear rate on the kinetics of asphaltene flocculation. While flocculation rate and floc size increased with precipitant and asphaltene concentrations, they were impaired by increased shear rate. Nevertheless, in virtually all their measurements, the change in amount precipitated over time was generally consistent with first-order kinetics.

The experimental results of Rahmani *et al.* (2003) also showed a reduction in "steady-state" aggregate size with shear rate. However, they observed that there exists an optimum aggregate size. Initially, both the aggregation rate and floc size increase with increasing shear rate due to enhanced collision frequency, but beyond the optimum size, further increase in shear rate induces shear erosion which fragments the aggregate. The erosion takes place at a lower rate compared to aggregation and ceases when an aggregate size is reduced to another stable configuration. Recently, Nabzar and Aguiléra (2008) reported a negative correlation between deposit thickness and shear rate.

The foregoing examples highlight the importance of kinetics in asphaltene precipitation and eventual deposition. Hence, realistic models of the process should account for kinetics. However, to the best of our knowledge, existing models do not incorporate such kinetics. In the current study, we propose a new DBF-based model which, despite including kinetics, has a much smaller number of model parameters. We show that it is possible to rationalise various experimental results, representing diverse porous media and suspensions, with this new model.

In complement to the impairment models derived in the earlier parts of this Chapter, the following theoretical studies develop deposition models for asphaltene, taking advantage of the DBF theory. In particular, we examine both constant and dynamic-filtration mechanisms.

5.3.1 Deposition under Dynamic Conditions

The porous medium is conceptualised as a homogenous filter bed, with capacity for particle retention. **Fig. 5.12** illustrates a 1-D convective transport of asphaltene-laden stream, accumulation and deposition. The main assumptions are:

- the porous medium is modelled as a 1-D, homogenous and isotropic system. While isotopic and homogeneous conditions may be valid for bead packs and most sandstone media, carbonate systems on micro scale can display sizeable heterogeneities. However, from the viewpoint of present modelling, which is focused on average behaviour, we neglect in the first instance these effects and assume homogeneous representation, even for carbonates;
- asphaltene suspension is injected at constant rate;
- dispersive transport is insignificant. At reservoir scale, advective transport typically dominates diffusion/dispersion component (high Peclet numbers), especially in the net flow direction (Vargas *et al.*, 2010);
- relative to the rate of deposition, kinetics of asphaltene precipitation and flocculation are negligible.
- negligible amount of external filter cakes is present; and
- formation damage is irreversible. Hence, we neglect the potential restorative effect of deposit erosion which, for a constant-rate process, could be triggered by increased interstitial velocity due to tighter flow areas. It is important to point out that the erosion of deposited asphaltene has been observed experimentally (Rahmani *et al.*, 2003; Ali and Islam, 1998; 1997).

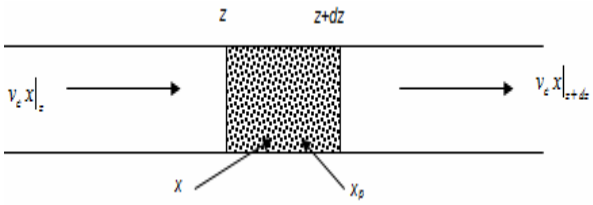


Fig. 5.12: Schematic of Asphaltene-Suspension Flow Process

Neglecting porosity changes, a mass balance on suspended flocs yields (Tchobanoglous *et al.*, 2003; Pang and Sharma, 1997):

$$-v_c \frac{\partial x}{\partial z} = \phi \frac{\partial x}{\partial t} + \frac{\partial x_p}{\partial t}, \tag{5.20}$$

where x and x_p refer to asphaltene concentration in suspension and deposit, respectively and t is elapsed time. The quantity v_c is the superficial (Darcy) flow velocity.

In a deep-bed filtration system, the deposition rate is governed by the rate of asphaltene availability. An empirical model for this relationship is given by (Guedes *et al.*, 2009; Iwasaki, 1937).

$$\frac{\partial x_p}{\partial t} = \lambda x v_c . \tag{5.21}$$

Considering that a granular deep filter is characterised by several particle removal mechanisms including straining, sedimentation, bridging, electrical forces, chemical/physical adsorption and flocculation (Tchobanoglous *et al.*, 2003), it would be expected that each mechanism requires an independent coefficient to account for its effect. However, based on recent investigations, the use of

an aggregate single coefficient is satisfactory (Guedes *et al.*, 2009). Thus, in our work, λ is the overall filtration coefficient. In reality, λ is a phenomenological parameter (Iwasaki, 1937) which, to the best of our knowledge, has no clear relation to underlying physics and is therefore difficult to estimate theoretically, limiting the predictive capabilities of the DBF model. In the current model, we treat it as an empirical parameter.

Combining **Eqs. 5.20** and **5.21**, we obtain the following partial differential equation (PDE) that approximates the deposition process,

$$\phi \frac{\partial x}{\partial t} + \lambda v_c x + v_c \frac{\partial x}{\partial z} = 0 , \tag{5.22}$$

that is subject to the following initial and boundary (inlet) conditions:

$$x(0,z) = 0 ; \;\; x_p(0,z) = 0 ; \;\; x(t,0) = x_a . \tag{5.23}$$

By solving **Eq. 5.22**, subject to the boundary conditions given by **Eq. 5.23**, for the asphaltene concentration in suspension, *x*, and substituting in **Eq. 5.21**, the temporal variation of asphaltene deposition concentration, x_p within the porous medium can be estimated. In order to derive an explicit solution, we require knowledge of the overall filtration coefficient, λ. As this is an empirical parameter in our model, we first examine two limiting cases of; (i) constant filtration coefficient or (ii) filtration coefficient that is time dependent.

Constant Filtration-Coefficient: For constant λ, the solution of **Eq. 5.22** is (Guedes *et al.*, 2009; Pang and Sharma, 1997),

$$x(t,z) = 0 , \;\; z > v_c t , \tag{5.24}$$

$$x(t,z) = x_a e^{-\lambda z} , \;\; z < v_c t . \tag{5.25}$$

For constant filtration coefficient, the time-dependence only enters the solution through the movement of the front, as the suspension traverses the porous medium at a constant superficial velocity, v_c. **Eq. 5.24**, which refers to the region ahead of the front, indicates that there is no suspended asphaltene in this region. However, behind the front (**Eq. 5.25**), the concentration decays exponentially from the boundary value. As our interest is in the region behind the front, we take **Eq. 5.25** as the solution.

In practice, we are more interested in the average deposition rate within the whole medium of length, *L* (in flow direction). Hence, the average asphaltene concentration, $\bar{x}$, is given by:

$$\bar{x}(t) = \int_0^L x(t,z) dz \Big/ L . \tag{5.26}$$

Evaluating **Eq. 5.26**, substituting the solution in **Eq. 5.21** and solving the resulting ordinary differential equation, we obtain a useful expression for the instantaneous, spatially-averaged deposit concentration, $\bar{x}_p$,

$$\bar{x}_p(t) = v_c x_a t\left(1 - e^{-\lambda L}\right)/L . \tag{5.27}$$

To ensure physical consistency, we impose the following restriction on **Eq. 5.27**,

$$\bar{x}_p(t) = 1 \quad \text{if } \bar{x}_p(t) \geq 1$$

which basically indicates that the pore volume has been filled by asphaltene particulates.

We can re-write **Eq. 5.27** in terms of pore volume (PV), resulting in,

$$\bar{x}_p(N) = \phi x_a N\left(1 - e^{-\lambda L}\right), \tag{5.28}$$

with the following constraint,

$$\bar{x}_p(N) = 1 \quad \text{if } \bar{x}_p(N) \geq 1 ,$$

The quantity *N* is the number of pore-volumes of suspension (crude) injected. The quantities *t* and *N* as well as τ and *N** are related by,

$$t = N\phi L / v_c , \qquad \tau = N^* \phi L / v_c . \tag{5.29}$$

As will be illustrated later, the solutions with constant filtration coefficient are limited to a handful of situations. Specifically, they apply to the situation where the formation damage begins as soon as asphalted crude is injected. However, numerous experimental datasets indicate the contrary, showing periods of delayed impairment as well as changing damage rate (Shedid and Abbas, 2005; Shedid, 2001; Minssieux *et al.*, 1998). Hence, one needs to also consider a time-dependent filtration coefficient model.

Dynamic Filtration-Coefficient: From experimental evidence (Maqbool *et al.*, 2011, 2009; Rastegari *et al.*, 2004; Rahmani *et al.*, 2003), one could argue that flocculation rate and floc-size increase over time, before asymptotically reaching a plateau. As most deposition mechanisms are characterised by a positive correlation between floc size and deposition rate (Chang and Chan, 2008; Rastegari *et al.*, 2004), inferences from flocculation studies should be reasonably valid for deposition kinetics. Hence, we assume first-order dynamics for the filtration-coefficient,

$$\lambda = \lambda_o\left(1 - e^{-t/\tau}\right). \tag{5.30}$$

The quantities τ and λ_o refer to time constant and stabilised (steady-state) filtration coefficient, respectively. The time constant, τ measures the 'speed' at which the filtration coefficient evolves,

and by implication, it provides an indication of the rate of potential damage. As would be expected, when deposition is instantaneous, $\tau \to 0$.

From the capillary flow experiments performed by Boek *et al.* (2010b), a key deduction is that, regardless of the Peclet number, the fraction of asphaltene particles deposited increases with time, before asymptotically reaching a saturation level. Nonetheless, the ultimate deposition fraction reduces, nonlinearly, with flow rate (Peclet number). Noting that pore-scale events are usually dominated by capillary forces, which are relatively negligible on a field scale, these results further support our assumption that the deposition process can be approximated by a first-order model, and that induced formation damage is less likely to be instantaneous at reservoir-level.

Please note that **Eq. 5.30**, in the absence of erosion, assumes that the amount of deposits increases over time, hence the particle-capture capacity (λ) increases as pore-size reduces, owing to multi-layer deposition, enhancing the main capture mechanisms of size-exclusion and interception until flow area becomes sufficiently small to stimulate erosion. This approach is fundamentally different from other works that account for the variation of λ by assuming mono-layer ("one particle - one pore") deposition (Altoe *et al.*, 2006; Al-Abduwani *et al.*, 2005), hence treating λ as a monotonic decreasing function of deposit concentration, implying continuous reduction of deposition rate as the process progresses. However, there is overwhelming experimental evidence that supports multi-layer deposition of asphaltenes in porous media, especially in the presence of precipitants (Gummel *et al.*, 2009; Nabzar and Aguiléra, 2008; Kuhnen *et al.*, 2000; Minssieux *et al.*, 1998; Todd *et al.*, 1990) and consequently, as explained above, deposition (particle precipitation/aggregation) rate generally increases over time until some steady state is reached (Maqbool *et al.*, 2011, 2009).

Substituting **Eq. 5.30** into **Eq. 5.22**, and employing the method of characteristics (Logan, 2008), subject to the boundary and initial conditions given by **Eq. 5.23**, the following solution applies to the region behind the front.

$$x(t,z) = x_a \exp\left\{-\frac{\lambda_o v_c \tau}{\phi} e^{-t/\tau} - \lambda_o z + \frac{\lambda_o v_c \tau}{\phi} e^{(\phi z - v_c t)/v_c \tau}\right\}, \quad z < v_c t\,. \tag{5.31}$$

However with respect to *z*, **Eq. 5.31** is not amenable to analytic integration. Nevertheless it is straightforward to perform the integration numerically. For the purposes of this work we made use of Simpson's rule and give the relevant expressions in Appendix **G**. Although the expressions are lengthy, they are easily programmable.

In summary, our semi-analytic model is based on just three empirical parameters: *n* which characterises the porous medium, and τ and λ_o which effectively describe the precipitation (and deposition) process and the effects on the characteristics of the porous medium. In principle, τ and λ_o account for all the effects that lead to asphaltene precipitation and eventual deposition including the nature and concentration of precipitants / flocculants and asphaltene as well as the continuous liquid phase, which is the transport agent. As the three empirical parameters are effective, they are

obtained by matching the prediction of the model to the given experimental data set. We performed the matching calculation in three steps: (i) estimate $\bar{x}_p(t)$ from **Eq. G.3**; (ii) calculate mixture density from **Eq. 5.9**; and (iii) depending on the property of interest, estimate instantaneous fractional damage from **Eq. 5.10**, **5.11** or **5.12**. This process allowed us to optimise the values of parameters *n,* τ and λ_o for a given experimental data set.

We refer to the procedure using **Eq. G.3** to evaluate the dynamics of deposited asphaltene as "dynamic filtration". Conversely, "constant filtration" is that which employs **Eq. 5.27**. While the former requires three tuning parameters (λ_o, τ and *n*), the latter is implemented with just two effective parameters (λ_o and *n*).

5.3.2 Validation of Open-System Models

To validate proposed models, a large body of published experimental datasets is used. The independent datasets covered the range of porous media of interest to petroleum engineering - sandstone, carbonate, glass beads and actual reservoir cores. Reported test conditions are generally diverse and cover a range of values relevant to petroleum applications. Properties of the oil samples and porous media, including media geometry and asphaltene content, are given in **Table 5.2**. Results of validation and the model parameters are presented in **Table 5.3**. In all cases, asphaltene density was 1.16 g/cm^3 (Mehrotra and Svrcek, 1987). Although pure asphaltene density ranges from 1.13 to 1.20 g/cm^3 (Ting *et al.*, 2007), sensitivity analysis showed negligible impact on the results. Maltene density was estimated from **Eq. 5.3**, using quoted crude density and asphaltene content. Very few authors discuss the accuracy of their experimental data. The lack of any estimate of accuracy is a major drawback for validating any model including ours and the subsequent results have to be viewed within this constraint.

As a measure of model performance, we used the AAD. The optimisation objective was to minimise the AAD by adjusting the empirical parameters. Overall, the dynamic-filtration model was capable of representing about 82% of the reference data within 7%. This is a remarkably good representation considering the model has only three effective parameters and the accuracy of experimental data are not known. The constant filtration model, which is, by its nature, less robust, could only explain about 64% of the available datasets within the same 7% accuracy.

As noted earlier, the empirical parameter λ_0 is an aggregation of several complex particle-capture mechanisms. Nevertheless, theoretical and experimental studies have shown that this parameter is primarily controlled by the process parameters (temperature, particle size, flow regime, etc) and the nature of porous medium (rock morphology, rock-surface characteristics, etc) (Chang and Chan, 2008; Tien and Payatakes, 1979). For our study, we have no specific information on the surface characteristics or the morphologies of the porous media used in the various experiments. But we know the main lithology (some of the media are mixed lithologies e.g. clayey sandstone in experiment GV5 of Minssieux *et al.* (1998)) and have estimated the average pore size from given permeability and porosity. By assuming that lithology is the main determinant of λ_0 in experiments

with comparable process conditions and pore size, we have deliberately fixed λ_0 for similar cores. This explains the same λ_0 in Minssieux *et al.*'s sets GF2/GF3 and GP9/HMD26 as well as all the runs of Fadili *et al.* (2009) and Shedid and Abbas (2005) in **Table 5.3**.

Table 5.2: Summary of Benchmark Datasets[**]

			Porous Medium Properties					Oil Properties	
Reference	Run	Injection velocity (cm/h)	Medium	Permeability (mD)	Porosity (%)	Length (cm)	PV (cm^3)	Oil API	Asphaltene Content (wt. %)
Ali & Islam (1997)	1	5.8	limestone	11.3	35	26.5	48	29.29	3
Ali & Islam (1997)	3	35.0	"	11.3	35	26.5	48	29.29	3
Minssieux *et al.* (1998)	GF1	12	sandstone	107	13.1	6	3.3	29	5.3
Minssieux *et al.* (1998)	GF2	2.4	"	87	13.6	6	3.4	29	5.3
Minssieux *et al.* (1998)	GF3	2.4	"	77.4	13.7	6	3.4	29	5.3
Minssieux *et al.* (1998)	GV5	2.4	"	29	24.7	6	6.2	29	5.3
Minssieux *et al.* (1998)	GP9	2.4	"	1.1	22.6	6	5.6	43	0.7
Minssieux *et al.* (1998)	HMD26	1.92	"	0.67	7.1	6	1.8	43	0.7
Minssieux *et al.* (1998)	GV10	2.4	"	12.2	24.3	6	6.1	29	5.3
Mousavi Dehghani *et al.* (2007)		22.8	limestone	1062.5	48.54	37.74	465	21	6.56
Mousavi Dehghani *et al.* (2007)		22.8	sandstone	1089.6	49.19	37.74	472	21	6.56
Mendoza de la Cruz *et al.* (2009)		0.88	limestone	18.7	15.4	5	9	29.3	2.86
Fadili *et al.* (2009)	1	200	glass beads	5000	27	1828.8	150	43.6	11
Fadili *et al.* (2009)	2	100	"	5000	27	1828.8	150	43.6	11
Fadili *et al.* (2009)	3	100	"	5000	27	1828.8	150	52.2	11
Fadili *et al.* (2009)	4	200	"	5000	27	1828.8	150	47.6	11
Fadili *et al.* (2009)	5	300	"	5000	27	1828.8	150	43.6	11
Fadili *et al.* (2009)	6	100	"	5000	27	1828.8	150	47.6	11
Shedid & Abbas (2005)	1	11.8	carbonate	12	21.6	5	5.5	37.32	1.871
Shedid & Abbas (2005)	2	11.8	"	6.07	16.1	5	4.1	37.32	1.871
Todd *et al.* (1990)		10.6	sandstone	260	14.6	20.3	102	water	1.0E-04
Todd *et al.* (1979)		71	ceramic	501	22	2.5	13	water	0.0025

[**] For runs GP9 and HMD26, Minssieux et al. (1998) indicated asphaltene content of 0.15 wt. % for the Hassi Messaoaud crude used. Because their composition does not sum to unity, we assume the balance is asphaltene hence we use 0.7 wt. %. However, in some reports (Leontaritis and Mansoori, 1988), asphaltene concentration as low as 0.062 wt. % has been indicated for the same crude. This range probably reflects the uncertainties associated with this variable.

Table 5.3: Summary of Validation Results

Reference	Run	Constant-Filtration Model			Dynamic-Filtration Model				
		n	λ_o (m^{-1})	AAD (%)	*n*	τ (N^*)	τ (h)	λ_o (m^{-1})	AAD (%)
Ali & Islam (1997)	1	*30*	*7.8*	*12.7*	*35*	*0.6*	*0.9*	*7.8*	*11.9*
Ali & Islam (1997)	3	*3.2*	*7.8*	*7.1*	8.8	37.7	10	7.8	3.1
Minssieux *et al.* (1998)	GF1	2.2	10	3.8	3.2	16.8	1.1	10	2.9
Minssieux *et al.* (1998)	GF2	5.6	8	2.1	6.9	6.5	2.2	8	1.6
Minssieux *et al.* (1998)	GF3	7.1	8	2.3	8.7	4.2	1.5	8	1.8
Minssieux *et al.* (1998)	GV5	*13*	*9*	*27.1*	*15*	*2.9*	*1.8*	*9*	*29.7*
Minssieux *et al.* (1998)	GP9	*27*	*13*	*4.6*	8.8	17.5	6	13	1.9
Minssieux *et al.* (1998)	HMD26	*5.4*	*13*	*8.5*	8.8	262	58	13	6.5
Minssieux *et al.* (1998)	GV10	6.4	15	3.0	8.1	0.16	0.1	15	2.6
Mousavi Dehghani *et al.* (2007)		3.3	7	3.5	3.9	0.77	0.62	7	3.0
Mousavi Dehghani *et al.* (2007)		3.2	3	4.0	3.9	0.39	0.32	3	3.8
Mendoza de la Cruz *et al.* (2009)		4.3	13	2.7	8.8	15.7	14	13	1.7
Fadili *et al.* (2009)	1	4.9	0.23	5.1	5.1	0.73	1.8	0.23	3.8
Fadili *et al.* (2009)	2	4.3	0.23	3.7	4.8	0.73	3.6	0.23	2.8
Fadili *et al.* (2009)	3	*17.5*	*0.23*	*3.1*	*19.6*	*0.97*	*4.8*	*0.23*	*2.1*
Fadili *et al.* (2009)	4	8.9	0.23	6.1	*10*	0.81	2.0	0.23	4.4
Fadili *et al.* (2009)	5	5.6	0.23	5.7	6.3	0.73	1.2	0.23	4.4
Fadili *et al.* (2009)	6	7.7	0.23	4.0	8.7	0.81	4.0	0.23	2.4
Shedid & Abbas (2005)	1	*7.4*	*300*	*10.1*	10	161	14.7	300	4.8
Shedid & Abbas (2005)	2	9.1	300	5.9	9.6	62	4.2	300	4.9
Todd *et al.* (1990)		7.7	1.8	2.9	9.3	547	60	1.8	2.8
Todd *et al.* (1979)		*12.1*	*10*	*20.6*	*14.9*	*12.7*	*0.1*	*10*	*20.5*

We now analyse the capabilities of both models in more detail, by analysing the results obtained for different selected datasets, starting with the data of Minssieux *et al.* (1998).

Fig. 5.13 illustrates the dataset GV10 of Minssieux *et al.* (1998) that exhibits sharp reduction in permeability at early times, while **Fig. 5.14** illustrates the dataset GP9 where the reduction in permeability at early times is low. The qualitative difference in behaviour can be related to the influent asphaltene concentration, which is 5.3 vs. 0.7 wt. %, for GV10 and GP9, respectively. Hence, sample GV10 is expected to lead to much higher initial and ultimate amount of damage, compared to sample GP9 (Yudin *et al.*, 1998). For the dynamic filtration model, the effect of influent concentration on damage rate follows directly from **Eqs. G.3** and **G.4**, in which the deposit concentration x_p varies directly as the influent x_a. The same explanation is valid for the constant filtration process (**Eq. 5.27**).

On the other hand, the observed behaviour is not consistent with the average pore-radius, which is 0.07 and 0.22 micron, for GP9 and GV10, respectively, as estimated from **Eq. 5.8**. As we shall show shortly, the average pore-radius correlates negatively with the stabilised filtration coefficient λ_o, which in turn, varies directly with x_p (**Eqs. G.3** and **G.4**). The difference in average pore-radius indicates that for similar operating conditions (based on comparable injection velocity, see **Table 5.2**), the trapping capacity, hence damage rate, of a sample with smaller pores (GP9) will be considerably larger but this is contradictory to the results depicted in **Figs. 5.13** and **5.14**. Here, the effect of x_a seems to override that of λ_o (pore size). This explanation is plausible when one

considers that the asphaltene concentration for GV10 is about 8 times (possibly more than 30 and 80 times if we consider asphaltene content of 0.15 and 0.062 wt. %, respectively, for the GP9 crude) that of GP9 while the latter's pore-size is only 3 times lower than that of the former.

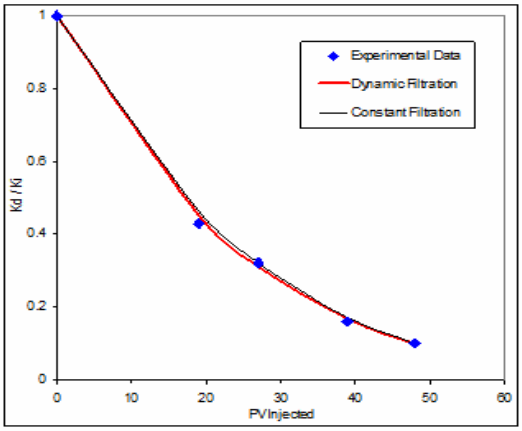


Fig. 5.13: Data of Minssieux *et al.* (1998) - Run GV10

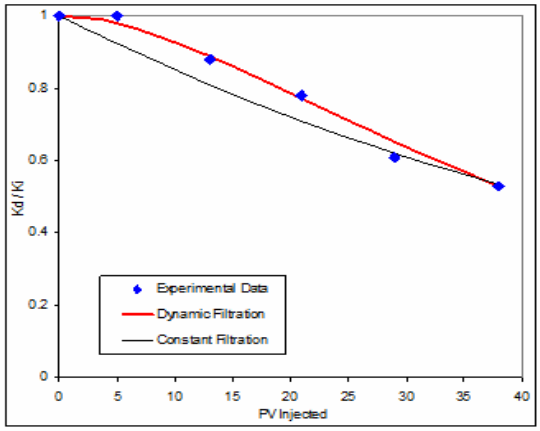


Fig. 5.14: Data of Minssieux *et al.* (1998) - Run GP9

As **Figs. 5.13** and **5.14** illustrate, our dynamic filtration model can fit both types of behaviour, with AAD better than 3%, and reasonable values of the three empirical parameters (n, τ and λ_o). A closer inspection indicates that the good fit to both sets of data was primarily achieved by varying the time-constant τ. For dataset GV10, the high initial precipitation rate, which leads to a rapid decrease in permeability, is a clear indication of a relatively small time-constant for the filtration coefficient. An inspection of the fitted time-constants in **Table 5.3** reveals that it is indeed negligible relative to the respective experimental time scale. As discussed earlier, in the limit of $\tau \to 0$ the dynamic filtration model will revert to constant filtration model. This explains the excellent agreement between the two models in representing the dataset GV10. However, for dataset GP9, illustrated in **Fig. 5.14**, the estimated time-constant τ, is equivalent to some 40% of the cumulative injection volumes, indicating that the filtration and deposition processes were probably very slow due to the overriding effect of dilute influent stream on the small pores. For such relatively passive systems, the inadequacies of the constant-filtration model become apparent. The difference in predictive power between the two models is further illustrated in **Fig. 5.15** for the dataset GF2 of Minssieux *et al.* (1998). A closer examination would reveal that the dynamic-filtration model provides a superior performance to that of the constant-filtration model, during the early times at the onset of precipitation. In fact, with the constant-filtration model, there is the tendency to treat the second data point as an outlier.

Petrophysical and fluid properties, as well as operating conditions, used by Minssieux *et al.* (1998) in generating the datasets GF2 and GF3 are very similar (**Table 5.2**). Hence, one would expect that the fitted parameters for the two datasets should be interchangeable. We examined this hypothesis by using the fitted parameters obtained for datasets GF2 to predict the reduction in permeability for the dataset GF3. **Fig. 5.16** illustrates the results that indicate that although the

original trend is well reproduced the values are overestimated. This is a surprising finding that indicates that either the porous media are not fully described by the parameters given in **Table 5.2** or that the experimental uncertainty is higher than anticipated. Minssieux *et al.* (1998) were aware of incompatibility of GF2 and GF3 datasets and using their model performed a similar investigation of compatibility of GF2 and GF3 parameters, concluding that it is due to the uniqueness of individual systems. In fact, their relative deviations were comparable to ours. They attributed the failure of interchangeability to differences in the surface properties of the cores. However, considering that the cores were of the same type (pure silica Fontainebleau sandstone) and clay-free, hence negligible mineralogy effect (Hamadou *et al.*, 2008); we do not think that this explanation is conclusive. Rather, we are of the opinion that the differences could be partially explained by differences in core geometry and average pore-size. In support of our position, we advance the following argument.

Using **Eq. 5.8**, we estimated the average pore radius of the GF2 core to be slightly higher (0.80 vs. 0.75 μm) than that of GF3. Providing the other characteristics are similar, as they are for GF2 and GF3, a larger pore system is likely to be less susceptible to plugging (Sim 2005; Pautz *et al.*, 1989). Hence, we would expect the damage process in GF2 to be less severe, as is confirmed in **Fig. 5.16**, where the permeability loss (after 50 PV injection) is 42.5% for GF2 and 58.5% in GF3. The experimental results of Todd *et al.* (1979), highlighting remarkable increase in formation impairment with increasing particulate-to-pore size ratio, further lends credence to our point.

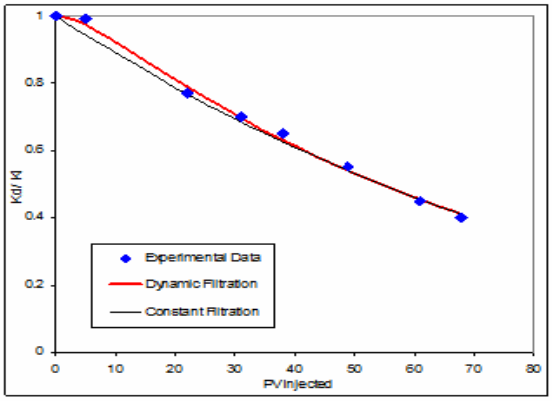


Fig. 5.15: Data of Minssieux *et al.* (1998) - Run GF2

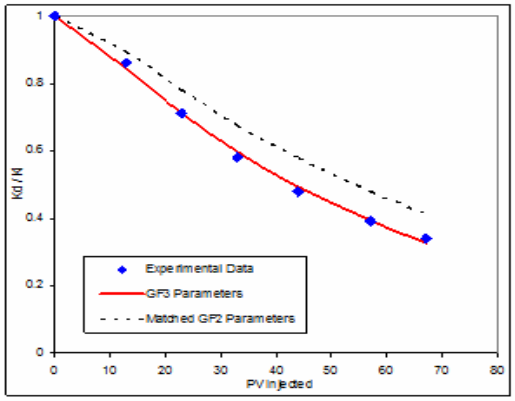


Fig. 5.16: Validating Minssieux *et al.* (1998), Run GF3: Using fitted GF2 Parameters

Finally we test the correlative power of both of our models using the dataset HMD26 (Minssieux *et al.*, 1998) from an actual reservoir core. The results are depicted in **Fig. 5.17**. Although this dataset exhibits higher uncertainty than the previous datasets, reasonable approximations are provided by both the dynamic-filtration model and constant-filtration model with AAD of 6.5% and 8.5%, respectively. However, the dynamic filtration model would indicate that there is a delay in onset of deposition. Perhaps with the exception of the complex simulation model used by the original authors (Minssieux *et al.*, 1998), no other model (Mendoza de la Cruz *et al.*, 2009; Wang and Civan, 2001) that we are aware of, has been able to fit the early behaviour as satisfactorily, in

spite of using higher number (up to 7) of tuning parameters. Although the contentious fourth data point may at first appear to be an outlier (indeed, some workers (Soulgani *et al.*, 2011; Mendoza de la Cruz *et al.*, 2009; Kariznovi *et al.*, 2008; Wang and Civan, 2001) implicitly treat it as an outlier), some background on the Hassi-Messaoaud field, the source of rock and crude used (Minssieux *et al.*, 1998; Hirschberg *et al.*, 1984), would indicate otherwise. For a light crude (43 ^{o}API) containing just 0.7 wt. % asphaltene, with resin/asphaltene ratio (R/A) in the region of 5-52[*], it is likely that the potential damage would be delayed, considering the empirical screening rule that R/A in excess of 2.5 suggests potential crude stability (Al-Atar, 2000). Furthermore, sample GP9, where the oil of same characteristic was injected displays clear low initial damage. The sample HMD26 has larger pore size (0.31 vs 0.22 μm) and lower injection velocity (1.92 vs. 2.4 cm/h), indicating lower initial damage is anticipated. However, the fitted time-constant for HMD26 sample is 35% of the respective test duration, compared to 46% for GP9. Finally, omitting the fourth data point from our fit results in a negligible change in the adjustable parameters, further supporting the argument that the initial rate of formation impairment may not be significant.

Further examples of possible delay in the damage process are observed in the data of Mendoza de la Cruz *et al.* (2009) who have also conducted core-flood experiments. As illustrated in **Fig. 5.18**, the dynamic-filtration model is capable of representing this behaviour with an AAD that does not exceed 2%.

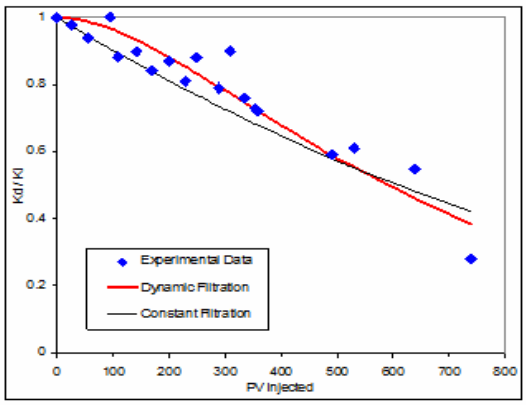


Fig. 5.17: Data of Minssieux *et al.* (1998) - Run HMD26

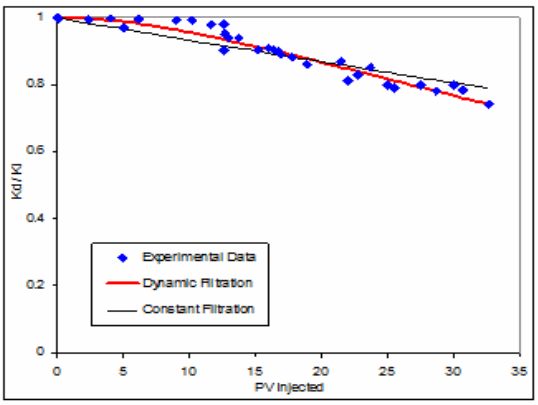


Fig. 5.18: Data of Mendoza *et al.* (2009): Limestone

Perhaps the strongest proof of the robustness of the dynamic-filtration model is provided by correlating the datasets reported by Shedid and Abass (2005) based on flow through carbonate rocks; reproduced here in **Figs. 5.19** and **5.20**. Of note is the remarkable accuracy in approximating the "inverted s-curve" described by the experimental data. Evidently, even for the processes characterised by complicated kinetics, the dynamic-filtration model, despite making use of only three adjustable parameters, is capable of representing the observed behaviour.

[*] Based on asphaltene contents of 0.062 and 0.7 wt. % but resin content of 3.3 wt. % (Minssieux *et al.*, 1998).

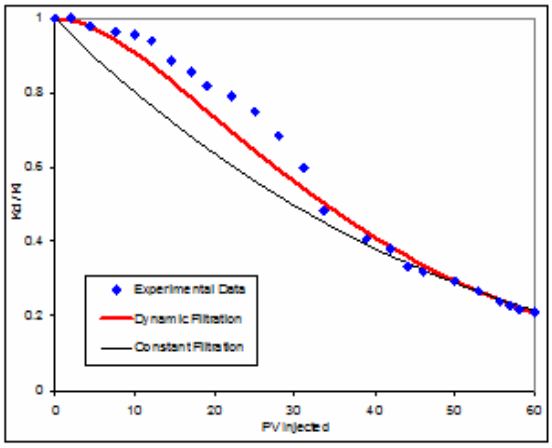


Fig. 5.19: Data of Shedid and Abbas (2005) - Run 1

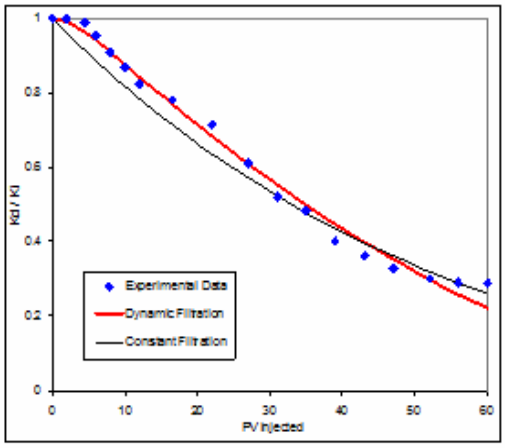


Fig. 5.20: Data of Shedid and Abbas (2005) - Run 2

We complete the analysis of the correlative power of our dynamic filtration model by making use of Fadili *et al.* (2009) data. The experiments were performed in a glass-bead medium, using slim-tube to host the glass beads, thereby inducing a helical and tortuous flow pattern, rather than the typical linear one observed in sandstones and carbonates hence providing a further stringent test of our models. In correlating the Fadili *et al.* data, we take a slightly different approach and take advantage of the fact that in a number of experiments, Fadili *et al.* examined the influence of varying one parameter while keeping the others constant. For instance, datasets 2, 1 and 5 differ only in the injection rates (velocities as the core area is the same) and so do the datasets 4 and 6. In our dynamic filtration model, the injection velocity enters as dimensionless group $v_c \tau / \phi L$ (or $v_c t / \phi L$) which implies that we can eliminate the influence of injection velocity by re-casting the model in terms of dimensionless time ($N = v_c t / \phi L$). If the model correctly depicts the experimental data, then the plot of the experimental data for different injection velocities against dimensionless time should result in a universal curve. **Figs. 5.21** and **5.22** demonstrate that this is indeed the case and that the relevant data do collapse on approximately the same curve.

We have further optimised the dynamic filtration model parameters by fitting to the three datasets (Tests 2, 1 and 5) depicted in **Fig. 5.21** as well as the two datasets (Tests 4 and 6) depicted in **Fig. 5.22**. Parameters of the universal fits are presented in **Table 5.4**. As would be expected, the overall deviation with the universal parameters is larger than could be obtained by fitting to the individual data sets (see **Table 5.3**) but the overall AAD, within 12%, is generally still satisfactory.

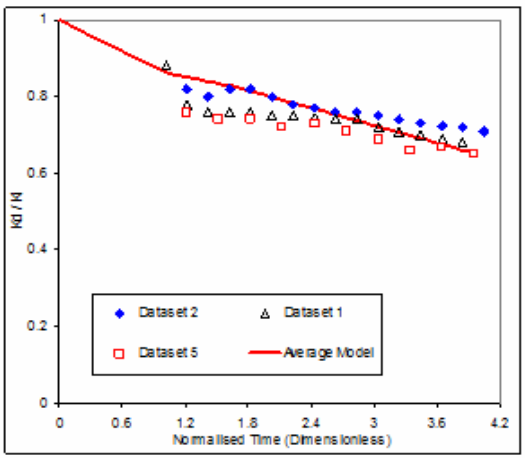


Fig. 5.21: Universal Fit for Tests 2, 1, 5 of Fadili *et al.* (2009)

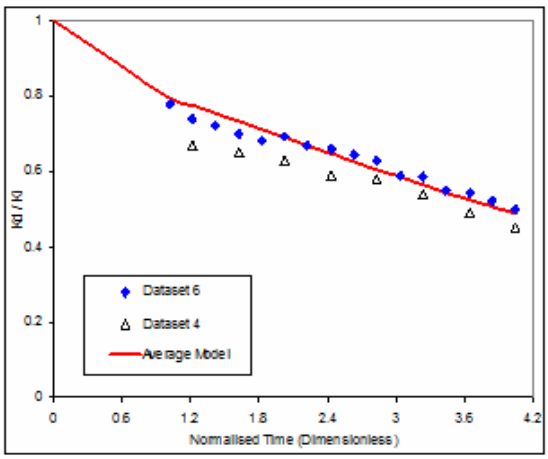


Fig. 5.22: Universal Fit for Tests 4 and 6 of Fadili *et al.* (2009)

Table 5.4: Parameters of the Universal Curves for the Datasets of Fadili *et al.* (2009)

Set	n	λ_o (m^{-1})	$v_c\tau$ (cm)	AAD (%)
2,1,5	5.4	0.23	360	9.5
6,4	9.3	0.23	400	12.2

As implied by our model (see **Eq. 5.21**) and supported by the data of Fadili *et al.* (2009), the damage rate increases with increased flowrate but the dependency is non-linear. However, this deduction ignores the effect of erosion which may become important as the interstitial velocity increases owing to deposition-induced reduction of flow area; but this is outside the scope of the current study. Incidentally, Bagheri *et al.* (2011) observed a similar relationship between the rates of damage (deposition) and injection in their experiments but attributed this effect to increased pressure drop caused by higher flowrate.

Fig. 5.23 illustrates how well the dynamic-filtration model correlates the datasets 2, 6 and 3 of Fadili *et al.* (2009). The difference between the experimental datasets is only in reported oil density, indicating that the damage is highest for the lightest oil. However, one can also view the observation of increased damage with respect to the change in viscosity. Although not indicated in **Table 5.2**, the oils used in runs 2, 6 and 3 have viscosities of 1.1, 0.71 and 0.59 cP, respectively, suggesting that damage rate is less pronounced in viscous crudes. This may partly explain the typical observation of lower rate and magnitude of impairment in viscous crudes, despite their much higher asphaltene content (Sohrabi *et al.*, 2008; Nghiem and Coombe, 1997; de Boer *et al.*, 1995; Leontaritis and Mansoori, 1988; Hirschberg *et al.*, 1984). A similar finding on the influence of viscosity in the damage process was recently reported by Lawal and Vesovic (2010b), see also the analysis of closed systems presented earlier (**Fig. 5.10**).

It is noteworthy that the runs of Fadili *et al.* (2009), notwithstanding the similarity of the porous medium, result in fitting parameters that differ significantly, see **Table 5.3**. This is due to the fact that when our model is used for history-matching, the empirical parameters reflect the historical

behaviour of the system, and not its initial state. Hence, a given system is not likely to yield the same set of parameters if taken through a different process either due to different flow conditions or crude composition.

Fig. 5.24 shows that the two models adequately represent the dataset of Todd *et al.* (1990), which involved water rather than oil flowing through sandstone. In both cases, AAD is less than 3%, implying that the models are independent of the nature of the particle-transporting fluid. Considering the excellent agreement between the two models, it may be deduced that the deposition kinetics was very fast, and there was immediate manifestation of damage. This suggests that λ reaches steady state (λ_0) as soon as injection commences, hence $\tau \to 0$ and, as expected; the fitting *n* should be the same because λ_0 is the same for both models. Contrary to expectation, this is not exactly the case here because the particle-capture and damage processes in this experiment may not be exactly instantaneous. We present the following argument to justify the inequality of the fitting *n* in the constant and dynamic-filtration models for this example, despite the seeming consistency of the fits obtained.

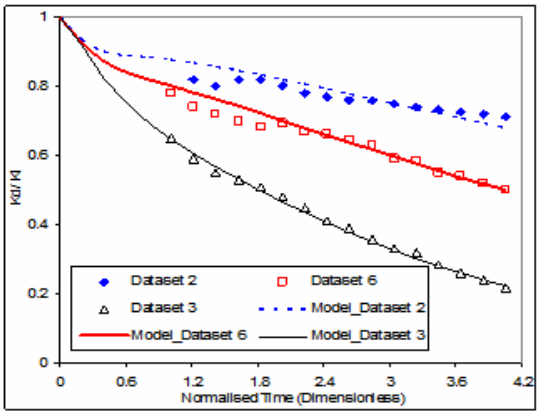


Fig. 5.23: Datasets 2, 6, 3 of Fadili *et al.* (2009)

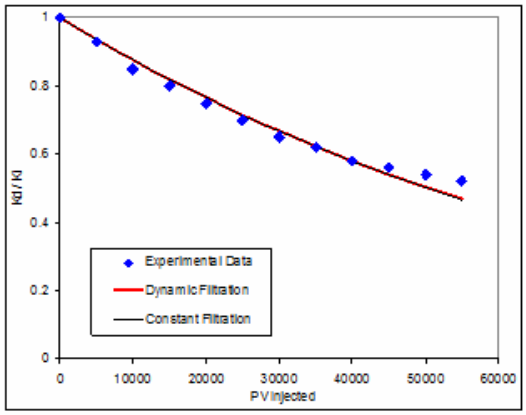


Fig. 5.24: Data of Todd *et al.* (1990) – their Dataset 2

The earliest data point (**Fig. 5.24**) corresponds to the cumulative injection of about 5000 PV, leaving a huge data gap between start-up and first measurement. Whereas the dynamic-filtration model indicates τ is about 550 PV, the absence of early-time measurements precludes analysing the dynamics before the first measurement point. Considering that the influent was very dilute (1 ppm), it is apparent that it would take a relatively long time for induced damage to manifest, which would have been better resolved with greater measurement frequency at early times, say before the injection of 1000 PV. Hence, the low resolution of data might have obscured the true damage dynamics.

A key conclusion from the above discussion is that for systems, such as very dilute suspensions (typical of water injection processes (Bedrikovetsky *et al.*, 2001; Pang and Sharma, 1997)) and porous media with relatively high average pore size, characterised by very slow deposition / damage kinetics, it may be necessary to have high measurement frequency at early times in order

to be able to obtain reliable description of the early damage mechanism. In principle, the same argument on the paucity of data for the early times may be used to explain the difference in the fitted *n* for run GV10 of Minssieux *et al.* (1998). For example, although the experiments GP9 and GV10 (**Figs. 5.13** and **5.14**) are of comparable duration, the first measurement point for the former was 5 PV, compared to 18 PV for the latter.

One of the few datasets not satisfactorily matched by our models is depicted in **Fig. 5.25**. In this work, we treat runs that required $n > 10$ as anomalies, probably caused by non-negligible localised damage (including mechanical plugging). Because our models are premised on *deep* (internal) filtration and uniform particle deposition, we postulate that $n > 10$ is an indication of either significant external *cake* filtration, usually restricted to the inlet area of the porous medium where filter cakes build up locally over time, or internal caking. It is worth noting that, in contrast to deep-bed filtration, cake filtration often dominates in relatively dense suspensions and / or when average particle and pore sizes are comparable (Tien and Payatakes, 1979). Interestingly, in all the experiments (including GV5) reported by Minssieux *et al.* (1998), external caking was not observed. Hence, the non-uniform deposition presumed by our model for GV5 dataset is probably a reflection of internal caking, which may not be surprising considering the adsorptive effects of the illite clay contained in the clayey sandstone medium employed for the GV5 run. However, Todd *et al.* (1979) did note that their tests were dominated by external caking, and in some cases, over 70% of injected particulates were retained as surface filter cake. This could explain the failure of our model for their test 2 presented here in **Tables 5.2** and **5.3**. Although less obvious, it could also be that the deposition kinetics was not first-order (**Eq. 5.30**), which is yet another violation of the assumptions underlying our model.

As a further measure of the robustness of the proposed damage model, we examine its sensitivity to the likely range of uncertainties in the adjustable parameters. We evaluate the limiting case in which all the parameters (n, λ_o and τ) change simultenesously. Here we consider a 10% change on each parameter.

Using one of the relatively more challenging datasets of Shedid and Abbas (2005), **Fig. 5.26** shows the result of the sensitivity. Considering that the AAD, which is 8.4%, compares reasonably with the 4.8% obtained for the “best” fit in **Table 5.3**, we conclude that the model fits are robust.

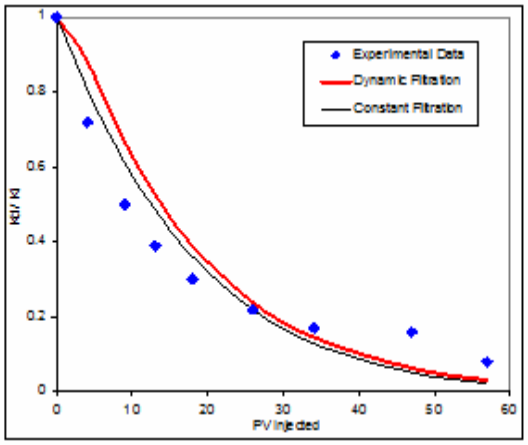


Fig. 5.25: Data of Minssieux *et al.* (1998) - Run GV5

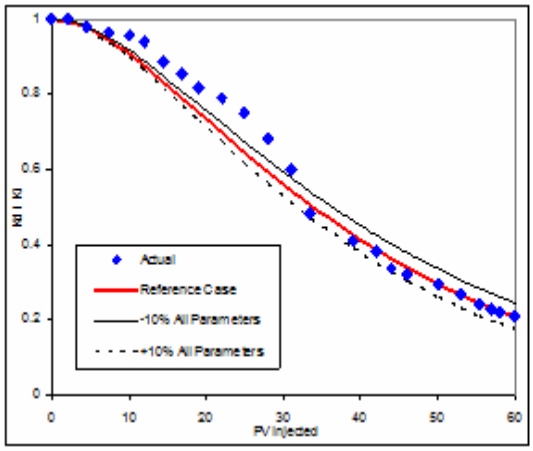


Fig. 5.26: Sensitivity on *n*, λ_o and τ for the fit to the Run 1 In Shedid & Abbas (2005)

5.3.3 Towards Predictive Open-System Models

One of the major drawbacks of existing theories is their limited predictive capability, which is partly due to the high number (up to 16) of fitting parameters, most of which do not have clear physical bounds. In addition, there are no clear guidelines for quantifying these parameters. As we shall show shortly, we correlate λ_0 with pore-radius for each of the lithologies. And for τ, which contributes to the characterisation of the filtration coefficient, we correlate it with the available process variables- injection velocity, oil (or water) density, and influent concentration of particles. With this rather simple approach, we are able to achieve a fairly approximate representation of the two main factors (process and medium effects) that govern the filtration coefficient. The characterisation of filtration coefficient appears to be of greater importance than the permeability-porosity exponent *n*, because the former, as evident in the results presented in **Table 5.3**, has a much larger range of uncertainties.

Using the parameters obtained from the regression studies earlier discussed, we plot λ_o against initial pore-size for each lithology. The plots are based on the data in **Tables 5.2** and **5.3** for cases having accuracy within 7% and $n \leq 10$. For sandstone, λ_o varies inversely as the average size of the flow-path. Apparently, this is intuitive, as the trapping capacity, represented by λ_o, is expected to increase as the pore-size reduces relative to the size of the suspended particulates. A similar trend was obtained for the experiments reportedly performed on carbonates but that of glass-bead media is constant at λ_o = 0.23 m^{-1} because exactly the same set up was used to accomplish all the runs reported by Fadili *et al.* (2009). It is interesting to note that this empirical relationship is consistent with a number of experimental observations that reported that formation damage increased either with an increase in the ratio of particulate-to-pore size (Todd *et al.*, 1979) or a decrease in some measure of flow-path size such as permeability (Sim *et al.*, 2005; Pautz *et al.*, 1989).

We also analysed the variation of time-constant τ with influent particulate concentration x_a. The analysis suggests that the rate of precipitation and deposition roughly increases (τ reduces) with

inlet concentration. Additionally, we found that time-constant also depends on other process parameters such as injection rate as well as crude density. Qualitatively, these findings are consistent with empirical observations (Rastegari *et al.*, 2004; Yudin *et al.*, 1998). For example, the increase in damage rate with asphaltene concentration is well established in qualitative terms (Yudin *et al.*, 1998). And in the absence of significant erosion, deposition is accelerated by increased rate of particle supply, given as v_c in the model formulation (**Eq. 5.21**).

Although the model parameters would ideally be determined from experiments, we develop simple correlations that should provide first-pass estimates in the absence of such data. In addition, they could serve as preliminary benchmarks for experimental results. While we have constructed "best-fit" response surfaces for these data points (see following equations), we do acknowledge their inherent uncertainties, which stem from the lack of theoretical basis on one hand, and uncertainty limits (which are not available) of the experimental datasets on the other hand. However, with additional experimental data, there is scope for improvement, hence reduction of the current range of uncertainties. Furthermore, whereas we limit ourselves to the range $2 \le n \le 10$ (Sisavath *et al.*, 2003) in constructing the following correlations, we admit there might be conditions that warrant relaxing this range (Bernabe *et al.*, 2003; David *et al.*, 1994), which may potentially affect the formation-based correlations presented here.

For sandstone media:

$$\lambda_{os} \approx \left(3.334 + 3.919\,r - 7.895\,r^2 + 3.003\,r^3\right)^2;\ \ \lambda_{os} \ge 0, \tag{5.32}$$

where r is average pore-radius of porous medium (μm) which, given the initial permeability and porosity, can be estimated from **Eq. 5.16**. λ_{os}, referring to λ_o of sandstone, has units of m^{-1}.

$$N_s^* \approx \left(-32.53 + 0.05512\,\rho_c - 222.89\,x_a - 250.36\,v_c\right)^2;\ N_s^* \ge 0, \tag{5.33}$$

where ρ_c is density of crude (or any other suspension medium such as water), kg/m^3; x_a is influent asphaltene (particulate) mass fraction; and v_c is injection superficial velocity, m/s. Note that these empirical correlations have correlation coefficient R^2 of 0.92 and 0.89 for λ_{os} and N_s^*, respectively, based on fitting 8 data points. Again, N_s^* is the pore-volume equivalence of the time-constant τ.

For carbonate media:

$$\lambda_{oc} \approx \left(-146.0 + 1.406\,x10^3\,r - 3.395\,x10^3\,r^2 + 1.699\,x10^3\,r^3\right)^2;\quad \lambda_{oc} \ge 0, \tag{5.34}$$

$$N_c^* \approx \exp\left(21.91 - 0.01941\,\rho_c - 73.38\,x_a + 10337.8\,v_c\right);\quad N_c^* \ge 0, \tag{5.35}$$

where λ_{oc} and N_c^* have R^2 of 0.76 and 0.97, respectively, based on fitting 4 data points.

For glass-bead media:

$$\lambda_{og} \approx 0.23, \tag{5.36}$$

$$N_g^* \approx \exp\left(6.950 - 4396.4 v_c - 0.00901 \rho_c + 5.466 v_c \rho_c\right);\ N_g^* \geq 0. \qquad (5.37)$$

Here, the N_s^* correlation has R^2 of 0.99, respectively, based on fitting 6 data points.

While the foregoing correlations reasonably represent the limited porous media examined in this study, considering that the reference data are based on laboratory-scale experiments, caution must be exercised in applying them to pore and field-scale problems, as there might be issues related to downscaling and upscaling, respectively. It is worth noting that unlike **Eqs. 5.33** and **5.35**, **Eq. 5.37** does not include x_a dependence because the asphaltene concentration was reportedly kept constant for all the experiments accomplished in the glass-bead medium (Fadili *et al.*, 2009).

From the datasets studied and the correlations in **Eqs. 5.33**, **5.35** and **5.37**, it can be deduced that the decreasing order of impact of available process variables on the rate of asphaltene deposition in porous-media is v_c > x_a > ρ_c (viscosity). Conversely, our rather simple analysis suggests that pore-size is the only parameter that influences λ_o. Therefore, in order to minimise uncertainties associated with our proposed models, especially for predictive purposes, it is important that the porous medium be adequately characterised (representative *r*) and the process parameters properly established and controlled.

From the results and correlations, it is apparent that our model parameters have physical bounds. A check on the range of the stabilised filtration coefficient shows they are consistent with the range 0.2-1000 m^{-1} established for industrial deep-bed filters and laboratory cores (Bedrikovetsky *et al.*, 2001; Tien and Payatakes, 1979; Rajagopalan and Tien, 1976; Payatakes *et al.*, 1974; Herzig *et al.*, 1970). Consequently, we presume they are suitable for typical petroleum reservoirs as well as laboratory-scale cores, carbonate, sand and glass-bead packs. This notwithstanding, we emphasise that researchers should be aware of the limitations and inherent uncertainty of the source data before applying the predictions to pore- and field-level processes.

Of all the empirical parameters in the proposed models, the time-constant appears to be inherently the most prone to low accuracy, as it ranges from 0.16 for concentrated suspensions to 547 PV for very dilute mixtures. In retrospect, this wide range is in line with the conclusion reached by Maqbool *et al.* (2009) that the time scale for precipitation (deposition) is of the order of few minutes to several months. Although we have correlated this parameter with influent concentration, velocity and crude density (viscosity), we recommend the establishment of specific relationship for common precipitants, such as CO_2, N_2, flue gas, natural gas, *n*-pentane and *n*-heptane, focusing on both the nature and concentration of respective precipitants on one hand, and the flow regime on the other hand. Shortly, we discuss the experiments we have performed in line with this recommendation.

In practice, we envisage that it would be difficult to establish the time constants (on the order of months and years) for very dilute solutions. To manage this challenge, we expand on an idea inferred from the experimental data published by Maqbool *et al.* (2009). Given few experimental data points on the kinetics of asphaltene precipitation/aggregation (and deposition) obtained at

relatively high concentration of asphaltene or precipitant, we may estimate the time constants for relatively low concentrations by extrapolating the high-concentration trend (time constant vs. concentration). In this approach, the implicit assumption is that the main mechanisms at play at high concentration would also be dominant at low concentrations.

Finally, though the primary interest of this work was asphaltene suspensions, we are of the opinion that the proposed models are applicable to any solid-suspension flow in porous media. A justification for this position is the quality of results obtained with the dataset reported by Todd *et al.* (1990), which was based on non-asphaltene particulates in water. Furthermore, although we have provided simple correlations for first-order estimation of the adjustable parameters, there is still scope for more fundamental research, both theoretical and experimental, that would enable the rigorous characterisation of these phenomenological parameters which, like other empirical constants relating to formation damage, are currently not well understood at the level where reliable predictions can be made (Civan, 2007).

5.4 Experimental Investigation of Asphaltene Deposition in Capillary Flow

In this section, we discuss a set of capillary-flow experiments conducted to improve our understanding of the mechanism of asphaltene deposition in reservoir pores. Specifically, we examine some of the assumptions underlying our earlier theoretical models and the simulation results. These include the deposition profile, pre-deposition kinetics and the effects of some process variables.

Although the fluids of interest in the alternating-injection processes are CO_2 and flue-gas, for convenience, we have employed *n*-heptane and selected alkane precipitants as analogues. In principle, most of the deductions reached from these experiments should be relevant for CO_2 and flue-gas.

Materials and Procedure: The extra-heavy oil sample, identified here as crude X, was from a field in South America. As *n*-heptane insoluble, its asphaltene content is about 18 wt.% (Li, 2011). At 1 atm and 20 ^{o}C, its density and viscosity are ~990 kg/m^3 and 200 Pa s, respectively. In order to achieve reasonable flowrates under atmospheric conditions and for the purpose of obtaining visible images (the crude is very dark), the oil was diluted with toluene (solvent). Although an aromatic solvent (toluene) was used, we assume that the critical micellisation concentration (CMC) was not reached, hence the asphaltene particles did not exist in micelle forms (Mousavi-Dehghani *et al.*, 2004; Priyanto *et al.*, 2001; Yudin *et al.*, 1998). In the range of dilution ratios examined, the oil viscosity was reduced from about 100 Pa s to the average of 20 mPa s (25 ^{o}C, 0.01 s^{-1} shear rate). As the asphaltene precipitant, *n*-C_7 was used. The purity of the toluene and *n*-C_7 exceeded 95 % (Sigma-Aldrich, UK). At 25 ^{o}C, their densities are 865 and 680 kg/m^3, respectively. **Fig. 5.27** illustrates the asphaltene-precipitation curves for the diluted crude when *n*-pentane, *n*-heptane and *n*-octane are used as precipitants (Li, 2011).

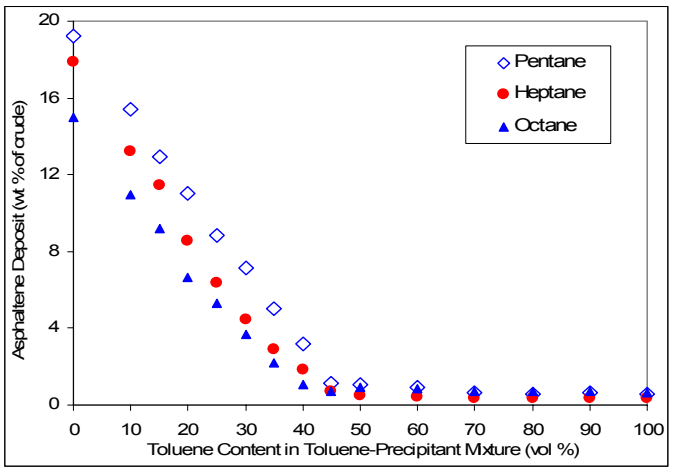


Fig. 5.27: Asphaltene-Precipitation Curves for the Crude Oil (after Li (2011))

The host medium (tube) was a cylindrical glass microcapillary pipette (71900-10 from Sigma-Aldrich, Germany). With internal volume of 10 μl ± 0.5%, the length and internal diameter (ID) of the microcapillary were 5 in. (127 mm) and 0.32 mm, respectively. Two dedicated constant-rate programmable syringe pumps (BS-8000/9000 from Braintree Scientific, USA), with designed throughput of 0.73 μl/h to 2120 ml/h, were used for each of the precipitant and crude/solvent streams. Whereas other workers used three pumps (Wang *et al.*, 2004; Broseta *et al.*, 2000), one for each of the crude, solvent and precipitant, this was presumably influenced by the relatively high mobility (viscosity and density below 60 mPa s and 883 kg/m^3) of their crudes under laboratory conditions. In the current case of 100 Pa s crude, it became imperative to premix the solvent and the oil prior to injection, hence eliminating a pump. Each of the pumps was equipped with a gastight syringe, through which they discharge the preset flowrates. The syringes had barrels of volume 10 ml and ID 14.6 mm (81601 from Hamilton, USA).

Imaging was performed with a camera-mounted Zeiss microscope (Axio Observer.A1m from Carl Zeiss, Germany), connected to a computer for image analysis (**Figs. 5.28** and **5.29**). More details are available elsewhere (Boek *et al.*, 2010b). A well-calibrated 0-5 V (1-bar range) pressure transducer, which output to a computer, was used to measure voltage (pressure) at the capillary entrance. Because the capillary was made to discharge to the atmosphere, the recorded gauge pressure was taken to be the pressure-drop across the capillary. In our discussions on the hydraulic design, we shall show that the 1-bar range was adequate for all the runs investigated.

The making-up of the assembly of capillary, PEEK Y-connector (from Upchurch, USA) and microscope glass slide holder have been detailed by Boek *et al.* (2010b). However, in contrast to their set up that employed a rectangular capillary, ours was cylindrical. Hence, our design had some obvious differences that are peculiar to the current capillary geometry. The assembly was subsequently mounted onto the microscope stage, and the injection lines (0.40 mm ID transparent rubber tubings) connected via the Y-connector to the capillary. Please note that for each run, a new capillary was used while the precipitant and crude/solvent lines were never interchanged. However,

before commencing a new run, the injection lines were adequately vacuum-cleaned to remove accumulations from the previous runs. In the case of the experimental-oil line, while being isolated from the heptane line, vacuum-cleaning was preceded by flowing toluene through it.

The microscope stage was movable, allowing for image-capture along the capillary length. Capillary movement was eliminated by holding it unto a rectangular glass slide which slid perfectly into the capillary holder. A rubber band was used to hold both the capillary and slide firmly unto the holder (**Fig. 5.28a**). Because the slide was transparent, the distortion of transmitted light to the capillary was minimal.

In this work, images were taken at 10, 50 and 100 mm along the capillary, taking the stage ~ 1 s to move between points. Apart from end effects (discussed shortly), the geometry of the capillary holder precluded taking images outside the 10-100 mm interval of the 127-mm long capillary (**Fig. 5.29**). The precipitant and crude/solvent injection lines had dead volumes of 250 and 170 μl, respectively. In determining the effective reacting volumes (elapsed times) in the capillary, these dead volumes were discounted.

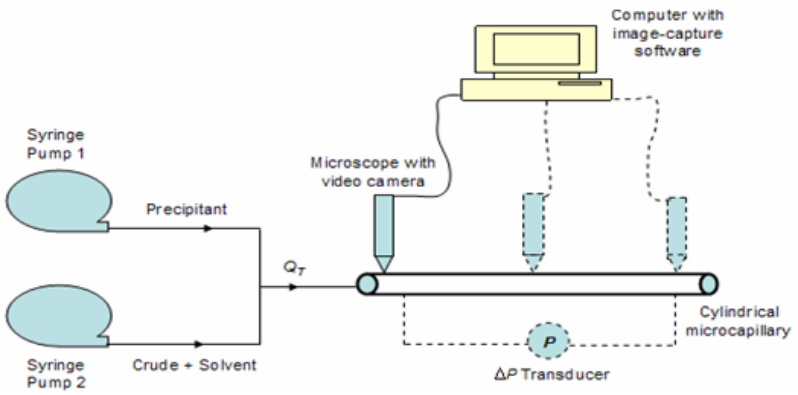
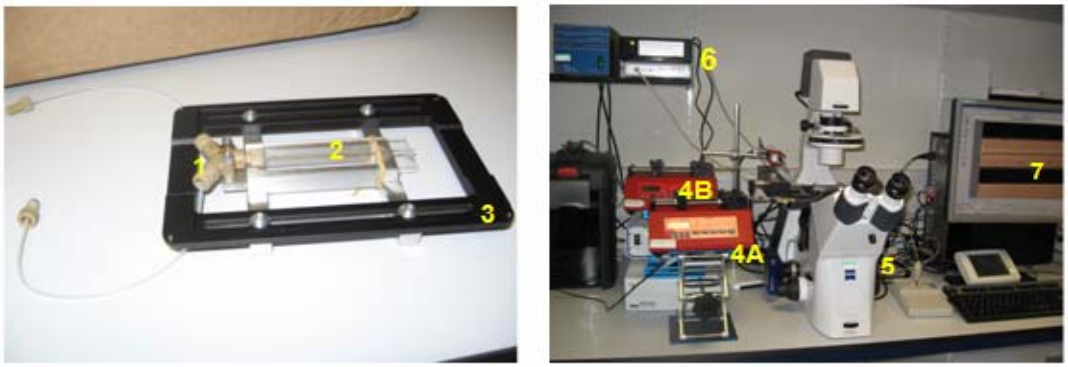


Fig. 5.28: Schematic of the Asphaltene-Deposition Experiment in a Capillary Tube (Modified after Boek *et al.* (2010b))



(a) Assembly of Capillary and its Holder **(b) Some Hardware**

Fig. 5.29: The Experimental Rig

(1 = Y-connector, 2 = capillary holder with model, 3 = microscope stage, 4A = experimental-oil pump, 4B = precipitant pump, 5 = microscope with the model mounted; 6 = pressure recorder; 7 = computer).

Asphaltene-Precipitation Onset (APO): using gravimetric analysis, Li (2011) established the APO for the sample crude. However, rather than the standard ASTM D2007 method (ASTM, 1993) of mixing one volume oil with 40 volumes *n*-C_7, Li (2011) used one volume oil and 40 volumes of the mixture of toluene and n-C_7, where toluene served as an oil solvent. As illustrated in **Fig. 5.27**, the APO is 52 vol.% *n*-C_7 to 48 vol.% toluene of the 40-volume precipitant/solvent mixture to 1-volume crude. However, because of the uncertainties associated with the measurements on one hand (Escobedo and Mansoori, 1995), and the disparity among various methods of determining the APO on the other hand (Mousavi-Dehghani *et al.*, 2004), we take the *n*-C_7/toluene volumetric ratio of 55:45 as the "minimum" APO for our studies, , which consider *n*-C_7 as the reference case..

Preparation of Experimental Oil: Given the APO of 55 vol.% *n*-C_7 (in mixture with toluene) which, in principle, is the lower bound of precipitation, we investigate higher precipitant concentrations. In order to enhance its flowrate, the crude was premixed with toluene to constitute one stream, which we call the "experimental oil". This was then injected through a dedicated line for onward dynamic mixing with the precipitant stream, injected through another line (see **Fig. 5.28**). The mixing and reaction of the co-injected streams commenced just at the entrance of the microcapillary and continued throughout its length. Essentially, the system approximated a plug-flow reactor (Levenspiel, 1999). Except stated otherwise, all the runs had the experimental oil prepared to honour the toluene fraction in the desired solvent-precipitant ratio and the fixed crude:precipitant/solvent volumetric ratio of 1:40.

Under the assumptions of steady-state and incompressible fluids, simple material balance yields the following expressions for the flowrates of the crude, solvent, and precipitant, respectively.

$$Q_c = \frac{Q_T}{R+1}, \tag{5.38}$$

$$Q_s = \frac{RQ_T}{(R+1)(f+1)}, \tag{5.39}$$

$$Q_p = \frac{fRQ_T}{(R+1)(f+1)}, \tag{5.40}$$

where R is the volumetric ratio of solvent and precipitant to crude, f is precipitant-to-solvent volumetric ratio, and Q_T is the total flowrate. Q_c, Q_s, and Q_p are crude, solvent and precipitant flowrates, respectively.

In line with **Eqs. 5.38-5.40**, for a given Q_T, R and f, while the experimental oil was prepared at crude:toluene ratio of Q_c:Q_s, and then injected at the rate (Q_c+Q_s), the precipitant was injected at the rate Q_p. Although we have studied diluted crudes in these experiments, the resulting states may not be too different (in terms of viscosity and flow regime) from the likely in-situ conditions in a reservoir undergoing either a thermal flood or miscible injection, or some combination of these exploitation techniques.

5.4.1 Hydraulic Design

It was necessary to determine the appropriate flowrates (Q_T) through the capillary as well as the rating of the pressure gauge. As a design philosophy, the hydraulics was governed by the following, where the limits are arbitrary:

- Capillary-dominated flow $N_{ca} = \mu Q_T / A\sigma < 0.01$.
- Low inertial forces $N_{\mathrm{Re}} = \rho_c Q_T D / A\mu < 0.5$.
- Negligible dispersion $N_{Pe} = Q_T D_a / A\alpha_m > 5$.
- Insignificant gravity effects $N_G = (\rho_a - \rho) g A D_a^{\,2} / 18\,\mu Q_T < 0.0001$.
- End-effect limited to 0.1% of capillary length $L_e = 0.035\,\rho_c Q_T D^2 / A\mu < 0.001\,L$.

The quantities N_{ca}, N_{Re}, N_{Pe}, and N_G refer to the capillary, Reynolds, Peclet, and gravity numbers, respectively. L_e is the minimum entrance (exit) length required to attain a fully-developed Hagen-Poiseuille flow (Bird *et al.*, 1960). The definitions of the other variables and the corresponding values used in this study are presented in **Table 5.5**. It is worth noting that the dispersion refers to the asphaltene particles rather than the bulk flow, hence the use of floc diameter D_a and not capillary internal diameter D. Furthermore, we used the stream viscosity of 20 mPa s, which applied to the solvent/crude mixture. Ideally, the precipitant would further lighten (~ 2 mPa s) this mixture but from a conservative viewpoint (maximum pressure-gauge rating), this effect was ignored.

The flowrates satisfying the various constraints are indicated in **Table 5.6**. From these results, it was straightforward to deduce that the most suitable range of total injection rate Q_T, was $5 \le Q_T \le 60$ μl/min.

Sensitivity Studies: As the reference case, we examined Q_T = 20 μl/min, R = 40, and f = 3. The primary objective was to assess the rate of asphaltene deposition on one hand, and the resulting impairment of the hydraulic conductivity of the microcapillary on the other hand. The latter is discussed shortly. As sensitivities, we also investigated the effects of Q_T, R and f on the experimental objectives. **Table 5.7** outlines all the cases studied in this work. Please note that we have deliberately included Q_T = 100 μl/min, which falls outside the "allowable" $5 \le Q_T \le 60$ μl/min, in order to evaluate the relative effect of inertia (erosion/re-entrainment). Given the capillary volume of 10 μl, the total rates of 10, 20 and 40 μl/min resulted in average oil-precipitant contact (reaction) times of 60, 30 and 15 s, respectively. To evaluate the influence of precipitant type (Luo *et al.*, 2010), we include *n*-pentane and *n*-octane, selected to assess the effect of increasing carbon number on the precipitation potentials of alkanes (Luo *et al.*, 2010). Depending on the process kinetics, pressure readings and images were taken every 10-60 s and 30-60 mins, respectively.

Table 5.5: Numerical Values of Some Hydraulic-Design Parameters

Quantity	Value	Reference / Comment
Viscosity, μ (Pa s)	0.02	
Crude density, ρ_c (kg/m^3)	990	
Interfacial tension, σ (N/m)	0.029	Mohamed *et al.* (1999)
Capillary length, *L* (m)	0.127	
Capillary ID, *D* (m)	3.2×10^{-4}	
Capillary flow area, *A* (m^2)	8×10^{-8}	
Dispersion coefficient, α_m (m^2/s)	1×10^{-10}	Chin (1986)
Asphaltene-floc diameter, D_a (m)	5×10^{-7}	Sim *et al.* (2005)
Asphaltene density, ρ_a (kg/m^3)	1160	Mehrotra and Svrcek (1987)
Asphaltene content, x_a (wt.%)	18	Li (2011)
Maltene density, ρ (kg/m^3)	865	assuming toluene is the continuous phase, as its density is between *n*-C_7 and the crude.

Table 5.6: Range of Total-Injection Rate

Constraint	Q_T (μl/min)
N_{ca}	< 70
N_{Re}	< 150
N_{Pe}	> 4.8
N_G	> 0.1
End-effect	< 3400

In **Table 5.7**, the limiting amounts of asphaltene deposits x_{pmax}, are listed for the various precipitant:solvent ratios (*f*) shown in **Fig. 5.27**. For an arbitrary cumulative injection-volume of 10 ml (1000 times the capillary volume), we have estimated the maximum thickness of asphaltene deposit expected in a capillary of 127 mm length. Assuming uniform deposition of all the injected "precipitable" asphaltenes, the upper limits of deposit thickness e_{tmax}, are also indicated in **Table 5.7**. It is worth stating that by "precipitable", we refer to the proportion of asphaltenes that can be precipitated at the prevailing precipitant concentration (*f* value) as illustrated in **Fig. 5.27**.

Apart from the flowrate-effect, the other effects (for same precipitant) are associated with varying amount of "precipitable" asphaltene and limitng deposit thickness. However, to obtain a fixed concentration of "precipitable" asphaltene in practice, some extracted asphaltenes can be dissolved in the dilute solutions (Boek *et al.*, 2008; Yudin *et al.*, 1998). But caution should be exercised with this option, as some workers have argued that extracted asphaltenes tend to aggregate faster (more sticky) than in-situ asphaltenes (Boek *et al.*, 2010b), hence may affect the overall kinetics.

Table 5.7: Matrix for Sensitivity Studies

Effect of Flowrate (R = 40; f = 3)			
Q_T (μl/min)	**x_{pmax} (wt.%)**	**e_{tmax} (μm)**	***Run No.***
10	6.8	380	1
20	*6.8*	*380*	*2*
40	6.8	380	3
100	6.8	380	4
Effect of Precipitant Concentration (R = 40; Q_T = 20 μl/min)			
Precipitant : Solvent	**x_{pmax} (wt.%)**	**e_{tmax} (μm)**	***Run No.***
55 : 45 (1.22)	0.5	100	5
75 : 25 (3)	*6.8*	*380*	*2*
90 : 10 (9)	12.9	530	6
Effect of Precipitant (f = 3; R = 40; Q_T = 20 μl/min)			
Precipitant	**x_{pmax} (wt.%)**	**e_{tmax} (μm)**	***Run No.***
n-pentane	8.8	440	7
n-heptane	*6.8*	*380*	*2*
n-octane	5.3	340	8

Pressure-Sensor Rating: In selecting a "suitable" pressure-gauge, we use the Hagen-Poiseuille equation (Bird *et al.*, 1960). As input parameters, we use the limiting values of μ, Q_T and D.

$$\Delta P < \frac{128\,\mu_{\max} L Q_{T\max}}{\pi D_{\min}^4}, \tag{5.41}$$

where μ_{max} = 0.02 Pa s, Q_{Tmax} = 100 μl/min, and D_{min} = 208 μm. Please note that we have assumed that, on average, not more than 35% of the capillary diameter (320 μm) would be clogged by the deposits, hence average minimum flow diameter of 208 μm.

Evaluation of **Eq. 5.41** with the given parameters yields ΔP < 0.93 bar. This indicates the suitability of a 1-bar gauge. It is re-assuring to note that the range of the selected gauge was not exceeded throughout the experiments, suggesting the robustness of the underlying assumptions.

5.4.2 Data-Interpretation Models

As earlier stated, pressure was the only dynamic parameter measured during the experiment. With this dataset, the following models are used to estimate the equivalent thickness of the deposits and variation of the capillary conductivity.

Deposit Thickness: the following analysis takes after Broseta *et al.* (2000) and Wang *et al.* (2004). However, while their final expressions are approximations of the average hydrodynamic thickness of the deposit, here, we present a more accurate expression. For a constant-rate Poiseuille flow (**Eq. 5.41**), the following is valid:

$$\frac{(\Delta P_t) r_t^4}{\mu_t} = \frac{(\Delta P_i) r_i^4}{\mu_i}, \tag{5.42}$$

where (ΔP_i) and (ΔP_t) refer to pressure-drop across the capillary at the beginning or some earlier steady-state (before precipitation) and time *t*, respectively; μ_i is viscosity of original crude that yields (ΔP_i); μ_t is average instantaneous viscosity of crude (with asphaltene precipitates) that yields (ΔP_t); r_i is initial tube radius; r_t is instantaneous effective tube radius after precipitation (and deposition).

For simplicity, we ignore changes in effective viscosity of the flowing crude i.e. $\mu_t \approx \mu_i$, thus:

$$r_t \approx r_i \left(\frac{(\Delta P_i)}{(\Delta P_t)} \right)^{1/4}. \tag{5.43}$$

But r_t is related to the instantaneous average asphaltene (deposit/suspension) hydrodynamic thickness e_t:

$$r_t = r_i - e_t. \tag{5.44}$$

Therefore, at any time, *e* can be estimated from the following expression:

$$e_t \approx r_i \left\{ 1 - \left(\frac{\Delta P_i}{\Delta P_t} \right)^{1/4} \right\}, \tag{5.45}$$

which is a less restrictive expression than $e_t \approx 0.25 r_i (\Delta P_t / \Delta P_i - 1)$ which, according to earlier workers, is only valid for $e_t << r_i$ (Wang *et al.*, 2004; Broseta *et al.*, 2000). Although the analysis leading to **Eq. 5.45** is about the same as that of Broseta *et al.* (2000), our manipulation of the algebraic equations differs slightly from theirs, hence the difference in the final expressions. Shortly, we evaluate the "consistency" of both models in the treatment of experimental results.

It should be borne in mind that, in principle, e_t is not limited to a deposit, as this may not even exist. Rather, it characterises the equivalent thickness of a hypothetical layer of deposited and suspended asphaltene particles (precipitates / flocs), which would effectively reduce the radius available for bulk flow.

According to **Eq. 5.45**, it is theoretically possible to have the case of $r_t > r_i$. This could occur either due to a "chipping" effect, in which suspended particles erode the tube walls as they are forcefully transported under high velocity (constant flowrate but reduced flow area), or re-dissolution of suspended particles. Apparently, for a constant viscosity, erosion (or infinite dissolution) may cause $\Delta P_i > \Delta P_t$ hence $e_t < 0$. Hence, $r_t > r_o$ is the limiting scenario in a non-rigid tube. In future

studies, it would be interesting to characterise the combined effects of simultaneous deposition and viscosity variations.

Hydraulic Conductivity: by drawing an analogy between the Hagen-Poiseuille (capillary) and Darcy (porous-media) flow equations, we can relate the instantaneous and initial conductivities (permeabilities) of the capillary to the corresponding pressure-drops (Appendix **H**):

$$\frac{k_d(t)}{k_i} \approx \sqrt{\frac{\Delta P_i}{\Delta P_t}} \,. \tag{5.46}$$

Again, we have neglected the effect of asphaltene drop-out on net fluid viscosity. According to **Eq. 5.46**, we only need to monitor the temporal variation of pressure-drop in order to estimate the conductivity changes of a capillary.

5.4.3 Experimental Results and Discussion

Fig. 5.30 shows the temporal variation of the pressure-drop and estimated capillary conductivity in the case of run 4 (100 μl/min). Because of the high sampling frequency, the plots are generally noisy. In order to render the datasets more amenable for analysis, we perform some filtering by averaging the data over specified time intervals. For consistency between runs, we use 40, 20, 10 and 4 mins as the averaging intervals for the 10, 20, 40 and 100 μl/min runs, respectively. As all the other runs were based on 20 μl/min, the 20-min interval was also used. To facilitate an objective comparison of different runs conducted at different injection rates Q_T, the following discussion considers the number of capillary-volume injected (CVI) as a measure of the elapsed time.

Fig. 5.31 depicts the variation of conductivity for different flowrates. Although some disparity can be seen after 600 CVI, it is still evident that deposition is independent of flowrate. In other words, within the range examined, the rate of particle supply appears to govern the deposition process, implying that erosion was not significant. This conclusion is consistent with that reached from our earlier analysis of the datasets of Fadili *et al.* (2009), see also Lawal *et al.* (2011), though they referred to porous media (see **Figs. 5.21** and **5.22**). As would be expected, the variation of deposit thickness in **Fig. 5.32** correlates with the impairment of conductivity (**Fig. 5.31**).

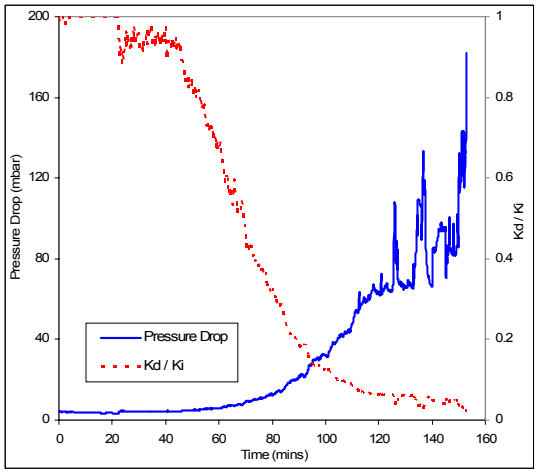


Fig. 5.30: Unfiltered Datasets (Run 4)

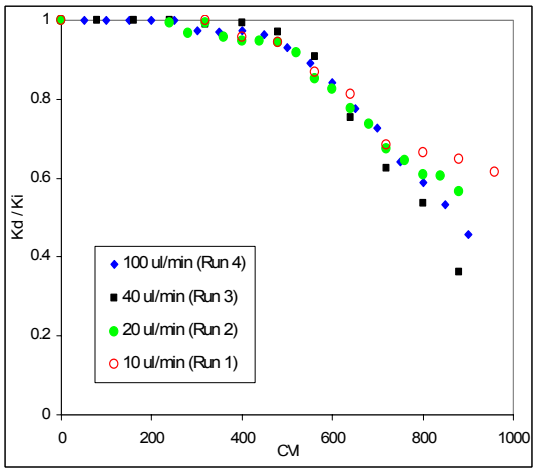


Fig. 5.31: Effect of Flowrate on Conductivity Impairment

In putting the analyses in context, we highlight the magnitude of potential error in the use of the deposit-thickness model of Broseta *et al.* (2000). As shown in **Fig. 5.33**, this model could yield estimates that are non-physical i.e. layer thickness exceeding the capillary ID. Additionally, compared to our model, the former could overestimate deposit thickness by more than a factor of two. In the light of this finding, it might be necessary to revisit some of the conclusions reached by Broseta *et al.* (2000) and Wang *et al.* (2004) on the geometry of asphaltene deposits in capillary flow systems.

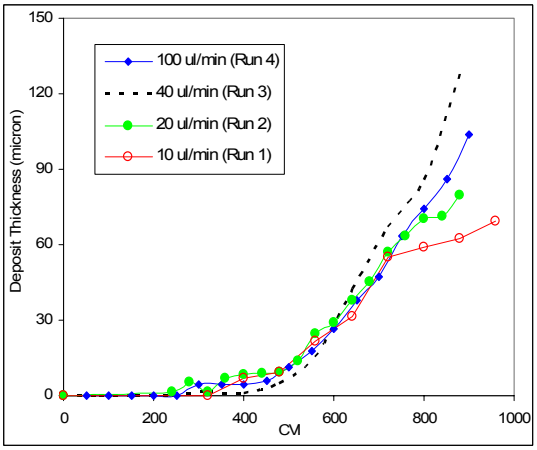


Fig. 5.32: Effect of Flowrate on Deposition

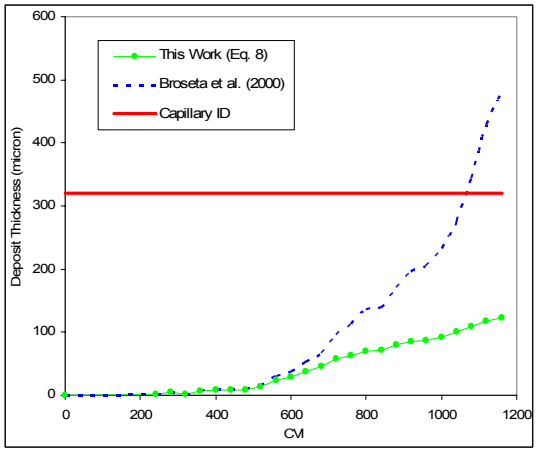


Fig. 5.33: Comparison of Thickness-Estimation Models

The effects of precipitant concentration are illustrated in **Fig. 5.34**. However in this case, unlike the approach taken in the earlier analysis, we consider “normalised” deposit thickness. Noting that the amount of precipitates varies with the precipitant concentration (**Fig. 5.27**), we obtain a normalised thickness by dividing the estimated deposit thickness by the corresponding e_{tmax} indicated in **Table 5.7**. A comparison of the results of runs 6 and 2 would indicate that, despite the ratio in the latter being a third of the former, the difference in the rates of deposition in the two cases is less pronounced.

It is surprising that there was no noticeable deposition in run 5 (f = 1.22), despite that its precipitant-solvent ratio exceeds the "minimum" threshold (f = 1.08) depicted in **Fig. 5.27** (Li, 2011). To some extent, this finding highlights the uncertainties associated with the determination of the APO and the need to be cautious in comparing results from different methods (Mousavi-Dehghani *et al.*, 2004; Escobedo and Mansoori, 1995). Because not all precipitates would effectively impede the bulk flow or be deposited to reduce the flow area, one would generally expect the amount of deposits estimated from the analysis of pressure-drop to be lower than that from gravimetry. From the viewpoint of enhanced oil recovery driven by deasphalting, this conclusion is quite interesting, as it implies that the actual oil recovery and upgrading would exceed that deduced from pressure analysis. However, the no-deposition observation could also be due to uncertainties in preparing the samples for this particular run, considering that the run is very close to the threshold of precipitation onset.

The inability to detect any deposition in run 5 can also be attributed to kinetics. Whereas the precipitation experiments presented in **Fig. 5.27** were generally based on 48 h contact between precipitant and crude (Li, 2011), the longest contact time in our deposition studies was just 1 min, which was probably too short to achieve significant aggregation and deposition of precipitated particles. The importance of kinetics in the analysis of asphaltene precipitation and deposition experiments has been noted by other workers (Lawal *et al.*, 2011; Maqbool *et al.*, 2009; Rastegari *et al.*, 2004).

In **Fig. 5.35**, which employs normalised deposit thickness, the deposition rate increases from n-C_8 to n-C_5. This is in agreement with the conclusion of other workers that within the alkane family, the asphaltene-precipitation potential increases with decreasing carbon number (Luo *et al.*, 2010; Wang *et al.*, 2004). Although this observation has been rationalised with the solubility parameter (Wang *et al.*, 2004), that explanation may not be conclusive. While solubility may control the events leading to precipitation, post-precipitation events of flocculation and eventual deposition are more likely to be influenced by particle transport. In this regard, we postulate that viscosity effect plays a key role in flocculation and deposition.

As can be seen in **Fig. 5.10**, the analysis by Lawal and Vesovic (2010b) as well as the experimental results of Al-Huraibi and Belhaj (2010), viscous drag inhibits particle aggregation and deposition. Therefore, noting that viscosity decreases from n-C_8 to n-C_5 (0.240 - 0.542 cP at 20 ^{o}C), it is expected that the viscous drag reduces accordingly. It is interesting to note that the viscosity-effect argument is partly supported by the results of Luo *et al.* (2010). From the analysis of the maltenes (asphaltene-free liquid) obtained from n-C_5 and n-C_7 as precipitants, they found that the maltene in the latter was about 50% more viscous than that of the former. In other words, even for the same precipitation rate and particle geometry, flocculation and deposition in the case of n-C_7 would be slower than obtained for n-C_5.

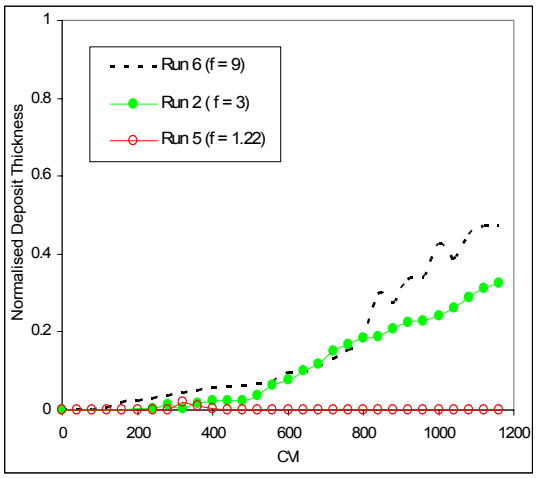


Fig. 5.34: Effect of Precipitant Concentration on Deposition

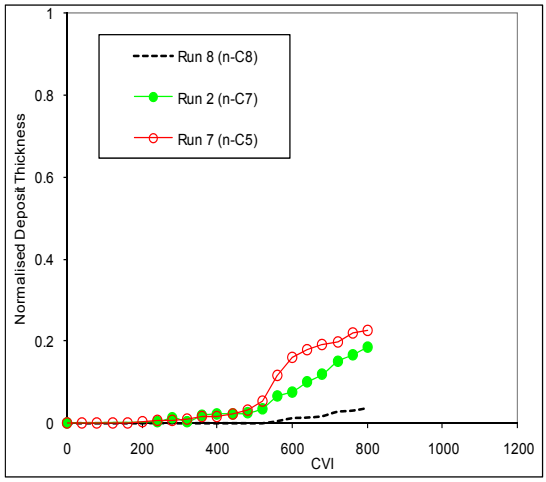


Fig. 5.35: Deposition for Different Precipitants

Fig. 5.36 presents the micrographs at different positions along the capillary at selected times. Please bear in mind that the images are in 2-D (plan view) hence, in qualitative terms, they show the particles in suspension and not necessarily those which adhere to the capillary walls. Within the microscope resolution, there is no noticeable asphaltene drop-out for the first 60 CVI. In essence, this observation reinforces the argument underlying our dynamic-filtration model that deposition is not a first-contact process. In other words, there is some time lag between *sustained* contact of the precipitant and asphaltene-laden crude, and the manifestation of asphaltene flocs.

A close observation of the images in **Fig. 5.36** would reveal that the "cloudiness", which in this case is used as a qualitative indicator of deposition, increases over time. This implies that deposit growth is generally monotonic, at least within the interval examined. This agrees with the pressure-drop trend, as evident in the temporal variations of estimated conductivity and deposit-thickness in **Figs. 5.30-5.35**.

Furthermore, at every instant, the images of this straight and relatively short capillary suggest that deposition is reasonably uniform behind the front. While this observation justifies some of the assumptions underlying our open-system theoretical models, it does not agree with the results of Boek *et al.* (2010, 2008). However, a careful analysis of the results of the latter authors would reveal that the reported non-uniform deposition might not be unconnected with erosion/entrainment, reportedly significant in their experiments.

For a uniform deposition, we could quantify the ''asphaltene-like'' particles retained within the capillary, thus estimating the extent of deasphalting. For instance, after 800 CVI, some 70 μm-worth of deposit layer had been formed in run-2. For a capillary length of 127 mm, the retained asphaltene volume was ~ 2.1 mm^3 which, for ρ_a =1.16 g/cm^3, was 2.4 mg. However, as at 800 CVI in run-2, about 12 mg of "precipitable" asphaltene had been injected, implying some 20% of the injected asphaltenes had been removed. As would be shown in Chapter 9, such in-situ deasphalting could have significant impact on oil recovery.

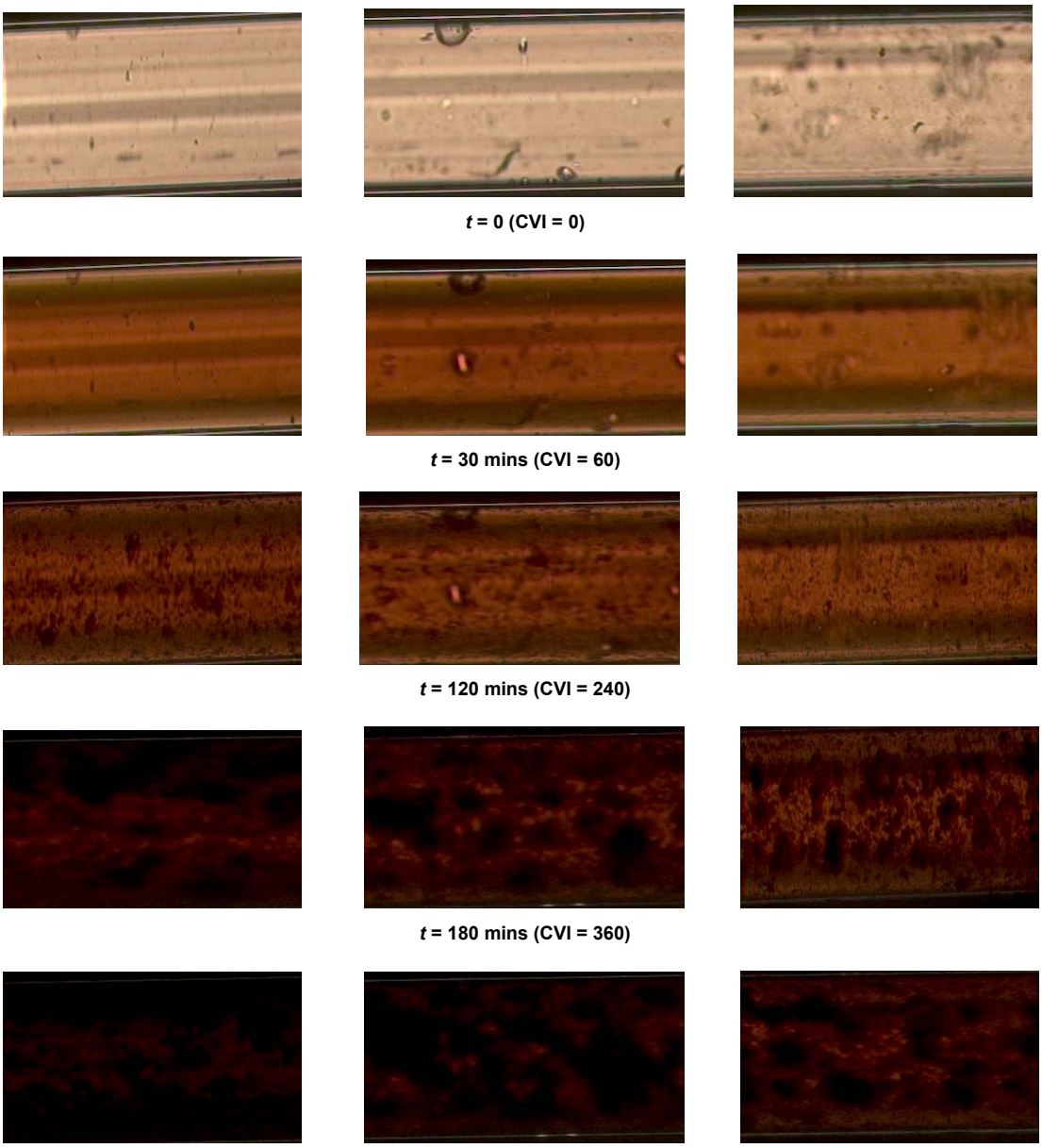


Fig. 5.36: Plan-View Photographs of Capillary Internals at Selected Times (Run 2)

5.5 Chapter Summary

The impairment of permeability and related porous-media properties due to asphaltene deposition has been studied. Here, we have distinguished between closed and open systems. The closed-system model tracks the deposition of a single asphaltene particle under the influence of gravity. The effects of rock and fluid properties as well as particle geometry on the deposition process have been elucidated.

The open-system modelling has taken advantage of the deep-bed filtration theory and studies on the kinetics of asphaltene deposition to develop a new asphaltene deposition and impairment

model, which has only three tuning parameters, characterising the deposition process and the hydraulic behaviour of the porous medium. Validation of the models against a large number of published experimental data sets, representing common types of porous media and particulate-laden streams, shows that they are robust. From the results of the validation, simple correlations have been proposed for predicting asphaltene-induced impairments in common porous media.

Finally, by performing capillary-flow experiments, we have examined some aspects of the deposition process at the pore scale and developed improved models for interpreting experimental data. From the results, some of the key assumptions, which include existence of deposition kinetics and uniform deposition behind the front, that underlie our theoretical models have been validated.

Chapter 6

Reservoir-Simulation Model for Nigerian Heavy-Oil Deposit

From the analyses and discussions in the last four chapters, it can be inferred that the dynamics of steam-based processes are overwhelming for analytic models. Specifically, current analytic models cannot handle, in sufficient details, key features such as multiphase and multi-dimensional flows, fluid-phase equilibria, well-related effects as well as realistic geologic and fluid models. Analysing the effects of in-situ oil upgrading and formation impairments due to asphaltene deposition is also a challenge for analytic methods.

On the prospects of experimental studies, there is a practical limit to which the effects of various parameters can be evaluated. Added to this, is the issue of upscaling, as the dimensions of typical laboratory models are orders of magnitude smaller than the field cases (Pujol and Boberg, 1972). Given these limitations of analytic and experimental studies, we continue the assessment of the feasibility of the alternating-injection processes by conducting numerical simulation studies. As a case study, the Nigerian heavy-oil system is considered though, in principle, most of the resulting deductions should be relevant for other tar deposits.

In this chapter, representative 3D reservoir-simulation models are constructed for an arbitrary sector of the Nigerian belt. The models are premised on rigorous assessment of the relative impacts of subsurface uncertainties on both hydrocarbon accumulation and recovery within the sector. To the best of our knowledge, the most comprehensive (and most cited) single work on the geosciences of this belt is that due to Adegoke *et al.* (1980), which was based on 40 boreholes in a 17 km^2 area. Hence, this work is the primary source of information for the current research. However, where data gaps exist, we supplement with other published studies on the Nigerian bitumen accumulation as well as analogous deposits from elsewhere, mainly the Athabasca region, Canada and the Orinoco belt, Venezuela.

6.1 Status of the Nigerian Heavy-Oil Sector

In southwestern Nigeria, a distinct bitumen belt has been mapped traversing present-day Ondo (7°10′N 5°05′E), Ogun (7°00′N 3°35′E) and Edo states (6°30′N 6°00′E) as well as parts of Lagos State (6°27′11″N 3°23′45″E). Within the belt, which is part of the Benin (Dahomey) Basin, unconventional hydrocarbons occur as outcrops, rich sands, lean sands and oil shale, distributed among three main (successive) horizons, which are generally continuous (Fayose, 2005). **Figs. 6.1a** and **b** illustrate the outcrop section of the belt, exposed over an approximate area of 120 km by 6 km (Enu, 1985). In terms of hydrocarbon potential, a recent study estimates that the entire belt (including areas, such as Lekki Lagoon, that are offset of the outcrop) hosts between 70 and 420 billion barrels of oil in association with some 1-13 Tscf of solution gas (Lawal, 2011a).

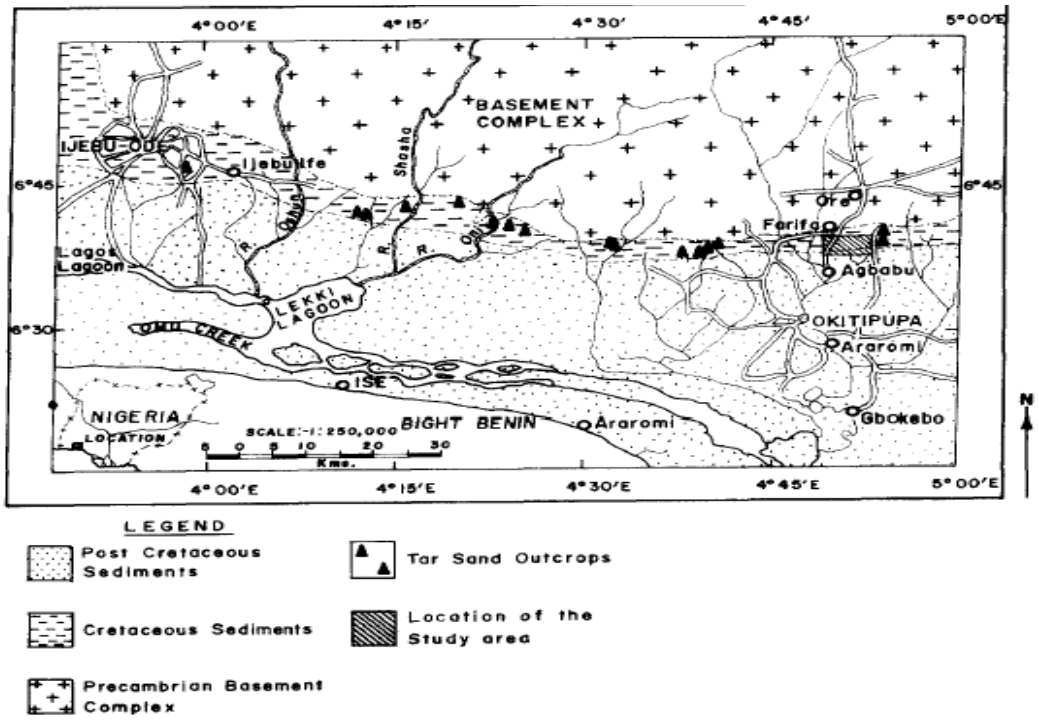


Fig. 6.1a: Tar Outcrop Belt of Southwestern Nigeria (after Enu (1985))



Fig. 6.1b: Some Exposed Tar-bearing Section at Agbabu, Southwestern Nigeria (Source: Tribune Newspapers (2011))

Since 1900 when this bituminous deposit was officially discovered in Nigeria, over 100 exploratory holes have been drilled followed by several independent studies (Gbadebo, 2010; Odunaike *et al.*, 2010, 2009; Akande, 2007; Oboh *et al.*, 2006; MSMD*, 2006; Sonibare *et al.*, 2003; Conoco, 2002; Ekweozor and Nwachukwu, 1989; Oluwole *et al.*, 1987; Enu, 1985; Adegoke *et al.*, 1980). However, most of these studies have focused primarily on rock and fluid characterisation (Asubiojo and Adebiyi, 2011; Akinmosin *et al.*, 2010; Adebiyi and Omode, 2007; Adebiyi *et al.*, 2006; Ukwuoma and Ademodi, 1999; Oderinde and Olanipekun, 1991; Ogunsola, 1991; Ogunsola

* Ministry of Solid Minerals Development.

and Williams, 1988). Although there are strong evidences that these vast resources are producible, including by natural flow (Akinmosin *et al.*, 2011; Akande, 2007; Steyn, 2006; Adegoke *et al.*, 1980; Nigerian Archives, 1909; BPA, 1936), commercial exploitation is yet to take off (Lawal, 2011a; KPMG, 2008; Nigeriafirst, 2006; Ayodele, 2006).

Ironically, Nigeria imports an average of 50,000 b/d of heavy crude from Venezuela, which is used as feedstock to the Kaduna Refining & Petrochemical Company (KRPC) (OnlineNigeria, 2009). With its installed capacity of 110,000 b/d, KRPC presently makes up some 25% of the total installed crude-refining capacity in Nigeria (NNPC[**], 2010). From heavy crude, KRPC produces asphalt, "base oils" for lubricants and greases as well as other refined products (NNPC, 2010). However, local road construction and other applications depend substantially on imported bitumen (Adedimila, 2000). Incidentally, earlier investigators (Adedimila, 2000; Adegoke *et al.*, 1980, 1974) have demonstrated the suitability of the Nigerian tar for road construction and petrochemical feedstock, among other industrial uses. On these evidences and for the purposes of sustainable development, there is a strong case for concerted efforts towards an efficient exploitation of these vast resources. Nevertheless, it is imperative that the commercial exploitations be premised on the outcome of rigorous technical studies, to which the current research is a modest contribution.

Although open-pit mining has been proposed for the relatively shallow (< 50 m) sections of the belt (Adegoke *et al.*, 1980, 1978, 1976), the suitability of in-situ recovery methods has been recognised for the deeper pools (Adegoke *et al.*, 1980). However, early researches appear to be driven by the surface-mining philosophy, as evident in the greater efforts expended on the surface treatment of the mined slurry (Adewusi and Adetona, 1998; Ademodi *et al.,* 1987). It is instructive to note that the limited studies on the surface treatment recommended the use of slightly alkaline hot water (< 85 ^{o}C) for winning oil from the mined tar sand (Adewusi and Adetona, 1998; Adegoke *et al.*, 1980; 1976). To some extent, this finding provides some impetus for thermal in-situ methods in general and hot water (steam) in particular. But as we shall show later, hot water, compared to steam, is not competitive for the deposit under discourse.

As far as we are aware, at least in the public domain, there is limited information on the reservoir engineering aspects of the deposit. In particular, except the field pilot reported by Akande (2007) and the core-flood experiments by Adewusi (1998a, b), Adewusi and Adetona (1998) as well as Omole and Omolara (1988), we are not aware of any other investigation on the prospects of steam injection in the belt. Taken further, apart from a recent paper by Lawal (2011b), numerical simulation studies on the reservoir engineering aspects of the system remain to be published. Perhaps, the current work is the first attempt at constructing a detailed reservoir-simulation model, entailing the integration of available and estimated data on the geology, petrophysics and fluids to evaluate potential performances of wells and exploitation strategies.

[**] Nigerian National Petroleum Corporation.

6.2 Geology

According to geoscientists, the Nigerian tar-bearing sands occur within the Dahomey Basin, which comprises three main formations (Enu, 1985; Adegoke *et al.*, 1980). From the shallowest to the deepest, the formations are identified as Ise, Afowo and Araromi (Omatsola and Adegoke, 1981; 1980). While the Ise formation is predominantly wet, there is evidence of hydrocarbons in Araromi formation but Afowo is the primary host of hydrocarbons within the Basin (Fayose, 2005; Enu, 1985; Adegoke *et al.*, 1980).

The Afowo Formation, with known maximum thickness of about 430 m in Afowo-1 well, comprises medium to fine-grained sandstones with relatively thick interbedded siltstones and shales, which are rich in organic matter. Shaliness increases progressively from bottom to top. It is bituminous in both surface and subsurface sections (Gbadebo, 2010; Fayose, 2005). The Afowo and Araromi shales are believed to be the source rocks for these unconventional oil deposits (Adegoke *et al.*, 1976). Within the Afowo Formation, there are six distinct stratigraphic units. From the base to the top, these are basal horizon, horizon 'Y', oil shale, horizon 'X', upper shales & limestones, and laterite & top soil.

The basal horizon comprises poorly sorted sand conglomerates and partially weathered basement materials, including silts and kaolinitic clays. It contains negligible amount of oil. Within the study area (Adegoke *et al.*, 1980), its thickness varies from 1 to 2.5 m. Deep boreholes (up to 90 m depth) encountered a confined (artesian) aquifer in the southern half of the study area but not in the north (Fayose, 2005; Adegoke *et al.*, 1980). Although neither the aquifer size nor its transmissibility is known, considering the quality of sand in this unit, it is fair to assume the aquifer is inactive, although it is a potential heat sink.

Horizon 'Y' is the lower bituminous horizon. Its average sand content, as penetrated by the boreholes, exceeds 94%. It consists of fine-medium grained sands interbedded with thin columns of sandy-clay and shales. As these shales contain large quantities of macrofossil shells, they are potential high-permeability pathways. Thus, in hydraulic terms, all the interbeds, reportedly less than 2 m thick, may be treated as "sands". In general, the sands are heavily saturated with bitumen. Within the explored area, the net thickness of this horizon lies between 10 and 26 m, with a mean of about 15 m (Enu, 1985).

Throughout the area of exploration, the so-called oil shale unit is continuous and overlies Horizon 'Y'. It is characterised by relatively uniform thickness and comprises of oil-saturated shales. Because of its unusually rich hydrocarbon and organic matter content (> 10 wt. %), the unit is referred to as an oil shale (Enu, 1985; Adegoke *et al.*, 1980). Despite that this layer physically separates the two pay zones, Horizons 'Y' and 'X', its hydraulic behavior, either as a flow baffle or barrier remains unknown, especially with its abundant quantity of macrofossil shell fragments (Adegoke *et al.*, 1980). However, based on geologic considerations, it is fair to anticipate that this unit would not exhibit similar hydraulics as the pay zones. Within the overall study area, this package is characterised by thickness variation of 6 to 15 m, averaging 8 m.

Horizon 'X' is the upper bituminous package, with average sand content exceeding 90%. Its geology is very similar to that of Horizon 'Y' but shows relatively less thickness variation, ranging from 10 to 22 m, with a mean of 15 m. A north-south section through the 17 km^2 area investigated by Adegoke *et al.* (1980) illustrates the stratigraphic sequence of the three main bitumen-impregnated units (**Fig. 6.2**).

The interval referred to as upper shales and limestones contains shale, sandy-clay and interbedded thin limestone bands as the dominant lithology. Although there may be local oil shows due to upward migration along fractures (Akinmosin *et al.*, 2011), this unit serves as the main cap rock, providing hydrodynamic barrier against fluid escape. In general, its thickness ranges from 3 to 55 m (Adegoke *et al.*, 1980).

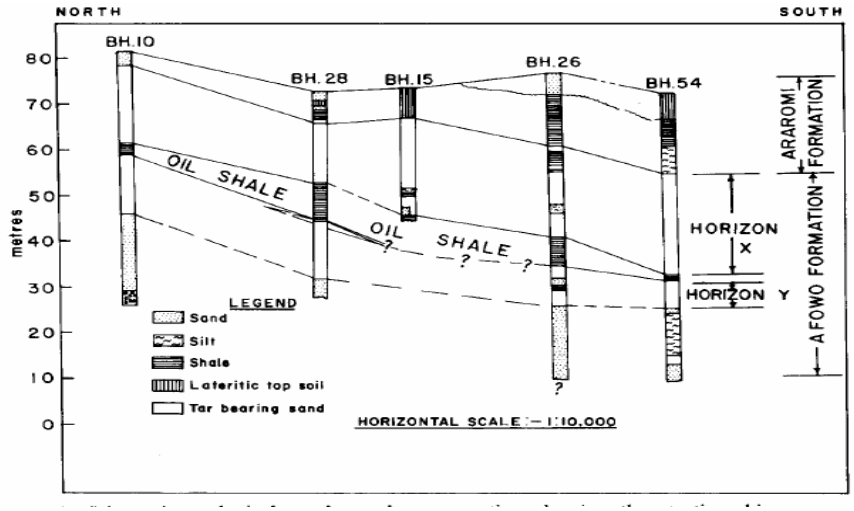


Fig. 6.2: Geologic N-S Cross-section of the Stratigraphy of Nigerian Tarsand Units (after Enu, 1985)

The overlying unit, which is the laterite and top soil, comprises laterised clay, sand and pebbles. It is 1.5-8 m thick. Given its relatively high clay content, this unit is a potential secondary cap rock. With the underlying layer (upper shales and limestones), they constitute the reservoir overburden.

As a composite, the overburden is predominantly silty-sand, making it of vulnerable sealing. Hence there is high risk of hydrocarbon loss by seepage and evaporation. In addition, this is a major concern for thermal recovery as heat and pressure containment may be threatened (Roche, 2010). In practice, one way of mitigating the risks of cap-rock failure is to inject below the fracture pressure (Bagci *et al.*, 2008). In units 'X' and 'Y', sediments are moderate to well sorted, indicative of relatively high-energy depositional environments (Enu, 1985). There is no evidence of intra-reservoir faults, and trapping mechanism is primarily stratigraphic.

Virtually all the layers are impregnated with reasonable amounts of bitumen but highest concentrations are in horizons 'X', 'Y' and the oil shale. Enclosed within the oil shale are lenses of heavily-saturated sands (Adegoke *et al.*, 1980), further suggesting that this unit is more likely to be flow baffle than barrier.

The foregoing is a summary of the geology that is relevant for the construction of a fit-for-purpose reservoir model for use in the current study, which primary focuses on reservoir engineering. More details on the geology and the other aspects of the geosciences of the belt can be found in a number of dedicated sources (Odunaike *et al.*, 2010, 2009; Conoco, 2002; Ekweozor and Nwachukwu, 1989; Enu, 1985; Omatshola and Adegoke, 1981; Adegoke *et al.*, 1980).

6.3 Petrophysics

From available sources (Lawal, 2011a; Fayose, 2005; Enu, 1985; Adegoke *et al.*, 1980), average net thicknesses of the main horizons are presented in **Table 6.1**. These estimates are somewhat conservative, as they ignore the thickening sequences towards the southern area, which is currently unexplored. Because neither a gas-cap nor contiguous basal water has been encountered, the thicknesses effectively refer to the oil sand.

Table 6.1: Average Net Thicknesses (metres)

Horizon	Low	Base	High
X	10	15	22
Oil shale	6	8	15
Y	10	15	26
Total	*26*	*38*	*63*

Although hydrocarbon contents were reported as mass fractions (relative to the bulk rock), we converted them to saturations (relative to pore volume), assuming equal-density bitumen and water, and negligible free gas. Using published data (Akinmosin and Shoyemi, 2010; Fayose, 2005; Adegoke *et al.*, 1980), we obtain the estimates in **Table 6.2**, as the averages. The relatively wide range reflects uncertainties in sampling, method of analysis and heterogeneity. In all cases, there is no initial free gas (S_{gi} = 0).

Porosity values presented in **Table 6.2** were estimated from the range published by Enu (1985); assuming the horizons are positively dependent and have equal porosities. Compared to core-based average porosity and oil saturation of 35% and 83% in Alberta's Surmont field (Wei and Gates, 2010), it is apparent that our estimates are satisfactory.

Table 6.2: Average Porosity and Bitumen Saturations (Fraction)

Horizon	Low		Base		High	
	ϕ	S_{oi}	ϕ	S_{oi}	ϕ	S_{oi}
X	0.24	0.61	0.30	0.80	0.35	0.91
Oil shale	0.24	0.50	0.30	0.68	0.35	0.82
Y	0.24	0.61	0.30	0.80	0.35	0.91

Owing to paucity of record on permeability and compressibility measurements on the Nigerian deposit, we use Athabasca pools as analogue. From a review of Canadian reservoirs, Dusseault (2001) reported permeability range of 0.5-5 D, with tar sands typically 1-3 D. Detailed analyses of core data from the McMurray sand formation in the Surmont field, northeast Alberta, showed average permeability of 5 D (Wei and Gates, 2010). Noting that the Nigerian tar sand is generally of superior textural characteristics and lower clay content (2-7% vs. 10-25%) to Athabasca accumulations (Enu, 1985; Carrigy, 1973), it is expected that the former would typically be more permeable than the latter. Hence, the use of Athabasca data in this study may be conservative.

Accordingly, for the Nigerian system, we assume 1, 2 and 5 D as the low, base and high absolute permeability, respectively. When compared to the 2-15 D indicated for Venezuelan heavy-oil sands, also reportedly of higher quality than Canadian sands (Dusseault, 2001), it is apparent that the assumed range for the Nigerian system would most likely be reviewed upwards.

Based on evidences of sand lenses and microfossils within the oil shale unit (Adegoke *et al.*, 1980), in all cases, we treat the oil shale as a baffle rather than a flow barrier. For simplicity, the oil shale permeability is some percentage of that of beds 'X' and 'Y', which are taken to be the same. With dependent combination of permeabilities, we arbitrarily assume percentages of 10, 20 and 50% in the low, base and high realisations, respectively. In other words, depending on the realisation, units 'X', 'Y' and the oil shale have low or high permeabilities at the same time.

Assumed values, typical of Athabasca deposits (Gotawala and Gates, 2009; Li and Chalaturnyk, 2009; Bagci *et al.*, 2008; McGee and Vermeulen, 2007; Law, 2004; Yee and Stroich, 2004; Doan *et al.*, 1999), of horizontal permeability and K_v/K_h are indicated in **Table 6.3**. Compared to the McMurray sandstone in Athabasca (Edmunds *et al.*, 2009, 1994), our permeability estimates seem conservative. In the horizontal direction, permeability is isotropic ($K_y = K_x$). Assumed rock compressibility and skin factor are presented (Chalaturnyk, 2009; Dusseault, 2001). Relative to the K_v/K_h data from micromodels (high-resolution) of the McMurray formation in Athabasca (Deutsch, 2010), our Nigerian estimates are largely conservative.

Table 6.3: Average Permeability, K_v / K_h, Rock Compressibility and Skin Factor

Horizon	Low		Base		High	
	K_h (D)	K_v / K_h	K_h (D)	K_v / K_h	K_h (D)	K_v / K_h
X & Y	1	0.2	2	0.5	5	0.7
Oil shale	0.1	0.2	0.4	0.5	2.5	0.7
Rock Compressibility (kPa^{-1})						
All horizons	0.5×10^{-6}		5×10^{-6}		50×10^{-6}	
Skin Factor						
All horizons & wells	0		5		15	

6.4 Wettability, Relative Permeability and Capillary Pressure

Adegoke *et al.* (1980) reported that the Nigerian tar sand is water-wet. However, the degree (contact angle) of wettability is unknown, especially at field scale, because their investigation was qualitative. This notwithstanding, we assume a strongly water-wet system, similar to the Athabasca sands (Enu, 1985).

Lack of relative-permeability data for the belt informed the application of Corey-type correlations (Corey, 1954) which, in spite of its simplicity, have been used successfully for theoretical studies as well as rationalisation of laboratory and field results (Lei *et al.*, 2010; Niz-Velasquez *et al.*, 2009; Pamukcu and Gumrah, 2008; Sedaee Sola *et al.*, 2007; Kisman and Yeung, 1995; Beattie *et al.*, 1991). However, to minimise uncertainties, the correlations were first constrained to limited Athabasca data (Bagci *et al.*, 2008; Law, 2004; Law *et al.*, 2003). Details of this procedure are discussed elsewhere (Lawal, 2011b).

Relevant Corey parameters are listed in **Table 6.4**. Except where indicated otherwise, the parameters are independent of lithology. Following the work of Valenti *et al.* (2002), we have assumed a positive correlation between S_{oi} and S_{orw} (and S_{org}). That is, high (low) S_{oi} corresponds to high (low) S_{orw}. In the presence of CO_2 (and flue gas), we reduce the S_{or} values in **Table 6.4** by 25%, thereby accounting for potential CO_2-induced improvement in the microscopic displacement efficiency due to oil swelling, dilution, reduced interfacial tension (IFT), vapourisation of intermediate components and other microscopic phenomena (Sohrabi *et al.*, 2008; Hornbrook *et al.*, 1991; Klins, 1984). In a subtle way, this also accounts for possible composition-dependency of relative permeabilities.

The Stone-2 model (CMG, 2010a; Stone, 1973) is used to estimate three-phase relative permeabilities from the resulting two-phase Corey functions. By neglecting hysteresis, drainage and imbibition curves are taken to be the same. The combination of high permeability and oil viscosity suggests that viscous forces would override capillary forces, especially at field scale. Given this point and the lack of data, we neglect capillarity.

On temperature-dependency of relative permeabilities, opinions are currently divided in the literature. While most researchers generally conclude that temperature enhances relative permeability of the non-wetting phase but undermines that of the wetting phase (Sedaee Sola *et al.*, 2007; Schembre *et al.*, 2006; Nakornthap and Evans, 1986; Kumar *et al.*, 1985), other workers did not notice any significant effect (Polikar *et al.*, 1986; Miller and Ramey, 1985; Sufi *et al.*, 1982). To capture the full range of possibilities, we consider temperature effects in our base and high-case models but not in the low-case model.

Recently, Saeed (2010) showed that the temperature-sensitivity of relative permeabilities is partly due to the dependency of residual oil saturation (ROS) on oil viscosity and IFT. As viscosity and IFT are affected by temperature, it follows that ROS, which affects relative permeabilities, also changes. Hence, the following semi-empirical correlation relates sandstone ROS at temperatures T_1 and T_2 (Saeed, 2010).

$$S_{or2} = S_{or1} + \frac{m(T_1 - T_2)}{T_1 T_2}; \quad S_{oi} \geq S_{or} \geq x_a S_{oi} \tag{6.1}$$

where S_{or2} and S_{or1} are ROS at T_1 and T_2, respectively. T and S_{or} are in K and fraction, respectively. The value of the constant m depends on the realisation under consideration. For the base and low (pessimistic) cases, the constant m equals 51.095 and 184.935 K, respectively. The lower limit of S_{or} for crude of asphaltene mass fraction x_a, is premised on the deposition of all the asphaltenes.

In the current study, we assume that only ROS varies with temperature, ignoring effects of temperature on other Corey parameters such as end-points, exponents and critical saturations (Shen *et al.*, 2010; Nakornthap and Evans, 1986). **Figs. 6.3** and **6.4** illustrate one of the examples using the base-case parameters in **Table 6.4**.

Table 6.4: Input Data for Corey-type Relative-Permeability Functions

	Low	Base	High	Comments / References
S_{orw}	0.48	0.40	0.30	Xin *et al.* (2010); Sedaee Sola *et al.* (2007); Wang *et al.* (2006); Valenti *et al.* (2002); Law *et al.* (2003); Polikar *et al.* (1989); Miller & Ramey (1985); Poston *et al.* (1970)
S_{wc}^{Ψ}	0.39 *(0.5)*	0.2 *(0.32)*	0.09 *(0.18)*	see **Table 6.2**
S_{wcrit}	0.39	0.2	0.09	Assuming $S_{wc} = S_{wcrit}$
S_{org}	0.15	0.1	0.05	Assuming $S_{org} = 0.5 S_{orw}$; Frauenfeld *et al.* (1988)
S_{gc}	0	0	0	See **Table 6.2**
S_{gcrit}	0.1	0.05	0.01	Gotawala & Gates (2009); Law (2004); Law *et al.* (2003); Smith *et al.* (1992)
K_{rwm}	0.5	0.4473	0.4	Bagci *et al.* (2008); Law (2004); Law *et al.* (2003)
K_{rgm}	0.9	0.9567	1	Bagci *et al.* (2008); Law (2004); Law *et al.* (2003)
K_{rowm}	0.9	0.9942	1	Law (2004); Law *et al.* (2003); Glandt & Malcolm (1991)[#]
K_{rogm}	0.834	0.9942	1	Bagci *et al.* (2008); Law (2004); Law *et al.* (2003)
N_w	3.5	2.5	1	CMG (2008a); Sedaee Sola *et al.* (2007); Law *et al.* (2003); Glandt & Malcolm (1991); Meldau *et al.* (1981)
N_{go}	3.5	2.5	1	”
N_{ow}	3.5	2.5	1	”
N_g	3.5	2.5	1	”

where S_{orw} = residual oil saturation (water/oil), S_{wc} = connate water saturation (water/oil), S_{wcrit} = critical water saturation, S_{gc} = connate gas saturation, S_{gcrit} = critical gas saturation, S_{org} = residual oil saturation (gas/oil), K_{rwm} = water relative permeability at residual oil saturation, K_{rgm} = gas relative permeability at residual oil saturation, K_{rowm} = oil relative permeability at connate water saturation, K_{rogm} = oil relative permeability at critical gas saturation, N_w = water relative permeability exponent (water/oil), N_g = gas relative permeability exponent (gas/oil), N_{ow} = oil relative

$^{\Psi}$ Values in bracket refer to the oil-shale horizon while those outside bracket apply to horizons ‘X’ and ‘Y’.
$^{\#}$ Data based on Peace River (Canada) bituminous rocks.

permeability exponent (water/oil), N_{go} = oil relative permeability exponent (gas/oil). While the saturations are in fraction, the other quantities are dimensionless.

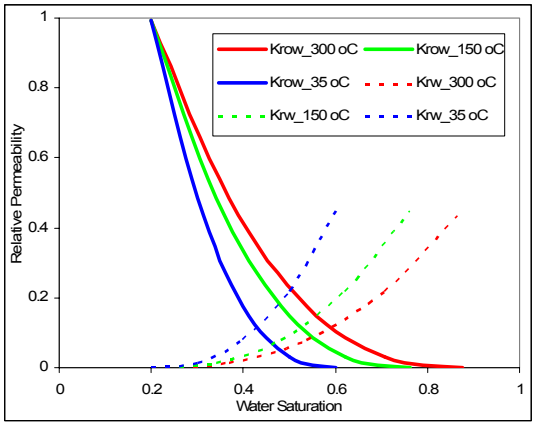


Fig. 6.3: Oil-Water Relperm Model (Base-Case)

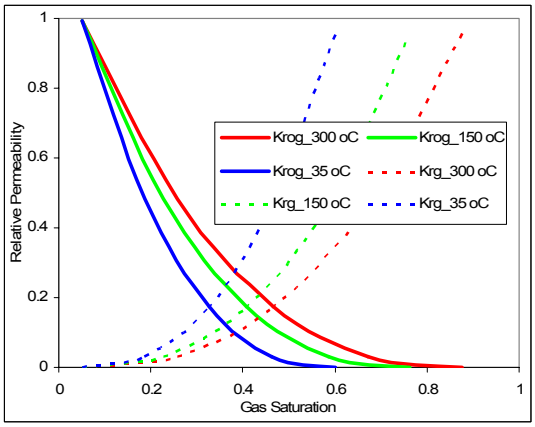


Fig. 6.4: Gas-Oil Relperm Model (Base-Case)

6.5 Thermal Properties and Aquifer Model

In the absence of thermal properties of the Nigerian bituminous rocks, we take recourse to published Athabasca data, from which we obtained the estimates shown in **Table 6.5**. The relatively wide ranges of these estimates reflect the order of uncertainties.

Table 6.5: Estimated Thermal Properties for Nigerian Bituminous Rocks

	Low	Base	High	Reference
Thermal conductivity (reservoir, over/under-burden), W m^{-1} K^{-1}	0.9	1.7	7.6	Bagci *et al.* (2008), Law (2004)
Heat capacity (overburden & underburden), MJ m^{-3} K^{-1}	1.3	2.6	5.8	Bagci *et al.* (2008), McGee and Vermeulen (2007), Law (2004), Butler (1997)

From exploratory data, pockets of normal-pressured basal water sand have been encountered (MMSD**, 2010; Fayose, 2005). At best, these water-bearing sands are artesian to sub-artesian (1 - 2.5 m thick), with limited prospects of recharge. However, large uncertainties remain with the southern limit of the belt, partly because it has not been explored and due to its proximity to the Atlantic Ocean. In this study, where an aquifer is considered, we assume bottom aquifer, whose thickness is a fraction of that of the reservoir but has similar properties as the reservoir (**Table 6.6)**.

** Ministry of Mines & Steel Development.

In the low realisation, no aquifer exists. But where it is modelled, the aquifer has the same area as the reservoir.

Table 6.6: Aquifer Properties

	Low	Base	High
Thickness (fraction of reservoir)	-	0.1	1.0
Permeability (D)	-	2	5

6.6 Reservoir Datum and Initial Conditions

Prognosis suggests that viscous oil in the zone occurs down to about 1000 m, especially in the southern limit (Adegoke *et al.*, 1980). For our analyses, we use an arbitrary datum of 500 m, referenced to the base of the reservoir. Because initial temperature and pressure of the accumulation are not known, we use typical trends of normal-pressured reservoirs in the onshore section of the neighbouring Niger Delta basin (Lawal and Adenuga, 2010).

$$T_r = 0.0191D + T_a\,, \tag{6.2}$$

$$P_r = 0.0098\,D + 0.1013\,, \tag{6.3}$$

where D is vertical depth (m), T_a is ambient temperature (^oC). T_r and P_r are in ^oC and MPa, respectively.

To estimate average T_a for the belt, we use the data for Akure (7°15′0″N 5°11′42″E), which is in proximity to Ore (6°45'0"N 4°52'0"E) and Agbabu (6°34'60''N 4°49'60''E), two of the areas straddled by the belt. From a 10-year (1992-2001) observation, Akinbode *et al.* (2008) reported annual mean-temperature of 21.9-30.4 ^oC for Akure. Taking 26.2 ^oC for the ambient, initial formation temperature and pressure are estimated to be 35 ^oC and 5 MPa, respectively. Note that only the reservoir-base is at 5 MPa, with the shallower layers at lower pressures determined by the hydrostatic gradient. However, we do not account for temperature gradient, as the formation is not very thick (< 80 m gross thickness).

6.7 Fluid Model

In contrast to light oils, which usually have a full suite of pressure-volume-temperature relationships and pure-component characterisation, heavy crudes are typically limited to viscosity vs. temperature relationships and their composition often available as chemical aggregates of saturates, aromatics, resins and asphaltenes (SARA) (Adebiyi and Omode, 2007; Alboudwarej *et al.*, 2006; Newley and Merrill Jr., 1991). Given the relatively less useful SARA characterisation and viscosity data, researchers have learnt to construct pseudocomponents (PC), which are then used to characterise the available viscosity measurements (Lawal, 2011b; Lawal and Adenuga, 2010;

Mehrotra and Svrcek, 1988; Johnson *et al.*, 1987). In this work, limited to just SARA analyses and viscosity data, we take the same approach.

As the base-case viscosity model, we use the limited data set representing a sample of the Nigerian bitumen published by Ukwuoma and Ademodi (1999). As noted elsewhere (Lawal, 2011b), although this dataset has some shortcomings, which include being based on outcrop rather than subsurface sample, we still employ it as the reference model due to the absence of other data on the Nigerian deposit.

The high-case (pessimistic flow) viscosity data set, taken from Bazyleva *et al.* (2010), represents typical "high"-case bitumen for Athabasca reservoirs. On the other hand, the low-case (optimistic flow) set is a typical viscosity relationship for heavy-oil pools in the Wabasca region, also in Canada, sourced from Svrcek and Mehrotra (1989). It is interesting to note that this Wabasca sample is much less viscous than typical Venezuelan heavy crudes (Zabel *et al.*, 2010), hence increasing the chances that the Nigerian accumulation, however heterogeneous, would not fall outside the range of viscosity values covered in our investigation. The reference sets of viscosity data are presented in **Fig. 6.5**.

It is worth mentioning that there is evidence that suggests that some areas of the belt contain oil of lower viscosity and higher quality than what we currently take as our optimistic viscosity data. For example, Steyn (2006), in discussing the oil exploration activities in Nigeria during the colonial era, cited an account that some 2,000 b/d of “good” quality oil was being produced (under natural drive) from the Lekki Lagoon concession (**Fig. 6.1a**) over a period of one year (1908-1909), and the exploitation was only stopped because of excessive water production (aquifer influx). Apparently, with this total rate, possibly from a maximum of 15 vertical wells (as at then 15 wells had been drilled, but the exact number of producers was not stated), and the indication that the oil quality was “good”, it is not likely that the in-situ viscosity of such oil would be up to 1000 cP. In addition, apart from documented cases of natural seepage (Akinmosin *et al.*, 2011), fairly recent records show that the vertical well NBC-10 produced 86 b/d of live heavy-oil naturally (Adegoke *et al.*, 1980). Furthermore, owing to improper abandonment, heavy-oil typically leaked from the well NBC-7 on hot days (Lawal, 2011a; Adegoke *et al.*, 1980). Based on this discussion, forecasts premised on **Fig. 6.5** may be somewhat conservative.

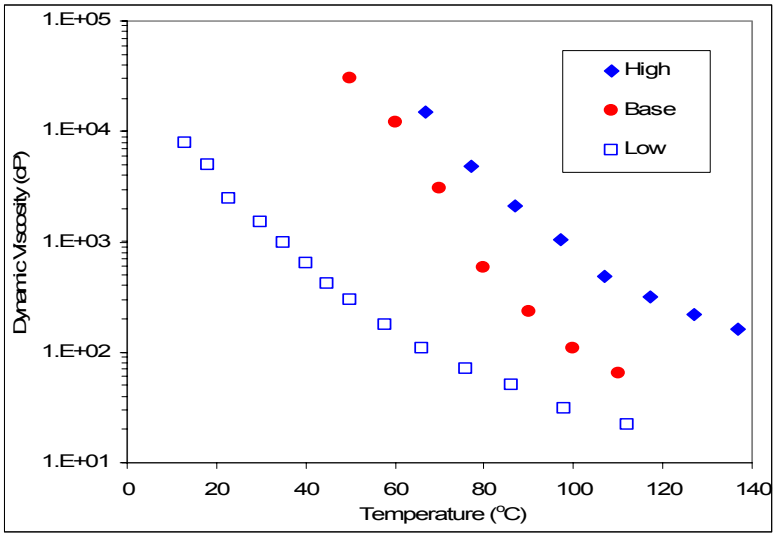


Fig. 6.5: Reference Viscosity-Temperature Relationships for Nigerian Heavy Oil

Field observations have shown that the bitumen in the Nigerian belt contains some dissolved gas under reservoir conditions (Adegoke *et al*., 1980). In order to take this into account, we use the range of initial gas-oil ratio (GOR) R_{si} and oil formation volume factor B_{oi} (**Table 6.7**) estimated elsewhere (Lawal, 2011a; Lawal and Adenuga, 2010). Hence, in addition to viscosity, we use gas solubility and oil shrinkage as constraints in generating the fluid models.

Table 6.7: Estimated R_{si} and B_{oi} for Nigerian Bitumen (Lawal, 2011a; Lawal and Adenuga, 2010)

Property	Low	Base	High
R_{si} (scf / stb)	6	22	50
B_{oi} (rb / stb)	1.10	1.04	1.00

To construct a model of the heavy oil under discourse, its composition is required. Due to non-availability of this composition, we employ the generic PC schemes recently proposed for the Nigerian bitumen (Lawal and Adenuga, 2010), reproduced here as **Table 6.8**. Fluid modelling is accomplished with the commercial pressure-volume-temperature (PVT) simulator, WinProp (version 2010.10), developed by the Computer Modelling Group (CMG) Ltd., Calgary.

To replicate the viscosity measurements and the estimated gas solubility by regression, we invoke the Peng-Robinson equation-of-state (EOS) (Peng and Robinson, 1976) and the viscosity correlation of Pedersen and Fredenslund (1987). In characterising the PC's, we only enter the corresponding molecular weight (MW) and specific gravity (SG), allowing the PVT simulator to estimate necessary parameters from selected correlations, listed in **Table 6.9**. In general, the correlation of Twu (1984), applicable for $SG \leq 1.436$ and normal boiling temperature $T_b \leq 715$ °C (CMG, 2010b), covers the range of our PC's and the foreseeable operating conditions. For the acentric factors and critical constants of petroleum fractions, the Lee-Kesler model (Lee and Kesler, 1975) is often adequate (Mehrotra and Svrcek, 1988). The parameters of the fluid models are tuned

until “satisfactory” match of the viscosity measurements and gas solubility are obtained. However, compared to the estimated gas solubility data, much higher weight was assigned to the viscosity data because the latter is derived from actual observations unlike the former that is estimated from correlations developed for other heavy crudes though trapped in formations of comparable geologic settings as Nigerian deposits (Enu, 1985). The regression parameters include PC properties such as critical constants and acentric factors as well as viscosity-model parameters such as coupling factors. For consistency, the same set of regression parameters are employed in all the cases.

Table 6.8: Pseudocomponent Groups for the Nigerian Bitumen (Lawal and Adenuga, 2010)

Scheme	Pseudocomponent	Composition (wt. %)	MW (g / mol)	SG	Composition (mol. %)
1-PC	Bitumen	100	657	1.01	100
2-PC	Gas	0.25	16	0.65	9.36
(2-phase basis)	Dead-Oil	99.75	659	1.01	90.64
	Total	**100**	**657**	**1.01**	**100**
3-PC	Gas	0.25	16	0.65	8.72
(3-phase basis)	Maltene	75.51	539	0.97	78.15
	Asphaltene	24.24	1030	1.16	13.13
	Total	**100**	**657**	**1.01**	**100**
4-PC	Gas	0.25	16	0.65	8.24
(Solubility basis)	Oil	37.26	382	0.86	51.44
	Precipitable-Asphaltene	8.93	1030	1.16	4.57
	Unprecipitable-Asphaltene	53.56	790	1.13	35.75
	Total	**100**	**657**	**1.01**	**100**
4-PC	Gas	0.25	16	0.65	8.40
(Distillation basis)	Distillable-Oil	5.59	368	0.81	8.16
	Undistillable-Oil	31.67	405	0.88	42.09
	Asphaltene-Resin	62.49	813	1.13	41.35
	Total	**100**	**657**	**1.01**	**100**
5-PC	Gas	0.25	16	0.65	8.37
(Solubility & Distillation)	Distillable-Oil	5.59	368	0.81	8.13
	Undistillable-Oil	31.67	405	0.88	41.95
	Precipitable-Asphaltene	8.93	1030	1.16	4.65
	Unprecipitable-Asphaltene	53.56	778	1.13	36.90
	Total	**100**	**657**	**1.01**	**100**

Table 6.9: Correlations Used for the PC Parameters (Lawal, 2011b)

Parameter	Correlation
Normal boiling point temperature	Twu (1984)
Acentric factor	Lee and Kesler (1975)
Critical constants	Lee and Kesler (1975)

At any condition, the following mole-average Arrhenius expression is used to estimate the mixture (oil-phase) viscosity from prevailing PC viscosities and mole fractions (Poling *et al.*, 2000):

$$\mu_m = \prod_{i=1}^{N} \mu_i^{x_i}, \tag{6.4}$$

where μ_m and μ_i are the dynamic viscosities of mixture and PC *i*, respectively; x_i is the mole fraction of PC *i* and *N* is the number of PC's making up the mixture at prevailing conditions.

As shown in **Fig. 6.6**, there is a good agreement between the actual and simulated viscosity-temperature relationships for all the PC schemes. But from a consideration of the relative accuracy, computational efficiency and dynamic performances, it was concluded that the 3-PC scheme is the optimum (Lawal, 2011b). Hence, in the current research, we use the 3-PC scheme for the construction of the fluid model. However, for the screening studies, the 1-PC (dead oil) scheme is employed.

Fig. 6.7 depicts the pseudo viscosity profiles of the PC's for the 3-PC model. These profiles are the products of tuning the EOS and viscosity models by least-squares regression, in combination with the mixing rule of **Eq. 6.4**, to reproduce the actual measurements. Having been constrained to available experimental data, the models and PC's can be used for predictive purposes, with the underlying assumption that the mechanisms that influenced the original experiments would still be dominant at other conditions (Lawal, 2011b). Please note that during the fluid characterisation, the component viscosities were used as fitting parameters with the asphaltene viscosity being the most uncertain while the properties of CH_4, being a standard component, were not adjusted. However, during reservoir simulations, the already characterised component viscosities were simply combined according to **Eq. 6.4** to estimate the crude viscosity at prevailing conditions.

Finally, based on the characterised EOS, fluid models are generated for each of the PC schemes for subsequent use in the thermal simulator. The distribution of PC's between phases is described by equilibrium ratios (*K*-values), which assume ideality of the PC's, thus the *K*-values only vary with temperature and pressure, neglecting compositional dependencies (Lolley and Richardson, 1998).

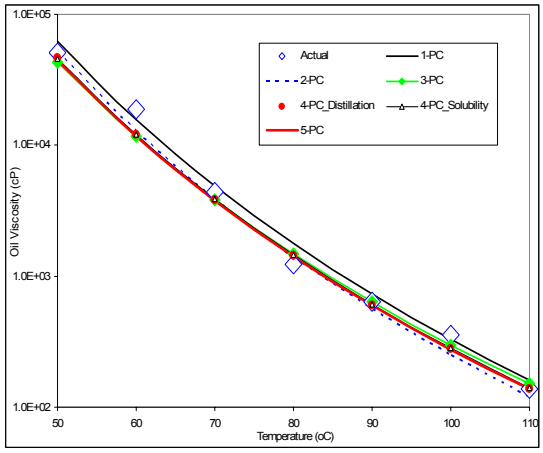


Fig. 6.6: Viscosity Matched to PC Schemes (Lawal, 2011b)

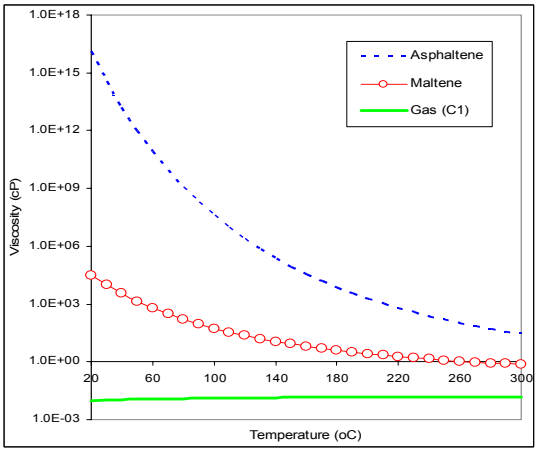


Fig. 6.7: PC Viscosities of Matched 3-PC Model (Lawal, 2011b)

As evident in the *K*-values presented in **Figs. 6.8-6.10**, within the range of temperature and pressure examined, the component C1 is most stable in the gaseous phase while the PC's maltene and asphaltene have considerable preference for the oleic phase. As shown in **Figs. 6.11** and **6.12**, both CO_2 and N_2 have much greater affinity for the gaseous phase than the oleic phase. However for the same conditions, CO_2 is more soluble in the oleic phase than N_2. Although these *K*-values are estimates, they are generally consistent with experimental values for typical crudes (Almehaideb *et al.*, 2001).

As input to the reservoir simulator, the component-phase distribution for the 3-PC system is presented in **Table 6.10**, which basically entails splitting the components among the three phases identified as aqueous, oleic and gaseous. In the dynamic-simulation output, all the components of the product stream are also found in these three phases. Note that this phase distribution ignores possible cracking of the oil and potential reactions (Sonibare *et al.*, 2003; Hayashitani *et al.*, 1978). This explains why the asphaltene is not modelled as existing in a distinct solid phase. As required by the simulator, asphaltene has been included in the gaseous phase. But, on the basis of the *K*-values (**Fig. 6.10**), it is not stable in the gaseous phase.

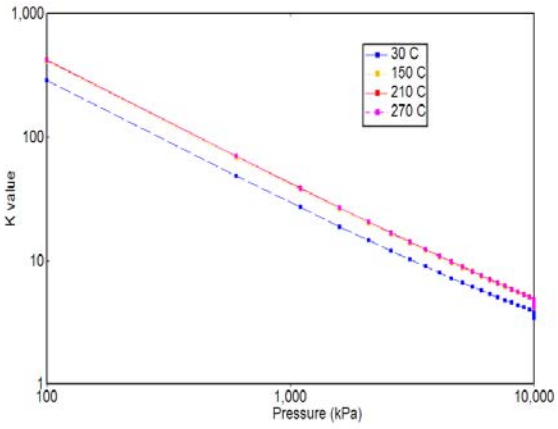


Fig. 6.8: Gas-Liquid (Oleic) Equilibrium Ratios for CH_4

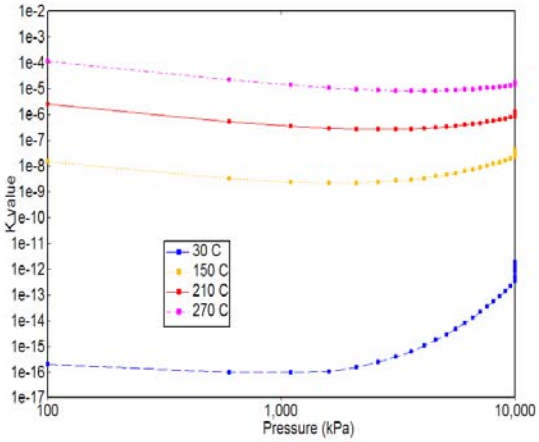


Fig. 6.9: Gas-Liquid Equilibrium Ratios for Maltene

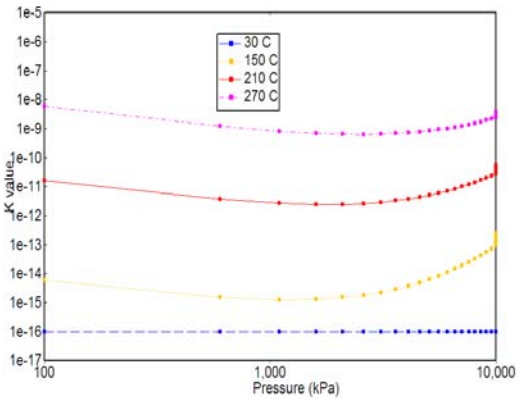


Fig. 6.10: Gas-Liquid Equilibrium Ratios for Asphaltene

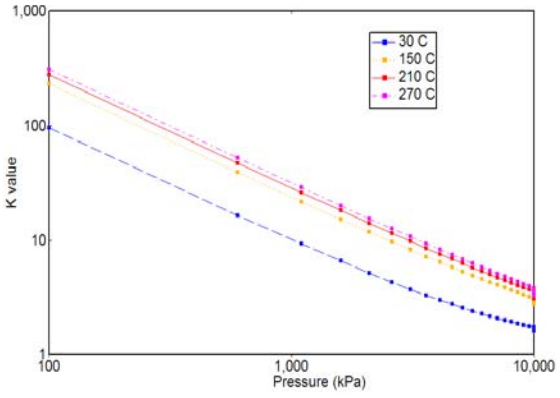


Fig. 6.11: Gas-Liquid (Oleic) *K*-values for CO_2

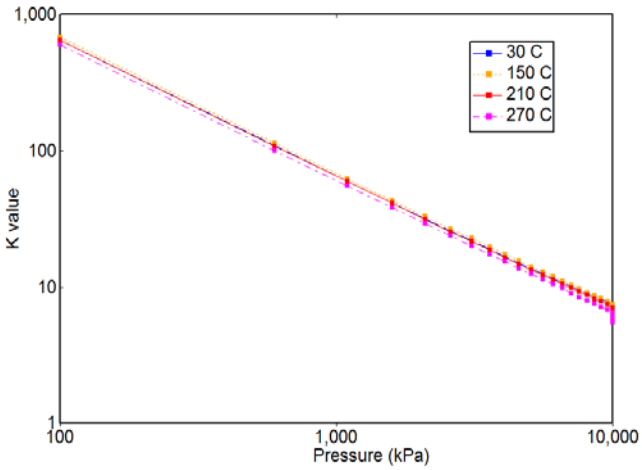


Fig. 6.12: Gas-Liquid (Oleic) *K*-values for N_2

Table 6.10: Phase-Distribution of Components

Component	Phase			
	Aqueous	Oleic	Gaseous	Solid
Water	X		X	
CO_2	X	X	X	
N_2	X	X	X	
Asphaltene (*asphalte*)		X	X	
Maltene (*maltene*)		X	X	
CH_4 (*C1*)	X	X	X	

6.8 Reservoir Model

Combining the foregoing input data, a 3-D homogenous (constant-property units X, oil-shale and Y) dynamic model is constructed with STARS (version 2010.11), a commercial thermal simulator developed by the CMG. The model uses Cartesian coordinates. At the preliminary stage vis-à-vis screening and assessment of uncertainties, we assume a layer-cake stratigraphy, with areally invariant rock and fluid properties. Despite its simplicity, the layer-cake model has been successful in history-matching actual steam-injection projects (Miller and Xiao, 2010). In later parts of this work (Chapter 9), we investigate effects of rock and fluid-property heterogeneities, including variable thermal properties. Due to lack of data on areal distribution of properties, we limit the heterogeneities to layering effects (vertical direction). The heterogeneous models, which are also based on very fine-scale simulations, serve as the basis of the final forecasts and input for subsequent economic analyses.

While the model thickness is fixed according to **Table 6.1**, the area dimensions for the three realisations are presented in **Table 6.11**. This relatively simple model is meant to represent a sector of the Nigerian heavy-oil belt. In principle, our understanding of the potential performance of a prospective exploitation technology in this robust sector model, which reasonably covers the full range of subsurface uncertainties and possible mix of operating options, could reasonably be

extrapolated to the entire belt. The dimensions in **Table 6.11** are comparable to those used in the simulations and actual field implementations of SAGD in heavy-oil accumulations in Athabasca and elsewhere (Zabel *et al.*, 2010; Gotawala and Gates, 2009; Gipson *et al.*, 2002; Ito and Suzuki, 1999). It is worth pointing out that in **Table 6.11** the variation in the cross-well (Y) reservoir dimensions is an indication of uncertainties associated with the effective drainage radius.

Table 6.11: Area (X-Y) Dimensions of Sector Model

Case	Length (m)	Width (m)
Low	500	100
Base	500	200
High	500	400

Whereas heat exchange is allowed through the cap and base rocks, the lateral boundaries of the model are adiabatic and are also closed, implying there is neither heat nor mass transfer across the sides of the model. Heat losses through the cap and base rocks are described with the semi-analytic method of Vinsome and Westerveld (1980), which treats these sinks as 1-D semi-infinite systems. **Fig. 6.13**, depicting the distribution of horizontal permeability, is a representation of the 0.1 km^2 base-case model. With this relatively small-sized sector model, it is fair to ignore any effect of reservoir dip. In this study, neither geomechanics nor chemical reaction is considered. Additionally, reservoir dip is neglected.

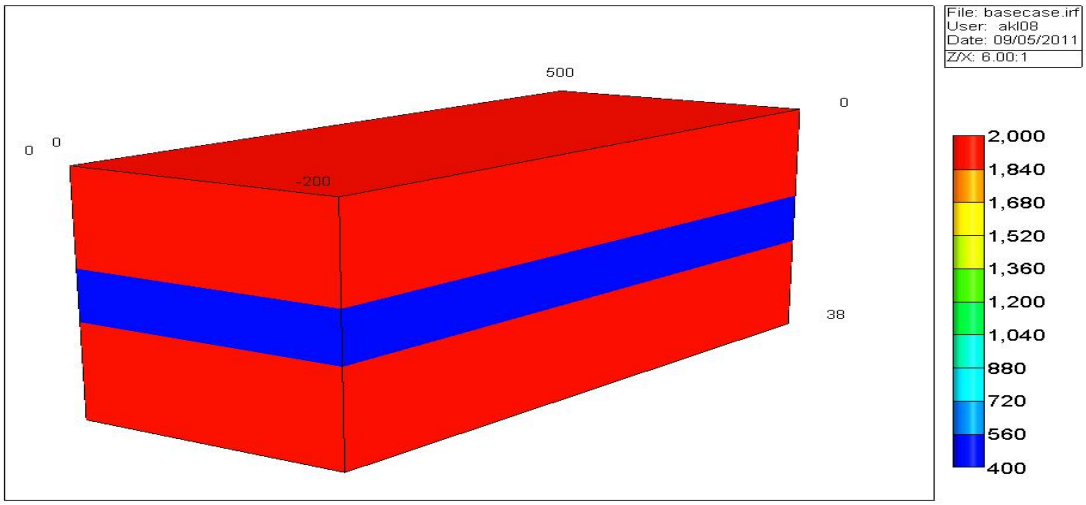


Fig. 6.13: Base-case Reservoir Geometry and Permeability ($K_x = K_y$) Field

Grid sensitivity studies show that the simulation results are sensitive to grid dimensions, with hydrocarbon recovery increasingly underestimated by the coarseness of the cells. This notwithstanding, for the screening studies, we use 5, 40 and 38 grid blocks in the *X* (length), *Y* (width) and *Z* (thickness) directions, respectively. However, in later studies, such as those on optimisation, heterogeneity and CO_2 (flue gas), much finer cells are employed in order to resolve the key physics of the processes under investigation. Most importantly, all the final forecasts used

for economic analyses are based on 152,000 cells (25 x 80 x 76). For simplicity, all the cells in a model are kept uniform, with no consideration for local grid refinement.

6.9 Well Model

This comprises two pairs of standard SAGD horizontal wells, each of length 500 m, radius 0.16 m, and perforated throughout their length (**Fig. 6.14**). In the base case, a skin factor of 5 applies to all wells. Considering the anticipated weak bottom aquifer in the base case, each injector-producer pair entails placing the producer about 2 m above the reservoir base. Some 5 m above the producer, in the same vertical plane, is the injector. In the lateral direction, the pairs are spaced 100 m apart. As the well configuration is such that symmetry is observed, it implies that each well-pair effectively influences a radius of 50 m within the 200 m wide reservoir model.

The fracture gradient is taken to be 21.1 kPa/m, which is about 80 % of actual value in typical Nigerian hydrocarbon fields (Ajienka *et al.*, 2009). Given a datum of 500 m, in order to avoid fracturing the reservoir, normal injection pressure does not exceed 10.5 MPa.

Saturated steam is injected at 70 % quality and 250 ^{o}C. At the screening stage, the injectors operate on maximum bottomhole pressure (BHP) of 5 MPa while the producers are constrained to 5 ^{o}C steam-trap. In the simulator (CMG, 2010a), steam trap is the minimum difference between saturation temperature (at well BHP) of injected steam and the temperature of produced water (and other components of the product stream). For computational efficiency during the screening phase of the current study, the injectors and producers are modelled as sinks and sources, respectively, neglecting pressure and heat losses along their lengths. The wells have 100 % uptime while simulation runs for just 10 years.

For simplicity, vertical sections of injectors and producers are not considered, thereby ignoring hydraulics between wellhead and sand face thus eliminating the need for lifting curves (Ito and Suzuki, 1999). When considered, to account for pressure and thermal losses along horizontal sections, the wellbore is discretised (multi-segment), with the semi-analytic model of Fontanilla and Aziz (1982) used to describe the hydraulics.

However with the discretised wellbore models, the producers experience significant nonlinearities and numerical instability due to sharp changes in the compositions of the phases and the drive to achieve thermodynamic equilibrium at every grid block and time-step. These cause unrealistic results (for example, cumulative water production exceeds the sum of initial water volume in-place and cumulative injection). At this point, as we do not have access to other thermal simulators, we cannot ascertain whether this difficulty is limited to STARS or it is common to all compositional thermal simulators (Perdomo *et al.*, 2008; Stone *et al.*, 2002). As a result of these stability issues, also reported by other researchers (Thorne and Zao, 2009; Oballa *et al.*, 1997), we discontinue the use of discretised wellbore model for the producers.

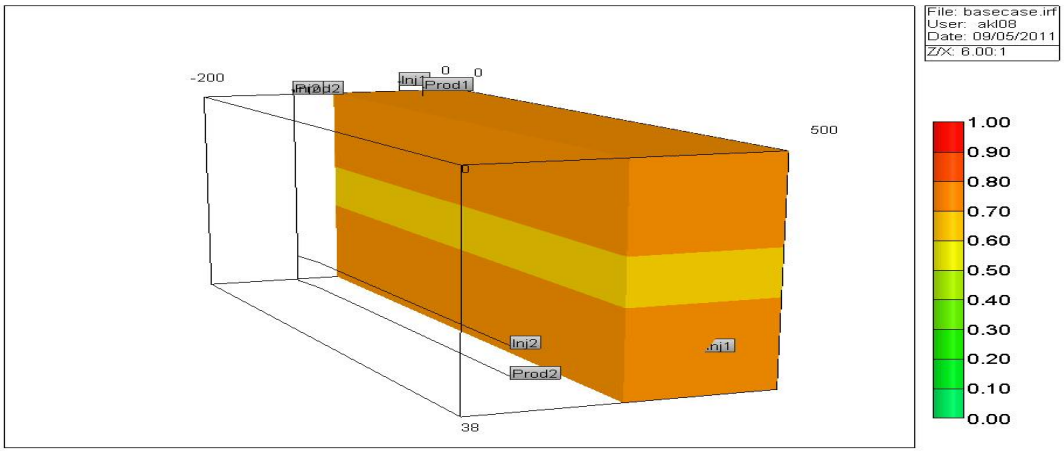


Fig. 6.14: Well Configuration and Initial Oil Saturation Field (Base Case)

A combination of high temperature and brine (formation water) would likely create corrosion-induced operational problems (Fontana and Greene, 1986). To minimise this threat, we select stainless steel as the completion material. In support of this decision, we refer to the work of Umoru *et al.* (2008) on the corrosion resistance of three commercial grades of stainless steel in a hot (95 ^{o}C) alkaline medium, stirred at 750 rpm. With corrosion rate below 0.13 mm/year, they concluded that the Nigerian bitumen is mild to stainless steel (see also Umoru (2008)). But the presence of CO_2 as well as higher flowrate (shear rate) and temperature envisaged in the alternating injection process could potentially aggravate the reported rate.

Typical roughness values of corroded and clean commercial stainless-steel pipes are 0.5 and 0.05 mm, respectively (ToolBox, 2010). However in this study, we assume 0.3 mm. In principle, this relatively high roughness partly accounts for downhole hardware (flow-control devices and sensors), possible solid deposits (scales, corrosion products, asphaltene and sands) as well as wellbore undulations.

Completion Model: From field experiences (Kisman and Yeung, 1995), for the same drawdown, horizontal wells typically achieve higher (up to five times) productivity and injectivity than vertical wells. Consequently, all wells are of the horizontal type in our base-case model. To minimise potential sand production, we expect that sand screens (or other sand-exclusion technologies) will be deployed, resulting in a reduction of well potentials. This additional flow restriction (mechanical skin) is implicit in the total skin factors presented in **Table 6.3**. As stated earlier, the scope of this study is limited to the horizontal section of the wellbore.

Fig. 6.15 is a generic schematic of proposed completion, highlighting some wellbore model variables. It is worth mentioning that the horizontal section is completed as open-hole (neither cased nor cemented) as typical for similar developments (Glenn *et al.*, 2008). Hence, in all cases, we assume that the slotted liner inner diameter (ID) is about 95% of open-hole diameter D_w which, contrary to the schematic, is assumed equal to the liner outer diameter (OD). Furthermore, the length L_w, refers to the liner and does not include the “rat hole” ahead of liner tip. All the well

process variables (steam quality, rate, temperature, pressure, etc) featured in this work are referenced to the liner inlet. Additionally, steam volumetric refers to cold-water equivalent (CWE). Although we have used slotted liners in our discussion, we recognise the prospects of wire-wrapped screens which though slightly more expensive, offer greater resistance to thermal stresses and load-induced mechanical failures (Glenn *et al.*, 2008; Xie *et al.*, 2007).

Concerning the discretised wellbore model, whereas our focus is on the horizontal section, the simulator requires that the vertical section, at least its length (completion depth), be specified. For computational efficiency, we have only included a short (1 m) segment just above the horizontal section. A similar approach was successfully implemented by Stone *et al.* (2002), though in another commercial simulator.

As part of a detailed optimisation study, we shall discuss the sensitivities performed on the well type, geometry, placements, and constraints in later chapters. The performances of other injectants such as cold and hotwater including non-condensable gases will also be presented.

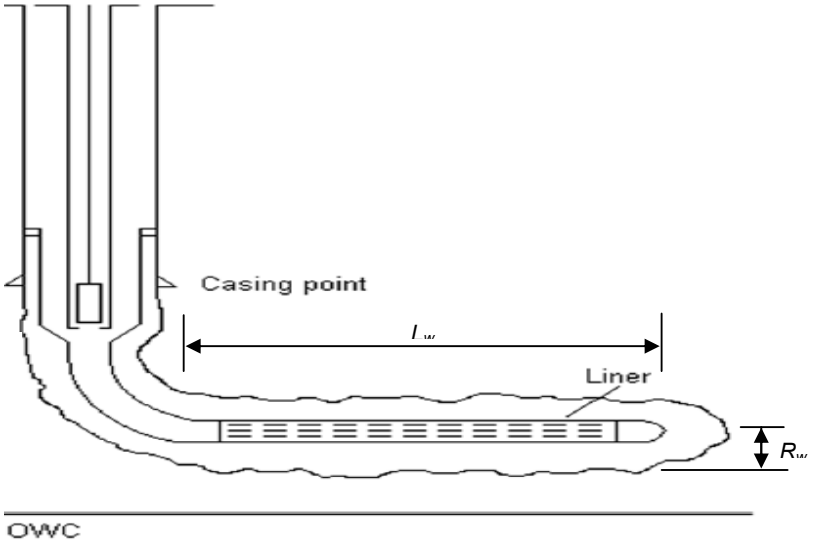


Fig. 6.15: Generic Wellbore Configuration (after Stone *et al.* (2002); Carpenter and Dazet (1992))

6.10 Assessment of Subsurface Uncertainties

In analysing the effects of the subsurface uncertainties, we differentiate between accumulative and dynamic properties. While the former refers to factors that impact primarily on the volume of hydrocarbons contained within the deposit, the latter represents variables that control the reservoir dynamics. First, single-variable sensitivity is conducted and then multi-variable analysis, the latter allowing for a simultaneous exploration of the entire parameter space.

6.10.1 Single-Variable Sensitivity

Considering the large number of variables, some screening is performed to eliminate those of "less" importance to the current model. Within the range of estimates discussed earlier, each

variable is perturbed (while keeping others at their reference state) and the impact on specific reservoir response is quantified.

Accumulative Properties: As an indication of the influence on the volume of hydrocarbons within the sector model, we consider the stock-tank oil initially in-place (STOIIP), estimated with the following expression.

$$N = Ah\phi S_{oi} / B_{oi} \quad , \tag{6.5}$$

where A is the area extent, h is net thickness, and ϕ is porosity. S_{oi} and B_{oi} are initial oil saturation and formation volume factor, respectively.

As illustrated with the sensitivity plot in **Fig. 6.16**, hydrocarbon accumulation within the representative model is most sensitive to the size and thickness of the structure as well as the fluid saturation.

Dynamic Properties: Although there are several indicators of reservoir performance, for this initial screening, we consider only the discounted (10% rate) recoverable oil volume. In a more detailed study presented shortly, other measures of dynamic response are evaluated.

Within the range of values examined, the sensitivity of discounted oil recovery to the various dynamic variables is illustrated in **Fig. 6.17**. On the evidence of this plot, it can be deduced that relative permeabilities, oil PVT, K_{shale}/K_{sand} and others are the primary uncertainties that would control the dynamics of a thermal exploitation of the sector model. Please note that K_{shale}/K_{sand} is the ratio of the absolute permeability of the oil-shale to that of the oil-sand. For convenience in subsequent discussions, the heavy-hitting accumulative and dynamic subsurface factors are assigned the notations in **Table 6.12**.

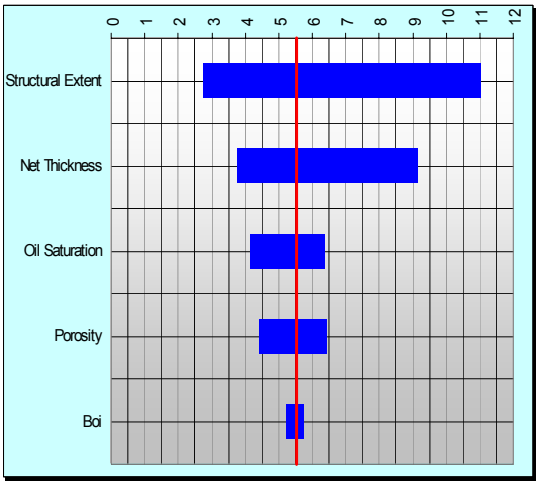


Fig. 6.16: Tornado Plot for STOIIP (MMstb)

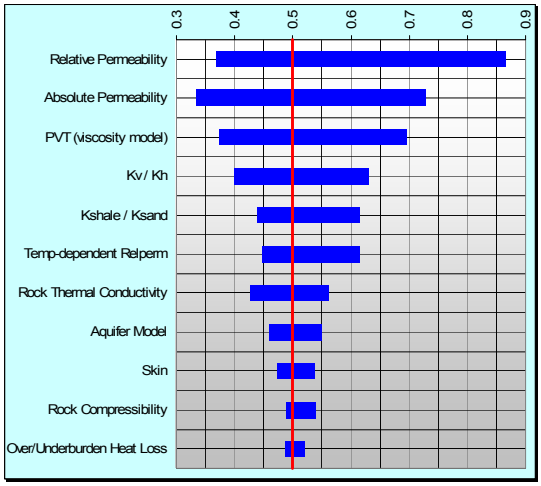


Fig. 6.17: Tornado Plot for Discounted Oil Recovery (MMstb)

Table 6.12: Definition of Main Subsurface Uncertainties

Factor	Definition
F_1	Structural extent
F_2	Porosity
F_3	Net thickness
F_4	Oil saturation
F_5	Horizontal permeability
F_6	K_v / K_h
F_7	Rock thermal conductivity
F_8	K_{shale} / K_{sand}
F_9	Relative permeability model
F_{10}	Oil PVT (viscosity) model
F_{11}	Relative-permeability temperature-dependency model

6.10.2 Multi-Variable Sensitivity (Experimental Design)

In theory, with two-level full factorial design (FD) involving 11 factors, we would need at least 2048 runs to describe all possible combinations. However, we employ fractional FD which, in principle, captures the main effects and the key interaction effects but at much lower computing costs (Montgomery, 1976). In this work, using the tool developed by Steppan e*t al.* (1998), we apply the Resolution IV design, requiring just 32 runs (2^{11-6}). To improve its ability to explain nonlinearity, we augment it with five centre points, hence yielding a total of 37 runs, which is only about 2% of the full design.

Table 6.13 shows the design matrix, including two arbitrary "blind" tests serving as benchmarks to evaluate the robustness of the resulting response surfaces. Theoretically, by performing 37 runs to model 11 factors, the response surface should explain 11 main effects and a maximum of 26 interaction effects. The factors are limited to just three states. These are low, base and high, denoted as -1, 0 and 1, respectively. Please note that in the case of F_{10}, -1 and 1 are the low (optimistic) and high (pessimistic) viscosity models, respectively.

In order to have a good understanding of the influence of these factors, all the simulations at this stage are neither constrained nor optimised. For example, there are no limitations on the injection and production rates as well as fluid ratios.

Table 6.13: ED Matrix for the Steam-alone Process

Run	*F1*	*F2*	*F3*	*F4*	*F5*	*F6*	*F7*	*F8*	*F9*	*F10*	*F11*
1	0	0	0	0	0	0	0	0	0	0	0
2	1	1	-1	-1	1	-1	1	1	1	1	-1
3	0	0	0	0	0	0	0	0	0	0	0
4	1	1	-1	1	1	-1	-1	-1	-1	-1	1
5	-1	1	-1	1	-1	1	-1	1	1	-1	-1
6	-1	-1	1	-1	1	1	1	-1	1	-1	1
7	-1	-1	-1	1	-1	-1	1	1	1	-1	1
8	0	0	0	0	0	0	0	0	0	0	0
9	-1	1	-1	-1	1	1	1	1	-1	-1	-1
10	1	-1	-1	-1	-1	1	-1	-1	1	-1	-1
11	1	-1	-1	1	1	1	1	-1	-1	-1	-1
12	-1	-1	-1	-1	-1	-1	-1	-1	-1	1	-1
13	1	-1	1	-1	1	-1	1	-1	-1	1	1
14	1	1	1	1	1	1	1	1	1	-1	1
15	-1	1	1	-1	-1	-1	-1	1	1	1	1
16	0	0	0	0	0	0	0	0	0	0	0
17	1	1	-1	1	-1	-1	-1	1	-1	1	-1
18	1	1	1	-1	-1	1	-1	1	-1	-1	1
19	-1	1	-1	1	1	1	-1	-1	1	1	1
20	-1	-1	-1	-1	1	-1	-1	1	-1	-1	1
21	-1	-1	-1	1	1	-1	1	-1	1	1	-1
22	-1	-1	1	1	-1	1	-1	-1	-1	-1	1
23	1	-1	1	1	1	-1	-1	1	1	-1	-1
24	0	0	0	0	0	0	0	0	0	0	0
25	1	-1	-1	-1	1	1	-1	1	1	1	1
26	1	1	-1	-1	-1	-1	1	-1	1	-1	1
27	1	1	1	-1	1	1	-1	-1	-1	1	-1
28	1	-1	1	-1	-1	-1	1	1	-1	-1	-1
29	1	1	1	1	-1	1	1	-1	1	1	-1
30	-1	1	-1	-1	-1	1	1	-1	-1	1	1
31	-1	1	1	1	-1	-1	1	-1	-1	-1	-1
32	-1	-1	1	-1	-1	1	1	1	1	1	-1
33	1	-1	1	1	-1	-1	-1	-1	1	1	1
34	1	-1	-1	1	-1	1	1	1	-1	1	1
35	-1	1	1	-1	1	-1	-1	-1	1	-1	-1
36	-1	-1	1	1	1	1	-1	1	-1	1	-1
37	-1	1	1	1	1	-1	1	1	-1	1	1
Blind test 1	*0*	*0*	*0*	*0*	*0*	*0*	*1*	*1*	*1*	*-1*	*1*
Blind test 2	*-1*	*-1*	*-1*	*-1*	*-1*	*-1*	*0*	*0*	*0*	*0*	*0*

6.10.2.1 Steam-alone Process

For convenience, the notations N_p, W_i, R_f, N, C_{SOR} and T_{WOR} denote cumulative oil recovery, cumulative steam injected as cold-water equivalent (CWE), oil recovery factor (RF), STOIIP, cumulative steam-oil ratio (CSOR), and ratio of cumulative steam injected and produced water to oil ratio, respectively. The terms N'_p, W'_i and W'_p refer to corresponding discounted results, which are used to account for time effects. Some of the responses are defined as:

$$C_{SOR} = W_i / N_p \ , \tag{6.6}$$

$$T_{WOR} = \left(W_i + W_p\right) / N_p \,, \tag{6.7}$$

with discounted CSOR and TWOR having same definitions but referred to the relevant discounted input.

Table 6.14 presents the simulation results for the various ED runs and blind tests for the steaming process. The results show wide disparity between the runs, with N_p varying by about two orders of magnitude while the difference in RF is up to 75 percentage units. Either in discounted or undiscounted states, results of produced water and injected steam indicate high sensitivity to subsurface uncertainties.

The oil recovery and CSOR plots for selected runs are illustrated in **Figs. 6.18** and **6.19**. The runs 1, 12 and 14 represent the base, "extreme" low and "extreme" high realisations, respectively. Please note that whereas the "extreme" low (high) realisation represents the "hypothetic" scenario in which the pessimistic (optimistic) states of all the factors occur simultaneously, the base realisation is premised on "best" engineering estimates of the factors. From the results obtained, it can be inferred that our base-case model has greater chances of being reviewed upward than downward, indicating that our base-case is somewhat conservative which, from a planning and risk management perspective, is suitable.

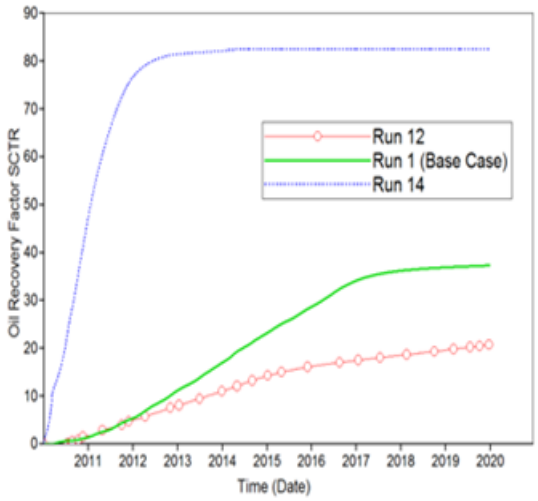


Fig. 6.18: Steaming Runs 1, 12 and 14 (Oil Recovery)

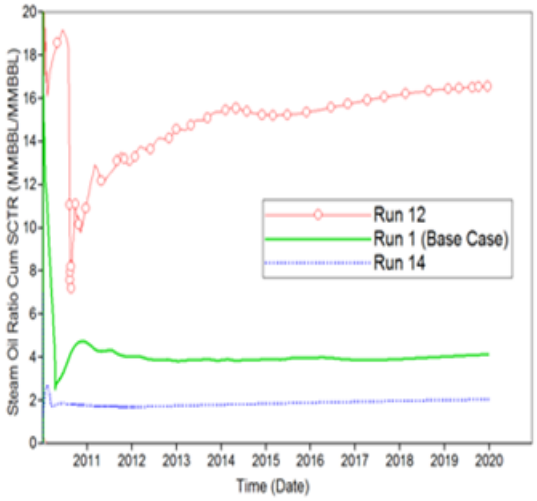


Fig. 6.19: Steaming Runs 1, 12 and 14 (CSOR)

Table 6.14: Results Matrix for Steam-alone Process

Run	N_p (MMb)	W_p (MMb)	W_i (MMb)	N'_p (MMb)	W'_p (MMb)	W'_i (MMb)	R_f (%)	N (MMb)	C_{SOR} (b/b)	T_{WOR} (b/b)	C'_{SOR} (b/b)	T'_{WOR} (b/b)
1	2.07	8.60	8.58	1.34	5.39	5.43	37.3	5.5	4.1	8.3	4.1	8.1
2	2.21	23.39	22.58	1.33	13.94	13.47	32.9	6.7	10.2	20.8	10.1	20.6
3	2.07	8.60	8.58	1.34	5.39	5.43	37.3	5.5	4.1	8.3	4.1	8.1
4	5.82	17.35	18.18	3.49	9.97	10.61	57.1	10.2	3.1	6.1	3.0	5.9
5	2.09	5.83	5.89	1.83	4.56	4.62	81.8	2.5	2.8	5.6	2.5	5.0
6	2.28	11.13	10.88	2.07	9.53	9.27	81.9	2.8	4.8	9.6	4.5	9.1
7	1.44	5.74	5.93	1.30	4.61	4.75	82.7	1.7	4.1	8.1	3.6	7.2
8	2.07	8.60	8.58	1.34	5.39	5.43	37.3	5.5	4.1	8.3	4.1	8.1
9	0.69	6.76	6.55	0.62	5.54	5.34	40.9	1.7	9.5	19.4	8.6	17.5
10	3.16	21.49	21.02	2.13	14.00	13.69	68.6	4.6	6.7	13.5	6.4	13.0
11	3.63	22.90	23.33	2.89	16.73	17.08	52.0	7.0	6.4	12.7	5.9	11.7
12	0.24	4.05	3.96	0.16	2.60	2.54	20.8	1.2	16.6	33.5	16.1	32.5
13	4.68	32.31	32.76	2.65	18.87	19.11	42.0	11.1	7.0	13.9	7.2	14.3
14	20.36	40.28	41.45	17.66	33.14	33.91	82.5	24.7	2.0	4.0	1.9	3.8
15	3.31	11.54	11.03	2.08	7.42	7.10	81.4	4.1	3.3	6.8	3.4	7.0
16	2.07	8.60	8.58	1.34	5.39	5.43	37.3	5.5	4.1	8.3	4.1	8.1
17	1.90	13.21	1.39	1.20	7.59	8.10	18.6	10.2	7.4	14.3	6.9	13.5
18	4.29	17.77	17.82	2.46	10.02	10.14	26.4	16.3	4.2	8.3	4.1	8.2
19	2.24	5.85	5.87	1.71	4.10	4.12	88.0	2.5	2.6	5.2	2.4	4.8
20	0.76	6.23	6.13	0.67	4.89	4.82	66.1	1.2	8.1	16.2	7.2	14.4
21	1.40	5.86	6.02	1.24	4.73	4.83	80.1	1.7	4.3	8.5	3.9	7.7
22	1.97	6.41	7.02	1.41	4.55	4.94	46.7	4.2	3.6	6.8	3.5	6.8
23	13.88	37.71	38.07	11.06	28.82	29.05	82.0	16.9	2.7	5.5	2.6	5.2
24	2.07	8.60	8.58	1.34	5.39	5.43	37.3	5.5	4.1	8.3	4.1	8.1
25	2.60	16.23	15.82	1.52	9.39	9.16	56.5	4.6	6.1	12.3	6.0	12.2
26	5.18	23.79	23.65	3.34	15.21	15.25	77.1	6.7	4.6	9.2	4.6	9.1
27	2.18	15.38	14.74	1.21	8.62	8.30	13.4	16.2	6.7	13.8	6.9	14.0
28	2.33	27.15	26.48	1.33	16.33	15.96	20.9	11.1	11.3	23.0	12.0	24.3
29	13.68	34.51	34.66	7.92	20.90	21.24	55.4	24.7	2.5	5.1	2.7	5.3
30	1.10	6.36	6.29	0.75	4.43	4.43	65.4	1.7	5.7	11.5	5.9	11.9
31	1.37	7.74	8.00	1.11	5.67	5.90	22.2	6.2	5.8	11.5	5.3	10.5
32	1.97	11.11	10.82	1.72	9.32	9.04	70.8	2.8	5.5	11.1	5.3	10.7
33	2.21	7.50	8.12	1.21	4.15	4.48	13.1	16.9	3.7	7.1	3.7	7.1
34	1.95	11.35	12.01	1.09	6.35	6.72	28.0	7.0	6.1	12.0	6.2	12.0
35	2.89	11.70	11.16	2.53	9.75	9.30	71.1	4.1	3.9	7.9	3.7	7.5
36	2.33	9.88	9.87	1.85	7.53	7.55	55.1	4.2	4.2	8.5	4.1	8.2
37	3.79	10.02	10.34	2.80	7.29	7.63	61.4	6.2	2.7	5.4	2.7	5.3
Blind 1	*4.37*	*13.71*	*13.86*	*3.56*	*10.49*	*10.60*	*78.8*	*5.6*	*3.2*	*6.3*	*3.0*	*5.9*
Blind 2	*0.52*	*4.43*	*4.37*	*0.37*	*2.95*	*2.94*	*45.5*	*1.2*	*8.3*	*16.8*	*8.0*	*16.1*

In order to identify the main response functions, we investigate potential redundancy by examining correlations between the responses. As shown in **Figs. 6.20-6.25**, some of the functions can be eliminated. With this analysis, we limit the main functions to N, N_p, W_i, CSOR and R_f.

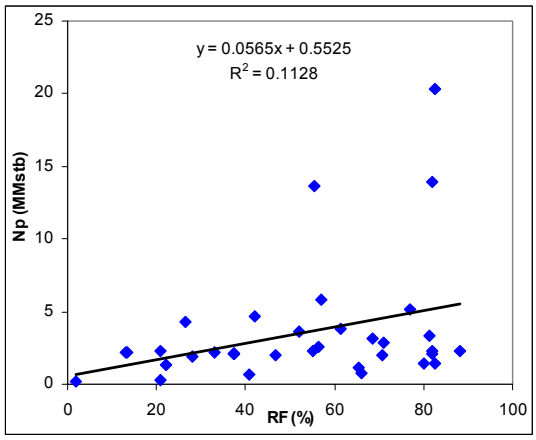


Fig. 6.20: N_p vs. R_f

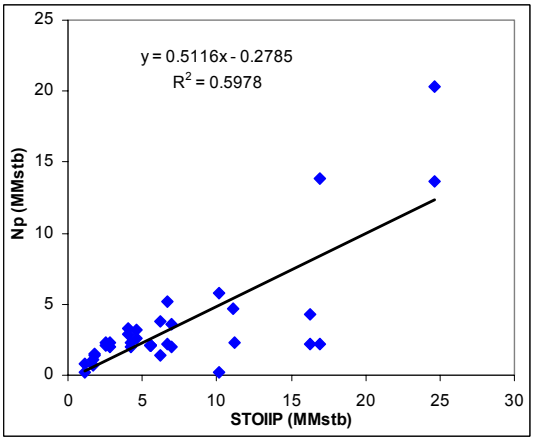


Fig. 6.21: N_p vs. N

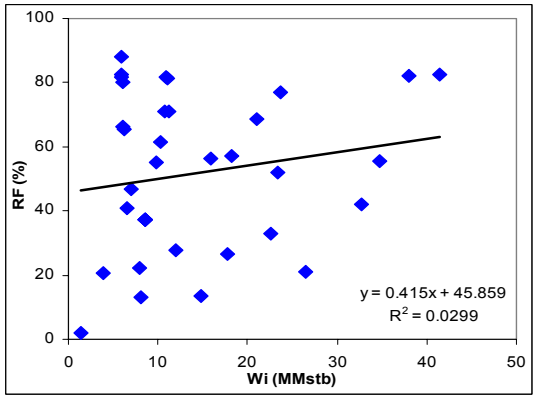


Fig. 6.22: R_f vs. W_i

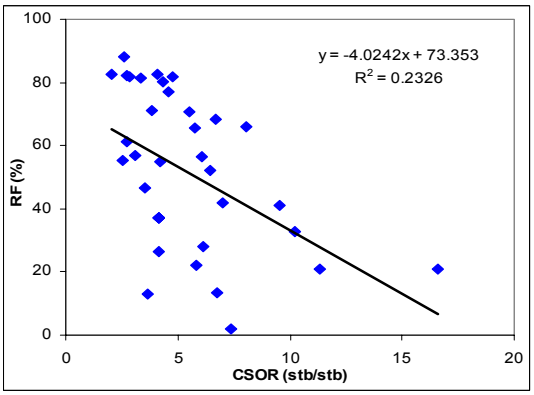


Fig. 6.23: R_f vs. C_{SOR}

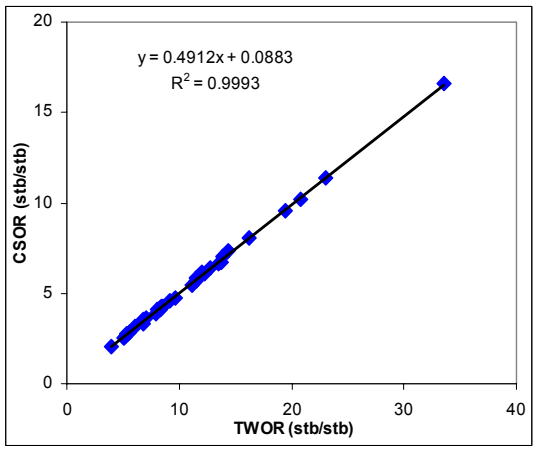


Fig. 6.24: C_{SOR} vs. T_{WOR}

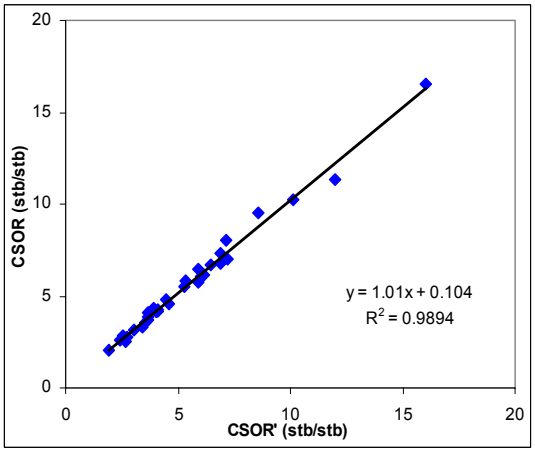


Fig. 6.25: C_{SOR} vs. C'_{SOR}

The application[**] of multiple (linear) regressions to the datasets in **Tables 6.13** and **6.14** yields the following proxy models (95% confidence). The model constants are presented in **Table 6.15**.

[**] Regression was performed with the statistical tool developed by Steppan *et al.* (1998).

$$\ln(N_p) = b_o + b_1F_3 + b_2F_1 + b_3F_9 + b_4F_1F_{10} + b_5F_5 + b_6F_5F_6 + b_7F_{10} + b_8F_{11} + b_9F_4 + b_{10}F_6 + b_{11}F_1F_8 + b_{12}F_1F_7 + b_{13}F_7 + b_{14}F_2F_8 + b_{15}F_2 + b_{16}F_1F_5 + b_{17}F_1F_2 \quad (6.8)$$

$$W_i = b_o + b_1F_1 + b_2F_3 + b_3F_7 + b_4F_1F_7 + b_5F_1^2 + b_6F_1F_{10} + b_7F_5 + b_8F_9 + b_9F_{10} + b_{10}F_1F_5 + b_{11}F_1F_9 + b_{12}F_5F_6 + b_{13}F_1F_3 + b_{14}F_2F_4 + b_{15}F_2F_5 + b_{16}F_3F_5 + b_{17}F_2F_8 + b_{18}F_1F_{11} \quad (6.9)$$

$$\sqrt{R_f} = b_o + b_1F_9 + b_2F_1 + b_3F_1F_{10} + b_4F_5 + b_5F_{10} + b_6F_{11} + b_7F_5F_6 + b_8F_1^2 + b_9F_1F_8 + b_{10}F_6 + b_{11}F_2F_8 + b_{12}F_1F_7 + b_{13}F_2F_5 + b_{14}F_7 + b_{15}F_1F_5 + b_{16}F_3F_5 + b_{17}F_3 \quad (6.10)$$

$$\ln(N) = b_o + b_1F_1 + b_2F_3 + b_3F_4 + b_4F_2, \quad (6.11)$$

$$\ln(C_{SOR}) = b_o + b_1F_4 + b_2F_9 + b_3F_{11} + b_4F_3 + b_5F_2 + b_6F_5F_6 + b_7F_1F_{10} + b_8F_6 + b_9F_1^2 + b_{10}F_7 + b_{11}F_1F_8 + b_{12}F_{10} + b_{13}F_2F_5 + b_{14}F_5 + b_{15}F_2F_8 + b_{16}F_1 \quad (6.12)$$

Table 6.15: Proxy Model Constants for Steam-alone Process

Coefficient / Statistic	N_p (MMstb)	W_i (MMstb)	R_f (%)	N (MMstb)	C_{SOR} (stb / stb)
b_o	0.8409	8.584	6.109	1.679	1.422
b_1	0.4300	7.071	1.114	0.693	-0.277
b_2	0.4088	3.394	-0.768	0.442	-0.209
b_3	0.3666	2.677	-0.643	0.209	-0.165
b_4	-0.2448	2.434	0.552	0.189	-0.161
b_5	0.2244	6.348	-0.518		-0.141
b_6	-0.2204	-2.205	0.488		0.087
b_7	-0.2119	2.176	-0.477		0.077
b_8	0.1956	2.128	0.958		-0.076
b_9	0.1745	-2.039	-0.333		0.175
b_{10}	0.1555	1.684	0.324		0.056
b_{11}	-0.1469	1.539	-0.280		0.056
b_{12}	0.1438	-1.366	0.271		0.051
b_{13}	0.1408	1.364	-0.271		0.047
b_{14}	-0.1292	0.921	0.254		-0.045
b_{15}	0.1142	-0.793	0.187		0.032
b_{16}	0.1043	0.655	0.153		0.030
b_{17}	-0.0817	-0.548	-0.143		
b_{18}		-0.428			
R^2	*0.958*	*0.995*	*0.969*	*1.000*	*0.982*

Although the statistics (R^2) give the impression of satisfactory fits, the results of the model adequacy tests (see **Figs. 6.26** and **6.27** for examples), using so-called “blind” runs, affirm that the regression equations have reasonable predictive power, hence can be reliably used as proxies to the simulator, at least within the normalised range (-1 to 1) of uncertainties evaluated.

As all the independent variables have been normalised, their values in the proxy equations are limited to the range -1 to 1. With the exception of the input F_{10} (PVT model) that correlates negatively with the responses, other variables have the high and low-realisation quantified by 1 and -1, respectively.

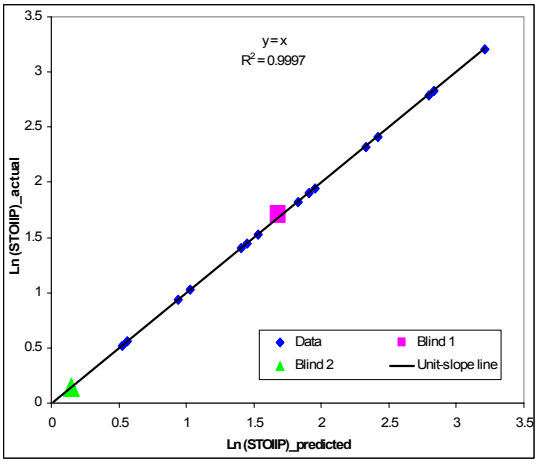


Fig. 6.26: Model Adequacy for *N*

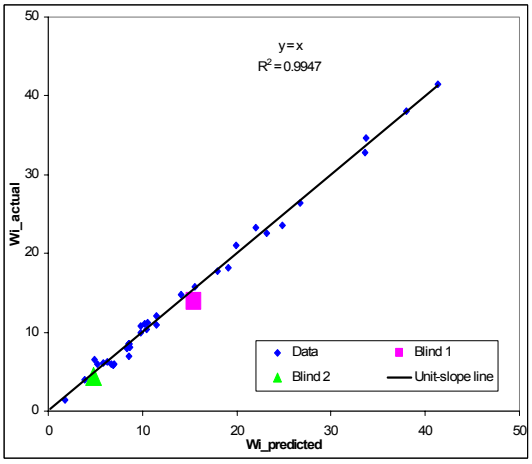


Fig. 6.27: Model Adequacy for W_i

Applying the response surfaces, Monte Carlo-type probabilistic simulations are conducted with the *Crystal Ball* package (Oracle, 2000). Although some of the input factors such as F_9, F_{10} and F_{11} are inherently discrete, for simplicity we treat them as continuous in order to perform random sampling within the range -1 to 1 during the stochastic simulations. The distribution curves of the various responses are presented in Appendix **I**, while relevant outcomes are summarised in **Table 6.16**. This includes the runs that coincide (approximate) with the selected probabilities. Here, $Px = b$ implies there is an *x*% chance of *exceeding* the value *b*.

Table 6.16: Responses and Inferred Probabilistic Realisations for Steam-alone Process

Response	P90		P50		P10	
	Value	Run	Value	Run	Value	Run
N_p (MMstb)	1.2	*30*	2.3	*19*	4.5	*18*
W_i (MMstb)	4.9	*19*	9.0	*1*	19.2	*4*
R_f (%)	25.6	*18*	41.5	*13*	61.0	*37*
N (MMstb)	2.7	*32*	5.4	*1*	10.4	*4*
C_{SOR} (stb/stb)	3.1	*4*	4.4	*21*	6.3	*11*

6.10.2.2 Alternating-Injection of Steam and CO_2 Process

However, in addition to N_p, W_i, CSOR and R_f, we consider the response G_{CO2}, which refers to the net mass (kton) of CO_2 retained in the reservoir. Being the same as in the steam-alone process, *N* is not considered again. In this case, we also ignore CSOR. The simulation results are shown in **Table 6.17**.

Table 6.17: Results Matrix for the SAC Process

Run	N_{p_CO2} (MMstb)	W_{i_CO2} (MMstb)	C_{SOR_CO2} (stb / stb)	R_{F_CO2} (%)	G_{CO2} (kton)
1	1.84	3.34	1.8	33.2	17.9
2	1.52	6.34	4.2	22.7	33.4
3	1.84	3.34	1.8	33.2	17.9
4	6.12	17.71	2.9	60.0	6.0
5	2.20	9.44	4.3	86.4	100.6
6	2.52	19.77	7.8	90.4	246.5
7	1.52	9.31	6.1	87.0	73.4
8	1.84	3.34	1.8	33.2	17.9
9	1.00	11.35	11.3	59.7	84.3
10	3.16	31.90	10.1	68.6	12.6
11	4.82	24.57	5.1	68.9	3.7
12	0.27	2.30	8.6	23.1	3.0
13	2.32	10.07	4.3	20.8	43.2
14	20.91	97.67	4.7	84.7	219.8
15	3.50	14.81	4.2	86.2	31.5
16	1.84	3.34	1.8	33.2	17.9
17	0.20	1.12	5.6	2.0	2.1
18	4.18	14.43	3.5	25.7	40.1
19	0.75	1.16	1.5	29.3	7.1
20	0.87	12.49	14.3	75.9	27.0
21	1.52	8.39	5.5	87.1	213.9
22	2.81	9.39	3.3	66.4	9.4
23	14.30	71.21	5.0	84.5	180.7
24	1.84	3.34	1.8	33.2	17.9
25	0.62	4.02	6.5	13.4	9.5
26	5.60	20.34	3.6	83.4	21.1
27	0.74	4.62	6.2	4.6	21.6
28	2.88	12.37	4.3	25.8	29.7
29	5.09	10.06	2.0	20.6	74.8
30	1.13	6.98	6.2	67.4	2.0
31	2.15	9.82	4.6	34.9	18.0
32	2.08	25.80	12.4	74.5	271.8
33	0.77	1.93	2.5	4.6	8.4
34	0.29	0.88	3.1	4.1	5.0
35	3.36	33.46	10.0	82.7	589.9
36	2.47	7.18	2.9	58.4	440.4
37	4.01	31.09	7.8	64.9	272.4
Blind 1	*4.83*	*12.9*	*2.7*	*87.0*	*86.7*
Blind 2	*0.73*	*5.14*	*7.1*	*63.0*	*9.9*

The following are the "best-fit" correlations for the various outputs, with the coefficients and correlation statistics shown in **Table 6.18**. Blind tests also indicate that the proxies have satisfactory predictability. The distribution curves are presented in Appendix **I** while the key results are summarised in **Table 6.19**.

$$\sqrt{N_{p_CO2}} = b_o + b_1F_{10} + b_2F_1F_{10} + b_3F_3 + b_4F_9 + b_5F_1 + b_6F_5 + b_7F_4 + b_8F_1F_5 + b_9F_1F_9 + b_{10}F_2 + b_{11}F_7 + b_{12}F_5F_6 + b_{13}F_1F_7 + b_{14}F_1F_4 + b_{15}F_3F_5 + b_{16}F_1^{\,2} + b_{17}F_{11} \quad ,(6.13)$$

$$In\left(W_{i_CO2}\right) = b_o + b_1F_{10} + b_2F_3 + b_3F_1F_{10} + b_4F_1^{\,2} + b_5F_5 + b_6F_5F_6 + b_7F_9 + b_8F_7 + b_9F_1F_8 + b_{10}F_1F_5 + b_{11}F_1F_9 + b_{12}F_4 + b_{13}F_1F_6 + b_{14}F_1 \quad , (6.14)$$

$$In\left(G_{CO2}\right) = b_o + b_1F_3 + b_2F_9 + b_3F_5 + b_4F_1 + b_5F_8 + b_6F_7 + b_7F_{11} + b_8F_5F_6 + b_9F_1F_{11} + b_{10}F_1F_5 + b_{11}F_{10} + b_{12}F_3F_5 + b_{13}F_1F_8 + b_{14}F_1^{\,2} + b_{15}F_1F_2 + b_{16}F_1F_4 \quad , \quad (6.15)$$

$$\sqrt{R_{f_CO2}} = b_o + b_1F_{10} + b_2F_1 + b_3F_1F_{10} + b_4F_9 + b_5F_5F_6 + b_6F_1F_8 + b_7F_5 + b_8F_7 + b_9F_1^{\,2} + b_{10}F_1F_5 + b_{11}F_2F_5 + b_{12}F_2F_4 + b_{13}F_3F_5 + b_{14}F_1F_3 \quad .(6.16)$$

Table 6.18: Proxy-Model Constants for the SAC Process

Coefficient / Statistic	N_{p_CO2} (MMstb)	W_{i_CO2} (MMstb)	R_{F_CO2} (%)	G_{CO2} (kton)
b_o	1.358	1.206	5.765	2.885
B_1	-0.417	-0.717	-1.378	0.818
b_2	-0.376	0.478	-1.338	0.619
b_3	0.351	-0.463	-0.982	0.580
b_4	0.234	1.017	0.820	-0.493
b_5	0.229	0.348	-0.499	0.471
b_6	0.188	-0.332	-0.490	0.318
b_7	0.182	0.322	0.460	-0.308
b_8	0.170	0.298	0.414	-0.286
b_9	0.152	-0.286	0.966	0.283
b_{10}	0.130	0.260	0.343	-0.279
b_{11}	0.122	0.226	-0.319	-0.273
b_{12}	-0.115	-0.209	-0.240	0.251
b_{13}	0.105	0.193	0.202	-0.232
b_{14}	0.102	-0.080	-0.183	0.592
b_{15}	0.0873			0.215
b_{16}	0.233			-0.168
b_{17}	0.0601			
b_{18}				
R^2	*0.972*	*0.988*	*0.964*	*0.985*

Table 6.19: Responses and Inferred Probabilistic Realisations for the SAC Process

Response	P90		P50		P10	
	Value	Run	Value	Run	Value	Run
N_{p_CO2} (MMstb)	0.87	*20*	2.0	*32*	4.2	*18*
W_{i_CO2} (MMstb)	1.8	*33*	4.6	*27*	11.6	*9*
R_{f_CO2} (%)	17.8	*29*	38.5	*31*	60.8	*4*
G_{CO2} (kton)	7.7	*19*	20.5	*26*	74.0	*7*

6.10.2.3 Comparing Steam-alone and Alternating Steam-CO_2 Processes

Fig. 6.28 is a cross-plot of the oil recovery factors of the two processes for the 37 simulation runs. Using the unit-slope line as a guide, it can be deduced that the alternating-injection process generally provides higher recovery. However, there is no clear correlation between the two processes. From an analysis of all the uncertainty parameters, we identify the viscosity model as the most appropriate parameter to correlate and explain the disparity between the two processes under discourse.

In **Fig. 6.29**, we focus on the runs that utilise the low-viscosity model. With the exception of an "outlier" (run 18), the steaming process consistently underperforms relative to the SAC process. Accordingly, it can be concluded that, keeping other variables the same, alternating-injection is more competitive than steam-alone in systems containing relatively low-viscosity heavy oil. In other words, this class of oils either have reasonable insitu mobility or can easily be mobilised by dilution as a complement to viscosity-reduction by temperature.

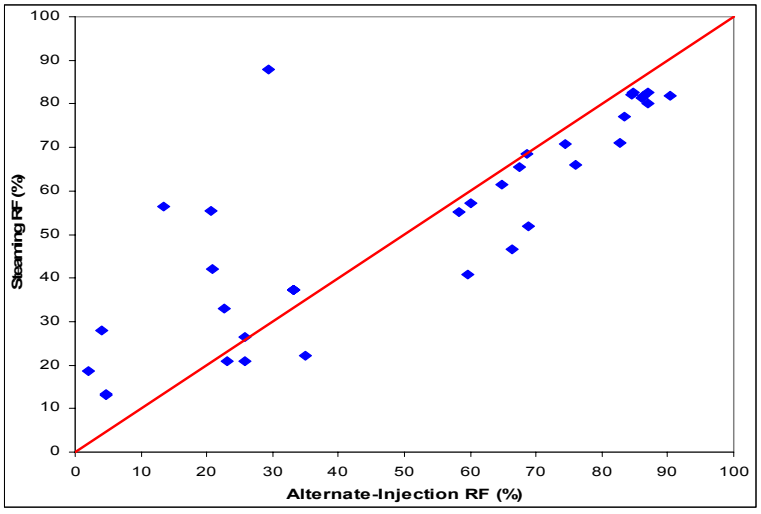


Fig. 6.28: Oil RF for Steaming and Alternating-Injection Runs (All Runs)

A critical evaluation of run 18, the outlier, reveals that it has large reservoir area but low permeability and thermal conductivity. As will be explained shortly in the case of reservoir area, this combination of parameters is not favourable for reservoir heating and fluid flow. While low permeability significantly inhibits CO_2 transport, the low thermal conductivity undermines conductive

heat transfer, which becomes more important in relatively low-permeability systems. Because the steaming process introduces higher enthalpy per unit mass, the convective transport partly compensates for the low conductivity.

Results for the high-viscosity runs are illustrated in **Fig. 6.30**. Compared to the low-viscosity case, several outliers are identified, though the inconsistency appears to be reasonably well-defined and uniform. Specifically, the outlying runs are 12, 15, 21, 30, 32, 36 and 37. A critical evaluation of these outliers reveals that they all have low-case structural extent (area). As this is the only feature common to them, we explore this parameter to rationalise the results.

From a heating perspective, it takes a shorter time to heat up a smaller reservoir, resulting in accelerated bitumen fluidisation and mobility enhancement. Therefore in this scenario, both processes have comparable heating rates. This suggests that temperature-induced viscosity reduction alone cannot fully explain the superior oil recovery noted for the alternating process in reservoirs of limited extent. But in addition to temperature effect, CO_2 miscibility also plays a role in the viscosity reduction. Hence, with comparable temperatures, CO_2 miscibility reduces insitu bitumen viscosity beyond that achievable by temperature only. Owing to the limited reservoir area, pressure tends to build up more rapidly and, with higher pressure, there is improved CO_2 miscibility in oil (**Fig. 6.11**).

A less apparent but complementary explanation is that a small reservoir area promotes the formation of a CO_2 cap, which supplements reservoir energy in pushing mobilised oil toward the producers. For equal amount of CO_2, the resulting gas-cap imposes a higher pressure (force-per-unit area effect) in a less extensive formation. Although steam also forms a vapour cap, this is much less stable (prone to condensation) in relation to a free-gas (non-condensable CO_2) cap.

Finally, the preliminary simulations presented in this chapter suggest that, in comparison to the steam-alone process, the SAC process becomes less competitive (using technical indices only) with increasing oil viscosity. However, in later chapters, when other important processes such as CO_2-induced deasphalting and consequent oil upgrading are examined, we shall show that the converse is more likely.

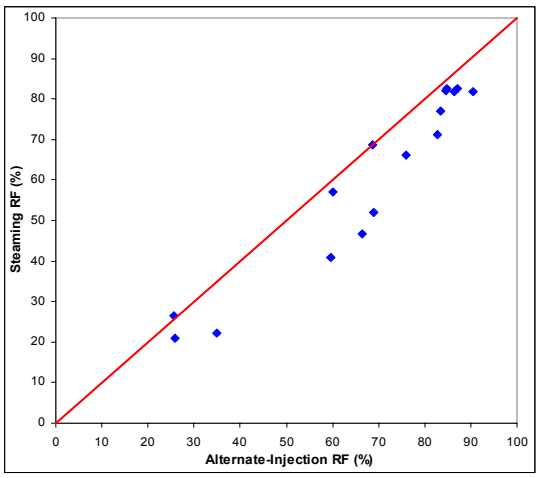


Fig. 6.29: Oil RF for SAC (Low-Viscosity Runs)

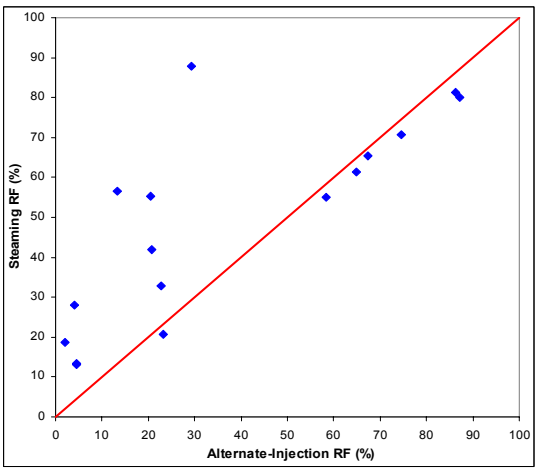


Fig. 6.30: Oil RF for SAC (High-Viscosity Runs)

6.11 Final Simulation Models

By considering the main response variables for both steam-alone and alternating-injection processes, the relative impacts of subsurface variables have been established. In a decreasing order of impact, the "heavy-hitting" factors are F_{10} (PVT model), F_1 (reservoir area), F_3 (reservoir thickness), F_9 (relative-permeability model), F_4 (oil saturation), F_5 (permeability), F_{11} (relative-permeability temperature sensitivity), F_6 (K_v / K_h), and F_8 (K_{shale} / K_{sand}). In essence, these include both accumulative and dynamic variables. On the basis of these heavy hitters, we construct a realistic set of simulation models.

However, from the results summarised in **Tables 6.16** and **6.19**, it is difficult to determine unique P10, P50 and P90 runs that satisfy all the responses at the same time. This dilemma, which has been noted by other workers (Lawal, 2009; Amudo *et al.*, 2009; Kabir *et al.*, 2002), is one of the current limitations of the ED technique of assessing reservoir uncertainties. Therefore, in constructing realistic simulation models, we complement ED with the structured deterministic approach (Lawal and Eweje, 2009; O'Dell and Lamers, 2003). Hence, the following are the final models used in subsequent simulations:

- **Low-Realisation Model:** In this case, all the heavy hitters (F_{10}, F_1, F_3, F_9, F_4, F_5, F_{11}, F_6, and F_8) take on their "pessimistic" estimates. In the case of F_{10}, the pessimistic realisation is the high-viscosity model. However, all other variables (F_7 and F_2 as well as skin factor, rock compressibility, over/underburden heat loss, aquifer, etc) refer to the base-case estimates.

- **Base-Realisation Model:** All variables, including the heavy-hitters, are in their base-case states.

- **High-Realisation Model:** Besides the heavy hitters, which refer to their "optimistic" estimates, all other factors use base-case values.

6.12 Chapter Summary

A generic, but representative, reservoir-simulation model has been constructed for the tar-bearing belt of southwestern Nigeria. Based on this model, the effects of reservoir parameters on the performances of the steam-alone and alternating-injection processes have been investigated. In assessing the impacts, we have employed both deterministic and probabilistic methods, and emphasised the difference between accumulative and dynamic effects.

The analysis of the results indicates that, within the range examined, the reservoir geometry, permeability distribution, relative-permeability functions and the fluid-property model are the primary determinants of project performance. We also found that the interactions between these high-impacting variables have significant influence on the set of performance indicators considered.

On the basis of these results, a set of realistic reservoir-simulation models have been constructed. In principle, these models describe the range of combinations that could be encountered in the belt. In the next chapter, we investigate the impacts of operating variables and how the geometric parameters related to the wells affect project performance.

Chapter 7

Optimisation of the Steam-Alone Process

The performance of the SAGD process, like all other in-situ recovery techniques, is very sensitive to reservoir, development (geometric) and operational parameters (Barillas *et al.*, 2006; Queipo *et al.*, 2002; Rahman *et al.*, 2001). Considering the limited ability to influence the reservoir parameters, the optimisation problem reduces to the establishment of the range of appropriate settings (design) of the development and operational parameters. The overall design objective is to achieve some performance measures within pre-defined bounds. While the last chapter addresses the impact of uncertainties in the reservoir model, the optimum settings of the design parameters remain to be investigated.

On the applicability of enhanced recovery methods to the Nigerian tar sand, a handful of promising results have been published for processes based on steam and hot water. From laboratory studies performed on a 20 ^{o}API (0.933 g/cm^3), 4800 cP crude sample, Adewusi (1998a, b) as well as Adewusi and Adetona (1998) indicated the technical feasibility of caustic, alcohol-caustic-steam and alkaline hotwater flooding, respectively. Similarly, Omole and Omolara (1988) as well as Akande (2007) reported favourable responses from steam stimulation. However, the fact that the oil samples used in most of these studies were initially mobile introduces uncertainties to the potentials of these methods in heavy-oil and bitumen pools. Given the general limitations of experiments in exploring realistic parameter space, only simulation studies can mitigate this shortcoming while allowing the extrapolation (and interpolation) of experimental results. However, as at date, we are not aware of any simulation studies on the response of the Nigerian system to thermal flooding, suggesting that the findings of the limited experiments may not be optimal, especially on a field scale.

This Chapter discusses the optimisation of the steam-alone process for possible application to the Nigerian heavy-oil deposit. Apart from assessing the applicability of this technology in Nigeria, a key objective of the current study is to establish the "optimum" steam rate for the steam-alone process, which would serve as the benchmark for the proposed alternating injection method. In particular, the data on optimum steam rate would give an indication of the steady load of direct process CO_2 emissions, required to be disposed of by the proposed thermal recovery technique.

7.1 Optimisation Studies

While the last chapter examines subsurface variables that are beyond the immediate control of the project developer, in this section, we investigate some variables that are within the influence of the project team either before start-up or during the operational phase. In general, we refer to these controllable variables as "design factors". We further categorise the design factors into fixed (static) and variable (dynamic).

Fixed design factors (FDF) are variables that can only be influenced (in practical terms) prior to project start-up. Essentially, they define the development concept (completion method). Although it is possible to modify them during the operational phase, such intervention usually requires expensive workover operations, and associated shutdowns. FDF's include:

- **Well Type:** vertical versus horizontal injectors and producers.
- **Well Spacing:** injector-producer vertical spacing.
- **Wellpair Spacing:** horizontal spacing between adjacent well pairs in the same plane.
- **Well Geometry**: length and radii (open-hole / tubing).
- **Well Count:** number of well pairs.
- **Well Pattern:** horizontal displacement of wells in a pair i.e. staggering/offsetting of injector and producer at different offset distances (Singhal *et al.*, 1998).
- **Perforation**: density, geometry, position, and orientation.

Unlike FDF, the variable design factors (VDF) or operating parameters are, subject to reliable information and experience, amenable to optimisation throughout the project life, and this can be achieved at much lower costs. Moreover, while the FDF's tend to take more of discrete values, the VDF's are mostly continuous, hence can readily be manipulated to achieve prevailing project objectives. In fact, most of the VDF's can be controlled remotely and almost in real time, for example using smart technology (Alhuthali *et al.*, 2010; Gotawala and Gates, 2009). Some VDF's are:

- **Injection:** pressure, temperature, rate, heating fluid (steam, hot water, cold water, saturated vs. superheated steam), steam quality.
- **Production:** liquid rate, vapour rate, GOR, BHP, water cut, steam-trap (subcool) temperature.
- **Preheating:** duration, rate.
- **Alternating Injection:** rates, frequency (weekly, monthly, quarterly, etc).

7.1.1 Basis for Discriminating the Optimisation Variables

Ideally, we should have subjected all the possible options (states of design factors) to economic analysis in order to arrive at the optimum set-up. However, this is virtually impractical. As qualitative indicators of the economics, we consider the following technical objectives, listed in a decreasing order of priority.

- Maximise discounted and undiscounted oil recovery per well but minimise steam injection per well.
- Maximise undiscounted and discounted oil (and gas) recovery.
- Minimise CSOR.
- Minimise enthalpy in-place and cumulative enthalpy injected.

While hydrocarbon production is proportional to revenue, it gives no insight into the project costs, which is also crucial for economic analysis. As a simple reflection of the possible capital

outlay, we use the recovery per well to penalise the incremental and accelerated recovery offered by higher well count.

CSOR provides a reasonable measure of the relative operating costs of different steaming alternatives. However being a ratio, CSOR can be misleading, as operations that involve very distinct oil recovery and steam consumption may be characterised by similar CSOR. Additionally, being strictly a volume-based quantity, CSOR does not account for energy costs in an explicit manner. For instance, whereas they may have equal CSOR, steaming operations at 300 and 150 ^{o}C are clearly not the same in energy terms.

To complement CSOR as a discriminating quantity, we consider the total enthalpy stored in the reservoir at the end of simulation. Technically, for the same initial reservoir temperature, enthalpy in-place is the net balance between cumulative heat injection and production. Apparently, leaving heat underground is not desirable, as such heat would be more valuable in the production stream such as mitigating rheology-related transport problems (flow assurance) and improving overall process efficiency. Additionally, heat retention in the produced water reduces the costs of recycling such water as steam.

Noting the potential pitfall in comparing the CSOR of two steaming processes at different temperatures, we use the cumulative enthalpy injected, which gets around the problem of steam being injected at different temperatures, thus providing a more objective basis to analyse the total thermal energy investment (fuel costs and possibly, size of steam generators).

7.1.2 Reference Development Concept

As the basis for optimisation, a reference development concept is defined, assigning values and states to the FDF's and VDF's. Basic details of the reference concept are listed in **Table 7.1**. For simplicity, only one variable is evaluated at a time, hence possible interactions are ignored. When there are interactions among the variables, it is assumed that such interactions are synergistic in favour of the outlined optimisation objectives. In this case of steam-alone injection, owing to the low solution gas (22 scf/stb) in the bitumen, coupled with the prospects of monetising the gas (mainly CH_4), no constraint is imposed on the gas production rate.

Table 7.1: Reference State for Optimisation

Fixed Design Factors		*Variable Design Factors*	
Well type	horizontal	Heating fluid	saturated steam
Wellbore length (m)	500	Injection temperature (^oC)	250
Wellbore radius (cm)	16	Maximum injector BHP (kPa)	5000
Wellpair count	2	Subcool temperature (^oC)	10
Injector-injector spacing (m)	100	Steam rate, CWE (stb/d/well)	5000
Producer-producer spacing (m)	100	Steam quality (%)	70
Vertical well spacing (m)	5	Water cut (%)	99
Perforation density	full wellbore	Gas production rate	unconstrained
Producer placement above OWC (m)	2		

7.2 Optimisation of Fixed Design Factors

In this section, the results of the optimisation studies conducted on selected FDF's are presented and analysed.

Well Type: In general, the productivity/injectivity of a typical horizontal well is at least twice of its vertical counterpart, despite that the cost of the former is just about twice the latter (Carpenter and Dazet, 1992). To compare vertical and horizontal completions, four options are evaluated. These include the reference case, involving two pairs of injectors and producers that are all horizontal. The other cases are 8 VI - 2 HP, 4 VI - 2 HP, 4 VI - 4 VP, and 2 HI - 8 VP. Here, VI and VP stand for vertical injector and producer, respectively. Similarly, HI and HP are horizontal injector and producer, respectively. In all the cases with vertical completion, we assume, in a dynamic sense, that two vertical wells are equivalent to one horizontal well. But the case of 8 VI - 2 HP is designed to assess the lower limits of vertical completions.

Fig. 7.1 shows predicted oil recovery for the various configurations. Apart from the short interval, vis-à-vis year 2011 to 2013, the reference case consistently outperforms the other cases. This is attributed to significantly larger contact area, resulting in higher injectivity and productivity, offered by horizontal completions. Furthermore, the apparently "balanced" injectivity and productivity minimises potential pooling of fluids around the wells. This is the so-called near-well congestion phenomenon (Rose and Deo, 1995), which impedes steam supply to the steam zone and, at the same time, blocks fluid flow to producers. It is worth pointing out that although the reference case is shown to have much higher recovery factor than others, this is primarily an accelerative (rather than reserves addition) effect, as the other cases ultimately yield similar recovery, which is not unexpected, because the petrophysical and fluid properties as well as operating conditions are the same.

Although the case of 8 VI - 2HP provides, in principle, the same productivity as the reference case, the relatively lower injectivity of the vertical producers could not sustain reservoir production

potential, as evident in the accelerated recovery in the first three years which, in relation to the reference concept, declines afterwards. Comparing the cases of 8 VI - 2 HP and 4 VI - 2 HP, which have similar fluid drainage potentials, the additional four injectors yield a slightly higher recovery for the former. As expected, due to inhibited injectivity and productivity, the all-vertical-well case yields the poorest performance. Accordingly, we select the concept of all-horizontal-completion.

A key learning point from this result is that the conventional rule-of-thumb on the improvement factor of horizontal completions over vertical wells should be used with caution, especially for heavy oil reservoirs. Unlike light oil formations, which are characterised by relatively high initial mobility as well as drainage volume and flowrates, the very low in-situ mobility of heavy oil requires significantly larger contact area to achieve reasonable productivity/injectivity on one hand, and propagate the viscosity-reducing mechanism on the other hand. As a result, it is recommended that detailed studies should always be conducted to discriminate between horizontal and vertical completions in prospective developments.

In the case of 2 HI - 8 VP, despite the high injectivity potential of the horizontal injectors, the inability of the vertical producers to drain mobilised fluids at comparable rate on one hand and the low pressure dissipativity of the reservoir on the other, causes pressure build-up, which then impedes injectivity. This scenario undermines early-time expansion of the steam chest and oil drainage. Instantaneous radius available for pressure dissipation can be estimated with this expression (Smith *et al*., 1992).

$$R_p = \sqrt{\frac{\bar{k}_h t}{\bar{\phi}\bar{\mu}_o\bar{c}_t}}\,, \tag{7.1}$$

where $\bar{k}_h$, $\bar{\phi}$ and $\bar{c}_t$ denote average horizontal permeability, porosity and total compressibility, respectively. $\bar{\mu}_o$ represents average oil viscosity at some *average* temperature (or composition) over elapsed time *t*.

Given a choice of one configuration-set for either producers or injectors, from an accelerated recovery standpoint, it would be more favourable to have horizontal producers as against horizontal injectors, especially in fairly homogenous formations. While injectivity trails productivity in the former, the reverse applies to the latter. This inference may partly explain the motivation for vertical-injector SAGD in some applications (Miller and Xiao, 2010; Bagci and Gumrah, 1992; Rose and Deo, 1995). However, mid-to-late life performances appear to favour horizontal injectors because in this period, effective injectivity is crucial to maintaining the steam chamber, hence recovery.

Wellbore (Open-hole) Radius: Forecasts of oil recovery and CSOR for different open-hole radius are presented in **Fig. 7.2**. Despite having the hole diameter varying by almost a factor of four, the impact of hole size on oil recovery and steam consumption is less than 10 % in this example. Accordingly, it may be concluded that the size of open hole does not appear to have considerable impact on reservoir dynamics.

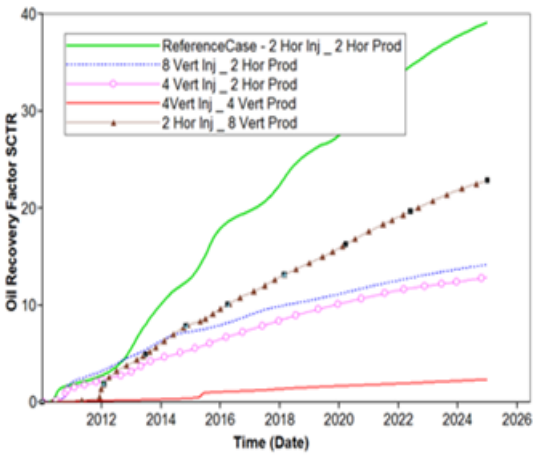


Fig. 7.1: Effect of Well Type on Oil Recovery

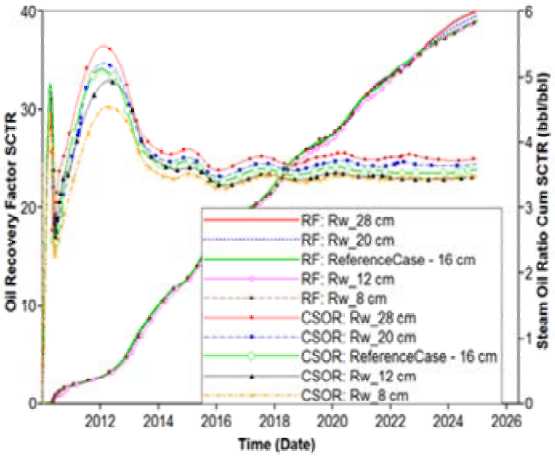


Fig. 7.2: Effect of Wellbore Radius on Oil Recovery and CSOR

Considering that open-hole radius appears as a logarithmic argument in the Darcy radial-flow model, the relative insensitivity of oil rate and production to this variable is not unexpected. Although apparently amplified by the scale of the abscissa, the CSOR seems a better discriminator of the impact of open-hole radius, with the process becoming more energy intensive as the hole expands. This can be attributed to the fact that larger hole causes a greater increase in injectivity because of the high steam mobility compared to low oil mobility that undermines productivity response to increased flow area for the same drawdown. On the basis of CSOR profiles, we select the 12 cm radius. On top of this, improved economics and the need to mitigate potential wellbore stability issues during drilling are other incentives for relatively slim holes (Nguyen *et al.*, 2010; Tubbs and Wallace, 2006).

Meanwhile, the plots in **Figs. 7.1** and **7.2** indicate that productivity and injectivity are insignificant at early times. This can be explained by a number of factors, which include: (i) low total fluid mobility caused by initially high oil viscosity (viscosity effect); (ii) low water saturation at start-up, resulting in low steam mobility (relative-permeability effect), hence delayed reservoir-heating; (iii) with small voidage, injection and reservoir pressures are comparable, resulting in low injectivity (drawdown effect); and (iv) with low average temperature, only the vicinity of the injectors, which are at relatively higher temperatures, operate on the more favourable temperature-dependent relative permeability models. However, as would be evident in other simulations, the viscosity effect appears to be the dominant factor, as the duration of the start-up period generally reduces as the *in-situ* oil becomes less viscous.

Wellbore (Horizontal Section) Length: For this analysis, the reservoir length in the along-well direction (x-axis) remains constant at 500 m. In principle, this sensitivity evaluates the effect of well exposure to the reservoir. To prevent eccentricity, the wells are consistently positioned to achieve symmetry along the x-axis of this homogenous model, with the entire length taken to be active (contributes to flow). Furthermore, the indicated length applies to all the wells simultaneously.

Lengths of 100, 200, 300, 400 and 500 m, representing 20, 40, 60, 80 and 100 % of the axis length, respectively, are investigated.

Fig. 7.3 depicts the oil-production profiles, with recovery increasing with wellbore length. Apart from the increased recovery, the production rate (gradient of recovery) also increases with the reservoir exposure. To discount the expected increase in drilling and completion costs due to increasing wellbore length, we analyse the oil-recovery per unit length, where the recovered oil is discounted at 10% per annum. From this analysis, we found the 500-m case to be the most competitive.

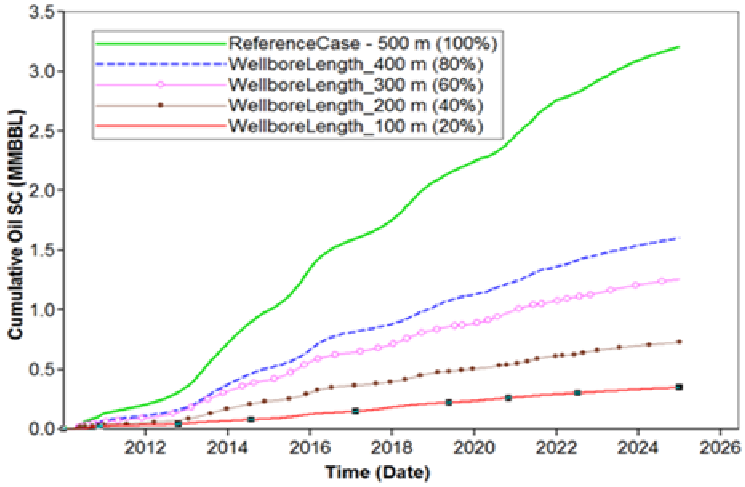


Fig. 7.3: Effect of Wellbore (Horizontal) Length on Oil Recovery

Wellpair Count: Performance plots for various number of injector-producer pairs are presented in **Fig. 7.4**, indicating that instantaneous oil recovery increases significantly with well density. This observation can be explained by two factors: (i) geometry and (ii) injection volume (enthalpy).

For instance, as well density increases, the effective volume attributed to each wellpair reduces, resulting in reduced capacity of the formation to store heat and mass while enhancing its ability to transmit same quantities through it. As a result of high well density (reduced effective geometry) in this homogenous model, it takes a shorter time for pressure, heat and mass to propagate through the formation.

However, the results in **Fig. 7.4** do not account for differences in injection volumes. For objective comparison of well count, it is necessary to use equal injection volume for all options. Hence, we conduct additional study, imposing an arbitrary maximum total injection rate of 1000 stb/d in all cases. Note that the injectors are constrained to the same rate in all the multiple wellpair cases.

Fig. 7.5 shows the production profiles for fixed total injection rate. Although it is still evident that recovery rate correlates positively with well density, this dependency reduces when similar enthalpy is injected. The results underscore the relative importance of the effective volume. A comparison of the 4 and 5-wellpair profiles highlights the effect of well interference, indicating the sub-optimal

benefit of the incremental wellpair. A similar inference can be drawn for the 2 and 3-wellpair configurations, especially during the mid-life. In theory, for the same injection conditions, the multiple-well operation may be viewed as a strategy for extending the instantaneous reach of the heat carrier and, at the same time, checking near-well congestion. This notwithstanding, because the absolute recovery does not account for the effects of time and incremental costs, it is not sufficient for discriminating the various options.

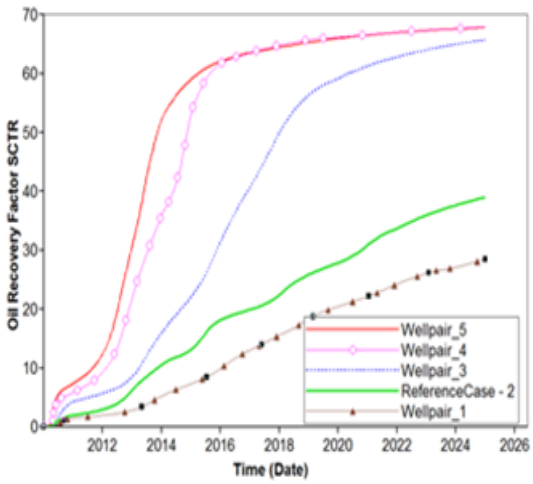


Fig. 7.4: Effect of Number of Wellpairs on Oil Recovery (Unequal Total Injection Rates)

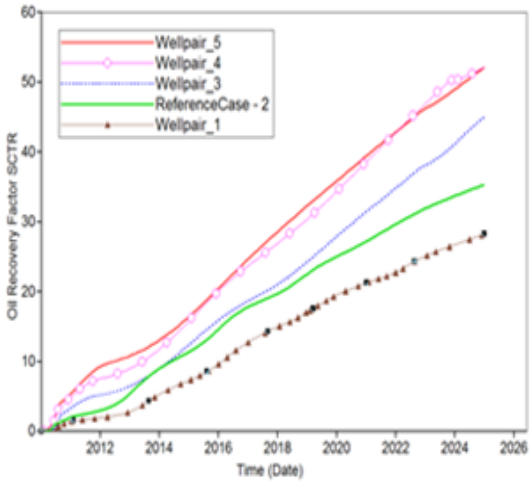


Fig. 7.5: Effect of Number of Wellpairs on Oil Recovery (Equal Total Injection Rates)

To adequately discount the effect of well count, a screening parameter N_x, which incorporates well count in addition to the time-value of oil recovery and steam consumption, is defined as follows:

$$N_x = \frac{N'_{pog}}{n_w W'_i} \quad , \tag{7.2}$$

where N'_{pog} is discounted sum of oil and gas UR, n_w is the number of wellpairs, and W'_i is the discounted steam volume (CWE) injected. In the definition of N_x, it is subtly implied that a linear relationship exists between total costs (capital and operating) and number of wells.

Contrary to the inference from the use of absolute recovery, **Fig. 7.6** shows that project becomes increasingly less competitive with the number of wellpairs. Although a one-wellpair concept is indicated to be the most competitive, considerations of geologic / engineering risks and lack of experience on heavy-oil development in Nigeria influence the decision to choose the two-wellpair alternative.

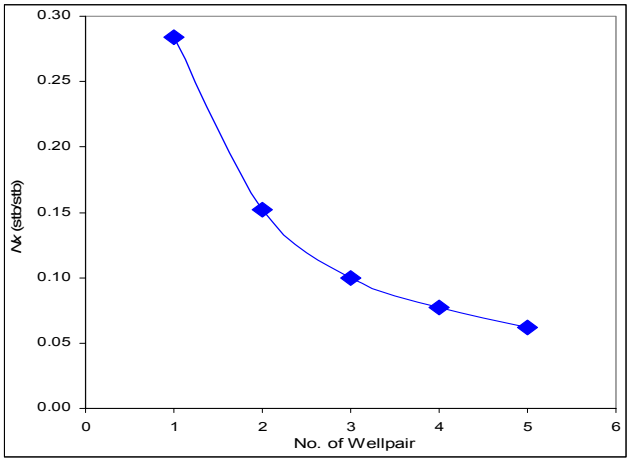


Fig. 7.6: N_x versus Wellpair Count

Vertical Well-spacing: Oil recovery for injector-producer vertical separations of 3, 5, 10 and 20 m are illustrated in **Fig. 7.7**. The separations are equivalent to 7, 12, 25 and 50 % of gross (including 2-m bottom-water sand) reservoir thickness, respectively. Corresponding average temperatures are depicted in **Fig. 7.8**. Beyond 10 m, there is a sharp decline in recovery rate. Although the late-time performance of the 10 m spacing compares reasonably with those of 3 and 5 m spacings, the 6-month initial production lag, due to delayed producer-injector communication, renders it less attractive. Despite similar early to mid-life profiles for the 3 and 5 m cases, the latter's higher ultimate recovery makes it the optimum option.

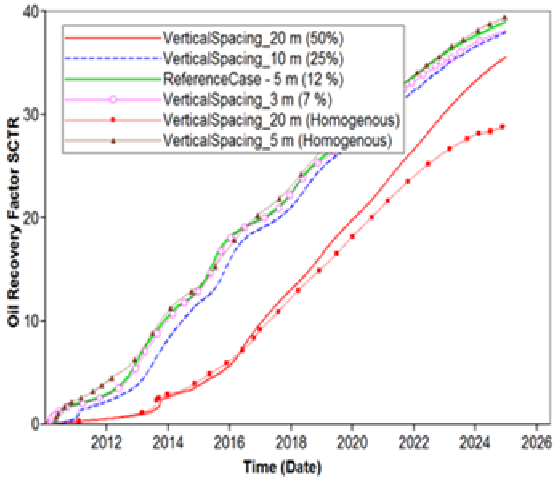


Fig. 7.7: Effect of Vertical Well-spacing on Oil Recovery

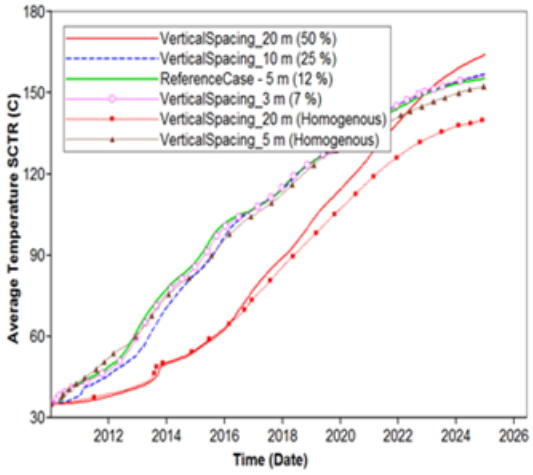


Fig. 7.8: Effect of Vertical Well-spacing on Average Reservoir Temperature

Despite that a low producer-injector spacing accelerates communication, simulations point to an optimum. In this study, 3-m spacing seems too close, as it promotes convective thermal losses through bulk production of hot fluids, steam breakthrough as well as heat flow to underlying water sand and underburden. These effects cause unnecessary temperature rise in the vicinity of the producers. Because the producers are primarily operated on steam-trap control (limiting allowable

pressure drop between wells), greater choking is experienced in the 3-m case, resulting in slightly lower recovery compared to the 5-m case. A less obvious contributor to the better performance of the 5 m case is its higher gravitational head relative to the 3 m option.

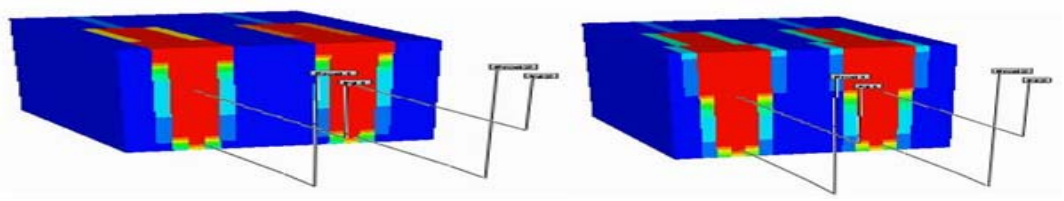
The 20-m case reveals the risks of placing injectors in a low-permeability layer (here, oil shale). The lower performance for this case is attributed to relatively poor injectivity, delay in establishing flow communication between injector and producer, and less importantly, thermal losses through the overburden because of relative proximity of injectors to the cap rock.

For greater clarity on the relative contributions of caprock thermal losses and delayed communication, we re-run the 5 and 20-m cases, but treating them as modified-homogenous models i.e. assigning equal permeability to the oil shale and sand units. These results are presented as 5 m (homogenous) and 20 m (homogenous) in **Figs. 7.7** and **7.8**.

Comparing the two 5-m cases, although the homogenous case predicts marginally higher oil recovery, more significantly, it leads to much lower average formation temperature. The higher oil recovery is attributable to the improved ability of the oil shale layer (now having higher permeability) to release its oil contents and at the same time, allowing enhanced passage of mobilised oil and condensates from the upper layers down to the producers. However, the homogenous case has a lower end-of-simulation average temperature because of higher convective losses due to higher volume of produced hot oil, water (and live steam) as well as gas.

Conversely, performance deteriorates with homogeneity for the 20-m case. Despite increased injectivity, the longer distance between injector and producer delays inter-well communication. As a result, it can be concluded that until adequate flow communication, i.e. mobilisation of oil column between producer and injector, is established, the primary heating mechanism remains conduction, which is not only very slow, but hampered by the longer injector-producer spacing in the 20-m case compared to the 5-m case.

Unlike the 5-m case, in the 20-m case, a combination of higher injectivity and proximity to overburden promotes heat losses to the caprock, hence the poorer oil recovery and lower average temperature for the 20-m homogenous case. To substantiate this argument for the 20-m runs, the relative rates of upward propagation of temperature front can be deduced from **Fig. 7.9**, illustrating the steam-chamber geometries after 7 years.



(a) "Heterogeneous" **(b) "Modified-Homogenous"**

Fig. 7.9: Steam-Chamber Geometry after 7 Years for 20-m Vertical Spacing

Wellpair Spacing: This refers to the cross-well separation of adjacent wellpairs, with the injector and producer in a pair placed in the same vertical plane. Spacings examined are 60, 80, 90, 100, 110, 120 and 140 m, corresponding to 30, 40, 45, 50, 55, 60 and 70 % of the reservoir width, respectively. **Fig. 7.10**, which illustrates the simulation results, suggests that production is accelerated with reduced spacing but ultimate recovery is jeopardised.

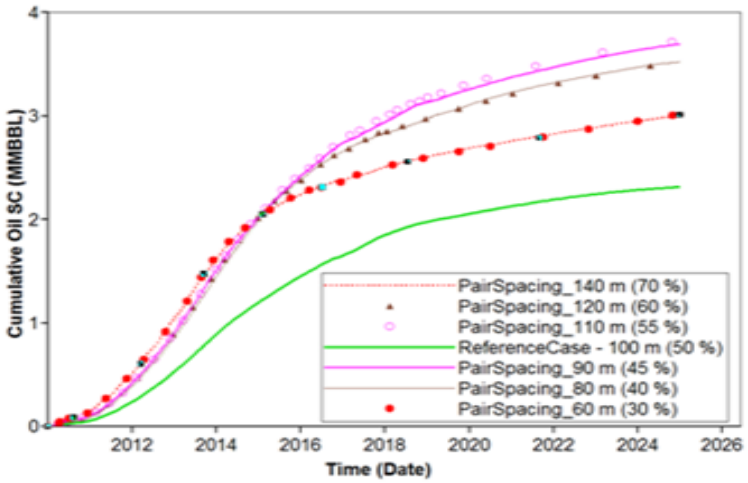
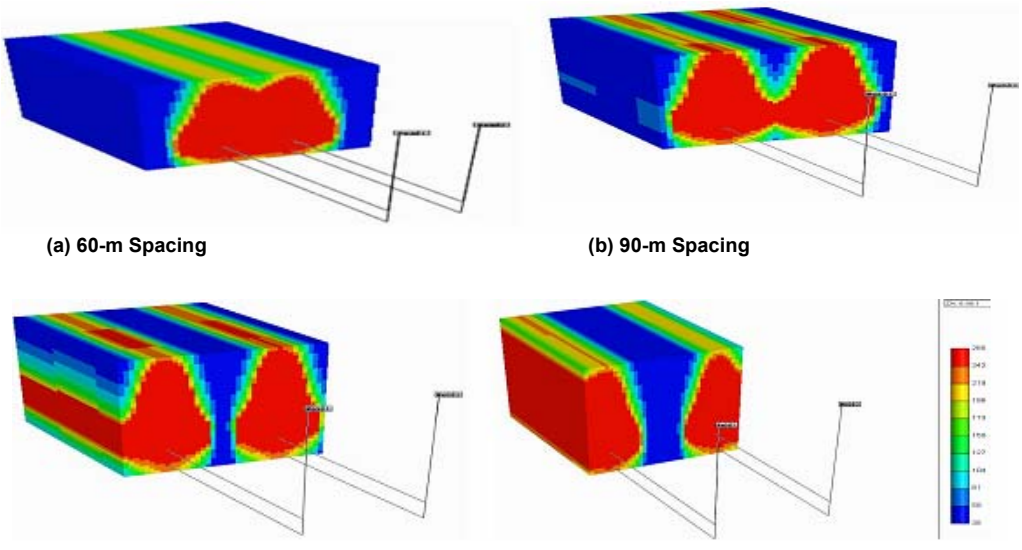


Fig. 7.10: Effect of Wellpair-Spacing on Oil Recovery

Fig. 7.11 depicts the steam-chamber geometry for selected cases after seven years. Although the closeness of the pairs accelerates the expansion and coalescence of adjacent chambers, it is important to ensure that the heating of the zones outside the inter-pair volume, vis-à-vis well-to-boundary areas, is not compromised. For the purpose of discussion, we refer to the sideward well-to-boundary areas as the “blind” zones.



(a) 60-m Spacing **(b) 90-m Spacing**

(c) 110-m Spacing **(d) 140-m Spacing**

Fig. 7.11: Steam-Chamber Geometry after 6 Years for Selected Wellpair Spacings

While it is critical to achieve effective heating of the "blind" zones, from a thermal-efficiency viewpoint, it is instructive to achieve a reasonable balance between blind-zone heating and heat "loss" through the side boundaries. Whereas the current model treats these boundaries as insulating, this may not be valid in practice, especially in full-field development, where the so-called losses for one "pad" would be gained by adjacent "pads", and vice-versa (depending on the direction of temperature gradient). But still, regardless of the number of pairs used to develop a particular field, the outermost wells would still interact with the formation boundaries, which define the reservoir (trap) in the first instance. Hence, the current analysis should be seen in the context of the furthest wells.

Because of the smaller inter-pair volume in the 60 m case, steam chambers form and coalesce rapidly, leading to early drainage of this volume (**Fig. 7.11**). As can be seen in **Fig. 7.10**, this case has its accelerated heating reflect as accelerated production. However, if one may ask, why would the 140 m case, whose inter-pair volume more than doubles that of 60 m, follow virtually the same performance trend? The answer lies in the "actual" heated volume.

In reality, the midpoint of two isothermal sources (maintained at the same temperature) heating or cooling a homogenous body through its ends, may be regarded as a no-flow boundary. In fact, in a homogeneous system, a plane through this midpoint is a plane of symmetry, as the temperature profiles from either source to the midpoint would be identical. To rationalise this argument, we use our numerical program (Chapter 3) to simulate conductive-heating of a 60-m section of this reservoir, initially at 35 ^{o}C, with its boundaries kept at 250 ^{o}C. The temperature profiles at selected times, shown in **Fig. 7.12**, reveal the symmetry of this system.

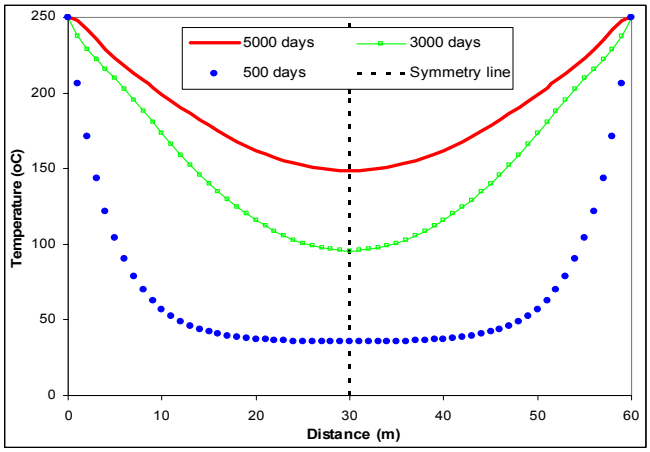


Fig. 7.12: Instantaneous Temperature Profiles for Conductive-Heating of Inter-well Volume

Therefore, in terms of heat propagation, heating the centre of a system by two sources at its ends would yield exactly the same results as would be obtained were only half of the volume be heated by either source. Accordingly, this midpoint may be regarded as a heat sink, whose temperature would continue to increase until it equilibrates with the sources.

In the 60 m case, the inter-pair length is being heated by two isothermal injectors, each effectively covering 30 m length between pairs and 70 m in the "blind" zone. But for the 140 m spacing, each injector essentially heats up a 30 m length in the blind zone, with the boundary serving as "sink", and another 70 m length in the inter-well zone. Due to the homogeneity of the formation, from a heating perspective, the 140 m and 60 m spacings are equivalent. Because oil recovery is primarily controlled by heat transport in this problem, performances of the two cases mirror one another. The same argument is valid for the 80 / 120 m and 90 / 110 m pairs. In retrospect, this result is another consequence of treating the lateral boundaries as insulators. But where there is significant lateral variation of thermal (and flow) properties, the symmetry analysis would cease to be valid.

From the simulation results, it can be deduced that closer well spacing, which allows for smaller-volume cold zones on either sides of the injector, enhances reservoir-heating. For the same amount of enthalpy injection, it takes a smaller time to heat up and mobilise the oil in such smaller-volume cold zones. However, for asymmetric well placement, once the smaller-volume zones have been depleted, production decline would be experienced, as it takes longer time to heat up and mobilise oil in the larger-volume cold zones on the other end. This explains the relative production decline, after 5 years, of the 60 and 140 m cases in **Fig. 7.10**.

Following the foregoing analysis, we hypothesise that it may be advantageous to displace the horizontal injector and producer in a well pair. Considering that the producer is somewhat a heat source, as the continuous presence of hot fluids raises its temperature above that of its immediate surroundings, placing the producer some horizontal distance away from the top injector may be analogous to creating two heat sources (in principle, extending the injector) and reducing the cold-zone volume in the direction of producer displacement. We investigate this hypothetic pattern, which was partly discussed by Chan *et al.* (1997), as a slight modification of the conventional SAGD configuration.

From the forecasts in **Fig. 7.10**, the 90 and 110 m spacings are the most attractive. But, given the need to mitigate subsurface and operational risks as well as the likelihood of incurring heat losses through the lateral boundaries, we select 90 m, i.e 45 % of reservoir width, as the optimum wellpair spacing.

Well Staggering: Here, the effect of placing injectors and producers in a repeated alternating pattern is examined. As shown in **Fig. 7.13**, the producer-producer and injector-injector spacings are consistently fixed at 100 m while the injector and producer in the same pair are staggered (horizontally displaced) by length, L_s. Essentially, the producers are kept in a fixed position as injectors are moved in the *same* direction. In addition to the reference case, in which there is no staggering, stagger lengths of 5, 20 and 50 m are studied.

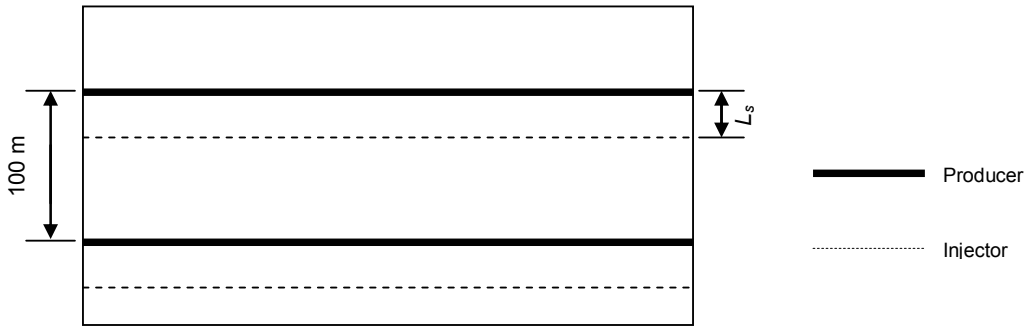


Fig. 7.13: Schematic of Staggered-Well Configuration (Plan View)

Predictions of oil recovery for the various cases are illustrated in **Fig. 7.14**, indicating that performance becomes increasingly less competitive with staggering length. However, providing the displacement does not exceed 5 m, there is some advantage in a staggered pattern. Overall, 5-m staggering is optimum.

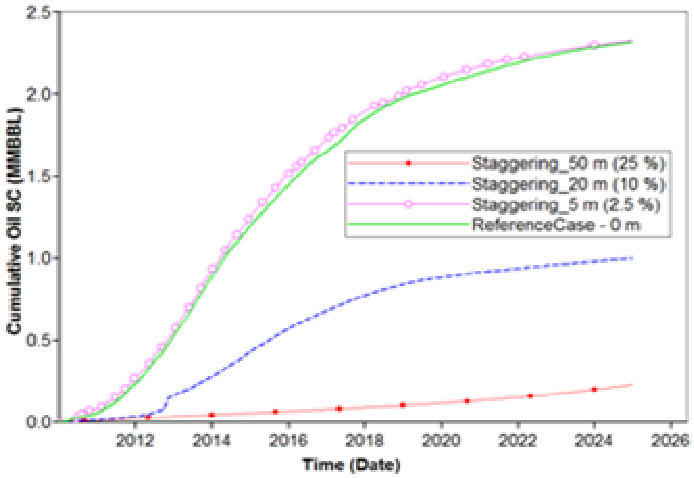
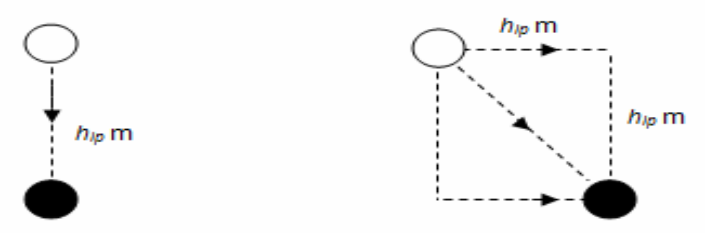


Fig. 7.14: Effect of Well-Staggering on Oil Recovery

The poor recovery observed for high stagger lengths can be rationalised by increased delay in establishing producer-injector configuration owing to the need to heat up a larger volume of colder region before oil is mobilised. But for the reference and 5-m cases, the smaller colder volume between wells accelerates heating, hence oil mobilisation and production. Moreover, as voidage is being created through fluid withdrawal, local pressure build-up and injectivity decline are minimal. The difficulty in creating voidage in the other cases is inimical to injectivity, forcing the system to rely on the less efficient conductive heating.

Fig. 7.15 is a simple conceptual model of flow paths for heat and mass exchange between a pair of injector and producer, displaced h_{ip} m along vertical and horizontal axes. Unlike the no-staggering case where there is effectively a single line of exchange, staggering introduces two flow paths, with the resultant greater than either path. This implies that, on a net basis and for the same conditions, fluids travel longer distances (~ 40 % more) to reach producer in the square-staggered

arrangement. As a result of the longer net travel distance (longer by $h_{ip}\left(\sqrt{2}-1\right)$ m), oil production start-up is prolonged in the staggered case, though this is not really obvious in **Fig. 7.14**. But how does this affect oil rate and recovery? This is examined shortly.



(a) No Staggering **(b) Staggered**

Fig. 7.15: Conceptualised Heat and Mass Flow Paths for Different Well-Placement Patterns

Producer-Producer Spacing: Unlike the arrangement under well staggering where injectors are moved in the *same* direction while producers are fixed, in the current analysis, the injectors, which are 100 m apart, are in fixed position while producers are moved in *opposite* directions to achieve desired spacing. Separations examined are 60, 80, 90, 100 and 120 m, equivalent to 30, 40, 45, 50 and 60 % of reservoir width, respectively.

The performance plots, presented in **Fig. 7.16**, suggest that the 90-m spacing is optimum. Although the 60 m run yields the highest recovery after 15 years, the considerable delay in achieving economic oil rates would be detrimental to project economics. This finding is consistent with the preceding suggestion on the merits of a square-pattern producer-injector displacement. With 90 m producer-producer spacing, the implication is that each producer is displaced 5 m horizontally from its injector, which is exactly 5 m above the producer.

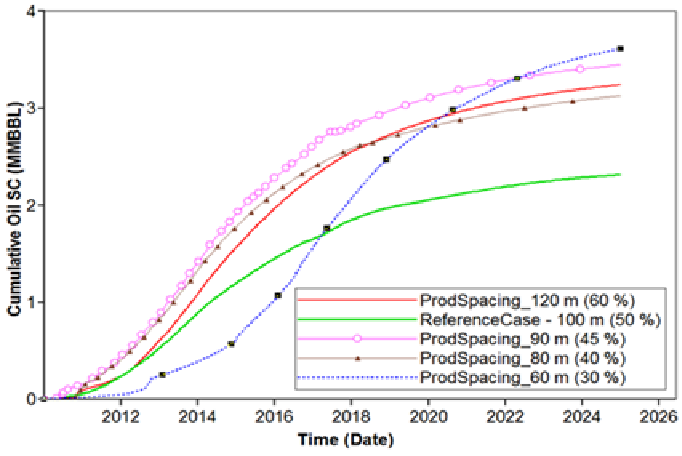
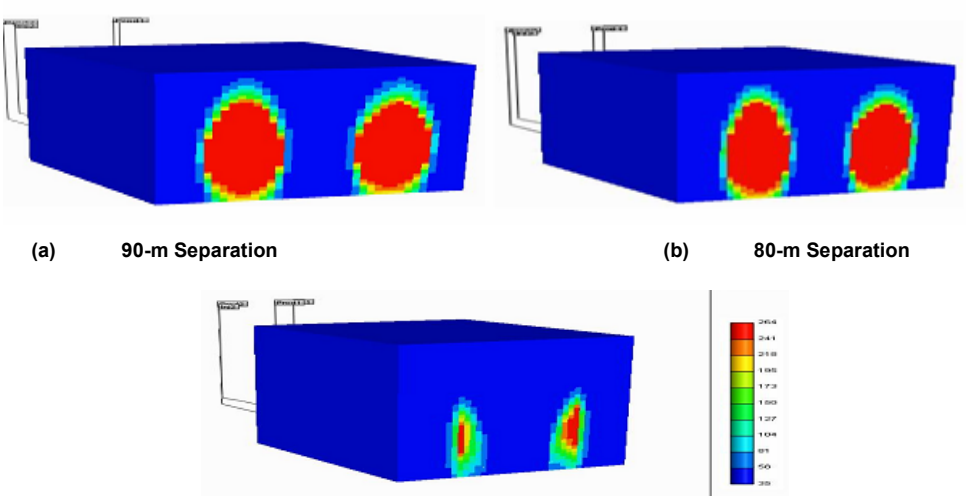


Fig. 7.16: Effect of Producer-Producer Spacing on Oil Recovery

Fig. 7.17 illustrates instantaneous steam chamber geometry for selected runs. From these schematics, the superior performance of the 90-m case, especially in the first three years, can be

rationalised. In particular, it is obvious that the time taken to heat up and mobilise the producer-injector cold zone becomes smaller with the proximity of the producer and injector (heat source) in a pair. Due to symmetry, the 80 and 120-m concepts have analogous heating behaviours. However, mid-to-late time interference, whereby the drainage radii of the producers overlap, accounts for the higher ultimate recovery of the 120 m option. And for the 100 m case, near-well congestion resulting from depending effectively on a single flow path makes it the least attractive development alternative.



(a) 90-m Separation **(b) 80-m Separation**

(c) 60-m Separation

Fig. 7.17: Steam-Chamber Geometry after 3 Years for Selected Producer Spacing

Injector-Injector Spacing: This is similar to the producer-producer spacing but here, producers are kept 100 m apart in fixed positions while injectors are shifted as required. In all runs, vertical spacing remains 5 m. From the performances in **Fig. 7.18**, unlike what obtains for producer-producer spacing, it is difficult to select between 100 and 90-m injector separations on the basis of recovery trends. As noted earlier, the significant delay in reservoir heating renders the 60, 80 and 120 m separations unattractive.

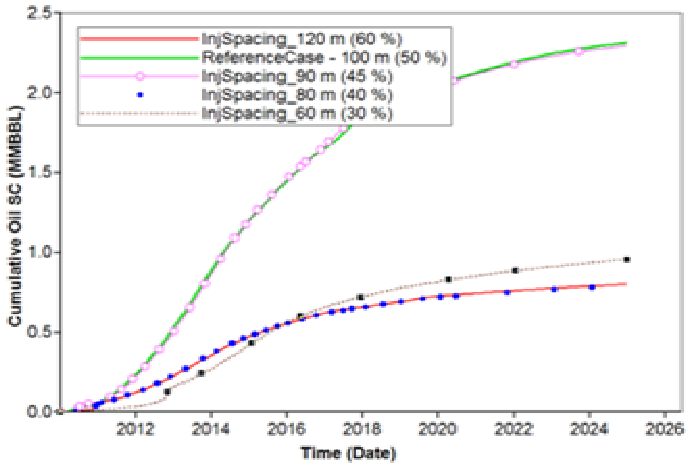
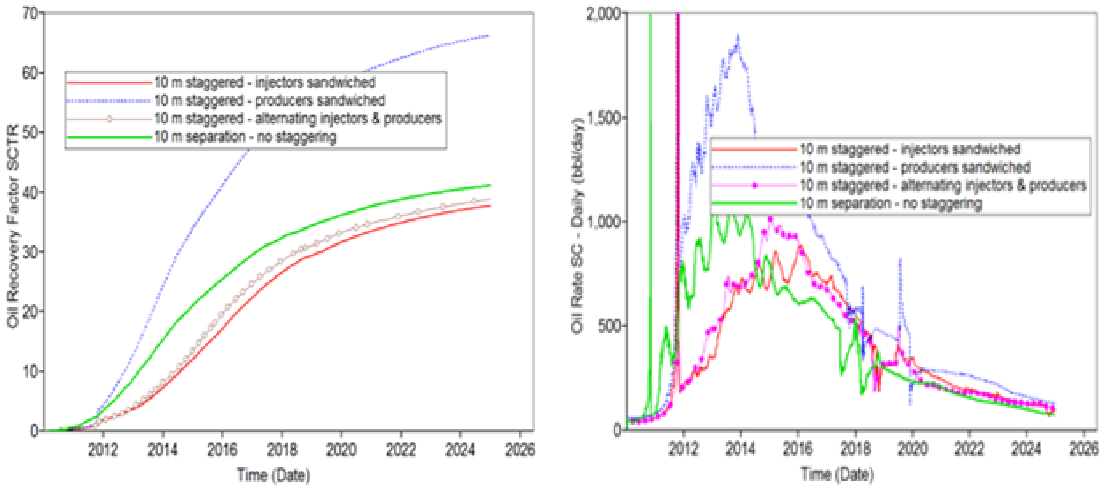


Fig. 7.18: Effect of Injector-Injector Spacing on Oil Recovery

But why would a 90-m producer-producer separation yield significant incremental recovery yet similar injector-injector spacing does not, despite that both arrangements describe exactly the same square-pattern staggering? Our preliminary explanation is that the orientation of the square pattern may also be important. The following analysis and sensitivity provide further clarity.

We imagine that the schematics in **Fig. 7.15** are also applicable to velocity, with component velocities v_v and v_h in the vertical and horizontal directions, respectively. Considering that horizontal permeability (2 D) exceeds vertical permeability (1 D), hence v_h is greater than v_v; it implies that the resultant velocity v, in the staggered case would always exceed that in the no-staggered concept (v_v). Accordingly, for the same flow area, it follows that mass and heat (convective) flow rates in the staggered case would be higher, resulting in higher oil rate and recovery. Evidently, this assertion applies in **Fig. 7.16** but not quite conclusive in **Figs. 7.14** and **7.18**.

To amplify the start-up delay in a staggered arrangement and understand the impact of square-pattern orientation, we simulate different well configurations but with each pair's producer and injector consistently 10 m apart. **Fig. 7.19**, depicting the results of these simulations, highlights the slight initial production delay associated with the staggered pattern. Incidentally, consistent with the simple analysis on net velocity (i.e. resultant permeability of 2.2 vs. 1 D), the peak oil rate of the sandwiched-producer staggering option almost doubles that of the no-staggering case.



(a) Cumulative Oil Production **(b) Oil Rate**

Fig. 7.19: Effects of Well-Arrangement on Oil Recovery

Based on the earlier analysis and the results in **Fig. 7.19**, we propose a simple rule-of-thumb for well arrangement as follows. For the same operating conditions in a homogenous system, a staggered well arrangement promises the most competitive performance, though with slightly delayed start-up, providing the staggering describes a square pattern and producers are sandwiched by injectors. Additionally, though not shown, as obtainable in horizontal versus vertical gas-liquid separators, by encouraging gravity segregation, the longer travel length that characterises staggered well configurations tends to limit steam (and CO_2) breakthrough for the same oil production.

7.3 Optimisation of Variable Design Factors

The following is an analysis and discussion of the key results obtained from the optimisation studies performed on some of the VDF's.

Injection Stream: This assesses different processes and injection streams, including cold-water flood (CWF), cold heavy-oil production with sand (CHOPS), hot-water flood (HWF), as well as the injection of saturated and superheated steams.

In CWF, water is injected at reservoir temperature, thus no net enthalpy is introduced. Although CHOPS is similar to CWF in terms of injectant, the difference lies in the permeability-increasing fractures induced in the former process. To simulate CHOPS without incorporating geomechanical effects, we have simply increased the base-case vertical and horizontal permeabilities ten-fold while doubling the injection pressure, which approximate potential fractures and enhanced injectivity, respectively.

HWF entails injecting water at 250 ^{o}C but with negligible steam quality, implying that, on a net basis, only sensible heat is available. Conversely, although saturated and superheated steams also involve water at 250 ^{o}C, they include the latent heat. But relative to the saturated steam, the

superheated case has 100 % quality (compared to the former's 70 %) and includes the equivalent of 20 ^{o}C (84 kJ/kg) excess heat.

Fig. 7.20 presents the simulation results of the various schemes. The plots, even with ten-fold increase in permeability in the case of CHOPS, suggest that oil mobility and recovery have much greater dependence on in-situ viscosity than permeability. Therefore, in order to be successful, potential development methods, currently thermal, should focus on drastic reduction of oil viscosity in-situ. On the basis of lifecycle costs per unit recovery, saturated steam emerges as the most competitive injectant.

Despite that superheated steam carries higher amount of steam per unit mass than its saturated counterpart, the inability of the former to release the more useful latent heat as early as possible inhibits its reservoir-heating potential, hence oil mobilisation. As shown in **Fig. 7.21**, due to the amount of cooling required before condensation, a large fraction of the superheated steam is reproduced along with oil, limiting the availability of a significant percentage of injected enthalpy for the intended application.

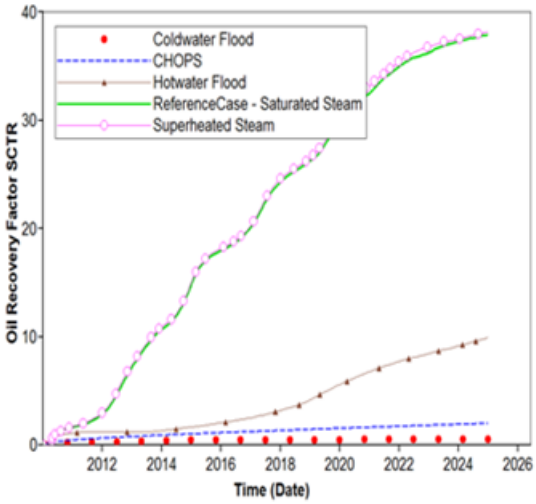


Fig. 7.20: Oil Recovery for Different Injection Streams

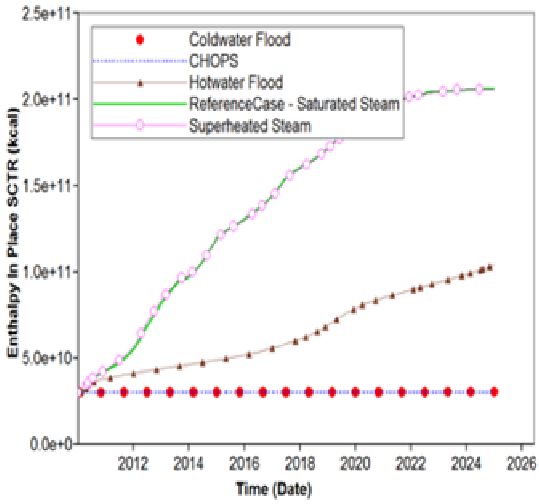


Fig. 7.21: Enthalpy In-place for Different Injection Streams

Injection Temperature: Given the fracture gradient of 21.1 kPa/m and 500 m datum, the maximum allowable injection BHP is 10.5 MPa. For a saturated steam process to satisfy this constraint, the downhole steam temperature must not exceed 315 ^{o}C. As a result, we limit the sandface injection temperature to 315 ^{o}C.

For an objective comparison of using different steam temperatures, rather than use a fixed maximum injection BHP of 5 MPa for all cases, the injection BHP constraint is set to the saturation pressure corresponding to the respective steam temperature. As a consequence, for injection temperatures of 200, 225, 250, 275, 300 and 315 ^{o}C, the injectors are set to maximum BHP of 1.6, 2.6, 4.0, 6.0, 8.6 and 10.5 MPa, respectively. By enforcing this conditionality of fully saturated steam, the difficulty of achieving significant injectivity for pressures below initial reservoir pressure

(5 MPa) becomes apparent. Intuitively, runs with BHP lower than 5 MPa should have been screened out due to poor injectivity, but we leave them for the sake of discussion.

For the same injection rate, **Fig. 7.22** indicates that oil rate and production increase with injection temperature. Although this inference can be explained by the increase in injection enthalpy with temperature, in the context of the current model, this explanation is not conclusive. Another key factor is temperature effect on relative permeability in the current model set-up. From the way the model is configured, high local temperature activates the correspondingly high relative permeability model, which is more favourable to oil recovery than the low-temperature model. Due to differences in instantaneous temperature distributions, at any instant, maps of active relative-permeability profiles differ between runs.

Fig. 7.23, showing the variation of average formation pressure for the five cases, stresses the injectivity problem associated with the 225 and 250 ^{o}C, both of which have saturation (injection) pressures below the initial reservoir pressure. In fact, in the two cases, the reservoir is continuously depressurised. Due to poor injectivity, we attribute predicted oil recovery to conduction-heating, a position reinforced by the end-of-simulation steam-chamber geometries (for example, compare 225 and 275 ^{o}C runs in **Fig. 7.24**), as well as the plots of CSOR, enthalpy in-place and enthalpy injected (**Figs. 7.25 - 7.27)**. Because of its very low CSOR but competitive oil recovery and enthalpy input, 275 ^{o}C is taken as the optimum temperature. However, in the following analysis, we present a different argument to reinforce the choice of 275 ^{o}C.

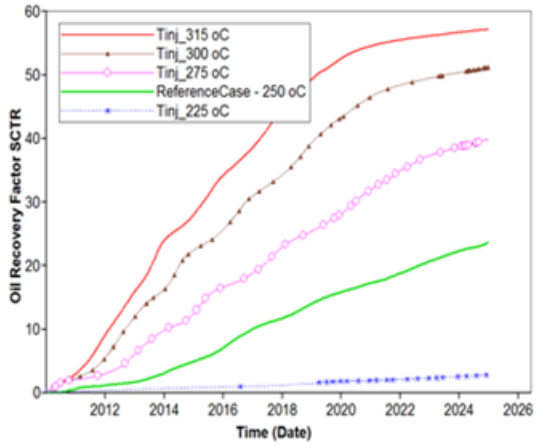


Fig. 7.22: Effect of Injection-Temperature on Oil Recovery

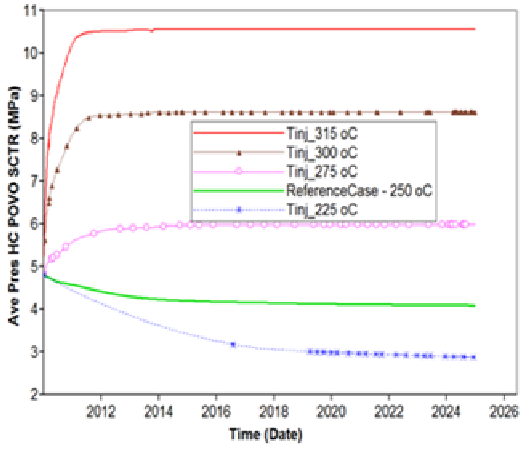
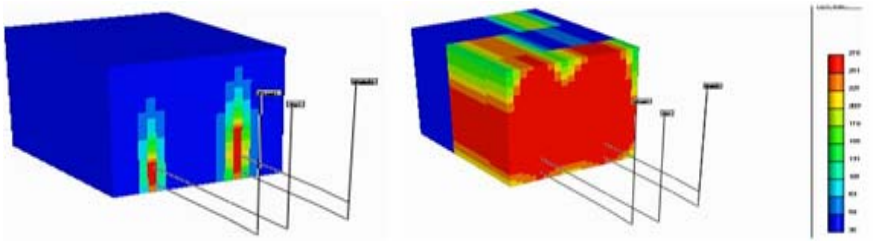


Fig. 7.23: Average Reservoir-Pressure for Different Injection Temperatures



(a) 225 °C (b) 275 °C

Fig. 7.24: Steam-Chamber Geometry after 15 Years for 225 and 275 °C Runs

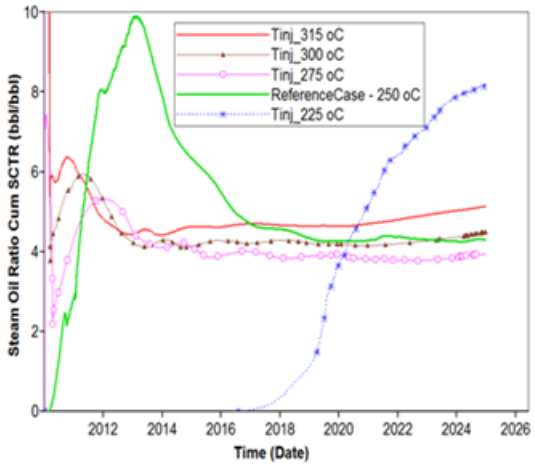


Fig. 7.25: Effect of Injection-Temperature on CSOR

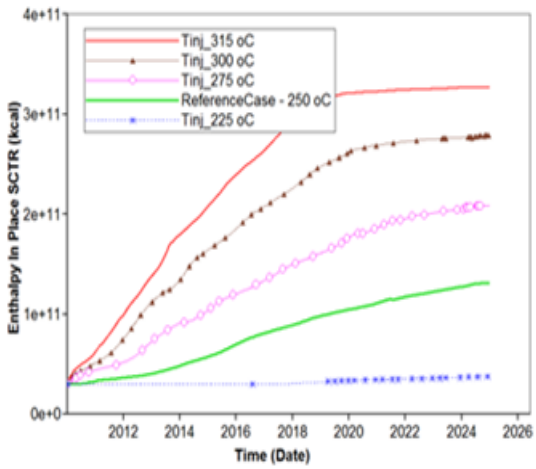


Fig. 7.26: Effect of Injection-Temp on Enthalpy In-place

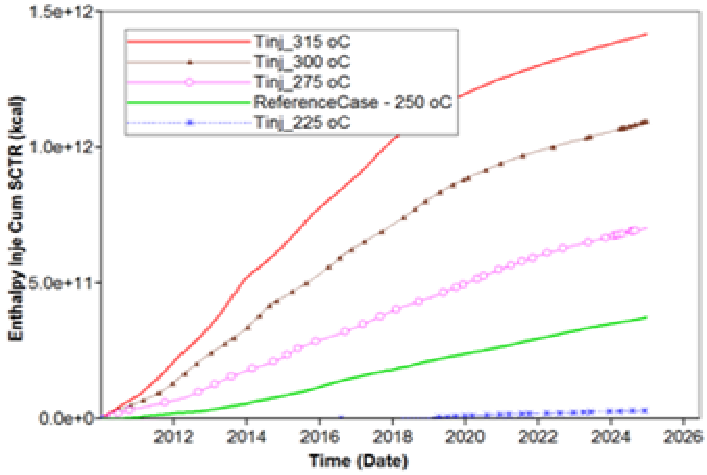


Fig. 7.27: Effect of Injection-Temperature on Enthalpy Injected

In the characterised viscosity-temperature relationship depicted in **Fig. 7.28**, it can be inferred that above 275 °C (as a guide, see the dashed tangent passing through 300 and 350 °C), the gradient becomes less steep. Hence, from the viewpoint of temperature-induced oil mobilisation, downhole temperature of 275 °C appears optimal, at least for the base-case oil PVT model. This implies that for a steam-alone process operating at this temperature, the lower limits of the oil phase viscosity are 0.9, 1.8 and 3.1 cP in the low, base and high-viscosity models, respectively.

However, lower viscosity is attainable in an alternating injection process if we can achieve reasonable dissolution of the CO_2 (or flue) in the oil phase at the same temperature. This is an interesting motivation for the alternating injection process.

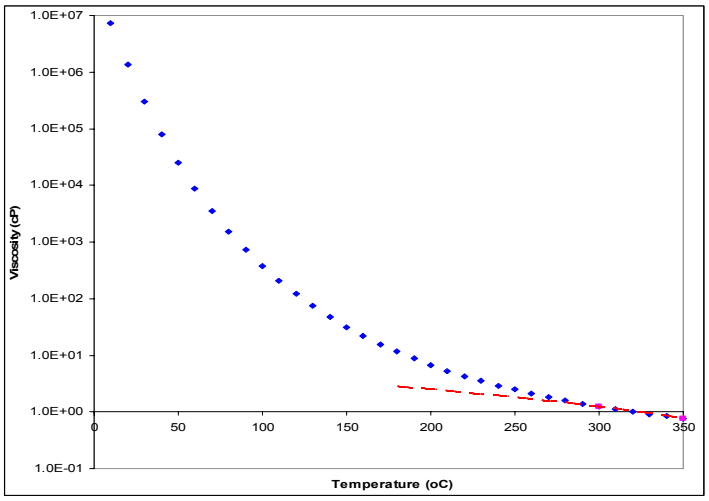


Fig. 7.28: Viscosity-Temperature Characteristics of the Bitumen (Base-case)

Injection BHP: Given the initial formation pressure of 5 MPa at the deepest layer, injection BHP's of 4, 5, 6, 7, 8, and 10 MPa are evaluated. The effects of injection BHP on oil production, CSOR and available enthalpy are presented in **Figs. 7.29**, **7.30**, and **7.31**, respectively.

On the basis of thermal efficiency and accelerated recovery, a downhole pressure of 6 MPa is appealing. Although it may be argued that 5 MPa is more attractive than 6 MPa, the realisation that steam at 250 ^{o}C and 5 MPa is not saturated, contradicts our earlier analysis which supports having saturated steam downhole. Coincidentally, 6 MPa is the saturation pressure of steam at 275 ^{o}C. In addition to thermal efficiency and oil recovery considerations, the viscosity curve favours operating at 275 ^{o}C. Hence, we select the injection of saturated steam at 275 ^{o}C and maximum downhole pressure of 6 MPa. Although not included in our models, relatively high injection pressure would induce geomechanical enhancements by increasing the porosity (dilation) and permeability, hence improving oil mobility (Collins, 2007b; Ito and Ipek, 2005; Ito, 1984).

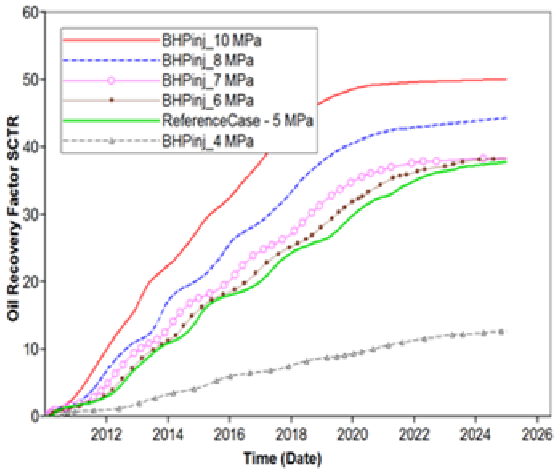


Fig. 7.29: Effect of Injection-BHP on Oil Recovery

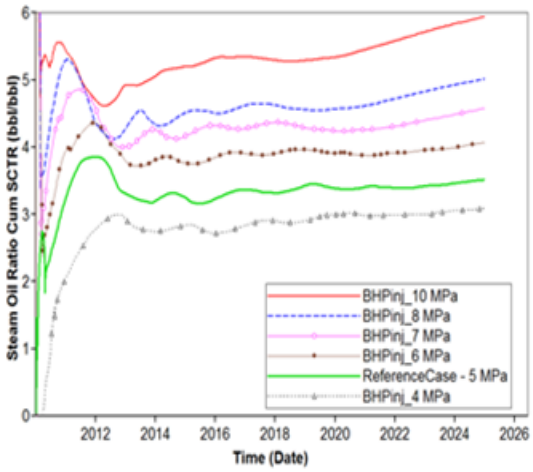


Fig. 7.30: Effect of Injection-BHP on CSOR

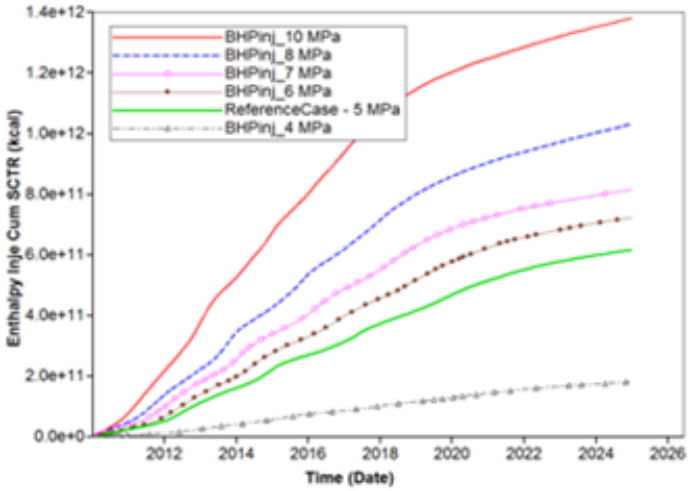


Fig. 7.31: Effect of Injection-BHP on Enthalpy Injected

Field experiences suggest that fluctuations and other nonlinearities would make it difficult to maintain an optimum point over a long time. Incidentally, a critical evaluation of the tangent in **Fig. 7.28** would indicate that competitive performances would still be realised providing we operate within the window $275 \pm 15\ ^{o}C$.

On how the simulator treats injection temperature and injector maximum BHP for saturated steam, a salient point is worth mentioning. In essence, the simulator overrides the injection temperature, replacing it with the saturation temperature corresponding to the specified injection BHP. Accordingly, for our reference case of 250 ^{o}C steam reaching the sandface at 5 MPa, the simulator effectively uses 265 ^{o}C, relating to 5 MPa. As this still falls within the optimum window just discussed, inferences (optimisation) drawn from this reference should still be valid for the optimum temperature, 275 ^{o}C.

Finally, to take advantage of accelerated production obtainable from high-pressure injection, a cascaded pressure approach is worth considering. In this approach, project start-up could be

implemented with relatively high-pressure injection (say 8 MPa), which should then be *ramped* (rather than *stepped*) down after 2-3 years to 6 MPa. After another 8-10 years, thermal efficiency considerations suggest that it is reasonable to wind-down at a lower pressure, say 4 MPa. In particular, this profiling of injection pressures is consistent with the simulation-based strategy proposed by other workers (Gates and Chakrabarty, 2006; Ferguson and Butler, 1988) for the reduction of CSOR and thermal losses to adjacent strata and, where it exists, top gas-zone (Gates *et al.*, 2007). Still at maturity, scope exists for other optimisations, including gradual reduction of heat injection rate to minimise fuel costs, emissions and water-related issues while enhancing project economic life (Messner, 1990). However, in the current study, given our limited knowledge of the subsurface uncertainties of the deposit, we are of the opinion that it would be pragmatic to keep the optimisation of the operating parameters simple. Hence, we do not explore the idea of pressure and enthalpy profiling.

Injection Rate Per Well: For the current homogeneous model, the injectors are operated on the same rates, hence injection rate per well. **Figs. 7.32** and **7.33** present the results for per-well steam rates of 500, 800, 1000, 2000, 5000, and 8000 stb/d, equivalent to injecting the equivalence of STOIIP over the period of 15, 10, 8, 4, 2, and 1 year, respectively.

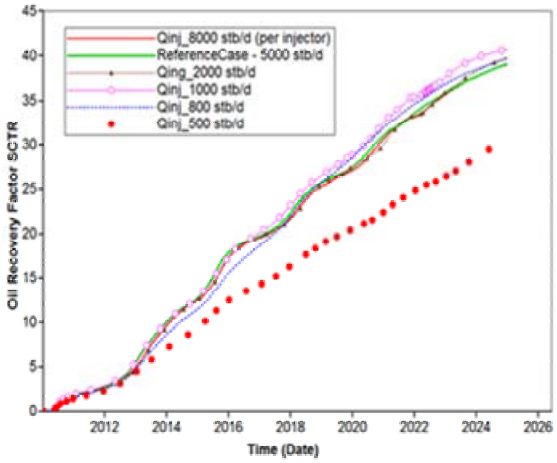


Fig. 7.32: Effect of Injection-Rate Per Well on Oil Recovery

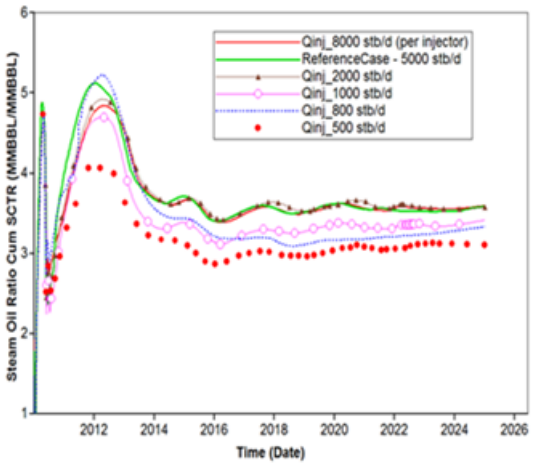


Fig. 7.33: Effect of Injection-Rate Per Well on CSOR

From an energy viewpoint, the 500 stb/d run is the most efficient, owing to low wellbore frictional losses. However, this relatively low rate has the least injection enthalpy, undermining the rates of reservoir heating and oil mobilisation.

Above 1000 stb/d per well, oil recovery and thermal efficiency are jeopardised, partly because of increasing frictional losses and lower injectivity, attributed to limited difference between injection and reservoir pressures. As shown in **Fig. 7.34**, due to pressure-limited injectivity, the desirable injection rate is only achievable in the case of 500 stb/d (though after about three years from start-up), implying that, for the injection pressure studied, net cumulative injection does not change

significantly above 1000 stb/d. As a result, we select 1000 stb/d as the optimum steam rate per injector i.e. total daily rate of 2000 stb.

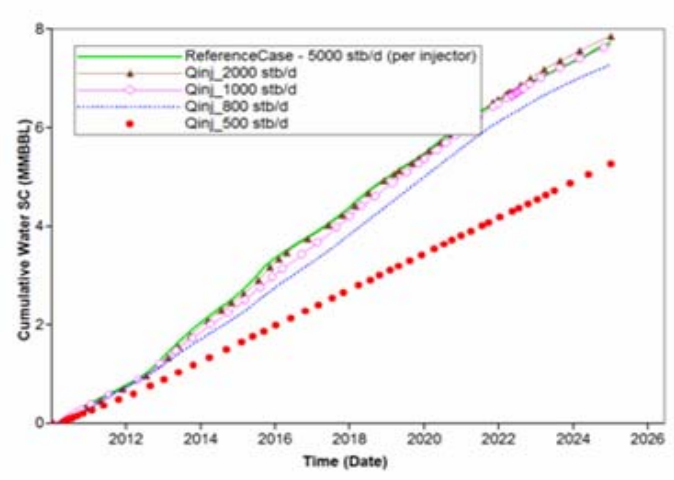


Fig. 7.34: Effect of Injection-Rate Per Well on Cumulative Injection

In line with the observation by other workers (Barillas *et al.*, 2006), injection rate is one of the most challenging variables to optimise conclusively. Being a VDF, we recommend that its optimisation should be done continuously, which should be driven by prevailing performance data. Indeed, this is one area that smart-well technology would likely be competitive (Alhuthali *et al.*, 2010; Gotawala and Gates, 2009).

Subcool Temperature: The simulation results of some steam-trap temperatures are shown in **Fig. 7.35**. Generally, recovery improves as the subcooling decreases but below the steam-trap of 15 ^{o}C, incremental recovery is less noticeable. This inference is attributed to increasing steam breakthrough via the lower-pressured producer, resulting in reduced contact time between fresh steam and the cold formation. However, when the subcooling becomes too low, near-well clogging causes unwarranted pressure build-up that undermines injectivity and productivity.

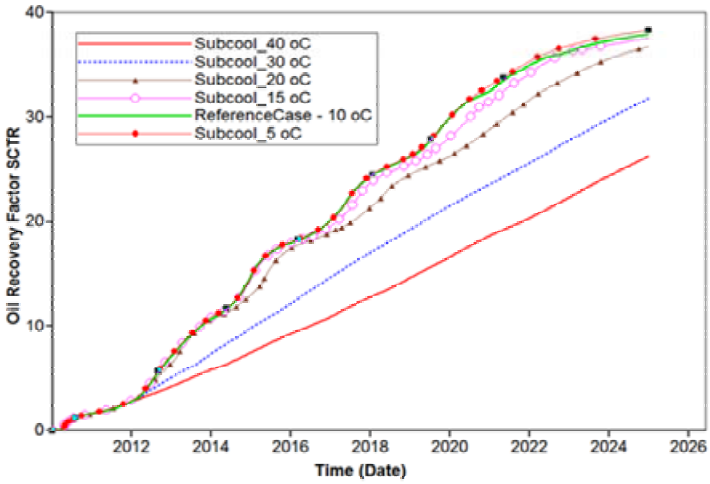


Fig. 7.35: Effect of Subcool-Temperature on Oil Recovery

With optimum injection range of 275±15 ^{o}C (6.0±1.4 MPa) and steam-trap of 15 ^{o}C, mean temperature of the production stream cannot exceed 260 ^{o}C (4.7 MPa). By operating at these optimum conditions, producer drawdown is limited to 1.3 MPa (190 psi). As an additional benefit, this relatively low drawdown would help mitigate potential ingress of water from the basal aquifer, if it turns out to be larger in volume and dynamically more active than currently suggested by the geologic data and assumptions used in our model. From the standpoint of CO_2 storage, low drawdown would serve as a choke, delaying and curtailing CO_2 breakthrough.

Steam Quality: The sensitivities of oil production and CSOR to steam quality are illustrated in **Fig. 7.36**. Within the range 50 to 100 % investigated, there is no marked impact on oil recovery but the effect on CSOR is noteworthy.

Although the injected heat per unit mass of steam increases with steam quality, this does not translate into significant difference in the average reservoir temperature, hence oil mobilisation, partly because steam flow in the reservoir is less dependent on its quality (within the range examined). As a result, at every instant, latent heat is released at roughly the same position in all the runs. Although the latent heat released varies between runs, most of these are removed through the out-flowing stream, implying that on a net basis, all the cases have approximately the same quantity of enthalpy in the reservoir at all times (**Fig. 7.37**). However, because of density segregation and greater availability of condensate, condensate (sensible heat) production increases with reducing steam quality, accounting for the inverse relationship between CSOR and steam quality. Furthermore, because of wellbore pressure losses, most of the injected steam condenses before entering the reservoir, downplaying the relative effects of differences in latent heat among the runs.

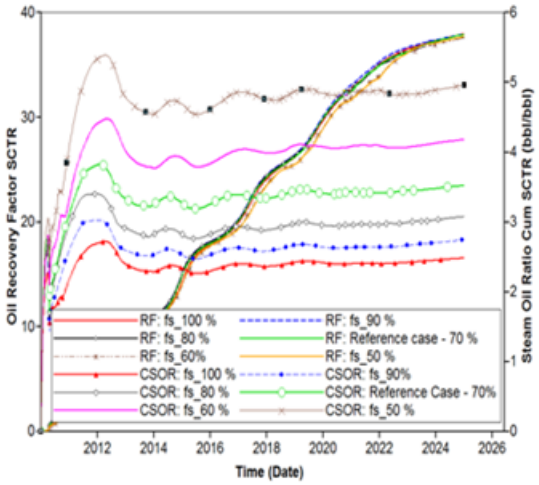


Fig. 7.36: Effect of Steam-Quality on Oil Recovery and CSOR

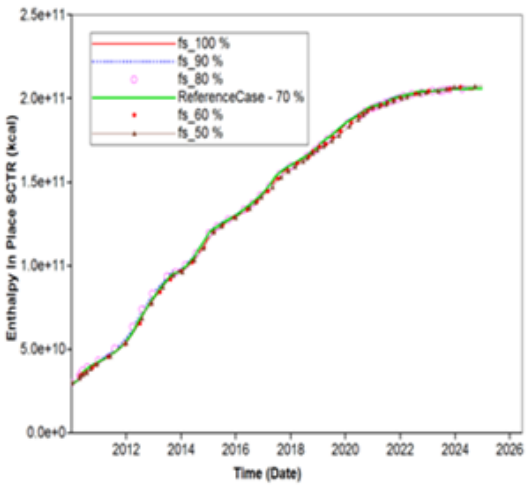


Fig. 7.37: Variation of Enthalpy In-place for the Runs

On account of the CSOR, the relative difficulty of maintaining high steam quality at downhole conditions and the incremental costs of higher quality steam, we select 80 % as the optimum. However, the best technical performance would be obtained with increasing steam quality but this would need to be balanced against the incremental costs. From a review of some field operations (Smith *et al.*, 1973; de Haan and Schenk, 1969), it can be deduced that, with good operational practices, downhole steam quality of 80 % is reasonably achievable. This position is further supported by the rigorous simulations conducted by Valbuena *et al.* (2009), involving coupled surface-subsurface network models. In their study, despite that steam travelled through more than 3 km length of pipe-network, including directional changes at the wellheads, the quality at the sandface was still within 80 %.

7.4 Summary of Optimum Development Concepts

On the assumption that the optimised parameters are not antagonistic of one another, we define the optimum development concept as that based on a combination of the optimum states of all the FDF's and VDF's. For the steam-alone process, a summary of the optimum states and values of the design factors is presented in **Table 7.2**. Although the perforation density (fraction of the horizontal wellbore that is perforated) and allowable water cut are also examined, space constraints preclude their discussion.

Table 7.2: Some Optimum States for the Steam-alone Process

Fixed Design Factors		*Variable Design Factors*	
Well type	horizontal	Heating fluid	saturated steam
Wellbore length (m)	500	Injection temperature (^oC)	275
Wellbore radius (cm)	12	Maximum injection BHP (kPa)	6000
Wellpair count	2	Subcool temperature (^oC)	15
Injector-injector spacing (m)	100	Steam rate per injector, CWE (stb/d/well)	1000
Producer-producer spacing (m)	90	Steam quality (%)	80
Vertical well spacing (m)	5	Maximum water cut (%)	unconstrained
Perforation density	full wellbore	Maximum gas production	unconstrained
Producer placement above OWC (m)	2		

The optimum states notwithstanding, we acknowledge the proverbial “chicken-and-egg” problem (Kabir *et al.*, 2002), which underscores the difficulty of independent optimisation of subsystems that are strongly interrelated. In this context, the concern centers on the robustness of an optimised reservoir development in the presence of huge subsurface uncertainties (Lawal, 2009). In other words, as long as the reservoir behaviour remains poorly understood, and may never be fully understood even at abandonment, any development optimisation is fundamentally at risk.

Unlike the FDF’s, the VDF’s can always be optimised thereby offering scope for the alleviation of project risks. As performance data become available, we advocate for dynamic optimisation, involving continuous review and refinement of the VDF’s. Apparently, for robust realisation of such optimisation scheme, it suffices to state that a “smart” operating philosophy (Alhuthali *et al.*, 2010; Gotawala and Gates, 2009) is worth considering. By deploying “smart” technology, there is a greater chance of achieving better control of some of the VDF’s, such as injection/production rate and pressure. Because of the continuous nature of the VDF’s and their relative flexibility, we foresee a scenario where the values of these parameters may vary significantly between wells and time intervals.

7.5 Chapter Summary

We have assessed the sensitivity of the steam-alone process to some geometric and operating parameters, referred to as fixed and variable design factors, respectively. The potentials of other recovery processes such as hot water, cold water and CHOPS have also been studied. For the reservoir and oil system studied, these alternative recovery methods have much less potential compared to the steam-injection technique. From the simulation studies and the detailed analysis, the optimum combination of geometric and operating parameters has been established for the steam-alone process. In essence, this optimum steam-alone development provides an indication of

the amounts of CO_2 and flue-gas emissions that need to be mitigated by the SAC and SAF processes.

It is also found that the current well arrangement, in which the injector and producer in a conventional SAGD wellpair are placed exactly in the same vertical plane, may not be optimum. Rather, the wells in a pair should be positioned such that they are displaced equally in the vertical and horizontal planes. We present a theoretical analysis to justify the new configuration. Although the proposed well arrangement may result in oil production being slightly delayed, simulation results indicate that it however yields higher oil recovery and lower steam consumption over time.

Given the set of optimum geometric and operating parameters for the steam-alone as the reference case, we continue our feasibility assessment in the next chapter, in which we investigate the optimum combination of the operating variables that are peculiar to the SAC and SAF processes.

Chapter 8

Alternating Injection of Steam and CO_2 for Heavy-Oil Recovery

The simulations performed in the last two chapters indicate that the steam-alone process is energy intensive, with steam requirement being on the order of four barrels of cold-water equivalent for each oil barrel. Moreover, the sourcing of feedwater for steam generation and the treatment of produced water introduce additional challenges that impact negatively on the project (Veil *et al.*, 2009; Jimenez, 2008; O'Rourke *et al.*, 1997). In cases where fossil fuel is burnt for steam generation, the management of resulting CO_2 emissions constitutes another difficulty (Charpentier *et al.*, 2009; Law, 2004).

As an improvement over the steam-alone process, we propose two techniques: (i) alternating injection of steam and CO_2, or simply steam-alternating-CO_2 (SAC); and (ii) alternating injection of steam and flue-gas i.e. steam-alternating-flue (SAF). In principle, these improvements take advantage of the dependency of heavy-oil viscosity on temperature and composition to alleviate the outlined drawbacks. While SAC employs a dedicated CO_2-capture train to obtain the required high-purity CO_2, SAF uses the "untreated" flue gas. Relative to SAC, the SAF method is meant to eliminate the CO_2-capture step which, at present, is one of the biggest challenges of the carbon-capture and storage technology (Kumar *et al.*, 2010; Aimard *et al.*, 2007).

In this chapter, we estimate the flowrates of CO_2 and flue-gas that could be obtained from the steam-alone, SAC and SAF processes. All the analyses presented herein are based on a closed-system operating philosophy. That is, the volumes of CO_2 and flue-gas are sourced from the "waste" stream of materials and heat emanating from the combustion of fossil fuels for steam generation. Hence, the starting point for the subsequent analyses refers to the "optimised" conditions of the steam-alone process, as presented in Chapter 7. Additional sources of CO_2 and flue-gas are the emissions from the capture, compression and transportation of CO_2 and flue-gas in the SAC and SAF processes.

Given the CO_2 load, we investigate the optimum operating conditions for the alternating-injection processes, using the SAC process as a reference case. However, in order to ascertain the best strategy for injecting steam and CO_2, we begin by evaluating the relative performances of the co-injection and alternating-injection schemes. Finally, the factors that underline the differences between the dynamics of the steam-alone and alternating-injection processes are discussed.

8.1 Co-injection versus Alternating-Injection of Steam and CO_2

As an alternative to the proposed alternating-injection processes, we examine the prospects of simultaneous injection of steam and CO_2 as a mixture. The latter, which is the co-injection process, is a common feature of relatively well established variants of steam-based recovery techniques

such as solvent-aided steaming and steam-gas push methods (Ayodele *et al.*, 2009; Nasr *et al.*, 2003; Butler, 2004; Nasr *et al.*, 1987).

For a total injection rate of 1000 b/d (159 m^3/d) CWE steam and 1 MMscfd (28,317 m^3/d) CO_2, we compare the co- and alternating-injection processes. Note that, as a total, these rates give CO_2 volume fraction of 99.45%. The relative rates for the two schemes are indicated in **Table 8.1**, with injection data in the co-injection case presented on a per-well basis. In principle, apart from the implementation of a similar set of constraints, the simulations of both processes are based on the same total injection of steam and CO_2.

Table 8.1: Injection Streams for Co- and Alternating-Injection of Steam and CO_2

Co-injection	
Total fluid injection rate per well (m^3/d/well)	14,238
CO_2 volumetric fraction (%)	99.45
Steam (CWE) volumetric fraction (%)	0.55
Alternating Injection	
CO_2 injector rate (sm^3/d)	28,317
Steam (CWE) injector rate (m^3/d)	159

As shown in **Fig. 8.1**, the forecasts of oil recovery and CSOR indicate that the alternating process is more attractive than its co-injection counterpart. As would be rationalised later, the immediate explanation for this is that in the current model, the effect of temperature on oil-viscosity reduction is greater than what is obtainable with dilution effect. Despite that the same amount of steam and CO_2 is being injected in both cases, the mixing of CO_2 and steam prior to reaching the reservoir depresses the steam saturation temperature. As a result of depressed saturation temperature, steam condensation is sub-optimal, reducing the total heat released to the formation.

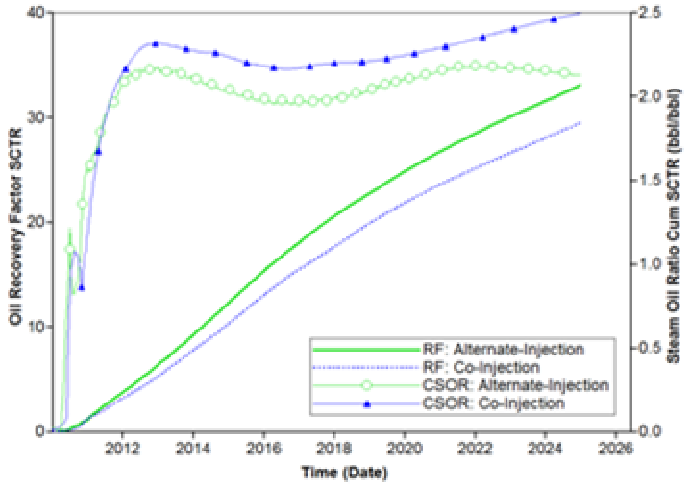


Fig. 8.1: Performance Plots for Co- and Alternating-Injection of Steam and CO_2

8.2 Basic Process Engineering and CO_2 Emissions Inventory

An underlying assumption in the analysis presented in this section and afterwards is that project implementation is based on a self-sustaining operating philosophy i.e. there is no net import of CO_2. **Fig. 8.2** is a simple schematic of the steaming process, which is the "business-as-usual" development concept. Here, the flue gas (including CO_2) associated with the combustion of fossil fuel for steam generation is continuously released into the atmosphere.

As a potential strategy for overcoming some of the challenges currently associated with CO_2 capture (Kumar *et al.*, 2010; Aimard *et al.*, 2007), for the proposed process of alternating injection of steam and CO_2, we conceptualise two options of injecting CO_2 during the CO_2 cycle. These options entail injecting CO_2 either as a pure stream or a mixture (flue gas).

In **Fig. 8.3**, schematic for the case of alternating steam and pure CO_2 process is illustrated. In this concept, CO_2 is captured from two main point sources. Apart from the CO_2 originating from the steam generators, additional emissions emanate from running compressors to raise the pressure of captured CO_2 stream to that required for subsequent transportation and injection.

An alternative to the pure-CO_2 injection process is shown in **Fig. 8.4**. A key difference with the scheme in **Fig. 8.3** is the elimination of the CO_2 capture train, implying that CO_2 is injected as a minor component (10 vol. %) in the flue gas stream. Apparently, for the same amount of CO_2, much higher gas volume is being compressed and injected in the flue gas case, requiring that the incremental compression costs would need to be evaluated against the costs of CO_2 capture that is being designed out. Furthermore, the relative impacts of higher (but low purity CO_2) gas injection rates on reservoir performance, vis-à-vis oil recovery, heat transport, dilution and pressure maintenance, would also need to be ascertained.

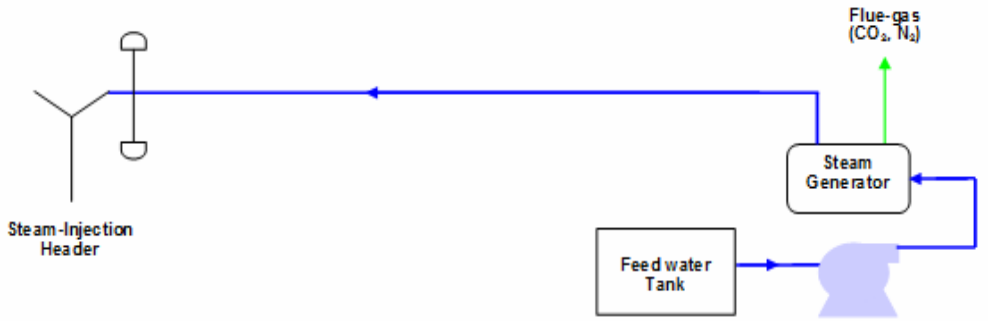


Fig. 8.2: Proposed Process Scheme for Steam-alone Process

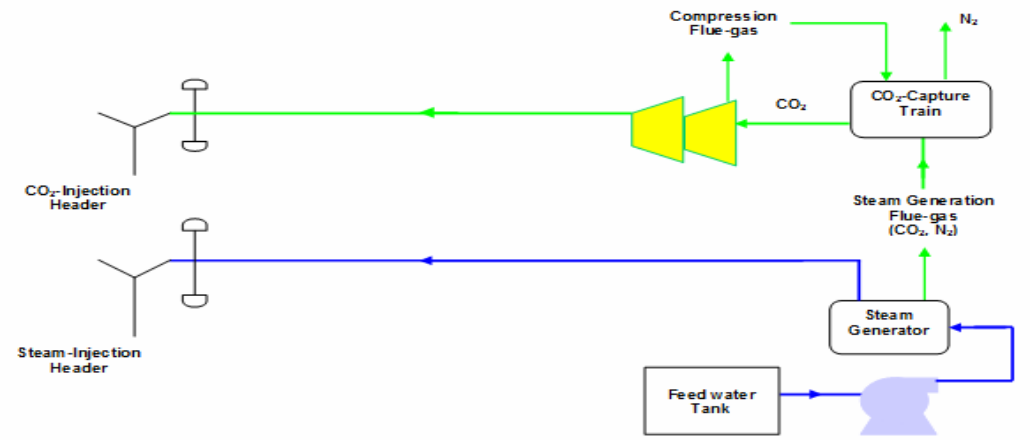


Fig. 8.3: Process Scheme for Alternating Steam and CO_2 (SAC) Injection Process

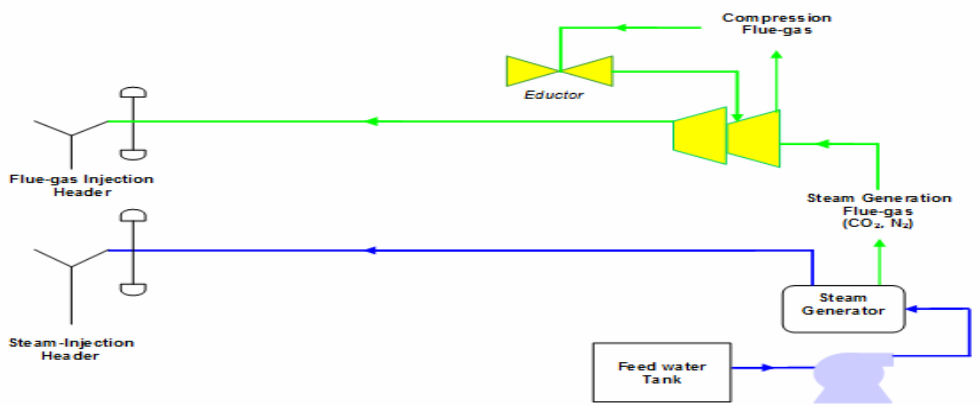


Fig. 8.4: Process Scheme for Alternating Steam and Flue-gas (SAF) Injection Process

8.3 Compressor Power Consumption

Theoretical analysis has shown that the isentropic process (adiabatic compression) is the least efficient compression process, setting the upper limits of compression work (Cengel and Boles, 2002). For a conservative estimate, we assume adiabatic compression in the current study.

Power required for steady-state adiabatic compression of a given gas of mass rate, $\dot{m}_g$ can be estimated from (Cengel and Boles, 2002):

$$\dot{E}_{comp} = \frac{\dot{m}_g \gamma R T_1}{\gamma - 1}\left[\left(\frac{P_2}{P_1}\right)^{(\gamma-1)/\gamma} - 1\right], \qquad (8.1)$$

where $\dot{E}_{comp}$ is compressor power output, $\dot{m}_g$ denotes gas mass flowrate, and γ is specific heat ratio. The quantities R, T_1, P_1, and P_2 represent gas constant, suction temperature, suction pressure, and discharge pressure, respectively.

For a given gas, γ depends primarily on temperature. However, for the gases of interest vis-à-vis CO_2 and N_2, this variable changes negligibly (< 6 %) over the expected operating interval 25-350 ^oC (Cengel and Boles, 2002). Accordingly, we assume average specific heat ratios of 1.24 and 1.39 for CO_2 and N_2, respectively. In this study, steam is not compressed, and the compressors are powered by the combustion of fossil fuel.

8.4 CO_2 Emissions due to Steam Generation and Compression Works

In this section, we estimate the rate at which CO_2 emissions would be released from the steam generators and compressors. In other words, these are the baseline emissions load to be mitigated by the proposed schemes. The following assumptions underlie the subsequent analyses.

- boiler thermal efficiency of 70 % (CIBO, 2003);
- boiler feed water temperature of 20-50 ^oC;
- compressor thermal efficiency of 70 % (Law, 2004);
- compression ratio of 100, taking boiler emissions from ambient pressure (0.1 MPa) to 10 MPa;
- taking air as the oxidant, regardless of the fossil burnt for the boiler and compressor, the flue-gas is a binary system of 10 vol.% CO_2 and 90 vol.% N_2 (Nogueira and Mamora, 2005; Chakravarti *et al.*, 2001; Srivastava *et al.*, 1999b); and
- for flue-gas compression, mixture molar mass and specific heat ratio are based on the volume-weighting of corresponding properties of CO_2 and N_2.

Noting that the optimum injection pressure is 6 MPa, the use of 10 MPa compressor output would overestimate the direct emissions. However, the excess accounts for transport-related emissions, as well as indirect emissions from running the CO_2-capture train, pumps, and other auxiliary equipment. In addition, the high pressure offers the flexibility of assessing prospective injection of CO_2 under supercritical conditions.

In the proposed process scheme, we have tacitly assumed post-combustion CO_2-capture process, whereby the combustion gas stream, formed by using air as oxidant for fuel combustion, is passed through a scrubbing system containing an amine-based CO_2 absorber (Aimard *et al.*, 2007). Despite our choice, we acknowledge other capture techniques vis-à-vis pre-combustion and oxyfuel combustion, as well as post-capture techniques not based on absorption technology (Aimard *et al.*, 2007). Although they yield more concentrated CO_2 streams (80-90 vol. % on a dry basis), compared to the post-combustion technique, the other options are largely immature and more energy-intensive, resulting in higher indirect emissions (ExxonMobil, 2010; British Petroleum, 2010; Aimard *et al.*, 2007; Haut and Thomas, 1989).

Details of the procedure used to estimate CO_2 emissions from the two point sources are presented in Appendix **J**. On the assumption that the steam generator(s) and compressor(s) operate independently, summation of estimated tranches of emissions from either sources gives the total daily CO_2 outlay.

Estimates of direct emissions from the generation of steam of different temperatures using 20-50 ^oC feedwater are plotted in **Fig. 8.5**. This shows that the intensity of the direct emissions depends more on the fuel, and less on the steam-temperature. Hence, in the context of the environment, there is no significant difference between high and low-temperature steaming, providing the same fossil is burnt. In subsequent discussions, we only consider heavy oil as fuel for running the boiler and compressors.

The distribution of emissions for the SAF scheme (**Fig. 8.4**) is presented in **Fig. 8.6**. In this case, because of the sharp increase in the compression load due to the relatively large volume of N_2, compression generally accounts for over 60% of the estimated total emissions.

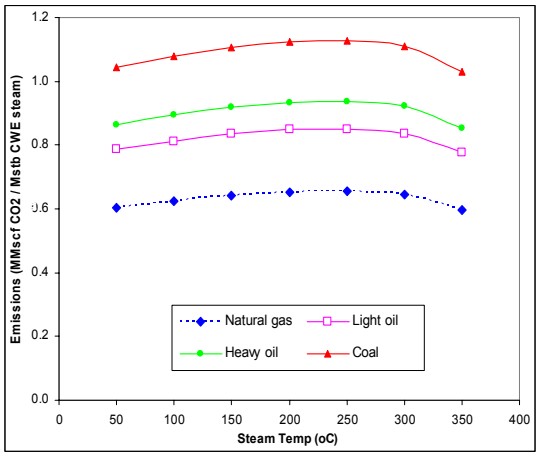


Fig. 8.5: Boiler-Emissions Intensity for Some Fossil Fuels

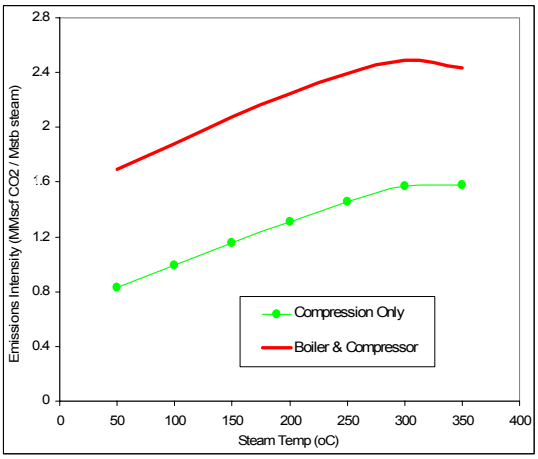


Fig. 8.6: Total CO_2 Intensity for the SAF Process

8.5 Optimisation of the Alternating-Injection Processes

In addition to the optimum states already established for the reference steam-alone process in Chapter 7, there are other operating parameters that are unique to the alternating injection processes. In this section, we investigate the "optimum" cycle time and gas-production rate for the latter process. In the ensuing discussion, we tacitly assume that both processes have similar optimum states of the FDF's and other VDF's. On the other hand, the injection rate of the CO_2 (and flue gas) is fixed at that corresponding to the optimum steam rate in line with the estimates presented in **Figs. 8.5** and **8.6**, using heavy-oil as the combustion fuel.

Cycle Time: This refers to the frequency of switching an injector between steam and CO_2 (or flue gas). For this variable, we investigate several options, ranging from monthly to annually. For simplicity, we maintain the same cycle time throughout each of the simulation runs.

Figs. 8.7 and **8.8** illustrate the impacts of cycle time on oil production and CSOR, respectively. Although neither recovery nor CSOR exhibits a clear trend with cycle time, it can be deduced that a 3-monthly switch of injectors between steam and CO_2 appears to be optimal.

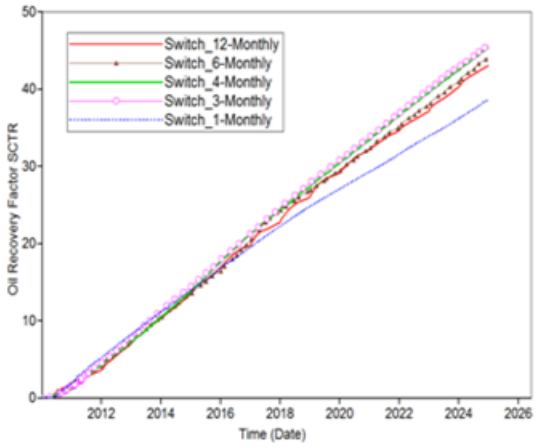


Fig. 8.7: Effect of Cycle Time on Oil Recovery for SAC



Fig. 8.8: Effect of Cycle Time on CSOR for SAC

Gas-Production Rate: From the *K*-value estimates (**Fig. 6.11)**, it is clear that gas solubility in the bitumen is very low, especially at high temperatures that characterise thermal processes. As a result, much of the injected CO_2 would remain in the gas phase downhole at high saturation. Given the high saturation, the relative permeability of CO_2 would also be high, promoting its reproduction along with oil and water.

As one of the objectives of the alternating-injection process is to provide an effective sink for process emissions, it follows that *net* CO_2 storage needs to be maximised. Therefore, in addition to the optimisation objectives outlined for the steam-alone case, the alternating-injection process seeks to optimise net CO_2 storage (as fraction of injection) with minimal negative impacts on oil recovery. Here, the CO_2 load is that associated directly with the steam generation and gas compression pertaining to upstream operations, leaving out emissions due to mid-stream treatments and upgrading of the produced oil. Generally, upgrading can increase the emissions due to *in-situ* exploitation by some 25% (Charpentier *et al.*, 2009).

Unlike the steaming process in which gas outflow is negligible, reproduced CO_2 (flue) renders the production stream too gassy in the case of alternating injection. Accordingly, the GOR, which refers to both *in-situ* CH_4 and injected CO_2, is unnecessarily exaggerated, making it difficult to achieve realistic controls during simulations. As a result, we apply gas production (mixture of CH_4 and injected gas) constraint, defined as a percentage of the total gas injection rate. In this study, we find it more convenient to implement a total gas rate constraint than the typical GOR constraint.

For selected constraints on gas curtailment, **Figs. 8.9 - 8.11** show the oil production, CO_2 injection and CO_2 reproduction, respectively. In general, oil recovery, CO_2 injection and re-production increase as the gas production constraint is relaxed. However, in the current model, the 80% constraint yields a higher amount of oil than the 100% case despite comparable cumulative injection and “leakage” of CO_2.

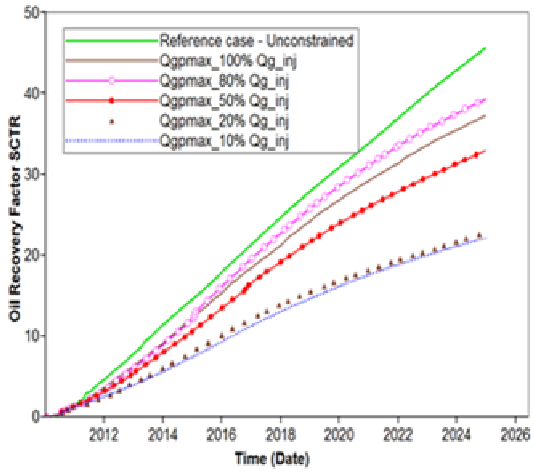


Fig. 8.9: Effect of Gas-Production on Oil Recovery (SAC)

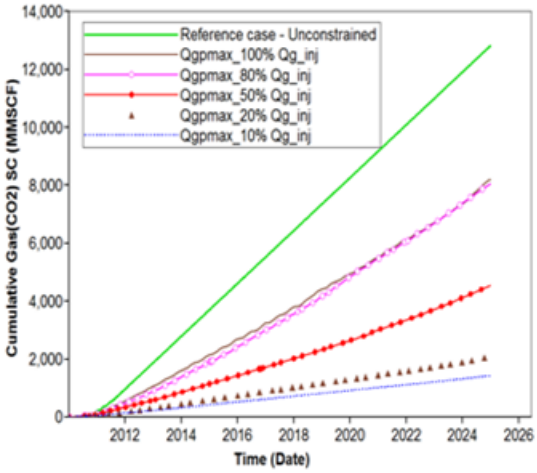


Fig. 8.10: Effect of Gas-Production on CO_2 Injection (SAC)

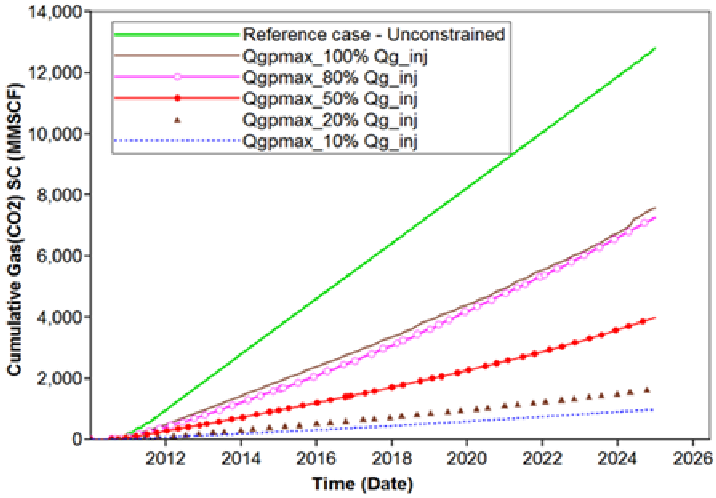


Fig. 8.11: Effect of Gas-Production Constraint on CO_2 Re-Production (SAC)

In order to obtain a more consistent comparison of the constraints, **Fig. 8.12** depicts instantaneous net CO_2 retention as a percentage of cumulative injection. As expected, net CO_2 retention increases with the stringency of production constraint. However, there is no marked difference between the 80% and 100% cases which, when oil recovery is considered, suggests that the former is a more attractive option.

From the results presented in **Fig. 8.12**, it is evident that irrespective of the gas production constraint imposed, the project would need to be a net polluter in order to recover reasonable and economic amount of oil. However, compared to the steam-alone process, a major advantage of the alternating injection processes is the improved environmental performance on a unit-oil basis. To make a decision on the optimum constraint, we conduct a simple economic screening.

We assume carbon credit of $ 30 /ton CO_2 stored, penalty of $ 50 /ton CO_2 flared as well as oil and gas (methane) prices of $ 50 /bbl and $ 5 /Mscf, respectively. We use the 15-year undiscounted net revenues for the various constraints. Although we found the “unconstrained” case

as the most economic, owing to environmental consideration, we limit gas-production rate to 80% in subsequent simulations.

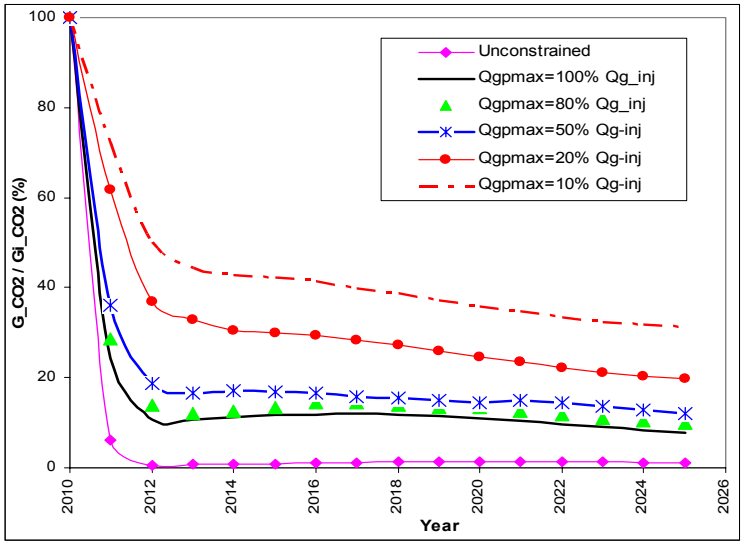


Fig. 8.12: Effect of Gas Constraint on Time Variation of Net CO_2-Retention (SAC)

At the "optimum" gas production constraint, which is 80% of total gas injection rate, a significant fraction of injected CO_2 is reproduced with oil and water (**Figs. 8.11** and **8.12**). However, for simplicity, we do not consider the prospects of recycling the produced CO_2. As a result, given a carbon-constrained scenario, we pay the penalty for emitting reproduced CO_2. Our decision not to embark on CO_2 recycling is partly influenced by the findings documented by Gaspar Ravagnani *et al.* (2009). In their work, despite assuming a somewhat optimistic CO_2 storage efficiency (fraction of pore volume used for storage) of 50% and a recycle ratio of 99%, there was only a 40% reduction in the net CO_2 emissions, compared to the no-recycle scenario. In essence, the reported 40% savings on the "do-nothing" total emissions may not justify the incremental costs due to the installation and operation of the recycling facilities. In an earlier study, Pamukcu and Gumrah (2008) also noted the economic unattractiveness of CO_2 recycling.

In conclusion, the optimum states of FDF and VDF for the alternating-injection processes are presented in **Table 8.2**. As earlier stated, where overlap exists, the parameters of the steam-alone process are retained, with the subtle assumption that they are also optimal for the alternating-injection techniques.

Table 8.2: Some Optimum Variables for the Alternating-Injection Processes

Fixed Design Factors		*Variable Design Factors*	
FDF's	as for steam-alone process (**Table 7.2**)	Other VDF's	as for steam-alone (**Table 7.2**)
		Maximum gas production rate (% of gas injection rate)	80
		CO_2 injection rate, (MMscf/d/well)	Depends on fuel burnt, and whether pure CO_2 or flue gas is injected
		Cycle time (month)	3

8.6 Final Injection and Production Schemes

In relation to the optimised steaming process (275 ^oC), a summary of the injection fluids and rates for the three process schemes under evaluation is presented in **Table 8.3**. Please note that the indicated rates assume that heavy oil is the fuel burnt to run the boilers and compressors. Hence, the tabulated rates are the optimum for implementing the steam-alone, SAC and SAF processes in the current sector model of the Nigerian accumulation. Again, in the alternating injection processes, we maintain our operating philosophy of a closed (self-sustaining) system in which there is no net import of CO_2 or N_2. In all the subsequent analyses, these relative rates are maintained while the FDF and VDF constraints in **Tables 7.2** and **8.3** are implemented.

Table 8.3: Injection Fluids and Rates for the Different Processes

Process	**Injectant / Injection Rate (per Well)**		
	Steam (stb/d)	**CO_2 (MMscfd)**	**N_2 (MMscfd)**
Steam	2000*	-	-
Alternating Injection (CO_2)	1000	1.0	-
Alternating Injection (Flue)	1000	2.5	22.5

8.7 Comparing Steam-alone and Alternating-Injection Processes

A comparison of corresponding simulation (using base-case reservoir model) results of the steam-alone (Chapter 7) and SAC processes (Chapter 8) would reveal that the former yields better oil recovery than the latter. One of the immediate explanations for this observation is that the alternating-injection process is consistently characterised by lower rates of injection and reservoir heating as well as ultimate reservoir temperature in relation to the steam-alone cases. In order to understand the physics underlying these results, we rationalise the observations along the following lines.

* 1000 stb/d per well.

- **Relative-Permeability Effect (Early Times):** in the current model set-up, steam attains mobility earlier because of the higher initial water saturation compared to the case of zero initial free-gas (CO_2) saturation. This effect is particularly more pronounced at early times.

- **Relative-Permeability Effect (Mid-Late Times):** this is related to the temperature-effect on relative permeability, especially during the mid-to-late times when the reservoir would have been sufficiently heated. Compared to the steam-alone, the SAC process has lower reservoir temperature at any instant. As a result, the simulator is unable to activate the more favourable higher-temperature relative-permeability functions.

- **Viscosity Effect:** at downhole conditions, viscosities of steam and CO_2 are 0.0185 and 0.0264 cP, respectively. A combination of higher viscosity and lower relative permeability, especially at early times, renders CO_2 less mobile than steam.

- **Enthalpy Effect:** for 70%-quality saturated steam at 275 ^oC, the specific enthalpy (referenced to 35 ^oC) is estimated to be 2.15 MJ/kg. With the injection rate of 160 tons/d, it implies that steam introduces a daily enthalpy of about 344 GJ into the formation. On the other hand, CO_2 has specific enthalpy (referenced to 35 ^oC) of 0.25 MJ/kg at 275 ^oC. At the rate 132 tons/d, the daily enthalpy supplied to the reservoir by hot CO_2 is approximately 33 GJ, which is less than 10 % of what is obtainable from steam.

- **Saturation-Depression Effect:** from a condensation viewpoint, the presence of CO_2, a non-condensable gas, is detrimental to steam. With CO_2, saturation temperature of steam at prevailing pressure is depressed, by an amount that depends on the relative steam-CO_2 mole fractions. This is the so-called partial pressure effect, partly used to rationalise the influence of the injection BHP in section **7.3**. With depressed saturation, effective steam temperature is reduced. This, in turn, reduces the effective quantity of total heat that is delivered, resulting in a steam chamber of relatively smaller size and poorer quality (Canbolat *et al.*, 2004; Butler; 2004, 1997). Because of this depression, the "new" steam saturation-temperature may be lower than the prevailing reservoir temperature. Considering that, with continuous injection, the reservoir is not likely to return to a lower temperature, the steam may not condense hence, the latent heat becomes stranded.

- **Volume Effect:** with maximum injection constraints of 1000 stb/d CWE and 2.5 MMscf/d for steam and CO_2, respectively, the equivalent mass rates are 160 tons/d and 132 tons/d, respectively. With downhole (275 ^oC, 6 MPa) densities of 30.5 and 59.4 kg/m^3 for steam and CO_2, the subsurface volumetric rates are 5246 and 2200 rm^3/d, respectively. Because the steam injector is effectively injecting higher volume, the rate of build-up of reservoir pressure is expected to be higher. With higher reservoir pressure, higher drawdown manifests at the producer, resulting in higher productivity. Similarly, for the same injectivity, because of higher injection volume in the case of steam, voidage replacement rate is more effective, leading to improved reservoir pressure maintenance.

- **Thermal-Insulation Effect:** owing to buoyancy, CO_2 and other non-condensable gases usually accumulate above the steam chamber (Ayodele *et al.*, 2009; Butler, 2004). Because of its lower thermal conductivity than steam (or water), the accumulated CO_2 effectively reduces the thermal diffusivity of the region ahead of the chamber, hampering the rate of heat propagation to the colder oil zone. As temperature effect dominates dilution effect in reducing the oil viscosity in the current model, the lower heat transport, despite the presence of a diluent, jeopardises oil recovery in the alternating process.

As a result of lower mobility and total enthalpy, CO_2-based convective heat transport is significantly less effective compared to the equivalent amounts of steam. To underscore our arguments, we examine steam-alone, alternating steam and CO_2, as well as CO_2–alone processes. Consequences of CO_2 as a poorer heat-carrier are evident in **Figs. 8.13 - 8.15** showing cumulative enthalpy injected, average reservoir temperature and recovery factor, respectively. An important, but less obvious, benefit of having a higher average temperature is the activation of the high-temperature relative permeability functions which, in the current model, are more favourable to oil production. This relative permeability effect complements the preceding arguments on the role of heat transport.

Meanwhile, it is worth pointing out that the foregoing analyses do not consider the effects of potential deasphalting by CO_2 and N_2. In the next chapter, the opposite effects of reduced bitumen viscosity and permeability impairment resulting from possible asphaltene precipitation and deposition within the porous media will be investigated.

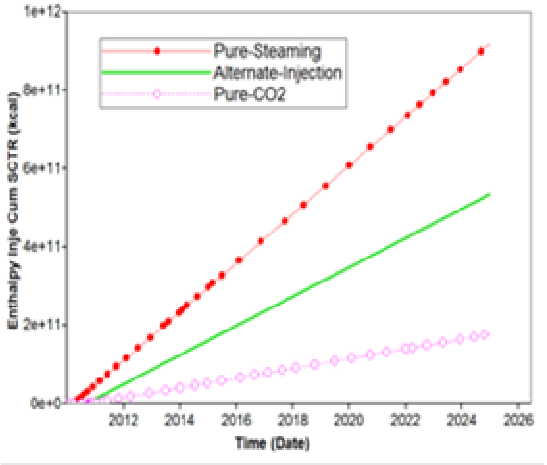


Fig. 8.13: Cumulative Injection-Enthalpy for Different Processes

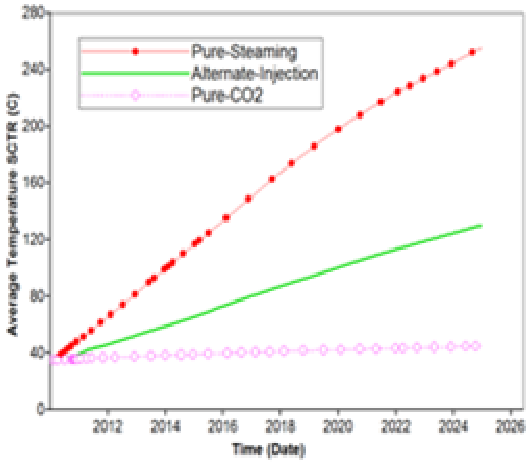


Fig. 8.14: Average Formation-Temperature for Different Processes

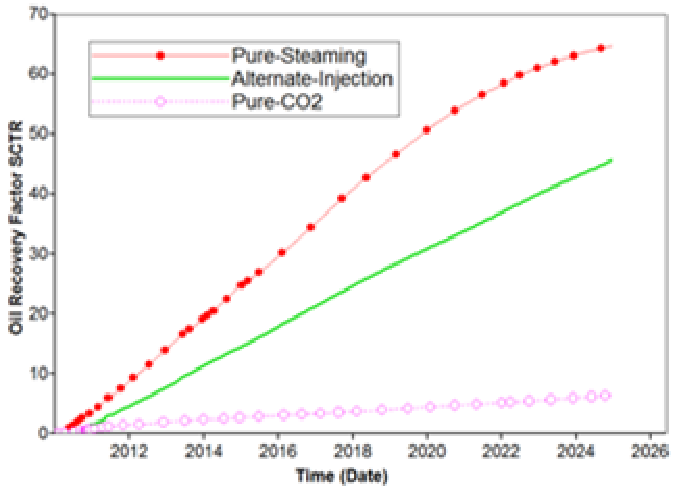


Fig. 8.15: Oil Recovery for Different Processes

8.8 Chapter Summary

Some process engineering aspects of the alternating-injection processes have been analysed, resulting in the estimation of the flowrates of CO_2 and flue-gas that are available to maintain these processes. For the same total injection rate and ratio of injectants, simulation results indicate that the alternating injection of steam and CO_2 yields higher oil recovery than its co-injection counterpart. At the same time, the former process is also thermally more efficient than the latter.

Building on the optimum operating conditions already established for the steam-alone process, the frequency of switching between steam and CO_2 (flue-gas) in the SAC and SAF processes is optimised. Additionally, in order to maximise the amount of CO_2 sequestered without jeopardising oil recovery, the limits of gas re-production have been established for the particular model under study.

Following the observation that the alternating-injection process recovers less amount of oil than the corresponding steam-alone process in this particular example, reasons for this competitive disadvantage have been discussed. Although oil recovery is lower in the alternating-injection process than its steam-alone counterpart, the steam consumption per unit oil production is higher in the latter process. In the next chapter, we investigate the effects of other technical factors such as reservoir heterogeneities and in-situ deasphalting on oil recovery, steam requirements, water production and CO_2 storage.

Chapter 9

Reservoir / Fluid-Property Heterogeneities and Deasphalting

All the analyses performed so far have been premised on homogeneous reservoirs that are saturated with crudes of uniform properties. However, virtually all formations are characterised by some spatial variation of rock and fluid characteristics, even over relatively short intervals (Wei and Gates, 2010; Chen *et al.*, 2008; Larter *et al.*, 2008; Yang and Butler, 1992; Adegoke *et al.*, 1980). Therefore, in order to have a good understanding of the physics of the processes under study, it is necessary to incorporate realistic features in the simulation models.

Employing numerical simulations, this chapter examines the robustness of the steam-alone and alternating-injection processes to the vertical variation of reservoir and fluid properties. Here, the reservoir properties considered are absolute and relative permeabilities as well as thermal conductivity. On the fluid properties, we evaluate viscosity. However, owing to the paucity of data on one hand, and simplicity on the other hand, we constrain the variation of properties to the vertical direction i.e. layering effect (Yang and Butler, 1992). This simplification looks reasonable considering that, over the same length scale, heterogeneity is often more pronounced vertically than horizontally (Larter *et al.*, 2008; Gibbons *et al.*, 1993). In addition, as buoyancy is a key drive mechanism in the processes being studied, it would be interesting to see how factors that relate to the hydraulics in the vertical direction influence the bulk flow.

In addition to the above-mentioned properties, for the alternating-injection processes, we investigate the sensitivities of reservoir dynamics to potential asphaltene drop-out as well as the dispersion of CO_2 and N_2. Finally, realistic simulation models are constructed as the ensemble of the insights gained from the earlier uncertainty studies, sensitivity analyses as well as the optimum operating conditions. From these final models, we generate representative set of forecasts for the different processes. On the basis of these forecasts, we conclude on the technical feasibility of the various processes for the exploitation of the Nigerian heavy-oil accumulation, as currently understood.

9.1 Permeability Heterogeneity (Layering)

From sedimentological characterisation of some outcrop tar-sand samples, geoscientists have identified two main facies and two sub-facies within the Afowo Formation, which is the primary host of the Nigerian heavy-oil accumulation (Akinmosin and Osinowo, 2008; Enu, 1985; Adegoke *et al.*, 1980). The facies are sandstone and shale, with the sandstone sub-divided into fine- and medium-grained sub-facies. While the medium-grained sub-facies dominate the upper sand unit *X*, the fine-grained is most represented in the sand unit *Y*, underlying the oil shale. Although particle size distribution reportedly varied irregularly, unit *Y* generally has a fining upward sequence while unit *X*,

though of coarser grains and greater uniformity, is interbedded with thin shales and siltstones. In constructing the permeability profiles, we treat these interbedded shales and siltstones as flow baffles rather than barriers.

In this study, we ignore heterogeneities associated with porosity and oil saturation which, in comparison to permeability, exhibit much less vertical variability (Adegoke *et al.*, 1980). An evaluation of the well/outcrop data from this belt (Akinmosin and Osinowo, 2008; Enu, 1985; Adegoke *et al.*, 1980) and the Surmont field in the analogous Athabasca region, would lend credence to the assumption of the relative insignificance of porosity and saturation heterogeneities (Wei and Gates, 2010). In all cases, areal variation of rock and fluid properties are neglected. Hence, the current analysis is limited to the effect of layered permeabilities.

In constructing the permeability profile (**Table 9.1**), we use the dataset of the Surmont field (Wei and Gates, 2010) as a guide while honouring available geologic description (gamma ray and texture) of the Nigerian deposit (Adegoke *et al.*, 1980). Although the estimates are arbitrary, the *average* permeability for each horizon coincides with the values used in the base-case homogenous model i.e. 2, 0.4 and 2 D for units *X*, oil shale and *Y*, respectively. Most importantly, the fining upward sequence (interpreted to be upwardly decreasing permeability) of unit *Y* and the baffle interbeds of the relatively uniform unit *X* are reasonably captured. Here, the permeability of well-defined shale streaks is 0.1 D (Wei and Gates, 2010).

It is worth pointing out that the *average* permeability refers to the geometric mean, which is generally regarded as the most representative of heterogeneous systems (Warren and Price, 1961). Although the viscosity distribution will be discussed shortly, the estimated oil-mobility profiles are shown in **Fig. 9.1**.

Table 9.1: Assumed Vertical Distributions of Some Properties

Horizon	Top (from caprock), m TVD*	Base (from caprock), m TVD	Absolute Horizontal Permeability, mD	Relative Permeability Model	Oil Composition (mole %); *(mass %)*		
					Methane	Maltene	Asphaltene
	0	1	2200	Base			
	1	2	3600	"			
	2	3	3800	"			
	3	4	100	Low			
	4	5	4100	Base	28.94	64.83	6.23
	5	6	4250	"			
X	6	7	4500	"			
	7	8	100	Low	*(1.11)*	*(83.54)*	*(15.35)*
	8	9	5500	Base			
	9	10	5300	"			
	10	11	5400	"			
	11	12	100	Low			
	12	13	4600	Base			
	13	14	4800	"			
	14	15	4000	"			
	15	16	490	Low			
	16	17	540	"			
	17	18	300	"	8.89	79.63	11.49
	18	19	450	"			
Oil Shale	19	20	500	"	*(0.26)*	*(78.19)*	*(21.55)*
	20	21	330	"			
	21	22	400	"			
	22	23	280	"			
	23	24	840	Low			
	24	25	920	"			
	25	26	1000	"			
	26	27	1200	"			
	27	28	1400	"	2.29	81.95	15.76
Y	28	29	1600	"			
	29	30	2000	"			
	30	31	2200	Base			
	31	32	2400	"	*(0.06)*	*(73.08)*	*(26.86)*
	32	33	2800	"			
	33	34	3000	"			
	34	35	3250	"			
	35	36	3600	"			
	36	37	3800	"			
	37	38	4000	"			

* True Vertical Depth.

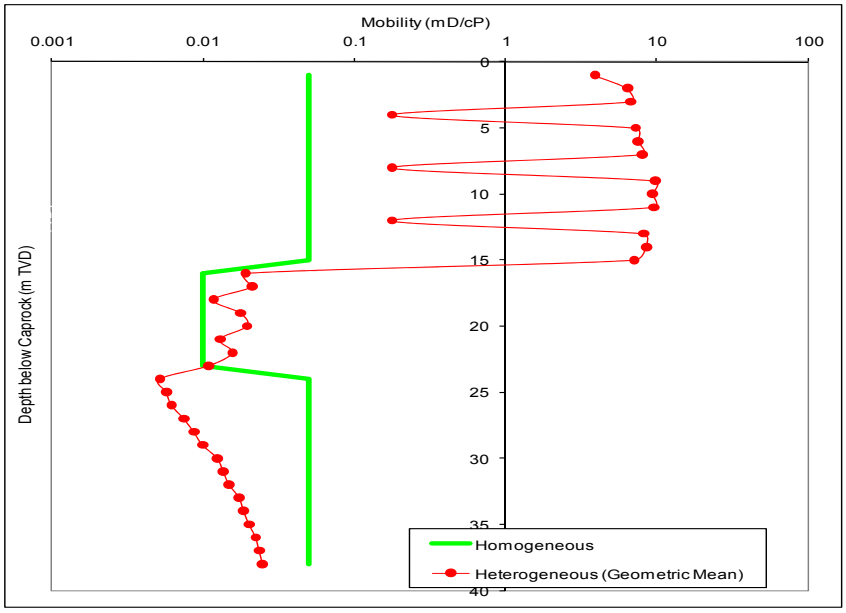


Fig. 9.1: Estimated Oil-Mobility Profiles at Initialisation (Base Case)

9.2 Viscosity Heterogeneity (Layering)

Owing to the paucity of data, we use compositional grading to infer possible viscosity heterogeneity. Here, an underlying assumption is that the fluids contained in the different horizons are not in thermodynamic equilibrium. The presence of flow baffles, microbial activities, the large time scales for molecular diffusion as well as the imbalance between the rates of oil charging and degradation, all point to the likelihood of compositional grading in the subject formation (Besong, 2009; Larter *et al.*, 2008).

Fig. 9.2 illustrates our concept of transposing composition of the homogenous model into compositional grading, where X_g, X_m and X_a are mole fractions of solution gas, maltene and asphaltene, respectively in unit X. Similarly, R, S and Y refer to the overall system, oil-shale, and unit Y, respectively. For simplicity, we retain homogeneity in each horizon. On the condition that the horizons have equal areal cross-section, the results of thickness-weighting of the horizon compositions are equivalent to those of volume-weighting. While details of the analysis are presented in Appendix **K**, the compositions in **Table 9.1** are estimated for the horizons.

Employing the Arrhenius mixing rule (**Eq. 6.4**), we estimate the initial (at 35 ^{o}C) distribution of oil-phase viscosity. The quotient of layer permeability and oil viscosity results in the mobility profiles depicted in **Fig. 9.1**. In this base-case model, the oil-mobility difference between some of the layers exceeds three orders of magnitude. Despite the drawbacks of Arrhenius-type mixing rules (de la Porte *et al.*, 2009; Mago *et al.*, 2005), the presence of maltene as intermediate component between the light-end methane and heavy-end asphaltene justifies its applicability in this case (Lawal, 2011b).

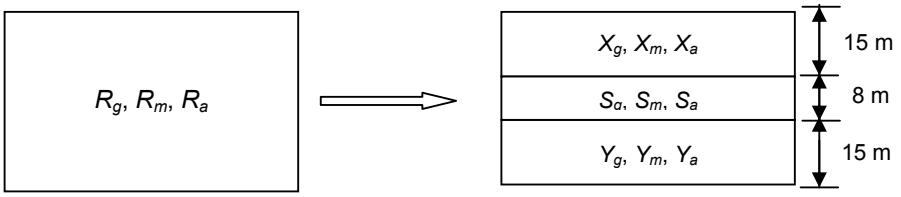


Fig. 9.2: Schematic of Oil-Phase Compositions in the Homogenous and Heterogeneous Models

9.3 Relative-Permeability Heterogeneity (Layering)

To describe possible relative permeability heterogeneity in the vertical direction, we employ facies-based relative permeability mapping. It is assumed that the relative permeability correlates positively with the hydraulic (textural) quality of the facies. Accordingly, in unit *X*, with the exception of the shale streaks (baffles) that are assigned the low-case relative permeability model, other layers have the base-case relative permeability model. For unit *Y*, the upper (top 50 %) and lower (bottom 50 %) sections are described by low- and base-case relative permeability functions, respectively. However, the entire oil shale unit is represented with the low-case relative permeability curves and, in all facies; the base-case temperature-dependency of relative permeability applies.

9.4 Rock-Thermal Conductivity Heterogeneity (Layering)

Following the approach undertaken for relative permeability, vertical variability of rock thermal conductivity is also evaluated on a facies basis. While shale-like layers have effective thermal conductivity of 1.4 W/mK (Khraisha, 2002), conductivity of the sandy layers is used as an adjustable parameter until the overall conductivity matches the homogenous input of 1.7 W/mK, which is taken to be a geometric mean. In particular, we found the fitting value for the sandy layers to be 2.0 W/mK, agreeing with published results for typical clean sandstones (Somerton, 1992).

Fig. 9.3 illustrates the impacts of layered heterogeneities on the alternating-injection technique. Reservoir response is very sensitive to viscosity heterogeneity, particularly during the early times. This can readily be attributed to the low initial total fluid mobility which, in turn, is due to the much more viscous oil that saturates the reservoir base where, incidentally, the producers and injectors are placed. This effect is more pronounced in the heterogeneous model because of inhibited injectivity and productivity, leading to delayed hydraulic communication between producers and injectors. However, some 10 years after start-up, oil rate from the heterogeneous model exceeds its homogeneous counterpart because the former's steam chamber has reached the interval 15-23 m, containing oil of lower viscosity than available anywhere in the latter (**Fig. 9.1**).

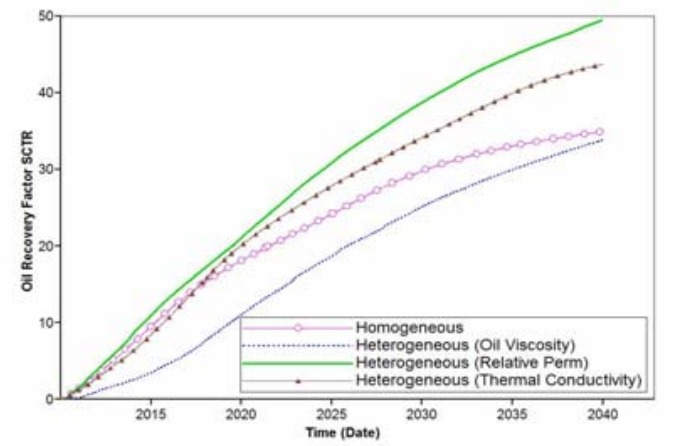


Fig. 9.3: Effects of Some Property Heterogeneities on the Alternating-Injection Process

9.5 Permeability-Impairment Due to CO_2-Induced Deasphalting

In the near-well region (5-m radius), dominated by convergent flow, we assume that the open-system model (see Chapter 5) of asphaltene deposition applies. Conversely, the closed-system model describes the far-field regions. Ideally, the vicinity of the injectors would be more consistent with the closed-system theory because the injection plane, in effect, is flow diverging. However, for a conservative analysis, it is treated as an open system. This is a fair assumption considering that some of the mobilised asphaltene-laden streams pass through, thus converging at, the injection plane on their way to the producers.

Employing our asphaltene-deposition correlations (**Eqs. 5.32** and **5.33**) and using properties of the Nigerian oil sand, we estimate the three model parameters required for the open-system model. Key input data and the estimated parameters are listed in **Table 9.2**. We assume an asphaltene-floc diameter of 20 nm (Minssieux *et al.*, 1998). From these parameters, we predict the time-variation of permeability impairments in the open and closed-system cases.

However, it was difficult to implement the resulting profiles during the simulation run-time. Hence as a first-order approximation, we apply a constant value, taken to be the average of predicted damage over the 40-year simulation period. For the open-system, the averages of predicted ratio of damaged-to-initial permeabilities are 0.90, 0.50 and 0.15 for the pessimistic (high oil-viscosity), base and optimistic (low oil-viscosity) cases, respectively. Corresponding values for the closed-system are 0.95, 0.92 and 0.74, respectively. The impacts of asphaltene-induced permeability and viscosity reduction are presented in **Fig. 9.4**, with the analysis provided shortly.

Table 9.2: Input Data and Estimated Model Parameters for the Open-system Model

	Pessimistic	Base	Optimistic	References / Comments
Length (m)	5	5	5	assumed near-well length.
Flow velocity (m/s)	5.8×10^{-8}	28×10^{-8}	480×10^{-8}	CO_2 buoyancy at 275 ^oC, 6 MPa.
Flow area (m^2)	5×10^3	5×10^3	5×10^3	product of well length (500 m) and assumed damaged width (10 m), centred at the well.
Asphaltene content (wt. %)	27.04	24.24	19.78	Lawal and Adenuga (2010).
n	8	4	2	assumption, but facies-independent.
λ_o (m^{-1})	15.8	156.5	4557.3	calculated (**Eq. 5.32**)
N^*	833	512	161	calculated (**Eq. 5.33**)

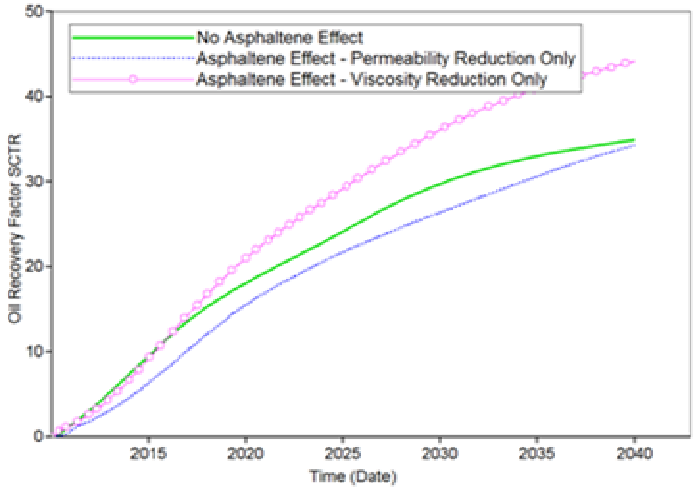


Fig. 9.4: Effects of Asphaltene-induced Permeability and Viscosity Reduction on Oil Recovery

9.6 Viscosity-Reduction Due to CO_2-Induced Deasphalting

As highlighted for permeability, crude composition and viscosity could not be manually updated during simulation run time. For simplicity, we employ a modified initial oil-phase molar composition to approximate cumulative deasphalting over the project lifetime.

Because asphaltene drop-out causes the simultaneous reduction of permeability and crude viscosity, it is necessary to ensure internal consistency in estimating the post-deposition values of these properties. For consistency, we back-calculate the average mass fraction of asphaltene required to achieve respective permeability impairments, using the proposed damage model (**Eqs. 5.9** and **5.11**):

$$\left(\frac{k_d}{k_i}\right)_{average} = \left(\frac{\rho_a\left(1-\bar{x}_a\right)}{\rho_o\bar{x}_a + \rho_a\left(1-\bar{x}_a\right)}\right)^n . \qquad (9.1)$$

This implies that, for time-averaged (open-system) damaged-to-initial permeability ratios of 0.90, 0.50 and 0.15 and the parameters in **Table 9.2**, corresponding $\bar{x}_a$ are 0.0174, 0.2045 and 0.6784 for the pessimistic, base and optimistic realisations, respectively. Taking the complements of these values of $\bar{x}_a$, percentages of the initial asphaltene mass retained in solution after a 40-year deasphalting are estimated to be 98.26, 79.55 and 32.16 % in the pessimistic, base and optimistic realisations, respectively. **Table 9.3** presents the compositions before and after predicted asphaltene drop-out. It is noteworthy that, in estimating the post-deasphalting compositions, initial masses of C_1 and maltene are preserved.

Table 9.3: Molar Compositions (in fractions) before and after Deasphalting (Average)

Component	Pessimistic		Base		Optimistic	
	Initial	Deasphalted	Initial	Deasphalted	Initial	Deasphalted
C1	0.0302	0.0303	0.0872	0.0896	0.2104	0.2242
Maltene	0.8121	0.8143	0.7815	0.8031	0.6986	0.7446
Asphaltene	0.1577	0.1554	0.1313	0.1073	0.0910	0.0312

Fig. 9.4 displays the performances with and without implementing asphaltene effects. Whereas the sensitivity to permeability impairment is evident almost from start-up, the viscosity-reduction effect is not noticeable until after 7 years. This is due to the initial dynamics being largely controlled by the oil mobility that does not change significantly with and without deasphalting in the base case, which is characterised by relatively small quantity of drop-out over the simulation time scale.

In the base-case model, thicknesses of the open- and closed-system regions are 12 and 26 m, respectively. After deasphalting, the open- and closed-system zones have permeability retention of 50 and 92 %, respectively. By thickness-averaging of the retained permeabilities, the reservoir is expected to retain about 79% of its initial permeability after 40 years of continuous operation and deasphalting.

On a net basis, the asphaltene drop-out predicted in the base realisation would reduce the average oil mobility by about 21 % when only permeability impairment is considered. Conversely, in the case of viscosity reduction only, oil viscosity is reduced by some 45 %, implying a mobility enhancement of about 80 %. Despite that effective permeability and viscosity have the same first-order impact on oil mobility ($\lambda_o = k_o/\mu_o$), the fact that, for the same amount of deasphalting, viscosity shows greater sensitivity than permeability, explains the higher effect obtained with viscosity-reduction in **Fig. 9.4**.

9.7 Effects of Dispersion

So far, the potential impacts of CO_2 and flue-gas dispersion on the reservoir dynamics have not been considered. While these are addressed in this section, for the sake of computational efficiency, we limit the dispersion effects to CO_2 and N_2 in the oil phase. Here, we assume

dispersion coefficient of 5 x 10^{-9} m^2/s, which accounts for both molecular diffusion and mechanical dispersion (Alkindi, 2009; Das and Butler, 1998; Dunn *et al.*, 1989). Due to paucity of data, we take it that the two components have the same dispersion coefficient, which does not depend on the viscosity, temperature and flow direction. By implementing physical dispersion for the alternating-injection processes, we have somewhat incorporated the effects of the VAPEX process which, in principle, is the non-thermal version of the SAGD steaming process (Das and Butler, 1998).

According to **Fig. 9.5**, the non-inclusion of dispersion would underestimate the potentials of the alternating-injection processes. The dispersed hot components extend the instantaneous size of the steam chamber, thereby improving heat propagation relative to the no-dispersion case (Sharma and Gates, 2010; Butler, 2004). Additionally, dispersion causes deeper penetration (**Fig. 9.6**) of these non-condensables which, following dilution of the in-situ oil, complements the viscosity reduction due to increased temperature.

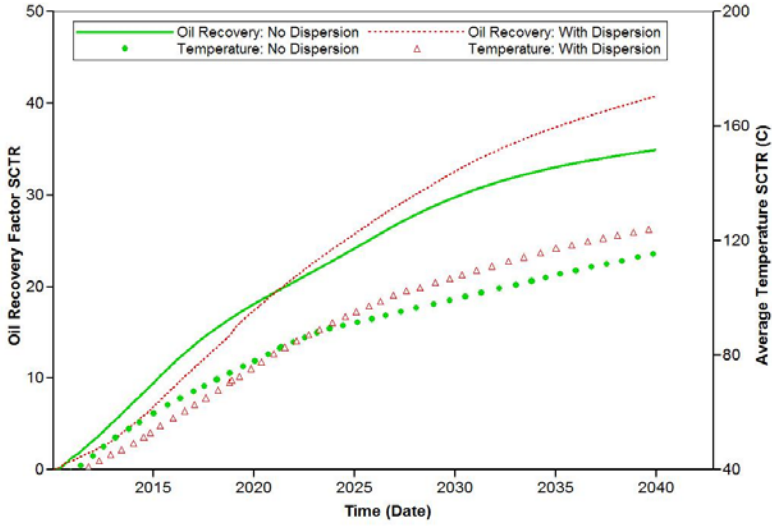
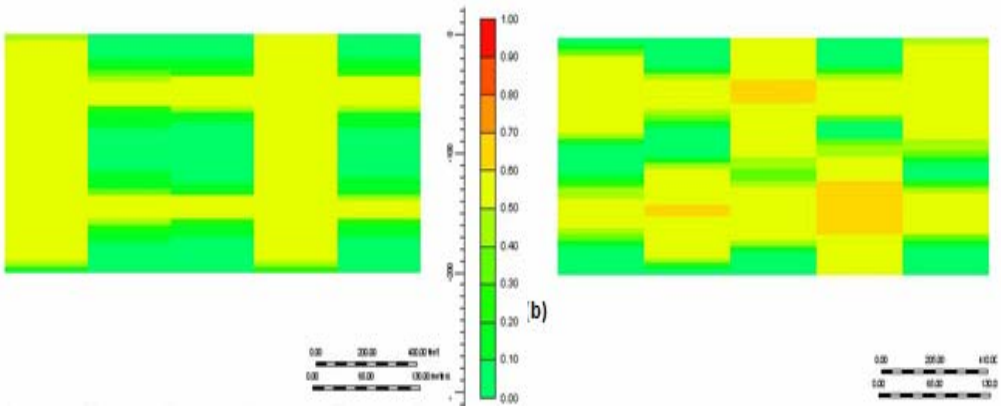


Fig. 9.5: Effects of Dispersion on the SAC Process



(a) No Dispersion **(b) With Dispersion**

Fig. 9.6: Gas-Saturation Profiles for the SAC Process (Topmost Layer after 15 Years)

As illustrated in **Fig. 9.5**, although dispersion reduces the heating rate at early times, this effect is compensated by larger chamber at later times. For clarity, it is worthwhile to state that dispersion, by itself, is not responsible for the retarded early-time heating but the poor heat-transport capacity of the dispersed components (see chapters 3 and 4). Were effective heat carriers such as steam, dispersed, the increased heating rate would have manifested from the onset. Similar result was noticed for the SAF. Specifically, in comparison to CO_2, the poorer heat-carrying capacity of N_2 (**Fig. 3.18**) and its lower solubility (**Figs. 6.11** and **6.12**) in the oil hamper both the thermal and miscibility effects on oil mobility.

On these results, it can be concluded that heating, as against dilution, is a more important mechanism for enhancing the in-situ mobility of the reference crude, particularly at early times (see discussions in Chapter 8). Therefore, in order to take advantage of both heating and dilution in a thermal process, it is essential that the dispersing components have very good heat-capacity in addition to excellent solubility in the in-situ crude.

9.8 Final Simulations

Following the integration of all the sensitivities, including heterogeneity and deasphalting, we now simulate the final models for the three cases. Although we found that dispersion improves oil recovery, for simplicity, the effect is limited to the base-case model. The relevant simulation results for the three processes are illustrated in **Figs. 9.7-9.9** while the key output is summarised **Tables 9.4-9.6**. Subsequent economic and risk analyses are based on the profiles in **Figs. 9.7-9.9**.

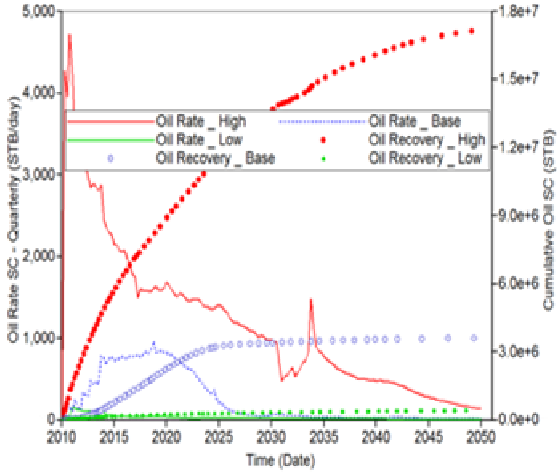


Fig. 9.7a: Oil Production for the Steam-alone Process

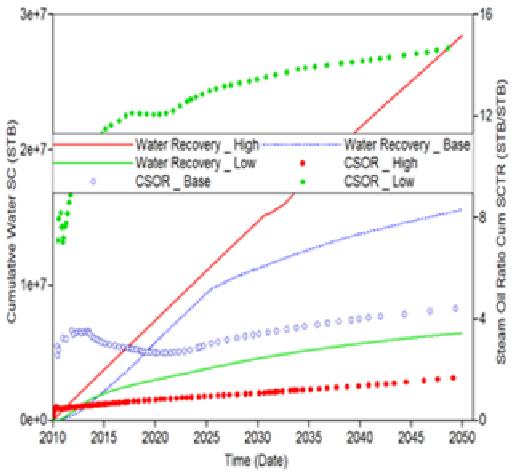


Fig. 9.7b: Water Production and Steam Consumption for the Steam-alone Process

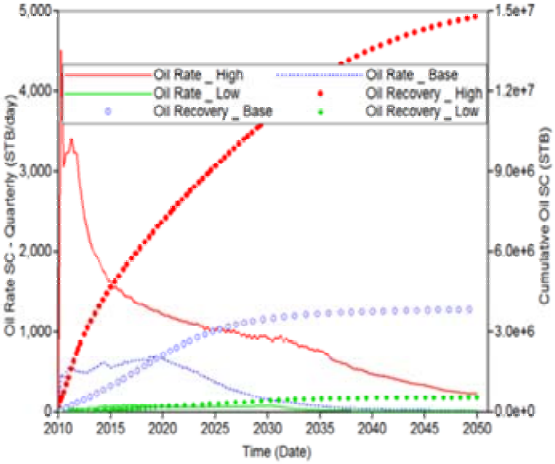


Fig. 9.8a: Oil Production for the SAC Process

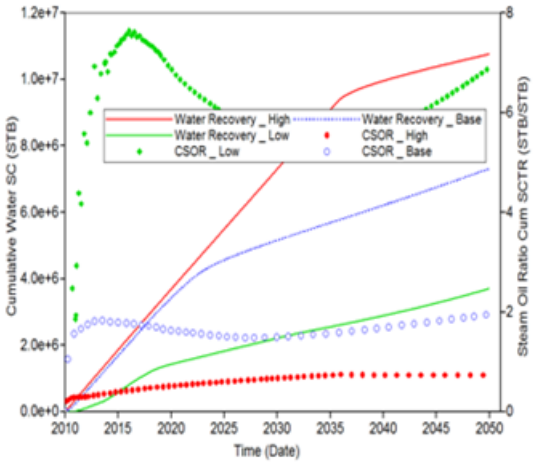


Fig. 9.8b: Water Production and Steam Consumption for the SAC Process

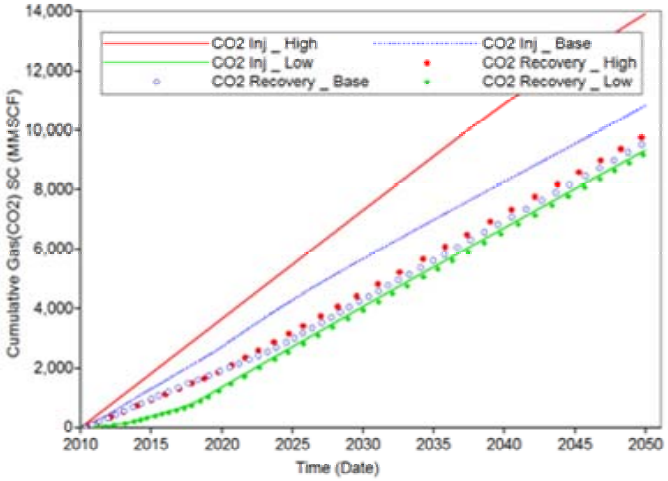


Fig. 9.8c: CO_2 Injection and Recovery for the SAC Process

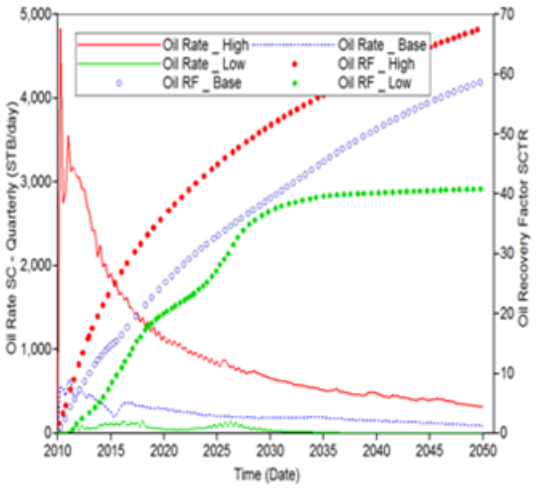


Fig. 9.9a: Oil Production for the SAF Process

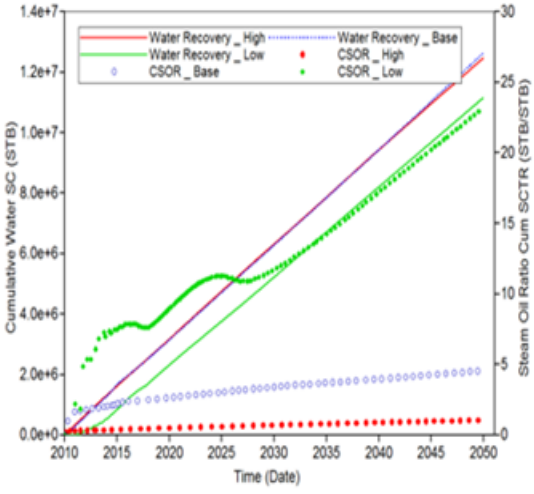


Fig. 9.9b: Water Production and Steam Consumption for the SAF Process

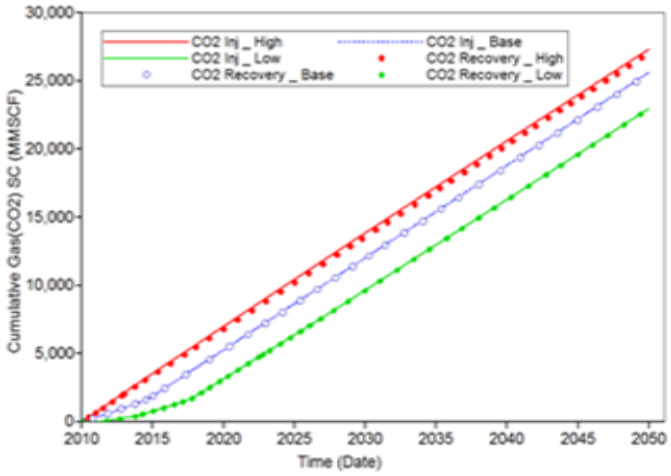


Fig. 9.9c: CO_2 Injection and Recovery for the SAF Process

Table 9.4: Performance Summary (High Case)

Quantity	Steam-alone	Steam - CO_2	Steam - Flue
STOIIP (MMstb)	21.1	21.1	21.1
GIIP, CH_4 (MMscf)	716.2	716.2	716.2
G_{max} (Bscf)	4.9	5.9	5.9
Steam Inj., CWE (MMstb)	29.2	10.9	14.8
CO_2 Load (Bscf)	-	13.9	27.3
N_2 Load (Bscf)	-	-	245.9
Oil RF (%)	81.4	70.1	66.9
Gas (CH_4) RF (%)	53.8	45.4	42.8
Water Produced (MMstb)	28.5	10.8	12.5
CO_2 Stored (Bscf)	-	3.9	0.3
N_2 Stored (Bscf)	-	-	2.8
Total CO_2 Stranded (Bscf)	29.2	10.0	27.0
Formation-Capacity Utilised by CO_2 (%)	-	65.8	5.5

Table 9.5: Performance Summary (Base Case)

Quantity	Steam-alone	Steam - CO_2	Steam - Flue
STOIIP (MMstb)	5.6	5.6	5.6
GIIP, CH_4 (MMscf)	80.3	80.3	80.3
G_{max} (Bscf)	1.2	1.5	1.5
Steam Inj., CWE (MMstb)	16.0	7.5	14.9
CO_2 Load (Bscf)	-	10.8	25.6
N_2 Load (Bscf)	-	-	230.5
Oil RF (%)	64.9	69.2	58.9
Gas (CH_4) RF (%)	33.6	34.3	28.5
Water Produced (MMstb)	15.6	7.3	12.6
CO_2 Stored (Bscf)	-	1.0	0.1
N_2 Stored (Bscf)	-	-	0.9
Total CO_2 Stranded (Bscf)	16.0	9.8	25.5
Formation-Capacity Utilised by CO_2 (%)	-	68.0	7.1

Table 9.6: Performance Summary (Low Case)

Quantity	Steam-alone	Steam - CO_2	Steam - Flue
STOIIP (MMstb)	1.4	1.4	1.4
GIIP, CH_4 (MMscf)	10.0	10.0	10.0
G_{max} (Bscf)	0.2	0.3	0.3
Steam Inj., CWE (MMstb)	6.3	3.7	13.5
CO_2 Load (Bscf)	-	9.3	22.9
N_2 Load (Bscf)	-	-	206.7
Oil RF (%)	29.9	37.8	40.8
Gas (CH_4) RF (%)	22.7	23.7	24.2
Water Produced (MMstb)	6.5	3.7	11.2
CO_2 Stored (Bscf)	-	0.1	0.01
N_2 Stored (Bscf)	-	-	0.1
Total CO_2 Stranded (Bscf)	6.3	9.2	22.9
Formation-Capacity Utilised by CO_2 (%)	-	45.0	4.3

With predicted oil recovery factor (RF) in the range 30-81%, which is typical of steam-based extraction methods (Dusseault, 2001; Farouq-Ali, 1994), all the processes can be regarded as technically feasible, at least for the system under study. However, a consideration of the production rates would reveal that the accumulation (STOIIP) also plays a key role in determining the eventual attractiveness of a prospective development. That is, the recovery rates are limited by the volume in-place rather than the dynamics. In this instance, despite that the RF of the high-case is less than three times the corresponding low-case, the plateau rate in the former generally exceeds that in the latter by a factor of 30. As the production rate impacts directly on project economics, it follows that the screening of prospective developments should not be based on just the RF.

The performances also indicate that the injection of either CO_2 or N_2 in alternating cycles with steam would only improve oil recovery if the crude is very viscous and there is reasonable in-situ deasphalting such that the resulting viscosity reduction far outweighs the plugging of pore throats. Otherwise, oil production is slightly jeopardised but there is significant saving in steam consumption and water-handling, especially in the SAC process. Contrary to expectation, the presence of either CO_2 or N_2 does not really induce the dilution effect required for further reduction of oil viscosity beyond that obtained from increased temperature. This lack of dilution is due to the poor miscibility of CO_2 and N_2 with the oil at the relatively high reservoir temperatures attained (see *K-values* in **Figs. 6.11** and **6.12**). Due to their characteristic high operating temperatures, this inference is instructive for thermal recovery methods in general. That is, for such operations where NCG's are used to augment a thermal flood, the prospects of achieving significant dilution-induced oil-viscosity reduction are relatively low.

The relatively high steam input in the low-case SAF is attributed to the poor injectivity of flue-gas in comparison to steam. Because of its relatively small volume in this case, the reservoir builds up pressure rapidly hence difficult to sustain high injection rates – compare 25 MMscfd flue-gas to 7.5 MMscfd steam (1000 stb/d CWE), resulting in considerable cut-back of flue-gas injection by the simulator in order to satisfy the imposed constraint of maximum injection pressure while aiming for the production targets. This accounts for the decrease in the total gas-to-steam injection ratio from the high to the low-case model in the SAF process. Conversely, this ratio decreases in the opposite direction for the SAC process because of relatively low CO_2 injection rate (1 MMscfd), hence lower rate of reservoir pressurisation.

On the basis of the foregoing analysis, the detrimental effect of CO_2 / flue-gas as steam additive reported by some workers (Bagci *et al.*, 2008; Law, 2004; Hornbrook *et al.*, 1991; Frauenfeld *et al.*, 1988) may partly be rationalised by the non-inclusion of deasphalting in their numerical models or very slow precipitation kinetics in the laboratory studies. By the same argument, where no significant difference was noted (Nasr *et al.*, 1987; Leung, 1983; Bader *et al.*, 1981; Fox *et al.*, 1981), it could be that the net beneficial effect of deasphalting and the unfavorable impact of reduced heat-transport are comparable.

Fig. 9.10 illustrates the final CSOR of the different processes for the three cases considered. From these results, it is evident that the SAC process consistently offers the highest savings on steam consumption per unit oil recovered. Indeed, in terms of CSOR, the competitiveness of SAC increases from the high case to the low-case model, underscoring the conclusion reached from the analysis of oil recovery that the attractiveness of the alternating-injection processes in general, and the SAC in particular, increases with the initial immobility of the crude. Given the general guideline that steam-based processes are likely to be economic at CSOR < 4 (Shin, 2008; Shin and Polikar, 2006), it follows that SAC is the most robust and competitive in this example, as it is the only process that meets the indicated screening criterion in both the high and base-case models while consuming the least amount of steam per unit oil in the low-case model.

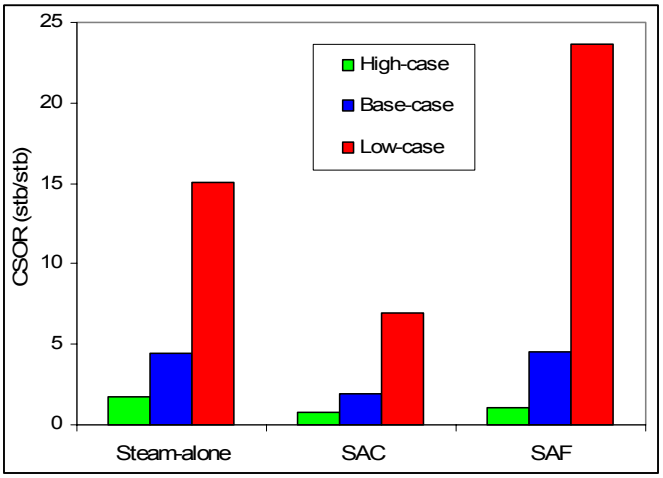


Fig. 9.10: Comparison of CSOR for the Different Processes

As shown in **Fig. 9.11**, for comparable amount of steam, the enrichment of flue-gas with CO_2 is favourable to oil production and water (energy) conservation. This relative advantage of CO_2 over N_2 is primarily due to the former's better heat-carrying capacity and its higher miscibility in the crude at all conditions examined in this example. Therefore, where permitted by economics and other considerations, the alternating-injection scheme should employ high-purity CO_2 stream.

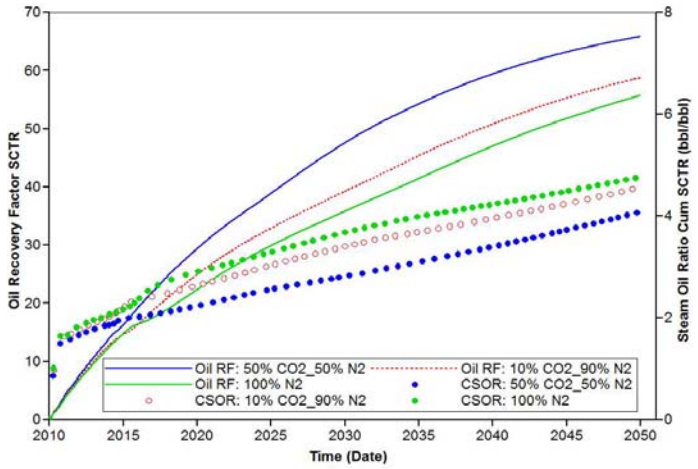
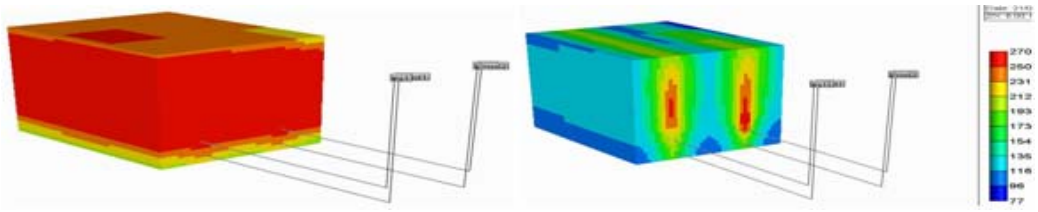


Fig. 9.11: Effects of CO_2-Composition on Performance of the SAF Process

Contrary to intuition, the methane RF is consistently lower than that of oil, despite that the former was initially dissolved in the latter. First, high temperature reduces the solubility of methane in oil (**Fig. 6.8**), hence in the high-temperature regions, CH_4 essentially exists in the gas (as free gas) rather than the oleic phase (in solution). Incidentally, due to its proximity to the injectors, the production area is always at relatively high temperature. Secondly, buoyancy plays a key role in the flow of fluids to the producers, placed almost at the base of the reservoir. As buoyancy is not favourable to downward migration of gas, most of the temperature-released solution gas is left in the formation.

Given the preceding arguments, it is surprising that the alternating-injection processes consistently have lower ratio of gas-to-oil RF than their steam-alone counterpart, notwithstanding the higher reservoir temperatures of the latter (**Fig. 9.12**). This can partly be explained by the solubility of CH_4 in the presence of other gas components. As can be seen in **Figs. 6.8** and **6.11**, for the range of temperature and pressure considered, CO_2 is more stable in the oil than does CH_4. Hence, CO_2 preferentially goes into the oleic phase for onward drainage along with the oil, at the expense of temperature-liberated CH_4.



(a) Steam-alone Process **(b) SAC Process**

Fig. 9.12: Distribution of Temperature after 40 Years

We speculate that, in practice, the effect of component relative-permeability may also contribute to a less-than-expected recovery of CH_4, as the large injection volumes of CO_2 and N_2 would reduce the CH_4 saturation, hence its relative permeabilities. However, this possibility cannot be explored here because the current models are based on phase, rather than component, relative permeabilities. Perhaps, where such data is available, it would be worthwhile to examine the influence of potential composition-dependency of the relative-permeability functions.

From **Figs. 9.8c** and **9.9c**, the fraction of injected CO_2 that is retained in the formation increases from the low-case to the high-case model. This is partly a result of the reservoir size, as the pressure-holding capacity generally increases with reservoir volume. Another factor is the voidage available. Considering that it has the most favourable reservoir dynamic properties, oil production rate is highest in the high-case model, creating more voidage, both in terms of number and rate, to be filled up by CO_2.

In order to assess the effective utilisation of the reservoir capacity by the alternating-injection processes, we estimate the maximum gas-storage capacity (at standard conditions), assuming a closed system:

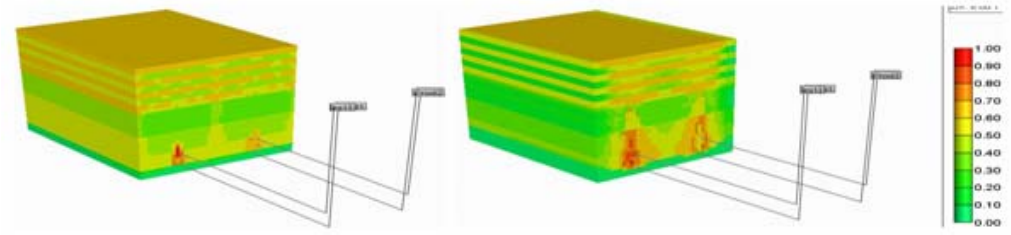
$$G_{\max} = \frac{G_{RV}\bar{\phi}\left(1-\bar{S}_{wc}\right)P_r T_s}{Z_r P_s T_r}, \qquad (9.2)$$

where G_{RV} is the gross-rock volume; $\bar{\phi}$ and $\bar{S}_{wc}$ are average porosity and connate-water saturation, respectively. T_r and P_r are the end-simulation average pressure and temperature, respectively. Z_r is CO_2 compressibility factor at T_r and P_r. T_s and P_s are at standard conditions. Here, T_r = 270 and 170 ^oC for the steam-alone and alternating-injection processes, respectively, and P_r = 6 MPa for all cases. The temperature effect accounts for corresponding differences in G_{max} in **Tables 9.4-9.6**.

In the summary tables, the CO_2 and N_2 loads refer to the total volumes (from steam generation as well as CO_2-N_2 compression and transportation) of these species available for disposal while the stranded amounts refer to the total volumes less the net storage.

As would be expected, the results indicate that the injection of N_2 consistently causes significant reduction in the carbon-storage capacity of the formation. While this may partly be explained by the much larger volume (90 v/v.%) of N_2 injected (**Fig. 9.13**), an equally important reason is the density effect. Given that N_2 and CO_2 have densities of 45 and 78 kg/m^3, respectively, at 6 MPa and 170 ^oC, for the same injection mass, the pore-volume occupied by N_2 would almost double that of CO_2. Because the reservoir has a finite pore-volume, its carbon-sequestration potential is thus undermined. With the exception of the base-case, formation-capacity utilisation increases from the low-case to the high-case model. The apparent violation of this trend in the base-case is due to the inclusion of dispersion.

On these simulation results, it can be concluded that all the processes are technically attractive for applicability in the Nigerian heavy-oil belt. This notwithstanding, as typical of fossil-fired steaming recovery methods, the three processes are still net carbon emitters. In order to establish their overall feasibility and relative competitiveness, we discuss economic and risk analyses in the next chapter.



(a) Alternating Steam and Flue-gas Process **(b) Alternating Steam and CO_2 Process**

Fig. 9.13: Distribution of Gas-Saturation after 40 Years

9.9 Chapter Summary

The effects of heterogeneity, deasphalting and dispersion on the dynamics of the steam-alone, SAC and SAF processes have been investigated. For this particular model, the vertical variation of reservoir and fluid properties has greater impact on the SAC and SAF processes. Reckoning that heat is the primary mechanism of mobilising the in-situ oil in the current system, the alternating-injection processes are more vulnerable to heterogeneity, mainly because of the lower heat-carrying capacities of CO_2 and N_2 in comparison to steam. Where heating is the main viscosity-reduction mechanism, dispersion would only be beneficial if the dispersing components are good heat carriers and at the same time miscible with the oil under reservoir conditions. Otherwise, dispersion may be detrimental to accelerated oil recovery.

Although the permeability impairment resulting from asphaltene deposition delays oil recovery, the associated viscosity reduction seems to override this effect. As a result, there is a net

enhancement of oil mobility which, in turn, accelerates oil production. In general, the mobility-improving benefits of deasphalting increase with oil viscosity (initial asphaltene content). With this in-situ upgrading, oil of higher quality is produced.

From a technical perspective (oil recovery), it can be concluded that the three processes have potentials in the Nigerian heavy-oil belt. However, they are all still plagued with the issues of carbon management, energy supply and water sourcing/handling. In order to further evaluate these processes, the next chapter assesses the economics as well as the associated risks, taking into consideration the penalties and rewards related to the outlined issues.

Chapter 10

Economics and Risk Analysis

The preceding chapters have shown that the steam-alone, SAC and SAF processes are technically feasible for the in-situ exploitation of heavy oil and bitumen deposits, particularly for the systems investigated. However, compared to the technical prospects, the commercial viability of a potential project often has greater influence on the decision-making process (Yang *et al.,* 2009; Frauenfeld *et al.*, 2006). Therefore, this chapter assesses the economics as well as the commercial risks of the three processes under discourse.

In conducting the economic and risk analyses, we apply the same workflow as that for the technical studies (Chapter 6). The workflow consists of screening, experimental design, response-surface construction and Monte-Carlo simulation (Yang *et al.*, 2009). But in the current case, the net present value (NPV) and value-to-investment ratio (VIR) are the objective functions. As commonly used in the industry (Shell, 2001), VIR is the quotient of NPV and discounted capital expenditure (CAPEX). Generally, for projects of different sizes and scopes such as the ones being evaluated, the VIR provides a better indication of the efficiency of capital than the NPV (Shell, 2001).

The analysis presented here evaluates the impacts of the reservoir models (production, injection and CO_2 storage profiles), costs, revenues as well as the fiscal regime on the afore-mentioned economic indicators. As a reference case, we apply the current petroleum fiscal laws in Nigeria (ETF, 1993; PTDF, 1990; PPT, 1990). Considering that Nigeria is yet to have a dedicated policy for the exploitation of her heavy oil and bitumen resources, we apply the laws currently guiding the exploitation of her light crude and gas. However, where data gap exists and for the sake of sensitivity studies, we make reasonable assumptions from information available on the well-established industries in Canada and elsewhere (Gaspar Ravagnani *et al.*, 2009; Shin and Polikar, 2006; Edwards, 2000).

10.1 Economic Model

In building an economic model, we need to establish the profile of net annual cash flow, which is the balance of the annual revenue and expenditure streams, including the "allowable" depreciation of fixed assets. The annual net cash flow is estimated from the following relation (Shell, 2001),

$$N_{CF} = R_v - C_{op} - C_{ca} - C_r - C_t - C_{CO2}\,, \tag{10.1}$$

where R_v is the gross revenue; C_{op}, C_{ca}, C_r and C_t are the OPEX* (fixed and variable), CAPEX, royalty and tax, respectively. C_{CO2} is the carbon-emissions penalty. R_v consists of receipts from oil

* Operating Expenditure.

and gas sales as well as the credits due to carbon storage. All the variables refer to the end of the year. Note that **Eq. 10.1** has been adapted to include the carbon penalty, C_{CO2}.

The quantities C_r and C_t are given by:

$$C_r = r_r R_v', \tag{10.2}$$

$$C_t = r_t \left(R_v - C_r - C_{op} - C_d \right), \tag{10.3}$$

where r_r and r_t are royalty and tax rates, respectively. C_d is the fiscal depreciation. R_v' refers to R_v less carbon-credit revenues. Again, these are annual estimates.

Royalty and tax payments, which are government takes, are in line with the Nigerian fiscal policy. Although carbon credit is also a revenue source, it only incurs tax but not royalty. This stems from the fact that the carbon credit, unlike oil and gas, is not associated with the sale of *extracted* minerals. Meanwhile, decommissioning costs are included in the computation of N_{CF} during the abandonment year.

The NPV is estimated from the annual net cash flow according to the following expression:

$$N_{PV} = \sum_{i=1}^{n_t} \frac{N_{CF}}{\left(1 + r_D\right)^i}, \tag{10.4}$$

where r_D and n_t are discount rate and number of years to abandonment, respectively. i is the year counter. All the analyses presented are based on 42 years (n_t = 42), comprising the 2-year pre-start and the 40-year operating lifetime, the latter conforming to the duration of the final simulation studies in Chapter 9.

In the following sub-sections, we discuss the key components of some of the variables in **Eqs. 10.1-10.4**. Furthermore, the main assumptions underlying the estimates applied in subsequent analyses are outlined.

10.1.1 CAPEX and OPEX Elements

The CAPEX items relate to the wells, flowlines, treatment facilities as well as provisions for gas-compression and transport. In the SAC process, the facilities for capturing CO_2 are included. As summarised in **Table 10.1**, provision is also made for contingency and decommissioning. For simplicity, we assume that all the CAPEX would be incurred in the two years preceding the project (production) start-up. Additionally, equal amounts of this CAPEX would be spent in these two years. The main components of the OPEX and their assumed reference values are given in **Table 10.2**.

Table 10.1: CAPEX Components

Cost Item	Quantity	Comments / References
Drilling & Completion		
- No. of injectors	2	Based on the optimised development (Chapters 7 & 8).
- No. of producers	2	"
Unit cost ($ mln / well)	*1.5*	Frauenfeld *et al.* (2006), Shin and Polikar (2006).
Surface Pipelines (Flowlines)		
- No. of injection lines	2	A "pessimistic" scenario of one flowline per injector.
- No. of production lines	2	A "pessimistic" scenario of one flowline per producer.
Length per line (km)	*1*	
Unit cost ($ mln / km)	*0.5*	EMT (2011), Cox *et al.* (2003)
Processing Facilities		
Peak steam rate, CWE (Mstb/d)	2	This is halved for SAC and SAF (see Chapters 7 & 8).
Peak gross liquid rate (Mstb/d)	8	Gross liquid is about 4 times CWE steam (Heins, 2010). But 2.5 times for SAC & SAF (see Chapters 7 & 8).
Unit cost of gross liquid facilities ($ mln / Mstb liquid)	*1.9*	Frauenfeld *et al.* (2006), Birrell *et al.*, (2005), Edmunds & Chhina (2001).
Unit cost of steam boiler ($ mln/ Mstb water)	*2.2*	Birrell *et al.*, (2005), Edmunds & Chhina (2001).
CO_2-Capture Facilities		
Peak CO_2 rate (MMscf/d)	1	Applies only to SAC (see Chapter 8).
Unit capture cost ($ mln / MMscf)	*13*	CAPEX of post-combustion capture process is ~ 10 times that of compression (US DOE**, 2008).
Gas-Compression Facilities		
Peak injection rate (MMscfd)	1	25 MMscfd for SAF and zero for steam-alone (Chapter 8).
Unit compressor cost ($ mln / MMscf)	*1.3*	Gaspar *et al.* (2009). But due to economies of scale, we assume the cost of the 25 MMscfd rating is only twice that of the 1 MMscfd rating.
Others		
CAPEX contingency (%)	10	Assumption (Shell, 2001).
Decommissioning costs (% CAPEX)	25	Allinson *et al.* (2010).
CAPEX phasing (% / year)	50	CAPEX spending spread over the first 2 years.

** US Department of Energy.

Table 10.2: OPEX Components

Cost Item	Rate
Fixed OPEX	5% of CAPEX
	Variable OPEX
- Gas injection	$ 580 / MMscf (Neal et al., 2010; Gaspar *et al.*, 2009; Frauenfeld *et al.*, 2006).
- CO_2 capture	$ 1600 / MMscf (Gaspar *et al.*, 2009; Nogueira & Mamora, 2005).
- Oil treatment	$ 12 / stb (NEB, 2006).
- CH_4 treatment	$ 400 / MMscf. Assumed to be 20% of the price of sales gas (CH_4).
- Water handling	$ 0.1 / stb (Anthony and Mohan, 2010).
- Heat injection	$ 16.8 / GJ i.e. 70% boiler thermal efficiency (CIBO, 2003) and heavy-oil as fuel.

10.1.2 Revenue and Penalty

Three revenue sources are considered in this work. The primary cash inflow is the conventional sale of produced oil and gas. But for the SAC and SAF processes, there is an addition to oil and gas sales. Potentially, revenue could accrue due to the underground storage of CO_2 that would have been released into the atmosphere. This is the so-called carbon credit (Pointcarbon, 2010; Kaarstad, 2004).

On the other hand, under the assumed carbon-constrained scenario, as the project attracts carbon credits for the CO_2 emissions that it effectively mitigates, penalties are also incurred for any release of such fugitive emissions. Hence, we pay the so-called carbon tax for stranded CO_2 (Kaarstad, 2004). For the reference-case analysis, the revenue and carbon-penalty rates are indicated in **Table 10.3**.

Table 10.3: Revenue and Penalty Components

Item	Rate
Oil price	$ 75 / stb (Bloomberg, 2010; Reuters, 2010).
Gas (CH_4) price	$ 2000 / MMscf (Nwachukwu and Adeoye, 2010).
Carbon credit	$ 16 / ton CO_2 (Pointcarbon, 2010; Kaarstad, 2004).
Carbon penalty	$ 60 / ton CO_2 (Kaarstad, 2004).

The oil price is relative to the West Texas Intermediate (WTI). As at Dec. 23, 2010, the price of WTI was $90.91/bbl (Bloomberg, 2010). As the price differential between the WTI and heavy oil is typically $15 (Reuters, 2010), this results in the reference-case oil price of $75/bbl as at 23/12/2010. The gas price is based on the guidelines recently released by the Nigerian government (Nwachukwu and Adeoye, 2010). Please bear in mind that the oil price does not reflect the potential upgrading by the SAC and SAF processes, hence the economics of these processes might be conservative with respect to the steam-alone case. Additionally, some upgrading could still result from all the processes as a result of heat-induced cracking and distillation (Richardson *et al.*, 2000).

10.1.3 Fiscal Terms

The Nigerian government currently operates three additive tax regimes in the upstream sector of its petroleum industry. These taxes are the corporate, Petroleum Technology Development Fund (PTDF) and Education Trust Fund (ETF)[**]. Although these policies were developed for its light-oil and gas industries, we assume that they are also applicable to its relatively immature heavy-oil industry. In this work, the reference-case fiscal terms are presented in **Table 10.4**.

Table 10.4: Fiscal-Term Components

Item	Rate
Corporate tax	40 % (Vanguard, 2010; PPT, 1990; 1999 Decree Nos. 9, 26).
PTDF tax	3 % (PTDF, 1990).
ETF tax	2 % (ETF, 1993).
Discount (inflation)	10 % / year (Yang *et al.*, 2009).
Depreciation	20 % / year (NIPC, 2010).
Royalty	10 % (PPT, 1990).

At present, the royalty rate varies from one basin to the other. For the inland basins, to which the bitumen-bearing Dahomey Basin belongs, the royalty rate is presently put at 10 % (PPT, 1990). As a comparison, the rate for the onshore sector of the Niger Delta is 20% (PPT, 1990). The disparity of fiscal rates is currently one of a number of efforts at attracting investors to this bitumen belt.

In the calculation of the annual net cash flow (**Eq. 10.1**), we assume that the prospective project developer is not an existing taxpayer (i.e. new investor) hence does not pay tax in the years when fiscal costs exceed gross revenue ($C_t < 0$). However, we implement the three-year tax holiday which is yet another incentive recently offered by the Nigerian government to attract investments to the heavy-oil industry (Vanguard, 2010).

As stipulated by the Nigerian government (NIPC, 2010), the straight-line method of depreciation is used to provide for the depreciable assets. Specifically, the CAPEX elements are depreciated in equal amounts over the first 5 years of incurring the costs (NIPC, 2010).

10.2 Parameter Space and Sensitivity Analysis

The set of variables, including the range of values, examined for the sensitivity analysis is presented in **Table 10.5**. Please note that the tax rate includes all the stipulated tax components i.e. corporate, PTDF and ETF, with the latter two consistently making up 5 percentage points (ETF, 1993; PTDF, 1990; PPT, 1990). As noted earlier, the three-year tax holiday is implemented in all cases. Due to space constraint, we limit the current discussion of sensitivity analysis to the results

[**] It has just been renamed Tertiary Education Trust Fund (Anuku, 2011).

of the SAC process which, unlike the steam-alone technique, highlights the relative impact of carbon credit.

Table 10.5: Range of Economic Variables for Sensitivity Analysis

Variable	Low-case	Base-case	High-case	Comments / References
Oil price ($/stb)	50	75	120	reflects oil-price uncertainties.
Gas price ($/MMscf)	1000	2000	5000	based on Nigerian gas pricing policy (Nwachukwu and Adeoye, 2010).
Carbon credit ($/ton CO_2)	8	16	60	Pointcarbon (2010), Kaarstad (2004). As a market incentive, high-case assumes carbon credit would, at least, equal the current penalty.
Carbon penalty ($/ton CO_2)	30	60	90	50% uncertainties on the base-case, Edwards (2000).
Discount / Escalation rate (%)	5	10	15	Yang *et al.* (2009).
CAPEX (% change)	-50	0	+50	50% uncertainties on the base-case (Gaspar Ravagnani *et al*., 2009).
OPEX (% change)	-50	0	+50	"
Royalty (%)	4	10	20	4% refers to deep offshore, Edwards (2000).
Tax (%)	28.65	45	90	Nwete (2004), PPT (1990). Low-case is Brazil's regime (Gaspar Ravagnani *et al*., 2009; Edwards (2000).
Reservoir model	Low	Base	High	refers to uncertainties in the production/injection/storage of oil, gas, water, steam, and CO_2 (flue).

Fig. 10.1 shows the NPV tornado plot for SAC. From this result, it can be concluded that, within the range investigated, the discounting, carbon credit/tax and gas price do not have significant control on the project economics. This follows directly from the fact that this project is primarily oil-driven rather than a gas development, as the gas accumulation is relatively insignificant.

On the other hand, the project commerciality, as represented by NPV, depends strongly on the reservoir model, oil price, OPEX, CAPEX, tax and royalty. Hence, to a large extent, the uncertainties inherent in these variables would contribute significantly to the commercial risks of the project. In essence, through the reservoir model, the technical risk controls the commercial risk. This conclusion reinforces the need to reduce the uncertainties in the subsurface models, which govern the technical risks.

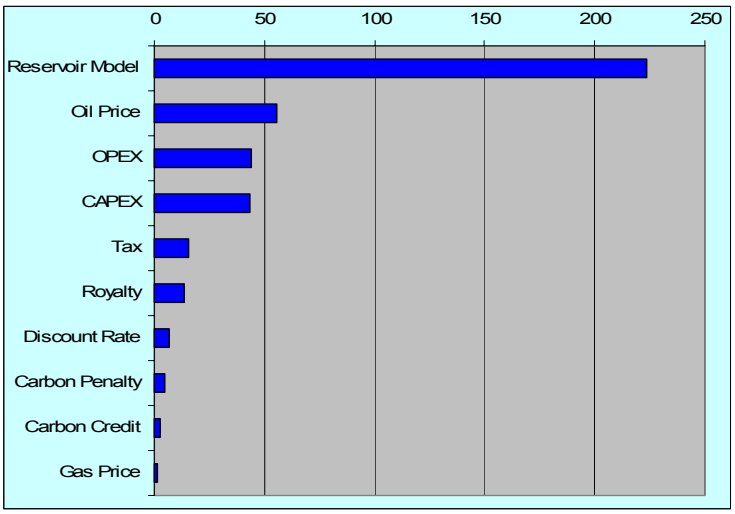


Fig. 10.1: Tornado Plot for NPV ($ mln) – SAC Process

10.3 Risk Analysis

Following the results of sensitivity analysis, the main variables controlling the economics are reservoir model, oil price, OPEX, CAPEX, tax and royalty. While the low-impact variables are maintained at their reference states, the six high-impacting variables are carried forward for the assessment of the risks associated with the processes. For convenience, these key variables are denoted by F_1, F_2, F_3, F_4, F_5, and F_6, respectively.

With fractional factorial design, the simulation matrix and responses are shown in **Table 10.6** for the case of SAC. Corresponding tables for the steam-alone and SAF are in Appendix **L**. In 50% of the possible parameter combinations examined, the project is expected to be economic (NPV > 0, VIR > 0). Although an equal number of runs is predicted to be uneconomic (NPV < 0, VIR < 0), the magnitude of the ultimate loss (< $ 98 mln, VIR < $ 2.3/$) is less than the corresponding profit (NPV > $ 370 mln, VIR > $ 20/$).

In **Fig. 10.2**, we examine the correlation between NPV and VIR as economic indicators for the SAC process. From this plot, the R^2 suggests that the two parameters need to be considered independently in order to make robust deductions on the project economics and commercial risks. It is interesting to note that similar inference was drawn from the analysis of the datasets of the steam-alone and SAF processes.

Table 10.6: Design Matrix and Output for the SAC Process

Run	*F1*	*F2*	*F3*	*F4*	*F5*	*F6*	*NPV ($ mln)*	*VIR ($/$)*
1	1	1	-1	-1	-1	1	331.56	20.56
2	1	1	1	-1	1	-1	169.24	9.58
3	-1	1	1	-1	-1	-1	-37.81	-2.14
4	-1	1	1	1	-1	1	-97.56	-1.84
5	1	1	1	1	1	1	93.56	1.77
6	-1	1	-1	-1	1	1	-17.94	-1.11
7	1	-1	1	-1	-1	1	39.06	2.21
8	-1	1	-1	1	1	-1	-54.27	-1.12
9	-1	-1	1	1	1	-1	-96.08	-1.81
10	-1	-1	1	-1	1	1	-40.27	-2.28
11	-1	-1	-1	-1	-1	-1	-21.51	-1.33
12	1	1	-1	1	-1	-1	374.05	7.73
13	1	-1	-1	1	1	1	25.46	0.53
14	-1	-1	-1	1	-1	1	-62.23	-1.29
15	1	-1	-1	-1	1	-1	70.40	4.37
16	1	-1	1	1	-1	-1	21.40	0.40
R^2							*0.984*	*0.858*

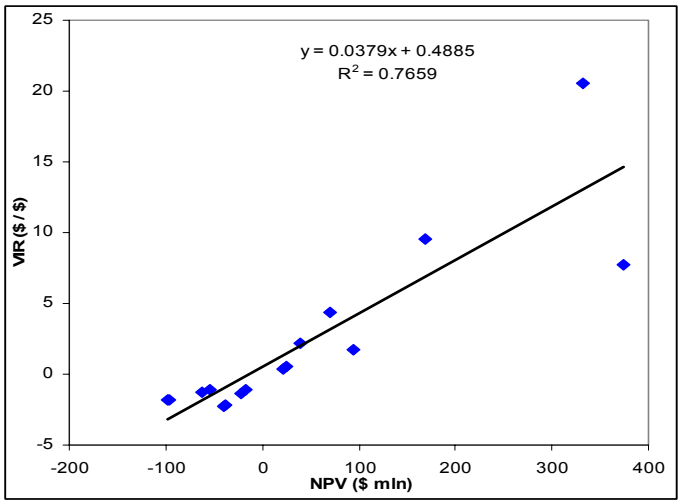


Fig. 10.2: VIR-NPV Crossplot for the SAC Process

Using the results of the experimental design, the following proxy models are obtained for the NPV and VIR of the three processes,

$$N_{PV_Steam} = 55.67 + 111.41F_1 + 59.93F_1F_2 + 59.21F_2 - 44.57F_3 - 33.07F_1F_5 - 30.26F_5 - 28.47F_1F_3 - 16.02F_4, \quad (10.5)$$

$$V_{IR_Steam} = 2.745 + 4.578F_1 + 2.489F_2 - 1.805F_3 - 1.863F_4 - 1.155F_5 + 0.250F_6, \quad (10.6)$$

$$N_{PV_SAC} = 43.57 + 97.03F_1 + 51.54F_2 + 49.97F_1F_2 - 37.12F_3 - 26.12F_1F_5 - 24.80F_5 - 22.65F_1F_3 - 18.02F_4, \quad (10.7)$$

$$V_{IR_SAC} = 2.139 + 3.755F_1 + 2.040F_2 + 1.977F_1F_2 - 1.694F_1F_4 - 1.593F_4 - 1.403F_3, \quad (10.8)$$

$$N_{PV_SAF} = 27.01 + 98.17F_1 + 59.38F_2 + 53.66F_1F_2 - 50.80F_3 - 22.74F_1F_3 - 18.73F_5 - 18.69F_1F_5, \quad (10.9)$$

$$V_{IR_SAF} = 2.234 + 6.367F_1 + 3.906F_2 + 3.530F_1F_2 - 3.224F_3 - 2.924F_1F_4, \quad (10.10)$$

where the factors *F* are numerical quantities ranging from -1 to 1.

An evaluation of the coefficients of the proxy equations would reveal that in addition to the reservoir model (F_1) and oil price (F_2) identified in the Tornado plot as the main uncertainties, the interaction between them (F_1F_2) also has high influence on the project economics, as represented by NPV and VIR. It is noteworthy that this conclusion is independent of the choice of process among the three processes under investigation.

Recall that the range of reservoir models, as used in the current economic analysis, is simply the aggregation of the uncertainties related to the subsurface (see Chapter 6). Considering the relative influence of the reservoir model on the economic indicators, it then follows that the technical risks are the main drivers of the commercial risks, which ultimately determine the commerciality of the development. As a consequence, the reduction of the main subsurface uncertainties would go a long way in reducing the commercial risks of the project. As highlighted in Chapter 6, in the current example, the reservoir-model uncertainties are governed by the reservoir geometry, oil-viscosity, relative permeability, oil saturation, and permeabilities.

In conducting the Monte-Carlo simulations of the above proxy models, we assume that all the input factors are uniformly distributed within the range -1 to 1. Following 10,000 stochastic simulations, the resulting NPV and VIR expectation curves are illustrated in **Figs. 10.3** and **10.4**, respectively. As discussed in Chapter 6, the notation $Px = b$ implies there is an *x*% probability of a given event *exceeding* the value *b*. From the curves, it follows that the steam-alone, SAC and SAF processes have 72, 68 and 55% chances of being economic (NPV > 0, VIR > 0), respectively.

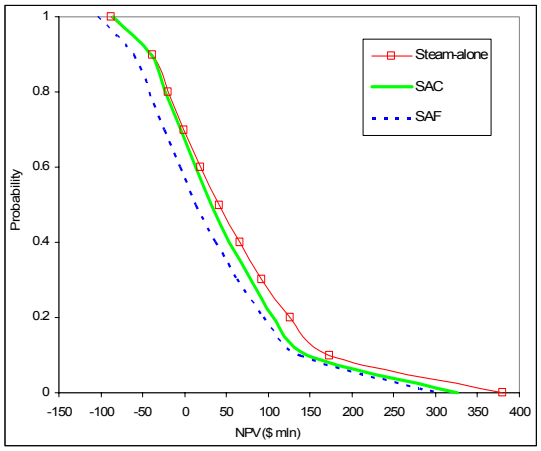


Fig. 10.3: Expectation Curves for NPV

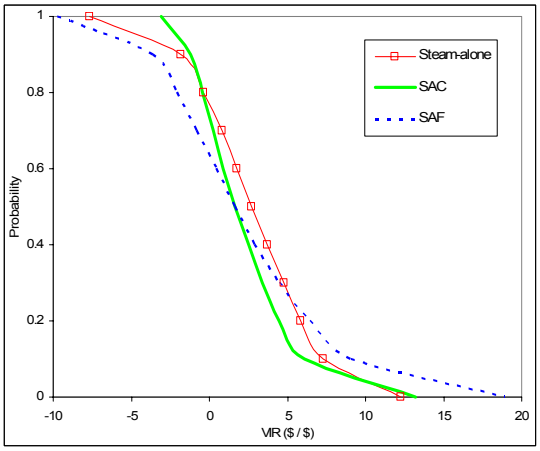


Fig. 10.4: Expectation Curves for VIR

In general, the spread of the expectation curves is a fair indication of the commercial risks associated with the processes (Cronquist, 2001). In other words, the larger the spread, the more risky is the process. Here, we use the difference (P10-P90) as an indication of the spread of the corresponding expectation curves. The main results of the probabilistic simulations are presented in **Table 10.7**, including the so-called "spread" (P10-P90).

Table 10.7: Summary of Economic Analysis

Parameter	P90	P50	P10	P10-P90
	Steam-alone			
NPV ($ mln)	-39.2	42.1	174.4	213.6
VIR ($ / $)	-1.7	2.8	7.3	9.0
	SAC			
NPV ($ mln)	-38.9	31.1	148.3	187.2
VIR ($ / $)	-1.2	1.6	6.2	7.4
	SAF			
NPV ($ mln)	-61.1	12.9	136.4	197.5
VIR ($ / $)	-3.7	1.5	9.2	12.8

On the downside (P90), all the processes are likely to incur losses after 40 years of operation (**Table 10.7**). However, it is expected that the SAC process would record the lowest loss, in terms of both NPV and VIR. Conversely, in an optimistic scenario (P10), implementing any of these processes in the Nigerian heavy-oil belt would yield large returns on investment although steam-alone is the most attractive in terms of NPV while the VIR favours the SAF method.

Overall, in terms of NPV and VIR, the results of **Table 10.7** indicate that the SAC process is the least risky. Therefore, on the basis of the example considered in this research, it may be concluded that the SAC process is the most robust among the three processes assessed for the exploitation of the Nigerian heavy-oil deposit, as it is currently understood.

Although we have been using the terms economic and commerciality interchangeably, they are not exactly the same. Technically, while a project is economic as long as its NPV > 0 (and VIR > 0), commerciality is a bit more tricky as it depends on some threshold i.e. NPV > x_1 and VIR > x_2, with the quantities x_1 and x_2 varying between investors. However, regardless of the subtle differences in these screening indicators, the three techniques are generally economic and apparently, commercially feasible for the Nigerian accumulation.

In spite of the several efforts and resources, which include incentives and competitive policies (Vanguard, 2010; KPMG, 2008), at attracting investments to the Nigerian bitumen belt, not much success has been recorded (Lawal, 2011a; Ayodele, 2007; 2006). This is partly because of limited knowledge on the appropriate recovery method and the commerciality of the belt (Ayodele, 2006). In the light of this, we recommend that the Nigerian government fund a demonstration (pilot) project with the primary objectives of assessing the technical and commercial feasibility of the SAC technique in the heavy-oil belt. In this way, the reservoir-model uncertainties would be reduced, thus narrowing the range of the commercial forecasts. With a relatively simple pilot of the same scope (2-wellpair sector development) as that investigated in this research, the CAPEX, including contingencies, is estimated to be within $ 20-40 mln. With this relatively small investment, there are chances that the much sought-after diversification of the upstream sector of the Nigerian petroleum industry could be realised in no distant time.

The finding that the factors related to the fiscal regime, vis-à-vis royalty and tax rates, do not have much impacts on the commerciality of the current example is particularly instructive. This implies that the current strategy in which the Nigerian government relies on fiscal instruments to attract investments to its undeveloped heavy-oil sector (Vanguard, 2010), may not be optimum. In line with this work, and as argued above, a more pragmatic approach is to fund relevant well-monitored demonstration projects evaluating the technical and commercial feasibility of the promising SAC and the related steam-alone and SAF techniques. In our opinion, the results from these pilot projects should serve as a motivating factor for investors, for instance see the Dover (Underground Test Facility) pilot in relation to the proliferation of SAGD technology in Canada and elsewhere (O'Rourke *et al.*, 1999, 1997; Butler, 1998; Edmunds *et al.*, 1994). Additionally, the results should be able to guide the formulation of informed and realistic policies for the sustainable development of the Nigerian heavy-oil industry.

Finally, it is noteworthy that the results of the current analysis should be taken with caution, as there are huge uncertainties with the range of input factors, especially the cost estimates. Considering that most of the estimates are based on the well-established Canadian industry, they may not be quite representative of Nigeria which does not yet have a heavy-oil industry. However, we are of the opinion that as more representative dataset becomes available, the ideas presented in this work would be found useful.

10.4 Chapter Summary

The economics and commercial risks of the steam-alone, SAC and SAF recovery methods have been investigated, using NPV and VIR as measures of project feasibility. Within the range examined, the uncertainties associated with the reservoir model, oil price, OPEX and CAPEX are found to be the main determinants of the commercial risks of the project. The fiscal policies do not appear to have much impact, at least within the parameter space examined.

With at least 55% chance of economic success (NPV > 0, VIR > 0), the analysis indicates that the three processes are commercially viable for the in-situ exploitation of the Nigerian bitumen. However, in terms of the commercial risks, the SAC process is the most robust. On this evidence, the proposed recovery method of alternating-injection of steam and CO_2 has high prospects in the Nigerian tar-bearing belt and similar heavy-oil plays elsewhere. Hence, the process is worthy of further investigation. In line with this promising assertion, some areas of improvement are outlined in the next chapter.

Chapter 11

Conclusion and Future Work

In this work, two new steam-based processes have been introduced and investigated for the in-situ exploitation of heavy-oil resources. These are: (i) alternating-injection of steam and CO_2 (SAC); and (ii) alternating-injection of steam and flue-gas (SAF). Compared to the steam-alone process in terms of oil recovery, environmental performance and economics, the new processes show much promise, with the SAC being more competitive while the SAF being only slightly less attractive. To reach this headline conclusion, a number of issues were addressed. The following is a summary of the main findings from this work.

In order to address the limitations of the current treatments of the heat transport during the steam-injection processes, we include the concepts of first-contact condensation (FCC) and multiple-contact condensation (MCC) into the traditional 1-D heat equations. To solve the resulting equations, numerical schemes, with well-defined convergence criteria, have been developed. With these enhancements, we show that laboratory and field observations are better rationalised.

In order to account for thermal losses in petroleum reservoirs, the new heat-transport equations have been extended to non-isothermal boundaries. We formulate new models for estimating heat losses through the overburden and underburden of reservoirs undergoing steam-injection operations. Conditions under which petroleum reservoirs may be analysed as adiabatic systems are also provided. From parametric studies, the relative influence of several reservoir and operating parameters is quantified. In principle, the deductions from these parametric studies should improve the design and management of steam-injection projects.

As CO_2 and flue-gas are known asphaltene precipitants, the mechanisms and impacts of asphaltene-induced impairment of formation permeability have been studied. With regards to the physics of asphaltene deposition, we distinguish between closed (non-flowing) and open (flowing) systems. As a result, three new models have been formulated for describing asphaltene-induced impairments in porous media. Application of the models to rationalise the experimental results from common porous media, which include sandstone, carbonate and glass-bead, validates their robustness. As further assessment of the underlying assumptions of our impairment models, we designed and performed capillary-flow experiments, which approximate asphaltene deposition at pore scale. The validity of most of the main theoretical assumptions has been confirmed.

As a case study for assessing the feasibility of the SAC and SAF processes, the Nigerian heavy-oil deposit is considered. Within the limits of data uncertainties, detailed (3-D) reservoir-simulation models are constructed for this deposit which, prior to the current study, may not have such models, at least in the public domain. Employing rigorous deterministic and probabilistic methods, the impacts of the various reservoir parameters on the performances of the steam-alone and

alternating-injection processes have been quantified. From these results, a realistic set of simulation models, covering all the possible combinations of uncertainties, have been constructed.

On the basis of the simulation models and detailed analyses, the optimum combination of geometric (well-related) and operating parameters has been established for the steam-alone process. Effectively, the optimum steam-alone development defines the amount of CO_2 and flue-gas emissions that need to be mitigated by the SAC and SAF processes. Given the CO_2 "load" and the optimum geometric parameters, we conduct optimisation studies on the operating variables of the SAC and SAF processes.

With simulation studies, the effects of reservoir and fluid heterogeneities, in-situ deasphalting and dispersion on the dynamics of the steam-alone, SAC and SAF processes have also been investigated. While all the processes are generally sensitive to heterogeneities, the oil-viscosity reduction that accompanies the in-situ precipitation of asphaltenes significantly enhances the productivity of the alternating-injection processes.

Finally, using the current fiscal policy on the Nigerian petroleum industry and reasonable estimates of project costs, carbon tax / credit and oil price, the economics and risks of the steam-alone, SAC and SAF processes have been examined. Within the range of parameters evaluated, these preliminary results indicate that the increasing order of economic competitiveness and commercial robustness of the processes is SAF < steam-alone < SAC. However, given the uncertainties in the input data and fiscal instruments, further studies are warranted.

11.1 Specific Conclusions

On the main issues investigated in this research, the following is an outline of the key conclusions that have been drawn.

11.1.1 Heat-Transport Modelling

- Condensation is an important contributor to the heat transport in steam-based processes. The inclusion of this term in the traditional conductive-convective equations significantly improves their performance. This eliminates the need to use unrealistic effective permeability and effective thermal diffusivity to rationalise experimental results.

- The presence of either CO_2 or flue-gas jeopardises the heat-carrying capacity of steam, hence the rate of reservoir-heating in steam-based operations. This effect is primarily due to the ineffective steam condensation as a result of the presence of these non-condensing gases. Additionally, because these gases have a lower product of specific-heat capacity and mobility compared to steam, they effectively reduce the heat-carrying capacity of steam, even when steam is not condensing.

- Except in low-permeability formations where the flow of the heating fluid is significantly impeded, the heat transport ahead of the advancing thermal front is a combination of

conduction, convection and condensation. Hence, the general assumption of conduction-dominated transport ahead of the front may not be valid.

- In the analysis of petroleum reservoirs undergoing steam-injection, the assumption of local thermal equilibrium (LTE) is valid within typical time scales. This may only be threatened if the injected fluid occupies less than 0.08% of the pore diameter or the heat-transfer coefficient of the pore-saturating fluid is below 0.05 W/m^2K.

- In the examples considered, for a buoyancy-driven constant-rate process, pressure-drop due to steam flow does not have significant impact (< 5%) on reservoir-heating. But, with non-condensing heat-carrying fluids, such as CO_2 and flue-gas, effects of pressure-drop would only be significant (> 5%) if the formation thickness exceeds 100 m.

- For a non-adiabatic reservoir, as the effectiveness of the heating process increases, it becomes less sensitive to the loss of heat to the adjacent formations. Generally, the effectiveness of the heating process increases with the quality of the injectant (steam > CO_2 > flue-gas), formation permeability and the thermal resistance of the boundaries.

11.1.2 Asphaltene-Induced Impairment

- The rate of asphaltene-induced impairment is controlled by rock and fluid properties. However, the initial asphaltene-content of the crude and the hydraulic quality of the formation determine the ultimate extent of permeability impairment.

- Compared to light crudes, rocks containing heavy oils, despite their higher asphaltene concentrations, are inherently less vulnerable to asphaltene-induced damage because of their greater ability (viscous-drag effects) to retard deposition.

Within the limits of experimental uncertainties, the capillary-flow experiments indicate that:

- Within the flow regime examined ($0.5 < N_{Re} < 20$), the deposition rate depends on the flowrate (i.e. rate of particle supply) as well as the nature and concentration of the precipitant. However, for the same cumulative injection, the amount of deposits is independent of flowrate.

- Asphaltene deposition is not a first-contact process. There is some time lag between the coming into contact of the asphaltene-laden crude and the precipitant, and the eventual deposition. In general, the time lag depends, among other factors, on the nature and concentration of precipitants as well as rock and crude characteristics.

- In the absence of significant particle erosion and entrainment, the deposition of asphaltenes in a straight and relatively short (127 mm used in this study) capillary tube is reasonably uniform.

- The current model (Broseta *et al.*, 2000) for estimating deposit thickness from pressure data may yield non-physical results. However, an improved model has been developed.

11.1.3 Numerical Reservoir-Simulations

Within the parameter space investigated:

- Reservoir geometry, permeability distribution as well as relative-permeability and fluid models are the main subsurface parameters controlling the responses of the steam-injection and alternating-injection processes.
- Where heating is the main viscosity-reduction mechanism, dispersion would only be beneficial if the dispersing components are good heat carriers and at the same time miscible with the oil under reservoir conditions. Otherwise, dispersion may be detrimental to oil recovery.
- Generally, injecting either CO_2 or N_2 in alternating cycles with steam would only improve oil recovery if the crude is very viscous (due to high initial asphaltene-content) and there is significant in-situ deasphalting such that the resulting viscosity reduction far outweighs the plugging of pores by the deposits. Otherwise, oil production is slightly jeopardised but there are considerable savings in steam consumption, water-handling and CO_2 emissions, especially for the SAC process.
- In the cases of SAC and SAF, the additional reduction of oil-viscosity by dilution is not significant. This is primarily due to the relatively high operating temperature, which inhibits CO_2 and N_2 from attaining significant miscibility (*K-value*) with oil.
- In terms of underground CO_2 storage, the SAC process is much more effective than the SAF. The poorer performance of the latter is attributed to the large volume of N_2 (~ 90%), which effectively takes up the pore volume that would have been used for CO_2.
- With predicted oil recovery factor in the range 30-81%, which compares with typical steam-based performances, the three processes of SAC, SAF and steam-alone can be regarded as technically feasible, at least for the Nigerian system investigated.

11.1.4 Economics and Risk Analysis

Within the limits of this study:

- Reservoir model (profiles of injection, production and CO_2 storage), oil price and costs are the primary determinants of project economics and commercial risks.
- The three processes are commercially feasible. However, in terms of economics and robustness against commercial risks, the order is SAC > steam-alone > SAF.

11.2 Future Work

In order to advance the contributions made by the current research, the following is a summary of some of the specific areas that worth further studies.

11.2.1 Heat-Transport Modelling

- Extend the current one-dimensional models to 3-D.
- Incorporate other drive mechanisms such as pressure gradient. Modelling currently limited to buoyancy drive.
- Include the effects of oil vapourisation and possible re-vapourisation of steam condensates. These are currently neglected.
- Incorporate reversal of heat flow between the reservoir and surroundings. Current modelling takes the surroundings as infinite heat sinks.

11.2.2 Asphaltene-Induced Impairment

- On the theoretical modelling:
  i. It would be interesting to incorporate the following features:
     - effects of erosion, temperature and dispersion. These are currently ignored;
     - higher-order kinetic models. Current treatment is based on first-order kinetics.
  ii. Decouple the kinetics of the precipitation, flocculation and deposition steps. The current analysis uses a lumped kinetic model. With decoupling, the relative contribution of the different steps to the overall damage would be quantified. This could lead to the development of better control strategies for problems relating to asphaltene and other particulates.
  iii. Develop techniques for upscaling asphaltene-deposition parameters from laboratory-scale experiments to field applications.
- On the experimental studies, consider:
  i. effects of capillary material and geometry (diameter and length). Current work is based on glass capillary of fixed geometry;
  ii. the use of CO_2 and flue-gas under anticipated reservoir conditions;
  iii. the use of “real” viscous crudes, rather than the diluted samples in the current experiments;
  iv. impacts of tortuosity and other aspects of flow such as flow pattern and regime - current studies limited to $0.5 < N_{Re} < 20$;
  v. impacts of viscosity changes on the estimated hydrodynamic thickness of deposits.

vi. conducting compositional analysis of the effluent stream. With the results, the amount of deposits can be obtained by difference. This would further validate our uniform-deposit thickness model.

11.2.3 Numerical Reservoir-Simulations

- Consider field-scale models that incorporate detailed heterogeneities. Only vertical (layering) heterogeneities have been modelled.
- Assess the influence of potential asphaltene-induced wettability alteration as well as compositional-dependency of relative permeabilities. These are currently not considered.
- Include geomechanical effects. In present treatments, they are insignificant.
- Consider carbonate reservoirs. Study currently limited to sandstone formations.

11.2.4 Feasibility of Alternating-Injection of Steam and CO_2

Although the current study has shown the feasibility (and risks) and competitiveness of the SAC process, it is necessary to conduct further assessments on the basis of more representative technical and economic datasets. Further investigations in the laboratory and the field are also recommended.

Appendix A

Thermophysical and Transport Properties

For rock matrix, density (ρ), isobaric specific heat capacity (c_p) and thermal conductivity (λ) are estimated at the average of the initial and injection temperatures.

For heavy oil, the following are Gambill (1957) and Cragoe (1929) correlations used to estimate specific heat and thermal conductivity respectively. Oil properties are referenced to the average of initial reservoir and injection temperatures. All the terms and their units are defined in the Nomenclature.

$$c_{po} = \gamma_o^{-0.5}\left(0.3881 + 0.00045\ T\right);\ \ \lambda_o = 1.62\left[1 - 3\times10^{-4}\left(T - 32\right)\right]/\gamma_o\ . \qquad \text{(A.1)}$$

Steam properties are estimated at injection temperature. Density and viscosity are estimated with the following correlations, valid within 273.15≤T≤645 K (Tortike and Farouq-Ali, 1989). For specific heat, the model of Kyle (1984), with validity range of 273.15≤T≤1800.15 K, is used.

$$\rho_s = \exp\left(-93.7072 + 0.833941T - 3.20809x10^{-3}T^2 + 6.57652x10^{-6}T^3 - 6.93747x10^{-9}T^4\right) + 2.97203x10^{-12}T^5\ , \text{(A.2)}$$

$$\mu_s = -5.46807x10^{-4} + 6.8949x10^{-6}T - 3.35009x10^{-8}T^2 + 8.29842x10^{-11}T^3 - 9.9706x10^{-14}T^4 + 4.71914x10^{-17}T^5\ , \quad \text{(A.3)}$$

$$c_{p_s}{}' = 32.24 + 1.923x10^{-3}T + 1.055x10^{-5}T^2 - 3.595x10^{-9}T^3\ . \qquad \text{(A.4)}$$

Connate water and condensate are treated as pure water. Referenced to the average of initial reservoir and injection temperatures, Tortike & Farouq-Ali (1989) models are used for water density and thermal conductivity. However, specific heat is assumed constant at 4200 J kg^{-1} K^{-1}. Over the range 0 - 300 ^oC, there is less than 2% change in specific heat (Smith and Van Ness, 1975).

$$\rho_w = 3786.31 - 37.2487T + 0.196246T^2 - 5.04708x10^{-4}T^3 + 6.29368x10^{-7}T^4 - 3.0848x10^{-10}T^5\ , \qquad \text{(A.5)}$$

$$\lambda_w = 3.51153 - 4.43602x10^{-2}T + 2.41233x10^{-4}T^2 - 6.05099x10^{-7}T^3 + 7.22766x10^{-10}T^4 - 3.37136x10^{-13}T^5\ . \qquad \text{(A.6)}$$

As indicated for steam, transport properties of CO_2 and N_2 are referenced to the injection temperature. Specific heats are computed from the model of Kyle (1984), with applicability range of $273.15 \le T \le 1800.15$ K. CO_2 and N_2 viscosity are estimated from the rigorous models of Vesovic *et al.* (1990) and Lemmon & Jacobsen (2004) respectively, valid over all liquid and vapour states as well as the critical point. However, we ignore the critical enhancement terms because their impact is negligible (maximum deviation <4%).

$$c_{p_{CO_2}}{}' = 22.26 + 5.981x10^{-2}T - 3.501x10^{-5}T^2 + 7.469x10^{-9}T^3\ , \qquad \text{(A.7)}$$

$$c_{p_{N_2}}{}' = 28.90 - 0.1571x10^{-2}T + 0.8081x10^{-5}T^2 - 2.873x10^{-9}T^3 . \quad \text{(A.8)}$$

Density is estimated from the real-gas equation of state. However, the compressibility factors are based on the acentric factor theory (Smith and Van Ness, 1975; Pitzer and Brewer, 1961).

In estimating the specific latent heat of steam condensation L_c (in J/kg) and specific enthalpy of water h_i (in J/kg), we use the correlations of Tortike and Farouq-Ali (1989), valid within the range $273.15 \leq T \leq 645$ K.

$$L_c = 1000\left(7184500 + 11048.6T_s - 88.4050\,T_s^{\,2} + 0.162561\,T_s^{\,3} - 1.21377\,x10^{-4}T_s^{\,4}\right)^{1/2} . \quad \text{(A.9)}$$

$$h_i = 1000\left(\begin{array}{l} 23665.2 - 366.232\,T_i + 2.26952\,T_i^{\,2} - 0.00730365\,T_i^{\,3} + 1.30241\,x10^{-5}T_i^{\,4} \\ - 1.22103\,x10^{-8}T_i^{\,5} + 4.70878\,x10^{-12}T_i^{\,6} \end{array}\right) . \quad \text{(A.10)}$$

where T_s and T_i are steam and initial-reservoir temperatures, respectively.

Although the L_c correlation is accurate within 1.5%, it is slightly less accurate than the correlations of Ejiogu and Fiori (1987) as well as Chien (1992). However, its wider temperature range of applicability, continuity of the function over this range and the lower number of coefficients are important advantages of the selected correlation over the others.

A.1 Mixing Rules

For flue gas mixtures (CO_2 and N_2), ρ and c_p are volume- and mass-weighted, respectively. However for viscosity, the model of Wilke (1950), as presented by Bird *et al.* (1960), is used. Bulk reservoir thermal diffusivity α, and volumetric heat capacity ρc_p, are estimated as follows.

$$\alpha = (1-\phi)\alpha_r + \phi\left(s_o\alpha_o + s_w\alpha_w\right) , \quad \text{(A.11)}$$

$$\rho c_p = (1-\phi)\rho_r c_{p_r} + \phi\left(s_o\rho_o c_{p_o} + s_w\rho_w c_{p_w}\right). \quad \text{(A.12)}$$

where s_o and s_w are oil and water saturations, respectively.

Appendix B

Estimation of Condensation Rate

For any operation, the rate of condensation per unit volume m_c, is not known beforehand. Hence, we present a simple analysis to estimate it. Considering the uncertainties in its estimate, m_c would ideally be one of the sensitivity parameters for history-matching project performance.

From the steam mass balance, we have

$$-\frac{\partial(\rho_s v_s)}{\partial z} = m_c + \rho_s \phi \frac{\partial s_s}{\partial t}. \tag{B.1}$$

Assuming steam condensation is always at steady state, the following is valid for the condensation flux, whose impact is assumed to be felt throughout the plane above the injector.

$$\int_{z=0}^{z=z_f(t)} m_c dz = -\int_{\rho_s v_s = f_s \rho_s v_s}^{\rho_s v_s = (1-f_c) f_s \rho_s v_s} d(\rho_s v_s), \tag{B.2}$$

where $z_f(t)$ is the instantaneous vertical distance covered, referenced to the injection point, by the condensable heating-fluid (front). The interval of the right-hand-side integral indicates that at injection point, steam mass flux rate (kg m^{-2} s^{-1}) is at maximum. However, just at the front, only uncondensed steam remains. f_c is the mass fraction of injected steam that effectively condenses. Evaluation of **Eq. B.2** gives

$$m_c = \frac{f_c f_s \rho_s v_s}{z_f}. \tag{B.3}$$

Appendix C

Spatial Variation of Latent Heat Due to Pressure-Drop

Recall that the temperature gradient of the steam depends on the prevailing pressure gradient and temperature-pressure relationship as follows:

$$\frac{dT}{dz} = \frac{dT}{dP}\frac{dP}{dz}, \tag{C.1}$$

and under a buoyancy drive, the pressure gradient is given by

$$\frac{dP}{dz} = -(\Delta\rho)g\ . \tag{C.2}$$

For saturated steam, its temperature and pressure are related by (Ejiogu and Fiori, 1987),

$$T = 273.15 + 7.0373P^{0.2350}, \tag{C.3}$$

where P and T are saturation pressure and temperature in Pa and K, respectively.

Here, we have modified the original correlation in order to have it in SI units. Although Ejiogu and Fiori (1987) limited the validity of this correlation to 3.4-17.2 MPa (514-626 K), we found that it still performs satisfactorily down to 0.1 MPa (373 K) and up to 22.0 MPa (646 K), with a maximum deviation of 5.6% in the extrapolated region.

Manipulating **Eqs. C.1 - C.3** in terms of saturation temperature T_s, we obtain

$$\frac{dT}{dz} = -948.524\,(\Delta\rho)g\,(T_s - 273.15)^{-3.2553}, \tag{C.4}$$

where T_s is saturation (injection) temperature, K.

The accompanying change in latent heat is given by

$$\frac{dL_c}{dz} = \frac{dL_c}{dT}\frac{dT}{dz}\ . \tag{C.5}$$

Employing the latent-heat correlation of Tortike and Farouq-Ali (1989), presented here as **Eq. A.9**, we obtain:

$$\frac{dL_c}{dT} = \frac{5x10^5\left(11048.6 - 176.810T + 0.487683\,T^2 - 4.85508\,x10^{-4}T^3\right)}{L_c}. \tag{C.6}$$

The combination of **Eqs. C.4** – **C.6** yields the following expression, which can be used to estimate the gradient of latent heat resulting from flow-induced drop in saturated-steam pressure and temperature, T_s.

$$\frac{dL_c}{dz} = \frac{-46.5251x10^5(\Delta\rho)\left(11048.6 - 176.810T_s + 0.487683T_s^{\,2} - 4.85508x10^{-4}T_s^{\,3}\right)}{\left(7184500 + 11048.6T_s - 88.4050T_s^{\,2} + 0.162561T_s^{\,3} - 1.21377x10^{-4}T_s^{\,4}\right)^{1/2}\left(T_s - 273.15\right)^{3.2553}} \quad \text{(C.7)}$$

Appendix D

Lumped-Parameter System Analysis

As lumped sub-systems, the reservoir and surroundings are modelled as individual thermal capacitors, which have thermal resistors at their inlets (**Fig. D.1**). In terms of heat flow, the reservoir and surroundings are assumed to be in series.

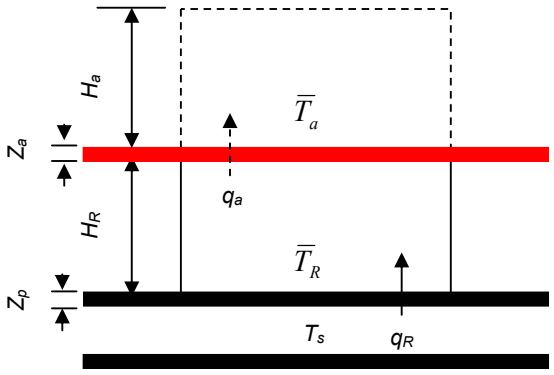


Fig. D.1: Lumped Model of Injector-Reservoir-Surroundings System

D.1 Reservoir and Surroundings are Non-Interacting

In this case, the reservoir dynamics affect the surroundings but the converse is not true. The following transfer functions relate the temperatures of the sub-systems in the Laplace domain (Coughanowr, 1991; Stephanopoulos, 1984). Here, we are interested in how the reservoir and surroundings respond to a temperature-change at the injection plane.

$$G_R(s) = \frac{\bar{\bar{T}}_R(s)}{\bar{\bar{T}}_s(s)} = \frac{1}{\tau_R s + 1}, \tag{D.1}$$

$$G_R(s) = \frac{\bar{\bar{T}}_a(s)}{\bar{\bar{T}}_R(s)} = \frac{1}{\tau_a s + 1}, \tag{D.2}$$

where T_s, T_R, and T_a are the temperatures of the injection plane, reservoir and surroundings, respectively. For the reservoir, its time-constant τ_R is given by

$$\tau_R = R_{t_R} C_{t_R}, \tag{D.3}$$

where the thermal resistance R_{tR} and capacitance C_{tR} are

$$R_{t_R} = Z_p / \kappa_p, \tag{D.4}$$

$$C_{t_R} = \rho_R c_{p_R} H_R, \tag{D.5}$$

in which H_R, c_{pR} and ρ_R are the reservoir thickness, specific-heat and density, respectively. Z_p and κ_R are the thickness and thermal-conductivity of the injector-reservoir boundary, respectively. Thus, both reservoir and boundary parameters characterise the time-constant which, in turn, influences heat flow.

In the case of reservoir-surroundings system, **Eqs. D.3-D.5** also apply but with appropriate parameters, which include ρ_a, H_a and Z_a. Here, C_{ta} refers to the surroundings while R_{tR} relates to the caprock (boundary).

For this *non-adiabatic* process, we combine **Eqs. D.1** and **D.2** to obtain the transfer-function for the injector-surroundings system (Stephanopoulos, 1984)

$$G(s) = \frac{\bar{T}_a(s)}{\bar{T}_s(s)} = \frac{1}{\tau_R s + 1} \cdot \frac{1}{\tau_R s + 1} \equiv \frac{1}{\tau^2 s^2 + 2\xi\tau s + 1}, \tag{D.6}$$

$$\tau = \sqrt{\tau_R \tau_a}\ ;\ \ \xi = \frac{(\tau_R + \tau_a)}{2\tau}, \tag{D.7}$$

where ξ is the damping coefficient.

For a step-increase in T_s, and arbitrary values for the reservoir and surroundings parameters, we simulate **Eqs. D.1** and **D.6**, resulting in the responses in **Fig. D.2**, which highlights significant delay between the responses. Here, the response-time ratio is ~ 200, implying that if it takes the reservoir ~ 5 years to reach a given average temperature, the surroundings would take about 1000 years for the same response. This is the characteristic transfer-lag between the reservoir and surroundings. This result justifies our assumption that the heat received from the injector, through the reservoir, does not change the sink temperature significantly.

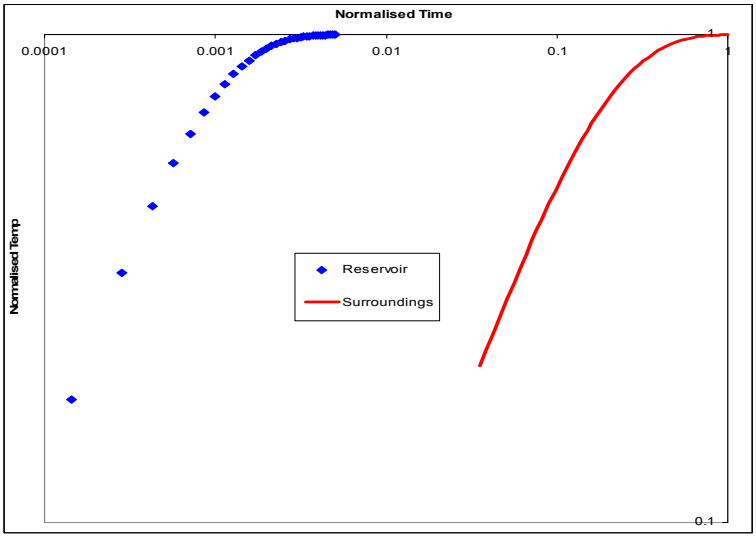


Fig. D.2: Reservoir and Surrounding Responses (Non-Interacting Subsystems in Series)

D.2 Reservoir and Surroundings Interact

Similar analysis for the case in which there is a two-way heat exchange between the surroundings and reservoir yields the following transfer functions

$$\frac{\bar{\bar{T}}_R}{\bar{\bar{T}}_s} = \frac{1+\tau_a s}{(\tau_a \tau_R)s^2 + (\tau_a + \tau_R + C_{t_a} R_{t_R})s + 1}, \tag{D.8}$$

$$\frac{\bar{\bar{T}}_a}{\bar{\bar{T}}_s} = \frac{1}{(\tau_a \tau_R)s^2 + (\tau_a + \tau_R + C_{t_a} R_{t_R})s + 1}. \tag{D.9}$$

These functions indicate that the surroundings dynamics is second-order, while the reservoir is approximately first-order ("first-over-second" order).

For a step-increase in T_s, and a set of reservoir and sink parameters, we solve **Eqs. D.8** and **D.9** (Marlin, 1995), resulting in the responses illustrated in **Fig. D.3**. As already noted in the case of interacting systems, there is significant transfer-lag between the reservoir and surroundings.

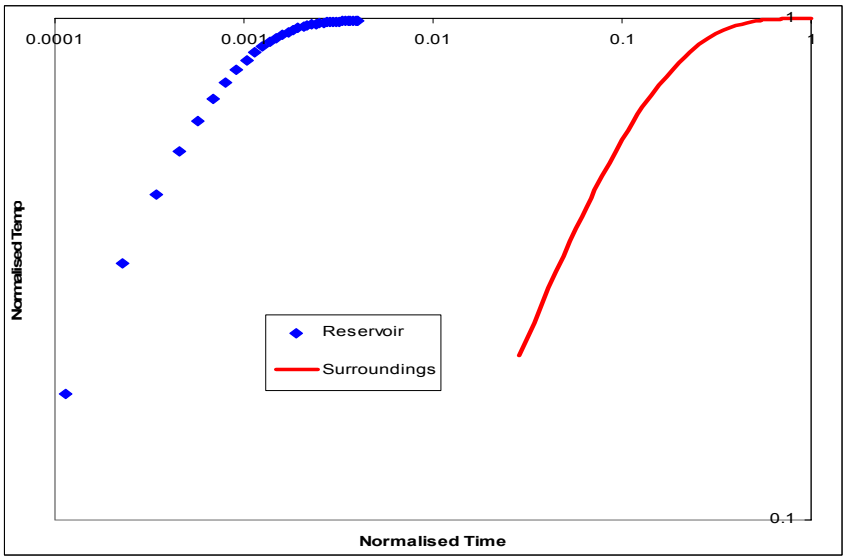


Fig. D.2: Reservoir and Surrounding Responses (Interacting Subsystems in Series)

Appendix E

Estimating Heat-Transfer Coefficients in Porous Media

Neglecting fluid-viscosity changes in a laminar flow (N_{Re} < 2100), heat-transfer coefficient for tubes can be estimated from (Sinnott, 1993; Sieder and Tate, 1936):

$$h_i \approx 1.86 \frac{\kappa}{D}\left[\frac{\rho v c_p D^2}{L\kappa}\right]^{1/3}. \quad \text{(E.1)}$$

As porous media and a bundle of tubes are fairly analogous (Civan, 2007), the correlation is useful. Ignoring tortuosity while considering a gravity-driven system (Darcy velocity), **Eq. E.1** becomes:

$$h_i \approx 1.48\kappa\left[\frac{\phi}{k}\right]^{1/2}\left[\frac{\rho c_p k^2 g(\rho - \rho_b)}{\kappa L \mu\phi}\right]^{1/3}, \quad \text{(E.2)}$$

in which the average pore-diameter is estimated from (Stolz and Graves, 2003):

$$D = 2\sqrt{k/\phi}, \quad \text{(E.3)}$$

where g, L, ϕ and k are gravitational acceleration, sink thickness, porosity and permeability, respectively; κ is fluid thermal conductivity; ρ, μ and c_p are sink-fluid density, viscosity and specific heat, respectively, at the injection temperature; ρ_b is sink-fluid density evaluated at the bulk temperature, $(T_i + T_s)/2$. For part of the sink within the reservoir (h_{ic}, h_{ib}), L is the thickness of the non-oil column e.g. gas-cap, bottom-water.

We consider gas and liquid-saturated sinks while using CH_4 and water as model gas and liquid, respectively. Water properties are estimated from the correlations of Tortike and Farouq Ali (1989).

In estimating gas specific heat, conductivity, and viscosity, pressure effects are neglected. Gas (CH_4) specific heat is given by the following expression, modified from Kyle (1984):

$$c_{pg} = 1243.1 + 3.14T + 7.93x10^{-4}T^2 - 6.88x10^{-7}T^3. \quad \text{(E.4)}$$

We adapt the Chapman-Enskog low-density gas formulae (Bird *et al*., 1960). In the case of CH_4, we derive

$$\kappa_g = 1.4243x10^{-3}\sqrt{T}/\Omega_\kappa, \quad \text{(E.5)}$$

$$\mu_g = 7.3184x10^{-7}\sqrt{T}/\Omega_\mu, \quad \text{(E.6)}$$

where T is absolute temperature, and $\Omega_\mu = \Omega_\kappa = \Omega_{\mu,\kappa}$ with $\Omega_{\mu,\kappa}$ being the collision integral.

Given the data in Bird *et al*. (1960), we fit the following piecewise functions to estimate methane $\Omega_{\mu,\kappa}$. Within the stated intervals, these correlations have accuracy of 6 and 1%, respectively.

$$\Omega_{\mu,\kappa} \approx 1.618\left(\varepsilon T\right)^{-0.4183}, \quad 0.3 \le \left(\varepsilon T\right) < 4.0, \tag{E.7}$$

$$\Omega_{\mu,\kappa} \approx 1.189\left(\varepsilon T\right)^{-0.1542}, \quad 4.0 \le \left(\varepsilon T\right) \le 100, \tag{E.8}$$

where ε is the Lennard-Jones parameter which, for CH_4, is ~ 7.3 x 10^{-3} K^{-1} (Bird *et al*., 1960).

Appendix F

Sensitivity of Other Processes to Boundary Thermal Losses

F.1 Non-Condensing Steam

Table F.1: Full-Factorial Design for Saturants in Non-Condensing Steam Process

Run	Base Sink	Bottom	Cap	Cap Sink	Steady-state Temp (°C)	Steady-state Time (days)	Steady-state Deviation (%)
1	*G*	*G*	*L*	*L*	*243.9*	*960*	*2.4*
2	L	G	G	L	244.9	820	2.0
3	G	L	L	G	245.8	870	1.7
4	G	L	L	L	243.8	770	2.5
5	G	G	G	L	244.9	770	2.0
6	L	G	L	G	245.7	780	1.7
7	G	L	G	L	244.9	780	2.0
8	G	L	G	G	246.3	820	1.5
9	*L*	*L*	*L*	*L*	*243.7*	*750*	*2.5*
10	*G*	*G*	*G*	*G*	*246.3*	*800*	*1.5*
11	L	G	L	L	243.8	800	2.5
12	L	G	G	G	246.3	890	1.5
13	L	L	L	G	245.7	840	1.7
14	*L*	*L*	*G*	*G*	*246.2*	*800*	*1.5*
15	G	G	L	G	245.8	810	1.7
16	L	L	G	L	244.8	770	2.1
17	Adiabatic boundaries $(U_b = U_c = 0)$				250	1980	0
18	Isothermal boundaries				223	1460	10.8

F.2 Flue Gas (50% CO_2, 50% N_2)

Table F.2: Full-Factorial Design for Saturants in Flue-Gas Process

Run	Base Sink	Bottom	Cap	Cap Sink	Steady-state Temp (°C)	Steady-state Time (days)	Steady-state Deviation (%)
1	*G*	*G*	*L*	*L*	*234.9*	*1740*	*6.0*
2	L	G	G	L	236.8	1540	5.3
3	G	L	L	G	238.6	1620	4.6
4	G	L	L	L	234.9	1920	6.0
5	G	G	G	L	236.9	1640	5.2
6	L	G	L	G	238.6	1700	4.6
7	G	L	G	L	236.9	1680	5.2
8	G	L	G	G	239.8	1760	4.1
9	*L*	*L*	*L*	*L*	*234.8*	*1960*	*6.1*
10	*G*	*G*	*G*	*G*	*239.8*	*1700*	*4.1*
11	L	G	L	L	234.8	1580	6.1
12	L	G	G	G	239.7	1600	4.1
13	L	L	L	G	238.5	1600	4.6
14	*L*	*L*	*G*	*G*	*239.7*	*1760*	*4.1*
15	G	G	L	G	238.6	1580	4.6
16	L	L	G	L	236.8	1700	5.3
17	Adiabatic boundaries $(U_b = U_c = 0)$				250	1980	0
18	Isothermal boundaries				223	1460	10.8

Appendix G

Numerical Integration of Asphaltene-Deposition Model

In order to integrate **Eq. 5.31** over z, we resort to Simpson's rule (Burden and Faires, 2007) to obtain an approximate analytical expression for $\bar{x}(t)$,

$$\bar{x}(t) \approx \frac{x_a}{6}\left\{\exp\left(-\beta_1 e^{-t/\tau} - \lambda_o L + \beta_1 e^{\left(\frac{\phi L}{v_c\tau}-\frac{t}{\tau}\right)}\right) + 1 + 4\exp\left(-\beta_1 e^{-t/\tau} - \frac{\lambda_o L}{2} + \beta_1 e^{\left(\frac{\phi L}{2v_c\tau}-\frac{t}{\tau}\right)}\right)\right\} \quad , \text{(G.1)}$$

where the parameter β_1, is given by:

$$\beta_1 = \lambda_o v_c \tau/\phi\,. \quad \text{(G.2)}$$

with respect to the time-integration of **Eq. G.1** in **Eq. 5.21**, we apply Simpson's rule again:

$$\bar{x}_p(t) \approx \frac{\beta_2 t}{36}\left\{\begin{array}{l} 5 + \exp\left(-\beta_1 e^{-t/\tau} - \lambda_o L + \beta_1 e^{\left(\frac{\phi L}{v_c\tau}-\frac{t}{\tau}\right)}\right) + 4\exp\left(-\beta_1 e^{-t/\tau} - \frac{\lambda_o L}{2} + \beta_1 e^{\left(\frac{\phi L}{2v_c\tau}-\frac{t}{\tau}\right)}\right) \\ + 4\exp\left(-\beta_1 e^{-t/2\tau} - \lambda_o L + \beta_1 e^{\left(\frac{\phi L}{v_c\tau}-\frac{t}{2\tau}\right)}\right) + 16\exp\left(-\beta_1 e^{-t/2\tau} - \frac{\lambda_o L}{2} + \beta_1 e^{\left(\frac{\phi L}{2v_c\tau}-\frac{t}{2\tau}\right)}\right) \\ - \exp\left(\frac{-t}{\tau}\right) - 4\exp\left(\frac{-t}{2\tau}\right) - \exp\left(-\beta_1 e^{-t/\tau} - \lambda_o L - \frac{t}{\tau} + \beta_1 e^{\left(\frac{\phi L}{v_c\tau}-\frac{t}{\tau}\right)}\right) \\ - 4\exp\left(-\beta_1 e^{-t/\tau} - \frac{\lambda_o L}{2} - \frac{t}{\tau} + \beta_1 e^{\left(\frac{\phi L}{2v_c\tau}-\frac{t}{\tau}\right)}\right) \\ - 4\exp\left(-\beta_1 e^{-t/2\tau} - \lambda_o L - \frac{t}{2\tau} + \beta_1 e^{\left(\frac{\phi L}{v_c\tau}-\frac{t}{2\tau}\right)}\right) \\ - 16\exp\left(-\beta_1 e^{-t/2\tau} - \frac{\lambda_o L}{2} - \frac{t}{2\tau} + \beta_1 e^{\left(\frac{\phi L}{2v_c\tau}-\frac{t}{2\tau}\right)}\right) \end{array}\right\}$$

. (G.3)

The parameter β_2, is defined as follows:

$$\beta_2 = \lambda_o v_c x_a\,. \quad \text{(G.4)}$$

For the time-constant, the equivalent number of PV required to be injected to reach some 63.2% of the ultimate filtration coefficient λ_o is:

$$\tau = N^* \phi L / v_c\ . \quad \text{(G.5)}$$

It should be noted that for $\tau = 0$, **Eq. G.3** does not reduce to **Eq. 5.27** analytically, but approaches it numerically as $\tau \to 0$. This is the consequence of approximating the exact integral. However, for all practical purposes, the numerical error is negligible.

Appendix H

Asphaltene-Induced Impairment in a Capillary Tube

In a capillary flow, the Hagen-Poiseuille equation describes fluid flow (Bird *et al.*, 1960):

$$Q_c = \frac{A(\Delta P)r^2}{8\mu L}, \tag{H.1}$$

where *A* is the effective flow cross-sectional area.

Making analogy with the Darcy equation for linear flow in porous media ($Q_c = kA(\Delta P)/\mu L$), the hydraulic conductivity (i.e. "permeability") becomes:

$$k = r^2/8. \tag{H.2}$$

In the following analysis, we assume a constant flowrate, rather than a constant velocity. Ideally, the injection rates are reasonably maintained during the runs. Owing to deposition, the flow area reduces, causing the flow velocity to vary as the experiment progresses.

For constant flowrate, *L* and μ, we can infer that $k \propto 1/(\Delta P)A$ from **Eqs. H.1** and **H.2**. Hence,

$$\frac{k_d(t)}{k_i} = \frac{A_i(\Delta P)_i}{A_t(\Delta P)_t}, \tag{H.3a}$$

$$\frac{k_d(t)}{k_i} = \frac{r_i^{\,2}(\Delta P)_i}{(r_i - e_t)^2(\Delta P)_t}, \tag{H.3b}$$

where e_t is the instantaneous average deposit thickness, expressed as (see **Eq. 5.45**):

$$e_t = r_i\left\{1 - \left(\frac{(\Delta P)_i}{(\Delta P)_t}\right)^{1/4}\right\}. \tag{H.4}$$

Combining **Eqs. H.3c** and **H.4**,

$$\frac{k_d(t)}{k_i} \approx \sqrt{\frac{(\Delta P)_i}{(\Delta P)_t}} \tag{H.5}$$

Appendix I

Some Additional Results of Uncertainty Assessment

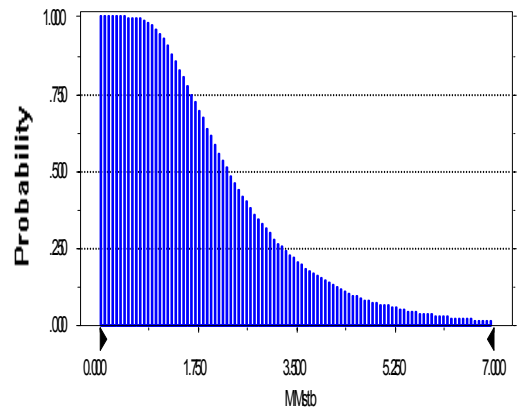


Fig. I.1: Reverse Cumulative Probability for N_p

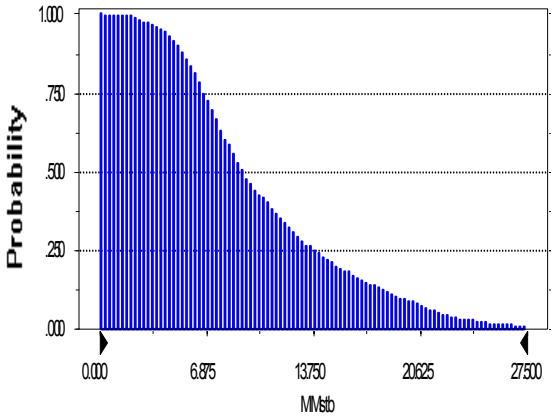


Fig. I.2: Reverse Cumulative Probability for W_i

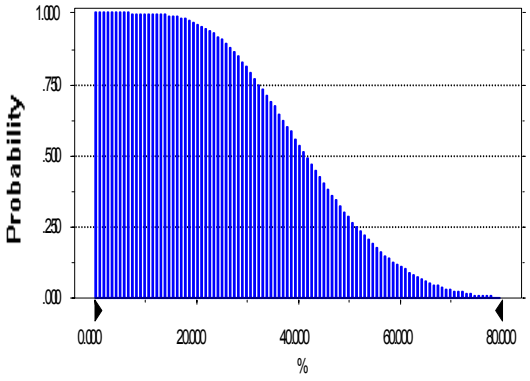


Fig. I.3: Reverse Cumulative Probability for R_f

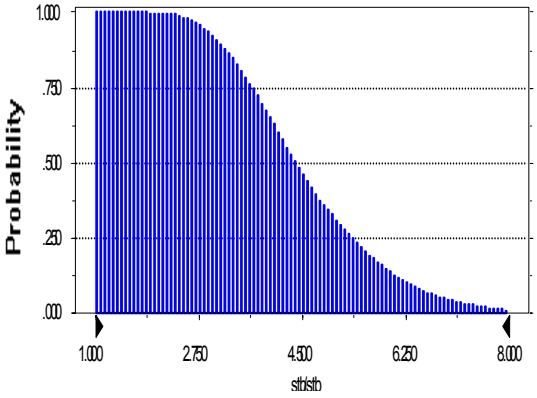


Fig. I.4: Reverse Cumulative Probability for C_{SOR}

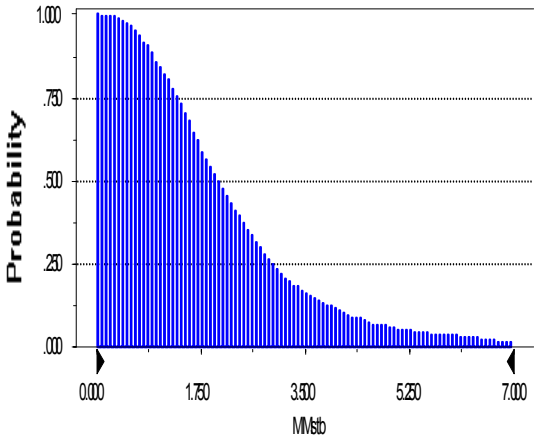


Fig. I.5: Reverse Cumulative Probability for N_{p_CO2}

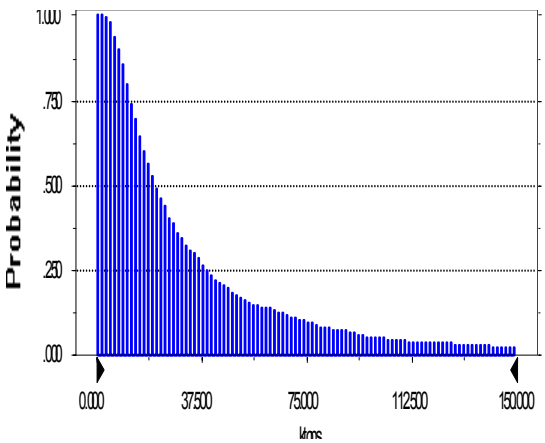


Fig. I.6: Reverse Cumulative Probability for G_{CO2}

Appendix J

Estimation of CO_2 Emissions

J.1 Boiler Emissions

The following analysis assumes 1 day of continuous operation.

Net steam specific enthalpy is:

$$h_{net} = h_g(T_s) - h_f(T_w), \tag{J.1}$$

where $h_g(T_s)$ is steam specific-enthalpy at T_s, $h_f(T_w)$ is boiler feedwater specific enthalpy at temperature T_w. All the enthalpy quantities are in J/kg.

Net thermal power generated (in J/d) is:

$$\dot{E}_{net} = 1000\ Q_s h_{net}\ , \tag{J.2}$$

where Q_s is cold-water equivalent (m^3/d) of steam produced, and the numeral 1000 refers to water density (kg/m^3).

Power (fuel) consumption (J/d) to generate this thermal power can be estimated from:

$$\dot{E}^b_{fuel} = \dot{E}_{net} / \eta_b\ , \tag{J.3}$$

in which η_b denotes the boiler thermal efficiency (fraction).

Amount of CO_2 emissions (ton/d) from the steam generator is approximately:

$$\dot{m}^b_{CO_2} = 44\,x10^{-12}\, e_f c_f \dot{E}^b_{fuel} / 12\ , \tag{J.4}$$

where e_f and c_f are fuel emission factor (ton C/TJ) and fraction of carbon oxidised, respectively.

Volume-equivalent of CO_2 (m^3/d) from the boiler is:

$$Q^b_{CO_2} = 1000\ \dot{m}^b_{CO_2} / 1.86\ , \tag{J.5}$$

where the factor 1.86 is CO_2 density (kg/m^3) at standard conditions.

J.2 Compressor Emissions

Compressor daily energy consumption (J) is estimated from:

$$E_{comp} = 86.4x10^3 \dot{E}_{comp} , \quad \text{(J.6)}$$

where $\dot{E}_{comp}$ is compressor power output (W).

Daily fuel consumption (J) in running the compressor is:

$$E_{fuel}^{comp} = E_{comp} / \eta_{comp} , \quad \text{(J.7)}$$

with η_{comp} denoting the compressor thermal efficiency (fraction).

The mass (ton/d) and volume (m^3/d) of CO_2 emitted from compression work are given by:

$$\dot{m}_{CO_2}^{comp} = 44x10^{-12} e_f c_f E_{fuel}^{comp} / 12 , \quad \text{(J.8)}$$

$$Q_{CO_2}^{comp} = 1000 \dot{m}_{CO_2}^{comp} / 1.86 . \quad \text{(J.9)}$$

Typical emission factor and oxidisable carbon-fraction for the common fossil fuels are listed in **Table J.1**.

Table J.1: Some Input Factors for Emission Calculations (Herold, 2003; IPCC, 1997)

Fuel	Emissions Factor (ton C / TJ fuel)	Fraction Carbon Oxidised
Natural gas	15.3	0.995
Light oil	20.0	0.990
Heavy oil (bitumen)	22.0	0.990
Coal	26.8	0.980

Appendix K

Analysis of Compositional Grading

Fig. K.1 shows a simple model of compositional grading.

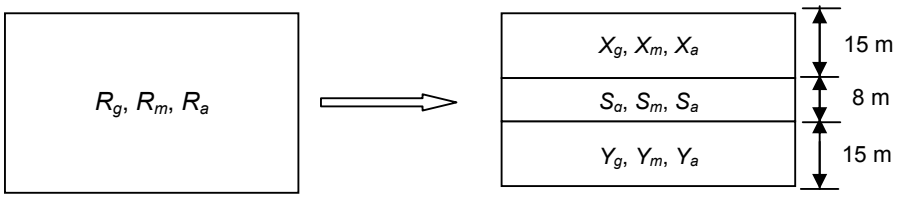


Fig. K.1: Schematic of Oil-Phase Compositions in the Homogenous and Heterogeneous Models

Given that the unit *X* consists of X_g, X_m and X_a mole fractions of solution gas, maltene and asphaltene, respectively, the following balance holds for this horizon.

$$15X_g + 15X_m + 15X_a = 15\,, \tag{K.1}$$

where the numeral "15" refers to the thickness (15 m) of this horizon.

Similar analysis for the oil-shale and *Y* units results in the following:

$$8S_g + 8S_m + 8S_a = 8\,, \tag{K.2}$$

$$15Y_g + 15Y_m + 15Y_a = 15\,. \tag{K.3}$$

Adding **Eqs. K.1-K.3** for the whole reservoir, and combining according to the components:

$$\left(15X_g + 8S_g + 15Y_g\right) + \left(15X_m + 8S_m + 15Y_m\right) + \left(15X_a + 8S_a + 15Y_a\right) = 38\,. \tag{K.4}$$

For consistency, each volume-weighted component mole fraction in **Eq. K.4** must equal the average component mole fraction (R_g, R_m and R_a for solution gas, maltene and asphaltene, respectively) in the homogenous model. Hence, the following component balances are valid:

$$\left(15X_g + 8S_g + 15Y_g\right)/38 = 0.0872\,, \tag{K.5}$$

$$\left(15X_m + 8S_m + 15Y_m\right)/38 = 0.7815\,, \tag{K.6}$$

$$\left(15X_a + 8S_a + 15Y_a\right)/38 = 0.1313\,, \tag{K.7}$$

where the numerals on the right hand side of **Eqs. K.5-K.7** are taken from **Table 6.8**.

To solve **Eqs. K.5**-**K.7** for the 9 unknowns, we assume the following component-level relationships between horizons.

$$S_g = 0.5X_g;\ S_m = 2X_m;\ S_a = 3X_a, \tag{K.8a}$$

$$Y_g = 0.25X_g;\ Y_m = 4X_m;\ Y_a = 8X_a. \tag{K.8b}$$

In general, the assumptions in **Eq. K.8** are reasonably consistent with the areal distribution reported by Ibisi *et al.* (2006) for the Nigerian belt. Additionally, the assumptions partly account for net biodegradation, which typically causes more dramatic compositional changes than obtainable with the transport processes of diffusion and advection (Besong, 2009; Larter *et al.*, 2008; Nasrabadi *et al.*, 2006; Koopmans *et al.*, 2002).

By substituting **Eqs. K.8a** and **b** into **Eq. K.5**, we obtain the amount of each component in unit *X* to satisfy the reservoir-level composition. The results are 0.1457, 0.3263 and 0.0314 mol for solution gas (g), maltene (m) and asphaltene (a), respectively. Normalising the moles yields the molar composition 28.94, 64.83 and 6.23 %, respectively for unit *X*.

Applying the molar mass 16, 539 and 1030 g/mol for the gas, maltene and asphaltene, respectively and normalising the results, we obtain the equivalent mass composition as 1.11, 83.54 and 15.35 %, respectively. Application of the same procedure for the other horizons gives the compositions presented in **Table 9.1**.

Appendix L

Additional Economic Results

Table L.1: Design Matrix and Output for the Steam-alone Process

Run	*F1*	*F2*	*F3*	*F4*	*F5*	*F6*	*NPV ($ mln)*	*VIR ($/$)*
1	1	1	-1	-1	-1	1	392.01	25.77
2	1	1	1	-1	1	-1	190.55	11.43
3	-1	1	1	-1	-1	-1	-46.98	-2.82
4	-1	1	1	1	-1	1	-103.78	-2.08
5	1	1	1	1	1	1	109.15	2.18
6	-1	1	-1	-1	1	1	-20.42	-1.34
7	1	-1	1	-1	-1	1	42.20	2.53
8	-1	1	-1	1	1	-1	-54.69	-1.20
9	-1	-1	1	1	1	-1	-94.55	-1.89
10	-1	-1	1	-1	1	1	-42.08	-2.53
11	-1	-1	-1	-1	-1	-1	-22.44	-1.47
12	1	1	-1	1	-1	-1	453.15	9.93
13	1	-1	-1	1	1	1	34.70	0.76
14	-1	-1	-1	1	-1	1	-61.04	-1.34
15	1	-1	-1	-1	1	-1	80.60	5.30
16	1	-1	1	1	-1	-1	34.27	0.69
R^2							*0.984*	*0.670*

Table L.2: Design Matrix and Output for the SAF Process

Run	*F1*	*F2*	*F3*	*F4*	*F5*	*F6*	*NPV ($ mln)*	*VIR ($/$)*
1	1	1	-1	-1	-1	1	320.43	33.12
2	1	1	1	-1	1	-1	158.89	15.00
3	-1	1	1	-1	-1	-1	-74.56	-7.04
4	-1	1	1	1	-1	1	-112.34	-3.53
5	1	1	1	1	1	1	95.66	3.01
6	-1	1	-1	-1	1	1	-27.24	-2.82
7	1	-1	1	-1	-1	1	-26.41	-2.49
8	-1	1	-1	1	1	-1	-47.62	-1.64
9	-1	-1	1	1	1	-1	-121.32	-3.82
10	-1	-1	1	-1	1	1	-88.64	-8.37
11	-1	-1	-1	-1	-1	-1	-36.17	-3.74
12	1	1	-1	1	-1	-1	377.97	13.02
13	1	-1	-1	1	1	1	31.25	1.08
14	-1	-1	-1	1	-1	1	-61.40	-2.12
15	1	-1	-1	-1	1	-1	65.28	6.75
16	1	-1	1	1	-1	-1	-21.56	-0.68
R^2							*0.981*	*0.846*

References

Adebiyi, F.M., Asubiojo, O.I. and Ajayi, T.R. (2006). "Multielement Analysis of Nigerian Bitumen by TXRF Spectrometry and the Physical Constants Characterisation of its Hydrocarbon Component", *Fuel* **85**, 3, 396-400.

Adebiyi, F.M. and Omode, A.A. (2007). "Organic, Chemical and Elemental Characterisation of Components of Nigerian Bituminous Sands Bitumen", *Energy Sources*, *Part A: Recovery, Utilisation, and Environ. Effects* **29***,* 8, 669-676.

Adedimila, A.S. (2000). "Bitumen: Nigeria's Other Black Gold?" Inaugural Lecture, Univ. of Lagos, Nigeria, www.nuc.edu.ng/nucsite/File, accessed May 23, 2011.

Adegoke, O.S., Ako, B.D., Enu, E.I., Afonja, A.A., Ajayi, T.R., Emofurieta, W.O., Jeje, L.K., Adegoke-Anthony, C.W., Omatsola, M.E. and Rahaman, M.A. (1980)[ξ]. *Geotechnical Investigations of the Ondo State Bituminous Sands- Vol. I. Geology and Reserves Estimate.* Geological Consultancy Unit, Dept. of Geology, Univ. of Ife (now Obafemi Awolowo University), Nigeria.

Adegoke, O.S., *et al.* (1978). *Tar Sand Project- Phase II. Delineation of Potential Mine Area.* Geological Consultancy Unit, Dept. of Geology, Univ. of Ife, Nigeria. *Cited in Adegoke et al. (1980).*

Adegoke, O.S., *et al.* (1976). *Tar Sand Project- Phase I. Estimation of Reserves, Materials Testing and Chemical Analyses.* Geological Consultancy Unit, Dept. of Geology, Univ. of Ife, Nigeria. *Cited in Adegoke et al. (1980).*

Adegoke, O.S., *et al.* (1974). *Preliminary Proposal for the Exploration and Utilisation of Tar Sands of Western State of Nigeria*. Geological Consultancy Unit, Dept. of Geology, Univ. of Ife, Nigeria. *Cited in Adegoke et al. (1980).*

Ademodi, B., Oshinowo, T., Sanni, S.A. and Dawodu, O.F. (1987). "Preliminary Studies on the Recovery of Bitumen from Nigerian Tar Sands. I. Beneficiation and Solvent Extraction", *Energy Sources* **9**, 3, 173-188.

Adewusi, V.A. (1998). "Alcohol-Caustic Steam Process - An Emerging Technology for Heavy Oil Recovery", *Pet. Sci. & Tech.* **16**, 5 & 6, 583-596.

Adewusi, V.A. (1998). "Transient Phenomena and Optimal Salinity Concept in Alkaline-Bitumen Recovery Systems", *Pet. Sci. & Tech.* **16**, 5 & 6, 521-538.

Adewusi, V.A. and Adetona, S.A. (1998). "Model Studies of Alkaline Hot Water Drive in Nigerian Tar Sands", *Pet. Sci. & Tech.* **16**, 5 & 6, 503-520.

Aherne, A.L. and Maini, B. (2008). "Fluid Movement in the SAGD Process: A Review of the Dover Project", *J. Can. Pet. Tech. (JCPT)* **47**, 1, 31-37.

Aimard, N., Lescanne, M., Mouronval, G. and Prébende, C. (2007). "The CO_2 Pilot at Lacq: An Integrated Oxycombustion CO_2 Capture and Geological Storage Project in the South West of France". Paper 11737 presented at Int. Petroleum Technology Conf., Dubai, 4-6 Dec.

Ajienka, J., Egbon, F. and Onwuemena, U. (2009). "Deep Offshore Fracture Pressure Prediction in the Niger Delta – A New Approach". Paper 128339 presented at SPE Int. Technical Conf. & Exhibition, Abuja, 3-5 Aug.

Akande, J.M. (2007). "Analysis of Steam Injection and In-situ Combustion Methods of Mining Agbabu Bitumen Deposit in Ondo State, Nigeria", *J. Eng. & Applied Sc.* **2**, 10, 1493-1496.

Akin, S. (2005). "Mathematical Modelling of Steam-Assisted Gravity Drainage", *SPEREE* **8***, 5,* 372-376.

Akinbode, O.M., Eludoyin, A.O. and Fashae, O.A. (2008). "Temperature and Relative Humidity Distributions in a Medium-Size Administrative Town in Southwest Nigeria", *J. Environ. Manage.* **87**, 1, 95-105.

Akinmosin, A. and Shoyemi, A. (2010). "Technical Feasibility of Direct Application of the Nigerian Tar Sand Deposits as Road Asphalt", *Pacific J. Sci. & Tech.* **11**, 1, 526-536.

Akinmosin, A and Osinowo, O.O (2008). "Sedimentological Characteristics of The Nigerian Tar Sand Deposits In Parts of Southwestern Nigeria", *Continental J. Earth Sciences* **3**, 8-21.

[ξ] Due to space constraints, only the major contributors are listed.

Akinmosin, A., Omosanya, K.O., Ariyo, S.O., Folorunsho, A.F. and Aiyeola, S.O. (2011). "Structural Control for Bitumen Seepages in Imeri, Southwestern Nigeria", *Int. J. Basic & Applied Sci.* **11**, 1, 93-103.

Akinmosin, A., Osinowo, O.O. and Adio, N.A. (2010). "Use of Stable Carbon Isotope in Characterisation of Tar Sand Deposit in Southwestern Nigeria", *J. Applied Sciences in Environmental Sanitation* **V**, N*,* 296-307.

Al-Abduwani, F.A.H., Hime, G., Alvarez, A. and Farajzadeh, R. (2005). "New Experimental and Modelling Approach for the Quantification of Internal Filtration". Paper 94634 presented at SPE European Formation Damage Conf., Scheveningen, 25-27 May.

Alajmi, A.F., Grader, A. and Halleck, P. (2008). "Visualisation of Steam Zone Advancement During Heavy Oil Recovery". Paper 120819 presented at SPE Saudi Arabia Section Technical Symp., Alkhobar, 10-12 May.

Alali, N., Pishvaie, M.R. and Jabbari, H. (2009). "A New Semi-analytical Modeling of Steam-assisted Gravity Drainage in Heavy Oil Reservoirs", *J. Pet. Sci. Eng.* **69**, 3-4, 261-270.

Al-Atar, E. (2000). "Effect of Oil Compatibility and Resins/Asphaltenes Ratio on Heat Exchanger Fouling of Mixtures Containing Heavy Oil", MSc thesis, Univ. British Columbia, Vancouver.

Albahlani, A.M. and Babadagli, T. (2009). "SAGD Laboratory Experimental and Numerical Simulation Studies: A Review of Current Status and Future Issues", *J. Pet. Sci. Eng.* **68**, 3-4, 135-150.

Albahlani, A.M. and Babadagli, T. (2008). "A Critical Review of the Status of SAGD: Where Are We and What is Next?" Paper 113283 presented at SPE Western Regional & Pacific Section AAPG Joint Meeting, Bakersfield, 31 Mar - 2 Apr.

Alberta Geological Survey (2009). "Cyclic Steam Stimulation", www.ags.gov.ab.ca/energy/oilsands/alberta_oil_sands3.html, accessed Nov. 16, 2010.

Alboudwarej, H. *et al.* (2006). "Highlighting Heavy Oil", *Oilfield Review*, summer, 34-53.

Al-Huraibi, N. and Belhaj, H. (2010). "Modelling of Crude Oil Asphaltenes Deposition: In-depth Colloidal Prospective". Paper 136087 presented at SPE Prod. & Operations Conf. and Exhibition, Tunis, 8-10 Jun.

Alhuthali, A.H., Datta-Gupta, A., Yuen, B. and Fontanilla, J.P (2010). "Field Applications of Waterflood Optimisation via Optimal Rate Control with Smart Wells", *SPEREE* **13**, 3, 406-422.

Ali, M.A. and Islam, M.R. (1997). "The Effect of Asphaltene Precipitation on Carbonate Rock Permeability: An Experimental and Numerical Approach". Paper 38856 presented at SPE Annual Technical Conf. & Exhibition, San Antonio, 5-6 Oct.

Ali, M.A. and Islam, M.R. (1998). "The Effect of Asphaltene Precipitation on Carbonate-Rock Permeability: An Experimental and Numerical Approach", *SPEPF* **13**, 3, 178-183.

Alkindi, A.S. (2009). *Experimental and Numerical Investigation of the Vapour Extraction (VAPEX) Process for Heavy Oil Recovery*, PhD Thesis, Imperial College London.

Allinson, W.G., Cinar, Y., Neal, P.R., Kaldi, J. and Paterson, L. (2010). "CO_2 Storage Capacity - Combining Geology, Engineering and Economics". Paper 133804 presented at SPE Asia Pacific Oil & Gas Conf. and Exhibition, Queensland, 18-20 Oct.

Almehaideb, R.A., Abdulkarim, M.A. and Al-Khanbashi, A.S. (2001). "Improved *K*-values Correlation for UAE Crude Oil Components using PVT Laboratory Data", *Fuel* **80**, 1, 117-124.

Al-Rabaani, A.S., Blunt, M.J. and Muggeridge, A.H. (2008). "Calculation of a Critical Steam Injection Rate for Thermally-Assisted Gas-Oil Gravity Drainage", Paper 113351 presented at SPE/DOE Improved Oil Recovery Symposium, Oklahoma, 19-23 Apr.

Altoe F, J.E., Bedrikovetsky, P., Siqueira, A.G., de Souza, A.L.S. and Shecaira, F.S. (2006). "Correction of Basic Equations for Deep Bed Filtration with Dispersion", *J. Pet. Sci. Eng.* **51**, 1-2, 68-84.

Amaefule, J.O., Altunbay, M., Tiab, D., Kersey, D.G. and Keelan, D.K. (1993). "Enhanced Reservoir Description: Using Core and Log Data to Identify Hydraulic (Flow) Units and Predict Permeability in Uncored Intervals/Wells". Paper 26436 presented at SPE Annual Technical Conf. & Exhibition, Texas, 3-6 Oct.

Amin, J.S., Nikooee, E., Ayatollahi, S. and Alamdari, A. (2010). "Investigating Wettability Alteration due to Asphaltene Precipitation: Imprints in Surface Multifractal Characteristics", *Applied Surface Science* **256**, 21, 6466-6472.

Amin, J.S. Nikooee, E., Ghatee, M.H., Ayatollahi, S., Alamdari, A. and Sedghamiz, T. (2011). "Investigating the Effect of Different Asphaltene structures on Surface Topography and Wettability Alteration", *Applied Surface Science* **257**, 20, 8341-8349.

Amro, M.M. (2005). "Effect of Scale and Corrosion Inhibitors on Well Productivity in Reservoirs Containing Asphaltenes", *J. Pet. Sci. Eng.* **46**, 4, 243-252.

Amudo, C., T. Graf, R. Dandekar, and J.M. Randle (2009). "The Pains and Gains of Experimental Design and Response Surface Applications in Reservoir Simulation Studies". Paper 118709 presented at SPE Reservoir Simulation Symposium, The Woodlands, 2 - 4 Feb.

Anthony, E.P. and Mohan, A. (2010). "Water Management vs. Water Control: Profitability, Not Cost, Driving the Paradigm Change". Paper 132253 presented at SPE Trinidad & Tobago Energy Resources Conf., Port of Spain, 27-30 Jun.

Anuku, W. (2011). "Senate Passes Bill to Rename ETF as Tertiary Education Trust Fund", www.elendureports.com, accessed May 23, 2011.

ASTM (1993). "Standard Test Method for Characteristic Groups in Rubber Extender and Processing Oils by the Clay-Gel Adsorption Chromatographic Method", ASTM D2007-93 05.01, 658-664.

Asubiojo, O.I. and Adebiyi, F.M. (2011). "Effects of Bitumen Deposit on Soil Physico-Chemical Characteristics", *Soil & Sediment Contamination: An Int. Journal* **20**, 2, 142-162.

Ayodele, O.R. (2006). "Strategies for Commercialising Nigerian Unconventional Oil", *Alexander's Gas & Oil Connections* **11**, 7.

Ayodele, O.R. (2007). "Unprecedented Transfer of Unconventional Oil Wealth in Venezuela: A Path Nigeria Should Avoid", *NigeriaWorld*, http://nigeriaworld.com/, accessed Jan. 20, 2011.

Ayodele, O.R., Nasr, T.N., Beaulieu, G. and Heck, G. (2009). "Laboratory Experimental Testing and Development of an Efficient Low Pressure ES-SAGD Process", *JCPT* **48**, 9, 54-61.

Bachu, S., Shaw, J.C, and Pearson, R.M. (2004). "Estimation of Oil Recovery and CO_2 Storage Capacity in CO_2 EOR Incorporating the Effect of Underlying Aquifers". Paper 89340 presented at SPE/DOE 14th Symposium on Improved Oil Recovery, Oklahoma, 17-21 Apr.

Bader, B.E., Fox, R.L. and Stosur, J.J. (1981). "The Potential of Downhole Steam Generation to the Recovery of Heavy Oils", *The Future of Heavy Crude and Tar Sands*, McGraw-Hill., New York, 369-377.

Badre, S., Goncalves, C.C., Norinaga, K., Gustavson, G. and Mullions, O.C. (2006). "Molecular Size and Weight of Asphaltene and Asphaltene Solubility Fractions from Coals, Crude Oils and Bitumen", *Fuel* **85**, 1-11.

Bagci, S. and Gumrah, F. (1992). "An Examination of Steam-injection Processes in Horizontal and Vertical Wells for Heavy-oil Recovery", *J. Pet. Sci. Eng.* **8**, 59-72.

Bagci, A.S. and Gumrah, F. (2004). "Effects of CO_2 and CH_4 Addition to Steam on Recovery of West Kozluca Heavy Oil". Paper 86953 presented at SPE Int. Thermal Operations & Heavy Oil Symposium and Western Regional Meeting, California, 16-18 Mar.

Bagci, A.S., Olushola, S. and Mackay, E. (2008). "Performance Analysis of SAGD Wind-Down Process with CO_2 Injection". Paper 113234 presented at SPE/DOE Improved Oil Recovery Symp., Tulsa, 19-23 Apr.

Bagheri, M.B., Kharrat, R. and Ghotby, C. (2011). "Experimental Investigation of the Asphaltene Deposition Process during Different Production Schemes", *Oil & Gas Sci. and Tech*. IFP, 1-13.

Bailey, L., Boek, E.S., Jacques, S.D.M., Boassen, T., Selle, O.M., Argillier, J.F. and Longeron, D.G. (2000). "Particulate Invasion from Drilling Fluids", *SPE J.* **5**, 4, 412-419.

Baker, R.O., Rodrigues, K., Sandhu, K.S. and Jong, E.S.W. (2010). "Key Parameters in Steam Chamber Development". Paper 138113 presented at SPE and Canadian Unconventional Resources & Int. Petroleum Conf., Alberta, 19-21 Oct.

Baker, H.L., Thomas, D.C., Doddridge, W.R. and McDougall, D.B. (1992). "Asphaltene Deposition Control Using Chemical Control Agent". Paper CIM 92-7 presented at CIM Annual Technical Conf., Calgary, 7-10 Jun.

Barillas, J.L.M., Dutra Jr., T.V. and Mata, W. (2006). "Reservoir and Operational Parameters Influence in SAGD Process", *J. Pet. Sci. Eng.* **54**, 1-2, 34-42.

Bazyleva, A.B., Anwarul Hasan, M.D., Fulem, M. Becerra, M. and Shaw, J.M. (2010). "Bitumen and Heavy Oil Rheological Properties: Reconciliation with Viscosity Measurements", *J. Chem. Eng. Data* **55**, 3, 1389-1397.

Beattie, C.I., Boberg, T.C. and McNab, G.S. (1991). "Reservoir Simulation of Cyclic Steam Stimulation in the Cold Lake Oil Sands", *SPERE* **6**, 2, 200-206.

Bedrikovetsky, P., Marchesin, D., Shecaira, F., Souza, A.L., Milanez, P.V. and Rezende, E. (2001). "Characterisation of Deep Bed Filtration System from Laboratory Pressure Drop Measurements", *J. Pet. Sci. Eng.* **32**, 2-4, 167-177.

Bennion, D.W., Moore, R.G. and Thomas, F.B. (1985). "Effect of Relative Permeability on the Numerical Simulation of the Steam Stimulation Process", *JCPT* **24**, 2, 40-44.

Bentein, J. (2009). "The Carbon Capture Cost Challenge", *Heavy Oil & Oil Sands Guidebook and Directory* **4**, 115-117.

Berger, S., Bergins, C., Strauβ, K., Bielfeldt, F.B., Elsen, R.O. and Erken, M. (1999). "Mechanical/Thermal Dewatering of Brown Coal", *VGB Power Tech*. **79**, 2, 44-49.

Bergins, C., Crone, S. and Strauss, K. (2005). "Multiphase Flow in Porous Media with Phase Change. Part II: Analytical Solutions and Experimental Verification for Constant Pressure Steam Injection", *Transp. Porous Media* **60**, 3, 275-300.

Bernabe, Y., Mok, U. and Evans, E. (2003). "Permeability-Porosity Relationships in Rocks Subjected to Various Evolution Processes", *J. Pure Appl. Geophys*. **160**, 937–960.

Besong, D.O. (2009). *Time-Scales for the Development of Thermodynamic Equilibrium in Hydrocarbon Reservoirs*, PhD Thesis, Imperial College London.

Bird, R.B., Stewart, W.E., and Lightfoot, E.N. (1960). *Transport Phenomena*, Wiley, New York.

Birrell, G.E. (2001). "Heat Transfer Ahead of a SAGD Steam Chamber, a Study of Thermocouple Data from Phase B of the Underground Test Facility (Dover Project)". Paper 71503 presented at SPE Annual Technical Conf. & Exhibition, New Orleans, 30 Sept - 3 Oct.

Birrell, G.E., Aherne, A.L. and Seleshanko, D.J. (2005). "Cyclic SAGD - Economic Implications of Manipulating Steam Injection Rates in SAGD Projects - Re-examination of the Dover Project", *JCPT* **44**, 1, 54-58.

Bloomberg (2010). "Energy and Oil Prices", www.bloomberg.com/energy, accessed Dec. 22, 2010.

Boberg, T.C. and Lantz, R.B. (1966). "Calculation of the Production Rate of a Thermally Stimulated Well", *J. Pet. Tech. (JPT)* **18**, 12, 1613-1623.

Bodvarsson, G.S. and Tsang, C.F. (1982). "Injection and Thermal Breakthrough in Fractured Geothermal Reservoirs", *J. of Geophysical Research* **87**, B2, 1031-1048.

Boek, E.S., Hall, C. and Tardy, P. (2010c). "Deep Bed Filtration Modelling of Formation Damage due to Particulate Invasion from Drilling Fluids", submitted to *Transport in Porous Media*.

Boek, E.S., Headen, T.F. and Padding, J.T. (2010a). "Multi-scale Simulation of Asphaltene Aggregation and Deposition in Capillary Flow", *Faraday Discussions* **144**, 271-284.

Boek, E.S., Ladva, H.K., Crawshaw, J.P. and Padding, J.T. (2008). "Deposition of Colloidal Asphaltene in Capillary Flow: Experiments and Mesoscopic Simulation", *Energy & Fuels* **22**, 2, 805-813.

Boek, E.S., Wilson, A.D., Padding, J.T., Headen, T.F. and Crawshaw, J.P. (2010b). "Multi-scale Simulation and Experimental Studies of Asphaltene Aggregation and Deposition in Capillary Flow", *Energy & Fuels* **24**, 4, 2361-2368.

Bourbiaux, B.J. and Kalaydjian, F.J. (1990). "Experimental Study of Cocurrent and Countercurrent Flows in Natural Porous Media", *SPERE* **5**, 3, 361-368.

Bowden, S.A., Wilson, R., Parnell, J. and Cooper, J.M. (2009). "Determination of the Asphaltene and Carboxylic acid Content of a Heavy Oil using a Microfluidic Device", *Lab Chip* **9**, 828–832.

BPA, BP 44063: Confidential Letter from the Petroleum Department, 12 Nov. 1936. *Cited in Steyn (2006)*.

Briggs, P., Redford, D.A. and Harris, P. (1982). "Core-sized Physical Simulator Experiments to Study the Effect of Naphtha and CO_2 Addition to Steam in the Recovery of Bitumen from Oil Sands". Paper presented at Petroleum Society's Annual Technical Meeting, Calgary, 6-9 Jun.

British Petroleum (2010). "BP Sustainability Review 2009", www.bp.com/sustainabilityreview2009, accessed 15 Aug. 2010.

Broseta, D., Robin, M., Savvidis, T., Fejean, C., Durandeau, M. and Zhou, H. (2000). "Detection of Asphaltene Deposition by Capillary Flow Measurements". Paper 59294 presented at SPE/DOE Improved Oil Recovery Symposium, Oklahoma, 3-5 Apr.

Bruining, J. and Marchesin, D. (2006). "Analysis of Nitrogen and Steam Injection in a Porous Medium with Water", *Transport in Porous Media* **62**, 251-281.

Bryant, S.L., Lakshminarasimhan, S. and Pope, G.A. (2008). "Buoyancy-Dominated Multiphase Flow and Its Effect on Geological Sequestration of CO_2", *SPE J.* **13**, 4, 447-454.

Burden, R.L. and Faires, J.D (2000). *Numerical Analysis*, 7th ed., Brooks/Cole, Boston.

Burns, J. (1969). "A Review of Steam Soak Operations in California", *JPT* **21**, 1, 25-34.

Butler, R.M. (1985). "A New Approach to the Modelling of Steam-assisted Gravity Drainage", *JCPT* **24**, 3, 42-51.

Butler, R.M. (1987). "Rise of Interfering Steam Chambers", *JCPT* **26**, 3, 70-75.

Butler, R.M. (1994). "Steam-assisted Gravity Drainage: Concept, Development, Performance and Future", *JCPT* **33**, 2, 44-50.

Butler, R.M. (1998). "SAGD Comes of Age", *JCPT* **37**, 7, 9-12.

Butler, R.M. (2004). "The Behaviour of Non-Condensable Gas in SAGD- A Rationalisation", *JCPT* **43**, 1, 28-34.

Butler, R.M. (1997). "The Steam and Gas Push (SAGP)". Paper 97-137 presented at the Petroleum Society's 48th Annual Technical Meeting, Calgary, 8-11 Jun.

Butler, R.M. and Mokrys, I.J. (1993). "Recovery of Heavy Oils Using Vapourised Hydrocarbon Solvents: Further Development of the VAPEX Process", *JCPT* **32**, 6, 56-63.

Butler, R.M. and Stephens, D.J. (1981). "The Gravity Drainage of Steam-heated Heavy Oil to Parallel Horizontal Wells", *JCPT* **20**, 2, 90-96.

Butler, R.M., McNab, G.S. and Lo, H.Y. (1981). "Theoretical Studies on the Gravity Drainage of Heavy Oil During In-situ Steam Heating", *Can. J. Chem. Eng.* **59**, 4, 455-460.

Canbolat, S., Akin, S. and Kovscek, A. R. (2004). "Noncondensable Gas Steam-assisted Gravity Drainage", *J. Pet. Sci. Eng.* **45**, 83-96.

Cao, H. and Aziz, K. (1999). "Evaluation of Pseudo Functions". Paper 54589 presented at SPE Western Regional Meeting, Anchorage, 26-28 May.

CAPP (Canadian Association of Petroleum Producers) (2008). "Environmental Challenges and Progress in Canada's Oil Sands", www.capp.ca/getdoc.aspx?DocID=135721, accessed June 20, 2011.

Carcoana, A. (1992). *Applied Enhanced Oil Recovery*, Prentice-Hall, New Jersey.

Carpenter, D.E. and Dazet, S.C. (1992). "Horizontal Wells in a Steamdrive in the Midway Sunset Field". Paper 24127 presented at SPE/DOE Symposium on Enhanced Oil Recovery, Oklahoma, 22-24 Apr.

Carrigy, M.A. (1973). "Mesozoic Geology of the Fort McMurray Area". In: Carrigy, M.A. and Kramers, J.W. (eds.), *Guide to the Athabasca Oil Sands Area*. Res. Counc. Inf. Ser. **65**, 78-101.

Carslaw, H.S. and Jaeger, J.C. (1959). *Conduction of Heat in Solids*, Oxford Univ. Press, Oxford, 387-388.

Cenegy, L.M. (2001). "Survey of Successful World-wide Asphaltene Inhibitor Treatments in Oil Production Fields". Paper 71542 presented at SPE Annual Technical Conf. & Exhibition, New Orleans, 30 Sept - 3 Oct.

Cengel, Y.A. and Boles, M.A. (2002). Thermodynamics*: An Engineering Approach*, McGraw-Hill, New York.

Chakma, A., Islam, M.R. and Berruti, F. (1994). "Asphaltene-Viscosity Relationship of Processed and Unprocessed Bitumen". In: *Asphaltene Particles in Fossil Fuel Exploration, Recovery, Refining and Production Processes;* M.K. Sharma and T.F. Yen (eds.), Plenum Press, New York.

Chakravarti, S., Gupta, A. and Hunek, B. (2001). "Advanced Technology for the Capture of Carbon Dioxide from Flue Gases". Proc. 1st National Conf. on Carbon Sequestration, Washington DC, 15-17 May.

Chan, M.Y.S., Fong, J. and Leshchyshyn, T. (1997). "Effects of Well Placement and Critical Operating Conditions on the Performance of Dual Well SAGD Well Pair in Heavy Oil Reservoir". Paper 39082 presented at SPE Latin American & Caribbean Petroleum Engineering Conf., 30 Aug. - 3 Sept., Rio de Janeiro.

Chandra, S. and Mamora, D.D. (2005). "Improved Steamflood Analytical Model". Paper 97870 presented at SPE Int. Thermal Operations & Heavy Oil Symposium, Calgary, 1-3 Nov.

Chang, Y.I. and Chan, H.C. (2008). "Correlation Equation for Predicting Filter Coefficient under Unfavourable Deposition Conditions", *AIChE J*. **54**, 5, 1235-1253.

Charpentier, A.D., Bergerson, J.A. and MacLean, H.L. (2009). "Understanding the Canadian Oil Sands Industry's Greenhouse Gas Emissions", *Environmental Research Letters* **4**, 1, 1-11.

Chase, C.A. and O'Dell, P.M. (1973). "Application of Variational Principles to Cap and Base Rock Heat Losses", *SPE J.* **13**, 14, 200 - 210.

Chen, Q., Gerritsen, M.G. and Kovscek, A.R. (2008). "Effects of Reservoir Heterogeneities on the Steam-Assisted Gravity-Drainage Process". *SPEREE* **11**, 5, 921-932.

Chien, S.F. (1992). "Empirical Correlations of Saturated Steam Properties", *SPERE* **7**, 2, 295-303.

Chin, D.A. (1986). "Estimation of Dispersion Coefficients in Porous Media", *J. Hydr. Eng.* **112**, 7, 591-609.

CIBO (Council of Industrial Boiler Owners) (2003). "Energy Efficiency and Industrial Boiler Efficiency: An Industry Perspective", http://cibo.org/pubs/whitepaper1.pdf, accessed May 20, 2010.

Civan, F. (2007). "Formation Damage Mechanisms and their Phenomenological Modelling – An Overview". Paper 107857 presented at SPE European Formation Damage Conf., Scheveningen, 30 May - 1 Jun.

Claridge, E.L. and Dietrich, T. (1983). "Viscous Fingers and Gravity Tongues in CO_2-Steam Stimulation". Paper 11707 presented at SPE California Regional Meeting, Ventura, 23-25 Mar.

Clark, N.J., Roberts, F.G. and Lindner, J.D. (Aug. 1964). "Engine Exhaust Gas Boosts Heavy Oil Recovery", *Pet. Eng.*, 36-43.

Closmann, P.J. (2010). "Saturated-Steam Pressure Drop in Flow through Porous Media", *SPEREE* **13**, 1, 105-108.

Closmann, P.J. (1995). "A Simplified Gravity-Drainage Oil-Production Model for Mature Steamfloods", *SPERE* **10**, 2, 143-148.

Closmann, P.J. (1984). "Steam Zone Growth in Cylindrical Channels", *SPE J.* **24**, 5, 481-483.

Closmann, P.J. and Smith, R.A. (1983). "Temperature Observations and Steam-Zone Rise in the Vicinity of a Steam-Heated Fracture", *SPE J.* **23**, 4, 575-586.

CMG (2010a). *STARS User's Guide*, Computer Modelling Group Ltd., Calgary.

CMG (2010b). *WinProp User's Guide*, Computer Modelling Group Ltd., Calgary.

Collins, P.M. (2007a). "The False Lucre of Low-Pressure SAGD", *JCPT* **46**, 1, 20-27.

Collins, P.M. (2007b). "Geomechanical Effects on the SAGD Process", *SPEREE* **10**, 4, 367-375.

Conoco Energy Nigeria Ltd. (2002*). Nigeria Heavy Oil and Tarsands Reserves Report*, Conoco Energy Nigeria Ltd.

Corey, A.T. (1954). "The Interrelation between Gas and Oil Relative Permeabilities", *Prod. Monthly* **19**, 1, 38-41.

Cornwell, K. (1977). *The Flow of Heat*, van Nostrand Reinhold, Berkshire.

Coughanowr, D.R. (1991). *Process Systems Analysis and Control*, 2nd ed., McGraw-Hill Inc., New York.

Cox, L., Forester, M., Hedden, J., Scroggin, J. and Smith, T. (2003). "Sequestering CO_2 in Houston: Capstone Design Project", Chemical Eng Dept., Univ. Oklahoma, Oklahoma.

Cragoe, C.S. (1929). Miscellaneous Publication No. 97, U.S. Bureau of Standards, Washington, DC.

Crank, J. and Nicolson, P. (1947), "A Practical Method for Numerical Evaluation of Solutions of Partial Differential Equations of the Heat Conduction Type", *Proc. Camb. Phil. Soc.* 43: 50–67, DOI 10.1007/BF02127704.

Crone, S., Bergins, C. and Strauss, K. (2002). "Multiphase Flow in Homogeneous Porous Media with Phase Change. Part I: Numerical Modelling", *Transport in Porous Media* **49**, 291-312.

Cronquist, C. (2001). *Estimation and Classification of Reserves of Crude Oil, Natural Gas, and Condensate*, SPE Inc., Texas.

Dahaghi, A.K., Gholami, V., Moghadasi, J. and Abdi, R. (2008). "Formation Damage through Asphaltene Precipitation Resulting from CO_2 Gas Injection in Iranian Carbonate Reservoirs", *SPE Prod. & Operations* **23**, 2, 210-214.

Dake, L.P. (1978). *Fundamentals of Reservoir Engineering*, Elsevier Science, Amsterdam.

Das, S.K. and Butler, R.M. (1998). "Mechanism of the Vapor Extraction Process for Heavy Oil and Bitumen", *J. Pet. Sci. Eng.* **21**, 1-2, 43-59.

David, C., Wong, T., Zhu, W. and Zhang, J. (1994). "Laboratory Measurement of Compaction-induced Permeability Change in Porous Rocks: Implications for the Generation and Maintenance of Pore Pressure Excess in the Crust", *PAGEOPH* **143**, 1/2/3, 425-456.

Davidson, L.B., Miller, F.G. and Mueller, T.D. (1967). "A Mathematical Model of Reservoir Response during the Cyclic Injection of Steam", *SPE J.* **7**, 2, 174-188.

de Boer, R.B., Leerlooyer, K., Eigner, M.R.P. and van Bergen, A.R.D. (1995). "Screening of Crude Oils for Asphalt Precipitation: Theory, Practice, and the Selection of Inhibitors", *SPEPF* **10**, 1, 55-61.

de Ghetto, G., Paone, F. And Villa, M. (1995). "Pressure-Volume-Temperature Correlations for Heavy and Extra Heavy Oils". Paper 30316 presented at SPE Int. Heavy Oil Symposium, Alberta, 19-21 Jun.

de Haan, H.J. and Schenk, L. (1969). "Performance Analysis of a Major Steam Drive Project in the Tia Juana Field, Western Venezuela", *JPT* **21**, 1, 111-119.

de la Porte, J.J., Riesco, N. and Vesovic, V. (2009). "Prediction of Heavy Oil Viscosity in Current Reservoir Simulators". Paper 125500 presented at SPE/EAGE Reservoir Characterisation & Simulation Conf., Abu Dhabi, 19-21 Oct.

Dehghan, M. (2004). "Weighted Finite Difference Techniques for the One-dimensional Advection-Diffusion Equation", *Appl. Math. Comput*. **147**, 307-319.

Demiral, B.M.R. and Erdogmus, T. (2003). "Investigation of Production Mechanism of Steam Assisted Gravity Drainage by Computerised Tomography". Paper 2003-157 presented at the Canadian Int. Petroleum Conf., Alberta, 10-12 Jun.

Deutsch, C.V. (2010). "Estimation of Vertical Permeability in the McMurray Formation", *JCPT* **49**, 12, 10-18.

Doan, L.T., Baird, H., Doan, Q.T. and Farouq Ali, S.M. (1999). "An Investigation of the Steam-Assisted Gravity-Drainage Process in the Presence of a Water Leg". Paper 56545 presented at SPE Annual Technical Conf. & Exhibition, Houston, 3-6 Oct.

Doan, L.T., Baird, H., Doan, Q.T. and Farouq Ali, S.M. (1998). "Combination Steam Drive Processes for Improving Sweep Efficiency". Paper 98-42 presented at Petroleum Society's 49th Annual Technical Meeting, Calgary, 8-12 Jun.

Dunn, S.G., Nenniger, E.H. and Rajan, V.S.V. (1989). "A Study of Bitumen Recovery by Gravity Drainage using Low-temperature Soluble-gas Injection", *Can. J. Chem. Eng.* **67**, 6, 978–991.

Dusseault, M.B. (2001). "Comparing Venezuelan and Canadian Heavy Oil and Tar Sands". Paper 2001-061 presented at Petroleum Society's Canadian Int. Pet. Conf., Alberta, 12-14 Jun.

E & P (Exploration & Production) (2007). "Technology Improves In-situ Recovery Efficiency", www.eandp.info, accessed Aug. 15, 2010.

Edmunds, N. (1999). "On the Difficult Birth of SAGD", *JCPT* **38**, 1, 14-17.

Edmunds, N. and Chhina, H. (2001). "Economic Optimum Operating Pressure for SAGD Projects in Alberta", *JCPT* **40**, 12, 13-17.

Edmunds, N., Barrett, K., Solanki, S., Cimolai, M. and Wong, A. (2009). "Prospects for Commercial Bitumen Recovery from the Grosmont Carbonate, Alberta", *JCPT* **48**, 9, 26-32.

Edmunds, N.R. (1998). "Investigation of SAGD Steam Trap Control in Two and Three Dimensions". Paper 50413 presented at SPE Int. Conf. on Horizontal Well Tech., Calgary, 1-4 Nov.

Edmunds, N.R. (1994). "The Case for SAGD: Theory and Practice of Heavy Oil and Bitumen Recovery". Paper presented at Can. SPE/CIM/CANMET Int. Conf. on Recent Advances in Horizontal Well Applications, Calgary, 20-23 Mar.

Edmunds, N.R., Kovalsky, J.A., Gittins, S.D. and Pennacchioli, E.D. (1994). "Review of Phase A Steam-Assisted Gravity-Drainage Test", *SPERE* **9**, 2, 119-124.

ETF (Education Trust Fund) Decree No. 7 of 1993, Federal Government of Nigeria.

Edwards, K. (2000). "CO_2 in Alberta – A Vision of the Future", *JCPT* **39**, 9, 48-53.

Ejiogu, G.C. and Fiori, M. (1987). "High-Pressure Saturated-Steam Correlations", *JPT* **39**, 12, 1585-1590.

Ekrann, S. and Mykkeltveit, J. (1995). "Dynamic Pseudos: How Accurate Outside Their Parent Case?" Paper 29138 presented at SPE Symposium on Reservoir Simulation, San Antonio, 12-16 Feb.

Ekweozor, C.M. and Nwachukwu, J.I. (1989). "The Origin of Tar Sands of Southwestern Nigeria", *Nig. Assoc. Petrol. Explor. Bull.* **4**, 2, 82-94.

Elliott, K (2008). "Examination of Oil Sands Projects: Gasification, CO_2 Emissions and Supply Costs". Paper 117524 presented at SPE Int. Thermal Operations & Heavy Oil Symposium, Calgary, 20-23 Oct.

EMT (2011). "Cost-Efficient Steam Pipe Insulation", www.emt-india.net/equipment, accessed Jan. 12, 2011.

Enu, E.I. (1985). "Textural Characteristics of the Nigerian Tar Sands", *Sedimentary Geology* **44**, 65-81.

Environment Canada (2007). "National Inventory Report 1990–2005: Greenhouse Gas Sources and Sinks in Canada", www.ec.gc.ca/Publications, accessed June 20, 2011.

Escobedo, J. and Mansoori, G.A. (1995). "Viscometric Determination of the Onset of Asphaltene Flocculation: A Novel Method", *SPEPF* **10**, 2, 115-118.

Esmail, M.N. (1985). "Problems in Numerical Simulation of Heavy Oil Reservoirs", *JCPT* **24**, 3, 80-82.

ExxonMobil (2010). "The Promise of Carbon Capture and Storage", www.exxonmobil.com, accessed Nov. 1, 2010.

Fadili, A., Alizadeh, N., Leung, E., Khaksar, A. and Ashoori, S. (2009). "Simulating the Permeability Reduction due to Asphaltene Deposition in Porous Media". Paper 13262 presented at Int. Pet. Tech. Conf., Doha, 7-9 Dec.

Fan, T. and Buckley, J.S. (2002). "Rapid and Accurate SARA Analysis of Medium Gravity Crude Oils", *Energy & Fuels* **16**, 6, 1571-1575.

Farouq-Ali, S.M. (1994). "CSS – Canada's Super Strategy for Oil Sands", *JCPT* **33**, 9, 16-19.

Farouq-Ali, S.M. (1997). "Is there Life after SAGD?", *JCPT* **36**, 6, 20-23.

Fayose, E.A. (2005). "Bitumen in Ondo State: Prospects and Promises", www.ondostategovernment.com/bitumen.html, accessed Oct. 25, 2009.

Fazelipour, W. (2005). "Reservoir Simulation of Asphaltene Precipitation", U. of Texas, Austin, www.pe.utexas.edu/Dept/Org/Students/PGEGSA/docs/waleed_pgegsa2005.pdf accessed Dec. 16, 2009.

Ferguson, F.R.S. and Butler, R.M. (1988). "Steam-assisted Gravity Drainage Model Incorporating Energy Recovery from a Cooling Steam Chamber", *JCPT* **27**, 5, 75-83.

Fisher, D., Yazawa, N., Sarma, N., Girard, M., Turta, A. and Huang, H. (2003). "A New Method to Characterise the Size and Shape Dynamics of Asphaltene Deposition Process in CO_2 Miscible Flooding". Paper 84893 presented at SPE Int. Improved Oil recovery Conf. in Asia Pacific, Kuala Lumpur, 20-21 Oct.

Fontana, M.G. and Greene, N.D. (1986). *Corrosion Engineering*, 3rd ed., McGraw-Hill Book Co., New York.

Fontanilla, P. and Aziz, K. (1982). "Prediction of Bottom-hole Conditions for Wet Steam Injection Wells", *JCPT* **21**, 2, 82-88.

Forsyth, P.A. and Vetzal, K.R. (2002). "Quadratic Convergence for Valuing American Options using a Penalty Method", *SIAM J. on Scientific Computing* **23**, 6.

Fox, R.L., Donaldson, B.A. and Mulac, A.J. (1981). "Development of Technology for Downhole Steam Production". Paper 9776 presented at SPE/DOE Symposium on Enhanced Oil Recovery, Tulsa, 5-8 Apr.

Frauenfeld, T.W., Deng, X. and Jossy, C. (2006). Economic Analysis of Thermal Solvent Processes". Paper 2006-164 presented at Petroleum Society's Canadian Int. Petroleum Conf., Alberta, 13-15 June.

Frauenfeld, T.W.J., Ridley, R.K. and Nguyen, D.M. (1988). "Effect of an Initial Gas Content on Thermal EOR as Applied to Oil Sands", *JPT* **40**, 3, 333-338.

Galoppini, M. and Tambini, M. (1994). "Asphaltene Deposition Monitoring and Removal Treatments: An Experience in Ultra Deep Wells". Paper 27622 presented at SPE European Prod. Operations Conf. & Exhibition, Aberdeen, 15-17 Mar.

Gambill, W.R. (Jun. 1957). "You Can Predict Heat Capacities", *Chem. Eng.*, 88-91.

Gaspar Ravagnani, A.T.F.S., Ligero, E.L. and Suslick, S.B. (2009). "CO_2 Sequestration through Enhanced Oil Recovery in a Mature Oil Field", *J. Pet. Sci. Eng.* **65**, 129-138.

Gates, I., Adams, J., and Larter, S. (2008b). "The Impact of Oil Viscosity Heterogeneity on Production from Heavy Oil and Bitumen Reservoirs: Geotailoring Recovery Processes to Compositionally Graded Reservoirs", *CSEG Recorder* **33**, 7, 42-48.

Gates, I. D., Adams, J. J., and Larter, S. R. (2008a). "The Impact of Oil Viscosity Heterogeneity on the Production Characteristics of Tar Sand and Heavy Oil Reservoirs. Part II: Intelligent, Geotailored Recovery Processes in Compositionally Graded Reservoirs", *JCPT* **47**, 9, 40 - 49.

Gates, I.D. and Chakrabart, N. (2006). "Optimisation of Steam Assisted Gravity Drainage in McMurray Reservoir", *JCPT* **45**, 9, 54-62.

Gates, I.D., Kenny, J., Hernandez-Hdez, I.L. and Bunio, G.L. (2007). "Steam-Injection Strategy and Energetics of Steam-Assisted Gravity Drainage", *SPEREE* **10**, 1, 19-34.

Gbadebo, A.M. (2010). "Environmental Implications of Bitumen Seep Induced Pollution in Parts of Ogun State, Southwestern Nigeria", *Environ. Earth Sci.* **59**, 1507-1514.

Gerald, C.F. and Wheatley, P.O. (1989). *Applied Numerical Analysis*, 4th ed., Addison-Wesley Inc., New York.

Gerl, S. and Stahl, W. (1996). "Improved Dewatering of Coal by Steam Pressure Filtration", *Coal Prep.* **17**, 137-146.

Gibbons, K., Halvorsen, C. and Siring, E. (1993). "Vertical and Horizontal Permeability Variation within a Sandstone Reservoir based on Minipermeameter Measurements", *Marine & Petroleum Geol.* **10**, 4, 325-334.

Giles, M.B. and Carter, R. (2006). "Convergence Analysis of Crank-Nicolson and Rannacher Time-marching", *J. Computational Finance* **9**, 4, 89-112.

Gipson, L.J., Owen, R. and Robertson, C.R. (2002). "Hamaca Heavy Oil Project – Lessons Learned and an Evolving Development Strategy". Paper 78990 presented at SPE Int. Thermal Operations & Heavy Oil Symposium and Int. Horizontal Well Technology Conf., Alberta, 4-7 Nov.

Glandt, C.A. and Malcolm, J.D. (1991). "Numerical Simulation of Peace River Recovery Processes". Paper 22645 presented at SPE Annual Technical Conf. & Exhibition, Dallas, 6-9 Oct.

Glenn, W., Ezio, T., Jueren, X., Brian, W. and Chengye, F. (2008). "Mechanical Evaluation of a New Sand Control Screen for SAGD Applications". Paper 117486 presented at SPE Int. Thermal Operations & Heavy Oil Symp., Alberta, 20-23 Oct.

Godze, S., Chhina, H.S. and Best, D.A. (1989). "An Analytical Cyclic Steam Stimulation Model for Heavy-Oil Reservoirs". Paper 18807 presented at SPE California Regional Meeting, Bakersfield, 5-7 Apr.

Gomaa, E.E. (1980). "Correlations for Predicting Oil Recovery of Steamflood", *JPT* **32**, 2, 325-332.

Gontijo, J.E. and Aziz, K. (1984). "A Simple Analytical Model for Simulating Oil Recovery by Cyclic Steam in Pressure-Depleted Reservoirs". Paper 13037 presented at SPE Annual Technical Conf. & Exhibition, Houston, 16-19 Sept.

Gotawala, D.R. and Gates, I.D. (2010). "On the Impact of Permeability Heterogeneity on SAGD Steam Chamber Growth", *Natural Resources Research* **19**, 2, 151-164.

Gotawala, D.R. and Gates, I.D. (2009). "SAGD Subcool Control with Smart Injection Wells". Paper 122014 presented at EUROPEC/EAGE Conf. & Exhibition, Amsterdam, 8-11 Jun.

Gotawala, D. R. and Gates, I. D. (2008). "Steam Fingering at the Edge of a Steam Chamber in a Heavy Oil Reservoir", *Can. J. Chem. Eng*. **86**, 6, 1011-1022.

Green, D.W. and Willhite, G.P. (1998). *Enhanced Oil Recovery*, SPE Inc., Texas.

Gruesbeck, C. and Collins, R. E. (1982). "Entrainment and Deposition of Fine Particles in Porous Media," *SPE J.* **22**, 12, 847–856.

Gu, F., Chan, M. and Fryk, R. (2011). "Geomechanical-Data Acquisition, Monitoring, and Applications in SAGD", *JCPT* **50**, 6, 9-21.

Guedes, R.G., Al-Abduwani, F., Bedrikovetsky, P. and Currie, P.K. (2009). "Deep-Bed Filtration under Multiple Particle-Capture Mechanisms", *SPE J.* **14**, 3, 477-487.

Gummel, J., Corvis, Y., Jestin, J., M'Hamdi, J. and Barre, L. (2009). "Asphaltene Multilayer Growth in Porous Medium Probed by SANS", *Eur. Phys. J. Special Topics* **167**, 1, 171–176.

Hamadou, R., Khodja, M., Kartout, M. and Jada, A. (2008). "Permeability Reduction by Asphaltenes and Resins Deposition in Porous Media", *Fuel* **87**, 10-11, 2178-2185.

Harding, T.G., Farouq Ali, S.M. and Flock, D.L. (1983). "Steam Performance in the Presence of Carbon dioxide and Nitrogen", *JCPT* **22**, 5, 30-37.

Hart Energy (Jul. 2006). "In Situ Production Technologies", *E&P Magazine* and *Oil & Gas Investor*. Available at www.heavyoilinfo.com/feature_items/e-p_heavyoil_article-1.pdf/download, accessed Apr. 29, 2009.

Hart Energy (2008). "Shaping Heavy Oil's Future", www.heavyoilinfo.com/feature_items/, accessed July 2, 2011.

Hassanzadeh, H. and Pooladi-Darvish, M. (2007). "Comparison of Different Numerical Laplace Inversion Methods for Engineering Applications", *App. Mathematics & Computation* **189**, 1966-1981.

Hassid, S. (2002). "Multi-layer Conductive Heat Transfer Including an Infinite Medium", *Energy & Buildings* **34**, 267-272.

Haut, R.C. and Thomas, E.R. (1989). "Development and Application of the Controlled-Freeze-Zone Process", *SPEPE* **4**, 3, 265-271.

Hayashitani, M., Bennion, D.W., Donnelly, J.K. and Moore, R.G. (1978). "Thermal Cracking Models for Athabasca Oil Sands Oil". Paper 7549 presented at SPE Annual Technical Conf. & Exhibition, Texas, 1-3 Oct.

Heins, W.F. (2010). "Is a Paradigm Shift in Produced Water Treatment Technology Occurring at SAGD Facilities?" *JCPT* **48**, 9, 10-15.

Hénaut, I., Barré, L., Argillier, J.F., Brucy, F. and Bouchard, R. (2001). "Rheological and Structural Properties of Heavy Crude Oils in Relation with Their Asphaltenes Content". Paper 65020 presented at SPE Int. Symposium on Oilfield Chemistry, Houston, 13-16 Feb.

Herold, A. (2003). "Comparison of CO_2 Emission Factors for Fuels used in Greenhouse Gas Inventories and Consequences for Monitoring and Reporting under the EC Emissions Trading Scheme", ETC/ACC Technical Paper 2003/10.

Herzig, J.P., Leclerc, D.M., and LeGoff, P. (1970). "Flow of Suspensions through Porous Media- Application to Deep Filtration", *Ind. Eng. Chem.* **62**, 5, 8-35.

Hirschberg, A., deJong, L.N.J., Schipper, B.A. and Meijer, J.G. (1984). "Influence of Temperature and Pressure on Asphaltene Flocculation", *SPE J.* **24**, 3, 283-293.

Hong, K.C. and Ault, J.W. (1984). "Effects of Noncondensable Gas Injection on Oil Recovery by Steamflooding", *JPT* **36**, 12, 2160-2170.

Hornbrook, M.W., Dehghani, K., Qadeer, S., Ostermann, R.D. and Ogbe, D.O. (1991). "Effects of CO_2 Addition to Steam on Recovery of West Sak Crude Oil", *SPERE* **6**, 3, 278-286.

Ibisi, N.E., Okwu, D.E. and Ekwenchi, M.M. (2006). "Evaluation of the Chemical Composition of Tar Sands of Southwestern Nigeria", *J. Eng. & Applied Sci.* **1**, 2, 138-142.

Ikwumonu, A., Rawnsley, K., Habsi, M. and Penney, R. (2007). "Key Learnings from History Matching a Thermally Assisted Gas / Oil Gravity-Drainage Pilot in Fractured Reservoirs". Paper 11411 presented at Int. Petroleum. Technology Conf., Dubai, 4-6 Dec.

IEA (2010). "World Energy Outlook 2010", International Energy Agency.

IPCC (1997). *Revised 1996 IPCC Guidelines for National Greenhouse Gas Inventories*, J.T. Houghton *et al.*, IPCC/OECD/IEA, Paris.

Ito, Y. (1984). "The Introduction of the Microchannelling Phenomena to Cyclic Steam Stimulation and its Application to the Numerical Simulation (Sand Deformation Concept", *SPE J.* **24**, 4, 417-430.

Ito, Y., Hirata, T. and Ichikawa, M. (2004). "The Effect of Operating Pressure on the Growth of the Steam Chamber Detected at the Hangingstone SAGD Project", *JCPT* **43**, 1, 47-53.

Ito, Y., Ichikawa, M. and Hirata, T. (2001). "The Growth of the Steam Chamber During the Early Period of the UTF Phase B and Phase I Projects", *JCPT* **40**, 9, 29-36.

Ito, Y. and Ipek, G. (2005). "Steam-Fingering Phenomenon During SAGD Process". Paper 97729 presented at SPE Int. Thermal Operations & Heavy Oil Symposium, Calgary, 1-3 Nov.

Ito, Y. and Susuki, S. (1999). "Numerical Simulation of the SAGD Process in the Hangingstone Oil Sands Reservoir", *JCPT* **38**, 9, 27-35.

Iwasaki, T. (1937). "Some Notes on Sand Filtration", *J. American Water Works Assoc.* **29**, 1591-1602.

Jamaluddin, A.K.M., Creek, J., Kabir, C.S., McFadden, J.D., D'Cruz, D., Manakalathil, M., Joshi, N. and Ross, B. (2002). "Laboratory Techniques to Measure Thermodynamic Asphaltene Instability", *J. Can. Pet. Tech.* **41**, 7, 44-52.

Jenkins, R. and Aronofsky, J.S. (1954). "Analysis of Heat Transfer Processes in Porous Media – New Concepts in Reservoir Heat Engineering", *Proc.* 18th Technical Conf. on Petroleum Prod., Pennsylvania State Univ., Pennsylvania

Jiang, Q., Butler, R. and Yee, C.T. (2000a). "The Steam and Gas Push (SAGP) - 2: Mechanism Analysis and Physical Model Testing", *JCPT* **39**, 4, 52-61.

Jiang, Q., Butler, R.M. and Yee, C.T. (2000b). "Steam and Gas Push (SAGP) – 4; Recent Theoretical Developments and Laboratory Results Using Layered Models". Paper 2000-51 presented at Canadian Int. Petroleum Conf., Alberta, 4-8 Jun.

Jimenez, J. (2008). "The Field Performance of SAGD Projects in Canada". Paper 12860 presented at the Int. Pet. Tech. Conf., Kuala Lumpur, 3-5 Dec.

Johnson, S.E., Svrcek, W.Y. and Mehrotra, A.K. (1987). "Viscosity Prediction of Athabasca Bitumen Using the Extended Principle of Corresponding States", *Ind. Eng. Chem. Res.* **26**, 11, 2290-2298.

Jones, J. (1977). "Cyclic Steam Reservoir Model for Viscous Oil, Pressure Depleted Reservoirs". Paper 6544 presented at SPE California Regional Meeting, Bakersfield, 13-15 Apr.

Jones, J. (1992). "Why Cyclic Steam Predictive Models Get No Respect", *SPERE* **7**, 1, 67-74.

Jones, J. (1981). "Steam Drive Model for Hand-Held Programmable Calculators", *JPT* **33**, 9, 1583-1598.

Kaarstad, O. (2004). "The Sleipner Project". Paper presented at IEA Asia Pacific Conf. on Zero Emissions Technologies, Queensland, 18 Feb.

Kabir, C.S., A. Chawathe, S.D. Jenkins, A.J. Olayomi, C. Aigbe, and D.B. Faparusi (2002). "Developing New Fields Using Probabilistic Reservoir Forecasting". Paper 77564 presented at SPE Annual Technical Conference & Exhibition, San Antonio, 29 Sep - 2 Oct.

Kariznovi, M., Nourozieh, H., Jamialahmadi, M. and Shahrabadi, A. (2008). "Optimisation of Asphaltene Deposition and Adsorption Parameter in Porous Media Search". Paper 114037 presented at SPE Western Regional & Pacific Section AAPG Joint Meeting, California, 31 Mar - 2 Apr.

Kawanaka, S., Leontaritis, K. J., Park, S. J. and Mansoori, G. A. (1989). "Thermodynamic and Colloidal Models of Asphaltene Flocculation", in: *Oil Field Chemistry*, Chapter 24, 443-458, ACS Symposium Series, Vol. 396, Am. Chem. Soc., Washington, DC.

Khalil, E.E. (1982). *Modelling of Furnaces and Combustors*, Abacus Press, Kent.

Khraisha, Y.H. (2002). "Thermal Conductivity of Oil Shale Particles in a Packed Bed", *Energy Sources, Part A: Recovery, Utilization & Environmental Effects* **24**, 7, 613-623.

Kisman, K.E. and Yeung, K.C. (1995). "Numerical Study of the SAGD Process in the Burnt Lake Oil Sands Lease". Paper 30276 presented at SPE Int. Heavy Oil Symposium, Alberta, 19-21 Jun.

Kjosavik, A., Ringen, J.K. and Skjaeveland, S.M. (2002). "Relative Permeability Correlation for Mixed-Wet Reservoirs", *SPEREE* **7**, 1, 49-58.

Klins, M.A. (1984). *Carbon dioxide Flooding Basic Mechanisms and Project Design*, Int. Human Resources Devt. Corp., Boston.

Kocabas, I. (2003). "Characterisation of Asphaltene Precipitation Effect on Reducing Carbonate Rock Permeability". Paper 81572 presented at SPE Middle East Oil & Gas Show and Conf., Bahrain, 9-12 Jun.

Koenig, H.A. (1988). *Modern Computational Methods*, Taylor & Francis, Philadelphia.

Kokal, S., Al-Dawood, N., Fontanilla, J., Al-Ghamdi, A., Nasr-El-Din, H. and Al-Rufaie, Y. (2003). "Productivity Decline in Oil Wells Related to Asphaltene Precipitation and Emulsion Blocks", *SPEPF* **18**, 4, 247-256.

Koopmans, M.P., Larter, S.R., Zhang, C., Mei, B., Wu, T. and Chen, Y. (2002). "Biodegradation and Mixing of Crude oils in Eocene Es3 Reservoirs of the Liaohe Basin, Northeastern China", *AAPG Bulletin* **86**, 10, 1833-1843.

Koots, J.A. and Speight, J.G. (1975). "Relation of Petroleum Resins to Asphaltenes", *Fuel* **54**, 179-184.

KPMG (2008). "Ondo State, Nigeria: Market Feasibility Study for Sustainable Development", Publication No: RRD-108984, 1-44.

Kuhn, S.Z. (1995). *Investigation of Heat-transfer from Condensing Steam-Gas Mixtures and Turbulent Films Flowing Downward Inside a Vertical Tube*, Ph.D. Thesis, U. of California, Berkeley.

Kuhnen, F., Barmettler, K., Bhattacharjee, S., Elimelech, M. and Kretzschmar, R. (2000). "Transport of Iron Oxide Colloids in Packed Quartz Sand Media: Monolayer and Multilayer Deposition", *J. Colloidal & Interface Sci*. **231**, 1, 32-41.

Kumar, S., Torabzadeh, S.J. and Handy, L.L. (1985). "Relative Permeability Functions for High- and Low-Tension Systems at Elevated Temperatures". Paper 13670 presented at SPE California Regional Meeting, Bakersfield, 27-29 Mar.

Kumar, S., Zarzour, O. and Gupta, A. (2010). "Challenges in Design of Post Combustion CO_2 Capture Facilities". Paper 137373 presented at Abu Dhabi Int. Petroleum Exhibition & Conf., Abu Dhabi, 1-4 Nov.

Kyle, B.G. (1984). *Chemical and Process Thermodynamics*, Prentice-Hall, New Jersey.

Kyte, J.R. and Berry, D.W. (1975). "New Pseudo Functions to Control Numerical Dispersion", *SPE J.* **15**, 4, 269-276.

Lapidus, L. and Pinder, G.F. (1980). *Numerical Solution of Partial Differential Equations in Science and Engineering*, Wiley Interscience, New York.

Larter, S., Adams, J., Gates, I.D., Bennett, B. and Huang, H. (2008). "The Origin, Prediction and Impact of Oil Viscosity Heterogeneity on the Production Characteristics of Tar Sand and Heavy Oil Reservoirs", *JCPT* **47**, 1, 52-61.

Law, D.H.S. (2004). "Disposal of Carbon Dioxide, a Greenhouse Gas, for Pressure Maintenance in a Steam-Based Thermal Process for Recovery of Heavy Oil and Bitumen". Paper 86958 presented at SPE Int. Thermal Operations & Heavy Oil Symposium and Western Regional Meeting, Bakersfield, 16-18 Mar.

Law, D.H.S., Nasr, T.N. and Good, W.K. (2003a). "Lab-Scale Numerical Simulation of SAGD Process in the Presence of Top Thief Zones: A Mechanistic Study", *JCPT* **42**, 3, 29-35.

Law, D.H.S., Nasr, T.N. and Good, W.K. (2003b). "Field-Scale Numerical Simulation of SAGD Process with Top-Water Thief Zone", *JCPT* **42**, 8, 32-38.

Lawal, A. K. (2011a). "Reconciling and Improving the Volumetrics of Nigerian Heavy Oil and Bitumen Resources", accepted for the Nigerian Annual SPE Int. Technical Conf. & Exhibition, Abuja.

Lawal, A. K. (2011b). "Validation of a Pseudocomponent Scheme for Nigerian Heavy Oil and Bitumen", accepted for the Nigerian Annual SPE Int. Technical Conf. & Exhibition, Abuja.

Lawal, A.K. (2009). "Modelling Subsurface Uncertainties with Experimental Design: Some Arguments of Non-Conformists". Paper 128350 presented at Annual SPE Int. Conf. & Exhibition, Abuja, 3-5 Aug.

Lawal, A.K. and Adenuga, A.O. (2010). "Pseudo-components for Nigerian Heavy Oil and Bitumen". Paper 136954 presented at Annual SPE Int. Conf. & Exhibition, Calabar, 31 Jul - 7 Aug.

Lawal, A.K. and Eweje, O. (2009). "On Field Development Planning: A Comparative Study of Experimental Design and Structured Deterministic Techniques". Paper presented at Offshore West Africa Conf. & Exhibition, Abuja, 27 - 29 Jan.

Lawal, A.K. and Onyekonwu, M.O. (2005). "A Robust Approach to Flow Unit Zonation". Paper 98830 presented at SPE Int. Technical Conf. & Exhibition, Abuja, 1-3 Aug.

Lawal, A.K. and Vesovic, V. (2009). "Analytic Investigation of Convection During Conduction Heating of a Heavy-Oil Reservoir". Paper 124072 presented at SPE Annual Technical Conf. & Exhibition, New Orleans, 4-7 Oct.

Lawal, A.K. and Vesovic, V. (2010a). "Modelling Asphaltene-Induced Formation Damage in Closed Systems". SPE Paper 138497 presented at Abu Dhabi Int. Petroleum Exhibition & Conf., Abu Dhabi, 1-4 Nov.

Lawal, A.K. and Vesovic, V. (2010b). "Modelling Multiple-Contact Condensation of Heat-Transporting Fluids in Thermal Floods". Paper 130568 presented at SPE EUROPEC/EAGE Annual Conf. & Exhibition, Barcelona, 14–17 Jun.

Lawal, A.K., Vesovic, V. and Boek, E.S. (2011). "Modelling Permeability Impairment in Porous Media due to Asphaltene Deposition under Dynamic Conditions", submitted to *Energy & Fuels* (in review).

Lee, B.I. and Kesler, M.G. (1975). "A Generalised Thermodynamic Correlation Based on Three-Parameter Corresponding States", *AIChE J.* **21**, 3, 510-527.

Lee, W.J. (2009). "Reserves in Nontraditional Reservoirs: How Can We Account for Them?", *SPE Econs. & Manag.* **1**, 1, 11-18.

Lei, Q., Wang, J. and Gates, I.D. (2010). "Impact of Oil-Water Relative Permeability Curves on SAGD Behaviour". Paper 132185 presented at SPE Int. Oil & Gas Conf. and Exhibition, Beijing, 8-10 Jun.

Lemmon, E.W. and Jacobsen, R.T. (2004). "Viscosity and Thermal Conductivity Equations for Nitrogen, Oxygen, Argon, and Air", *Int. J. Thermophysics* **25**, 1, 21-69.

Leontaritis, K.J. (1989). "Asphaltene Deposition: A Comprehensive Description of Problem Manifestation and Modelling Approaches". Paper 18892 presented at SPE Production Operations Symposium, Oklahoma, 13-14 Mar.

Leontaritis, K.J., Amaefule, J.O. and Charles, R.E. (1994). "A Systematic Approach for the Prevention and Treatment of Formation Damage Caused by Asphaltene Deposition". *SPEPF* **9**, 3, 157-164.

Leontaritis, K.J. and Mansoori, G.A. (1988). "Asphaltene Deposition: A Survey of Field Experiences and Research Approaches", *J. Pet.Sci. Eng.* **1**, 3, 229-239.

Leung, L.C. (1983). "Numerical Evaluation of the Effect of Simultaneous Steam and Carbon dioxide Injection on the Recovery of Heavy Oil", *JPT* **35**, 9, 1591-1599.

Levenspiel, O. (1999). *Chemical Reaction Engineering*, 3rd ed., John Wiley & Sons, New York.

Lewis, R.W., Morgan, K. and Roberts, P.M. (1985). "Infinite Element Modelling of Heat Losses during Thermal Recovery Processes". Paper 13515 presented at SPE Reservoir Simulation Symp., Texas, 10-13 Feb.

Li, P. and Chalaturnyk, R.J. (2009). "History Match of the UTF Phase A Project with Coupled Reservoir Geomechanical Simulation", *JCPT* **48**, 1, 29-35.

Li, X. (2011). "Asphaltene Onset Precipitation for Crude X", Personal Communication, April 10, 2011.

Logan, D.L. (2008). *An Introduction to Nonlinear Partial Differential Equations*, 2nd ed., Wiley, New Jersey.

Lolley, C.S. and Richardson, W.C. (1998). "Minimum Pseudocomponent Requirements for Compositional Thermal Simulation of Heavy Oil". Paper 39640 presented at SPE/DOE Improved Oil Recovery Symp., Oklahoma, 19-22 Apr.

Luo, P. and Gu, Y. (2007). "Effects of Asphaltene Content on the Heavy Oil Viscosity at Different Temperatures", *Fuel* **86**, 7-8, 1069-1078.

Luo, P. and Gu, Y. (2005). "Effects of Asphaltene Content and Solvent Concentration on Heavy-Oil Viscosity". Paper 97778 presented at SPE Int. Thermal Operations & Heavy Oil Symposium, Calgary, 1-3 Nov.

Luo, P., Wang, X. and Gu, Y. (2010). "Characterisation of Asphaltenes Precipitated with Three Light Alkanes under Different Experimental Conditions", *Fluid Phase Equilibria* **291**, 103-110.

Macchietto, S., Hewitt, G.F., Coletti, F., Crittenden, B.D., Dugwell, D.R., Galindo, A., Jackson, G., Kandiyoti, R., Kazarian, S.G., Luckham, P.F., Matar, O.K., Millan-Agorio, M., Müller, E.A., Paterson, W., Pugh, S.J., Richardson, S.M. and Wilson, D.I. (2011). "Fouling in Crude Oil Preheat Trains: A Systematic Solution to an Old Problem", *Heat Transfer Eng.***32**, 3-4, 197-215.

Mago, A.L., Barrufet, M.A. and Nogueira, M.C. (2005). "Assessing the Impact of Oil Viscosity Mixing Rules in Cyclic Steam Stimulation of Extra-Heavy Oils". Paper 95643 presented at SPE Annual Technical Conf. & Exhibition, Texas, 9-12 Oct.

Maini, B.B. and Batycky, J.P. (1983). "Effect of Temperature on Heavy-Oil/Water Relative Permeabilities in Horizontally and Vertically Drilled Core Plugs". Paper 12115 presented at SPE Annual Fall Tech. Meeting, San Francisco, 5-8 Oct.

Mane, P.A. (2007). "Angola – Water-Alternating Gas – First Surface Deepwater Well Gas to Water Injection Conversion". Paper 11378 presented at Int. Pet. Tech. Conf., Dubai, 4-6 Dec.

Maqbool, T., Balgoa, A.T. and Fogler, H.S. (2009). "Revisiting Asphaltene Precipitation from Crude Oils: A Case of Neglected Kinetic Effects", *Energy & Fuels* **23**, 7, 3681-3686.

Maqbool, T., Srikiratiwong, P. and Fogler, H.S. (2011). "Effect of Temperature on the Precipitation Kinetics of Asphaltenes", *Energy & Fuels* **25**, 2, 694-700.

Marlin, T.E. (1995). *Process Control: Designing Processes and Control Systems for Dynamic Performance*, McGraw-Hill Inc., New York.

Marx, J.W. and Langenheim, R.H. (1959). "Reservoir Heating by Hot Fluid Injection", *Trans.* AIME **216**, 312-315.

McCain, W.D., Jr. (1990). *The Properties of Petroleum Fluids*, 2nd ed., PennWell Publishing Co., Oklahoma.

McGee, B.C.W. and Vermeulen, F.E. (2007). "The Mechanisms of Electrical Heating for the Recovery of Bitumen from Oil Sands", *JCPT* **46**, 1, 28-34.

Mehrotra, A.K. and Svrcek, W.Y. (1988). "Characterisation of Athabasca Bitumen for Gas Solubility Calculations", *JCPT* **27**, 6, 107-110.

Mehrotra, A.K. and Svrcek, W.Y. (1987). "Corresponding States Method for Calculating Bitumen Viscosity", *JCPT* **26**, 5, 60-66.

Meldau, R.F., Shipley, R.G. and Coats, K.H. (1981). "Cyclic Gas Steam Injection in Heavy-Oil Wells", *JPT* **33**, 10, 1990-1998.

Mendoza de la Cruz, J.L., Arguelles-Vivas, F.J., Matias-Perez, V., Duran-Valencia, C.A. and Lopez-Ramirez, S. (2009). "Asphaltene-Induced Precipitation and Deposition During Pressure Depletion on a Porous Medium: An Experimental Investigation and Modelling Approach", *Energy & Fuels* **23**, 11, 5611-5625.

Messner, G.L. (1990). "A Comparison of Mass Rate and Steam Quality Reductions to Optimise Steamflood Performance". Paper 20761 presented at SPE Annual Technical Conf. & Exhibition, New Orleans, 23-26 Sept.

Metwally, M. (1990). "Effect of Gaseous Additives on Steam Processes for Lindbergh Field, Alberta", *JCPT* **29**, 6, 26-30.

Meyer, R.F., Attanasi, E.D. and Freeman, P.A. (2007). "Heavy Oil and Natural Bitumen Resources in Geological Basins of the World", US Geological Survey Open-File Report 2007-1084, available at http://pubs.usgs.gov/of/2007/1084/.

Miller, J.S. and Jones, R.A. (1981). "A Laboratory Study to Determine Physical Characteristics of Heavy Oil after CO_2 Saturation". Paper 9789 presented at SPE/DOE Symposium on Enhanced Oil Recovery", Tulsa, 5-8 Apr.

Miller, K.A. and Xiao, Y. (2010). "Lloydminster, Saskatchewan Vertical Well SAGD Field Test Results", *JCPT* **49**, 1, 22-29.

Miller, M.A. and Ramey, H.J., JR. (1983). "Effect of Temperature on Oil-Water Relative Permeabilities of Unconsolidated and Consolidated Sands". Paper 12116 presented at SPE Annual Fall Tech. Meeting, San Francisco, 5-8 Oct.

Miller, M.A. and Ramey, H.J., Jr. (1985). "Effect of Temperature on Oil-Water Relative Permeabilities of Unconsolidated and Consolidated Sands", *SPE J.* **25**, 6, 945-953.

Ministry of Mines & Steel Development (2010). *Tarsands and Bitumen Exploration Opportunities in Nigeria*, www.mmsd.gov.ng/Downloads/Tarsand%20&%20Bitumen.pdf , accessed July 29, 2010.

Ministry of Solid Minerals Development (2006). *Technical Overview: Nigeria's Bitumen Belt and Development Potential*, www.mmsd.gov.ng/privatisation/docs/bitumen%20overview.pdf, accessed Jan. 16, 2011.

Minssieux, L., Nabzar, L., Chauveteau, G., Longeron, D. and Bensalem, R. (1998). "Permeability Damage due to Asphaltene Deposition: Experimental and Modelling Aspects", *Rev. Inst. Franc. Pet.* **53**, 3, 313-327.

Mohamed, R.S., Ramos, A.C.S. and Loh, W. (1999). "Aggregation Behaviour of Two Asphaltenic Fractions in Aromatic Solvents", *Energy & Fuels* **13**, 2, 323-327.

Mohammadzadeh, O., Rezaei, N. and Chatzis, I. (2010). "Pore-Level Investigation of Heavy Oil and Bitumen Recovery Using Hybrid SAGD Process". Paper 130011 presented at SPE Improved Oil Recovery Symp., Oklahoma, 24-28 Apr.

Montgomery, D.C. (1976). *Design and Analysis of Experiments*, John Wiley & Sons Inc., New York.

Morton, K.W. and Mayers, D.F. (2005). *Numerical Solution of Partial Differential Equations*, 2nd ed., Cambridge U. Press, Cambridge.

Mousavi-Dehghani, S.A., Riazi, M.R., Vafaie-Sefti, M., and Mansoori, G.A. (2004). "An Analysis of Methods for Determination Onsets of Asphaltene Phase Separations", *J. Pet. Sci. & Eng.* **42**, 2-4, 145-156.

Mousavi Dehghani, S.A., Vafaie Sefti, M., Mirzayi, B. and Fasih, M. (2007). "Experimental Investigation on Asphaltene Deposition in Porous Media During Miscible Gas Injection", *Iran J. Chem. Chem. Eng.* **26**, 4 39-48.

Myhill, N.A. and Stegemeier (1978). "Steam-Drive Correlation and Prediction", *JPT* **30**, 2, 173-182.

Nabzar, L. and Aguiléra, M.E. (2008). "The Colloidal Approach. A Promising Route for Asphaltene Deposition Modelling", *Oil & Gas Science and Tech. – Rev. IFP* **63**, 1, 21-35.

Nadella, N.M. (2010). "Improving Energy Efficiency in Thermal Oil Recovery Surface Facilities". Paper presented at the World Energy Congress, Montreal.

Nakornthap, K. and Evans, R.D. (1986). "Temperature-Dependent Relative Permeability and its Effect on Oil Displacement by Thermal Methods", *SPERE* **1**, 3, 230-242.

Nasr, T.N., Beaulieu, G., Golbeck, H. and Heck, G. (2003). "Novel Expanding Solvent-SAGD Process "ES-SAGD"", *JCPT* **42**, 1, 13-16.

Nasr, T.N., Golbeck, H. and Lorimer, S. (1996). "Analysis of the Steam Assisted Gravity Drainage Process Using Experimental/Numerical Tools". Paper 37116 presented at SPE Int. Conf. on Horizontal Well Tech., Calgary, 18-20 Nov.

Nasr, T.N., Law, D.H.S., Golbeck, H. and Korpany, G. (2000). "Counter-current Aspect of the SAGD Process", *JCPT* **39**, 1, 41-47.

Nasr, T.N., Prowse, D.R. and Fraunfeld, T.W.J. (1987). "The Use of Flue Gas with Steam in Bitumen Recovery from Oil Sands", *JCPT* **26**, 3, 62-69.

Nasrabadi, H., Ghorayeb, K. and Firoozabadi, A. (2006). "Two-Phase Multicomponent Diffusion and Convection for Reservoir Initialisation", *SPEREE* **9**, 5, 530-542.

Nasri, Z. and Dabir, B. (2009). "Effects of Asphaltene Deposition on Oil Reservoir Characteristics Including Two-phase Flow", *J. Jpn. Petrol. Inst.* **52**, 1, 1-8.

Neal, P.R., Hou, W., Allinson, W.G. and Cinar, Y. (2010). "Costs of CO_2 Transport and Injection in Australia". Paper 133900 presented at SPE Asia Pacific Oil & Gas Conf. & Exhibition, Queensland, 18-20 Oct.

NEB (National Energy Board of Canada) (July 2006). "Canada's Oil Sands, Opportunities & Challenges to 2015: An Update", Calgary.

Newley, T.M.J. and Merrill Jr., R.C. (1991). "Pseudocomponent Selection for Compositional Simulation", *SPERE* **6**, 4, 490-496.

Nghiem, L.X. and Coombe, D.A. (1997). "Modelling Asphaltene Precipitation during Primary Depletion", *SPE J.* **2**, 2, 170-176.

Nigeriafirst (2006). "Bitumen Production", Office of Public Communications, Abuja, www.nigeriafirst.org, accessed Dec. 5, 2009.

Nigerian National Archives, Enugu Branch, CSE 8/4/59-CSO368/09: Mr Crewe-Sir W. Egerton, Governor of Nigeria, 30 Aug. 1909 (letter); Carland, *The Colonial Office and Nigeria*, p. 193; *The Times*, 11 Dec. 1908, p. 16f. *Cited in Steyn (2006)*.

NIPC (Nigerian Investment Promotion Commission) (2010). "Investors' Guide to Nigeria", 5th ed., www.cbcglobal.org/CBCG_Library, accessed Dec. 19, 2010.

Niz-Velasquez, E., Van Fraassen, K., Moore, R.G. and Mehta, S.A. (2009). "An Experimental Study on Three-Phase Flow in High Pressure Air Injection (HPAI)", *JCPT* **48**, 9, 47-53.

No, H.C. and Park, H.S. (2002). "Non-iterative Condensation Modelling for Steam Condensation with Non-condensable Gas in a Vertical Tube", *Int. J. Heat Mass Transfer* **45**, 845-854.

Nogueira, M.C. and Mamora, D.D. (2005). "Effect of Flue Gas Impurities on the Process of Injection and Storage of CO_2 in Depleted Gas Reservoirs". Paper 94906-STU presented at SPE/EPA/DOE E&P Environmental Conf., Texas, 7-9 Mar.

NNPC (Nigerian National Petroleum Corporation) (2010). "Kaduna Refining & Petrochemical Company", www.nnpcgroup.com/NNPCBusiness, accessed May 22, 2011.

Nwachukwu, C. and Adeoye, Y. (2010). "FG Unveils New Gas Prices", Vanguard Newspapers, Aug. 19, 2010.

Nwete, B.O.N. (2004). "Mineral and Petroleum Taxation: How Can Tax Allowances Promote Investment in the Nigerian Petroleum Industry?" www.dundee.ac.uk, accessed Dec. 18, 2010.

Oballa, V., Coombe, D.A. and Buchanan, L. (1997). "Aspects of Discretised Wellbore Modelling Coupled to Compositional/Thermal Simulation", *JCPT* **36**, 4, 45-51.

Oboh, B.O., Ilori, M.O., Akinyemi, J.O. and Adebusoye, S.A. (2006). "Hydrocarbon Degrading Potentials of Bacteria Isolated from a Nigerian Bitumen (Tar sand) Deposit", *Nature & Science* **4**, 3, 51-57.

O'Dell, M. and Lamers, E. (2003). "Subsurface Uncertainty Management in the Harweel Cluster, South Oman". SPE 84189 presented at Annual Technical Conf. & Exhibition, Denver, Colorado, 5 - 8 Oct.

Oderinde, R.A. and Olanipekun, E.O. (1991). "Composition Analysis of the Oil Component of the Nigerian Bitumen", *J. African Earth Sci.* **12**, 3, 483-487.

Odunaike, R.K., Laoye, J.A., Fasunwon, O.O., Ijeoma, G.C. and Akinyemi, L.P. (2010). "Geophysical Mapping of the Occurrence of Shallow Oil Sands in Idiopopo at Okitipupa Area, South-western Nigeria", *African J. Environ. Sci. & Tech.* **4**, 1, 34-44.

Odunaike, R.K., Ijeoma, G.C., Edigbe, R.O. and Babatope, A.H. (2009). "Oil Sands Exploration in Ijebu-Imushin Using Magnetic and Electrical Resistivity Methods", 11th SAGA Biennial Technical Meeting & Exhibition, Swaziland, 16-18 Sept.

Ogunsola, O.I. (1991). "Thermal Behaviour of Nigerian Oil Sands in Inert and Oxidising Atmospheres", *J. Analytical & Applied Pyrolysis* **21**, 1-2, 103-109.

Ogunsola, O.I. and Williams, P.C. (1988). ""Particle Size Effects on Compositional Analysis of Nigerian Tarsands", *J. African Earth Sciences* **7**, 4, 653-655.

Oil & Gas Journal (2006). "Historical Enhanced Oil Recovery Survey". *Cited in Meyer et al. (2007).*

Oluwole, A.F., Hannan, A.H.M.A., Kehinde, L.O., Borishade, A.B. and Adegoke, O.S. (1987). "Trace Elements in Nigerian Oil Sands and Extracted Bitumens", *J. Radioanalytical & Nuclear Chem.* **110**, 1, 275-282.

Omatsola, M.E. and Adegoke, O.S. (1981). "Tectonic Evolution and Cretaceous Stratigraphy of the Dahomey Basin", *J. Min. Geol.* **18**, 1, 130-137.

Omole, O. and Omolara, D. A. (1988). "Model Experiments of Steam Stimulation in Nigerian Tar Sands", *Energy Sources, Part A: Recovery, Utilisation & Environ. Effects* **10**, 2, 81-94.

OnlineNigeria (2009). "Bituminous Sands", www.onlinenigeria.com/geology accessed May 22, 2011.

Oracle (2000). "Oracle Crystal Ball", www.oracle.com, accessed May 20, 2011.

O'Rourke, J.C., Begley, A.G., Boyle, H.A., Yee, C.T., Chambers, J.I. and Luhning, R.W. (1997). "UTF Project Status Update", . Paper 97-08 presented at Petroleum Society's 48th Annual Technical Meeting, Calgary, 8-11 Jun.

O'Rourke, J.C., Begley, A.G., Boyle, H.A., Yee, C.T., Chambers, J.I. and Luhning, R.W. (1999). "UTF Project Status Update, May 1997", *JCPT* **38**, 9, 44-54.

Ozisik, M.N. (1993). *Heat Conduction*, John Wiley & Sons Inc., New York.

Palmgren, C.T.S. and Bruining, J. (1992). "An Interface Model to Predict Vertical Sweep During Steamdrive". Paper 24077 presented at SPE Western Regional Meeting, Bakersfield, 30 Mar - 1 Apr.

Pamukcu, Y.Z. and Gumrah, F. (2008). "Simulating Oil Recovery During CO_2 Sequestration Into a Mature Oil Reservoir", *JCPT* **47**, 8, 34-40.

Pang, S. and Sharma, M.M. (1997). "A Model for Predicting Injectivity Decline in Water-Injection Wells", *SPE Form. Eval.* **12**, 3, 194-201.

Paracha, O.R. (1985). *Experimental Investigation of the Effect of Carbon dioxide on Steam Drive Recovery*, PhD Thesis, U. of Oklahoma, Norman.

Park, H.S. and No, H.C. (1998). "A Condensation Experiment in the Presence of Noncondensables in a Vertical Tube of PCCS and its Assessment with RELAP5/MOD3.2", *Nucl. Technol.* **127**, 2, 160-169.

Patzek, T. (1996). "Field Applications of Steam Foam for Mobility Improvement and Profile Control", *SPERE* **11**, 2, 79-86.

Pautz, J.F., Crocker, M.E. and Walton, C.G. (1989). "Relating Water Quality and Formation Permeability to Loss of Injectivity". Paper 18888 presented at SPE Production Operations Symp., Oklahoma, 13-14 Mar.

Payatakes, A.C., Rajagopalan, R. and Tien, C. (1974). "Application of Porous Media Models to the Study of Deep Bed Fitration", *Can. J. Chem. Eng.* **52**, 722-731.

Pedersen, K.S., and Fredenslund, Aa. (1987). "An Improved Corresponding States Model for the Prediction of Oil and Gas Viscosities and Thermal Conductivities", *Chemical Eng. Sci.* **42**, 1, 182-186.

Peng, D.-Y. and Robinson, D.B. (1976). "A New Two-Constant Equation of State", *Ind. Eng. Chem. Fundam.*, **15**, 1, 59-64.

Perdomo, L., Damas, C.P. and Rincon, E.F. (2008). "The Impact of Steam Placement Control on SAGD Performance: A Numerical Study from the Orinoco Heavy Oil Belt". Paper 2008-450 presented at World Heavy Oil Congress, Edmonton, 10-12 Mar.

PPT (Petroleum Profits Tax) Act Cap 354 Laws of the Federation of Nigeria (LFN) 1990.

PTDF (Petroleum Technology Development Fund) Act Cap.355 Laws of the Federation of Nigeria (LFN) 1990.

Pfeiffer, J. Ph. and Saal, R. N. J. (1940). "Asphaltic Bitumen as Colloid System", *Phys. Chem.* **44**, 2, 139–149.

Pitzer, K.S. and Brewer, L. (1961). *Thermodynamics*, 2nd ed., McGraw-Hill, New York.

Pointcarbon (2010). "Value of Global Carbon Markets Up 5% in H1 2010", www.pointcarbon.com, accessed Dec. 19, 2010.

Polikar, M., Ferracuti, F., Decastro, V., Puttagunta, V.R. and Farouq Ali, S.M. (1986). "Effect of Temperature on Bitumen-Water End Point Relative Permeabilities and Saturations", *JCPT* **5**, 4, 44-50.

Poling, B.E., Prausnitz, J.M. and O'Connell, J.P. (2000). *The Properties of Gases and Liquids*, 5th ed., McGraw-Hill, New York.

Pooladi-Darvish, M., Tortike, W.S. and Farouq-Ali, S.M. (1994). "Steam Heating of Fractured Formations Containing Heavy Oil: Basic Premises and a Single-Block Analytical Model". Paper 28642 presented at SPE Annual Technical Conf. & Exhibition, New Orleans, 25-28 Sept.

Poston, S. W., Israel, S., Hossain, A. K. M. S., Montgomery III, E. F. and Ramey, H. J. Jr. (1970). "The Effect of Temperature on Irreducible Water Saturation and Relative Permeability of Unconsolidated Sands," *SPEJ.* **10**, 2, 171-180.

Prats, M. (1982). *Thermal Recovery*, SPE Monograph Vol. 7, SPE, Texas.

Priyanto, S., Mansoori, G.A., and Suwono, A. (2001). "Measurement of Property Relationships of Nano-structure Micelles and Coacervates of Asphaltene in a Pure Solvent", *Chem. Eng. Sci.* **56**, 24, 6933-6939.

Pujol, L. and Boberg, T.C. (1972). "Scaling Accuracy of Laboratory Steam Flooding Models". Paper 4191 presented at SPE Regional Meeting, Bakersfield, 8-10 Nov.

Pursley, S.A. (1975). "Experimental Studies of Thermal Recovery Processes". Paper presented at the Maracaibo Heavy Oil Symposium, Maracaibo, 4 Jun.

Queipo, N.V., Goicochea, J.V. and Pintos, S. (2002). "Surrogate Modelling-based Optimisation of SAGD Processes", *J. Pet. Sci. Eng.* **35**, 1-2, 83-93.

Rahman, M.M., Rahman, M.K. and Rahman, S.S. (2001). "An Integrated Model for Multiobjective Design Optimisation of Hydraulic Fracturing", *J. Pet. Sci. Eng.* **31**, 1, 41-62.

Rahmani, N.H.G., Masliyah, J.H. and Dabros, T. (2003). "Characterization of Asphaltenes Aggregation and Fragmentation in a Shear Field", *AIChE J.* **49**, 7, 1645-1655.

Rajagopalan, R. and Tien, C. (1976). "Trajectory Analysis of Deep Bed Filtration Using the Sphere-in-Cell Porous Media Model", *AIChE J.* **22**, 523.

Ramey Jr., H.J. (Nov. 1964). "How to Calculate Heat Transmission in Hot Fluid Injection", *Petroleum Engineer*.

Rastegari, K., Svrcek, W.Y. and Yarranton, H.W. (2004). "Kinetics of Asphaltene Flocculation", *Ind. Eng. Chem. Res.* **43**, 6861-6870.

Redford, D.A. and McKay, A.S. (1982). "The Use of Solvents and Gases in the Recovery of Bitumen from Oil Sands", *JCPT* **45**.

Reis, J.C. (1993). "A Steam-assisted Gravity Drainage Model for Tar Sands: Radial Geometry", *JCPT* **32**, 8, 43-48.

Reis, J.C. (1992). "A Steam-assisted Gravity Drainage Model for Tar Sands: Linear Geometry", *JCPT* **31**, 10, 14-20.

Reuters (2010). "Canada Heavy Oil Prices Weaken with Refinery Work", www.reuters.com, accessed Dec. 19, 2010.

Rezaei, N., Mohammadzadeh, O. and Chatzis, I. (2010). "Warm VAPEX: A Thermally Improved Vapor Extraction Process for Recovery of Heavy Oil and Bitumen", *Energy & Fuels* **24**, 11, 5934-5946.

Riaz, A. and Tchelepi, H.A. (2008). "Dynamics of Vertical Displacement in Porous Media Associated With CO_2 Sequestration", *SPE J.* **13**, 3, 305-313.

Rice, R.G. and Do, D.D. (1995). *Applied Mathematics and Modelling for Chemical Engineers*, John Wiley, New Jersey.

Richardson, W.C., Beladi, M.K. and Wu, C.H. (2000). "Steam Distillation Studies for the Kern River Field", *SPEREE* **3**, 1, 13-22.

Richtmyer, R.D. and Morton, K.W. (1967). *Difference Methods for Initial-value Problems*, 2nd ed., Wiley Inter., New York.

Ring, J.N., Wattenbarger, R.A., Keating, J.F. and Peddibhotla, S. (1994). "Simulation of Paraffin Deposition in Reservoirs", *SPEPF* **9**, 1, 36-42.

Rintoul, B. (Sept. 1979). "GATEOR Project at Edison", *Pacific Oil World*, 40-41.

Rivero, J.A. and Mamora, D.D. (2002). "Production Acceleration and Injectivity Enhancement Using Steam-Propane Injection for Hamaca Extra-Heavy Oil". Paper 75129 presented at SPE/DOE Improved Oil Recovery Symposium, Oklahoma, 13-17 Apr.

Robenstein, A.L. (1972). *Introduction to Ordinary Differential Equations*, Academic Press, Inc., New York.

Robertson, E.P. (1998). "Selection of Analytical Steam Stimulation Models Based on Common Reservoir Parameters". Paper 39607 presented at SPE/DOE Improved Oil Recovery Symposium, Tulsa, 19-22 Apr.

Roche, P. (May 2010). "Keep Your Cap On", *New Technology Magazine*, 1-6.

Roche, P. (Oct. 2008). "SAGD Report Card", *New Technology Magazine*, 1-12.

Rogner, H.H. (1997). "An Assessment of World Hydrocarbon Resources", *Annual Review of Energy & Env.* **22**, 217-262.

Rose, P.E. and Deo, M.D. (1995). "Steam-assisted Gravity Drainage in Oil Sand Reservoirs Using a Combination of Vertical and Horizontal Wells", *Fuel* **74**, 8, 1180-1184.

Rossen, R.H. and Dalton, R.L. (1990). "Selecting Grid and Timestep Sizes". In: *Reservoir Simulation*: C.C. Mattax and R.L. Dalton (eds.), SPE Monograph Series, Vol. 13, SPE, Texas.

Rowell, D. (2004). "Review of First- and Second-Order System Response", Dept. of Mechanical Engineering, Massachusetts Institute of Technology, Massachusetts.

S & S Geological Consultants Inc. (2008). "Steam Assisted Gravity Drainage", http://ssgeo.com/SAGD.html, accessed Nov. 16, 2010.

Saeed, M.S. (2010). *Effect of Temperature-Dependent Relative Permeability Functions on Thermal Recovery of Heavy Oil*, MSc Thesis, Imperial College London.

Sanchez, N.L. (1999). "Management of Water Alternating Gas (WAG) Injection Projects". Paper 53714 presented at SPE Latin American & Caribbean Petroleum Eng. Conf., Caracas, 21-23 Apr.

Sasaki, K., Akibayashi, S., Yazawa, N. and Kaneko, F. (2002). "Microscopic Visualisation with High Resolution Optical-Fibre Scope at Steam Chamber Interface on Initial Stage of SAGD Process". Paper 75241 presented at SPE/DOE Improved Oil Recovery Symposium, Tulsa, 13-17 Apr.

Sasaki, K., Akibayashi, S., Yazawa, N., Doan, Q.T. and Farouq Ali, S.M. (2001). "Experimental Modelling of the SAGD Process- Enhancing SAGD Performance with Periodic Stimulation of the Horizontal Producer", *SPE J*. **6**, 1, 89-97.

Satter, A. (1967). "A Prediction Method for Conduction Heating of Reservoirs by Steam Injection". Paper 1950 presented at 42nd Annual Fall Meeting of the SPE of AIME, Houston, 1-4 Oct.

Schapery, R.A. (1962). "Approximate Methods of Transform Inversion for Viscoelastic Stress Analysis". Proc. 4th US National Congress of Applied Mechanics, 1075-1085.

Schembre, J.M., Tang, G.Q. and Kovscek, A.R. (2006). "Interrelationship of Temperature and Wettability on the Relative Permeability of Heavy Oil in Diatomaceous Rocks", *SPEREE* **9**, 3, 239-250.

Schenk, L. (1989). "Further Discussion of Effect of an Initial Gas Content on Thermal EOR as Applied to Oil Sands", *JPT* **41**, 1, 94.

Schmidt, R., Gudbjerg, J., Sonnenborg, T.O. and Jensen, K.H. (2002). "Removal of Non-aqueous Phase Liquids from the Unsaturated Zone using Steam: Prevention of Downward Migration by Injecting Mixtures of Steam and Air", *J. Contam. Hydrol.* **55**, 233-260.

Schlumberger (2011). "Enhanced Oil Recovery", *Oilfield Glossary*, www.glossary.oilfield.slb.com, accessed June 28, 2011.

Schlumberger (2009). "Thermal Simulation Performance: Benchmarking ECLIPSE Thermal against another Leading Thermal Simulator", www.slb.com/media/services/software/whitepaper/whitepaper_benchmarking_eclipse_thermal.pdf, accessed Nov. 1, 2009.

Seba, R.D. and Perry, G.E. (1969). "A Mathematical Model of Repeated Steam Soaks of Thick Gravity Drainage Reservoirs", *JPT* **21**, 1, 87-94.

Sedaee Sola, B. and Rashidi, F. (2004). "Experimental Investigation of Steam/Methane Flooding in a Heavy Oil Reservoir". Paper 91968 presented at SPE Int. Petroleum Conf., Puebla, 8-9 Nov.

Sedaee Sola, B., Rashidi, F., and Babadagli, T (2007). "Temperature Effects on the Heavy Oil/Water Relative Permeabilities of Carbonate Rocks", *J. Pet. Sci. Eng.* **59**, 27 – 42.

Sharma, G.D. *et al.*[*] (1992). "Characterisation of Oil and Gas Reservoir Heterogeneity", DOE/ID/12839-8, Univ. Alaska, Fairbanks.

Sharma, J. and Gates, I. D. (2010). "Multiphase Flow at the Edge of a Steam Chamber", *Can. J. Chem. Eng*. **88**, 3, 312-321.

Shedid. A.S. (2001). "Influences of Asphaltene Deposition on Rock/Fluid Properties of Low Permeability Carbonate Reservoirs". Paper 68229 presented at SPE Middle East Oil Show, Bahrain, 17-20 Mar.

Shedid, A.S. and Abbas, E.A.A. (2005). "An Experimental Approach of the Reversibility of Asphaltene Deposition Under Dynamic Flow Conditions". Paper 92159 presented at SPE Middle East Oil & Gas Show and Conf., Bahrain, 12-15 Mar.

Shell (2001). *EP00- Introducing the E & P Business*, Vol. II, Shell Learning Centre, The Netherlands.

Shen, P., Zhu, B., Li, X-B. and Wu, Y-S. (2010). "An Experimental Study of the Influence of Interfacial Tension on Water-Oil Two-Phase Relative Permeability", *Transport in Porous Media* **85**, 2, 505-520.

Sheu, E.Y. and Storm, D.A. (1995). "Colloidal Properties of Asphaltenes in Organic Solvents". In: *Asphaltenes: Fundamentals and Applications*; E.Y. Sheu and O.C. Mullins (eds.), Plenum Press, New York.

Shin, H. (2008). "A Reservoir Economic Indicator to Evaluate a SAGD Project". Paper 2008-072 presented at Petroleum Society's Annual Technical Meeting, Alberta, 17-19 Jun.

Shin, H. and Polikar, M. (2006). "Fast-SAGD Application in the Alberta Oil Sands Areas", *JCPT* **45**, 9, 46-53.

Siddique, M., Golay, M.W. and Kazimi, M.S. (1993). "Local Heat Transfer Coefficients for Forced-convection of Steam in a Vertical Tube in the Presence of a Noncondensable Gas", *Nucl. Tech.* **102**, 386-402.

Sieder, E.N. and Tate, G.E. (1936). "Heat Transfer and Pressure Drop of Liquids in Tubes", *Ind. Eng. Chem.* **28**, 1429-1436.

Silin, D., Patzek, T. and Benson, S.M. (2009). "A Model of Buoyancy-Driven Two-Phase Countercurrent Fluid Flow", *Transport in Porous Media* **76**, 449-469, DOI 10.1007/s11242-008-9257-1.

Sim, S.S.K., Takabayashi, K., Okatsu, K. and Fisher, D. (2005). "Asphaltene-Induced Formation Damage: Effect of Asphaltene Particle Size and Core Permeability". Paper 95515 presented at SPE Annual Technical Conf. & Exhibition, Dallas, 9-12 Oct.

Simangunsong, R.A., Jaiswal, N.J. and Mamora, D.D. (2006). "Improved Analytical Model and Experimentally Calibrated Studies of Steam Injection With Hydrocarbon Additives to Enhance Heavy-Oil Recovery". Paper 100703 presented at SPE Annual Technical Conf. & Exhibition, Texas, 24-27 Sept.

Singhal, A. K., Ito, Y. and Kasraie, M. (1998). "Screening and Design Criteria for Steam Assisted Gravity Drainage (SAGD) Projects". Paper 50410 presented at SPE Int. Conf. on Horizontal Well Technology, Alberta, 1-4 Nov.

Sinnott, R.K. (1993). *Chemical Engineering Design*, 2nd ed., Butterworth-Heinemann, Oxford.

Siow, E.C., Ormiston, S.J. and Soliman, H.M. (2004). "A Two-phase Model for Laminar-film Condensation from Steam-Air Mixtures in Vertical Parallel-plate Channels", *Int. J. Heat Mass Transfer* **40**, 5, 365-375.

Siow, E.C., Ormiston, S.J. and Soliman, H.M. (2002). "Fully-coupled Solution of a Two-phase Model for Laminar-film Condensation of Vapour-Gas Mixtures in Horizontal Channels", *Int. J. Heat Mass Transfer* **45**, 18, 3689-3702.

Siow, E.C., Ormiston, S.J. and Soliman, H.M. (2007). "Two-phase Modelling of Laminar-film Condensation from Vapour-Gas Mixtures in Declining Parallel-plate Channels", *Int. J. Thermal Sciences* **46**, 458-466.

Sisavath, S., Al-Yaarubi, A., Pain, C.C. and Zimmerman, R.W. (2003). "A Simple Model for Deviations from the Cubic Law for a Fracture Undergoing Dilation or Closure", *Pure appl. Geophys.* **160**, 1009-1022.

Sissom, L.E. and Pitts, D.R. (1972). *Elements of Transport Phenomena*, McGraw-Hill Inc., New York.

Sjølyst, S.J. (2006). "Steam-Assisted Gravity Drainage in Heavy Oil", Statoil, Grieghallen; available in the public domain.

Smith, C.R., Tracy, G.W. and Farrar, R.L. (1992). *Applied Reservoir Engineering*, Vol. 1, Oil & Gas Consultants Int. Inc., Tulsa.

[*] On the document, only the principal investigator is named.

Smith, G.D. (1985). *Numerical Solution of Partial Differential Equations: Finite Difference Methods*, 3rd ed., Oxford U. Press, Oxford.

Smith, J.M. and Van Ness, H.C. (1975). *Introduction to Chemical Engineering Thermodynamics*, McGraw-Hill, New York.

Smith, R.V., Bertuzzi, A.F., Templeton, E.E., and Clampitt, R.L. (1973). "Recovery of Oil by Steam Injection in the Smackover Field, Arkansas", *J. Pet. Tech.* **25**, 8, 883-889.

Sohrabi, M., Emadi, A., Jamiolahmady, M., Ireland, S. and Brown, C. (2008). "Mechanisms of Extra-Heavy Oil Recovery by Gravity-Stable CO_2 Injection". Paper presented at Int. Symp. of Society of Core Analysts, Abu Dhabi, 29 Oct. - 2 Nov.

Somerton, W.H. (1958). "Some Thermal Characteristics of Porous Rocks", *Trans. AIME* **213**, 375.

Somerton, W.H. (1992). *Thermal Properties and Temperature-Related Behaviour of Rock/Fluid Systems*, Elsevier, Amsterdam.

Sonibare, O.O., Egashira, R. and Adedosu, T.A. (2003). "Thermo-oxidative Reactions of Nigerian Oil Sand Bitumen", *Thermochimica Acta* **405**, 195-205.

Sorokhtin, O.G., Chilingar, G.V. and Khilyuk, L.F. (2007). *Global Warming and Global Cooling: Evolution of Climate on Earth*, Elsevier, Amsterdam. Cited in Sorokhtin *et al.* (2007).

Sorokhtin, O.G., Chilingar, G.V., Khilyuk, L.F. and Haroun, M.R. (2010). "Impact of Increasing Anthropogenic CO_2 and CH_4 Gases Emission on Cooling of the Earth's Climate". Paper 127665 presented at SPE Oil & Gas India Conf. and Exhibition, Mumbai, 20-22 Jan.

Soulgani, B.S., Tohidi, B., Jamialahmadi, M. and Rashtchian, D. (2011). "Modelling Formation Damage due to Asphaltene Deposition in the Porous Media", *Energy & Fuels* **25**, 2, 753-761.

Speight, J.G. (1991). *The Chemistry and Technology of Petroleum*, 2nd ed., Marcel Dekker Inc., New York.

Srivastava, R.K., Huang, S.S. and Dong, M. (1999a). "Asphaltene Deposition during CO_2 Flooding", *SPEPF* **14**, 4, 235-245.

Srivastava, R.K., Huang, S.S. and Dong, M. (1999b). "Comparative Effectiveness of CO_2, Produced Gas, and Flue Gas for Enhanced Heavy-Oil Recovery", *SPEREE* **2**, 3, 238-247.

Stephanopoulos, G. (1984). *Chemical Process Control: An Introduction to Theory and Practice*, Prentice-Hall, New Jersey.

Steppan, D.D., Werner, J. and Yeater, R.P. (1998). *Essential Regression and Experimental Design for Chemists and Engineers*, http://www.jowerner.homepage.t-online.de/download.htm, accessed Aug. 22, 2010.

Steyn, P. (2006). "Oil Exploration in Colonial Nigeria", paper presented at 14th Int. Economic History Congress, Helsinki.

Stolz, A. and Graves, R.M. (2003). "Sensitivity Study of Flow Unit Definition by Use of Reservoir Simulation". Paper 84277 presented at SPE Annual Technical Conf. & Exhibition, Denver, 5-8 Oct.

Stone, H.L. (1991). "Rigorous Black Oil Pseudo Functions". Paper 21207 presented at SPE Symposium on Reservoir Simulation, Anaheim, 17-20 Feb.

Stone, H.L. (1973). "Estimation of Three-Phase Relative Permeability and Residual Oil Data", *JCPT* **12**, 4, 53-61.

Stone, T.W., Bennett, J., Law, D.H.S. and Holmes, J.A. (2002). "Thermal Simulation with Multisegment Wells", *SPEREE* **5**, 3, 206-218.

Strikwerda, J.C. (2004). *Finite Difference Schemes and Partial Differential Equations*, 2nd ed., SIAM, Philadelphia.

Sufi, A.H., Ramey, H.J. Jr., and Brigham, W.E. (1982). "Temperature Effects on Relative Permeabilities of Oil-Water Systems". Paper 11071 presented at SPE Annual Fall Tech. Meeting, New Orleans, 26-29 Sept.

Sukhatme, S.P. (1989). *A Textbook on Heat Transfer*, 3rd ed., Sangam Books Ltd., London.

Sumnu, M.D., Brigham, W.E., Aziz, K. and Castanier, L.M. (1996). “An Experimental and Numerical Study on Steam Injection in Fractured Systems”. Paper 35459 presented at SPE Symposium on Improved Oil Recovery, Tulsa, 21-24 Apr.

Svrcek, W.Y. and Mehrotra, A.K. (1989). "Properties of Peace River Bitumen Saturated with Field Gas Mixtures", *JCPT* **28**, 2, 50-56.

Sylvester, N.B. and Chen, H.L. (1988). “An Improved Cyclic Steam Stimulation Model for Pressure-Depleted Reservoirs”. Paper 17420 presented at SPE California Regional Meeting, Long Reach, 23-25 Mar.

Tarhuni, H., Shirif, E., Ayub, M. and Henni, A. (2004). “Theoretical Analysis of Steam Assisted Gravity Drainage Process”. Paper 2004-057 presented at the Canadian Int. Petroleum Conf., Alberta, 8-10 Jun.

Tchobanoglous, G., Burton, F.L. and Stensel, H.D. (2003). *Wastewater Engineering: Treatment and Reuse*, 4th ed., McGraw-Hill, New York.

Thorne, T. and Zhao, L. (2009). “The Impact of Pressure Drop on SAGD Process Performance”, *JCPT* **48**, 9, 41-46.

Tien, C. and Payatakes, A.C. (1979). “Advances in Deep Bed Filtration”, *AIChE J.* **25**, 5, 737-759.

Ting, P.D., Gonzalez, D.L., Hirasaki, G.J. and Chapman, W.G. (2007). “Application of the PC-SAFT Equation of State to Asphaltene Phase Behaviour”. In: *Asphaltenes, Heavy Oils, and Petroleomics*; O.C. Mullins, E.Y. Sheu, A. Hammami and A.G. Marshall (eds.), Springer, New York.

Todd, A.C., Brown, J., Noorkami, M. and Tweedie, J.A. (1979). “Review of Permeability Damage Studies and Related North Sea Water Injection”. Paper 7883 presented at SPE Int. Symp. Oilfield & Geothermal Chemistry, Texas, 22-24 Jan.

Todd, A.C., Kumar, T. and Mohammadi, S. (1990). “The Value and Analysis of Core-based Water-Quality Experiments as Related to Water Injection Schemes”, *SPEFE* **5**, 2, 185-191.

ToolBox (2010). “Roughness and Surface Coefficients of Ventilation Ducts”, www.engineeringtoolbox.com, accessed May 18, 2010.

Tortike, W.S. and Farouq Ali, S.M. (1989). “Saturated-Steam-Property Functional Correlations for Fully Implicit Thermal Reservoir Simulation”, *SPERE* **4**, 4, 471-474.

Tribune Newspapers (2011). “Agbabu Bitumen: Century of Neglect, Tales of Woes”, African Newspapers of Nigeria, http://tribune.com.ng/sun/, accessed June 26, 2011.

Twu, C.H (1984). "An Internally Consistent Correlation for Predicting the Critical Properties and Molecular Weights for Petroleum and Coal-Tar Liquids", *Fluid Phase Equilibria* **16**, 2, 137-150.

Ukwuoma, O. and Ademodi, B. (1999). “The Effects of Temperature and Shear Rate on the Apparent Viscosity of Nigerian Oil Sand Bitumen”, *Fuel Processing Technology* **60**, 95-101.

Umoru, L.E. (2008). “Effect of Weld Type and Post Weld Heat Treatment on the Corrosion Resistance of AISI 321 Stainless Steel in A Tar Sand Digester”, *Emirates J. for Eng. Research* **13**, 2, 45-50.

Umoru, L.E., Afonja, A.A. and Ademodi, B. (2008). “Corrosion Study of AISI 304, AISI 321 and AISI 430 Stainless Steels in a Tar Sand Digester”, *J. Minerals & Materials Characterisation & Eng.* **7**, 4, 291-299.

US DOE (2008). "The Cost of Carbon Dioxide Capture and Storage in Geologic Formations", www.netl.doe.gov, accessed Dec. 17, 2010.

Valbuena, E., Bashbush, J.L. and Rincon, A. (2009). “Energy Balance in Steam Injection Projects: Integrating Surface-Reservoir Systems”. Paper 121489 presented at SPE Latin American & Caribbean Pet. Eng. Conf., Cartagena, 31 May - 3 Jun.

Valenti, N.P., Valenti, R.M. and Koederitz, L.F. (2002). “A Unified Theory on Residual Oil Saturation and Irreducible Water Saturation”. Paper 77545 presented at SPE Annual Technical Conf. & Exhibition, San Antonio, 29 Sept - 2 Oct.

Vanguard (2010). "Nigeria Woos Mining Investors, Offers 3-year Tax Holiday", Vanguard Newspapers, Feb. 22, 2010.

van der Maas, J. and Maldonaldo, E. (1997). “A New Thermal Inertia Model based on Effusivity”, *Int. J. Solar Energy* **19**, 131-160.

van Lookeren, J. (1983). “Calculation Methods for Linear and Radial Steam Flow in oil Reservoirs”, *SPE J.***23**, 3, 427-439.

van Wunnik, J.N.M. and Wit, K. (1992). “Improvement of Gravity Drainage by Steam Injection into a Fractured Reservoir: An Analytical Evaluation”, *SPERE* **7**, 1, 59-66.

Vardoulakis, I., Stavropoulou, M. and Papanastasiou, P. (1996). ”Hydro-Mechanical Aspects of the Sand Production Problem”. *Transport in Porous Media* **22**, 225-244.

Vargas, F.M., Creek, J.L. and Chapman, W.G. (2010). “On the Development of an Asphaltene Deposition Simulator”, *Energy & Fuels* **24**, 4, 2294-2299.

Veil, J.A., Quinn, J.J. and Garcia, J.P. (2009). “Water Issues Relating to Heavy Oil Production”. Paper 120630 presented at SPE Americas E&P Environmental & Safety Conf., Texas, 23-25 Mar.

Vesovic, V., Wakeham, W.A., Olchowy, G.A., Sengers, J.V., Watson, J.T.R. and Millat, J. (1990). “The Transport Properties of Carbon Dioxide”, *J. Phys. & Chem. Data* **19**, 3, 763-808.

Vinsome, P.K.W. and Westerveld, J. (1980). “A Simple Method for Predicting Cap and Base Rock Heat Losses in Thermal Reservoir Simulators”, *JCPT* **19**, 3, 87-90.

Vogel, J.V. (Nov. 1992). “Gravity Drainage: Vital Factor for Understanding Steamfloods”, *Oil & Gas J*., 42-47.

Waldron, J. (2005). “Produced Water Reuse at the Kern River Oil Field”, *Southwest Hydrology* **4**, 6, 26-27.

Wang, J., Buckley, J.S. and Creek, J.L. (2004). “Asphaltene Deposition on Metallic Surfaces”, *J. Dispersion Sci. & Tech.* **25**, 3, 287-298.

Wang, J., Dong, M., and Asghari, K. (2006). "Effect of Oil Viscosity on Heavy-Oil / Water Relative Permeability Curves". Paper 99763 presented at SPE/DOE Symposium on Improved Oil Recovery, Tulsa, 22–26 Apr.

Wang, S. and Civan, F. (2005). “Modelling Formation Damage by Asphaltene Deposition during Primary Oil Recovery”, *J. Energy Resources Tech.* **127**, 310-317.

Wang, S. and Civan, F. (2001). “Productivity Decline of Vertical and Horizontal Wells by Asphaltene Deposition in Petroleum Reservoirs”. Paper 64991 presented at SPE Int. Symposium on Oilfield Chemistry, Houston, 13-16 Feb.

Warren, J.E. and Price, K.S. (1961). “Flow in Heterogeneous Porous Media”, *SPE J*. **1**, 3, 153-169.

Wei, W. and Gates, I.D. (2010). “On the Relationship between Completion Design, Reservoir Characteristics, and Steam Conformance Achieved in Steam-based Recovery Processes Such as SAGD”. Paper 129694 presented at SPE Improved Oil Recovery Symposium, Oklahoma, 24-28 Apr.

Weinstein, H.G. (1972). “A Semi-Analytic Method for Thermal Coupling of Reservoir and Overburden”, *SPE J*. **12**, 5, 439-447.

Weinstein, H.G. (1974). “Extended Semianalytic Method for Increasing and Decreasing Boundary Temperatures”, *SPE J*. **14**, 2, 152-164.

Wennberg, K.E., Batrouni, G.G., Hansen, A. and Horsrud, P. (1996). “Band Formation in Deposition of Fines in Porous Media”, *Transport in Porous Media* **25**, 3, 247-273.

Wilke, C.R. (1950). *J. Chem. Phys.* **18**, 517-519.

Williams, R.L., Ramey Jr., H.J., Brown, S.C., Sanyal, S.K. and Raghavan, R. (1980). “An Engineering Economic Model for Thermal Recovery Methods”. Paper 8906 presented at SPE Annual California Regional Meeting, California, 9-11 Apr.

Wojtanowicz, A.K., Krilov, Z. and Langlinais, J.P. (1987). “Study on the Effect of Pore Blocking Mechanisms on Formation Damage”. Paper 16233 presented at SPE Production Operations Symp., Oklahoma, 8-10 Mar.

Xie, J., Jones, S.W., Mathews, C.M., Wagg, B.T., Parker, P. and Ducharme, R. (2007). “Slotted Liner Design for SAGD Wells – Staggered Slot and Gang Slot Patterns Show Better Performance in Finite Element Analysis Model than Overlapping Slot Pattern”. *World Oil* **228**, 6, 667-675.

Xin, Z., Yongbin, W., Baofeng, W., Panqing, G., Huiying, Z., Bateer, H. and Yu, Q. (2010). “Investigation of Steam Injection at Critical Condition and a Pilot Test in 119-52, Chao-601”. Paper 130968 presented at CPS/SPE Int. Oil & Gas Conf. and Exhibition, Beijing, 8-10 Jun.

Yang, G. and Butler, R.M. (1992). "Effects of Reservoir Heterogeneities on Heavy Oil Recovery by Steam-Assisted Gravity Drainage", *JCPT* **31**, 8, 37-43.

Yang, C., Card, C. and Nghiem, L. (2009). "Economic Optimisation and Uncertainty Assessment of Commercial SAGD Operations", *JCPT* **48**, 9, 33-40.

Yang, W. and Wattenbarger, R.A. (1991). "Water Coning Calculations for Vertical and Horizontal Wells". Paper 22931 presented at SPE Annual Technical Conf. & Exhibition, Texas, 6-9 Oct.

Yee, C.T. and Stroich, A. (2004). "Flue Gas Injection Into a Mature SAGD Steam Chamber at the Dover Project (Formerly UTF)", *JCPT* **43**, 1, 54-61.

Yortsos, Y.C. and Gavalas, G.R. (1981a). "Analytical Modelling of Oil Recovery by Steam Injection: Part I – Upper Bounds", *SPE J.* **21**, 2, 162-178.

Yortsos, Y.C. and Gavalas, G.R. (1981b). "Analytical Modelling of Oil Recovery by Steam Injection: Part II – Asymptotic and Approximate Solutions", *SPE J.* **21**, 2, 179-190.

Yortsos, Y.C. and Gavalas, G.R. (1982). "Heat Transfer Ahead of Moving Condensation Fronts in Thermal Oil Recovery Processes", *Int. J. Heat Mass Transfer* **25**, 3, 305-316.

Yudin, I.K., Nikolaenko, G.L., Gorodetskii, E.E., Kosov, V.I., Melikyan, V.R., Markhashov, E.L., Frot, D. and Briolant, Y. (1998). "Mechanisms of Asphaltene Aggregation in Toluene-Heptane Mixtures", *J. Pet. Sci. & Eng.* **20**, 297-301.

Zabel, F., Law, D.H.S., Taylor, S. and Zuo, J. (2010). "Impact of Uncertainty of Heavy Oil Fluid Property Measurements", *JCPT* **49**, 3, 28-35.

Zalan, T.A., Badruzzaman, A., Julander, D. and Whittlesey, K. (2003). "Steamflood Surveillance in Sumatra, Indonesia and San Joaquin Valley, California Using Steam Identification, Carbon/Oxygen, and Temperature Logs". Paper 80435 presented at SPE Asia Pacific Oil & Gas Conf. and Exhibition, Jakarta, 9-11 Sept.

Zekri, A.Y., Shedid, S.A. and Alkashef, H. (2001). "A Novel Technique for Treating Asphaltene Deposition Using Laser Technology". Paper 70050 presented at SPE Permian Basin Oil & Gas Recovery Conference, Texas, 15-16 May.

Zhang, F., Fan, X. and Ding, J. (2000). "Field Experiment of Enhancing Heavy Oil Recovery by Cyclic Fuel Gas Injection". Paper 64724 presented at SPE Int. Oil & Gas Conf. and Exhibition, Beijing, 7-10 Nov.

Zhang, L. and Dusseault, M.B. (2004). "Sand-Production Simulation in Heavy-Oil Reservoirs", *SPEREE* **7**, 6, 399-407.

Zhang, W., Youn, S., and Doan, Q. (2007). "Understanding Reservoir Architectures and Steam Chamber Growth at Christina Lake, Alberta, by using 4D Seismic and Crosswell Seismic Imaging", *SPEREE* **10**, 5, 446-452.

Zhang, X., Zhang, Y., Yue, Q., Gao, Y. and Shen, D. (2009). "Conformance Control of CSS and Steam Drive Process with a Carbamide Surfactant", *JCPT* **48**, 9, 16-18.

Zienkiewicz, O.C. and Morgan, K. (1983). *Finite Elements and Approximation*, Wiley, New York.